Characterisation of a novel *GBA*-L444P BAC transgenic mouse model of Parkinson's disease

A thesis submitted for the degree of

Doctor of Philosophy



TARA DIVINEY

St. John's College

Department of Physiology, Anatomy and Genetics

University of Oxford

Trinity Term 2025

DECLARATION OF AUTHORSHIP

I declare that the data presented in this thesis are my own work. Where data have been provided by other individuals, due acknowledgement has been given in the main text and relevant figure legends. No part of this work has been submitted for the award of any other degree at the University of Oxford or any other university.

ACKNOWLEDGEMENTS

Firstly, I would like to express my gratitude towards my supervisors Richard Wade-Martins, Stephanie Cragg and Natalie Connor-Robson. To Richard and Steph, thank you for giving me the opportunity to take ownership of this project and to develop as a scientist across both of your labs. I appreciate all of the advice and guidance that you have given me throughout my DPhil. To Natalie, thank you for being a fountain of encouragement when the going got tough and for your advice to "jump through the hoop" in the final stretch. You have been an incredible support over the past years, both professionally and personally, and even from a distance in Cardiff! I will miss our catch-ups over Zoom!

I would also like to thank my viva examiners, Mark Walton and Patrick Lewis, for thoroughly reviewing my thesis and for an interesting discussion.

I am grateful to many members of the Wade-Martins and Cragg labs, past and present, who have helped me along the way. I would especially like to thank Emmanuel Lopes for his sage advice in all FCV-related matters, his patience as I was learning the ropes and for always being so generous with his time. A big thank you also to Milena Cioroch, Peter Kilfeather and Kamila Blachowiak for their help with mouse-related procedures, advice around colony management and good company. I would also like to thank to Nora Bengoa-Vergniory for training me in the mouse behavioural assays and to Elliot Mock for helpful discussions, especially around lipidomics. To Bethan O'Connor, Jess Livesey, Lucille Duquenoy and Shinil Raina thank you for contributing to some of my most enjoyable times in the lab and for always being so willing to lend a "hand", especially when I needed it most.

Related to this, I am eternally grateful to my thoracic surgeon and my physiotherapist at the Nuffield Orthopaedic Centre. Regaining the power and functionality in my right hand has been indispensable to finishing my lab work and to typing my thesis.

I would like to express my most sincere appreciation to those who have contributed data that is presented in this thesis. These collaborative research efforts have enriched my DPhil experience. Kateryna Bila and Martijn van der Lienden in the lab of Johannes Aerts (Leiden University) and Benjamin Jenkins (University of Cambridge) conducted lipidomic analysis on our model. Also, Clara Obensa Bertroli in Tim Bartels' lab (UK DRI at UCL) executed subcellular alpha-synuclein distribution assays. A huge thank you also to Georgina Menzies at the University of Cardiff for introducing me to the world of modelling protein-protein interactions and for extremely helpful discussions around the topic.

I am also indebted to my college advisor, Sandra Campbell, whose advice and encouragement over cups of coffee in the Senior Common Room have helped me tremendously, especially while navigating some of the more challenging phases of this project.

To Denise, thank you for pushing me in the right direction and for reminding me to trust in myself. I am very glad to have met you. To Anna and Patricia, our friendship is so important to me. I feel very lucky to have had your support throughout the highs and lows of the DPhil rollercoaster- we did it! I also want to give a shout out to the Horsebox Coffee Co., whose flat whites helped me to power through long days in the lab.

To Alex, you have been right by my side throughout this journey, no matter where we are in the world. Thank you for caring, for always believing in me and for cheering me on. You are very precious to me.

To my Mom and Dad, Kathy and Fergal, words cannot do justice to describe how vital your contribution has been to this project. I hope you already know that I could not have completed (or started) this DPhil had it not been for your unwavering encouragement and support. I look forward to making up for times that I have been absent during this phase.

ABSTRACT

Parkinson's disease (PD) is a progressive, age-related, multifactorial disorder, primarily characterised by motor symptoms associated with the loss of dopaminergic neurons of the substantia nigra and alpha-synuclein accumulation in Lewy bodies. Despite being the second most common neurodegenerative disorder worldwide, the underlying molecular mechanisms of PD remain poorly understood. An enigmatic interplay of genetic and environmental factors is thought to form the core of PD aetiology in most patients. Of the numerous genes that are implicated in PD pathology, *GBA* has emerged as the strongest genetic risk factor for the disease. This gene encodes for glucocerebrosidase (GCase), a lysosomal hydrolase that converts GlcCer to glucose and ceramide. Although approximately 10% of PD patients harbour a *GBA* variant, the mechanisms of GCase dysfunction in PD remain elusive. Indeed, the limitations of existing strategies to model *GBA*-associated PD in mice pose a barrier to progress in this field. To enhance our understanding of mutant GCase-related pathology in PD, our lab created the first humanised mouse model of *GBA*-associated PD, using BAC transgenic technology. To achieve this, the full-length human *GBA*-L444P gene, along with its endogenous promoter and regulatory elements, was specifically integrated into the mouse Rosa26 locus. We chose to model the L444P mutation because it is one of the most common *GBA* variants found in PD patients and typically predisposes to severe clinical manifestations. The overarching aim of this thesis was to characterise pathology in our *GBA*-L444P mice from a molecular to a behavioural level. The experiments presented herein identified that GCase activity is impaired and immature mutant GCase accumulates in our L444P mice, thereby illustrating that this model can successfully recapitulate both loss- and gain-of-function effects related to the L444P mutation. Furthermore, evoked dopamine release is diminished in the dorsolateral striatum of the L444P mice from an early age. This marks the first demonstration of striatal dopaminergic transmission deficits in a genetic mouse model of *GBA*-associated PD. Notably, this phenotype was not accompanied by loss of striatal dopamine content or dopaminergic neurodegeneration in the substantia nigra. Finally, our model displays subtle gait impairments in their hindlimbs but generally does not replicate the overt motor and non-motor clinical manifestations of PD in patients. Taken together, these findings highlight the usefulness of our L444P BAC transgenic mice as a resource for future research that aims to illuminate mutant GCase dysfunction in the early stages of *GBA*-associated PD.

CONFERENCE PRESENTATIONS

Diviney, T., Connor-Robson, N., Roberts, B.M., Brimblecombe, K.R., Cragg, S.J., Wade-Martins, R. Characterisation of a novel *GBA*-L444P BAC transgenic mouse model of Parkinson's disease. *Invited guest speaker*, ARUK Thames Valley Network Research day, University of Oxford, United Kingdom. June 2024.

Diviney, T., Connor-Robson, N., Roberts, B.M., Brimblecombe, K.R., Cragg, S.J., Wade-Martins, R. Characterisation of a novel *GBA*-L444P BAC transgenic mouse model of Parkinson's disease. *Selected poster presentation*, Gordon Research Conference and Seminar, Les Diablerets, Switzerland. May 2023.

Diviney, T., Connor-Robson, N., Roberts, B.M., Brimblecombe, K.R., Cragg, S.J., Wade-Martins, R. Characterisation of a novel *GBA*-L444P BAC transgenic mouse model of Parkinson's disease. *Invited guest speaker*, UK Dementia Research Institute- Parkinson's disease early career researchers workshop. Hybrid: online and University of Manchester, United Kingdom. March 2023.

Diviney, T., Connor-Robson, N., Roberts, B.M., Brimblecombe, K.R., Cragg, S.J., Wade-Martins, R. Characterisation of a novel *GBA*-L444P BAC transgenic mouse model of Parkinson's disease. *Invited guest speaker (Data Blitz presentation) and selected poster presentation,* The BRAIN conference, Online. February 2022.

Diviney, T., Connor-Robson, N., Roberts, B.M., Brimblecombe, K.R., Cragg, S.J., Wade-Martins, R. Characterisation of a novel *GBA*-L444P BAC transgenic mouse model of Parkinson's disease. *Runner-up poster prize*, DPAG Second year DPhil poster day, University of Oxford, United Kingdom. November 2021.

Diviney, T., Connor-Robson, N., Roberts, B.M., Brimblecombe, K.R., Cragg, S.J., Wade-Martins, R. Characterisation of dopamine release in a BAC transgenic *GBA*-L444P mouse model of Parkinson's disease using fast-scan cyclic voltammetry. *Selected poster presentation*, Virtual Dopamine Conference, Online. June 2021.

TABLE OF CONTENTS

DECLARATION OF AUTHORSHIP ..... **I**

ACKNOWLEDGEMENTS ..... **II**

ABSTRACT ..... **IV**

CONFERENCE PRESENTATIONS ..... **V**

LIST OF FIGURES ..... **XI**

LIST OF TABLES ..... **XIV**

LIST OF ABBREVIATIONS ..... **XV**

CHAPTER 1: INTRODUCTION **1**

1.1 OVERVIEW OF PARKINSON'S DISEASE **1**

1.1.1 Worldwide prevalence and burden 1

1.1.2 Symptomatology 3

1.1.3 Neuropathological hallmarks and therapeutic strategies 5

1.1.4 Aetiology 9

1.1.4.1 Age and sex 9

1.1.4.2 Dietary and lifestyle factors 11

1.1.4.3 Exposure to environmental toxicants 12

1.1.4.4 Genetics 13

1.2 *GBA* AS THE STRONGEST GENETIC RISK FACTOR FOR PD **15**

1.2.1 The historical background to *GBA*'s association with PD 15

1.2.2 The prevalence and penetrance of *GBA* variants in PD patients 19

1.2.3 The clinical profile of *GBA*-associated PD 23

1.2.4 Symptom management in PD patients with *GBA* mutations 28

1.3 GCASE: PHYSIOLOGICAL FUNCTION AND PD-RELATED DYSFUNCTION **29**

1.3.1 GCase structure and catalytic activity 29

1.3.2 The cellular lifecycle of GCase 32

1.3.3 Pathological pathways of *GBA*-associated PD 35

1.3.3.1 Loss-of-function: GCase enzymatic deficiency 35

1.3.3.2 Gain-of-function: the ER-retention of misfolded, mutant GCase 39

1.3.3.3 The pathogenic exchange between GCase and αS 40

1.3.4 Disease-modifying therapeutic strategies targeting GCase function 44

1.4 MODELLING *GBA*-ASSOCIATED PD IN MICE **46**

1.4.1 A brief introduction to animal models of PD 46

1.4.2 Current mouse models of GCase dysfunction in PD: strategies and key phenotypes.....48
1.4.3 Limitations of existing approaches to model *GBA*-associated PD.....53
1.4.4 Creation of a novel, humanised *GBA*-L444P transgenic mouse model and thesis overview.....56
1.4.5 Aims of this thesis.....59

CHAPTER 2: MATERIALS AND METHODS.....61

2.1 GENERATION AND MAINTENANCE OF TRANSGENIC MICE.....61
2.1.1 Creation of humanised *GBA* transgenic mice.....61
2.1.2 Breeding strategies.....61
2.1.3 Husbandry and ethical declaration.....62
2.2 MOUSE GENOTYPING.....64
2.2.1 DNA extraction from mouse tissue biopsies.....64
2.2.2 Amplification of extracted DNA lysates.....64
2.2.3 DNA restriction enzyme digest.....65
2.2.4 Agarose gel preparation and electrophoresis.....65
2.2.5 Representative genotyping results on agarose gels.....67
2.3 METHODS PERTAINING TO CHAPTER 3.....68
2.3.1 Generation and treatment of mixed primary cortical cultures from neonatal mice.....68
2.3.2 Immunocytochemistry on primary cortical cell cultures.....69
2.3.3 GCase activity assay.....70
2.3.4 BCA assay to quantify protein concentration.....73
2.3.5 Western blotting.....73
2.3.6 Lipidomic analysis.....75
2.3.7 αS quantification in membrane and soluble tissue fractions.....76
2.3.8 Computational characterisation of GCase-LIMP2 interactions.....77
2.4 METHODS PERTAINING TO CHAPTER 4.....81
2.4.1 Voltammetric detection of striatal DA dynamics in *ex vivo* slices.....81
2.4.1.1 Microelectrode fabrication.....81
2.4.1.2 Acute slice preparation.....81
2.4.1.3 FCV recordings.....82
2.4.2 Immunofluorescence of paraffin-embedded striatal sections.....84
2.4.2.1 Tissue fixation via transcardiac perfusion of PFA.....84
2.4.2.2 Paraffin embedding and sectioning.....85
2.4.2.3 Tissue staining and imaging.....85
2.4.3 HPLC with electrochemical detection.....87
2.5 METHODS PERTAINING TO CHAPTER 5.....89
2.5.1 Locomotion in the open field.....89

2.5.2 Accelerating rotarod 89
2.5.3 Vertical pole test 90
2.5.4 Inverted screen test 90
2.5.5 The CatWalk XT gait analysis system 91
2.5.6 Stool collection 91
2.5.7 The T-maze assessment of spontaneous alternation behaviour 92
2.5.8 The elevated plus maze 92
2.6 STATISTICAL ANALYSIS 93

CHAPTER 3: ELUCIDATING GAIN-OF-FUNCTION AND LOSS-OF-FUNCTION EFFECTS OF THE L444P MUTATION 96

3.1 INTRODUCTION 96
3.2 RESULTS 102
3.2.1 Human GCase expression in cortical tissue 102
3.2.2 GCase activity in primary cortical cell cultures and tissue 103
3.2.3 BiP, LAMP1 and LC3 expression in cortical tissue 106
3.2.4 Lipidomic analysis in the brain, liver and spleen 108
3.2.5 Subcellular αS distribution in the brain 113
3.2.6 The nature of the GCase-LIMP2 interaction across disease-states and species 115
3.3 DISCUSSION 130
3.3.1 L444P mice display phenotypes related to gain-of-function and loss of GCase activity 130
3.3.2 Ambroxol failed to rescue GCase activity deficits in L444P primary cortical cultures 131
3.3.3 Changes to GCase activity, ER homeostasis or lysosomal/autophagic function were not detected in L444P cortex tissue 133
3.3.4 GlcSph accumulates in the brain and viscera of *Gba*$^{+/-}$ mice 135
3.3.5 The subcellular distribution of αS was unchanged across genotypes 138
3.3.6 The strength and conformation of GCase-LIMP2 interactions in our humanised *GBA* mice may differ from the human environment 140
3.3.7 Conclusion 144

CHAPTER 4: THE IMPACT OF THE L444P MUTATION ON STRIATAL DOPAMINERGIC TRANSMISSION 146

4.1 INTRODUCTION 146
4.2 RESULTS 151
4.2.1 Characterisation of DA release in the aged striatum with multisite FCV recordings ... 151
4.2.2 Quantification of striatal dopaminergic axon density and striatal DA content 153
4.2.3 The regulation of DA reuptake and short term plasticity by the DAT 156
4.2.4 D_2R-mediated inhibition of DA release 162

4.2.5 Tonic GABAergic inhibition of DA release in response to single-pulse and phasic stimulations 166

4.3 DISCUSSION 171

4.3.1 The DLS $[DA]_o$ deficit in L444P mice is a marker of early stage selective vulnerability in the absence of neuronal loss....171

4.3.2 Elevated L444P NAcC $[DA]_o$ may be a manifestation of early compensatory mechanisms 173

4.3.3 Aberrant DA release in L444P mice is not accompanied by striatal DA depletion or perturbed DA turnover 176

4.3.4 PD-related disturbances to the local control of DA transmission by the striatal microcircuitry 178

4.3.5 Future research avenues to shed light on the mechanistic basis of impaired $[DA]_o$ in L444P mice....184

4.3.6 Conclusion....187

CHAPTER 5: BEHAVIOURAL CHARACTERISATION OF AGED MICE.....189

5.1 INTRODUCTION....189

5.2 RESULTS....192

5.2.1 Characteristics of the behavioural cohort....192

5.2.2 Spontaneous locomotion in the open field 193

5.2.3 Motor coordination and balance on the accelerating rotarod....194

5.2.4 Speed and coordination on the vertical pole 196

5.2.5 Muscle strength using the inverted screen test....198

5.2.6 Automated gait analysis with the CatWalk XT 199

5.2.7 GI function with the stool collection test 202

5.2.8 Spatial working memory using the T-maze spontaneous alternation test 204

5.2.9 Anxiety-like behaviour in the EPM....205

5.3 DISCUSSION 207

5.3.1 Motor dysfunction in *GBA*-associated PD is poorly recapitulated in mouse models ...207

5.3.2 Abnormal gait signatures of rodent models imitates gait deficits in PD patients 214

5.3.3 Mouse models of *GBA*-associated PD have mild or inconsistent non-motor phenotypes 218

5.3.4 Factors influencing the validity and reproducibility of behavioural data in PD models 227

5.3.4.1 The relevance of ageing to symptom manifestation is largely disregarded in behavioural studies with *Gba* rodent models 227

5.3.4.2 Behavioural characterisation across both sexes is necessary to encapsulate the diverse clinical profile of PD patients....229

5.3.4.3 Many rodent behavioural studies lack adequate power....230

5.3.4.4 Novel, automated technologies show promise to improve the reliability of behavioural data 231

5.3.5 Conclusion....232

CHAPTER 6: DISCUSSION....234

6.1 STRENGTHS OF OUR L444P MODEL AND SUMMARY OF KEY FINDINGS IN THIS THESIS....234

6.2 LIMITATIONS OF OUR L444P MICE AND GENERAL CHALLENGES OF MODELLING *GBA*-ASSOCIATED PD....239

6.3 FUTURE RESEARCH DIRECTIONS....241

6.3.1 Identifying novel disease features in our model and probing the mechanisms of observed phenotypes....242

6.3.2 Exploring the multifactorial nature of *GBA*-associated PD....244

6.4 CONCLUDING REMARKS....248

APPENDIX....250

REFERENCES....263

LIST OF FIGURES

Figure 1.1: Schematic of the *GBA* gene illustrating the positions of PD-relevant mutations. 20
Figure 1.2: Glycosphingolipid metabolism in the lysosome. 31
Figure 1.3: The physiological lifecycle of GCase and GCase dysfunction in PD. 34
Figure 1.4: Summary of the experimental genotypes used in this thesis and insights from individual genotypic pairwise comparisons. 58
Figure 2.1: Breeding strategy for experimental mice. 63
Figure 2.2: Representative genotyping results from the PCRs and restriction enzyme digest reactions described in this thesis. 67
Figure 2.3: The computationally predicted structures of proteins used as inputs for HADDOCK docking. 78
Figure 2.4: Cross-species sequence alignment of residues on GCase and LIMP2 that previous studies have determined as important for mediating the GCase-LIMP2 interaction. 80
Figure 3.1: Characterisation of midbrain pathology in L444P mice. 100
Figure 3.2: L444P mice have elevated high MW GCase, whereas total human GCase levels are comparable across hWT and L444P mice. 103
Figure 3.3: Primary cortical cultures from L444P and *Gba*$^{+/-}$ mice have impaired GCase activity, which is not rescued by ambroxol. 104
Figure 3.4: GCase activity in cortex tissue is not significantly different across genotypes. 105
Figure 3.5: Cortical BiP levels are similar across genotypes. 106
Figure 3.6: Cortical LAMP1 and LC3 levels are comparable across genotypes. 107
Figure 3.7: Quantification of sphingolipid species that are directly influenced by GCase activity across brain regions. 110
Figure 3.8: Cholesterol and GlcChol levels are comparable across genotypes in various brain regions. 111
Figure 3.9: Quantification of sphingolipid species that are directly influenced by GCase activity in visceral organs. 112
Figure 3.10: The subcellular distribution of αS is similar across genotypes in 3-month-old mice. 114
Figure 3.11: The subcellular distribution of αS is not significantly different across genotypes in aged mice. 115
Figure 3.12: The structure and intermolecular energies of the docked HuGCase-MuLIMP2 complex. 118
Figure 3.13: The structure and intermolecular energies of the docked HuL444PGCase-MuLIMP2 complex. 119

Figure 3.14: The structure and intermolecular energies of the docked MuGCase-MuLIMP2 complex. 120
Figure 3.15: The structure and intermolecular energies of the docked HuGCase-HuLIMP2 complex. 121
Figure 3.16: Parameters mediating the strength of the GCase-LIMP2 interaction across complexes. 123
Figure 3.17: The structural conformation and polar interactions of the HuGCase-MuLIMP2 and HuL444PGCase-MuLIMP2 complexes. 124
Figure 3.18: The structural conformation and polar interactions of the HuGCase-MuLIMP2 and MuGCase-MuLIMP2 complexes. 127
Figure 3.19: The structural conformation and polar interactions of the HuGCase-MuLIMP2 and HuGCase-HuLIMP2 complexes. 129
Figure 4.1: Multisite FCV recordings of 1p-evoked $[DA]_o$ in the striatum of 3-month-old mice. ..149
Figure 4.2: Local control of striatal DA release from striatal axons. 150
Figure 4.3: Multisite FCV recordings of 1p-evoked $[DA]_o$ in the striatum of aged mice. 152
Figure 4.4: Dopaminergic axon area is preserved in the DLS of L444P mice. 154
Figure 4.5: DA and DOPAC levels are maintained in the striatum of aged L444P mice. 155
Figure 4.6: The dynamics of DAT-mediated DA uptake is similar across genotypes at 3-6 months. 157
Figure 4.7: No genotype-related differences in DA uptake by the DAT were observed in aged mice. 158
Figure 4.8: Short term plasticity of DA release is comparable across genotypes in aged mice prior to and during cocaine exposure. 160
Figure 4.9: DAT expression levels are similar across genotypes in the DLS. 161
Figure 4.10: Inhibition of DA release by D_2Rs is unaltered in 3-6-month-old L444P mice. 163
Figure 4.11: D_2R-mediated inhibition of DA release remains similar across genotypes in aged mice. 164
Figure 4.12: The abundance of D_2Rs in the DLS is comparable across genotypes. 165
Figure 4.13: The extent of GABAergic inhibition of DA release is not different across genotypes in 3-6-month-old mice. 167
Figure 4.14: The levels of striatal GABA tone remained comparable across genotypes in aged mice. 168
Figure 4.15: The frequency sensitivity of DA release is similar across genotypes in the absence and presence of $GABA_{A+B}$R antagonism. 170
Figure 5.1: The age, weight and sex distribution of the behavioural analysis cohort. 192
Figure 5.2: Spontaneous LMA is similar across genotypes. 194
Figure 5.3: Aged L444P mice did not display coordination or balance deficits on the rotarod. 196

Figure 5.4: No genotype-related differences were observed in the vertical pole test. 197
Figure 5.5: Grip strength was normal across genotypes in the inverted screen test. 198
Figure 5.6: Heatmap summarising the results from gait analysis using the CatWalk XT. 200
Figure 5.7: Swing duration and swing speed are exclusively altered in the hindlimbs of L444P mice. 201
Figure 5.8: Assessment of GI function using the stool collection test. 203
Figure 5.9: All genotypes had similar activity and spontaneous alternation rates in the T-maze. ..205
Figure 5.10: Total activity and open arm activity were similar across genotypes in the EPM. 206

Figure A-1: GalCer and GalSph levels are comparable across genotypes in various brain regions. 250
Figure A-2: The structural conformation of the GCase-LIMP2 complexes, illustrating polar contacts within and outside the main interaction interface. 255
Figure A-3: DA neurons in the SN are preserved in aged L444P mice. 256
Figure A-4: Striatal DA and DOPAC levels are comparable across genotypes in 3-month-old mice. 257
Figure A-5: The relationship of rotarod performance with age and bodyweight.....258
Figure A-6: Bodyweight did not influence the total descent time from the vertical pole.....259
Figure A-7: Various temporal gait parameters recorded by the CatWalk XT were not different across genotypes.....260
Figure A-8: Spatial gait parameters recorded by the CatWalk XT were not different across genotypes.....261
Figure A-9: Support and coordination gait parameters recorded by the CatWalk XT were not different across genotypes. 262
Figure A-10: Print gait parameters recorded by the CatWalk XT were not different across genotypes.....262

LIST OF TABLES

Table 1.1: Clinical and demographic features of the three GD subtypes. 18
Table 1.2: Summary of observational cohort studies that illustrate the distinctive clinical features of *GBA*-associated PD. 27
Table 1.3: Overview of key phenotypes in *Gba* transgenic mice used to model *GBA*-associated PD. 51
Table 2.1: Mouse colonies used for maintenance purposes. 62
Table 2.2: Lysis buffer recipe for DNA extraction. 64
Table 2.3: PCR parameters for genotyping mouse DNA lysates in this thesis. 66
Table 2.4: Cell plating conditions for cortical primary cultures. 69
Table 2.5: Primary antibodies used for immunocytochemistry. 70
Table 2.6: CP-buffer recipe for GCase activity assay. 71
Table 2.7: GCase activity assay protocol specifics for cells and tissue. 72
Table 2.8: BCA assay parameters. 73
Table 2.9: Composition of buffer solutions used in western blot sample preparation. 74
Table 2.10: Recipe for western blot reagents. 75
Table 2.11: Primary antibodies used for western blots. 75
Table 2.12: αS antibodies used in the MSD immunoassay. 76
Table 2.13: Composition of solutions used for acute slice preparation and FCV recordings. 82
Table 2.14: Details of drugs used in FCV wash-on experiments. 84
Table 2.15: Primary antibodies used for immunofluorescence in tissue. 86
Table 2.16: Parameters for loading standards and samples for HPLC experiments. 88
Table 2.17: Recipe for mobile phase used for HPLC. 88
Table 5.1: Studies investigating motor function in existing genetic mouse models of *GBA*-associated PD and GD. 208
Table 5.2: Studies investigating motor function in existing multifactorial genetic mouse models of *GBA*-associated PD and GD. 210
Table 5.3: Description of CatWalk XT gait parameters analysed in this thesis. 215
Table 5.4: Studies investigating non-motor behaviour in existing genetic mouse models of *GBA*-associated PD and GD. 220
Table 5.5: Studies investigating non-motor behaviour in existing genetic multifactorial mouse models of *GBA*-associated PD and GD. 222

Table A-1: List of interacting residues across complexes determined by PRODIGY and RING analyses. 251

LIST OF ABBREVIATIONS

$[DA]_o$	Concentration of extracellular dopamine
4-MUG	4-methylumbelliferyl-β-D-glucopyranoside
6-OHDA	6-hydroxydopamine
AAV	Adeno-associated virus
ACDase	Acid ceramidase
aCSF	Artificial cerebrospinal fluid
AJ	Ashkenazi Jewish
ANCOVA	Analysis of covariance
ANOVA	Analysis of variance
αS	Alpha-synuclein
BAC	Bacterial artificial chromosome
BCA	Bicinchoninic acid
BiP	Binding immunoglobulin protein
CBE	Conduritol B epoxide
CFM	Carbon-fibre microelectrode
CMA	Chaperone-mediated autophagy
CPu	Caudate putamen
CSF	Cerebrospinal fluid
CTSD	Cathepsin D
CTSL	Cathepsin L
D_2R	Dopamine D_2 receptor
DA	Dopamine
DAT	Dopamine transporter
DBS	Deep brain stimulation
DHβE	Dihydro-β-erythroidine hydrobromide
DIV	Day *in vitro*
DLS	Dorsolateral striatum
DOPAC	3,4-dihydroxyphenylacetic acid
Endo-H	Endoglycosidase-H
EPM	Elevated plus maze

ER	Endoplasmic reticulum
ERAD	Endoplasmic reticulum-associated degradation
FCV	Fast-scan cyclic voltammetry
$GABA_{A+B}R$	$GABA_A$ and $GABA_B$ receptor
GalCer	Galactosylceramide
GalSph	Galactosylsphingosine
GCase	Glucocerebrosidase
GCase2	Glucocerebrosidase-2
GD	Gaucher disease
GI	Gastrointestinal
GlcCer	Glucosylceramide
GlcChol	Cholesteryl glucoside (1-*O*-cholesteryl-b-D-glucopyranoside)
GlcSph	Glucosylsphingosine
GPi	Globus pallidus internus
GWAS	Genome-wide association studies
HPLC	High-performance liquid chromatography
hWT	Human wild-type
IF	Immunofluorescence
iPSC-DAns	iPSC-derived DA neurons
KI	Knock-in
KO	Knockout
L-Dopa	Levodopa
LAMP1	Lysosomal-associated membrane protein-1
LAMP2A	Lysosomal-associated membrane protein-2A
LB	Lewy body
LC-MS	Liquid chromatography-mass spectrometry
LC-MS/MS	Liquid chromatography-tandem mass spectrometry
LC3	Microtubule-associated protein 1 light chain 3
LIMP2	Lysosomal integral membrane protein 2
LMA	Locomotor activity
LRRK2	Leucine-rich repeat kinase 2
MPTP	1-methyl-4-phenyl-1,2,3,6-tetrahydropyridine
MSD	Mesoscale discovery

MW	Molecular weight
NAc	Nucleus accumbens
NAcC	Nucleus accumbens core
nAChR	Nicotinic acetylcholine receptor
nTG	Non-transgenic
PBS	Phosphate-buffered saline
PCR	Polymerase chain reaction
PD	Parkinson’s disease
PDD	Parkinson’s disease dementia
PFA	Paraformaldehyde
PFF	Preformed fibril
PGRN	Progranulin
PIGD	Postural instability and gait difficulty
PLA	Proximity ligation assay
PND	Postnatal day
PPR	Paired pulse ratio
PSAP	Prosaposin
RBD	REM-sleep behaviour disorder
ROS	Reactive oxygen species
SapC	Saposin C
SEM	Standard error of the mean
SN	Substantia nigra
SNCA-OVX	Alpha-synuclein overexpressing
SNPs	Single nucleotide polymorphisms
STN	Subthalamic nucleus
TEM	Transmission electron microscopy
TH	Tyrosine hydroxylase
UPR	Unfolded protein response
VGLUT2	Vesicular glutamate transporter 2
VTA	Ventral tegmental area
WT	Wild-type

CHAPTER 1: INTRODUCTION

1.1 OVERVIEW OF PARKINSON'S DISEASE

1.1.1 WORLDWIDE PREVALENCE AND BURDEN

Parkinson's disease (PD) stayed largely inconspicuous to clinicians until 1817, when James Parkinson first formally described the clinical manifestations of the disorder in *An Essay on the Shaking Palsy* (Parkinson, 1817). In the initial years post-publication, Parkinson's monograph was largely overlooked and PD remained understudied (Fahn, 2018, Louis, 1997). Indeed, Jean-Martin Charcot described the disease as "generally not well known" in the mid 1800s (Charcot and Vulpian, 1861, Walusinski, 2018). Nowadays, it is well-established that the symptoms Parkinson described are associated with dopaminergic neurodegeneration of the substantia nigra (SN) and alpha-synuclein (αS) accumulation in Lewy bodies (LBs) (Poewe et al., 2017), although these realisations were over 100 years in the making (Fahn, 2018). In addition, relatively few PD cases and related-deaths had been documented by the turn of 20th the century, altogether indicating that PD was a rare condition (Dorsey et al., 2018b, Garcia-Ruiz and Espay, 2017, Morris, 1989). Fast-forward 200 years since Parkinson's pioneering work, we are now facing a PD pandemic (Dorsey et al., 2018b).

Today, PD is known to affect over 11 million people worldwide (Luo et al., 2024), making it the second most common neurodegenerative disorder in the world after Alzheimer's disease (Feigin et al., 2017, Steinmetz et al., 2024). PD predominantly affects older generations: its estimated prevalence is just below 1% of the global population over 60 years of age (Zhu et al., 2024) and peaks among individuals aged over 80-years-old (Dorsey et al., 2018a). On a global stage, regions with a higher sociodemographic index and human development index also tend to report a higher crude and age-standardised

prevalence of PD (Dorsey et al., 2018a, Peng et al., 2025, Zhu et al., 2024). This finding appears counterintuitive considering that regions' sociodemographic index positively correlates with overall population health (Lim et al., 2016). However, increased population longevity in nations with relatively high economic status is thought to play a role in driving the higher frequency of cases overall. Superior diagnostic infrastructure and increased exposure to occupational- and lifestyle-related PD risk factors that result from industrialisation and urbanization, e.g. heavy metal pollution, physical inactivity, may also contribute to the elevated age-standardized prevalence in these geographies (Dorsey et al., 2018a, Peng et al., 2025, Zhu et al., 2024). Notably, historical trends in the age-adjusted incidence are conflicting across nations, which suggests region-specific fluctuations in exposures to certain risk factors (Darweesh et al., 2016, Dorsey et al., 2018a, Okunoye et al., 2022, Savica et al., 2016, Xu et al., 2024). Some of these risk factors are further discussed in **Section 1.1.4**. Alternatively, the relative-scarcity of data in low-income countries may give rise to an underestimation of the true prevalence of the disease in these regions (Dorsey et al., 2018a, Pereira et al., 2024). It should also be highlighted that race/ethnicity is rarely incorporated into research investigating PD risk factors (Siddiqi et al., 2025) and that various ethnic minorities are underrepresented in PD research at large (Aamodt et al., 2023, Sanchez et al., 2022, Schumacher-Schuh et al., 2022). Studies in multi-ethnic North American populations have largely demonstrated that PD is most common among white people (Aamodt et al., 2023). However, it has been suggested that poor study design, differential access to healthcare and clinician-related biases may confound prevalence estimates across ethnicities (Aamodt et al., 2023, Harris et al., 2023, Siddiqi et al., 2025).

PD is also the fastest growing neurological disorder internationally (Dorsey et al., 2018a, Feigin et al., 2017). According to a Global Burden of Disease study, the overall prevalence of the disease increased by 74% between 1990 and 2016 (Dorsey et al., 2018a).

This concerning growth rate cannot be exclusively explained by increased life-expectancy in the global population (Schumacher et al., 2024) because the age-standardised prevalence has also risen by 22% over the same period (Dorsey et al., 2018a). In addition, the estimated worldwide incident cases experienced a 1.6-fold increase since 1990 (Ou et al., 2021) and stood at 1.02 million cases in 2017 (James et al., 2018). By 2040, it is estimated that 13-14 million individuals globally will be living with PD (Dorsey and Bloem, 2018). In parallel with the rise in cases over the past three decades, mortality and disability attributed to PD has also surged (Dorsey et al., 2018a, Lampropoulos et al., 2022, Ou et al., 2021, Peng et al., 2025). Indeed, these factors exacerbate the overall burden that the disease places on caregivers (Mosley et al., 2017, Schrag et al., 2006) and the economy (Chaudhuri et al., 2024, Yang et al., 2020b).

Clearly, there is a critical need for increased research investment, patient access to healthcare and risk prevention strategies to futureproof against this global public health challenge (Dorsey and Bloem, 2018, Schiess et al., 2022). Despite this, the aetiology and pathophysiology of PD remain elusive and there are no therapies that can halt or reverse disease progression (Kouli et al., 2018, Stocchi et al., 2024). Although the field has made remarkable progress over the past two centuries (Obeso et al., 2017), there remains a long road ahead.

1.1.2 SYMPTOMATOLOGY

The clinical profile of PD is canonically defined by the four cardinal motor signs of the disorder: bradykinesia, tremor, rigidity and postural instability (Jankovic, 2008). Motor deficits tend to present unilaterally in early phases of disease and progress bilaterally in later stages (Mirelman et al., 2019). Depending on the predominant motor symptom, patients can to be classified into two clinical subtypes: tremor-dominant or postural instability and gait difficulty (PIGD)-dominant (Jankovic et al., 1990), although the relevance of this

classification system has faced criticism (Kotagal, 2016, Nutt, 2016). The motor phenotype of PIGD-dominant patients is primarily characterised by bradykinesia with gait impairments. These patients typically have more severe, accelerated motor impairment than the tremor-dominant patients (Jankovic and Kapadia, 2001, Jankovic et al., 1990, Thenganatt and Jankovic, 2014). Postural instability, characterised by balance deficits due to lack of postural reflexes, usually emerges in late stages of disease course but can arise earlier in PIGD-dominant patients (Crouse et al., 2016, Palakurthi and Burugupally, 2019). It has been described as the most debilitating motor symptom and increases patients' risk of falling (Crouse et al., 2016). On the other hand, bradykinesia, tremor and rigidity tend to feature earlier in the disease course and therefore form the bedrock of clinical diagnosis of Parkinsonism (Postuma et al., 2015).

Although the International Parkinson and Movement Disorder Society (MDS) diagnostic criteria recognizes PD as "primarily a motor disorder" (Postuma et al., 2015), a wide range of non-motor symptoms also occur in the disease (Schapira et al., 2017). The significant burden that these symptoms place on patient quality of life is increasingly recognized, despite being historically neglected by clinicians (Chaudhuri et al., 2020, LeWitt and Chaudhuri, 2020, Martinez-Martin et al., 2011, Todorova et al., 2014). Firstly, a broad spectrum of cognitive difficulties, such as issues with memory, attention and executive function, are frequently observed in PD patients (Aarsland et al., 2021, Muslimovic et al., 2005). These symptoms often progress to dementia in later disease stages (Gibson et al., 2024, Hely et al., 2008, Pedersen et al., 2017). Psychiatric disturbances, including depression, anxiety and psychosis are also highly prevalent in PD but poorly understood (Weintraub et al., 2022). Cognitive and psychiatric dysfunction have been determined to significantly deteriorate patients' quality of life and functional ability (Balestrino and Martinez-Martin, 2017, Bock et al., 2022, Leroi et al., 2012, Soh et al., 2011). In addition,

sleep disturbances e.g. REM-sleep behaviour disorder (RBD) (Stefani and Hogl, 2020), gastrointestinal (GI) dysfunction (Fasano et al., 2015) and olfactory impairments (Fullard et al., 2017) are common features of the disease.

Importantly, non-motor symptoms typically arise during the prodromal phase of PD (Berg et al., 2015, Fengler et al., 2017). This prodromal period precedes the manifestation of cardinal motor signs and is thought to span approximately 10 years in most patients (Berg et al., 2015, Stern et al., 2012), although it was shown to last longer in patients with RBD (Schenck et al., 2013). Therefore, early identification of clinical markers of prodromal PD could help to detect at-risk individuals, expedite diagnosis, facilitate differential diagnoses, monitor early disease progression and select appropriate patients for clinical trials of disease-modifying therapies (Hustad and Aasly, 2020, Postuma and Berg, 2016, Salat et al., 2016). Indeed, various diagnostic tools are in the development pipeline to detect both non-motor symptoms (Janssen Daalen et al., 2024) and subtle motor deficits e.g. oculomotor abnormalities (Antoniades and Spering, 2024, Maetzler et al., 2024) that manifest in the prodromal phase of disease.

1.1.3 NEUROPATHOLOGICAL HALLMARKS AND THERAPEUTIC STRATEGIES

The progressive degeneration of dopamine (DA) neurons in the SN combined with αS accumulation in LBs and Lewy neurites define the neuropathological diagnosis of PD (Poewe et al., 2017).

An estimated 30-50% of DA neurons in the SN have insidiously degenerated by the time of motor symptom onset in patients (Cheng et al., 2010, Fearnley and Lees, 1991). Despite this, neighbouring DA neurons in the ventral tegmental area (VTA) remain relatively unscathed in the disease. The factors governing the selective vulnerability of SN DA neurons in PD is a long-standing mystery (Brichta and Greengard, 2014). However, the uniquely

large axonal arbour and pacemaking activity of these neurons likely plays a role by increasing their susceptibility to bioenergetic insufficiency and oxidative stress (Giguere et al., 2018). Many studies have also supported that neurodegeneration starts at striatal axon terminals and follows a "dying-back" process (Tagliaferro and Burke, 2016). Supporting this, Cheng et al. (2010) estimated that at clinical diagnosis, 50-60% of DA axon terminals in the striatum are lost, whereas only 30% of DA neurons in the SN have degenerated. Unsurprisingly, therapeutic strategies that act to replace lost dopamine are the cornerstone of PD symptom management (Armstrong and Okun, 2020). Levodopa (L-Dopa), a synthetic DA precursor, has remained the typical first-line treatment of PD symptoms for over 50 years (Cotzias et al., 1969, LeWitt, 2015, Salat and Tolosa, 2013). However, the prolonged use of L-Dopa can lead to motor complications, including dyskinesia and motor fluctuations (Aquino and Fox, 2015, Armstrong and Okun, 2020). Compared to oral L-Dopa intake, the direct infusion of levodopa-carbidopa intestinal gel (LCIG) increases the stability of the L-Dopa concentration in patient plasma (Nyholm et al., 2003). LCIG treatment is therefore effective against motor fluctuations and has been shown to improve patient quality of life, alongside various motor and non-motor symptoms, in the advanced stages of PD (Antonini et al., 2017, Fasano et al., 2023). DA receptor agonists are an alternative treatment option to manage motor symptoms in the disorder. The most common DA agonists used for PD, e.g. pramipexole, ropinirole and rotigotine, are selective for D_2-like DA receptor subtypes ($D_2/D_3/D_4$) (Isaacson et al., 2023). These medications can be prescribed in the early stages of disease to delay the need for L-Dopa or as an adjunct to L-Dopa therapy in later stages (de Bie et al., 2020, Fox et al., 2018). DA agonists are regarded as "clinically useful" in the treatment of motor fluctuations (Fox et al., 2018) and studies have demonstrated that these drugs confer lower risk of motor complications vs L-Dopa when administered as an initial therapy (Hauser et al., 2007, Parkinson Study Group, 2009, Pringsheim et al., 2021, Stowe

et al., 2008). However, compared to L-Dopa, DA agonists are associated with increased risk of non-motor adverse effects, including impulse control disorders, and were shown to be less effective at improving motor symptoms and overall quality of life (de Bie et al., 2020, Fox et al., 2018, Gray et al., 2014, Pringsheim et al., 2021, Stowe et al., 2008). Notably, the advent of deep brain stimulation (DBS) was a major milestone in the treatment of motor symptoms in patients with advanced PD who no longer respond to L-Dopa or who experience L-Dopa related complications. This neurosurgical approach involves the insertion of electrodes into specific nuclei of the basal ganglia motor circuitry (Hariz and Blomstedt, 2022). The subthalamic nucleus (STN) is the most common site targeted in PD patients, followed by the globus pallidus internus (GPi). High frequency stimulation of the STN or GPi is thought to improve patients' motor function by alleviating hyperactivity in these regions; however, it remains subject to debate whether STN-DBS confers greater clinical benefit than GPi-DBS (Hariz and Blomstedt, 2022, Lachenmayer et al., 2021, Mansouri et al., 2018). According to the classical basal ganglia model, overactivation of the STN and GPi in PD largely arises due to loss of striatal DA causing increased activity in the indirect pathway (McGregor and Nelson, 2019). Related loss of signalling in the direct pathway also has a disinhibitory effect on the GPi. The net effect of increased GPi output in PD patient brains is to increase inhibition of the thalamus and motor cortex, thereby attenuating movement and giving rise to the cardinal motor symptoms of the disease (McGregor and Nelson, 2019). It follows that both STN-DBS and GPi-DBS have widely demonstrated efficacy to treat motor symptoms of the disorder including akinesia, rigidity and tremors (Hariz and Blomstedt, 2022, Lachenmayer et al., 2021, Mahlknecht et al., 2022, Machado and Reppold, 2015). In addition, DBS was the advanced treatment option associated with the greatest improvement in quality of life in a meta-analysis of PD patients (Nijhuis et al., 2021). However, various aspects of cognitive function have been shown to

decline following DBS (Bucur and Papagno, 2023, Nassery et al., 2016, Troster, 2024, Wang et al., 2016) and evidence is lacking surrounding the longer-term effects of DBS on disease progression (Mahlknecht et al., 2022). Indeed, disease-modifying treatments that can reverse or halt neurodegeneration remain highly sought-after but are currently unavailable (Vijiaratnam et al., 2021). Notably, restoring DA neurons via stem cell transplantation has recently demonstrated safety and tolerability in phase I/II clinical trials (Sawamoto et al., 2025, Tabar et al., 2025) and many other trials investigating this approach are currently ongoing (Barker et al., 2024).

Lewy pathology was discovered in PD patient brains in 1912 (Lewy, 1912); however, it was not until the late 1990s that aggregated αS was identified as the main component of LBs and Lewy neurites (Spillantini et al., 1997, Spillantini et al., 1998). Physiologically, αS plays a role in neurotransmitter release and is thought to exist in equilibrium between a monomeric and stable tetrameric state (Bartels et al., 2011, Calabresi et al., 2023, Sharma and Burre, 2023). On the other hand, the accumulation of αS oligomers and fibrils is known to be at centre-stage of PD pathology (Alam et al., 2019). These toxic species are involved in various pathological processes including inflammation, oxidative and endoplasmic reticulum (ER) stress, mitochondrial dysfunction and lysosomal/autophagic deficits (Calabresi et al., 2023, Fields et al., 2019). However, there are many controversies and unknowns surrounding αS's physiological and pathological forms and functions (Burre et al., 2018, Fauvet et al., 2012, Fields et al., 2019), including whether αS fibrils are present in LBs (Lashuel, 2020, Shahmoradian et al., 2019). Nevertheless, it remains the general consensus that Lewy pathology spreads throughout the PD brain in a relatively stereotypical pattern with disease progression, as initially proposed by Braak in his staging hypothesis (Braak et al., 2003a). According to Braak's hypothesis, inclusions first manifest in the olfactory bulb or the brainstem and subsequently propagate through the midbrain, eventually

infiltrating the cortex in later disease stages (Goedert et al., 2013). Although initial Lewy pathology in the olfactory bulb has been connected to hyposmia as an early disease symptom (Fullard et al., 2017), many have criticised the relevance of Braak staging to the progression of clinical symptoms and neuronal loss (Braak and Del Tredici, 2017, Rietdijk et al., 2017). Moreover, it is estimated that Lewy pathology in up to 20% of PD patients does not follow the typical Braak staging pattern (Jellinger, 2019). In spite of this, the prion-like spread of αS helped to spark the gut-brain axis hypothesis of PD. This paradigm-shifting theory speculates that PD originates from αS aggregates in the enteric nervous system that propagate to the brainstem via the vagus nerve (Braak et al., 2003b, Breen et al., 2019, Tan et al., 2022). Therefore, GI dysfunction may be both a manifestation (Fasano et al., 2015) (**Section 1.1.2**) and mediator of PD pathology. Considering αS's pivotal role in PD pathology, clinical trials of disease-modifying therapies that target its aggregation and accumulation are ongoing (Baggett et al., 2024, Grosso Jasutkar et al., 2022).

1.1.4 AETIOLOGY

The idiom "genetics loads the gun but environment pulls the trigger" comes to mind when describing the elusive, complex interplay between genetic and environmental risk factors that predispose to PD development. The heterogeneity of these risk factors, see Ascherio and Schwarzschild (2016) and Ben-Shlomo et al. (2024) for detailed reviews, has contributed to viewpoint that PD should not be considered as a single entity (Weiner, 2008). This section describes some of the major intrinsic, environmental and genetic influences that can predispose to this multi-aetiological condition.

1.1.4.1 Age and sex

Ageing is the single biggest risk factor for PD (Reeve et al., 2014), as indicated by the predominance of the disease among older individuals (**Section 1.1.1**). On an international

scale, PD prevalence, alongside disease-related mortality and disability, sharply increases with age between 50 and 85 years (Dorsey et al., 2018a) but declines thereafter. This decrease is likely related to higher rates of underdiagnosis and co-morbidities among individuals older than 85 (Dorsey et al., 2018a). According to the Parkinson's Progression Markers Initiative (PPMI) database, the mean age of symptom onset is 61.6 years-old and less than 15% of patients experience symptoms before the age of 50 (Pagano et al., 2016). Indeed, the alarming rate at which PD cases are growing worldwide has largely been attributed to increased longevity in the global population (Dorsey et al., 2018a, Mathers et al., 2015, Schumacher et al., 2024). A slew of age-related pathological changes, including mitochondrial, proteasomal and autophagic dysfunction, have been proposed to underlie the association between ageing and PD (Reeve et al., 2014). These dysfunctional changes are likely to occur years before diagnosis, considering the long-spanning prodromal phase in many patients (Kalia and Lang, 2015).

Sex is also known to influence the risk of PD development (Cerri et al., 2019): the global age-standardised prevalence of the disease is approximately 1.4-1.5 fold higher in men than women (Dorsey et al., 2018a, Steinmetz et al., 2024), although the extent of this difference was shown to be variable across geographies (Pringsheim et al., 2014, Zirra et al., 2023). This unequal sex-distribution may contribute to the underrepresentation of women in PD clinical trials (Tosserams et al., 2018) and to sex-related disparities in PD diagnosis and the provision of care (Subramanian et al., 2022, Willis et al., 2011). The factors governing why men are more susceptible to PD are not understood but the preponderance of pesticide exposure among men and neuroprotective effects of oestrogen in women have been suggested to contribute (Cattaneo and Pagonabarraga, 2025, Frigerio et al., 2006, Haaxma et al., 2007, Savica et al., 2013).

1.1.4.2 Dietary and lifestyle factors

Epidemiological studies have indicated that physical activity and exercise can protect against the development of PD later in life (LaHue et al., 2016, Sasco et al., 1992). This benefit may be attributed to an exercise-related release of neurotrophic factors and reduction in inflammation and oxidative stress (LaHue et al., 2016). Diet patterns and overall diet quality may also influence PD risk, as supported by recent meta-analyses (Liu et al., 2021, Zhang et al., 2025a, Zhao et al., 2025). Individuals who follow diets that are rich in fruit, vegetables and whole grains, such as a Mediterranean-style diet, were consistently found to be at lower risk for the disease (Alcalay et al., 2012b, Gao et al., 2007, Zhang et al., 2025a, Zhao et al., 2025). Adherence to a Mediterranean-style diet was also suggested to play a role in the decline of PD incidence in Italy (Li et al., 2025, Ou et al., 2021, Peng et al., 2025). However, reports looking at specific dietary factors have produced inconsistent results (Boulos et al., 2019). For instance, a high intake of refined sugar and saturated fats may the increase the risk of developing PD and prodromal PD symptoms (Anderson et al., 1999, Wang et al., 2025, Zhang et al., 2025a) but this lacks definitive evidence (reviewed by Seidl et al. (2014)). Moreover, consumption of certain dairy products were found to modestly increase PD risk in US cohorts (Chen et al., 2007, Hughes et al., 2017) but not in European cohorts (Groninger et al., 2024, Strikwerda et al., 2021). Nevertheless, dietary components' effect on PD patients' gut microbiota is a current hot topic and may help to delineate a causal basis between the intake of certain foods and PD susceptibility (Jackson et al., 2019, Kwon et al., 2024, Solch et al., 2022).

In addition, cigarette smoking has been connected to a lower risk of PD (Li et al., 2015). Accordingly, the cessation in smoking habits worldwide (Dai et al., 2022, Ng et al., 2014) may contribute to the heightened global prevalence of PD (Dorsey et al., 2018a, Savica et al., 2016) and has been predicted to exacerbate the future escalation in PD cases (Rossi et

al., 2018). However, a causal relationship between PD and smoking has not been established (Rossi et al., 2018).

1.1.4.3 Exposure to environmental toxicants

It can be challenging to establish causal inferences between environmental toxicants and PD development (Aravindan et al., 2024). However, a clear case arose in the 1980s when a group of illicit drug users in California developed advanced parkinsonism overnight after injecting themselves with a "synthetic heroin" (Langston, 2017, Langston et al., 1983). The compound responsible for their symptoms was identified as 1-methyl-4-phenyl-1,2,3,6-tetrahydropyridine (MPTP), which has since been widely used to model PD in mice (Meredith and Rademacher, 2011) and non-human primates (Porras et al., 2012). It was later highlighted that MPTP has a similar chemical structure to paraquat, a well-known herbicide widely used in agricultural practises (Barbeau, 1984). Since then, many studies have supported that occupational exposure to various pesticides, including paraquat and rotenone, and other agricultural toxicants can increase individuals' susceptibility to PD (Aravindan et al., 2024, Berry et al., 2010, Cao et al., 2018, Tanner et al., 2011). The mechanism(s) of toxicity for these compounds include mitochondrial dysfunction, inflammation and oxidative stress (Cao et al., 2018). Contact with industrial chemicals such as chlorinated solvents (Gash et al., 2008, Goldman et al., 2023) and heavy metals (Willis et al., 2010) via water, air or soil pollution has also been linked to PD; however, some epidemiological studies have produced conflicting results (De Miranda et al., 2022, Goldman, 2014, Willis et al., 2010). Notably, China has the highest age-adjusted incidence and prevalence of PD in the world, which has been linked to high levels of pesticide and industrial pollution exposure among inhabitants of the country (Dorsey et al., 2018a, Li et al., 2025, Xu et al., 2024).

1.1.4.4 Genetics

A mere 40 years ago, the possibility that PD has a genetic component was rejected by some in the field (Duvoisin, 1984). Nowadays, approximately 15% of patients have been shown to carry a PD-related genetic mutation (Westenberger et al., 2024, Cook et al., 2024) and family history for the disease is a known risk factor (Noyce et al., 2012). The genetic landscape of PD has been broadly been divided into two classes, according to genetic variants' penetrance and prevalence in patients.

The first class, monogenic PD, can be directly attributed to Mendelian inheritance of a known pathogenic variant. These variants are typically rare but highly penetrant (Day and Mullin, 2021). Of the 19 genes that are implicated in monogenic PD, 10 are autosomal dominant e.g. *SNCA, LRRK2* and the rest are autosomal recessive e.g. *PINK1, PRKN* (Deng et al., 2018). Notably however, many rare monogenic variants lack functional validation and their relevance to the disease is controversial (Blauwendraat et al., 2020). The first insights into the genetic architecture of monogenic PD came in the late 1990s, with the discovery of the *SNCA*-A53T mutation in families with autosomal dominant inheritance of the disease (Polymeropoulos et al., 1997). Since this landmark study, eight further *SNCA* missense variants, along with *SNCA* duplications and triplications (Ibanez et al., 2004, Singleton et al., 2003), have been causally associated with autosomal-dominant PD (Deng et al., 2018, Jia et al., 2022). However, the pathogenicity of *SNCA*-H50Q has been contested (Blauwendraat et al., 2018b). Duplications are the most common *SNCA* monogenic variant (Lesage et al., 2020, Trinh et al., 2018) and are associated with milder clinical manifestations and a later age-of-onset than triplications, thereby suggesting a dosage-effect (Book et al., 2018, Ross et al., 2008). To note, *SNCA* is the gene encoding for αS and this toxic protein accumulates in *SNCA* mutation carriers in a similar fashion to idiopathic patients (**Section 1.1.3**). However, different types of *SNCA* mutations facilitate αS aggregation and

accumulation via heterogenous mechanisms, which are not fully understood (Rosborough et al., 2017, Serratos et al., 2022, Vidovic and Rikalovic, 2022). Although αS pathology occurs universally in PD patients, pathogenic *SNCA* variants have only been observed in up to 0.2% of patients in recent observational clinical studies (Cook et al., 2024, Westenberger et al., 2024).

On the other hand, mutations in *LRRK2*, the gene encoding leucine-rich repeat kinase 2 (LRRK2), are the most common cause of monogenic PD and have been identified 2.5-3% of PD patients overall (Cook et al., 2024, Lunati et al., 2018, Westenberger et al., 2024). *LRRK2*-G2019S has the highest prevalence out of the 10 pathogenic *LRRK2* variants that have been associated with the disease thus far (Simpson et al., 2022). This mutation is most frequently observed in North-African Arabs, accounting for approximately 40% of total cases in this population, while it is typically found in less than 5% of European patients overall (Correia Guedes et al., 2010, Lesage et al., 2006). Although most monogenic variants are highly penetrant in the disease, penetrance estimates of the G2019S mutation range between 9-74%, according to the population studied and patient age (Healy et al., 2008, Kmiecik et al., 2024). Typically, PD-related *LRRK2* mutations serve to increase LRRK2 function, either by increasing the protein's kinase activity or by reducing its GTPase activity (Reed et al., 2019, West et al., 2005). The mechanisms underlying how *LRRK2* mutations lead to neurodegeneration are not fully established, although lysosomal, autophagic and synaptic recycling deficits are likely to play a role (Martin et al., 2014).

The 2nd class of genetic mutations in PD are referred to as risk variants. These variants are more prevalent than monogenic mutations but their penetrance is too low to be designated as causative in the disease (Day and Mullin, 2021). The advent of genome-wide association studies (GWAS) has been instrumental to the discovery of these genetic risk factors (Bandres-Ciga et al., 2020, Satake et al., 2009, Simon-Sanchez et al., 2009). To date,

GWAS have identified up to 90 risk loci in the disease (Nalls et al., 2019) and have helped to unravel diversity in the genetic basis of the disorder across populations (Foo et al., 2020, Kim et al., 2024a, Loesch et al., 2021, Nalls et al., 2019, Rizig et al., 2023). Notably, many of the variants identified by GWAS are located close to genes that are implicated in monogenic PD, including *SNCA* and *LRRK2*. These pleomorphic risk loci suggest that pathogenic mechanisms are shared between monogenic and non-monogenic disease forms (Reed et al., 2019). Despite the importance of GWAS, the strongest genetic risk factor for PD, *GBA*, was first connected to the disease through astute clinical observations (**Section 1.2.1**). *GBA* encodes for glucocerebrosidase (GCase), a lysosomal enzyme that hydrolyses glucosylceramide (GlcCer) to glucose and ceramide (**Section 1.3.1**). *GBA* mutations have been found in approximately 10% of PD patients (Cook et al., 2024, Westenberger et al., 2024); however, they are canonically referred to as risk variants due to their relatively low penetrance in the disease compared to monogenic variants (Balestrino et al., 2020) (**Section 1.2.2**). Despite this, some recent reports have described *GBA* variants as "causal" in the disease (Blauwendraat et al., 2020, Reed et al., 2019, Rossi et al., 2025) and the distinction between genetic causal and risk factors becomes somewhat blurred considering that *LRRK2* variants have mixed penetrance but are still classed as monogenic causes (Day and Mullin, 2021). Nevertheless, this thesis will refer to *GBA* variants as genetic risk factors for PD. These variants are described further in the next section.

1.2 *GBA* AS THE STRONGEST GENETIC RISK FACTOR FOR PD

1.2.1 THE HISTORICAL BACKGROUND TO *GBA*'S ASSOCIATION WITH PD

Early clues of *GBA*'s involvement in PD came from a series of clinical case reports of parkinsonism in Gaucher disease (GD) patients (Bembi et al., 2003, McKeran et al., 1985,

Neudorfer et al., 1996, Tayebi et al., 2001, Turpin et al., 1988, Varkonyi et al., 2003). GD is a rare, autosomal-recessive, lysosomal storage disorder (Stirnemann et al., 2017), first described in 1882 by Philippe Gaucher (Gaucher, 1882). There are three recognized clinical types of GD, based on the presence and rate of neurological decline (**Table 1.1**). However, the heterogenous, multisystemic nature of disease symptoms can sometimes render it challenging to assign patients to a disease category (Hertz et al., 2024). GD is caused by GCase deficiency due to the inheritance of pathogenic biallelic (homozygous or compound heterozygous) *GBA* mutations (Brady et al., 1965b, Horowitz et al., 2022, Hruska et al., 2008). This results in the lysosomal accumulation of GCase lipid substrates in macrophages, thereby causing their transformation into Gaucher cells (Stirnemann et al., 2017). The infiltration and amassment of Gaucher cells in various tissues and organs is the clinical hallmark of GD and is thought to be primarily responsible for symptoms of the disorder (Furderer et al., 2022, Stirnemann et al., 2017). Different *GBA* mutations predominate across each type of GD (**Table 1.1**). *GBA*-N370S is the most prevalent variant in type 1 GD and is not found in neuronopathic forms (Hruska et al., 2008, Koprivica et al., 2000, Theophilus et al., 1989a). The *GBA*-L444P mutation is another highly common variant, which has been observed in all three disease types but typically predisposes to type 2 in a compound heterozygous state and type 3 in a homozygous state (Grabowski et al., 2015, Koprivica et al., 2000, Theophilus et al., 1989a). To note, the GD3c subtype (**Table 1.1**) is exclusively caused by homozygous D409H mutations (Abrahamov et al., 1995, Kurolap et al., 2019).

Whilst all pathogenic *GBA* variants cause GD in a biallelic state, carriers of heterozygous (monoallelic) variants are at increased risk of PD. The first screening studies that demonstrated increased prevalence of heterozygous *GBA* mutations in PD patients were published over 20 years ago (Aharon-Peretz et al., 2004, Lwin et al., 2004). Around the same time, other reports identified an increased incidence of PD among relatives of GD patients

(Goker-Alpan et al., 2004, Halperin et al., 2006). An international multicentre screening study later confirmed that heterozygous *GBA* mutations are a risk factor for PD (Sidransky et al., 2009). These findings have been corroborated by many reports in the past 15 years to firmly establish *GBA* as the strongest genetic risk factor for the disease (Gabbert et al., 2023, Zhang et al., 2018a).

Two recent multicentre observational clinical studies identified *GBA* variants in approximately 10% of screened PD patients (Cook et al., 2024, Westenberger et al., 2024). *GBA* mutations are most common in patients of Ashkenazi Jewish (AJ) origin, with an estimated prevalence around 20% in this population (Gan-Or et al., 2015a, Goldstein et al., 2019, Rossi et al., 2025, Ruskey et al., 2019). However, the frequency of individual *GBA* mutations in PD varies considerably across demographics, described further in the next section (**Section 1.2.2**) (Gabbert et al., 2023, Koros et al., 2024).

Table 1.1: Clinical and demographic features of the three GD subtypes.

Type	GD1	GD2	GD3
Relevant mutations	N370S/N370S, N370S/84GG, N370S/L444P.[1]	L444P/RecNciI, RecNciI/RecNciI*[2-3] D409H + H255Q/D409H + H255Q.[6]	L444P/L444P, L444P/D409H[1] V394L/RecNciI[#], N188S/RecNciI[#] [4] D409H/D409H[†].[5]
Primary CNS involvement	Conventionally absent but Gaucher cells observed in post-mortem brains and Parkinsonism can develop.[7-8]	Acute neuronopathic form: rapid aggressive neurodegeneration.[9-10]	Chronic neuronopathic form: slower neurological deterioration vs GD2, mixed reports of neurodegeneration.[1-2, 7]
Symptom onset	Typically, during childhood but can also first present later in life. Earlier onset observed in N370S/84GG patients.[1]	Usually within one year of birth after a symptom-free period. Can present prenatally or neonatally in rare cases*.[2-3, 10-11]	Generally, by 20 years old.[11]
Severity	Variable: patients can develop severe symptoms early or be asymptomatic into adulthood.[1, 11]	The most severe type: mortality generally occurs in infancy/ early childhood. Prenatal and neonatal death are also observed*.[3, 9, 11]	Variable across clinical subtypes (see below). Patients usually survive into their 20s-30s.[12]
Clinical manifestations	Diverse symptoms observed across and within mutations. Splenomegaly, hepatomegaly, cytopenia, skeletal disease and pulmonary disease are commonly observed. N370S/N370S is considered to convey milder symptoms.[12, 14]	Opisthotonus, spontaneous apnoea, strabismus, poor sucking and swallowing reflexes are common neurological symptoms. Hydrops fetalis and congenital ichthyosis (collodion baby phenotype) can also be observed in pre-term foetuses or neonates*.[2, 9-10, 12]	Slowed horizontal saccades are a defining feature. Patients also share symptoms with GD1. Three subtypes with distinct phenotypes: *GD3a:* Myoclonic epilepsy, *GD3b:* Less severe neurological symptoms than GD3a, *GD3c:* Cardiac defects associated with valvular and aortic calcification.[2, 4, 5, 12]
Estimated prevalence	Most common type in western and AJ populations. Affects 0.26-0.63:100,000 of European populations and up to 1:850 of the AJ population. Represents 90-95% of cases in Europe and North America.[11, 13-14]	The rarest type overall. Affects 0.02-0.08:100,000 of European populations. Generally, accounts for < 5% of cases across cohorts.[9, 11, 13]	Prevalence 0.02-0.04:100,000 in European populations and typically represents 5% of cases. Observed more frequently in the Asia-Pacific region and in some Swedish populations (Norrbottnian subtype).[11, 13, 15-16]

* = refers to perinatal lethal Gaucher disease (PLGD), a rare subtype of GD2. RecNciI homozygosity is exclusively observed in this subtype and symptoms present prenatally in stillborn foetuses or at full-term birth, [#] = identified in patients with the GD3a subtype, [†] = observed in GD3c only; AJ = Ashkenazi Jewish.

References: 1 = (Grabowski et al., 2015); 2 = (Daykin et al., 2021); 3 = (Mignot et al., 2003); 4 = (Park et al., 2003); 5 = (Abrahamov et al., 1995); 6 = (Michelakakis et al., 2006); 7 = (Furderer et al., 2022); 8 = (Imbalzano et al., 2024); 9 = (Gupta et al., 2011); 10 = (Weiss et al., 2015); 11 = (Stirnemann et al., 2017); 12 = (Hughes and Pastores, 2023); 13 = (Castillon et al., 2022); 14 = (Mistry et al., 2011); 15 = (Tajima et al., 2009); 16 = (Tsitsi et al., 2022).

1.2.2 THE PREVALENCE AND PENETRANCE OF *GBA* VARIANTS IN PD PATIENTS

The *GBA* gene, located on chromosome 1q21, is composed of 11 exons and 10 introns that span across 7604 bps (Ginns et al., 1985, Horowitz et al., 1989). Exons 8-10 are a hotspot for GD- and PD-relevant pathogenic *GBA* variants (Parlar et al., 2023, Zhang et al., 2018a). (**Fig. 1.1**). These mutations can be classed as "risk", "mild" or "severe" in PD according to their pathogenicity for GD in a biallelic state (Parlar et al., 2023). Risk variants (e.g. E326K and T369M) are non-pathogenic in GD, whereas mild (e.g. N370S) and severe (e.g. L444P) variants cause non-neuronopathic and neuronopathic GD, respectively[1]. However, most of the ~400 *GBA* variants that have been observed in PD patients are classed as "unknown" because their pathogenicity in GD and PD is poorly established due to their rarity in the conditions (Parlar et al., 2023, Rossi et al., 2025). The N370S, L444P, E326K and T369M missense mutations are regarded as the most common variants in PD, validated by a recent systematic reviews (Gabbert et al., 2023, Rossi et al., 2025) and large multicentre observational clinical studies (Cook et al., 2024, Westenberger et al., 2024). Together, these variants accounted for over 80% of cases in a UK cohort (Malek et al., 2018). However, the frequency of these mutations varies across populations (Gabbert et al., 2023, Koros et al., 2024) (**Fig. 1.1**).

[1] The nomenclature for *GBA* variants in this thesis excludes GCase's 39-amino acid signal peptide (Sorge et al., 1987) and thereby follows the canonical system of describing sequence variations. Current Human Genome Variation Society (HGVS) guidelines (den Dunnen and Antonarakis, 2001, den Dunnen et al., 2016) recommend describing sequence variants according to their position in the cDNA sequence. Therefore, updated nomenclature for *GBA* variants incorporates GCase's signal peptide (Hruska et al., 2008). For instance, N370S and L444P are named N409S and L483P, respectively, according to current guidelines.

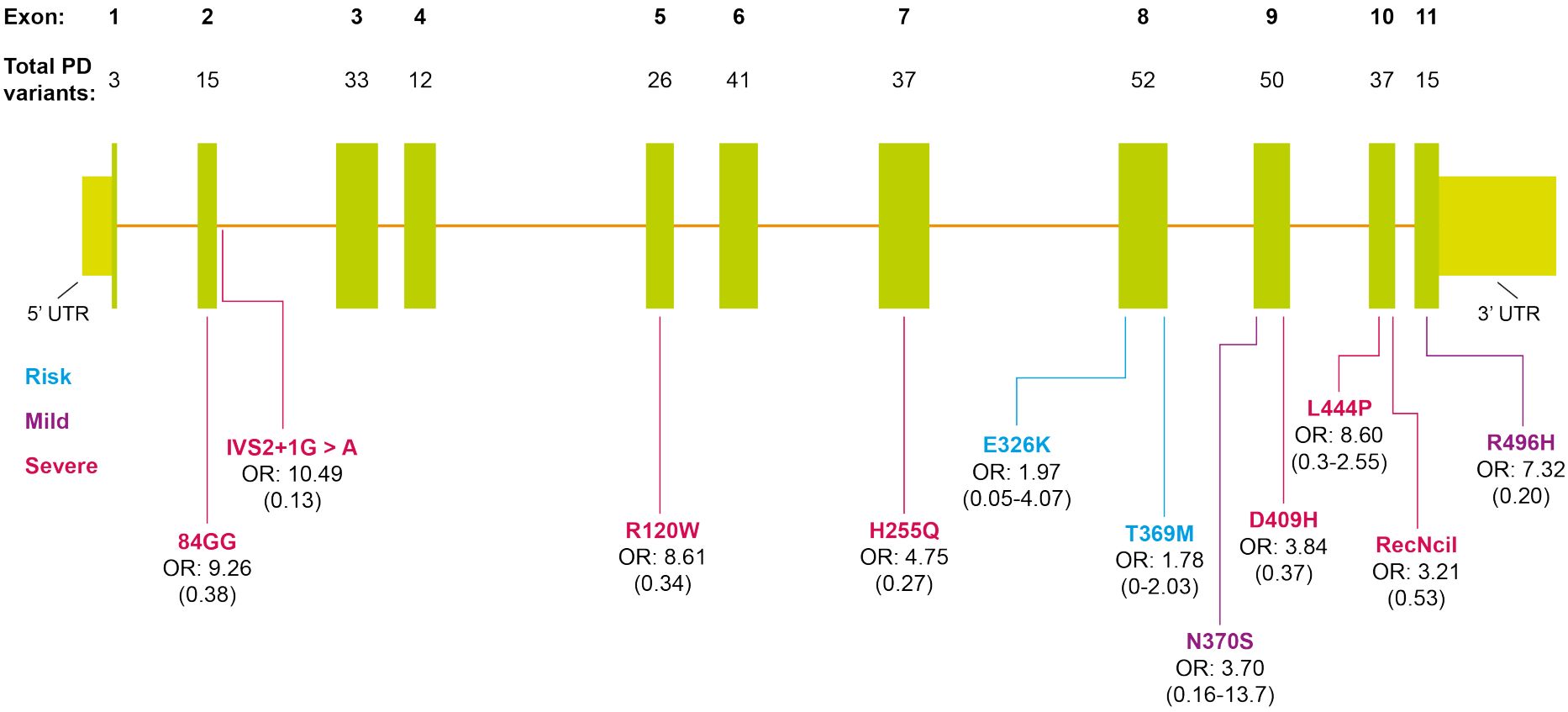


Figure 1.1: Schematic of the *GBA* gene illustrating the positions of PD-relevant mutations. The total number of variants that have been reported in PD patients across exons is from Parlar et al. (2023). Most PD-related variants have been observed in exons 8-10. Mutations are coloured according to their severity classification in the disease (Parlar et al., 2023). The odds ratio (OR) of individual variants is taken from a meta-analysis conducted across ethnicities by Zhang et al. (2018a). Mutation prevalence is indicated in brackets underneath the OR as a percentage of the total PD patients screened in relevant studies. The prevalence of the most common PD-related variants (N370S, L444P, E326K and T369M) is shown as a range across ethnic groups from Gabbert et al. (2023). The prevalence of rarer variants is expressed as the average prevalence across populations from Zhang et al. (2018a).

For instance, the N370S mutation (c.1226A>G, causing the substitution of the asparagine residue at position 370 with a serine in the mature GCase protein) (Tsuji et al., 1988) is the most common variant in AJ PD patients (Gan-Or et al., 2015a, Ruskey et al., 2019, Sidransky et al., 2009) and has been frequently observed in multi-ethnic North American groups (Cook et al., 2024, Mata et al., 2016) and various European populations (den Heijer et al., 2020, Lesage et al., 2011, Malek et al., 2018, Petrucci et al., 2020). Conversely, this variant is rare (Zhou et al., 2023) or absent (Choi et al., 2012, Kamath et al., 2024, Lim et al., 2022, Mitsui et al., 2009, Zhao et al., 2020) across East Asian and Indian demographic groups.

On the other hand, the L444P mutation has been shown to predominate in Asian populations (Chen et al., 2014, Gabbert et al., 2023, Kamath et al., 2024, Lim et al., 2022). This mutation is also widely observed across other geographies (Koros et al., 2024), including Europe (den Heijer et al., 2020, Lesage et al., 2011, Petrucci et al., 2020, Ran et al., 2016), North America (Cook et al., 2024, Mata et al., 2016) and Latin America (Velez-Pardo et al., 2019). Notably, L444P was shown to be the most prevalent GD-related mutation overall in UK cohorts (Malek et al., 2018, Neumann et al., 2009). This missense mutation (c.1448T>C) is located on exon 10 (**Fig. 1.1**) and leads to the replacement of the leucine residue at position 444 of the mature enzyme with a proline residue (Tsuji et al., 1987). Individuals can carry the L444P variant by itself or as part of a recombinant allele such as RecNciI (Hruska et al., 2008, Tayebi et al., 2003). The RecNciI allele has been observed in PD patients across various demographic groups (Han et al., 2016, Mata et al., 2016, Mitsui et al., 2009, Neumann et al., 2009); however, its disease prevalence is likely underestimated in screening studies that do not incorporate Sanger sequencing or that do not sequence the entire length of the *Gba* gene (Olszewska et al., 2020, Woo et al., 2021). This null allele, harbouring the L444P, A456P and V460V mutations, is the product of DNA rearrangements

between *GBA* and its neighbouring pseudogene, *GBAP* (Eyal et al., 1990, Latham et al., 1990, Liu et al., 1998). These genes are highly susceptible to aberrant recombination events due to their close proximity (16 kb apart) and 96% sequence homology (Horowitz et al., 1989, Sorge et al., 1990, Tayebi et al., 2003, Winfield et al., 1997, Woo et al., 2021). This high level of sequence similarity also hinders accurate gene sequencing, quantification of gene expression and transcript annotation at this locus (Gustavsson et al., 2024, Woo et al., 2021, Zampieri et al., 2017).

Unlike N370S and L444P, the E326K (c.1093G>A) and T369M (c.1223C>T) variants are not recognized as pathogenic in GD due to their relatively high prevalence in healthy individuals and because they only occur alongside known pathogenic variants in GD patients (Park et al., 2002, Walker et al., 2003). Indeed, controversy surrounded whether these mutations are risk factors for PD or just simply polymorphisms and early studies produced mixed results (Clark et al., 2007, Duran et al., 2013, Lesage et al., 2011, Sidransky et al., 2009). Meta-analyses of screening studies (Huang et al., 2018, Mallett et al., 2016, Pankratz et al., 2012) alongside large-scale genotyping studies (Berge-Seidl et al., 2017, Blauwendraat et al., 2018a, Goldstein et al., 2019) established that these variants increase PD susceptibility. However, despite the high prevalence of these variants across diverse ethnicities (Cook et al., 2024, Gabbert et al., 2023, Koros et al., 2024, Westenberger et al., 2024), they were not universally associated with increased PD risk across European or North American populations (Brolin et al., 2025, Crosiers et al., 2016, Han et al., 2016, Olszewska et al., 2020). Aside from these common variants, GWAS in underrepresented populations have continued to identify novel *GBA* risk factors for PD. Many of these variants are highly penetrant in these populations but have not previously been observed in other demographics (Rizig et al., 2023, Velez-Pardo et al., 2019). This further highlights the diversity in the distribution of *GBA* variants across geographies and ethnicities.

Although the prevalence of *GBA*-associated PD has been studied across various demographics, investigations into the sex distribution of *GBA* variants in the disease have produced contradictory results. Ortega et al. (2022) and Thaler et al. (2023) reported that the prevalence of *GBA*-associated PD is significantly higher among males. However, this supposed male predominance did not reach significance in an international observational clinical study (Westenberger et al., 2024) and the age-related cumulative incidence of PD was similar among male and female carriers of various *GBA* mutations (Straniero et al., 2020). Conversely, a meta-analysis of observational studies demonstrated that the disease frequency was higher among females from certain demographic groups (Li et al., 2021). It also remains inconclusive whether a male or female sex bias exists across different mutation classes (Kresojevic et al., 2023, Ortega et al., 2022, Panteghini et al., 2023, Thaler et al., 2023).

The penetrance of individual *GBA* mutations in PD also varies according to patient ethnicity (Zhang et al., 2018a) and is widely acknowledged to increase with age (Anheim et al., 2012, Balestrino et al., 2020, Straniero et al., 2020). Balestrino et al. (2020) estimated that the overall penetrance of *GBA* mutations in PD patients is 10% at 60 years-old and increases to 20% by 80 years-old, whereas the penetrance estimates reached up to 30% in 80-year-old patients from familial PD cohorts (Anheim et al., 2012). Severe *GBA* mutations also tend to confer a greater risk of developing PD (**Figure 1.1**) (Balestrino et al., 2020, Gan-Or et al., 2015a, Gan-Or et al., 2008) and are associated with a more aggressive clinical profile (**Section 1.2.3**) vs risk or mild variants.

1.2.3 THE CLINICAL PROFILE OF *GBA*-ASSOCIATED PD

The range of symptoms that manifest in *GBA*-associated PD is equivalent to idiopathic PD (**Section 1.1.2**). Patients harbouring *GBA* mutations display all of the cardinal motor signs of the disorder, although the PIGD motor subtype may predominate over other clinical

subtypes (Davis et al., 2016, Malek et al., 2018, Zhou et al., 2023). Consistent with this, PD patients that carry *GBA* mutations have increased prevalence and severity of bradykinesia, gait deficits and balance issues vs non-carriers (Gan-Or et al., 2010, Lesage et al., 2011, Maple-Grodem et al., 2021a, Morris et al., 2022), whereas tremor has been reported to occur less frequently (Jesus et al., 2016). The severity and rate of overall motor decline also tends to be greater in *GBA*-associated PD patients (**Table 1.2**) (Crosiers et al., 2016, Mata et al., 2016, Ren et al., 2022, Zhang et al., 2018b).

The three major clinical features that distinguish *GBA*-associated PD from idiopathic PD are earlier symptom onset, accelerated disease progression and increased prevalence of cognitive deficits (Clark et al., 2007, Gan-Or et al., 2008, Neumann et al., 2009, Winder-Rhodes et al., 2013). These phenotypic distinctions have been demonstrated by a myriad of observational studies (**Table 1.2**) and corroborated by meta-analyses (Creese et al., 2018, Iwaki et al., 2019, Zhang et al., 2018b, Zhang et al., 2015). Notably, the clinical profile of *GBA*-associated PD largely depends on the class of *GBA* variant. Severe mutations were shown to pre-dispose to disease onset earlier and further exacerbate cognitive decline vs mild mutations (**Table 1.2**). In a large meta-analysis, carriers of severe mutations displayed symptoms up to five years earlier than mild mutation carriers (Gan-Or et al., 2015a). Impaired cognition has been connected to gait and balance deficits in PD and is therefore also a canonical manifestation of the PIGD subtype (Alves et al., 2006, Kelly et al., 2015, Morris et al., 2022). Patients with *GBA* mutations have problems with non-verbal memory, executive function and visuospatial processing, in particular (Alcalay et al., 2012a, Leocadi et al., 2022, Mata et al., 2016, Morris et al., 2022). However, the timepoint at which patients' cognitive function begins to deteriorate is unclear. Various studies identified reduced cognitive abilities in non-PD *GBA* mutation carriers vs non-carriers (Moran et al., 2021, Roeben et al., 2024, Simuni et al., 2020), indicating that cognitive impairment may be one

of the earliest signs of PD in individuals with *GBA* mutations and could help to predict conversion to PD. Moreover, a longitudinal UK-based study demonstrated significantly worse cognition in non-PD *GBA* mutation carriers vs genetically unrelated controls at baseline and two-year follow-up (Beavan et al., 2015, McNeill et al., 2012) but not at six-year follow-up (Avenali et al., 2019). In contrast, other reports failed to detect differences in cognition between idiopathic and *GBA*-associated PD patients at diagnosis or in the early phases of disease (Brockmann et al., 2015, Liu et al., 2016, Malek et al., 2018).

There is strong evidence that other non-motor symptoms also occur more frequently in patients carrying *GBA* variants. Studies in AJ (Swan et al., 2016, Thaler et al., 2018), European (Cilia et al., 2016, Jesus et al., 2016, Petrucci et al., 2020) and Asian (Ren et al., 2022, Zhou et al., 2023) populations have shown that psychosis and mood disorders, in particular depression and anxiety, are more common in *GBA*-associated PD. In addition, anxiety progression was indicated to be more rapid in *GBA*-associated PD patients (Sang et al., 2024) and undiagnosed *GBA* mutation carriers display increased apathy vs non-carriers and *LRRK2* mutation carriers (Pachi et al., 2021). Similar to cognitive dysfunction, depression tends to be worse in carriers of severe vs mild mutations (Ren et al., 2022, Thaler et al., 2018). Moreover, Petrucci et al. (2020) reported that overall dysautonomia is increased in *GBA*-associated PD patients vs non-carrier patients. Supporting this, the prevalence of constipation and hyposmia was found to be higher in *GBA*-associated PD patients vs non-carriers of *GBA* mutations (Jesus et al., 2016, Malek et al., 2018, Wang et al., 2014, Zhou et al., 2023). Furthermore, other cross-sectional studies have found increased prevalence of orthostatic hypertension and other cardiovascular deficits in patients carrying *GBA* mutations vs idiopathic PD patients (Carandina et al., 2022, De Santis et al., 2025, Devigili et al., 2023, Usnich et al., 2022). A higher rate of sleep disturbances has also been identified in some *GBA*-associated PD cohorts (Brockmann et al., 2011, Iwaki et al., 2019, Jesus et al.,

2016, Ren et al., 2022). In accord with this, non-PD *GBA* mutation carriers are also more likely to develop RBD (Gan-Or et al., 2015b, Krohn et al., 2020). As observed in PD, severe *GBA* mutations may expedite RBD onset and confer a greater risk for the disease (Krohn et al., 2020).

Table 1.2: Summary of observational cohort studies that illustrate the distinctive clinical features of *GBA*-associated PD.

Reference	Type of study (average follow-up)	Demographic (# *GBA*-PD / # NC-PD)	Earlier age at onset	Accelerated disease progression					Presence of CI	
				↑ HY staging	↑ UPDRS-III	↓ Survival	↑ Cognitive decline	↑ Progression to dementia	↑ General CI	↑ Dementia
(Zhou et al., 2023)	Cross-sectional analysis	China (301/3733)	* # §						* #	
(Szwedo et al., 2022)	MA LT cohorts [a] (7.2 y)	European [a] (102/876)	*				*	* #		
(Leocadi et al., 2022)	Prospective LT (5.0 y)	Serbia (10/20)		*	*		*			
(Stoker et al., 2020)	Prospective LT (5.8-8.0 y)	UK (48/214)		*		* [i]		*		
(Straniero et al., 2020)	Cross-sectional analysis	Italy (248/3433)	* #							* #
(Lunde et al., 2018, Maple-Grodem et al., 2021a)	MA LT cohorts [b] (7.0 y)	European [b] (53/389), (53/386)	*		*			*		
(Iwaki et al., 2019)	MA LT cohorts [c] (1.2-6.8 y)	International [c] (446/3861)		*			*		*	
(Cilia et al., 2016)	Retrospective LT (7.2 y) [i]	Italy (123/2641)	*	* #	* #	* #		* # §	* §	
(Liu et al., 2016)	MA LT cohorts [d] (1.7-7.0 y)	International [d] (198/1723)	*				* #			
(Davis et al., 2016)	Prospective LT (3.0 y)	USA (58/675)			*		* [ii]			*
(Jesus et al., 2016)	Retrospective LT [i]	Spain (62/470)	*				* [ii]		* [ii]	
(Mata et al., 2016)	Cross-sectional analysis [i]	USA (56/1055)	*						*	*
(Brockmann et al., 2015)	Prospective LT (3.0 y) [i]	Germany (13/26)	*	*	*	*	*			
(Petrucci et al., 2020)	Retrospective LT	Italy (124/713)	* §	* §			* § [ii]		* [ii]	*
(Zhang et al., 2015)	Cross-sectional analysis	China (34/1113)	#							
(Winder-Rhodes et al., 2013)	Prospective LT (5.9 y) [i]	UK (4/106)		*				*		
(Alcalay et al., 2012a)	Cross-sectional analysis [i]	USA (26/39)							*	* [ii]

Key: *GBA*-PD = patients with a *GBA* mutation; NC-PD = patients not carrying *GBA* mutation; * = significant change *GBA*-PD vs NC-PD; # = significant change severe *GBA*-PD vs NC-PD; § = significant change severe *GBA*-PD vs mild/risk *GBA*-PD; CI = cognitive impairment; HY = Hoehn and Yahr; UPDRS = Unified Parkinson's Disease Rating Scale; MA = meta-analysis; LT = longitudinal; y = years. a. six cohorts (UK, Norway, Sweden); b. three cohorts (Scotland, Norway, Sweden), also included in (Szwedo et al., 2022); c. 13 cohorts (Europe, North America and Australia); d. seven cohorts (North America and Europe); i. analysis does not include risk variants e.g. E326K, T369M; ii. progression to/ occurrence of either mild cognitive impairment or dementia.

1.2.4 SYMPTOM MANAGEMENT IN PD PATIENTS WITH *GBA* MUTATIONS

Akin to idiopathic PD, oral L-Dopa is a mainstay therapy for alleviating symptoms in PD patients with *GBA* mutations. L-Dopa's efficacy in *GBA*-associated PD has been validated across various patient cohorts (Neumann et al., 2009, Rossi et al., 2022, Wu et al., 2007). However, patients carrying *GBA* mutations were shown to require a higher daily dose compared to idiopathic PD patients (Jesus et al., 2016, Malek et al., 2018), consistent with their heightened symptom severity (**Table 1.2**). Moreover, *GBA*-associated PD patients may be at higher risk of developing L-Dopa-related motor complications, including wearing-off and dyskinesia (Jesus et al., 2016, Lesage et al., 2011, Tonin et al., 2025) but these complications were equivalent across *GBA* mutation carrier and non-carrier PD patients in other studies (Cilia et al., 2016, Maple-Grodem et al., 2021b, Oeda et al., 2015). *GBA* mutation carriers were also more likely to be prescribed cholinesterase inhibitors in a study of AJ PD patients (Barrett et al., 2014). These findings align with the increased prevalence of cognitive deficits in *GBA*-associated PD (**Table 1.2**), considering that these drugs can effectively ameliorate cognitive difficulties in PD (Wang et al., 2015) and are the only approved pharmacotherapy to treat PD dementia (PDD) (Sun and Armstrong, 2021).

Smaller studies have indicated that LCIG is effective and well-tolerated in late-stage *GBA*-associated PD patients (Balestrino et al., 2024, Thaler et al., 2024). On the other hand, whether *GBA*-associated PD patients are appropriate candidates for STN-DBS remains inconclusive and the importance of pre-surgical screening for *GBA* mutations has been emphasized (Artusi and Lopiano, 2023). Despite showing improved motor function, patients carrying *GBA* mutations had worse cognitive outcomes following STN-DBS vs patients with idiopathic or other genetic forms of the disorder and vs *GBA*-associated PD patients who did not receive DBS (Artusi et al., 2019, Avenali et al., 2024, Pal et al., 2022). GPi-DBS may be

a better option for *GBA*-associated PD patients (Artusi and Lopiano, 2023, Lythe et al., 2017) because it has been associated with improved post-operative cognitive function vs STN-DBS (Wang et al., 2016). However, these types of DBS have not been directly compared in *GBA*-associated PD owing to the low amount of data on GPi-DBS in these patients (Artusi and Lopiano, 2023, Avenali et al., 2024, Pal et al., 2022).

1.3 GCASE: PHYSIOLOGICAL FUNCTION AND PD-RELATED DYSFUNCTION

1.3.1 GCASE STRUCTURE AND CATALYTIC ACTIVITY

GCase is a membrane-associated lysosomal hydrolase, composed of three discontinuous domains (Dvir et al., 2003). The enzyme's active site comprises an E235-E340 catalytic dyad and is located in domain three, a (β/α)8 triosephosphate isomerase (TIM) barrel. Seven cysteine residues across domains one and three maintain GCase integrity and activity, to varying degrees (Dvir et al., 2003, Liou et al., 2006). Glycosylation of GCase at four out of its five N-glycosylation sites is also essential for its functionality and stability (Bergfussman et al., 1993, Pol-Fachin et al., 2016).

GCase belongs to the family of retaining β-glucosidases and displays optimal activity around pH 5.6, consistent with the acidic environment of the lysosome (Liou et al., 2006). It mediates substrate hydrolysis via a two-step, double-displacement mechanism at the surface of intra-lysosomal membranes (Liou and Grabowski, 2009, Schulze et al., 2009). The putative acid/base catalyst is E235 (Fabrega et al., 2000, Liou and Grabowski, 2009, Premkumar et al., 2005) and the nucleophilic residue is E340 (Miao et al., 1994). GCase's primary function is to cleave the β-glucosyl linkage of GlcCer to yield ceramide and a glucose moiety (**Fig. 1.2***) (Brady et al., 1965a). Subsequently, acid ceramidase (ACDase) deacetylates ceramide to form sphingosine. After exiting the lysosome, sphingosine is degraded or recycled back to ceramide in the salvage pathway of ceramide synthesis

(Kitatani et al., 2008, Colacios et al., 2015). However, in conditions of GCase deficiency e.g. in GD, excess GlcCer is deacetylated by ACDase to form glucosylsphingosine (GlcSph) (Ferraz et al., 2016, Yamaguchi et al., 1994). GlcSph is a cytotoxic glycolipid that is barely detectable in tissue from healthy individuals but is elevated in the spleen, liver and brain of GD patients (Nilsson et al., 1982, Nilsson and Svennerholm, 1982, Orvisky et al., 2002, Schueler et al., 2003). There is also some evidence of GlcSph accumulation in PD patients (**Section 1.3.3.1**). Notably, GCase is also capable of hydrolysing GlcSph (Vaccaro et al., 1985). However, this reaction is much slower than GCase-mediated GlcCer hydrolysis and is likely to be spatially constrained by GlcSph's propensity to exit the lysosome due to its amphiphilic properties (Ferraz et al., 2016, Vaccaro et al., 1985). Therefore, a hypothetical deficit in GCase-mediated GlcSph degradation would be unlikely to exacerbate GlcSph accumulation in GD (Dekker et al., 2011), considering that this reaction seems to have limited relevance *in vivo*.

GCase can also catalyse the reversible exchange of glucose between GlcCer and cholesteryl glucoside (1-*O*-cholesteryl-β-D-glucopyranoside) (GlcChol) (**Fig. 1.2**[†]) (Akiyama et al., 2013, Marques et al., 2016). The direction of this transglucosylation reaction at equilibrium is determined by the relative concentration of the glucose donors and acceptors. Although GCase-mediated degradation of GlcChol is thought to be favoured in healthy lysosomes, GCase can also synthesize GlcChol in response to elevated lysosomal cholesterol (Marques et al., 2016). On the other hand, GCase does not act on GlcCer's isobaric enantiomer galactosylceramide (GalCer) (**Fig. 1.2**) (Milenkovic et al., 2022). GalCer is typically hydrolysed to ceramide by galactosylceramidase (GALC) (Reza et al., 2021). However, reduced GALC activity, e.g. in Fabry disease, results in GalCer deacetylation to galactosylsphingosine (GalSph) (Hawkins-Salsbury et al., 2013), a cytotoxic isobaric enantiomer of GlcSph (Matsumoto et al., 2022).

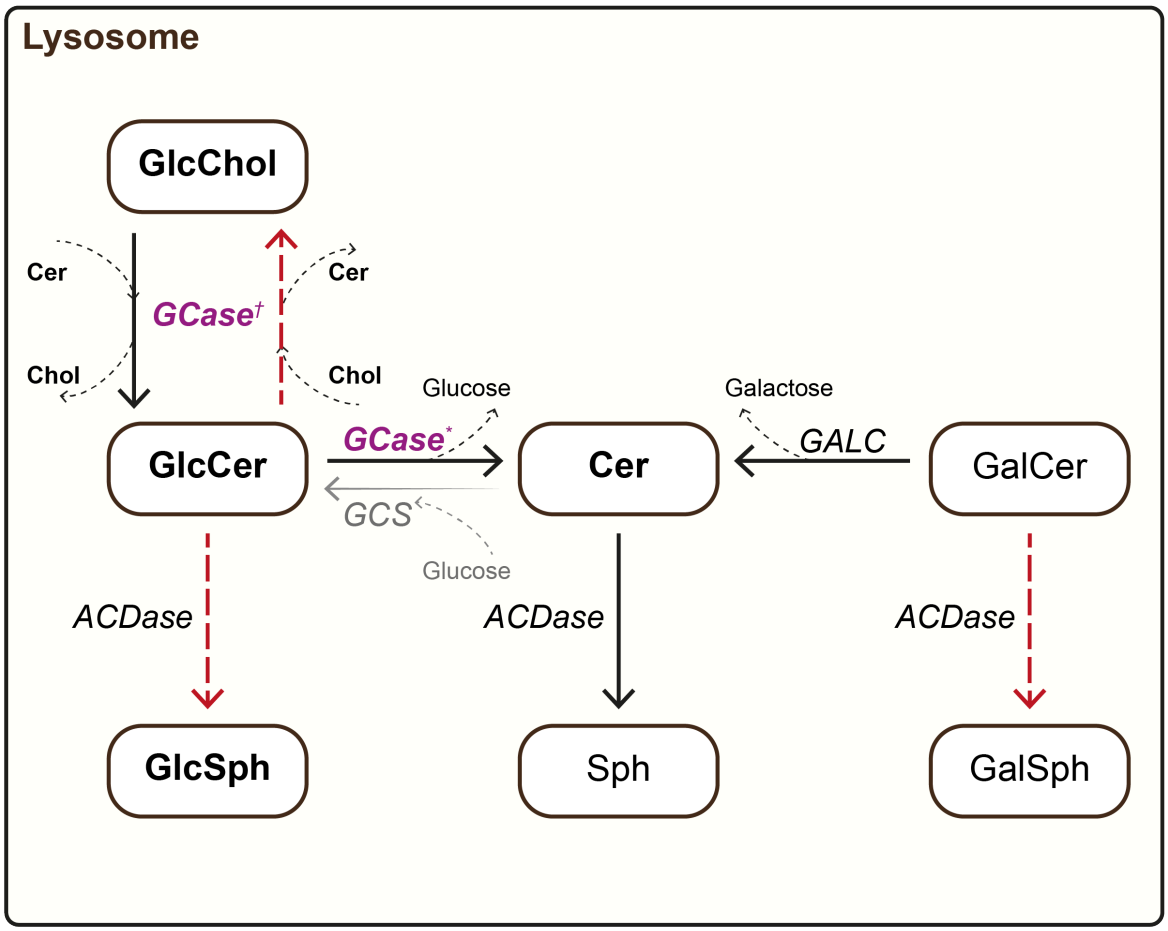


Figure 1.2: Glycosphingolipid metabolism in the lysosome. GCase hydrolyses GlcCer to glucose and ceramide (*). Ceramide is subsequently deacetylated to sphingosine by ACDase. In disease states, GCase deficiency results in ACDase-mediated GlcCer deacetylation to GlcSph (*red arrow*). GCase can also catalyse the transfer of a glucose moiety between GlcCer and GlcChol (†). Typically, GCase degrades GlcChol but it can also promote GlcChol formation (*red arrow*) in conditions of elevated lysosomal cholesterol e.g. Niemann-Pick type C disease. GCase does not act on GlcCer's isobaric enantiomer GalCer. GalCer is hydrolysed to ceramide by GALC in physiological states and deacetylated to GlcSph (*red arrow*) when GALC is deficient e.g. in Krabbe disease. To note, GCS (*grey arrow*) converts Cer to GlcCer in the Golgi and not the lysosome. This reaction is indicated here because GCS inhibitors recently failed to demonstrate efficacy in clinical trials for *GBA*-associated PD (**Section 1.3.4**). The lipid species shown are explored further in **Section 3.2.4**. GlcCer = glucosylceramide; Cer = ceramide; Sph = sphingosine; GlcSph = glucosylsphingosine; GlcChol = cholesteryl glucoside; Chol = cholesterol; GalCer = galactosylceramide; GalSph = galactosylsphingosine; GCase = glucocerebrosidase; GCS = glucosylceramide synthase; ACDase = acid ceramidase; GALC = galactosylceramidase.

To note, a second form of GCase, glucocerebrosidase-2 (GCase2), encoded for by the *GBA2* gene, is also highly abundant in the brain (Boot et al., 2007, van Weely et al., 1993, Yildiz et al., 2006). This enzyme catalyses GlcCer hydrolysis to glucose and ceramide and GlcCer transglucosylation to form GlcChol (Marques et al., 2016, van Weely et al., 1993, Yildiz et al., 2006); but, unlike GCase, it is localised to the cytosolic surface of the ER and Golgi membranes (Korschen et al., 2013). It has been suggested that GCase2's GlcCer substrate originates from lysosomal GlcCer that leaked into the cytoplasm due to GCase deficiency (Mistry et al., 2014); however, GCase2's physiological role and crosstalk with GCase activity are not fully understood (Woeste and Wachten, 2017). Some studies have shown that reduced GCase activity results in loss of GCase2 activity via negative-feedback inhibition of GCase2 by GlcSph and sphingosine (Korschen et al., 2013, Schonauer et al., 2017). In contrast, others have found that GCase deficiency is associated with increased GCase2 activity (Aureli et al., 2012, Burke et al., 2013). *GBA2* mutations do not cause GD or predispose to PD but are associated with hereditary spastic paraplegia and autosomal-recessive cerebellar ataxia (Woeste and Wachten, 2017).

1.3.2 THE CELLULAR LIFECYCLE OF GCASE

GCase is synthesized in the rough ER as a precursor protein with a 19 or 39 amino acid leader sequence (Erickson et al., 1985, Ginns et al., 1985, Sorge et al., 1987). The leader sequence is subsequently cleaved to yield the mature protein, which comprises 497 amino acids and harbours four N-linked high-mannose glycan chains (Dvir et al., 2003, Erickson et al., 1985, Takasaki et al., 1984). GCase binds to lysosomal integral membrane protein 2 (LIMP2) before exiting the ER (Reczek et al., 2007) and the complex subsequently passes through the Golgi apparatus (**Fig. 1.3**). Here, GCase undergoes various post translational modifications, including glycosylation changes: GCase's molecular weight (MW) ranges

between 55-69 kDa during its lifecycle depending on the degree of glycosylation (Bergmann and Grabowski, 1989, Erickson et al., 1985).

LIMP2, a transmembrane glycoprotein encoded by *SCARB2*, is responsible for GCase translocation from the Golgi to the lysosome (Fujita et al., 1991, Reczek et al., 2007). This distinguishes GCase from most other lysosomal enzymes, which rely on mannose-6-phosphate-dependent mechanisms for lysosomal trafficking (Braulke and Bonifacino, 2009, Reczek et al., 2007). In addition to its role as a GCase transporter, LIMP2 (and LIMP2-derived peptides) have been shown to allosterically enhance GCase activity using recombinant proteins and in cell cultures (Dobert et al., 2024, Zunke et al., 2016). The GCase-LIMP2 complex dissociates once it reaches the acid environment of the lysosome, presumably via pH-dependent conformational changes. LIMP2's H150 and H171 residues have been proposed to act as pH sensors; however, the exact mechanism remains to be resolved (Arnold and Zunke, 2025, Dobert et al., 2025, Zachos et al., 2012, Zhao et al., 2014).

GCase-association with anionic phospholipids, e.g. phosphatidylserine, in the membrane of intra-lysosomal vesicles is required for optimal enzymatic activity (Wilkening et al., 1998, Yap et al., 2015). The activity of lysosomal GCase is further enhanced by its cofactor saposin C (SapC), a glycoprotein produced from cleavage of prosaposin (PSAP) (Ho and O'Brien, 1971, Tamargo et al., 2012). SapC is thought to facilitate GCase catalysis primarily by increasing GlcCer accessibility, although the precise mechanisms have not been fully elucidated (Blanz and Saftig, 2016, Romero et al., 2019, Tamargo et al., 2012, Vaccaro et al., 1993). SapC also functions to shield GCase from degradation by lysosomal proteases (Sun et al., 2003). GCase has a rather short half-life in lysosomes of approximately 24-36 hours (Jonsson et al., 1987) and the cysteine protease cathepsin L (CTSL) was recently shown to mediate its lysosomal proteolytic degradation (Kim et al., 2024b).

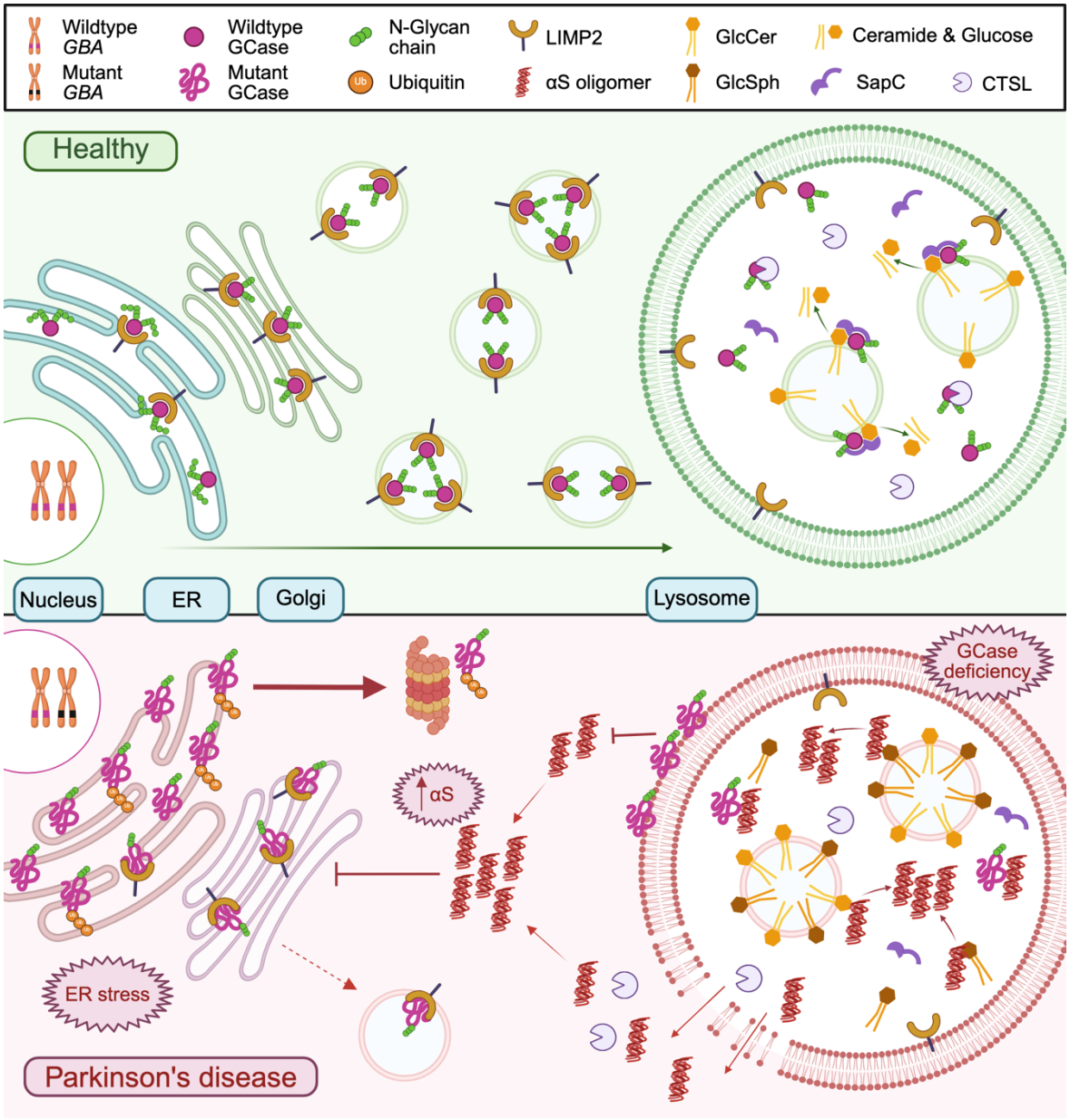


Figure 1.3: The physiological lifecycle of GCase and GCase dysfunction in PD. ***Top:*** GCase synthesis and subsequent association with lysosomal integral membrane protein 2 (LIMP2) occurs in the ER. GCase next undergoes post-translational processing, including modification of its N-glycan chains, in the Golgi. LIMP2 then traffics GCase to the lysosome, where GCase dissociates from LIMP2 and binds to its cofactor saposin C (SapC). SapC facilitates GCase-mediated hydrolysis of glucosylceramide (GlcCer) to glucose and ceramide on intralysosomal membranes. Cathepsin L (CTSL) degrades lysosomal GCase. ***Bottom:*** Heterozygous *GBA* mutations impair GCase folding, causing its entrapment in the ER. This can induce ER stress and premature GCase degradation via the proteasome (bold red arrow). Mutations may also interfere with GCase-LIMP2 binding, thereby reducing GCase transport to the lysosome. Meanwhile, loss of lysosomal GCase activity may elevate levels of GlcCer and glucosylsphingosine (GlcSph). These glycolipids have been shown to promote αS pathology. Toxic αS aggregates can also directly bind to GCase, potentially aggravating GCase activity deficits and related lysosomal dysfunction. Intralysosomal build-up of GlcSph and αS can lead to lysosomal membrane permeabilization, which serves to augment the levels of cytosolic αS. Mutant GCase accumulation on the lysosome surface can also inhibit chaperone mediated autophagy of αS, thereby exacerbating the cytosolic αS burden. αS pathology in the cytosol can further impede GCase translocation to the lysosome in a toxic feedforward loop. Created with BioRender.com.

1.3.3 PATHOLOGICAL PATHWAYS OF *GBA*-ASSOCIATED PD

PD-related GCase variants are dispersed across all three of GCase's domains (Dvir et al., 2003, Smith et al., 2017). However, the direct impact of these mutations on protein structure and related functionality remains largely enigmatic. This has made it challenging to specifically map the nature and severity of disease to mutations' location in the protein (Lieberman, 2011). Nevertheless, diverse *GBA* variants have been shown to confer PD pathology through many common loss- and gain-of-function related mechanisms. These loss- and gain-of-function effects have various downstream deleterious consequences, including lysosomal dysfunction, ER stress and αS accumulation, which are discussed further in the following sections.

1.3.3.1 Loss-of-function: GCase enzymatic deficiency

Attenuated GCase activity is a key pathological feature of *GBA*-associated PD (**Fig. 1.3**). This loss-of-function related phenotype has consistently been demonstrated in cellular and animal models of the disorder, including fibroblasts (Ambrosi et al., 2015, Collins et al., 2017, Garcia-Sanz et al., 2017, McNeill et al., 2014) and iPSC-derived DA neurons (iPSC-DAns) (Fernandes et al., 2016, Schondorf et al., 2014) from *GBA*-associated PD patients, *Drosophila* expressing N370S- or L444P-mutant GCase (Sanchez-Martinez et al., 2016) and a plethora of *Gba* transgenic mice (**Table 1.3**). GCase deficiency has also been observed in post-mortem brain samples (Gegg et al., 2012, Huebecker et al., 2019, Murphy et al., 2014, Rocha et al., 2015a), cerebrospinal fluid (CSF) (Parnetti et al., 2017) and dried blood spots (Alcalay et al., 2015) from PD patients with and without *GBA* mutations. GCase activity levels were shown to be associated with mutation status: carriers of severe variants tend to display lower GCase activity than those who carry mild or risk variants (Lerche et al., 2021, Omer et al., 2022). The extent of GCase deficiency in PD patient samples may also relate to disease duration (Alcalay et al., 2015) and predict the development of dementia in later

disease stages (Oftedal et al., 2023). However, other studies did not find evidence to support an association of GCase activity with PD risk and clinical phenotypes (Alcalay et al., 2020, Avenali et al., 2019, Omer et al., 2022).

There is a dearth of information on the conformational changes that underlie loss-of-function effects of *GBA* mutations (Lieberman, 2011). These changes are most well understood for N370S-GCase, facilitated by the availability of a crystal structure for this variant (Lieberman, 2011, Wei et al., 2011). Although the N370S mutation, located at the interface of domains 2 and 3 (Dvir et al., 2003), is relatively distant from the catalytic dyad, it is thought to slow GCase's catalytic cycle (Liou and Grabowski, 2009) by interfering with hydrogen bonding surrounding the active site (Offman et al., 2010, Wei et al., 2011). In turn, this reduces the flexibility of loops that flank the enzyme's active site, which likely hinders substrate accessibility (Lieberman et al., 2007, Offman et al., 2010, Premkumar et al., 2005, Wei et al., 2011). Conformational changes may also indirectly reduce GCase activity by perturbing GCase binding to membrane phospholipids, LIMP2 and SapC. For instance, the N370S mutation has also been shown to impair GCase's interaction with negatively charged membrane phospholipids and SapC (Romero et al., 2019, Salvioli et al., 2005), although this was not corroborated by others (Liou et al., 2006). Furthermore, the L444P mutation may diminish GCase activation by phosphatidylserine membrane lipids and SapC (Atrian et al., 2008, Grace et al., 1994, Liou et al., 2006, Romero et al., 2019). In line with this, Atrian et al. (2008) demonstrated that GCase residues 443-445 are involved in GCase binding to SapC. E326K-GCase also displayed reduced association with SapC in molecular dynamics simulations (Pietrafesa et al., 2024). In addition, the D409H mutation, primarily associated with GD but also observed in PD patients (**Fig. 1.1**), is located within GCase's binding interface for LIMP2 (Liou et al., 2014) and has been associated with increased endoplasmic reticulum-associated degradation (ERAD) of the GCase-LIMP2 complex (Dobert et al.,

2025). *GBA*-D409H may also directly impede GCase's interaction with LIMP2 and subsequent lysosomal trafficking because direct contacts between LIMP2 and D409 on wild-type (WT) GCase are essential to the formation of the GCase-LIMP2 complex (Dobert et al., 2025).

Although both mild and severe heterozygous *GBA* mutations unequivocally decrease GCase activity, the jury is out on whether this deficit induces GlcCer and GlcSph accumulation in PD. Despite GlcCer amassment being the pathological hallmark of GD (**Section 1.2.1**), there is no definitive evidence for GlcCer build-up in PD patient brains (Blumenreich et al., 2022, Leyns et al., 2023, Milenkovic et al., 2022), although two reports demonstrated a subtle, region-specific elevation (Blumenreich et al., 2022, Huebecker et al., 2019). GlcCer levels are also normal across many transgenic mouse models of *GBA*-associated PD and GD (**Table 1.3**). Conversely, GlcCer accumulation and altered distribution of GlcCer species has been demonstrated in iPSC-DAns (Burbulla et al., 2019, Fernandes et al., 2016, Schondorf et al., 2014). GlcCer levels were also increased in CSF from *GBA*-associated PD patients (Huh et al., 2021, Lerche et al., 2021), whereas studies in PD patient plasma have produced mixed results (den Heijer et al., 2023a, Surface et al., 2022, Te Vruchte et al., 2022).

On the other hand, GlcSph is elevated in plasma (Surface et al., 2022) and dried blood spots (Kopytova et al., 2022)[2] of *GBA*-associated PD patients vs idiopathic patients. This has sparked interest in GlcSph being a potential biomarker for PD, especially considering its existing use as a biomarker in GD (Dekker et al., 2011, Revel-Vilk et al., 2020, Rolfs et al., 2013). However, the clinical relevance of this has been negated considering that GlcSph levels were comparable in *GBA* mutation carriers with and without PD (Gleason et al.,

[2]Kopytova et al. (2022) reported increased hexosylsphingosine (HexSph) in dried blood spots from patients. This study therefore did not distinguish between glucosylsphingosine and galactosylsphingosine species.

2022a, Gleason et al., 2022b). GlcSph also accumulates in post-mortem brains from *GBA*-associated PD and idiopathic PD patients (Huebecker et al., 2019, Rocha et al., 2015a) and in mice harbouring heterozygous and homozygous *Gba* mutations (**Table 1.3**). Notably, GlcSph has been suggested to be responsible for neuropathology in GD patients, as the extent of GlcSph accumulation is higher in neuronopathic vs non-neuronopathic GD brains (Nilsson and Svennerholm, 1982, Orvisky et al., 2002). In further support of this, GlcSph was shown to accelerate loss of tyrosine hydroxylase (TH) mRNA in a zebrafish model of GD (Lelieveld et al., 2022). TH is the rate limiting enzyme in the DA synthesis pathway; it catalyses the hydroxylation of tyrosine to DOPA (Daubner et al., 2011). GlcSph has also been shown to impair lysosomal biogenesis and autophagy in iPSC-derived neurons from GD and PD patients (Kumar et al., 2023, Srikanth et al., 2021) and can facilitate αS aggregation (**Section 1.3.3.3**). Recently, recombinant GCase was also shown to catalyse the deglucosylation of glucosylated phytosterols and the accumulation of certain glycosyl-phytosterol species was observed in GD patient spleens (Bannink et al., 2024). A reduction in this GCase-mediated catalytic effect may also be relevant to PD pathology, considering that administration of the glucosylated phytosterol β-sitosterol β-D-glucoside (BSSG) to rats triggers dopaminergic degeneration and is used to model PD (Van Kampen and Robertson, 2017). However, this remains to be directly investigated.

Although the degree to which glycolipids accumulate and contribute to pathology in *GBA*-associated PD remains uncertain, many studies have directly linked reduced GCase activity with dysregulation of the lysosomal-autophagy pathway. Cellular models of GCase deficiency, either via *GBA* knockout (KO) or pharmacological GCase inhibition with conduritol B epoxide (CBE), display many signs of lysosomal dysfunction. These include accumulation of lysosomal substrates and lysosomal-associated membrane protein-1 (LAMP1), reduced intralysosomal acidity, perturbed lysosomal membrane integrity and

impaired lysosomal exocytosis and recycling (Bae et al., 2015, Lunghi et al., 2022, Magalhaes et al., 2016, Navarro-Romero et al., 2022). The abundance and size of lysosomes are also increased in heterozygous *GBA*-N370S iPSC-DAns (Fernandes et al., 2016, Schondorf et al., 2014) and fibroblasts (Garcia-Sanz et al., 2017). These lysosomal phenotypes are accompanied by dysregulation of macroautophagy and chaperone-mediated autophagy (CMA) in many of these *in vitro* models (Fernandes et al., 2016, Garcia-Sanz et al., 2017, Navarro-Romero et al., 2022, Schondorf et al., 2014). Lysosomal/autophagic deficits in mouse models of *GBA*-associated PD are summarised in **Section 1.4.2**.

1.3.3.2 Gain-of-function: the ER-retention of misfolded, mutant GCase

The entrapment of immature, misfolded GCase in the ER can induce ER stress and consequently trigger the unfolded protein response (UPR) and ERAD of mutant GCase (**Fig. 1.3**). ER stress and UPR activation have been identified in iPSC-DAns (Fernandes et al., 2016, Schondorf et al., 2018) and fibroblasts (Garcia-Sanz et al., 2017, Sanchez-Martinez et al., 2016) from *GBA*-associated PD patients, *GBA*-mutant neuronal-like cell lines (Navarro-Romero et al., 2022), midbrain organoids (Frattini et al., 2024) and *Drosophila* (Sanchez-Martinez et al., 2016), as well as post-mortem *GBA*-associated PD brains (Gegg et al., 2012). Notably, some studies have indicated that the UPR is not triggered by GCase deficiency alone (Farfel-Becker et al., 2009, Maor et al., 2013) underscoring its nature as a gain-of-function manifestation of *GBA* mutations. GCase confinement in the ER can induce Golgi fragmentation in PD patient fibroblasts (Garcia-Sanz et al., 2017), whilst ER stress has been demonstrated to stimulate apoptosis in GD patient cell lines (Wei et al., 2008). In accord with this, GD severity was shown to positively correlate with the extent of GCase retention in the ER and subsequent ERAD (Ron and Horowitz, 2005).

The L444P variant has been associated with elevated UPR induction compared to other common variants, including N370S and E326K (Schmitz et al., 2005, Smith et al., 2023).

Studies in GD cells have also found that L444P-GCase undergoes substantial ERAD (Bendikov-Bar et al., 2011, Dobert et al., 2024). Despite this, the structural underpinnings of L444P-GCase's susceptibility to imprisonment in the ER remain enigmatic (Lieberman, 2011). As this mutation is located in the hydrophobic core of domain II, it has been suspected to disturb hydrophobicity in this region (Dvir et al., 2003, Smith et al., 2017). It may also reduce flexibility in the protein's backbone or interfere with the stabilising effects of GCase glycosylation at residue N19 (Lieberman, 2011, Pol-Fachin et al., 2016, Smith et al., 2017). Furthermore, it has been demonstrated that L444P-GCase does not interact with the ER chaperone binding immunoglobulin protein (BiP), which likely also contributes to its folding difficulties (Schmitz et al., 2005).

Notably, the proteasomal degradation of L444P- and N370S-GCase was shown to be mediated by the E3 ubiquitin ligase parkin (Ron et al., 2010). Loss-of-function mutations in the parkin-encoding gene, *PRKN*, are also implicated in PD development (Wasner et al., 2020) and the accumulation of various parkin substrates is known to have deleterious effects on neuronal viability (Quinn et al., 2020, Shin et al., 2011). It follows that mutant GCase can also contribute to neuronal toxicity by preventing the ubiquitination and subsequent degradation of other parkin substrates (Bendikov-Bar et al., 2014). Aside from ER stress-related phenotypes, gain-of-function effects have been shown to underlie lipid droplet accumulation in *GBA*-E326K fibroblasts (Smith et al., 2023). In addition, misfolded mutant GCase can directly perturb CMA via a gain-of-function effect by accumulating on the lysosomal surface and impeding the multimerization of lysosomal-associated membrane protein-2A (LAMP2A) (Kuo et al., 2022).

1.3.3.3 The pathogenic exchange between GCase and αS

A seminal study from Mazzulli et al. (2011) proposed that αS and GCase are ensnared in a toxic feedforward cycle in PD. According to Mazzulli's model, GCase deficiency promotes

αS aggregation, which subsequently drives further GCase deficits by inhibiting GCase translocation to the lysosome. This self-perpetuating loop has been suggested to act as the potential missing link between GD and PD pathology (Cookson, 2011).

Indeed, αS levels are elevated in cell cultures in response to pharmacological GCase inhibition (Cleeter et al., 2013, Manning-Bog et al., 2009) or *GBA* KO (Bae et al., 2015, Navarro-Romero et al., 2022) and in cells that harbour *GBA* mutations (Kumar et al., 2023, Kuo et al., 2022, Labrador-Garrido et al., 2023, Navarro-Romero et al., 2022). αS accumulation and aggregation have also been demonstrated mouse models of *GBA*-associated PD and GD (**Table 1.3**) (Cullen et al., 2011, Xu et al., 2011). In addition, *GBA* mutations and GCase depletion can facilitate the propagation of αS pathology in cell culture (Bae et al., 2014, Cerri et al., 2021, Gegg et al., 2020) and *in vivo* (Migdalska-Richards et al., 2020, Papadopoulos et al., 2018). Vice versa, mice harbouring *SNCA*-A53T mutations display reduced GCase activity (Rockenstein et al., 2016, Sardi et al., 2013) and GCase levels (Kim et al., 2018a). Pharmacological studies have also corroborated an inverse correlation between αS levels and GCase activity in the disease. In mice harbouring *Gba* or *SNCA* mutations, αS pathology was ameliorated by augmenting GCase activity with small molecule activators (Burbulla et al., 2019), pharmacological chaperones (Migdalska-Richards et al., 2016) or viral-mediated *GBA* expression (Glajch et al., 2021, Rockenstein et al., 2016, Sardi et al., 2011, Sardi et al., 2013). Although these phenotypes are consistent with the pathological GCase-αS interplay that Mazzulli et al. (2011) described, the mechanistic basis of the self-perpetuating loop remains poorly understood.

According to Mazzulli's model, GlcCer forges the link between GCase deficiency and αS accumulation by directly stabilising αS oligomers (Mazzulli et al., 2011). Others have since demonstrated that incubation of αS with GlcCer or GlcSph directly promotes αS aggregation and proteinase K resistivity (Paul et al., 2021, Suzuki et al., 2015, Taguchi et

al., 2017, Zunke et al., 2018). GlcSph can also indirectly promote αS accumulation by driving autophagic deficits via mTOR hyperactivation (Kumar et al., 2023). Furthermore, the degree of αS pathology was found to be a significant determinant of GlcSph levels in post-mortem PD patient brains (Leyns et al., 2023). Consistent with these findings, pharmacological depletion of GlcCer and GlcSph protected against αS pathology in *Gba*$^{D409V/409V}$ and *SNCA*^{A53T} mice (Sardi et al., 2017) and in *GBA* mutant iPSC-DAns (Kumar et al., 2023). Despite this, there is a lack of evidence for the accumulation of glycosphingolipids, particularly GlcCer, in PD patient brains (**Section 1.3.3.1**). Therefore, glycosphingolipid-induced αS aggregation has questionable relevance to PD pathology.

Reduced ceramide resulting from GCase deficiency is another potential culprit involved in αS pathology in *GBA*-associated PD. Ceramide is a known activator of protein-phosphatase 2A (PP2A), which dephosphorylates pathogenic αS (Dobrowsky et al., 1993, Lee et al., 2011). It also activates cathepsin D (CTSD), an aspartyl protease that degrades lysosomal αS (Heinrich et al., 1999, Sevlever et al., 2008). Ceramide depletion may therefore be responsible for αS accumulation in GCase deficient cells that also display diminished PP2A or CTSD activity (Du et al., 2015, Yang et al., 2020a). In addition, enhancing ceramide levels in *GBA*-associated PD iPSC-DAns reduced oxidised αS by restoring secretory autophagy (Kim et al., 2018b). However, there are only limited reports of ceramide deficiency in PD patient brains (Abbott et al., 2014, Murphy et al., 2014) and studies investigating ceramide levels in GCase deficient cells and L444P-mutant fibroblasts from PD patients have yielded inconsistent results (Galvagnion et al., 2022, Kim et al., 2018b).

Altogether, this suggests that gain-of-function effects of *GBA* mutations may also contribute to promoting αS accumulation and aggregation. This was supported by studies that failed to identify a direct link between GCase deficiency and αS accumulation *in vitro*

(Cullen et al., 2011, Dermentzaki et al., 2013). Moreover, some CBE-treated mice (Mus et al., 2019), *Gba*$^{+/-}$ mice (Migdalska-Richards et al., 2017b, Sardi et al., 2011, Tayebi et al., 2017) and conditional *Gba* KO mice (Soria et al., 2017) do not accumulate αS, despite having reduced GCase activity. Kuo et al. (2022) identified a potential gain-of-function effect of *GBA* mutations on αS accumulation by demonstrating that misfolded mutant GCase can directly inhibit the lysosomal uptake and subsequent CMA of αS by impeding LAMP2A multimerization.

Although the mechanisms underlying how GCase deficiency modulates αS aggregation remain elusive, it has been shown to depend on the extent of pre-existing αS pathology (Henderson et al., 2020). GCase inhibition with CBE did not induce *de novo* αS accumulation in primary neurons but did exacerbate αS preformed fibril (PFF)-induced αS aggregation in these neurons and in mice (Henderson et al., 2020). This strongly indicates that αS pathology instigates the toxic exchange with GCase in PD. αS can reduce GCase activity by blocking its translocation to the lysosome (**Fig. 1.3**) (Mazzulli et al., 2011, Mazzulli et al., 2016). Furthermore, accumulation of this toxic protein may impair GCase folding in the ER via direct interaction with and sequestration of ER chaperone proteins (Stojkovska et al., 2022). αS can also bind to and directly inhibit GCase at intralysosomal membranes (Yap et al., 2011, Yap et al., 2015, Yap et al., 2013b). This interaction is thought to perturb substrate access to GCase's the active site, either by steric hindrance, inducing conformational changes or reducing GCase's proximity to lipid membranes (Yap et al., 2015, Yap et al., 2013b). Conversely, GCase's association with αS was also suggested to also confer protection by facilitating αS degradation (Yap et al., 2013b) or by inhibiting αS association with lipid membranes and subsequent membrane-facilitated acceleration of αS aggregation (Barber et al., 2018). In line with this, the N370S mutation has been shown to

impair GCase's interaction with αS (Yap et al., 2011). Regardless of the mechanism underlying αS-mediated GCase deficiency, αS pathology could be responsible for reduced GCase activity in post-mortem brain samples (Gegg et al., 2012, Huebecker et al., 2019, Murphy et al., 2014, Rocha et al., 2015a) and CSF (Parnetti et al., 2017) from PD patients who don't carry a *GBA* mutation.

1.3.4 DISEASE-MODIFYING THERAPEUTIC STRATEGIES TARGETING GCASE FUNCTION

Disease-modifying therapies for *GBA*-associated PD are highly sought-after but currently unavailable (Menozzi et al., 2023, Stoker and Barker, 2020). The use of GCase chaperone compounds, which act to stabilise mutant, misfolded GCase and thereby facilitate its lysosomal transport, is one strategy that has garnered considerable interest in the field (Fan, 2003, Han et al., 2020). Among the wide range of GCase chaperones that have been investigated, ambroxol has received the most attention in recent years (Han et al., 2020, Menozzi et al., 2023). Notably, ambroxol has been available over-the-counter as an expectorant since 1979 but its ability to chaperone GCase was only recognized 30 years later (Maegawa et al., 2009). Since then, reports in cells (Ambrosi et al., 2015, Galvagnion et al., 2022, Magalhaes et al., 2018, McNeill et al., 2014, Sanchez-Martinez et al., 2016), midbrain organoids (Frattini et al., 2024), mice (Migdalska-Richards et al., 2016) and non-human primates (Migdalska-Richards et al., 2017a) have demonstrated the effectiveness of ambroxol in enhancing GCase activity. Ambroxol has also been shown to reduce αS accumulation, neuroinflammation and ER stress, along with rescuing motor and cognitive deficits in various preclinical models (Migdalska-Richards et al., 2016, Sanchez-Martinez et al., 2016, Ullah et al., 2025). Following positive findings in preclinical studies, ambroxol's safety and tolerability was confirmed in PD and PDD patients in phase 2 clinical trials (Mullin et al., 2020, Silveira et al., 2025, Silveira et al., 2019). Many other phase 2 trials are

currently ongoing to assess this compound's efficacy to improve symptoms in PD (Colucci et al., 2023, Siemeling et al., 2024) and a phase 3 trial assessing whether it can slow PD progression is in the patient recruitment stage (NCT05778617, ASPro-PD). Notably however, ambroxol was not shown to improve cognition in PDD patients in a recent phase 2 trial (Silveira et al., 2025).

Aside from chaperone therapies, a small-molecule GCase allosteric activator, LTI-291 (BIA-28-6156), has demonstrated tolerability in healthy individuals (den Heijer et al., 2021) and in *GBA*-associated PD patients in a Phase 1B clinical trial (den Heijer et al., 2023b). A phase 2 trial to test its efficacy in *GBA*-associated PD (NCT05819359, ACTIVATE) began dosing patients in early 2025. GCase enhancement with viral-mediated delivery of *GBA* is also currently in the clinical development pipeline for *GBA*-associated PD (Uspenskaya et al., 2020) (NCT04127578, PROPEL). Previously, this strategy effectively increased GCase activity, protected against αS insults and ameliorated behavioural deficits in *Gba*$^{D409V/D409V}$ mice and *SNCA* transgenic mice (Morabito et al., 2017, Rocha et al., 2015b, Rockenstein et al., 2016, Sardi et al., 2013).

GlcCer synthase, the enzyme responsible for the conversion of ceramide to GlcCer (**Fig. 1.2**), was also investigated as a potential target for disease-modifying therapies. However, substrate reduction therapy using GlcCer synthase inhibitors has been unsuccessful in *GBA*-associated PD, despite its use in GD patients (Gary et al., 2018). This strategy showed promise in preclinical models by reducing GlcCer and αS accumulation and rescuing behavioural deficits (Sardi et al., 2017, Viel et al., 2021) and one compound, venglustat, progressed to clinical trials. Venglustat was determined as safe in patients (Peterschmitt et al., 2022) but failed to demonstrate efficacy (Giladi et al., 2023) (NCT02906020, MOVES-PD), leading to termination of the trial.

Indeed, unravelling the loss- and gain-of-function effects of *GBA* mutations in PD, including the toxic reciprocity between GCase and αS, should facilitate the future development of disease-modifying therapies. I believe that investigations employing valid mouse models of *GBA*-associated PD will play a fundamental role in furthering our understanding GCase's role in the disorder. Various mouse models have already been created to study GCase dysfunction in PD. The primary phenotypes and limitations of these models will be described further in the next section (**Section 1.4**).

1.4 MODELLING *GBA*-ASSOCIATED PD IN MICE

1.4.1 A BRIEF INTRODUCTION TO ANIMAL MODELS OF PD

Animal models are instrumental in the ongoing quest to elucidate the basic pathological mechanisms of PD and to develop disease-modifying therapies. Since 1990, animals have been incorporated into over 23000 PD-related publications (Konnova and Swanberg, 2018). These models can be divided into two main classes: toxin-based and genetic (Blesa and Przedborski, 2014). Since each animal model has its own unique strengths and limitations, the choice of model should be specifically tailored to the scientific objectives of the study (Fisher and Bannerman, 2019). Broady speaking, administration of neurotoxins, e.g. MPTP or 6-hydroxydopamine (6-OHDA), evokes widespread neurodegeneration and consequential severe behavioural deficits (Dovonou et al., 2023). However, the acute nature of pathology renders toxin-based models unsuitable to monitor longitudinal disease progression (Lama et al., 2021). In contrast, genetic models can be used to track the age-related evolution of disease but typically display milder behavioural phenotypes and can lack nigral dopaminergic neurodegeneration (Bezard and Przedborski, 2011, Blesa and Przedborski, 2014). Notably, the use of genetic models in PD research has grown steadily

since the early 2000s (Kin et al., 2019), in tandem with our increased awareness of genetics' role in disease aetiology (**Section 1.1.4.4**).

Rodents, and in particular mice, are the most common species used to model genetic PD (Kin et al., 2019). There are multiple advantages of using mice to study genetic PD: their genome is highly similar to the human genome, it contains many homologues of human PD-related genes and it is relatively easy to manipulate with the wealth of advanced gene-editing technologies at our disposal (Perlman, 2016, Zhang et al., 2022a). Furthermore, the anatomical organisation of the mouse and human basal ganglia are comparable (Gerfen and Bolam, 2010) and the extent of DA neurodegeneration tends to correlate with the severity of behavioural symptoms in both species (Konnova and Swanberg, 2018). However, despite the high level of genetic homology between mice and humans, species-related differences in gene regulation and splicing can create issues for recapitulating neurodegenerative disease in mice (Fisher and Bannerman, 2019). It can also be challenging to study age-related dysfunction in mice, considering that common laboratory strains e.g. C57BL/6J typically do not survive past 24 months (Fisher and Bannerman, 2019). Indeed, many mouse models of genetic PD do not display DA neurodegeneration or PD-relevant behavioural phenotypes (Dawson et al., 2010, Vingill et al., 2018), which limits their translatability to PD patients. It has been proposed that compensatory processes may mask neuropathology in these models and that reduced complexity in the mouse nigrostriatal DA neuron network contributes to mice's natural resistance to PD (Dawson et al., 2010, Garcia-Ruiz and Espay, 2017).

The vast array of genetic mouse models in the PD researcher's arsenal has been extensively reviewed elsewhere (Bobela et al., 2014, Crabtree and Zhang, 2012, Koprich et al., 2017, Volta and Melrose, 2017). The following sections will specifically focus on mice used to model *GBA*-associated PD.

1.4.2 CURRENT MOUSE MODELS OF GCASE DYSFUNCTION IN PD: STRATEGIES AND KEY PHENOTYPES

GBA-associated PD is predominantly modelled in mice (**Table 1.3**), although *Drosophila* (Maor et al., 2016, Sanchez-Martinez et al., 2016) and zebrafish (Keatinge et al., 2015) models have also been created. Both pharmacological and genetic approaches have been employed in mice to gain insights into GCase dysfunction in PD. Intraperitoneal injection of CBE is the most frequently used strategy to pharmacologically inhibit GCase activity *in vivo* (Farfel-Becker et al., 2019, Vardi et al., 2016). CBE-mediated loss of GCase activity is associated with glycolipid and αS accumulation, autophagic-lysosomal deficits, neuroinflammation and impaired evoked-DA release (Ginns et al., 2014, Mus et al., 2019, Papadopoulos et al., 2018, Rocha et al., 2015c, Rockenstein et al., 2016).

A wide range of genetically engineered mouse models of *GBA*-associated PD have been developed (**Table 1.3**). Many of these models are *Gba* haploinsufficient ($Gba^{+/-}$) or harbour a knock-in (KI) pathogenic variant in the endogenous mouse *Gba* gene. Notably, mouse models of GD, carrying biallelic *Gba* mutations or a mutated allele on a *Gba* KO background ($Gba^{-/-}$), have also been used to study *GBA*-associated PD (Furderer et al., 2024, Polinski et al., 2021, Sardi et al., 2011, Vidyadhara et al., 2025).

Loss of GCase activity is the most widely investigated and reproducible phenotype across *Gba* transgenic mouse models (**Table 1.3**). This reflects findings in cellular models and PD patients (**Section 1.3.3.1**), thereby further highlighting the central role of GCase activity deficits in *GBA*-associated PD pathology. Reduced GCase activity typically induces the accumulation of GlcSph, but not GlcCer, in these models, analogous to neuropathology in PD patients (**Section 1.3.3.1**). Notably, GlcCer elevation is primarily restricted to models carrying homozygous *Gba* mutations (Kweon et al., 2024, Polinski et al., 2021).

Overall, loss-of-function related deficits in the lysosomal-autophagy pathway are identified less frequently in *Gba* transgenic mice vs cellular models (**Section 1.3.3.1**), perhaps because studies using whole tissue homogenates may further mask lysosomal-specific impairments (Navarro-Romero et al., 2022). LAMP1 levels were normal across various models (**Table 1.3**); however, late endosomal/ lysosomal activity was reduced in primary hippocampal neurons from *Gba*$^{+/L444P}$ mice, as determined using a DQ-BSA assay (Mahoney-Crane et al., 2023). Furthermore, various autophagy markers were dysregulated in the same *Gba*$^{+/L444P}$ mouse model (Li et al., 2019a). These included p62, beclin and microtubule-associated protein 1 light chain 3 (LC3), specifically in its lipidated state (LC3-II). Similar to this, other studies identified increased p62 in *Gba*$^{+/L444P}$ mice (Yun et al., 2018), reduced beclin in *Gba*$^{D409V/D409V}$ mice (Sardi et al., 2011) and increased LC3-II in *SNCA*^{A53T} transgenic mice with viral-mediated overexpression of *GBA*-N370S (Papadopoulos et al., 2018). Primary neurons from *Gba*$^{+/L444P}$ mice also displayed accumulation of autolysosomes, accompanied by diminished responses to pharmacological autophagy inducers and lysosomal protease inhibitors (Li et al., 2019a). This indicates that autophagy induction and lysosomal degradation is impaired in these mice. However, these observations require further validation since LC3 was reduced or unchanged in other studies using this *Gba*$^{+/L444P}$ mouse model (Migdalska-Richards et al., 2017b, Yun et al., 2018).

It is somewhat surprising that ER stress-related phenotypes are seldom investigated or found in transgenic *Gba* mice (**Table 1.3**), considering that UPR activation has been identified in many other models of the disorder (**Section 1.3.3.2**). αS pathology also tends to be milder overall in mouse models of *GBA*-associated PD vs *in vitro* models (**Section 1.3.3.3**). In accord with this, Fishbein et al. (2014) found that αS accumulates in primary hippocampal neurons but not in hippocampus tissue from *Gba*$^{+/L444P}$ mice that co-express the *SNCA*-A53T transgene. The lack of αS elevation in tissue was attributed to extra-

neuronal αS clearance mechanisms (Fishbein et al., 2014). Although there is mixed evidence for *de novo* αS pathology in *Gba* transgenic mice (**Table 1.3**), *Gba* mutations or haploinsufficiency can augment αS pathology driven by injection of αS PFFs (Kweon et al., 2024, Mahoney-Crane et al., 2023, Migdalska-Richards et al., 2020), *SNCA*-A53T mutations (Fishbein et al., 2014, Kim et al., 2018a) or human *SNCA* transgene expression (Ikuno et al., 2019). These phenotypes support that GCase dysfunction can increase neuronal vulnerability to pre-existing αS, as proposed by Henderson et al. (2020).

Table 1.3: Overview of key phenotypes in *Gba* transgenic mice used to model *GBA*-associated PD.

Model (original reference)	GCase activity	Glycolipid accumulation		Lysosomal-autophagy pathway	ER stress	αS pathology	SN DAn count	Reference
		GlcCer	GlcSph					
Gba$^{+/L444P}$ (*)	↓	NC	↑	–	–	↑ total, NC p-αS	–	(Lado et al., 2024)
Gba$^{+/L444P}$ (*)	↓	NC	↑	↓ Late endosomal/ lysosomal activity	–	Pre PFF: NC total, ↓ p-αS PFF-mediated: ↑ p-αS (HC only)	NC	(Mahoney-Crane et al., 2022)
Gba$^{+/L444P}$ (*)	↓	–	–	↓ LC3-II, ↑ p62	–	↑ total	NC	(Yun et al., 2018)
Gba$^{+/L444P}$ (*)	↓	–	–	NC LAMP1, LC3, p62, CTSD	NC BiP	↑ total (Str), NC total (MB & BS)	NC	(Migdalska-Richards et al., 2017b)
Gba$^{+/L444P}$ (*)	↓	–	–	↑ LC3-II, p62, ↓ BECN, AMBRA1	–	↑ total	–	(Li et al., 2019a)
GBA^{L444P}*Gba*$^{-/-}$ (***)	↓	–	–	–	–	–	NC	(Chen et al., 2024)
Gba$^{E326K/E326K}$ (§)	↓	↑ [a]	–	–	–	Pre PFF: ↑ insoluble PFF-mediated: ↑ p-αS, insoluble	NC	(Kweon et al., 2024)
Gba$^{D409V/D409V}$ (‡‡)	↓	NC	↑	↓ BECN, NC LC3, p62	–	↑ proteinase K resistant αS (HC)	NC	(Sardi et al., 2011)
Gba$^{D409V/D409V}$ (‡)	↓	↑	↑	NC LAMP1	–	NC total, p-αS	NC	(Polinski et al., 2021)
Gba$^{+/D409V}$ (‡)	↓	NC	↑	–	–	–	–	
Gba$^{+/-}$ (††)	↓	–	–	NC LAMP1, LC3, p62, CTSD	–	NC total	–	(Migdalska-Richards et al., 2017b)
Gba$^{+/-}$ (†)	↓	NC	NC	NC LAMP1, CTSD, CTSL	–	NC total	–	(Tayebi et al., 2017)
Gba$^{L444P/L444P}$ (**)	↓	NC	NC	–	–	NC total	NC	(Furderer et al., 2024)
Gba$^{D409H/D409H}$ (‡‡)	↓	NC	↑	–	–	NC total	NC	
Gba$^{+/D409H}$ (‡‡)	↓	NC	–	–	NC BiP	NC total	NC	(Kim et al., 2018a)

Key: NC = no change; – = not investigated; ↓ = significant decrease; ↑ = significant increase; DAn = dopaminergic neuron; LC3(-II) = microtubule-associated protein 1 light chain 3(-lipidated form); LAMP1 = lysosomal associated membrane protein-1; p62 = sequestosome-1; BECN = beclin; AMBRA1 = autophagy/beclin 1 regulator 1; CTSD = cathepsin D; CTSL = cathepsin L; BiP = binding immunoglobulin protein; p-αS = phosphorylated αS; SN = substantia nigra; HC = hippocampus; Str = striatum; MB= midbrain; BS = brainstem. [a] determined by immunofluorescence. Models: * (Liu et al., 1998); ** (Ginns et al., 2014); *** (Sanders et al., 2013); † (Tybulewicz et al., 1992); †† (Enquist et al., 2007); ‡ (Ikuno et al., 2019) & (Polinski et al., 2021); ‡‡ (Xu et al., 2003); § (Kweon et al., 2024).

GCase dysfunction in CBE-based or genetic mouse models does not culminate in DA neurodegeneration in the SN (**Table 1.3**) (Mus et al., 2019, Rocha et al., 2015c). This is consistent with *GBA* mutations' incomplete penetrance in the disease, contributing to its status as a risk factor and not a causal agent. Additional genetic and environmental "hits" are therefore likely to play a role in disease onset and progression. To emulate the multifactorial nature of *GBA*-associated PD and to augment pathological phenotypes in mouse models of the disease, various studies have exposed *Gba* transgenic mice to additional insults. These include injection of MPTP or αS PFFs, co-expression of pathogenic mutations in other PD-related genes and αS overexpression (Ikuno et al., 2019, Kim et al., 2018a, Mahoney-Crane et al., 2023, Migdalska-Richards et al., 2017b, Nam et al., 2024, Yun et al., 2018). For instance, a significant loss of SN DA neurons was observed in $Gba^{+/L444P}$ mice injected with αS PFFs (Mahoney-Crane et al., 2023) and in dual-mutant mice: $Gba^{+/-}$ *SNCA*-Tg/Tg, $Gba^{+/D409H}SNCA^{A53T}$ and $Gba^{+/L444P}Park7^{-/-}$ (Ikuno et al., 2019, Kim et al., 2018a, Nam et al., 2024). Notably, the extent of nigral DA neurodegeneration in MPTP-treated $Gba^{+/L444P}$ mice and αS-overexpressing $Gba^{+/L444P}$ mice surpassed DA neuron depletion caused by MPTP or adeno-associated virus (AAV)-mediated αS overexpression in WT mice (Migdalska-Richards et al., 2017b, Yun et al., 2018). This highlights that the L444P mutation can significantly enhance neuronal susceptibility to toxicity, despite being insufficient to independently drive DA neuron loss. A gain-of-function effect of the L444P mutation may mediate this phenomenon, since CBE-mediated GCase inhibition or conditional *Gba* KO did not exacerbate nigral DA neurodegeneration in MPTP-treated mice or αS overexpressing mice, respectively (Mus et al., 2019, Soria et al., 2017).

1.4.3 LIMITATIONS OF EXISTING APPROACHES TO MODEL *GBA*-ASSOCIATED PD

Although numerous studies over the past two decades have sought to illuminate *GBA*-associated PD pathology, the mechanisms underlying GCase dysfunction in the disease remain poorly understood (**Section 1.3.3**). In addition, no disease-modifying therapy that can ameliorate GCase function is currently available for PD patients (**Section 1.3.4**). The challenges of developing valid mouse models of *GBA*-associated PD, especially considering *GBA* mutations' incomplete penetrance in the disorder, can stall progress in elucidating mechanisms of GCase dysfunction. Although existing models can recapitulate various disease features (**Table 1.3**), their limitations must not be overlooked.

Firstly, models that are based on genetic or pharmacological GCase inhibition neglect the contribution of gain-of-function effects' to pathology. Furthermore, GCase depletion is typically more severe in CBE-treated models compared to *GBA*-associated PD patients, resulting in phenotypes with contentious clinical relevance to PD. For instance, an ≥80% loss of GCase activity in the brains of CBE-treated WT and *SNCA*^{A53T} mice yielded significant GlcCer accumulation (Rocha et al., 2015c, Rockenstein et al., 2016); however, loss of GCase activity does not exceed 60% in *GBA*-associated PD postmortem brains and there is little evidence for GlcCer elevation (Gegg et al., 2012, Gegg et al., 2015, Leyns et al., 2023, Milenkovic et al., 2022). Other studies have failed to report the level of GCase inhibition achieved with CBE (Ginns et al., 2014), which makes it challenging to ascertain the model's relevance to PD. Moreover, the nature and severity of CBE-mediated pathology depends on the administered dose and the mouse's age (Vardi et al., 2016). Indeed, the effects of CBE administration on αS accumulation and lysosomal/autophagic dysfunction are inconsistent across studies that employ different compound dosage regimens (Farfel-Becker et al., 2019, Mus et al., 2019, Papadopoulos et al., 2018, Rocha et al., 2015c, Rockenstein et

al., 2016). Another drawback of CBE-based models is that the acute nature of GCase inhibition prevents the assessment of age-related disease progression. Lastly, CBE can have off-target effects on GCase2 (Ridley et al., 2013): 100mg/kg of CBE for 6 days decreased GCase2 activity by 30% (Kuo et al., 2019). These effects should not be ignored, especially considering that the potential cross-talk between GCase and GCase2 in PD pathology remains elusive (**Section 1.3.1**).

Gba transgenic mice also have various weaknesses as models of *GBA*-associated PD. In particular, the inferences drawn from mice harbouring biallelic *Gba* variants undermine the distinct genetic-basis, neuropathological features and clinical profile of GD and PD (**Table 1.1**) (Furderer et al., 2024, Kim et al., 2018a, Polinski et al., 2021, Sardi et al., 2011, Vidyadhara et al., 2025). For example, studies have used *Gba*$^{D409H/D409H}$ mice to gain insights into PD-related biochemical and behavioural phenotypes (Furderer et al., 2024, Kim et al., 2018a) even though homozygous *GBA*-D409H mutations in humans exclusively cause a distinctive subtype of GD (GD3c), characterised by valvular and aortic calcification (**Table 1.1**). Akin to CBE-based models, loss of GCase activity in GD mice also exceeds GCase activity deficits in PD patients and has been shown to evoke GlcCer build-up in the brain and viscera (Furderer et al., 2024, Polinski et al., 2021, Sanders et al., 2013).

The relevance of a *Gba* transgenic mouse to *GBA*-associated PD is also informed by the prevalence of their specific *Gba* variant among PD patients. Considering this, the popularity of *Gba*$^{D409V/D409V}$ and *Gba*$^{+/D409V}$ mice as models of *GBA*-associated PD is counterintuitive since the *GBA*-D409V variant has not been identified in PD patients (Farfel-Becker et al., 2019). This variant has only been reported once in GD patients, exclusively in a compound heterozygous state (Theophilus et al., 1989b). In addition, models that combine *Gba* mutations with a human *SNCA*-A53T transgene also lack construct validity (Fishbein et al., 2014, Kim et al., 2018a) because co-occurrence of the *SNCA*-A53T variant with a

GBA mutation has not been described in PD patients. Out of approximately 20,000 PD patients recently screened for a PD-relevant mutation, only one co-expressed pathogenic *GBA* and *SNCA* mutations (Cook et al., 2024, Westenberger et al., 2024). The exact variants were not reported.

Importantly, although PD exclusively affects humans (Garcia-Ruiz and Espay, 2017), no humanised models of *GBA*-associated PD have been described to date. On the other hand, two GD models have been developed that overexpress a human *GBA*-L444P or *GBA*-N370S transgene on a $Gba^{-/-}$ background (Sanders et al., 2013). These mice express human GCase at supraphysiological levels because they harbour up to eight copies of the *GBA* transgene. The transgene copy number also varies across WT and mutant mice, which limits the validity of genotype-related comparisons. Notably, $GBA^{L444P}Gba^{-/-}$ mice display splenic infiltration of Gaucher cells alongside visceral GlcCer accumulation (Sanders et al., 2013), highlighting their unsuitability to model PD. Therefore, it is surprising that "experts at MJFF [the Michael J. Fox foundation]" consider these mice to be transgenic models of *GBA*-associated PD (Alzforum, 2025). Concordant with this view, Chen et al. (2024) used the $GBA^{L444P}Gba^{-/-}$ model to study PD-related sleep disturbances and αS pathology.

A valid humanised mouse model of *GBA*-associated PD would open novel avenues to longitudinally explore disease mechanisms and related behavioural phenotypes conferred by human mutant GCase within an *in vivo* system. Modelling human GCase may also yield enhanced reproducibility across studies, considering that hepatic GCase activity in WT mice is strain-dependent (Duran et al., 2021). It follows that disease-related phenotypes due to mouse KI *Gba* mutations or haploinsufficiency may also vary across strains, as previously observed for genes implicated in psychiatric disorders (Sittig et al., 2016). A humanised model could also offer superior predictive validity in pre-clinical trials for disease-modifying therapies. Supporting this, the efficacy of various pharmacological GCase

activators has previously been shown to differ across human and mouse GCase (Berger et al., 2015). Furthermore, ambroxol failed to elevate human N370S- or L444P-GCase activity in the CNS of *GBA*^{L444P}*Gba*$^{-/-}$ and *GBA*^{N370S}*Gba*$^{-/-}$ GD mice (Sanders et al., 2013), despite significantly enhancing mouse GCase activity in a *Gba*$^{+/L444P}$ model (Migdalska-Richards et al., 2016). This could indicate that ambroxol has a greater therapeutic effect on mouse vs human GCase activity, although differences in the dosing regimen across studies may have also contributed to these inconsistent findings. The recently failed MOVES-PD trial for venglustat in *GBA*-associated PD (**Section 1.3.4**) (Giladi et al., 2023) exemplified the general discrepancy in therapeutic efficacy of potential drugs between preclinical and clinical testing (Athauda and Foltynie, 2015), thereby further highlighting the need for improved disease models. Indeed, much of the rationale for this trial came from preclinical studies in *Gba*$^{D409V/D409V}$ and *Gba*$^{+/D409V}$ mice (Sardi et al., 2017, Viel et al., 2021) and the speed at which the drug progressed to testing in PD patients alarmed some in the field (Sidransky et al., 2020).

1.4.4 CREATION OF A NOVEL, HUMANISED *GBA*-L444P TRANSGENIC MOUSE MODEL AND THESIS OVERVIEW

Considering the shortcomings of existing models and our limited understanding of *GBA*-associated PD pathology, there is a clear unmet need for improved mouse models of the disorder. A humanised model that is heterozygous for a common *GBA* mutation would create unprecedented opportunities for researchers to unravel the mechanisms of GCase dysfunction in the disease. It may also help to accelerate the development of disease-modifying PD therapies by narrowing the "translation gap" from preclinical models to patients.

To address this need, our lab sought to create a novel humanised *GBA*-L444P mouse model of PD. The L444P mutation was chosen because this is the most frequently observed

"severe" *GBA* variant in PD patients (Rossi et al., 2025). It is also the most common *GBA*-variant overall in some populations (**Section 1.1.2**). Dr Javier Alegre-Abarrategui developed the model and Dr Natalie Connor-Robson subsequently expanded the lines and led the model's initial characterisation, prior to this DPhil. To create the humanised mice, a bacterial artificial chromosome (BAC) vector (Yang and Gong, 2005, Yang et al., 1997) was used to insert the full-length human *GBA* transgene, either WT or L444P-mutant, into the mouse genome. Our lab has previously used a BAC transgenic approach to create humanised *SNCA* and *LRRK2* rodent models of PD (Janezic et al., 2013, Sloan et al., 2016, Taylor et al., 2014). These models successfully recapitulate various aspects of PD pathology and our αS overexpressing (*SNCA*-OVX) mice have been used to assess potential disease-modifying therapeutic strategies (Bengoa-Vergniory et al., 2020). A key strength of the BAC vector is that it can accommodate large genomic sequences (up to 300 kb) (Mogi et al., 2025). This enabled the full-length human *GBA* gene to be inserted into the mouse genome, along with its endogenous promoter and regulatory elements. Another advantage of our novel model is that the human *GBA* transgenic construct is specifically integrated into the mouse Rosa26 locus. Therefore, the position and expression levels of the human transgene are equivalent in L444P mice and mice that harbour the human wild-type (hWT) *GBA* construct, making these genotypes directly comparable (**Fig. 1.4**). This site-specific insertion approach is superior to traditional BAC technology, which is limited by the random nature of transgene integration into the host's genome (Mogi et al., 2025). Random integration can result in unphysiological expression levels due to the insertion of multiple copies of the transgene (Chandler et al., 2007). It may also lead to insertional mutagenesis and aberrant position effects, whereby the patterns of transgene expression differ from its intrinsic regulation (Mogi et al., 2025). On the other hand, the Rosa26 locus offers a safe harbour for targeted transgene insertion because the mouse *Rosa26* gene does not serve a known critical function

and is therefore not essential for mouse viability (Biggs et al., 2023, Zambrowicz et al., 1997). Targeting the Rosa26 locus has been shown to produce ubiquitous, stable and highly efficient transgene expression, which has contributed to its popularity in the creation of genetically engineered mouse models (Casola, 2010).

Four genotypes are compared in all experiments throughout this thesis (**Fig. 1.4**): *Gba*$^{+/+}$ (non-transgenic, nTG), *Gba*$^{+/-}$, *Gba*$^{+/-}$*GBA*^{WT} (hWT) and *Gba*$^{+/-}$*GBA*^{L444P} (L444P). These genotypes allow my experiments to identify pathological phenotypes caused by the human L444P mutation and to probe whether such phenotypes could specifically be attributed to loss- or gain-of-function effects of the mutation (**Fig. 1.4**). Namely, a disease-feature that is observed across both L444P and *Gba*$^{+/-}$ mice is likely driven by a loss-of-function effect, whereas a gain-of-function effect would more plausibly underpin phenotypes that are present in L444P mice but absent in *Gba*$^{+/-}$ mice.

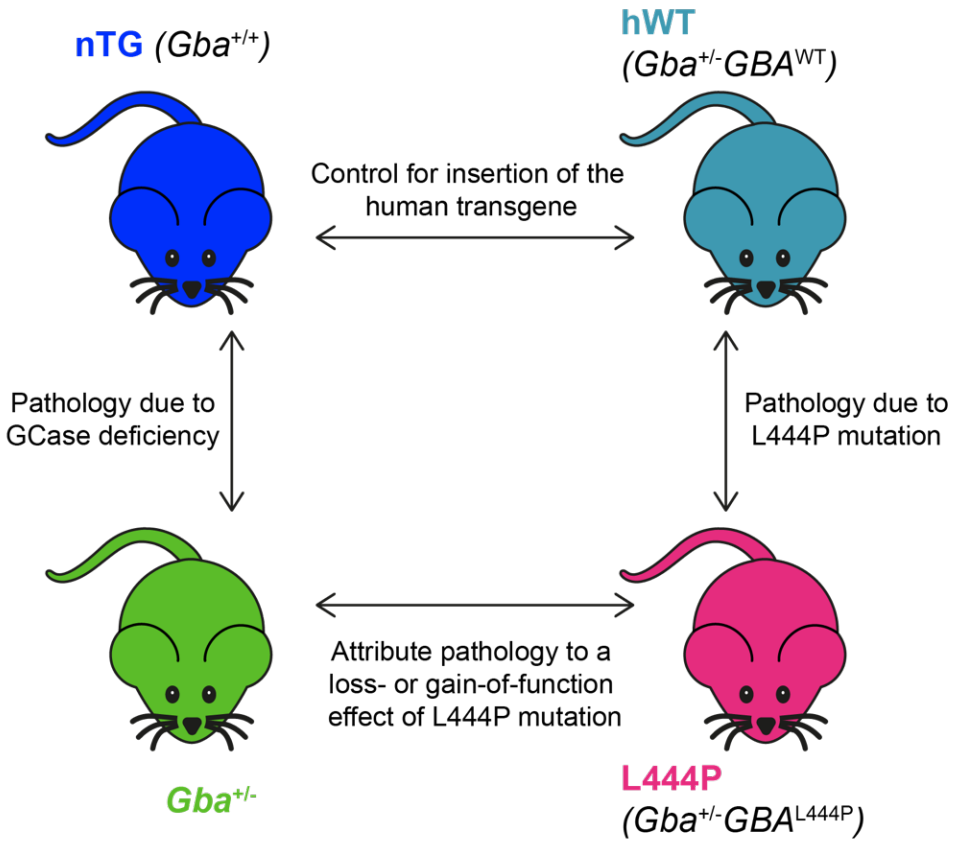


Figure 1.4: Summary of the experimental genotypes used in this thesis and insights from individual genotypic pairwise comparisons.

1.4.5 AIMS OF THIS THESIS

The overarching goal of this DPhil is to comprehensively characterise pathology in our novel *GBA*-L444P BAC transgenic mouse model from a molecular to a behavioural level. It is hoped that this thorough evaluation will contribute to advancing our understanding of the pathological mechanisms underlying *GBA*-associated PD and will pinpoint the strengths and limitations of our model to help inform future research avenues. This thesis contains three results chapters, each addressing different aspects of *GBA*-associated PD pathology. The specific aims of this thesis are as follows:

1. **To unravel pathology related to gain- and loss-of-function effects of the L444P mutation across brain regions** (*Chapter 3*).

In chapter three, I first seek to confirm that our model can recapitulate both gain- and loss-of-function effects of the L444P mutation in the cortex. These experiments build on initial characterisation of midbrain pathology in our L444P model conducted by Dr Natalie Connor-Robson (**Fig. 3.1**). Subsequent experiments in this chapter examine downstream consequences of these effects on ER, lysosomal and autophagic function, glycolipid homeostasis, αS distribution and GCase's interaction with LIMP2. These phenotypes are investigated using biochemical assays in cells and tissue alongside *in silico* modelling of protein-protein binding.

2. **To explore DA transmission and homeostasis in the L444P striatum** (*Chapter 4*).

Experiments in chapter four endeavour to determine if evoked DA release is impaired in the striatum of aged L444P mice and if potential deficits are associated with reduced striatal DA levels. Subsequently, I set out to elucidate if mechanisms that govern striatal DA dynamics are dysregulated by the L444P mutation in young and aged mice. These questions are addressed using fast-scan cyclic voltammetry (FCV) in *ex vivo* striatal slices, high-

performance liquid chromatography (HPLC) and immunofluorescence (IF) in paraffin-embedded sections.

3. **To determine whether the L444P mutation evokes PD-relevant behavioural deficits in an aged mouse cohort** (*Chapter 5*).

In chapter five, various aspects of spontaneous motor function, including overall locomotion, coordination, grip strength and gait, are characterised in a battery of tests. Spatial working memory, anxiety-like behaviour and GI function are also evaluated given the high prevalence of non-motor symptoms in *GBA*-associated PD patients.

CHAPTER 2: MATERIALS AND METHODS

2.1 GENERATION AND MAINTENANCE OF TRANSGENIC MICE

2.1.1 CREATION OF HUMANISED *GBA* TRANSGENIC MICE

The humanised *GBA*-transgenic model characterised in this thesis was created in our lab prior to this DPhil by Dr Javier Alegre-Abarrategui. Briefly, a BAC vector, retrofitted with the full-length human *GBA* transgenic construct (either WT or L444P) and PhiC31 integrase exchange machinery, was transfected into embryonic stem cells. Subsequently, co-transfected PhiC31 integrase mediated the site-specific insertion of this BAC vector into the Rosa26 locus of the mouse genome. Therefore, the location of the *GBA* transgene is consistent across hWT and L444P mice, which enables a more refined comparison of the functionality of the WT and mutant transgene vs a random insertion approach. Experimental mice, hemizygous for the BAC *GBA* transgene, were produced on a mouse *Gba* heterozygous background by crossing to $Gba^{+/-}$ mice, procured from the Jackson Laboratory (Strain name: B6.129S6-Gba-^{tm1Nsb}/J, Jackson Laboratories stock number: 003321) (**Fig. 2.1**). Heterozygous *Gba* KO was achieved in these mice via a neomycin resistance gene inserted at exon 9 and 10 of one *Gba* allele, as described by Tybulewicz et al. (1992).

2.1.2 BREEDING STRATEGIES

Three maintenance colonies were bred on a tick-over basis (**Table 2.1**). These colonies were maintained on a C57BL/6J background by pairing males of relevant genotypes with C57BL/6J females ($Gba^{+/+}$) that were procured at 8-weeks-old from Charles River Laboratories.

The breeding strategy for experimental mice is outlined in **Fig. 2.1**. Briefly, male *Gba*$^{+/-}$ mice (bred in the GBAN colony, **Table 2.1**) were paired with *Gba*$^{+/+}$*GBA*^{WT} or *Gba*$^{+/+}$*GBA*^{L444P} females (from crosses in the 2711 or 311 colonies, **Table 2.1**) to generate *Gba*$^{+/-}$*GBA*^{WT} (hWT) or *Gba*$^{+/-}$*GBA*^{L444P} (L444P) mice, respectively. *Gba*$^{+/+}$ (nTG) and *Gba*$^{+/-}$ mice were also produced by both crosses and were used for experiments (**Fig. 2.1**). Mice that were hemizygous for the *GBA* transgene and homozygous for the native *Gba* gene (*Gba*$^{+/+}$*GBA*^{WT} and *Gba*$^{+/+}$*GBA*^{L444P}) were not used for experiments because total GCase expression in these mice is higher than physiological levels. Males and females with the same parents were not paired in any crosses.

Table 2.1: Mouse colonies used for maintenance purposes. All female tick-over breeders were ordered from Charles River Laboratories at 8-weeks-old.

		Genotype of tick-over breeders	
Name	**Purpose**	♂	♀
GBAN	To maintain heterozygosity for mouse *Gba*	*Gba*$^{+/-}$	*Gba*$^{+/+}$
2711	To retain hWT *GBA* transgene expression	*Gba*$^{+/+}$*GBA*^{WT}	*Gba*$^{+/+}$
311	To retain L444P *GBA* transgene expression	*Gba*$^{+/+}$*GBA*^{L444P}	*Gba*$^{+/+}$

2.1.3 HUSBANDRY AND ETHICAL DECLARATION

Mice were group-housed in the Biomedical Sciences Building at the University of Oxford. Food and water were available *ad libitum*. Holding conditions were maintained at 20-24°C, 45-65% humidity on a 12:12 light cycle with 30 min dawn and 30 min dusk. A mixture of male and female mice were used for all experiments. All procedures involving mice were conducted in compliance with the United Kingdom Home Office Regulations under the Animals (Scientific Procedures) Act 1986. For collection of experimental tissue, mice were euthanised by cervical dislocation (confirmed with exsanguination) or by intraperitoneal injection of a terminal dose of anaesthetic (pentobarbitone) followed by transcardiac

perfusion-fixation. Neonatal mouse pups, up to postnatal day (PND) 5, were sacrificed by decapitation.

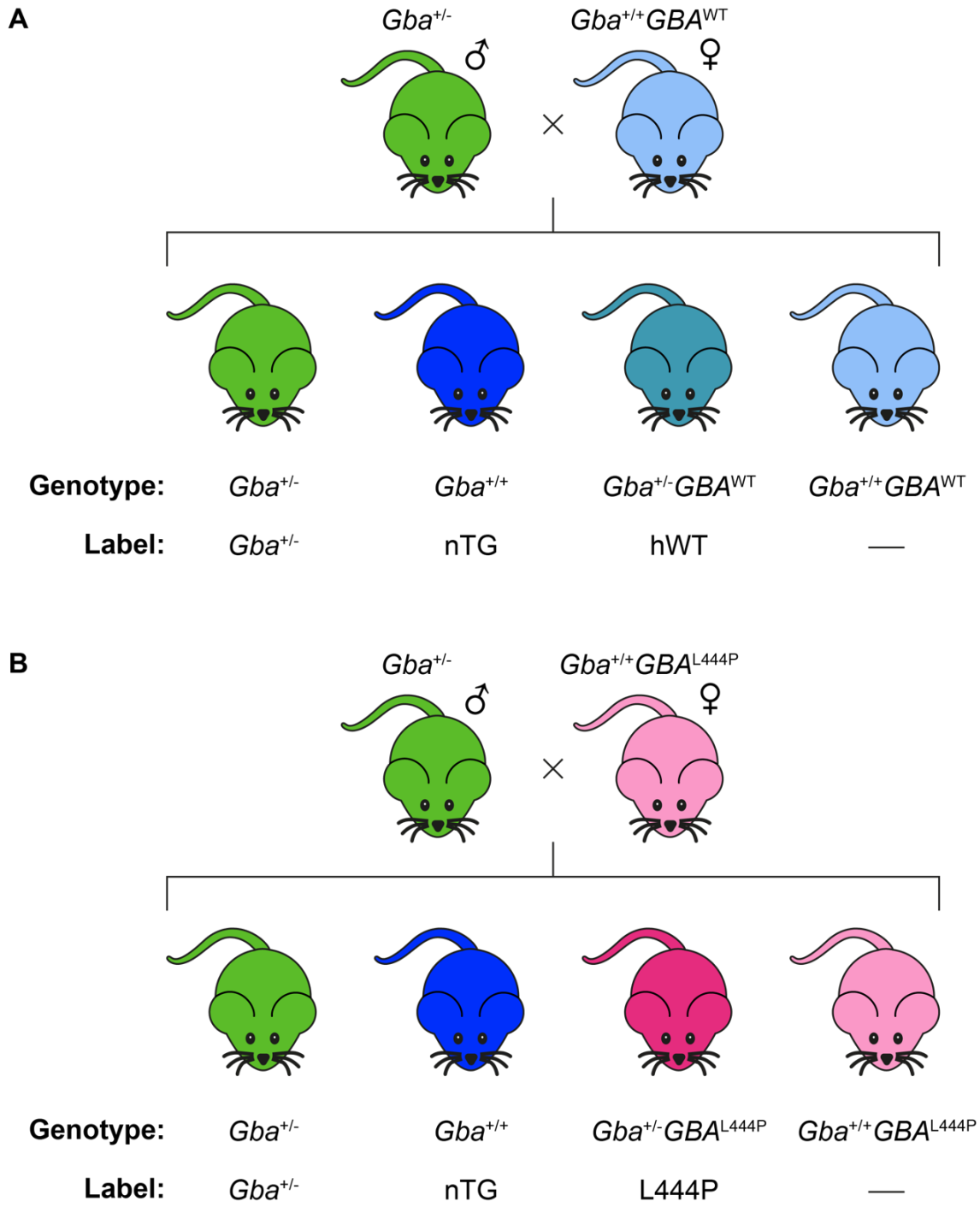


Figure 2.1: Breeding strategy for experimental mice. *Gba*$^{+/-}$ males were paired with *Gba*$^{+/+}$*GBA*^{WT} (**A**) or *Gba*$^{+/+}$*GBA*^{L444P} (**B**) females. Potential genotypes of offspring from both crosses are listed, along with their experimental labels. The "–" denotes that the genotype is not used for experiments.

2.2 MOUSE GENOTYPING

2.2.1 DNA EXTRACTION FROM MOUSE TISSUE BIOPSIES

Mouse ear or tail clips were individually submerged in 450 µL of lysis buffer (**Table 2.2**), supplemented with 13 µL of proteinase K (stock concentration: 20 mg/mL) (Invitrogen). Samples were vortexed for 30 s and then incubated at 65°C for 1-1.5 hours, followed by 95°C for a further 30 min. Heating at 95°C served to inactivate proteinase K. Lysates were cooled on ice for 5 min before centrifuging at 2400 rcf for 1 min.

Table 2.2: Lysis buffer recipe for DNA extraction.

Reagent	Final Concentration
KCl	50 mM
$MgCl_2$	1.5 mM
Tris pH 8.5	10 mM
IGEPAL CA-630	0.45%
Tween 20	0.45%

2.2.2 AMPLIFICATION OF EXTRACTED DNA LYSATES

Lysed DNA was amplified in up to three polymerase chain reactions (PCRs) (**Table 2.3**), depending on the mouse colonies from which samples came and the purpose of the genotyping. Briefly, DNA lysates were first pipetted into individual wells of a 96-well PCR plate and the appropriate PCR master mix (**Table 2.3 A**) was subsequently added. An equivalent volume of Milli-Q H_2O was used instead of lysed DNA in negative control samples and previously genotyped lysates with known positive results acted as positive controls. For the deoxynucleoside triphosphate (dNTP) mix (**Table 2.3 A**), individual dNTPs (dATP, dCTP, dGTP, dTTP) (Invitrogen) were co-diluted in Milli-Q H_2O, each to a final concentration of 2 mM. Primers were resuspended according to manufacturer's specifications (IDT) and primer pair mixes (**Table 2.3 A-B**) were prepared by diluting both

forward (F) and reverse (R) primers 1:10 in Milli-Q H_2O. DNA was amplified using a T100 Thermal Cycler (Bio-Rad) as per the cycling conditions in **Table 2.3 C**.

2.2.3 DNA RESTRICTION ENZYME DIGEST

To determine if the PCR products from **Reaction (iii), Table 2.3** harboured the L444P mutation, I assessed whether they could be digested by the NciI restriction enzyme. NciI specifically recognizes CC^SGG nucleotide sequences and thereby cuts the L444P transgenic construct at its mutation site, yielding DNA fragments of 263 and 246 base pairs (bps) (**Fig. 2.2**). The hWT construct is not cleaved by NciI. A master mix was first prepared to a final working concentration of 5% NciI and 2X rCutSmart buffer (both New England Biolabs) in Milli-Q H_2O. Next, 10 µL of this mix was added to 10 µL of each amplified DNA lysate. Samples were subsequently incubated for 60 min at 37°C before running on a 2% agarose gel (**Section 2.2.4**).

2.2.4 AGAROSE GEL PREPARATION AND ELECTROPHORESIS

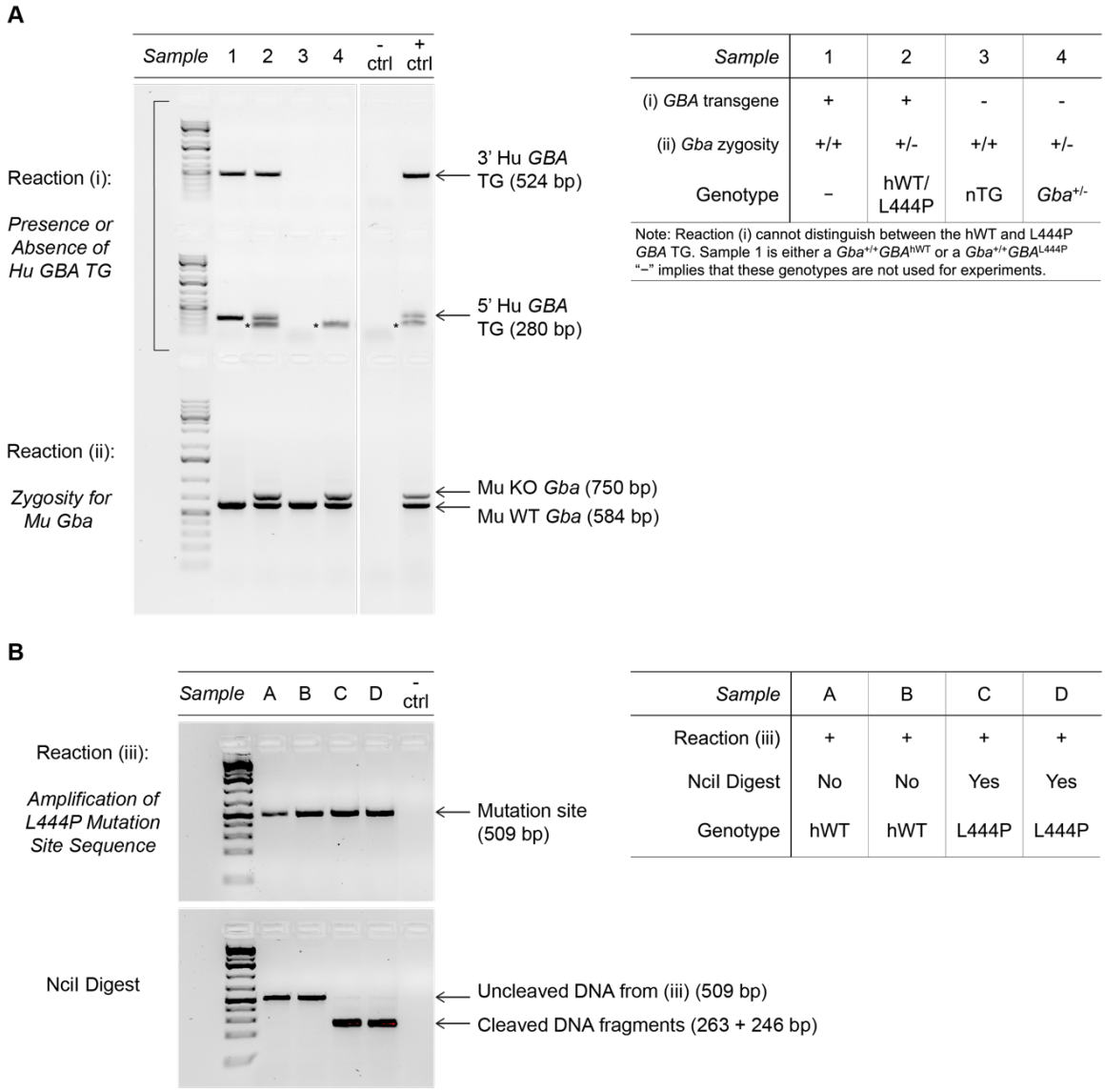
The % concentration of agarose gels are shown on **Table 2.3 D**. Agarose powder was first dissolved in 150 mL of 1X Tris-Borate-EDTA (TBE) buffer by microwaving for 2.5 min. The solution was allowed to cool for 1-2 min and 10 µL of Ethidium bromide (stock concentration: 10 mg/mL) (Sigma-Aldrich) was added. The mixture was poured into a casting tray, pre-fitted with plastic combs, and left to set at room temperature for at least 30 min. Once set, the gel was transferred to a horizontal electrophoresis tank (Sub-cell GT, Bio-Rad), filled with 1X TBE buffer. Each PCR product was mixed with 5 µL of loading buffer (15% Ficoll 400 solution supplemented with trace amounts of Orange G and bromophenol blue) and subsequently loaded into the gel at 10 µL per well. The leftmost well contained 5 µL of GeneRuler 1 kb Plus DNA Ladder (Thermo Scientific). Gels were run at 100 V for 30-50 min to achieve sufficient band separation.

Table 2.3: PCR parameters for genotyping mouse DNA lysates in this thesis. The PCR buffer and DNA polymerase for **reaction (i-ii)** were purchased from Qiagen. **For reaction (iii)**, the PCR buffer, DNA polymerase and $MgCl_2$ were from Applied Biosystems and the Q-Solution was from Qiagen. bp = base pairs.

Reaction:	**(i) To detect the presence or absence of the human *GBA* transgene**	**(ii) To determine mouse *Gba* zygosity**	**(iii) To amplify the transgene sequence spanning the L444P mutation site**
(A) PCR master mix recipe *Volumes are expressed per sample and were scaled according to the number of samples. Components are expressed as their stock concentration.*	2 µL 10X-PCR buffer with 15 mM $MgCl_2$ 1.5 µL F & R primer pair mix 0.4 µL 2 mM dNTP mix 0.1 µL HotStarTaq DNA Polymerase 14 µL Milli-Q H_2O 18 µL Total volume (added to 2 µL DNA lysate)		1.5 µL 10X-PCR Buffer II 0.9 µL 25 mM $MgCl_2$ 3 µL 5X Q-Solution 1.5 µL F & R primer pair mix 0.75 µL 2 mM dNTP mix 0.2 µL AmpliTaq Gold DNA Polymerase 6.15 µL Milli-Q H_2O 14 µL Total volume (added to 1 µL DNA lysate)
(B) Primer pairs Forward (F) & Reverse (R) sequences (Predicted band size)	5' *GBA* transgenic construct: (280 bp) F:CACGCTTCAAAAGCGCACGTCTG R:GTTGTGCCCAGTCATAGCCGAATAG 3' *GBA* transgenic construct: (524 bp) F: TTAGGTCCCTCGACCTGCAGG R: CGGGAGAAATGGATATGAAGTAC TGGGC	Mouse WT *Gba* allele: (584 bp) F: CGTAACTGGATGGACGGACT R: ACACGACCACAACTGCAGAG Mouse KO *Gba* allele - Neomycin resistance gene: (750 bp) F: GCTATCAGGACATAGCGTTGG R: ACACGACCACAACTGCAGAG	L444P mutation site in *GBA* transgenic construct: (509 bp) F: AGCAACAGAAAACCCCAATG R: GCCACAGGTAGGTGTGAATG
(C) PCR thermal cycling parameters	1. 95°C for 15 min 2. 95°C for 30 s 3. 65°C for 30 s 4. 72°C for 2 min 5. Cycle to step two x 34 more times 6. 72°C for 5 min 7. 12°C for 10 min	1. 95°C for 15 min 2. 95°C for 30 s 3. 62°C for 30 s 4. 72°C for 2 min 5. Cycle to step two x 34 more times 6. 72°C for 5 min 7. 12°C for 10 min	1. 95°C for 10 min 2. 95°C for 30 s 3. 58°C for 30 s 4. 72°C for 2 min 5. Cycle to step two x 34 more times 6. 72°C for 8 min 7. 12°C for 10 min
(D) Agarose gel %	1% : 1.5 g agarose in 150 mL 1X TBE		2% : 3 g agarose in 150 mL 1X TBE

2.2.5 REPRESENTATIVE GENOTYPING RESULTS ON AGAROSE GELS

Once electrophoresis was complete, DNA bands were visualised on agarose gels using a Chemidoc MP Imaging System (Bio-Rad). Representative agarose gels with genotype annotations are illustrated in **Fig. 2.2**.



Sample	1	2	3	4
(i) *GBA* transgene	+	+	-	-
(ii) *Gba* zygosity	+/+	+/-	+/+	+/-
Genotype	–	hWT/ L444P	nTG	*Gba*$^{+/-}$

Note: Reaction (i) cannot distinguish between the hWT and L444P *GBA* TG. Sample 1 is either a *Gba*$^{+/+}$*GBA*^{hWT} or a *Gba*$^{+/+}$*GBA*^{L444P}
"–" implies that these genotypes are not used for experiments.

Sample	A	B	C	D
Reaction (iii)	+	+	+	+
NciI Digest	No	No	Yes	Yes
Genotype	hWT	hWT	L444P	L444P

Figure 2.2: Representative genotyping results from the PCRs and restriction enzyme digest reactions described in this thesis. Samples on representative agarose gels (*left*) are presented with their corresponding genotype annotations (*right*). (**A**) Separate PCRs determined the presence of the human (Hu) *GBA* transgene (i) and the zygosity of mouse (Mu) *Gba* (ii). Bands marked with an * are non-specific. (**B**) The DNA sequence at the position of the L444P mutation site was amplified by reaction (iii) and the subsequent digest with NciI distinguished between hWT and L444P transgenic constructs.

2.3 METHODS PERTAINING TO CHAPTER 3

2.3.1 GENERATION AND TREATMENT OF MIXED PRIMARY CORTICAL CULTURES FROM NEONATAL MICE

Mouse pups (PND 0-5) were decapitated and their brains immediately extracted and individually submerged in ice-cold cell culture media (Neurobasal Plus, Gibco). Tail clips were also collected for genotyping (**Section 2.2**). As mice were genotyped post-cell plating, brains and resultant cell cultures from each mouse were kept separate. Meninges were first removed and cortices subsequently dissected under a dissection microscope (Lynx Stereo, Vision Engineering) using Jewelers forceps (No. 5, Dumont). Cortices were then minced with a scalpel and kept in media on ice until all brains were processed.

Afterwards, the media was aspirated and samples were trypsinised for 20 min at 37°C, using 3.33% trypsin-EDTA in fresh media. To inactivate the trypsin, an equal part of 20% foetal bovine serum (FBS) in fresh media was added to each sample. Samples were next centrifuged at 200 rcf for 5 min, the supernatant was discarded and pellets were resuspended in fresh media. Centrifugation and resuspension were repeated two more times to wash away residual FBS. After the final centrifugation, pellets were resuspended in growth media: sterile Neurobasal Plus supplemented with B-27 (Gibco) and MycoZap Plus-PR (Lonza) at final working concentrations of 2% and 0.2%, respectively. Samples were subsequently triturated approximately 30 times using a P1000 pipette, then 30 times with a P200 pipette and a final 30 times with a P20 pipette.

For cell counting, a portion of the cell suspension from each mouse was diluted 1:10 in growth media. Trypan blue or Solution 18 (ChemoMetec) was then diluted 1:20 in this suspension to determine cell viability and cells were counted using a NucleoCounter NC-250 (ChemoMetec). Cells were diluted in growth media to the required density (**Table 2.4**) and seeded in Geltrex- (Gibco) coated sterile well plates. Cultures were maintained at 37°C,

5% CO_2, 95% relative humidity and received a full media change after 72 hours i.e. on the 3rd day *in vitro* (DIV) post-plating. A 50% media replacement was made in 96-well half-area plates every 2nd day thereafter and in 24-well plates on DIV 5 and DIV 7. Subsequently, 24-well plates were treated for 5 days with ambroxol (Suppelco) or dimethyl sulfoxide (DMSO) (Sigma-Aldrich) as a vehicle control, each prepared to a final working concentration of 10 μM in growth media. Compounds were initially applied as part of a full media change on DIV 9[3] and concentrations were maintained during a subsequent media replacement 2-3 days later. On DIV 14, cells were either fixed in paraformaldehyde (PFA) (**Section 2.3.2**) and kept at 4°C or snap frozen on dry ice and stored at -80°C (**Section 2.3.3**).

Table 2.4: Cell plating conditions for cortical primary cultures.

Plate	Seeding density per well	Growth media volume per well
24-well	500,000 cells	500 mL
96-well half-area	50,000 cells	50 mL

2.3.2 IMMUNOCYTOCHEMISTRY ON PRIMARY CORTICAL CELL CULTURES

On DIV 14, cells in 96-well half-area plates were washed in 1X phosphate-buffered saline (PBS) and fixed using 4% PFA in 1X PBS, for 20 min at room temperature. Cells were re-washed in PBS to remove residual PFA and were kept in PBS with sodium azide (PBS-Azide) (Santa Cruz Biotechnology) at 4°C until needed for immunocytochemistry.

On the staining day, cells were permeabilised and blocked for 20 min at room temperature using 4% FBS in 1X PBS, supplemented with Tween 20 (final concentration: 0.1%). Thereafter, cells were incubated in primary antibodies, diluted in the permeabilization/blocking solution, overnight at 4°C (**Table 2.5**). The next day, cultures

[3] 24-well plates from one culture were treated with compounds on DIV 10. This culture also received a 5-day treatment and was therefore frozen on DIV 15.

were washed three times, for 1 min, 10 min and 20 min, in 1X PBS at room temperature. Cells were then treated with DAPI and appropriate Alexa Fluor-conjugated secondary antibodies (Invitrogen), diluted 1:1000 in 1X PBS, for 2 hours at room temperature. Plates were kept protected from light following application of secondary antibodies and cells were subsequently re-washed three times as before. All washes and antibody incubations were conducted on a mechanical rocker. Cells were imaged using an Opera Phenix (Perkin Elmer) at 20X magnification and stored longer-term in PBS-Azide at 4°C.

Table 2.5: Primary antibodies used for immunocytochemistry.

Antibody	Dilution	Species raised (class)	Supplier	Catalogue #
MAP2	1:500	Rabbit (polyclonal)	Sigma-Aldrich	AB5622
GFAP	1:500	Chicken (polyclonal)	Abcam	ab4674

2.3.3 GCase ACTIVITY ASSAY

GCase activity was measured in cortical cell and tissue lysates using a 4-methylumbelliferyl-β-D-glucopyranoside (4-MUG) fluorescent substrate-based assay. A solution of 4-MUG (Sigma-Aldrich) was prepared in citrate phosphate buffer pH 5.4 (CP-buffer) (**Table 2.6**) to a final working concentration of 10 mM (3.4 mg/mL). To increase 4-MUG solubility, the solution was kept at 30°C and vortexed regularly until needed. The specifics of the assay protocols for cortical cells and tissue are outlined in **Table 2.7**.

Briefly, samples were first lysed in CP-buffer on ice and membranes were removed by centrifuging at 4°C. The protein concentration of the supernatant was determined using a bicinchoninic acid (BCA) assay (**Section 2.3.4**) and samples were diluted accordingly in CP-buffer to a consistent protein concentration (**Table 2.7**). A portion of the neat supernatant from one sample per genotype was separated and used as a negative control sample. These samples were treated with 100 μM (final concentration) of CBE (Sigma-Aldrich), diluted in

CP-buffer. Non-CBE treated samples from the same mice were diluted in an equivalent volume of CP-buffer. CBE-treated samples were thereafter incubated for 30 min at 37°C. All samples were then pipetted in triplicate into a 96-well plate (50 µL per well) and 20 µL of the 10 mM 4-MUG solution was subsequently added to each well. Plates were incubated at 37°C for 60 min, protected from light. Afterwards, the reaction was terminated by pipetting 70 µL of 0.2 M glycine solution (pH 10.8) into each well. The fluorescence was read immediately using a PHERAstar FSX microplate reader (BMG Labtech) at excitation/emission wavelengths of 350/450 nm. During analysis, the average fluorescence of CBE-treated samples served as a background reading for GCase activity and was subtracted from the fluorescence readout of other samples.

Table 2.6: CP-buffer recipe for GCase activity assay.

Reagent	**Final Concentration**
Na_2HPO_4	111 mM
$C_6H_8O_7$	44 mM
Triton X-100	0.25%
Taurocholic acid	0.25%
cOmplete protease inhibitor cocktail tablets (Roche)	1 tablet per 10 mL
PhosSTOP phosphatase inhibitor tablets (Roche)	1 tablet per 10 mL

Table 2.7: GCase activity assay protocol specifics for cells and tissue.

Assay parameter or procedure	Cortical cell cultures	Cortex tissue
CP-buffer volume	50 µL per well*	1 mL per sample
Sample lysis	1. Wells incubated in CP-buffer, (approx. 30-60 s) 2. Cells scraped & transferred to Eppendorf tubes 3. Sonicated at 50 kHz (10 s)	1. Homogenised with a handheld homogenizer (20 s) 2. Sonicated at 50 kHz (30 s)
Centrifugation	1200 rcf (5 min)	3 m = 8000 rcf (10 min) 15-21 m = 2700 rcf (5 min) then 5200 rcf (4 min)
Final concentration	10 µg protein/ 50 µL	25 µg protein/ 50 µL

* CP-buffer in wells from the same mouse and treatment condition were combined into the same Eppendorf tube after cell harvesting by scraping. GCase activity was only assessed in cultures from 24-well plates and not 96-well half-area plates. Cell samples were left to settle on ice for 15 min after sonicating and before centrifuging. 3 m = 3 months, 15-21 m = 15-21 months.

2.3.4 BCA ASSAY TO QUANTIFY PROTEIN CONCENTRATION

The protein concentration of cell and tissue samples was measured using a BCA assay, according to manufacturer's instructions (Pierce BCA Protein Assay Kit, Thermo Scientific). Briefly, one part of reagent B was added to 50 parts of reagent A to make the BCA working reagent. A series of bovine serum albumin (BSA) protein standards (range 0-1 mg/mL) was prepared and pipetted in triplicate into a 96-well plate. Samples were diluted in CP-buffer (**Table 2.6**) and added to the plate in triplicate (**Table 2.8**). Subsequently, the BCA working reagent was added to each well (**Table 2.8**) and plates were incubated at 37°C for 30 min. Absorbance was read at 562 nm using a PHERAstar FSX microplate reader (BMG Labtech).

Table 2.8: BCA assay parameters.

		Volume per well of a 96-well plate	
Sample type	**CP-buffer dilution**	**Sample/ standard**	**BCA working reagent**
Cortex tissue	1:10	10 µL	100 µL
Cortex cell cultures	1:5	5 µL	45 µL

2.3.5 WESTERN BLOTTING

To prepare samples for western blotting, cortex tissue was first homogenised in CP-buffer and protein concentration determined as described in **Section 2.3.3-2.3.4**. Tissue homogenates were then diluted to a final concentration of 1 µg protein/µL in radioimmunoprecipitation assay (RIPA) buffer (**Table 2.9 A**), supplemented with 6X Laemmli sample buffer (diluted 1:6) (**Table 2.9 B**). Samples were boiled at 95°C for 5 min to reduce and denature proteins and stored at –20°C until required for the assay.

A pre-cast polyacrylamide gradient gel (Criterion TGX, Bio-Rad) was transferred to an electrophoresis tank (Criterion Blotter, Bio-Rad) filled with 1X running buffer (**Table 2.10 A**). The leftmost well was loaded with the MagicMark XP standard (Invitrogen) and 7 µL

of each sample (containing 7 μg protein) was added to the other wells. Gels were run at 200 V until the dye front had just run off the gel, or longer depending on the protein of interest.

Table 2.9: Composition of buffer solutions used in western blot sample preparation.

(A) RIPA buffer		(B) Laemmli sample buffer (6X)	
Reagent	**Final Concentration**	**Reagent**	**Final Concentration**
Tris pH 8	50 mM	SDS	12%
NaCl	150 mM	β-mercaptoethanol	30%
IGEPAL CA-630	1%	Glycerol	60%
Na-deoxycholate	0.5%	Bromphenol blue	0.012%
SDS	0.1%	Tris pH 6.8	375 mM
cOmplete protease inhibitor cocktail	1 tablet per 10 mL solution		
PhosSTOP phosphatase inhibitors	1 tablet per 10 mL solution		

Following electrophoresis, proteins were transferred to a polyvinylidene fluoride (PVDF) membrane (Trans-Blot Turbo Transfer Pack, Bio-Rad) using a Trans-Blot Turbo Transfer System (Bio-Rad). The membrane was rinsed in 1X Tris-buffered saline (**Table 2.10 B**), supplemented with Tween 20 (final concentration: 0.1%) (TBS-T), before blocking with 4% milk (skim milk powder dissolved in TBS-T) for 60 min at room temperature. Afterwards, the membrane was incubated with the primary antibody, diluted in 4% milk, overnight at 4°C (**Table 2.11**). The primary antibody was removed the next day by washing the membrane three times in TBS-T at room temperature (5 min per wash). Afterwards, the membrane was incubated in the appropriate horseradish peroxidase- (HRP) conjugated secondary antibody (Bio-Rad), diluted 1:3000 in TBS-T, for 60 min at room temperature. Residual secondary antibody was then removed with three washes in TBS-T (5 min each) at room temperature. Membranes were developed with the Immobilon (Millipore) or Amersham (GE Healthcare) chemiluminescent HRP substrate as per manufacturers'

instructions and immediately visualised using a Chemidoc MP Imaging System (Bio-Rad). Subsequently, membranes were rinsed in TBS-T and incubated for 60 min at room temperature with HRP-conjugated β-Actin in 4% milk, as a protein loading control. After three 5 min washes in TBS-T at room temperature blots were re-developed and visualised as before. Membranes were rocked on a mechanical rocker for all antibody incubations and washes. The volume of protein bands was quantified using Image Lab (Bio-Rad).

Table 2.10: Recipe for western blot reagents.

Running buffer (10X)		**Tris buffered saline (10X)**	
Reagent	**Final Concentration**	**Reagent**	**Final Concentration**
Glycine	192 mM	Tris-HCL	154 mM
Tris base	250 mM	NaCl	1.38 M
SDS	35 mM		
1X working solutions were prepared in dH_2O			

Table 2.11: Primary antibodies used for western blots.

Antibody	**Dilution**	**Species raised (class)**	**Supplier**	**Catalogue #**
GCase	1:500	Rabbit (monoclonal*)	Abcam	ab128879
αS	1:250	Mouse (monoclonal)	Abcam	ab1903
BiP	1:1000	Rabbit (polyclonal)	Abcam	ab21685
LAMP1	1:250	Rabbit (polyclonal)	Abcam	ab24170
LC3-B	1:1000	Rabbit (polyclonal)	Cell Signalling Technology	2775
HRP-conjugated β-Actin	1:50000	Mouse (monoclonal)	Abcam	ab49900
* antibody made using recombinant technology.				

2.3.6 LIPIDOMIC ANALYSIS

Mice were sacrificed by cervical dislocation (confirmation with exsanguination) and their liver, spleen and brain were immediately extracted. Midbrain, striatum and cortex from each

hemisphere were dissected on ice. Brain and visceral tissue were subsequently snap-frozen in dry ice and transported externally for lipidomic analysis. Dr Benjamin Jenkins (University of Cambridge) analysed cholesterol levels using liquid chromatography-mass spectrometry (LC-MS), as previously described (Jenkins et al., 2020). All other lipid species presented in this thesis were quantified by Ms Kateryna Bila and Dr Martijn van der Lienden (Leiden University) using liquid chromatography with tandem mass spectrometry (LC-MS/MS) coupled with either a C-18 column or a HILIC column, in accordance with previous reports (Lelieveld et al., 2022, Marques et al., 2016, Mirzaian et al., 2017). The HILIC column enabled the separation of glucosyl- and galactosyl- lipid species (Lelieveld et al., 2022).

2.3.7 αS QUANTIFICATION IN MEMBRANE AND SOLUBLE TISSUE FRACTIONS

Mice were sacrificed and brains extracted as per **Section 2.3.6**. The cerebellum, midbrain, striatum and cortex from each hemisphere were dissected on ice and immediately snap-frozen in dry ice. Dr Clara Obensa Bertroli (University College London) used these samples to measure the intracellular distribution of αS across the membrane and cytosol. Briefly, tissue was first manually homogenised and sonicated. Thereafter, membrane and soluble tissue fractions were sequentially extracted by serial ultracentrifugation. αS was quantified in these tissue fractions using a mesoscale discovery (MSD) immunoassay. The capture and Sulfo-tagged SOY1 detection antibodies against αS (**Table 2.12**) have been previously described (Dettmer et al., 2015, Sanderson et al., 2020).

Table 2.12: αS antibodies used in the MSD immunoassay.

Antibody	Final concentration	Species raised (class)	Supplier	Catalogue #
αS 2F12	6.67 μg/mL	Mouse (monoclonal)	Sigma-Aldrich	MABN1817
αS SOY1	6.67 μg/mL	Mouse (monoclonal)	Sigma-Aldrich	MABN1818

2.3.8 COMPUTATIONAL CHARACTERISATION OF GCASE-LIMP2 INTERACTIONS

To generate GCase-LIMP2 structural complexes, protein-protein docking was performed using HADDOCK v2.4 (Dominguez et al., 2003, Honorato et al., 2024). The inputs for the docking runs were AlphaFold2's computationally predicted structures of human GCase (AF-P04062), mouse GCase (AF-P17439), human LIMP2 (AF-Q14108) and mouse LIMP2 (AF-O35114) (Jumper et al., 2021, Varadi et al., 2024) (**Fig. 2.3 A, C-E**). These structures have low Prediction Aligned Error (PAE) scores and high predicted local distance difference test (pLDDT) scores, which indicates that AlphaFold is highly confident that the predicted structures accurately resemble the true protein structure (Guo et al., 2022). Notably, experimental structures for human, but not mouse, GCase and LIMP2 have previously been reported (Dvir et al., 2003, Neculai et al., 2013). The human L444P GCase structure used for HADDOCK docking was kindly generated by Dr Georgina Menzies (Cardiff University) by replacing the leucine residue with a proline residue at position 444 of the human GCase structure (AF-P04062) (**Fig. 2.3 B**).

HADDOCK docks proteins in three stages: rigid-body energy minimization, semi-flexible simulated annealing and flexible final refinement (Dominguez et al., 2003). The amino acids on human GCase and LIMP2 that have been experimentally determined to be involved in GCase-LIMP2 binding were defined as "active residues" in the input parameters for the docking runs (Liou et al., 2014, Reczek et al., 2007, Zunke et al., 2016) (**Fig. 2.3-2.4**). The active residues on the mouse proteins were defined as those that aligned to the active residues on their respective human proteins following sequence alignment with Clustal Omega (Sievers et al., 2011) (**Fig. 2.4**). Other docking parameters were kept at their default values.

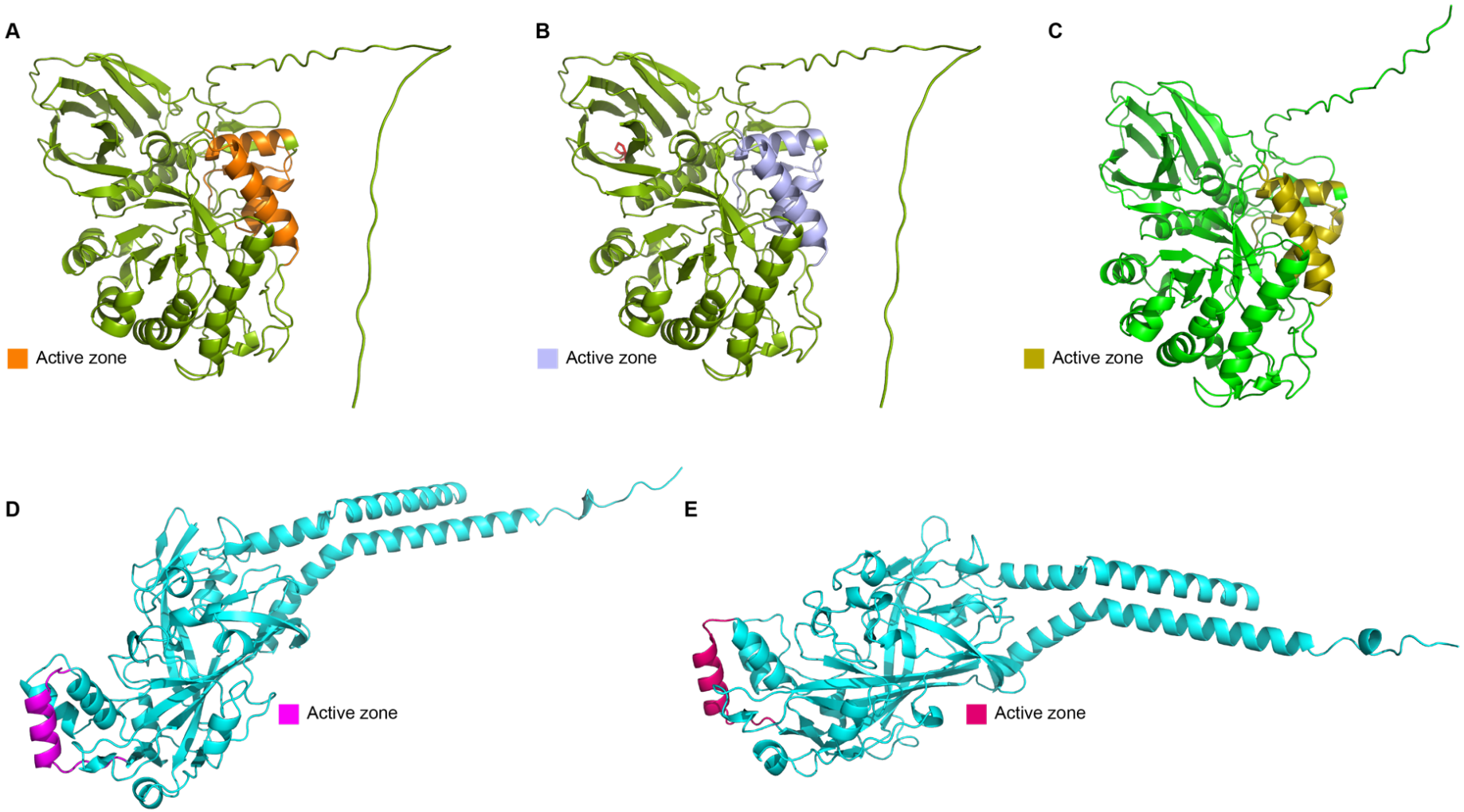


Figure 2.3: The computationally predicted structures of proteins used as inputs for HADDOCK docking. (**A**) Human WT GCase; (**B**) human L444P GCase, the mutated residue is indicated in red; (**C**) mouse WT GCase; (**D**) human LIMP2; (**E**) mouse LIMP2. The "active zone" refers to the residues that were previously found to be implicated in GCase-LIMP2 binding.

To note, the amino acid reference sequence for human GCase used for protein-protein docking (excerpts on **Fig. 2.4**) includes the protein's 39-residue signal peptide (Sorge et al., 1987). For example, residue L444 on WT GCase is labelled as L483 on this reference sequence. I therefore refer to individual human GCase amino acids on my computationally docked structures (**Sections 3.2.6** and **3.3.6**) according to their position on this reference sequence; I did not employ the traditional nomenclature for numbering human GCase residues that is used elsewhere throughout this thesis.

The binding affinity of the complexes docked by HADDOCK was predicted using the PRODIGY (Vangone and Bonvin, 2017, Vangone and Bonvin, 2015) and RING web servers (Clementel et al., 2022, Martin et al., 2011). PRODIGY predicts binding affinity with an algorithm that accounts for the number of interatomic contacts between chains and the properties of the non-interacting surface (Vangone and Bonvin, 2015). RING represents protein structures as residue interacting networks to calculate various types of non-covalent interactions within the complex (Piovesan et al., 2016). The inputs for the PRODIGY and RING analyses were the docked GCase-LIMP2 complexes generated by HADDOCK. Other analysis parameters were kept at their default values.

The structures of the GCase-LIMP2 complexes and the polar contacts formed between interacting residues were visualised using PyMOL (The PyMOL Molecular Graphics System, Schrödinger). The bond length cut-off for strong polar contacts was set at 3.8 Å, and weaker polar contacts had a defined bond length of 3.8-4.2 Å.

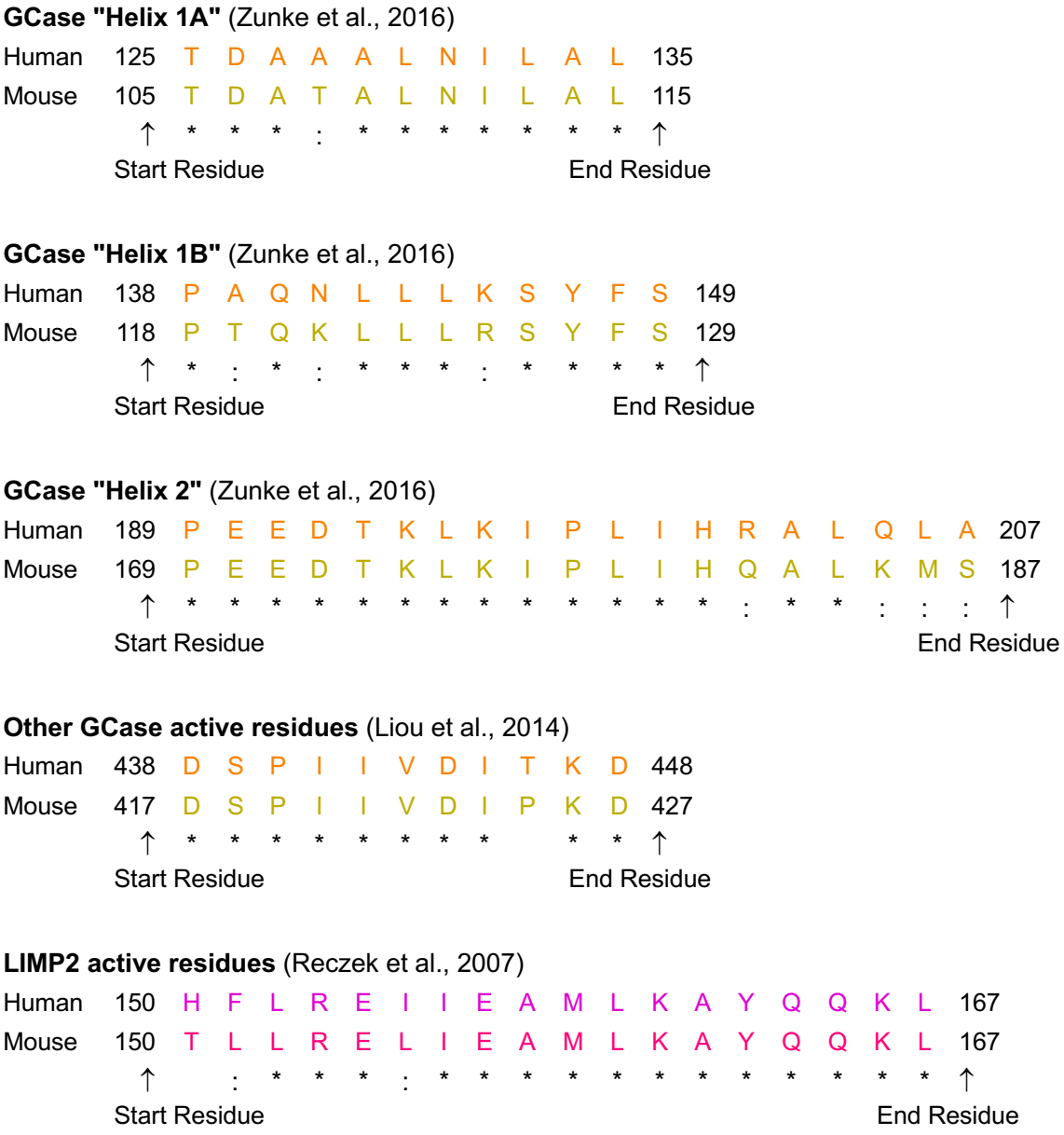


Figure 2.4: Cross-species sequence alignment of residues on GCase and LIMP2 that previous studies have determined as important for mediating the GCase-LIMP2 interaction. These amino acid sequences were classed as "active residues" for protein-protein docking with HADDOCK. The reference sequence for human GCase includes the protein's 39-amino acid signal peptide. Therefore, the nomenclature for the position of individual residues on human GCase in my docked structures incorporates this signal peptide. The symbols represent the degree of conservation between residue pairs assigned by Clustal Omega: * = Fully conserved residues; : = Partially conserved residues (residues share strongly similar properties equivalent to a Gonnet PAM 250 matrix score > 0.5); No symbol: Non-conserved residues.

2.4 METHODS PERTAINING TO CHAPTER 4

2.4.1 VOLTAMMETRIC DETECTION OF STRIATAL DA DYNAMICS IN *EX VIVO* SLICES

2.4.1.1 Microelectrode fabrication

Carbon-fibre microelectrodes (CFMs) were used to detect DA release during fast-scan cyclic voltammetry (FCV) experiments. An epoxy-free carbon-fibre (diameter: 7 μm, Goodfellow Cambridge Ltd.) was threaded through a borosilicate glass capillary tube (outside diameter: 2 mm, inside diameter: 1.16 mm, Harvard Apparatus), submerged in acetone. Residual acetone was subsequently removed by tapping one end of the capillary tube on tissue paper. Next, the capillary tube with the inserted carbon-fibre was pulled using a PE-2 vertical glass microelectrode puller (Narishige) at a high heat setting (approximately 6.7). High temperatures allow a tight seal to form around the carbon-fibre, which heightens the signal to noise ratio for DA detection. The exposed tip of carbon-fibre was cut 50-100 μm from the seal under a microscope at 100X magnification (Laborlux D, Leitz). CFMs with an exposed tip length of 50-100 μm offer optimal sensitivity for DA detection within our experimental setup. Next, both ends of a core from a data cable were stripped and the copper wires at one end were clipped to leave one wire remaining. This copper wire (diameter: 100 μm) was dipped in silver conductive lacquer (RS components) and inserted into the open end of the capillary tube. The core was fixed to the capillary tube with cyanoacrylate glue once the copper wire made contact with the carbon-fibre. Each CFM was used across experiments in a single day only as CFM sensitivity and kinetics are altered by repeated exposure to tissue.

2.4.1.2 Acute slice preparation

On the day of FCV recording, the mouse was euthanised by cervical dislocation (confirmation of death by exsanguination) and decapitated. Its brain was extracted and immediately immersed in ice-cold, HEPES-buffered cutting solution (**Table 2.13 A**),

saturated with 95% O_2/ 5% CO_2. Acute 300 μm coronal sections containing caudate putamen (CPu) and nucleus accumbens (NAc), 1.4-0.2 mm anterior of bregma, were prepared using a VT1200 S vibratome (Leica). Slices were subsequently transferred to a holding chamber filled with oxygenated cutting solution at room temperature and allowed to recover for a minimum of 60 min prior to recording.

Table 2.13: Composition of solutions used for acute slice preparation and FCV recordings.

(A) HEPES-buffered cutting solution		**(B) aCSF recording solution**	
Reagent	**Final Concentration**	**Reagent**	**Final Concentration**
NaCl	120 mM	NaCl	124 mM
KCl	5 mM	KCl	3.8 mM
$NaHCO_3$	20 mM	$NaHCO_3$	26 mM
HEPES acid	6.7 mM	$MgSO_4(7H_2O)$	1.3 mM
HEPES salt	3.3 mM	KH_2PO_4	1.2 mM
$MgSO_4(7H_2O)$	2 mM	Glucose	10 mM
KH_2PO_4	1.25 mM	$CaCl_2(2H_2O)$	2.4 mM
Glucose	10 mM		
$CaCl_2$	2 mM		

2.4.1.3 FCV recordings

FCV, in conjunction with CFMs, can measure changes to the concentration of extracellular DA ($[DA]_o$) with sub-second temporal resolution at distinct sites in *ex vivo* striatal sections (John and Jones, 2007, Venton and Cao, 2020).

In the recording chamber, hemisected slices were superfused with oxygenated artificial cerebrospinal fluid (aCSF) (**Table 2.13 B**), flowing at 2.25 mL/min (MINIPULS 3, Gilson) and maintained between 31-33°C. Each slice was allowed to acclimatize to the recording chamber conditions for at least 20 min before starting the experiment. CFMs were charged for 45-60 min at the start of the day by inserting the tip 100 μm deep into a part of the slice that would not be recorded from e.g. the cortex. Once charged, the CFM was positioned at

the recording site, either in the dorsolateral quadrant of the striatum (DLS) or NAc core (NAcC), and re-inserted 100 μm deep into the tissue (representative recording sites on the inset of **Fig. 4.3**). The full signal gain was adjusted to allow a 5 V working range and was changed as needed during the experiment to prevent saturation of the signal. Only CFMs with a starting full signal gain between 3-10 nA/mV were used for experiments. The opposite end of the CFM was connected to a Millar voltameter (Julian Millar, Barts and the London School of Medicine and Dentistry). The voltammeter passed a biphasic triangular voltage waveform across the CFM from -0.7 to +1.3 V relative to an Ag/AgCl reference electrode (World Precision Instruments), at a scan rate of 800 V/s and a sampling frequency of 8 Hz. The CFM was switched out of circuit between scans. The background signal was subtracted by the voltammeter and the resultant current was digitized using a Digidata 1440A (Molecular Devices). A TDS 1001B oscilloscope (Tektronix) enabled real-time visualisation of signals during experiments.

To evoke DA release, electrical pulses (amplitude: 0.65 mA, width: 200 μs) were generated using a DS3 Isolated Current Stimulator (Digitimer). These electrical stimuli were delivered at 2.5 min intervals during experiments via a concentric bipolar Pt/Ir electrode (diameter 25 μm, FHC). This electrode was positioned lightly touching the surface of the slice, approximately 100 μm from the CFM. Stimuli were delivered out of phase with the FCV scans and the number and frequency of electrical pulses was manually adjusted according to the experiment. In **Section 4.2.5**, high-frequency electrical stimulation trains (5 pulses delivered at 100 Hz) and related evoked $[DA]_o$ are referred to as “phasic” stimulations and “phasic” DA release, respectively.

For FCV recordings in **Sections 4.2.3-4.2.5**, DA dynamics were manipulated via wash-on of various drugs (**Table 2.14**). Working solutions of these compounds were prepared in oxygenated aCSF immediately prior to application.

Once all recordings were completed on an experimental day, the CFM was calibrated with 2 μM DA (final concentration) in aCSF, prepared from a stock solution of 2.5 mM DA in 0.1 M $HClO_4$. Experimental signals were confirmed as DA because oxidation and reduction peaks on the recording voltammograms were consistent with the characteristic peak oxidation and reduction potentials of DA (+0.5-0.6 V and -0.2 V, respectively) (**Fig. 4.3**, *inset*). On each voltammogram, the current at the peak oxidation potential was measured from baseline and used to plot fluctuations in $[DA]_o$ over time. Data was acquired using Axoscope, version 11 (Molecular Devices) and analysed using Microsoft Excel macros, written in-house.

Table 2.14: Details of drugs used in FCV wash-on experiments.

Drug	Mechanism of action	Final concentration	Supplier
DHβE	nAChR antagonist	1 μM	Tocris Bioscience
Cocaine	DAT inhibitor	5 μM	Sigma-Aldrich
Quinpirole	D_2R agonist	44 nM and 1 μM	Tocris Bioscience
Bicuculine	$GABA_AR$ antagonist	10 μM	Abcam
CGP 55845	$GABA_BR$ antagonist	4 μM	Abcam

Abbreviations: DHβE = dihydro-β-erythroidine hydrobromide, nAChR = nicotinic acetylcholine receptor, DAT = dopamine transporter, D_2R = dopamine D_2 receptor, $GABA_AR$ = $GABA_A$ receptor, $GABA_BR$ = $GABA_B$ receptor.

2.4.2 IMMUNOFLUORESCENCE OF PARAFFIN-EMBEDDED STRIATAL SECTIONS

2.4.2.1 Tissue fixation via transcardiac perfusion of PFA

Transcardiac perfusions were performed by Dr Natalie Connor-Robson and Ms Milena Cioroch. Mice were sacrificed via intraperitoneal injection of a terminal dose of anaesthetic

(pentobarbitone). When the mouse had lost its tail-pinch, pedal and blink reflexes, its beating heart was exposed. The left ventricle was pierced with a butterfly needle connected to a syringe containing 1X PBS and the right atrium was cut. PBS was manually circulated to flush the blood out of the mouse's system; administration was terminated once the discharged fluid ran clear. Keeping the butterfly needle in the same position, approximately 30 mL of 4% PFA in PBS was steadily perfused through the mouse's system. Afterwards, the brain was extracted and post-fixed in approximately 20 mL of 4% PFA for 24 hours at 4°C. Samples were then transferred to PBS-azide for longer-term storage at 4°C.

2.4.2.2 Paraffin embedding and sectioning

Samples were embedded and sectioned by Dr Natalie Connor-Robson. Briefly, fixed brains underwent consecutive 10 min incubations in 95% EtOH, 100% EtOH twice and Histoclear thrice. Subsequently, brains were embedded by incubating three times in Paraplast for 60 min each, using a HistoStar Embedding workstation (Thermo Scientific). Next, 8 μm coronal sections were prepared from paraffin-embedded brains with a manual rotary microtome (Microm HM 325, Thermo Scientific).

2.4.2.3 Tissue staining and imaging

Sections were rehydrated via sequential 10 min incubations in xylene, 100% EtOH, 95% EtOH and finally 70% EtOH. Residual EtOH was removed by immersion in dH_2O for 5 min. Sections were next incubated in 10% H_2O_2 (VWR) for 5 min to inhibit endogenous peroxidase activity and re-washed with dH_2O. Afterwards, heat-mediated antigen retrieval was performed in 1X citrate buffer pH 6.0 (Abcam). Samples were heated by microwaving once for 5 min and subsequently three times for 1.5 min each. Samples were left to stand at room temperature for 4 min between microwave heating and were cooled on ice after the last heating step.

A hydrophobic barrier was created around sections with a PAP pen (ImmEdge, Vector Laboratories). Samples were then blocked for 60 min at room temperature using 10% donkey serum in 1X PBS with Tween 20 (final concentration: 0.4%) (PBS-T). This was followed by an overnight incubation at 4°C in primary antibodies, diluted in blocking solution (**Table 2.15**). Secondary-only control samples received an overnight incubation in blocking solution instead of primary antibodies. The next day, samples were washed three times in PBS-T and incubated in the appropriate Alexa Fluor-conjugated secondary antibodies (Invitrogen), diluted 1:1000 in PBS-T, for 60 min at room temperature. Samples were kept protected from light subsequent to application of secondary antibodies. After three more washes in PBS-T, sections were mounted with FluorSave (Millipore). Three images of dorsolateral striatum were captured in each section using a FluoView FV1000 confocal microscope (Olympus). The area of fluorescent stain on auto-thresholded images was analysed using Fiji (Schindelin et al., 2012) with locally-written custom macros.

Table 2.15: Primary antibodies used for immunofluorescence in tissue.

Antibody	Dilution	Species raised (class)	Supplier	Catalogue #
TH	1:250	Sheep (polyclonal)	Sigma-Aldrich	AB1542
DAT	1:250	Rabbit (monoclonal*)	Abcam	ab184451
D_2R	1:500	Rabbit (polyclonal)	Sigma-Aldrich	AB5084P

Abbreviations: TH = tyrosine hydroxylase, DAT = dopamine transporter, D_2R = dopamine D_2 receptor. * antibody made using recombinant technology.

2.4.3 HPLC WITH ELECTROCHEMICAL DETECTION

High-performance liquid chromatography (HPLC) was coupled to an electrochemical detector to measure the concentration of DA and 3,4-dihydroxyphenylacetic acid (DOPAC) in the striatum. Tissue punches were taken from the CPu (diameter: 2 mm) and NAc (diameter: 1.2 mm) of 300 μm coronal sections and submerged in 0.1 M $HClO_4$. Typically, four punches from each region were taken per mouse and two punches from the same region were combined in 200 μL of $HClO_4$. Samples were snap frozen in dry ice and stored at –80°C until required.

On the assay day, samples were defrosted on ice, sonicated at 25 kHz for 20 s and centrifuged at 14000 rcf for 15 min at 4°C. Next, standard solutions of DA (Suppelco) and DOPAC (Sigma-Aldrich) were individually prepared to a final working concentration of 100 nM each in 0.1 M $HClO_4$. These standards and the supernatant of centrifuged samples were subsequently transferred to glass vials (Jaytee Biosciences) (**Table 2.16**) and loaded into an AS2057 plus autosampler (JASCO). The autosampler injected samples interspersed with standards, one at a time, into a stream of filtered mobile phase at pH 4.5-4.6 (**Table 2.17**), which was pumped through the system at 1 mL/min (PU-2080 plus, JASCO). Compounds were separated across a column (Microsorb 100 - 5 C18, S150 x 4.6, Agilent) and detected using a DECADE II SDC detector (Antec Scientific). The detector was fitted with a glassy carbon working electrode set at +0.7 V relative to an Ag/AgCl reference electrode. Chromatograms were analysed using Clarity (DataApex) by comparing the height of the peaks produced by samples with those produced by corresponding standards. Prior to each run, I confirmed that the system and $HClO_4$ were not contaminated with analytes because no peaks were evident on chromatograms of 0.1 M $HClO_4$.

Table 2.16: Parameters for loading standards and samples for HPLC experiments.

Run	Sample Dilution	Volume in vial	Volume injected
CPu DA	1:10 in 0.1 M $HClO_4$	100 µL	50 µL
CPu DOPAC	Ran Neat	130 µL	100 µL
NAc DA & DOPAC	Ran Neat	130 µL	100 µL

Table 2.17: Recipe for mobile phase used for HPLC.

Reagent	Final Concentration
MeOH (HPLC grade)	13%
NaH_2PO_4	120 mM
EDTA	0.8 mM
OSA	0.5 mM

2.5 METHODS PERTAINING TO CHAPTER 5

2.5.1 LOCOMOTION IN THE OPEN FIELD

Spontaneous locomotor activity (LMA) in the open field was assessed using the Photobeam Activity System-Home Cage (PAS-HC) (SD instruments). Each testing station comprises an acrylic container with wood chippings spread across the floor, surrounded by a 4 x 8 photobeam frame. The apparatus tracks ambulation by recording photobeam breaks made as the mouse freely moves around the arena. Beam disruptions were automatically recorded and collated into 15 min intervals during the trial, starting from when the mouse was placed into the container. Each mouse was assessed in one trial only and up to 12 mice could be tested simultaneously using 12 separate stations. All trials started at 09:00 and lasted for 4 hours. Food and water were not available for the duration of the trial. To minimise noise disruption during the trial, an "Experiment in progress" sign was placed on the testing room door and no experimenter was present in the room.

2.5.2 ACCELERATING ROTAROD

Coordination and balance were assessed using an ENV-577M rotarod (Med Associates). Firstly, mice were placed on the rotarod facing opposite to the direction of rotation and were allowed to settle on the stationary rod for 1-2 min before acceleration was started. The rotarod subsequently accelerated from 2.5-25 rpm over the 5 min trial. The time that mice were able to stay on the rotarod before falling, i.e. their latency to fall, was used as an indicator of coordination and balance. This was automatically recorded by the apparatus via disruption of a photobeam underneath the rod when a mouse fell. All mice were tested in three trials per day across five consecutive days and 3-5 mice were tested simultaneously in each trial. Days 1-3 were classed as training days. Latency to fall was averaged across trials on days 4-5 and used for genotype comparison.

2.5.3 VERTICAL POLE TEST

The vertical pole test, first described by Ogawa et al. (1985), was used to examine coordination and bradykinesia. A 60 cm wooden pole was wrapped in bandage gauze and fixed standing upright in the centre of a cage akin to the mouse's home cage. The base of the apparatus was concealed by wood chippings to mimic a familiar environment. The mouse was positioned within approximately 5 cm from the top of the pole, with its head facing upwards toward the ceiling. The time taken for the mouse to rotate its body to point downwards (complete a T-turn) and to subsequently walk down the pole was recorded. The "total descent" time was the sum of the "T-turn" time and "walk-down" time. Mice underwent three trials per day across three consecutive days. Mice were acclimatized to the apparatus on trials across days 1-2 and performance on day 3 was used for genotype comparison. Trials on day 3 were excluded from the analysis if the mouse climbed over the top of the pole rather than completing a T-turn or if the total descent time was longer than 20 s. One mouse (L444P) was excluded based on this criteria.

2.5.4 INVERTED SCREEN TEST

Mice's grip strength was assessed using Kondziella's inverted screen test (Kondziella, 1964) with an 1849 cm^2 wire-mesh square grid. As described by Deacon (2013b), the screen was surrounded by a 4 cm thick wooden frame to prevent the mouse from climbing over the side and individual squares of the grid (1.44 cm^2) were made from 1 mm diameter wire. The mouse was first placed standing upright in the centre of the grid. The screen was subsequently inverted over a soft surface, which forced the mouse to cling to the underside. The time at which the mouse fell from the grid was recorded. The trial was terminated at 60 s if the mouse was still holding on to the grid; therefore, 60 s was the maximum score. Each mouse was tested in one trial only.

2.5.5 THE CATWALK XT GAIT ANALYSIS SYSTEM

The CatWalk XT gait analysis system automatically records various gait parameters (**Table 5.3**) in real-time as the mouse voluntarily transverses a 130 cm glass walkway (Garrick et al., 2021). The mouse's pawprints are captured using a high speed camera via the reflection of a green light-emitting diode (LED) at contact points with the walkway. The ceiling of the apparatus is illuminated with a red LED, which provides a backlight to contour the mouse's body. Lights in the testing room were switched off during data acquisition to enhance visualisation and to minimise stress on the mice. The walkway was calibrated at the start of each testing session and was wiped clean between mice. The CatWalk XT software classed runs as compliant if they lasted between 0.5-5 s and if the maximum variation in speed was less than 35%. For each mouse, gait parameters were averaged for analysis across a maximum of five compliant runs.

2.5.6 STOOL COLLECTION

Stool production was characterised as an indicator of mice's GI function. Mice were held separately in clean, dry acrylic containers for the trial and did not have access to food or water. During the trial, stool pellets were collected into individual Eppendorf tubes (one tube per mouse) and the number of pellets that each mouse produced was recorded. Faecal samples were weighed at the end of the trial, "wet weight". The stool was then dried at 65°C overnight and re-weighed the next morning, "dry weight". The % water content of the stool was calculated by: (wet weight – dry weight) / wet weight *100. All trials started at 16:00 and lasted for 60 min. Each mouse was assessed in one trial only.

2.5.7 THE T-MAZE ASSESSMENT OF SPONTANEOUS ALTERNATION BEHAVIOUR

Mice's spatial working memory was assessed by measuring spontaneous alternations in the T-maze. This test takes advantage of mice's natural inclination to explore new environments; therefore, a mouse with normal spatial working memory will tend to alternate their choice of goal arm, i.e. make a spontaneous alternation, upon re-exposure to the maze (d'Isa et al., 2021). The apparatus consists of a start arm and two opposite facing goal arms, configured in the shape of the letter T. The dimensions of the T-maze used in this thesis were previously described by Deacon and Rawlins (2006). At the start of each trial, the mouse was placed at the base of the start arm and allowed to move into either goal arm. Once the mouse's four paws had entered one of the goal arms, a sliding door was lowered to confine it in its chosen arm. The mouse was returned to the starting area after 30 s, while the sliding door was simultaneously raised. The mouse was then free to make a second choice of goal arm. A spontaneous alternation was recorded if the mouse entered the opposite goal arm on its second choice. The mouse was immediately removed from the maze after making its second choice of goal arm and was left to rest for 1-2 min before a second trial was conducted.

Mice underwent two trials per day over five consecutive days. However, only trials across days 1-3 were used for analysis of spontaneous alternation due to a decline in participation across days (**Fig. 5.9 A**). Trials were excluded from the analysis if the mouse failed to move into a goal arm within 120 s on either their first or second choice. Mice that completed less than five trials in total across days 1-3 were excluded (n = 6).

2.5.8 THE ELEVATED PLUS MAZE

The elevated plus maze (EPM) examines anxiety-like behaviour in mice using an approach-avoidant paradigm, based on mice's innate tendency to explore enclosed spaces over open spaces (Handley and Mithani, 1984, Montgomery, 1955, Pellow et al., 1985). This maze

consists of two “open arms”, arranged perpendicularly to two “closed arms”, in the shape of a plus sign. The EPM used for this thesis has arms measuring 35 x 6 cm that are elevated 70 cm above the floor. The closed arms are surrounded by a 20 cm wall, while the open arms are exposed to the surroundings. The mouse was placed at the intersection of the arms, facing toward the open arm that was opposite to the experimenter. It was then free to explore the maze undisturbed for the 5 min trial. The total number of entries into all arms (open and closed) and the time spent in the open arms was recorded. Each mouse was assessed in one trial only. One mouse (hWT) was excluded from the analysis because the complete video recording of this mouse’s run was not captured due to technical issues with the camcorder.

2.6 STATISTICAL ANALYSIS

Data was analysed using GraphPad Prism 10 (GraphPad Software). Firstly, normality was assessed using a Shapiro-Wilk test to determine whether parametric or non-parametric analysis methods should subsequently be used to assess differences between experimental groups. For data provided by collaborators (**Sections 3.2.4-3.2.5**), the ROUT method was used to detect outliers at Q = 0.1% before running statistical analysis and exclusions are detailed in the relevant figure legends. For experiments comparing two groups only, parametric data was analysed using either a two-tailed unpaired t-test or a two-tailed paired t-test, depending on the nature of the data. For experiments involving three or more experimental groups, parametric data was analysed with either a one-way analysis of variance (ANOVA), two-way ANOVA, two-way repeated measures ANOVA or a mixed-effects analysis. Non-parametric data was analysed using a Wilcoxon matched-pairs signed rank test when comparing two experimental groups and a Kruskal-Wallis test for comparisons across more than two groups. A Tukey’s or Dunn’s post-hoc test were only conducted if any significant effects were identified in the preceding ANOVA or Kruskal-Wallis test, respectively. Both the Tukey’s and Dunn’s post-hoc tests correct for multiple

comparisons by controlling the type I error rate for the family of comparisons. The GraphPad Prism software also calculates a multiplicity adjusted p-value for each comparison at a significance threshold of 0.05 when performing these tests (Motulsky, 2025). Spearman's correlation analysis was conducted on some datasets to investigate relationships between two continuous variables. This was followed by an analysis of covariance (ANCOVA) to assess if these relationships significantly differed across genotypes. Data is presented as the mean ± the standard error of the mean (SEM), unless stated otherwise in the figure legend. Significance was determined at $p < 0.05$ for all statistical tests. Sample sizes for experiments were chosen based on previous transgenic mouse characterisations conducted by our lab (Hunn et al., 2019, Janezic et al., 2013, Sloan et al., 2016). The experimental unit, "n", is one mouse for most experiments with some exceptions, which are clearly reported in the relevant figure legends. In the drug wash-on FCV experiments (**Fig. 4.6-4.8, 4.10-4.11, 4.13-4.15**) $[DA]_o$ was measured from a single recording site in each slice before and during drug application. In this design, each slice is treated as one experimental unit. We consider that individual slices meet the three criteria for genuine replication set out by Lazic et al. (2018): each slice can be randomly and independently assigned to a drug treatment intervention, drug treatments can be independently applied to individual slices without affecting other slices and the recordings in one slice do not influence the recordings in any other slice. Slices were used from a minimum of 4 mice per genotype in these experiments, as stated in the corresponding figure legends. In the multisite FCV experiments (**Fig. 4.1 and 4.3**), $[DA]_o$ is recorded from multiple sites in each slice and the recording site is regarded as the experimental unit. A minimum of two slices in each mouse across five mice per genotype were used for these experiments. Sampling across multiple sites in each slice from different mice reflects biological variability because, in our experience, the variation observed in $[DA]_o$ within a given slice is largely equivalent to the variation in $[DA]_o$ observed across

slices. We therefore consider each recording site to be an independent unit and this approach allows us to capture the variability in DA release across the striatum. Previous multisite FCV experiments that characterised DA release in other transgenic rodent models developed by our lab also treated the recording site as the experimental unit (Janezic et al., 2013, Taylor et al., 2014). Data was collected blind to genotype in **Sections 3.2.4, 3.2.5, 4.2.1** and for all behavioural tests in **Chapter 5**.

CHAPTER 3: ELUCIDATING GAIN-OF-FUNCTION AND LOSS-OF-FUNCTION EFFECTS OF THE L444P MUTATION

3.1 INTRODUCTION

Gain-of-function and loss-of-function effects of *GBA* mutations are intertwined in a pathological web in *GBA*-associated PD (**Fig. 1.3**) (Yoon et al., 2024). Briefly, the ER-retention of mutant, misfolded GCase confers a gain-of-function effect by triggering ER stress and UPR activation (**Section 1.3.3.2**), whereas loss of GCase activity has been associated with deficits in the lysosomal-autophagy pathway and may induce glycosphingolipid accumulation (**Section 1.3.3.1**). Prior to the start of this DPhil, Dr Natalie Connor-Robson illustrated that our L444P BAC transgenic model recapitulates gain- and loss-of-function effects of the L444P mutation in the midbrain (**Fig. 3.1**).

She first demonstrated that high molecular weight (MW) human GCase accumulates in the midbrain of our L444P model from 3-months-old (**Fig. 3.1 A**). This high MW form of GCase was sensitive to cleavage by endoglycosidase-H (Endo-H), as shown by the downward shift in the position of the band on a western blot in response to Endo-H treatment (**Fig. 3.1 B**). Endo-H selectively cleaves high-mannose N-linked glycan chains (Freeze and Kranz, 2010), which are primarily observed on immature forms of GCase soon-after synthesis in the ER (Erickson et al., 1985). Therefore, the predominance of Endo-H-sensitive GCase in the L444P midbrain indicates that immature mutant GCase is retained in the ER of these mice. Additionally, total human GCase levels were significantly reduced in the aged L444P midbrain (**Fig. 3.1 A**), which may demonstrate elevated proteolytic degradation of L444P GCase. These gain-of-function related effects were accompanied by a progressive,

age-related, loss of GCase activity in the L444P midbrain (**Fig. 3.1 C**). Building on these findings, this chapter explores if these gain- and loss-of-function hallmarks of *GBA*-associated PD pathology extend to the cortex of the L444P mice. I also sought to determine whether the GCase chaperone ambroxol can enhance GCase activity in primary cortical cultures from our L444P model. Ambroxol was chosen because its ability to restore GCase activity has been demonstrated in various preclinical models of *GBA*-associated PD and its potential as a disease-modifying therapy for PD is currently being investigated in clinical trials (**Section 1.3.4**).

Subsequent experiments aimed to investigate downstream pathological consequences related to both gain- and loss-of-function effects of the L444P mutation in our model. ER stress, autophagic deficits and lysosomal dysfunction have not been widely examined in existing mouse models of *GBA*-associated PD (**Table 1.3**). Therefore, the expression levels of BiP, LC3 and LAMP1 were measured in the cortex of 3-month-old mice. It also remains subject to debate whether the GCase activity deficit induced by heterozygous *GBA* mutations is sufficient to elevate GlcCer and GlcSph in PD patients (**Section 1.3.3.1**). Mouse models of *GBA*-associated PD have largely failed to demonstrate GlcCer accumulation, although some display significantly increased GlcSph levels (**Table 1.3**). Notably GlcChol levels were elevated in a mouse model of GD and in GD patient plasma (Marques et al., 2016); however, this lipid species has not been investigated in mice harbouring heterozygous *Gba* mutations. Considering the enigmatic role of glycolipid accumulation in *GBA*-associated PD, experiments this chapter set out to elucidate the relationship between GCase deficits and lipid dyshomeostasis in our L444P mice.

On the other hand, αS is widely recognized as a major protagonist in the pathology of *GBA*-associated PD (**Section 1.3.3.3**). Supporting this, Dr Connor-Robson demonstrated an increase in the mean levels of oligomeric αS in the SN of aged L444P and *Gba*$^{+/-}$ mice, using

the αS proximity ligation assay (αS-PLA) (**Fig. 3.1 D**) (Roberts et al., 2019). Although a significant effect of genotype on oligomeric αS levels was identified in 18-month-old mice using a Kruskal-Wallis test (Kruskal-Wallis statistic = 8.538, p = 0.0084), a Dunn's post-hoc test failed to detect significant pairwise differences. To the best of my knowledge, this is the first time that *in situ* endogenous αS oligomerisation has been investigated in a mouse model of *GBA*-associated PD. Considering that interactions between αS and lipid membranes promote αS oligomerisation and aggregation (Galvagnion et al., 2015, Lee et al., 2002), we may hypothesize that αS co-localisation with lipid membranes is elevated in our L444P and *Gba*$^{+/-}$ mice. However, the subcellular distribution of αS has not previously been explored in existing mouse models of *GBA*-associated PD. To probe this in our model, experiments in this chapter set out to quantify the proportion of soluble (cytosolic) and membrane-associated αS from sequential tissue fractions across brain regions.

Lastly, impaired lysosomal translocation of mutant GCase is another key feature of *GBA*-associated PD (Chatterjee and Krainc, 2023). The D409H mutation has previously been suggested to directly impede GCase delivery to the lysosome by weakening GCase's interaction with its transporter, LIMP2 (Dobert et al., 2025). In theory, L444P-mediated protein misfolding may also directly perturb L444P-GCase's association with LIMP2; however, this potential gain-of-function effect has not previously been investigated. Moreover, the association between murine GCase and LIMP2 has not previously been examined, despite increased efforts to characterise the mouse interactome in recent years (Zhang et al., 2022b). To further understand the nature of the GCase-LIMP2 interactions in our model, I sought to examine the L444P mutation's influence on GCase-LIMP2 binding and to explore the structure and affinity of the GCase-LIMP2 complexes formed by human and mouse proteins.

The specific aims of this chapter are:

1. To investigate whether gain- and loss-of-function related phenotypes of the L444P mutation are recapitulated in the cortex of our L444P mice.
2. To shed light on pathological mechanisms related to gain- and loss-of-function effects of the L444P mutation including:
    i) ER stress and dysfunction in the lysosomal-autophagy pathway.
    ii) Dyshomeostasis of lipid species that are related to GCase function.
    iii) Subcellular αS re-distribution.
3. To computationally predict and compare the conformation and affinity of the GCase-LIMP2 interaction across disease-states and species.

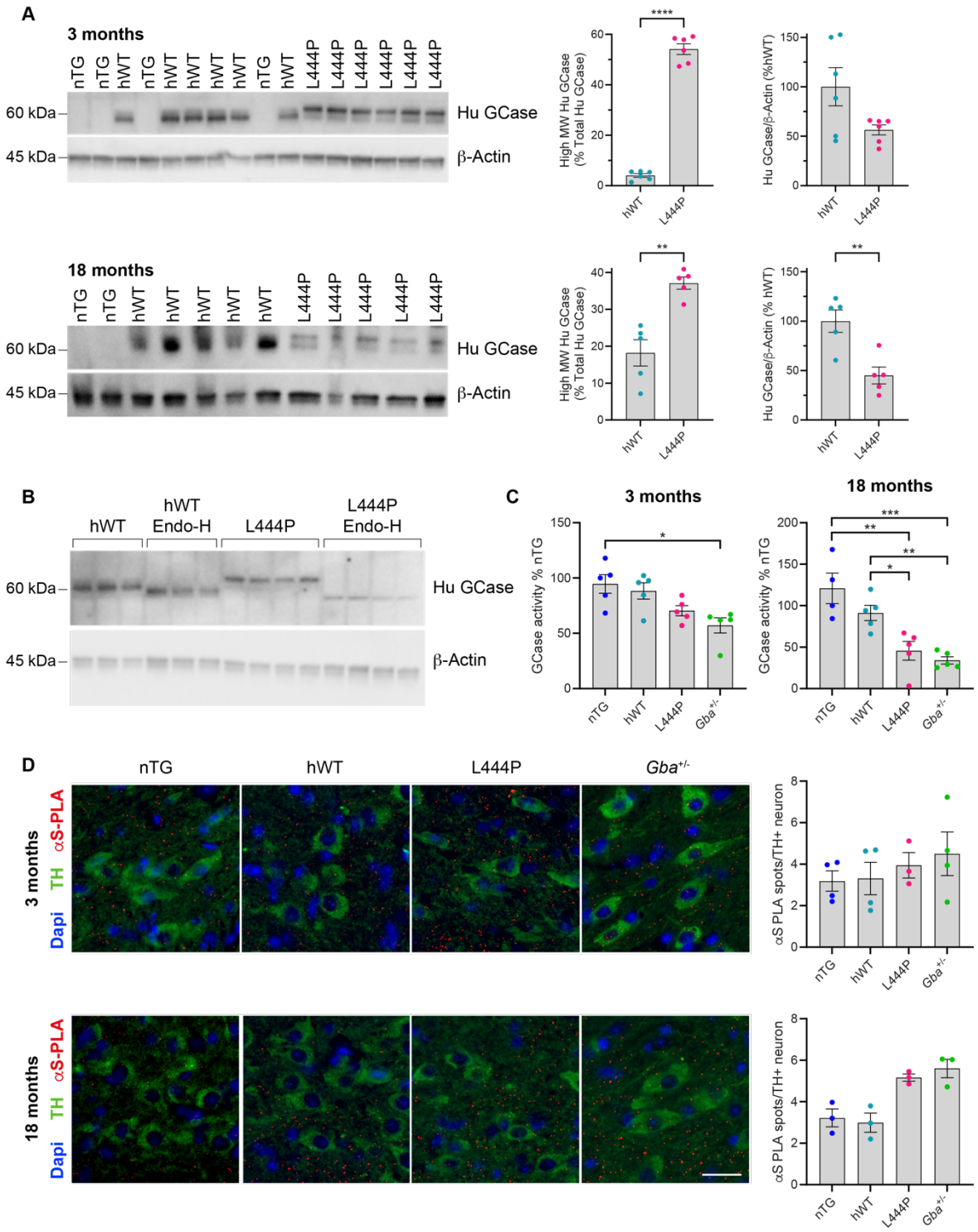


Figure 3.1: Characterisation of midbrain pathology in L444P mice. (**A**) *Left:* representative western blots for human GCase and β-Actin in midbrain homogenates from mice aged 3 and 18 months. *Right:* corresponding quantification of high MW human GCase (expressed as a percentage of the total human GCase present) and total human GCase normalised to β-Actin (expressed as a percentage of the mean total human GCase in hWT mice). (**B**) Representative western blot for human GCase and β-Actin in untreated and Endo-H-treated midbrain homogenates from 3-month-old mice. Endo-H sensitivity indicates that human L444P GCase possesses high-mannose oligosaccharides and is therefore retained in the ER. (**A-B**) MW = molecular weight, Hu = human. (**C**) Midbrain GCase activity is progressively lower with age in L444P mice. Data are expressed normalised to the

mean GCase activity of nTG mice at each age. (**D**) *Left:* representative immunohistochemical images of αS-PLA signal (red punctate spots) in TH+ neurons (green) of the SN from 3- and 18-month-old mice. Scale bar = 50 μm. *Right:* corresponding quantification of αS-PLA puncta count per TH+ neuron. 35 TH+ neurons per mouse were counted blind to genotype. (**A**) Two-tailed unpaired t-test: 3 months high MW $p < 0.0001$, 3 months total $p = 0.0527$, 18 months high MW $p = 0.0013$, 18 months total $p = 0.0048$. (**C**) Kruskal-Wallis test with Dunn's post-hoc test (3 months): Kruskal-Wallis statistic = 10.03 $p = 0.0183$, one-way ANOVA with Tukey's post-hoc test (18 months): $F_{(3,15)} = 12.68$ $p = 0.0002$. (**D**) one-way ANOVA (3 months): $F_{(3,11)} = 0.6289$ $p = 0.6114$, Kruskal-Wallis test with Dunn's post-hoc test (18 months): Kruskal-Wallis statistic = 8.538 $p = 0.0084$. * $p < 0.05$, ** $p < 0.01$, *** $p < 0.001$, **** $p < 0.0001$; n = 3-6 mice per genotype. Data are presented as mean ± SEM and each datapoint represents one mouse. Data collected and analysed by Dr Natalie Connor-Robson.

3.2 RESULTS

3.2.1 HUMAN GCASE EXPRESSION IN CORTICAL TISSUE

GBA mutations confer gain-of-function effects in PD via the ER-retention of immature, misfolded, mutant GCase, and consequential ER stress (**Section 1.3.3.2**) (Fernandes et al., 2016, Garcia-Sanz et al., 2017, Gegg et al., 2012, McNeill et al., 2014, Ron and Horowitz, 2005, Sanchez-Martinez et al., 2016). The predominance of high MW, Endo-H-sensitive human GCase in the midbrain of our L444P mice strongly indicates that mutant GCase is entrapped in the ER (**Fig. 3.1 A-B**).

Since GCase is ubiquitously expressed in the human brain (Uhlen et al., 2015, proteinatlas.org, 2024) and pre-existing mouse models that harbour L444P-GCase display disease-relevant phenotypes in various brain regions (Lado et al., 2024, Mahoney-Crane et al., 2023, Vidyadhara et al., 2025), I sought to examine whether this gain-of-function related effect extends to the cortex of our L444P mice. To do this, human GCase expression was measured in cortical tissue homogenates from 3-month-old mice (**Fig. 3.2**). Similar to observations in the midbrain (**Fig. 3.1 A-B**), two forms of human GCase with distinct MWs around 60 kDa were apparent on a western blot (**Fig. 3.2 A**). The proportion of high MW human GCase, relative to the total human GCase present, was significantly higher in L444P vs hWT mice (**Fig. 3.2 B(i)**). On average, this form accounted for 42% of the total GCase in L444P mice and only 5% of the total GCase in hWT mice. On the other hand, total expression levels of human GCase were similar across hWT and L444P mice (**Fig. 3.2 B(ii)**). In agreement with phenotypes in the midbrain, the accumulation of high MW GCase in the cortex of L444P mice (**Fig. 3.2 B(i)**) suggests that mutant misfolded GCase is retained in the ER. Therefore, this phenotype likely relates to a gain-of-function effect of the mutation.

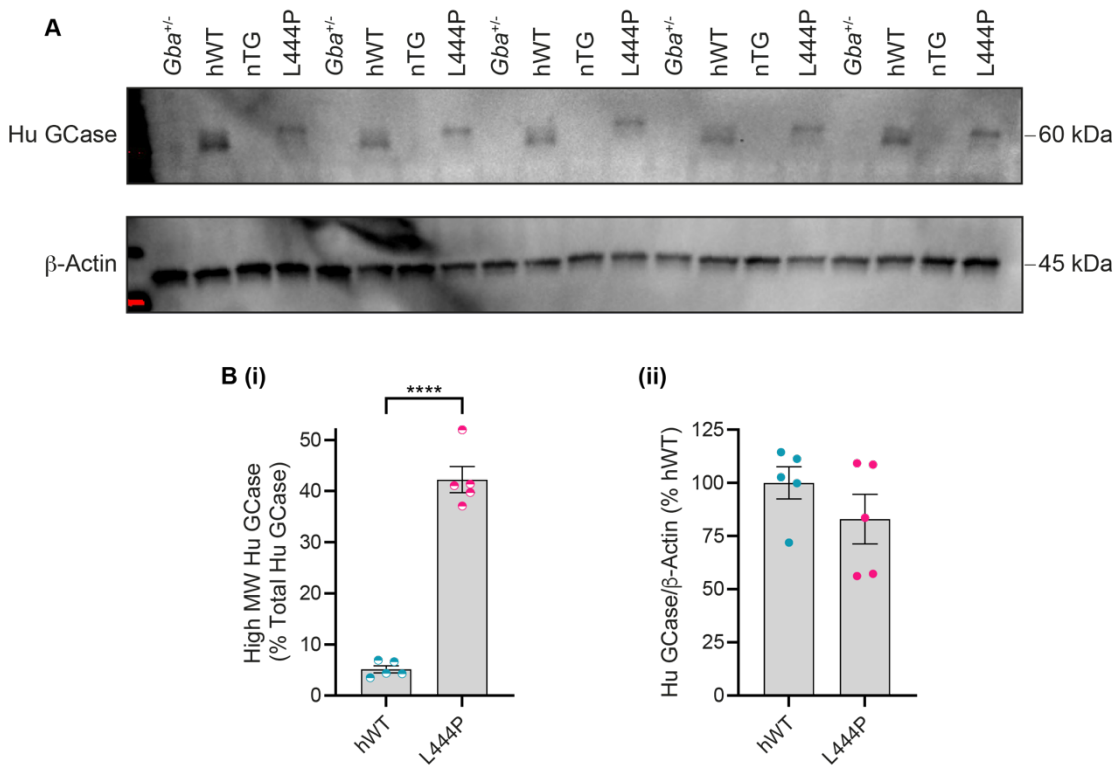


Figure 3.2: L444P mice have elevated high MW GCase, whereas total human GCase levels are comparable across hWT and L444P mice. (**A**) Representative western blots for human GCase and corresponding β-Actin from cortical homogenates of 3-month-old hWT and L444P mice. Human GCase is represented by two bands around 60 kDa on the blot. (**B(i)**) Quantification of high MW human GCase (upper band), expressed as a percentage of the total GCase per mouse (upper + lower bands). (**B(ii)**) Quantification of total human GCase normalised to its own β-Actin per mouse and expressed as a percentage of the mean total human GCase in hWT mice. MW = molecular weight, Hu = human. (**B(i-ii)**) Two-tailed unpaired t-test: (**i**) $p < 0.0001$, (**ii**) $p = 0.2545$; **** $p < 0.0001$; n = 5 mice per genotype. Data are presented as mean ± SEM and each datapoint represents one mouse.

3.2.2 GCase ACTIVITY IN PRIMARY CORTICAL CELL CULTURES AND TISSUE

Loss of GCase activity is another key pathological hallmark of *GBA* mutations in PD and has been widely demonstrated across cell and rodent models and in PD patient brains (**Section 1.3.3.1 and Table 1.3**) (Munoz et al., 2021). In line with this, our L444P mice have significantly reduced GCase activity in the midbrain at 18-months-old (**Fig. 3.1 C**). Having illustrated gain-of-function related effects of the L444P mutation in cortex tissue (**Fig. 3.2**), I sought to measure cortical GCase activity in cells and tissue from our mice and to determine if potential deficits could be rescued by the GCase chaperone, ambroxol.

Firstly, mixed primary cell cultures were established from the cortex of neonatal mouse pups up to PND 5 (**Fig. 3.3 A**). Cultures were treated with 10 µM of ambroxol or vehicle (DMSO) for 5 days and GCase activity was subsequently measured in cell lysates using a 4-MUG assay. GCase activity was significantly impaired in both vehicle- and ambroxol-treated cultures from L444P and *Gba*$^{+/-}$ mice (**Fig. 3.3 B**). Somewhat surprisingly, ambroxol only increased GCase activity in cultures from nTG mice; it had no significant effect on GCase activity in hWT, L444P or *Gba*$^{+/-}$ cortical cells. As ambroxol did not restore GCase activity in L444P cortical cultures, its potential therapeutic effect on other pathological phenotypes was not examined further in subsequent experiments.

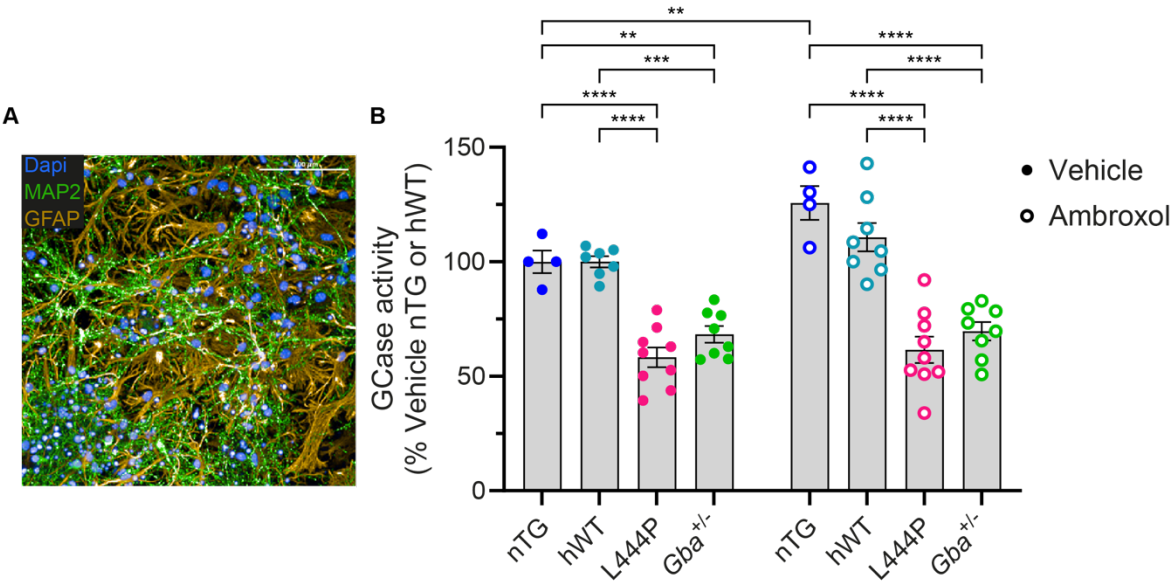


Figure 3.3: Primary cortical cultures from L444P and *Gba*$^{+/-}$ mice have impaired GCase activity, which is not rescued by ambroxol. (**A**) Representative immunocytochemical image of mixed primary cortical cultures, obtained from mice ≤ PND 5, co-stained with DAPI (nuclei), MAP2 (neurons) and GFAP (astrocytes). Scale bar = 100 µm. (**B**) GCase activity was measured in primary cortical cultures via 4-MUG hydrolysis following a 5-day treatment with 10 µM vehicle (DMSO) or 10 µM ambroxol. Individual assays were conducted on a culture-by-culture basis; data was normalised to the mean GCase activity of vehicle treated nTG or hWT cells within each assay before pooling assays for analysis. Two-way ANOVA with Tukey's post-hoc test: genotype $F_{(3,49)} = 51.57$ $p < 0.0001$, drug treatment $F_{(1,49)} = 7.715$ $p = 0.0077$, interaction $F_{(3,49)} = 1.764$ $p = 0.1663$; ** $p < 0.01$, *** $p < 0.001$, **** $p < 0.0001$ from Tukey's post-hoc test; n = 4-9 mice per genotype. Data are presented as mean ± SEM and each datapoint represents one mouse.

Following this, GCase activity was measured in cortical tissue homogenates from mice aged 3 and 15-21 months using the 4-MUG assay. The mean GCase activity was slightly reduced in cortex tissue from L444P and *Gba*$^{+/-}$ mice at both ages; however, this did not reach significance in either genotype (**Fig. 3.4**).

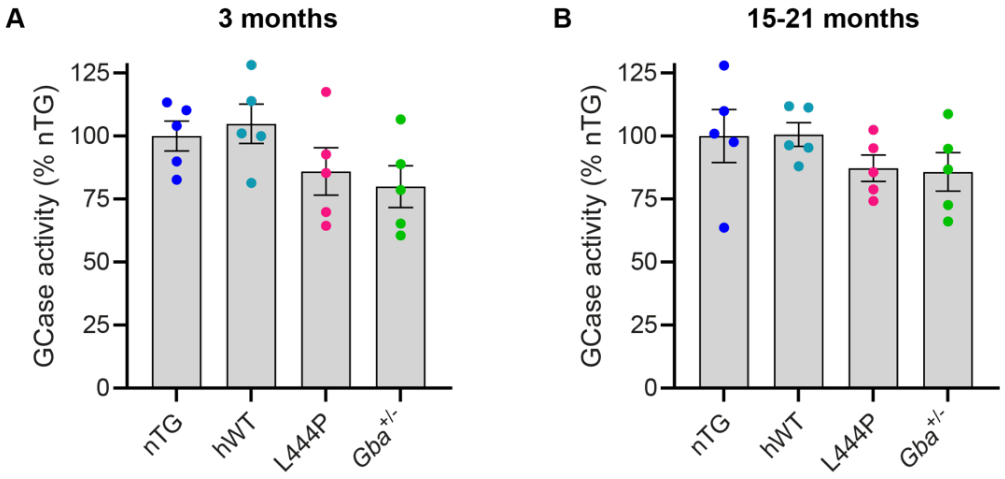


Figure 3.4: GCase activity in cortex tissue is not significantly different across genotypes. GCase activity was measured via 4-MUG hydrolysis in cortical tissue homogenates from mice aged 3 months (**A**) and 15-21 months (**B**). Data are expressed normalised to the mean GCase activity of nTG mice at each age point. (**A-B**) One-way ANOVA: all $F_{(3,16)} < 2.162$ and all $p > 0.1324$; n = 5 mice per genotype. Data are presented as mean ± SEM and each datapoint represents one mouse.

3.2.3 BiP, LAMP1 and LC3 expression in cortical tissue

As our L444P mice display an accumulation of high MW GCase in cortex tissue and a significant loss of GCase activity in primary cortical cultures, I sought to investigate if these gain- and loss-of-function effects were associated with ER stress or lysosomal/autophagic dysfunction in our model. To do this, the expression of BiP, LAMP1 and LC3 were probed on western blots using cortical tissue homogenates from mice aged 3-months-old.

Firstly, the levels of BiP, an ER chaperone with elevated expression in response to ER stress (Gething, 1999), was not different across genotypes (**Fig. 3.5**).

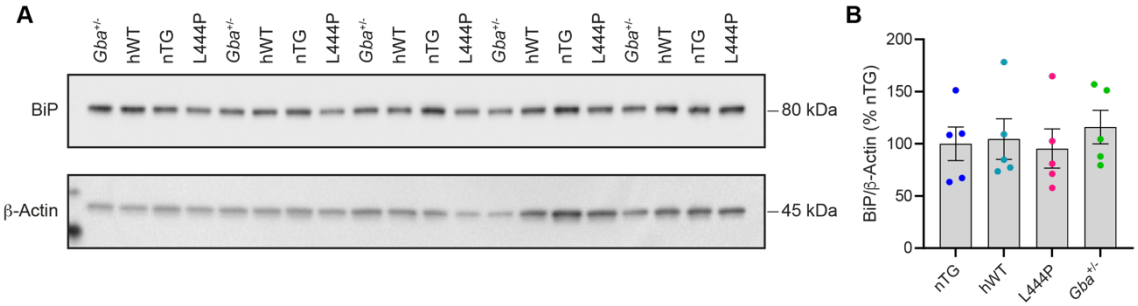


Figure 3.5: Cortical BiP levels are similar across genotypes. (**A**) Representative western blots for BiP and corresponding β-Actin from cortical tissue homogenates of mice aged 3 months. (**B**) Quantification of BiP normalised to its own β-Actin per mouse and expressed as a percentage of the mean BiP levels in nTG mice. One-way ANOVA: $F_{(3,16)} = 0.2492$ $p = 0.8607$; n = 5 mice per genotype. Data are presented as mean ± SEM and each datapoint represents one mouse.

Next, expression of the lysosomal membrane protein, LAMP1 (Schwake et al., 2013), was also comparable across genotypes (**Fig. 3.6 B(i)**). This indicates that the number of lysosomes is not grossly changed according to genotype. My western blots also did not detect autophagic deficits in the cortex of L444P mice; the expression of the autophagosomal marker, LC3-II (Tanida et al., 2008), (**Fig. 3.6 B(ii)**), and the ratio of LC3-II to its cytosolic precursor, LC3-I (**Fig. 3.6 B(iii)**), were similar across genotypes.

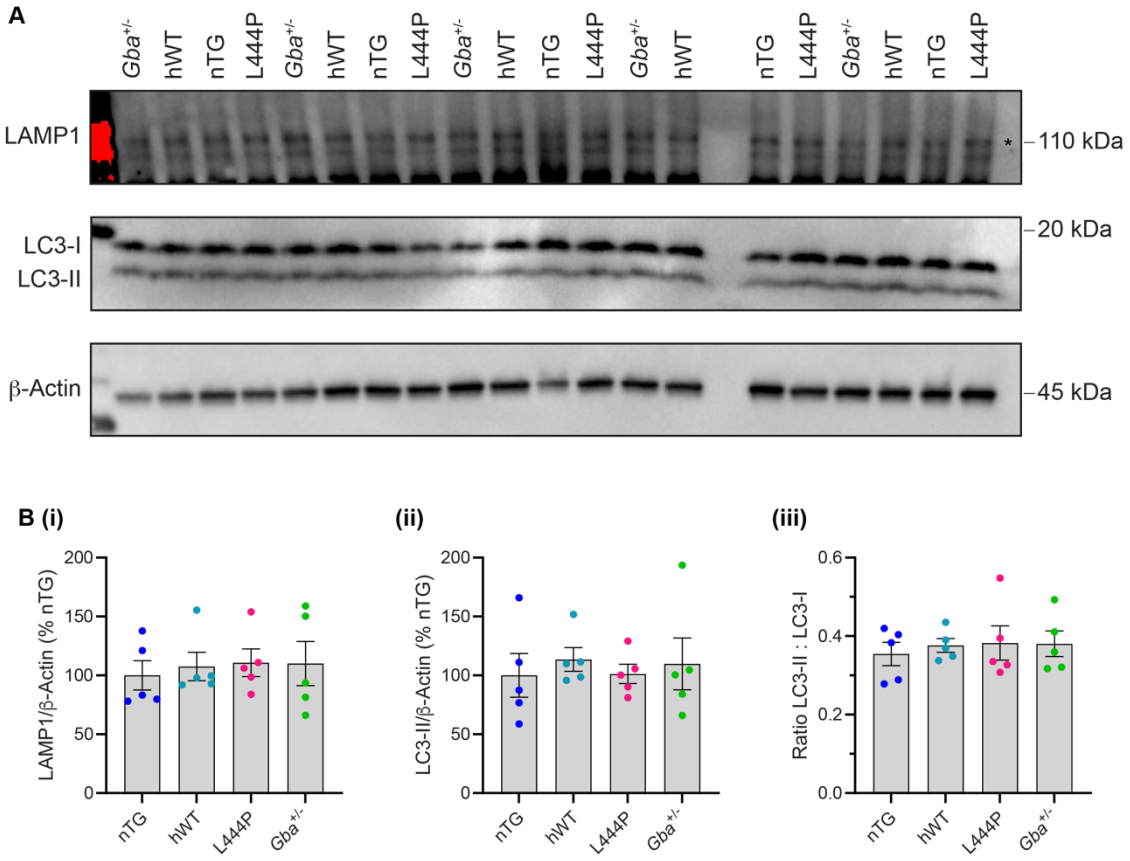


Figure 3.6: Cortical LAMP1 and LC3 levels are comparable across genotypes. (**A**) Representative western blots for LAMP1, LC3 and corresponding β-Actin from cortical tissue homogenates of mice aged 3 months. The * indicates the position of the LAMP1 band used for quantification. (**B**) Quantification of LAMP1 (**i**), LC3-II (**ii**) and the ratio of LC3-II : LC3-I (**iii**). (**B(i-ii)**) LAMP1 and LC3 are normalised to their own β-Actin per mouse and expressed as a percentage of the mean protein levels value in nTG mice. (**B(i)**) Kruskal-Wallis test: Kruskal-Wallis statistic = 1.354 p = 0.7163, (**B(ii-iii)**) one-way ANOVA: all $F_{(3,16)} < 0.1714$ and all $p > 0.9141$; n = 5 mice per genotype. Data are presented as mean ± SEM and each datapoint represents one mouse.

3.2.4 LIPIDOMIC ANALYSIS IN THE BRAIN, LIVER AND SPLEEN

The accumulation of GlcCer and GlcSph resulting from loss of GCase activity are undisputed hallmarks of GD pathology (**Section 1.2.1**) (Dekker et al., 2011, Revel-Vilk et al., 2020, Rolfs et al., 2013, Stirnemann et al., 2017). GlcChol elevation has also been demonstrated in GD patient plasma and GD rodent models (Marques et al., 2016). However, whether these lipid species accumulate and contribute to PD pathology remains controversial (**Section 1.3.3.1**) (Blumenreich et al., 2022, Gleason et al., 2022a, Huebecker et al., 2019, Leyns et al., 2023, Milenkovic et al., 2022, Surface et al., 2022).

To determine if lipid species related to GCase function (**Fig. 1.2**) are altered in our mice, lipidomic analysis was conducted using LC-MS/MS by Ms. Katerina Bila and Dr Martijn van der Lienden (Leiden University). Cholesterol was also measured using LC-MS by Dr Benjamin Jenkins (University of Cambridge). Lipids were quantified in 3-month-old mice across various brain regions (midbrain, striatum and cortex). GlcCer, ceramide and GlcSph were also measured in liver and spleen, as these organs are major sites of glycosphingolipid accumulation in GD (Stirnemann et al., 2017). A HILIC column made it possible to separate glucosylated sphingolipids, GlcCer and GlcSph, from their galactosylated isobaric isomers GalCer and GalSph, respectively (**Fig. 1.2**) (Lelieveld et al., 2022). Changes to GalCer and GalSph have not been implicated in PD pathology (Leyns et al., 2023). In accord with this, these lipids were similar across genotypes in the midbrain, striatum, and cortex (**Fig. A-1**).

GlcCer and ceramide levels were also comparable in all genotypes across brain regions (**Fig. 3.7 A-B**). Moreover, GlcSph was not significantly different across genotypes in the midbrain, striatum and cortex, according to a one-way ANOVA (**Fig. 3.7 C(i)** $F_{(3, 20)} = 2.878$ $p = 0.0616$; **C(ii)** $F_{(3,19)} = 3.070$ $p = 0.0527$; **C(iii)** $F_{(3,20)} = 1.037$ $p = 0.3977$). Although the one-way ANOVAs failed to detect a significant effect of genotype on GlcSph levels across all groups in these regions, I questioned if the GCase deficit specifically in the *Gba*$^{+/-}$ mice

was sufficient to induce significant GlcSph accumulation. To address this, I used a Šídák's multiple comparisons test to assess GlcSph levels in *Gba*$^{+/-}$ mice vs nTG mice and vs hWT mice in each brain region. Like the Tukey's and Dunn's tests, the Šídák's test corrects for multiple comparisons by controlling the type I error rate for the family of comparisons. Using the Šídák's test, the mean GlcSph level was shown to be significantly elevated in *Gba*$^{+/-}$ mice vs nTG mice in the midbrain (**Fig. 3.7 C(i)**) and the striatum (**Fig. 3.7 C(ii)**). No significant differences were observed in the cortex (**Fig. 3.7 C(iii)**). Levels of cholesterol and GlcChol were also not different across genotypes in the midbrain, striatum or cortex (**Fig. 3.8**).

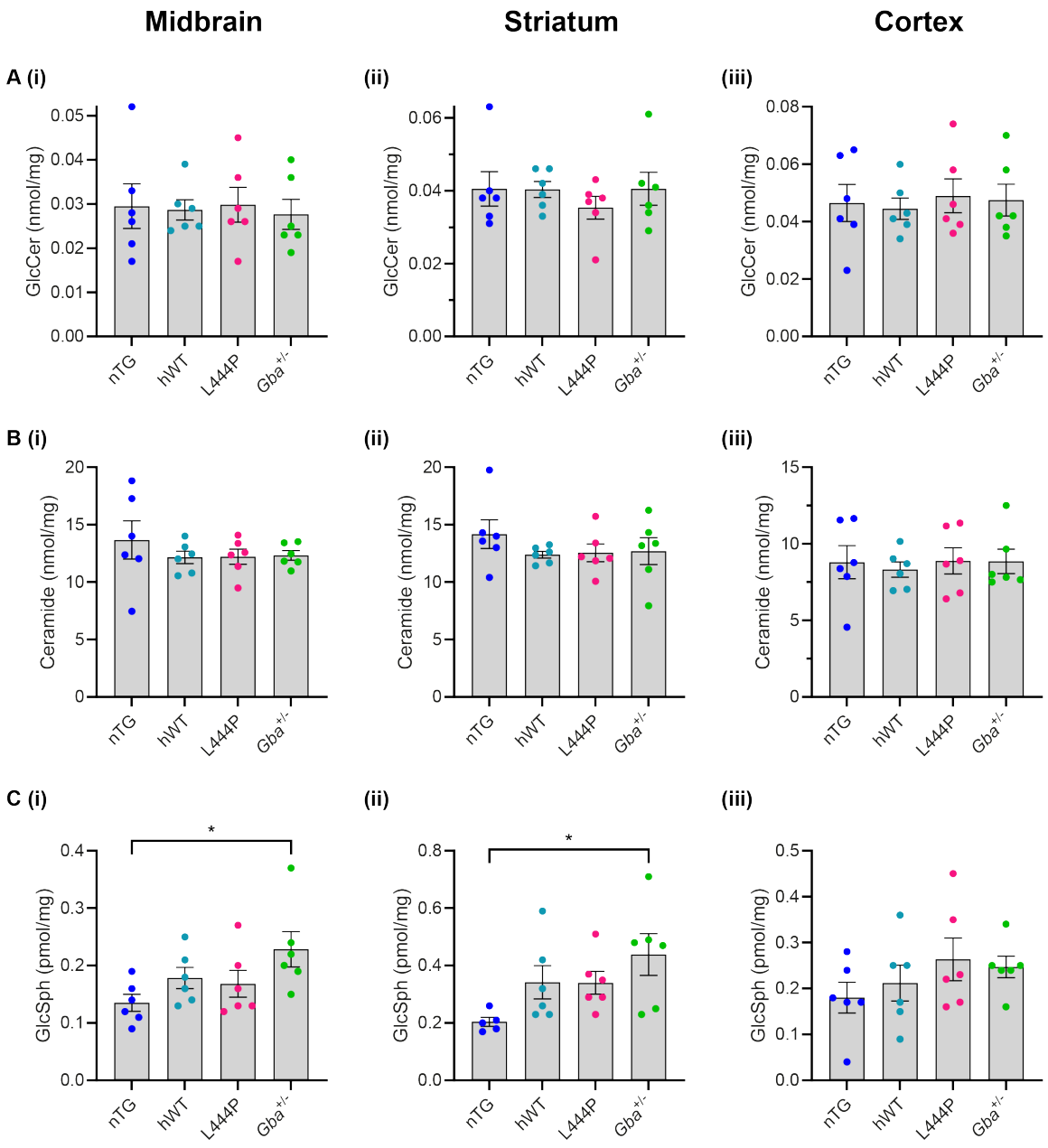


Figure 3.7: Quantification of sphingolipid species that are directly influenced by GCase activity across brain regions. Lipids were extracted from midbrain (**i**), striatal (**ii**) and cortical (**iii**) tissue homogenates from 3-month-old mice and were detected using LC-MS/MS. GlcCer (**A**) and ceramide (**B**) levels are similar across genotypes in all brain regions investigated. (**C**) GlcSph is significantly increased in the midbrain (**i**) and striatum (**ii**), but not the cortex (**iii**), of *Gba*$^{+/-}$ vs nTG mice using Šídák's multiple comparisons test. (**A-C**) Lipid species are normalised to protein concentration per sample, determined with a BCA assay. (**A(i, iii), B(i-ii)**) One-way ANOVA: all $F_{(3,20)} < 0.7514$ and all $p > 0.5344$, (**A(ii)**, **B(iii)**) Kruskal-Wallis test: all Kruskal-Wallis statistics < 1.103 and all $p > 0.7763$, (**C**) one-way ANOVA followed by Šídák's multiple comparisons test: all $F < 3.070$ and all $p > 0.0527$ in the one-way ANOVA; * $p < 0.05$ from Šídák's multiple comparisons test; n = 6 mice per genotype, except for **C(ii)** n = 5 nTG mice (one nTG mouse identified as an outlier (ROUT, Q = 0.1%) and excluded from statistical analysis). Data are presented as mean ± SEM and each datapoint represents one mouse. Data collected and analysed by Ms. Katerina Bila and Dr Martijn van der Lienden.

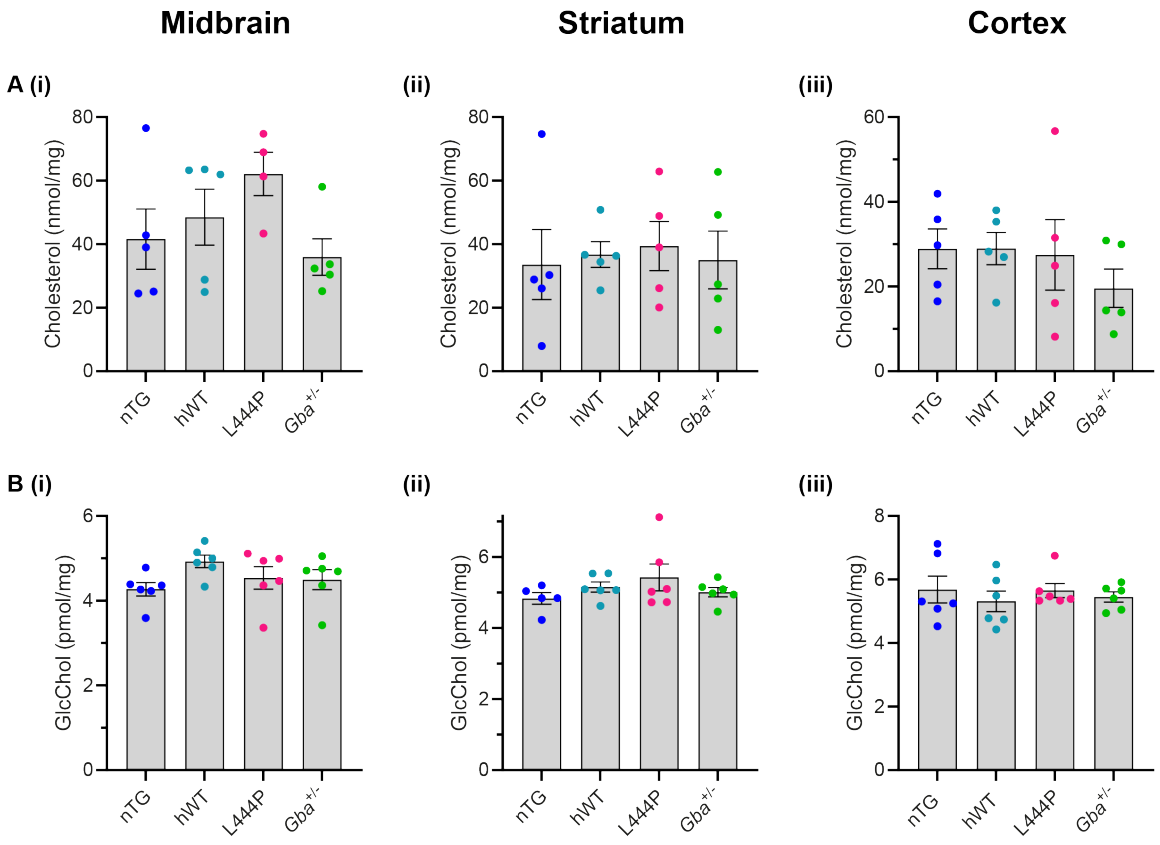


Figure 3.8: Cholesterol and GlcChol levels are comparable across genotypes in various brain regions. Lipids were extracted from midbrain (**i**), striatal (**ii**) and cortical (**iii**) tissue lysates from 3-month-old mice and were detected using LC-MS (**A**) or LC-MS/MS (**B**). No changes to cholesterol (**A**) or GlcChol (**B**) were observed across regions. Lipid species are normalised to tissue weight per sample (**A**) or protein concentration per sample, determined with a BCA assay (**B**). (**A(i), B(iii)**) Kruskal-Wallis test: all Kruskal-Wallis statistics < 4.347 and all $p > 0.2264$, (**A(ii-iii), B(i-ii)**) one-way ANOVA: all $F < 1.737$ and all $p > 0.1917$; n = 4-6 mice per genotype, (**B(ii)**) n = 1 outlier identified (ROUT, Q = 0.1%) and excluded from statistical analysis. Data are presented as mean ± SEM and each datapoint represents one mouse. Data collected and analysed by Dr Benjamin Jenkins (**A**) and Ms. Katerina Bila and Dr Martijn van der Lienden (**B**).

Reflecting observations in the brain, all genotypes had similar levels of GlcCer and ceramide in the liver and the spleen (**Fig. 3.9 A-B**). On the other hand, GlcSph accumulated in the liver of hWT and *Gba*$^{+/-}$ mice vs nTG mice (**Fig. 3.9 C(i)**). Although the mean GlcSph concentration in the L444P liver (0.15 pmol/mg) was similar to hWT and *Gba*$^{+/-}$ mice (both 0.16 pmol/mg), the difference between nTG vs L444P mice did not reach significance ($p = 0.069$, one-way ANOVA with Tukey's post-hoc test). GlcSph was also significantly elevated in the spleen of hWT, L444P and *Gba*$^{+/-}$ mice vs nTG mice (**Fig. 3.9 C(ii)**).

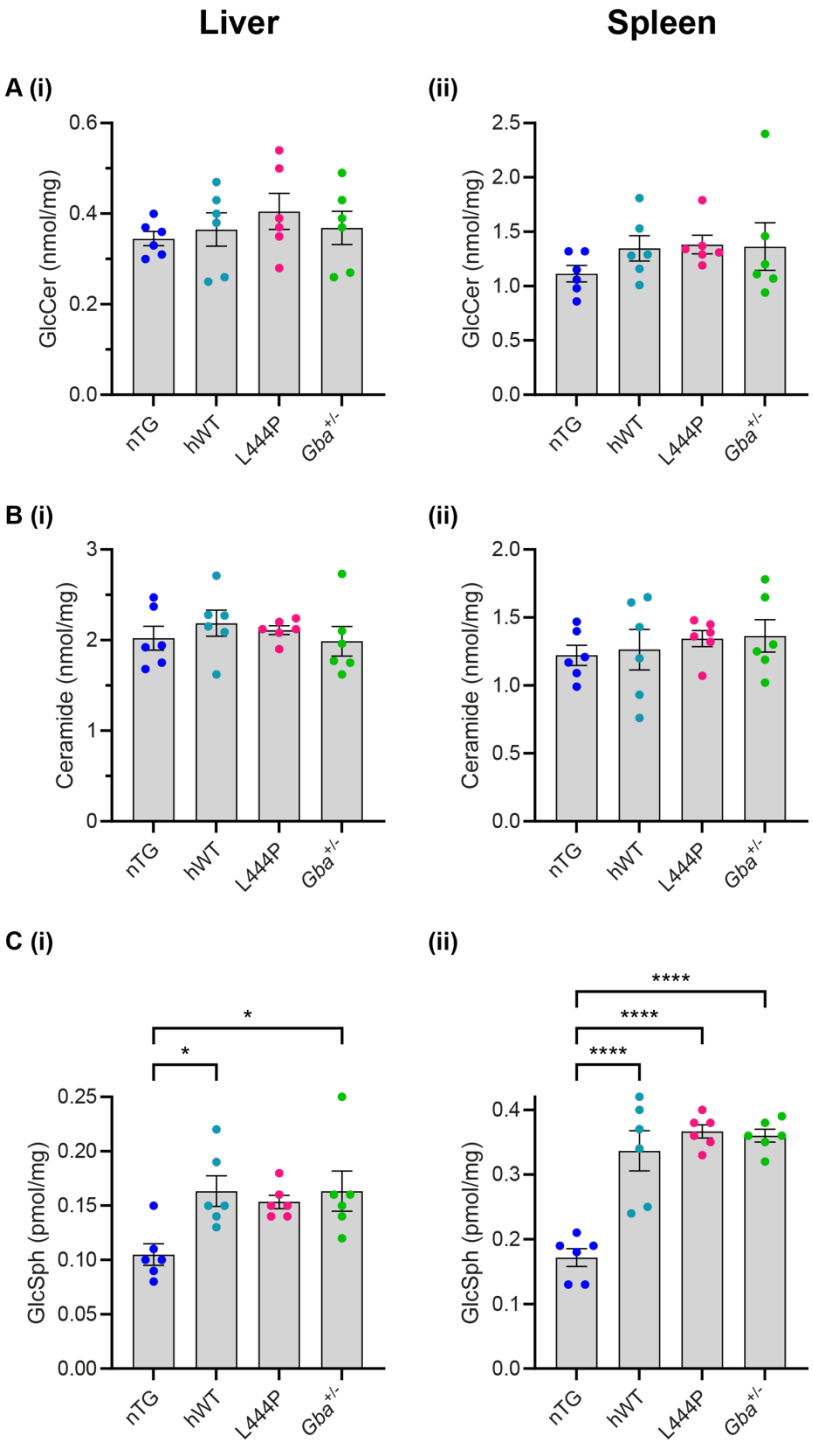


Figure 3.9: Quantification of sphingolipid species that are directly influenced by GCase activity in visceral organs. Lipids were extracted from liver (**i**) and spleen (**ii**) tissue lysates from 3-month-old mice and were detected using LC-MS/MS. GlcCer (**A**) and ceramide (**B**) levels are similar across genotypes in liver and spleen. (**C(i)**) Liver GlcSph is significantly increased in hWT and *Gba*$^{+/-}$ mice vs nTG mice. (**C(ii)**) Spleen GlcSph is significantly increased in hWT, L444P and *Gba*$^{+/-}$ mice vs nTG mice. (**A-C**) Lipid species are normalised to protein concentration per sample, determined with a BCA assay. (**A(i), B**) One-way ANOVA: all $F_{(3,20)} < 0.5509$ and all $p > 0.6534$, (**A(ii)**) Kruskal-Wallis test: Kruskal-Wallis statistic = 4.045 p = 0.2566, (**C**) one-way ANOVA with Tukey's post-hoc test: (**i**) $F_{(3,20)} = 4.636$ p = 0.0128, (**ii**) $F_{(3,20)} = 25.08$ $p < 0.0001$; * $p < 0.05$, **** $p < 0.0001$ from Tukey's post-hoc test; n = 6 mice per genotype. Data are presented as mean ± SEM and each datapoint represents one mouse. Data from Ms. Katerina Bila and Dr Martijn van der Lienden.

3.2.5 SUBCELLULAR αS DISTRIBUTION IN THE BRAIN

Many studies have supported that a toxic interplay between GCase deficiency and αS accumulation is central to *GBA*-associated PD pathology (**Section 1.3.3.3**) (Aflaki et al., 2017). Corroborating this, loss of GCase activity in the midbrain of our L444P and *Gba*$^{+/-}$ mice is associated with an increase in the mean αS-PLA signal in dopaminergic neurons of the SN (**Fig. 3.1 C-D**). Given that interactions between αS and lipid membranes accelerate αS aggregation (Galvagnion et al., 2015, Lee et al., 2002), we hypothesized that the subcellular distribution of αS may be altered in the brains of L444P and *Gba*$^{+/-}$ mice. To investigate this, Dr Clara Obensa Bertroli (University College London) performed sequential fractionation on cerebellar, midbrain, striatal and cortical tissue homogenates from 3-month-old and aged mice (15-22-months-old). She subsequently quantified αS in the soluble fraction ($\alpha S_{sol.}$), representing cytosolic αS, and in the membrane fraction ($\alpha S_{mem.}$), using an MSD immunoassay.

The relative proportions of $\alpha S_{mem.}$ and $\alpha S_{sol.}$ were similar across genotypes in 3-month-old mice; both forms of αS accounted for approximately 50% of the total αS detected (αS_{total}) across brain regions (**Fig. 3.10 A**). In accord with this, the ratio of $\alpha S_{mem.}$ to $\alpha S_{sol.}$ was also not significantly different across genotypes at 3 months (**Fig. 3.10 B**).

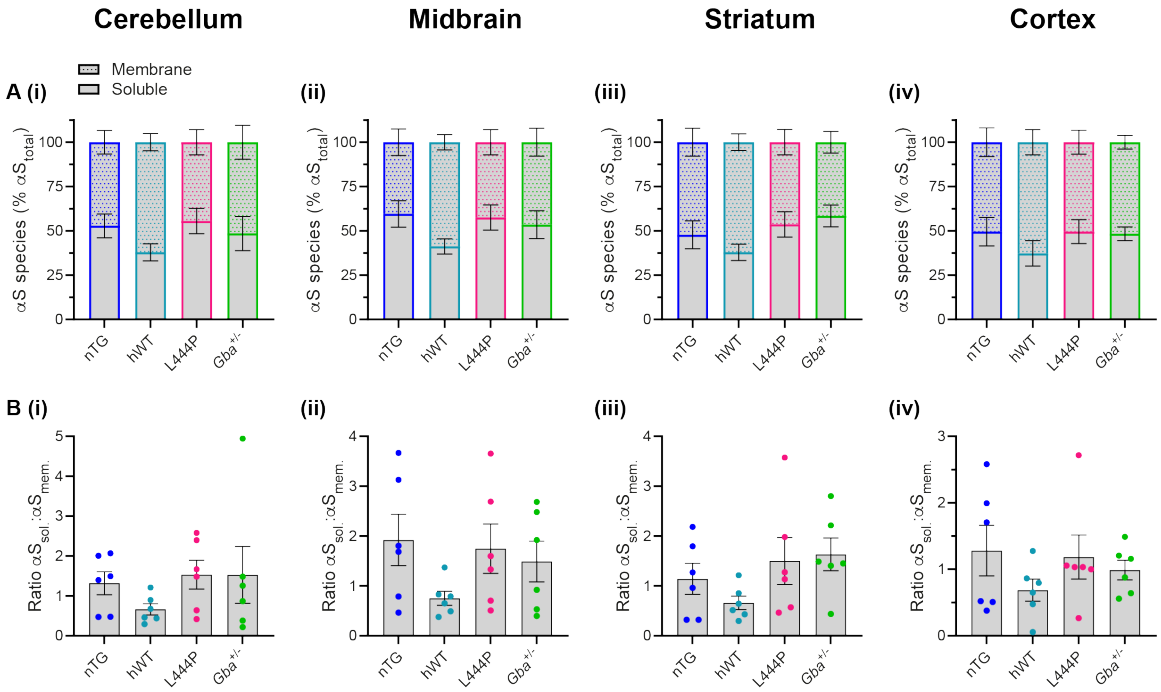


Figure 3.10: The subcellular distribution of αS is similar across genotypes in 3-month-old mice. Tissue homogenates from the cerebellum (**i**), midbrain (**ii**), striatum (**iii**) and cortex (**iv**) underwent sequential fractionation and the proportions of $\alpha S_{sol.}$ and $\alpha S_{mem.}$ were subsequently quantified using an MSD immunoassay. (**A**) Levels of $\alpha S_{sol.}$ and $\alpha S_{mem.}$, expressed as a percentage of the αS_{total} per sample. (**B**) The ratio of $\alpha S_{sol.}$ to $\alpha S_{mem.}$ displayed per sample. $\alpha S_{sol.}$ = soluble (cytosolic) αS, $\alpha S_{mem.}$ = membrane αS, αS_{total} = total αS. (**B(i, iv)**) Kruskal-Wallis test: all Kruskal-Wallis statistics < 4.407 and all $p > 0.2208$, (**B(ii-iii)**) one-way ANOVA: all $F_{(3,20)} < 1.702$ and all $p > 0.1986$; n = 6 mice per genotype. Data are presented as mean ± SEM and each datapoint in (**B**) represents one mouse. Data collected by Dr Clara Obensa Bertroli.

In aged mice, the proportion of $\alpha S_{sol.}$ tended to be slightly higher than $\alpha S_{mem.}$ across genotypes in the cerebellum, midbrain and striatum (**Fig. 3.11 A(i)-(iii)**), whereas the proportions of $\alpha S_{mem.}$ and $\alpha S_{sol.}$ were relatively even in the aged cortex (**Fig. 3.11 A(iv)**). Nevertheless, the relative proportions of $\alpha S_{mem.}$ and $\alpha S_{sol.}$ appeared comparable across genotypes in these mice (**Fig. 3.11 A**). Reflecting this, no genotype-related differences were observed in the ratio of $\alpha S_{mem.}$ to $\alpha S_{sol.}$ (**Fig. 3.11 B**).

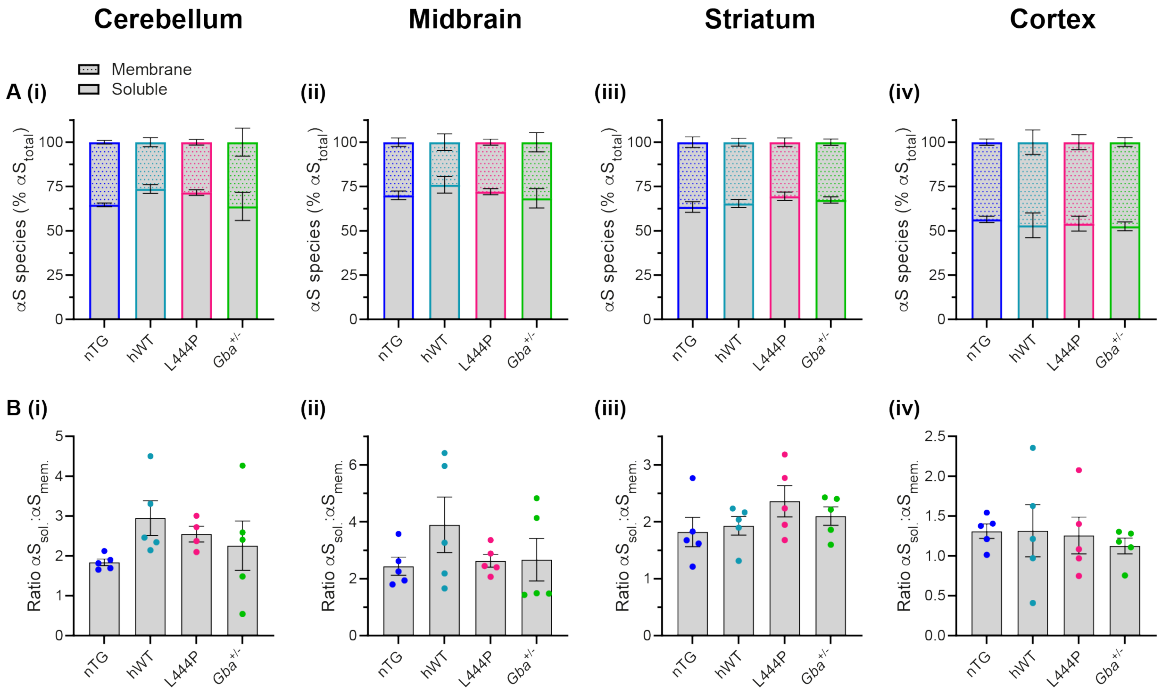


Figure 3.11: The subcellular distribution of αS is not significantly different across genotypes in aged mice. Tissue homogenates from the cerebellum (**i**), midbrain (**ii**), striatum (**iii**) and cortex (**iv**) of mice aged 15-22 months underwent sequential fractionation and the proportions of $\alpha S_{sol.}$ and $\alpha S_{mem.}$ were subsequently quantified using an MSD immunoassay. (**A**) Levels of $\alpha S_{sol.}$ and $\alpha S_{mem.}$, expressed as a percentage of the αS_{total} per sample. (**B**) The ratio of $\alpha S_{sol.}$ to $\alpha S_{mem.}$ displayed per sample. $\alpha S_{sol.}$ = soluble (cytosolic) αS, $\alpha S_{mem.}$ = membrane αS, αS_{total} = total αS. (**B(i, iii-iv)**) one-way ANOVA: all $F < 1.356$ and all $p > 0.2940$, (**B(ii)**) Kruskal-Wallis test: Kruskal-Wallis statistic = 1.834 $p = 0.6075$; n = 5 mice per genotype, except for (**A(i), B(i)**) n = 4 L444P mice (one L444P mouse identified as an outlier (ROUT, Q = 0.1%) and excluded from statistical analysis). Data are presented as mean ± SEM each datapoint in (**B**) represents one mouse. Data collected by Dr Clara Obensa Bertroli.

3.2.6 The nature of the GCase-LIMP2 interaction across disease-states and species

Various pathophysiological mechanisms have been proposed to mediate lysosomal GCase trafficking deficits in *GBA*-associated PD (Chatterjee and Krainc, 2023). Since GCase's interaction with LIMP2 is integral to its delivery to the lysosome (Reczek et al., 2007), I questioned if the L444P mutation directly hinders GCase trafficking by weakening its association with LIMP2. I also sought to elucidate similarities and differences in GCase-LIMP2 complex formation between humans and mice to further understand interactions between GCase and LIMP2 in our humanised mice.

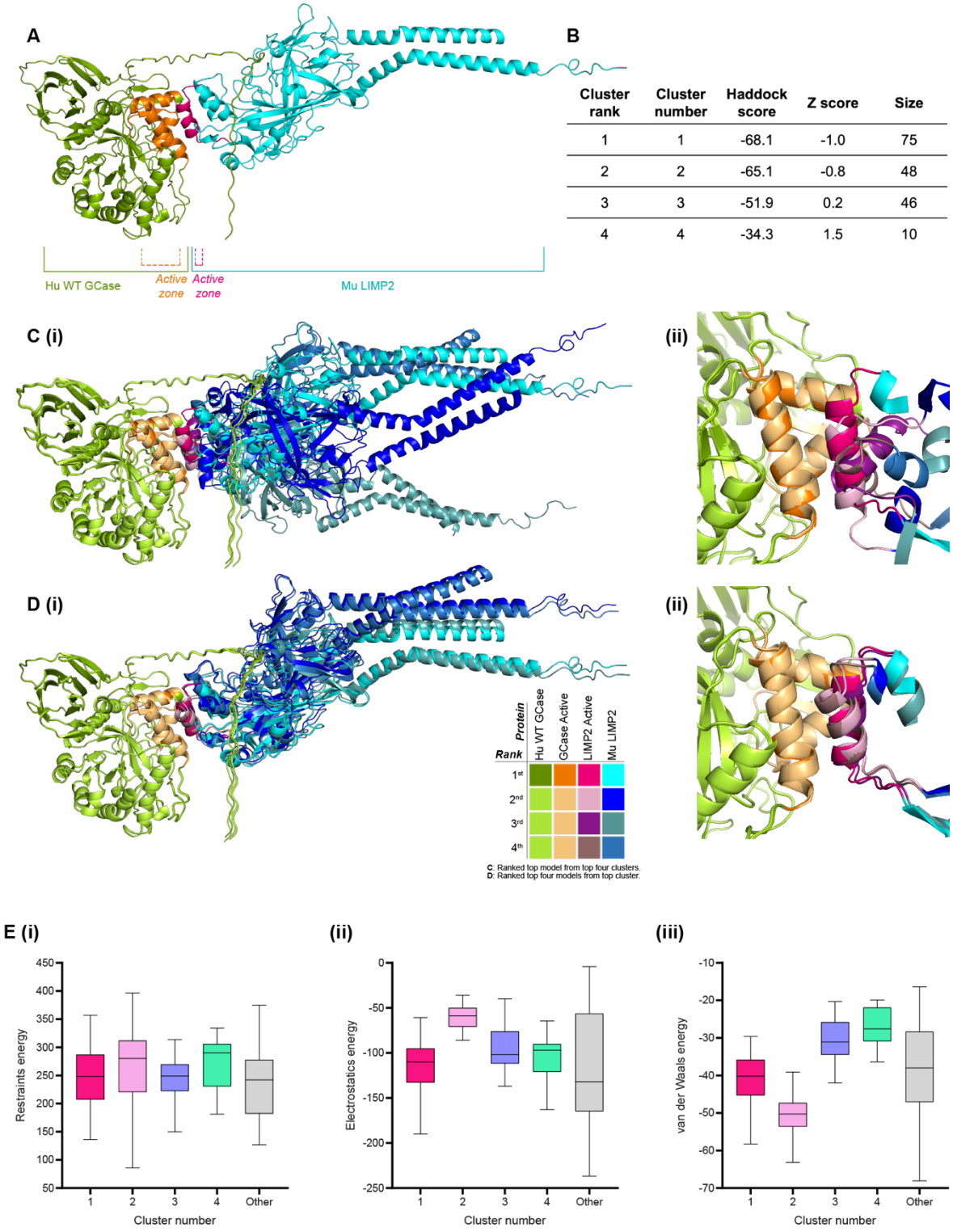
Firstly, the conformation of four GCase-LIMP2 complexes of interest was predicted using protein-protein docking:

1. Human WT GCase and mouse LIMP2 (HuGCase-MuLIMP2) (**Fig. 3.12**).
2. Human L444P-mutant GCase and mouse LIMP2 (HuL444PGCase-MuLIMP2) (**Fig. 3.13**).
3. Mouse WT GCase and mouse LIMP2 (MuGCase-MuLIMP2) (**Fig. 3.14**).
4. Human WT GCase and human LIMP2 (HuGCase-HuLIMP2) (**Fig. 3.15**).

The HADDOCK web server docks proteins according to user-inputted information on residues that have been proposed to mediate the interaction (Honorato et al., 2024). The amino acids on human GCase and human LIMP2 that were previously determined to be critical for GCase-LIMP2 binding (Liou et al., 2014, Reczek et al., 2007, Zunke et al., 2016), and their aligned sequences on mouse GCase and mouse LIMP2, were classed as "active residues" in the docked structures (**Fig. 2.3-2.4**). HADDOCK generates many structural models for each complex and calculates a HADDOCK docking score for each model; a weighted sum of various energies and the buried surface area in the model (Vangone et al., 2017). The lower the HADDOCK score, the more energetically favourable the model is. Models are subsequently clustered according to their fraction of common contacts (by default) (Rodrigues et al., 2012). Clusters are then ranked based on the average HADDOCK score of the four lowest-scoring models in the cluster; the lower the HADDOCK score of a cluster, the higher that cluster will be ranked (Honorato et al., 2024). It follows that the lowest-scoring model from the lowest-scoring cluster is the most energetically favourable model generated by HADDOCK (**Fig. 3.12-3.15 A**). This model is therefore presumed to be the most reliable prediction of the true structure of the complex. Each cluster also has a Z score (**Fig. 3.12-3.15 B**), which indicates the number of standard deviations that separate the HADDOCK score of that cluster and the mean HADDOCK score of all the clusters

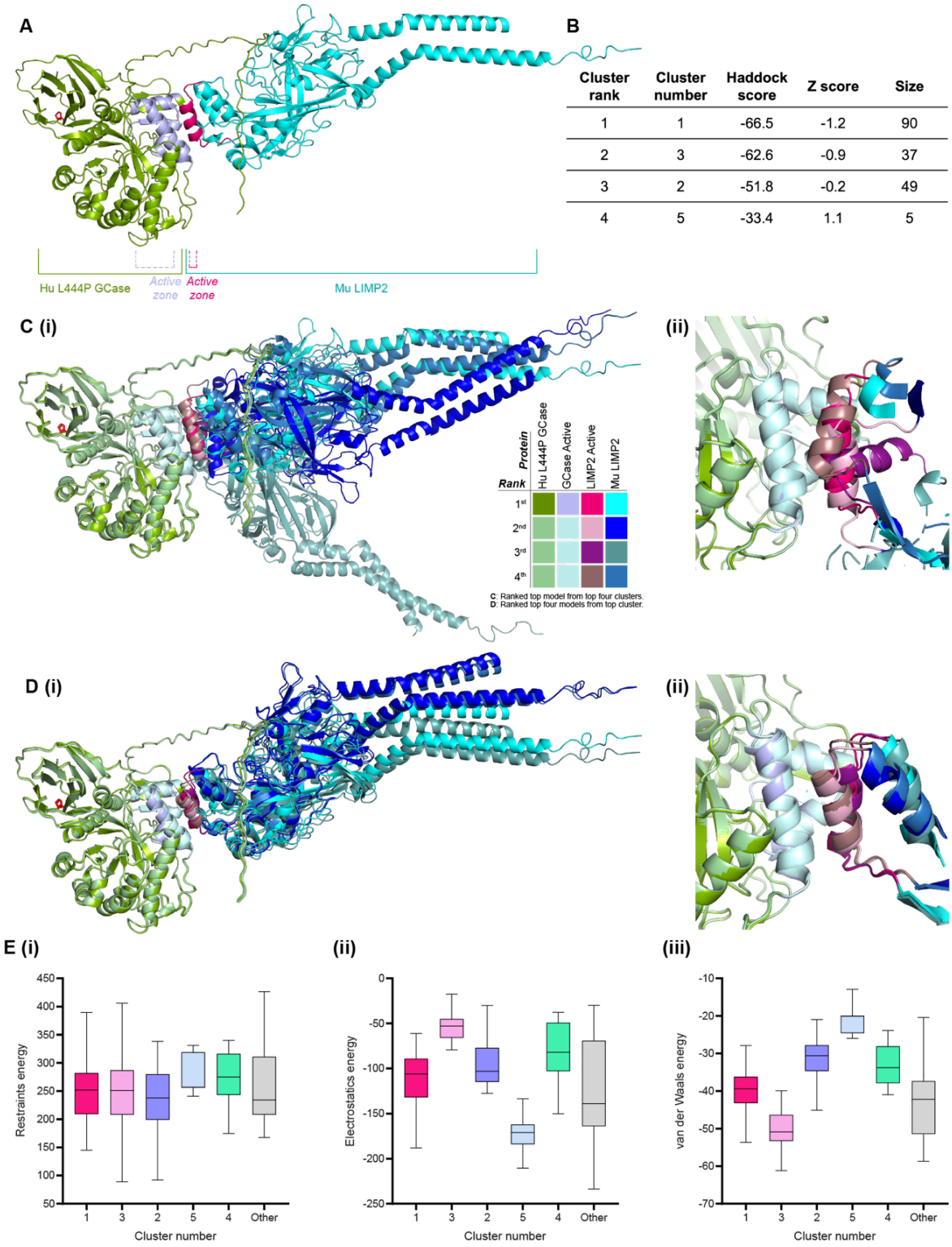
generated. In summary, the highest-ranked cluster has the lowest negative Z score, the lowest average HADDOCK score and contains the most energetically favourable models overall (van Zundert et al., 2016).

Structural alignment of the lowest scoring model from the top four ranked clusters is variable for each complex (**Fig. 3.12-3.15 C**). This variability mirrors the range of Z scores across clusters in each complex (**Fig. 3.12-3.15 B**) and highlights that models across clusters have different conformations. HuGCase-MuLIMP2 and HuL444PGCase-MuLIMP2 appear to have the most variable structural alignment and have the largest range of Z scores across the four highest-ranked clusters (**Fig. 3.12-3.13 B-C**). On the other hand, the four lowest-scoring models in the top ranked cluster were closely aligned in each complex (**Fig. 3.12-3.15 D**). These models therefore have a similar structural conformation, which lends confidence to the reliability of HADDOCK's protein-protein docking predictions. The restraints, electrostatics and van der Waals energies across clusters for each complex are summarised in **Fig. 3.12-3.15 E**. A combination of relatively negative electrostatic and van der Waals forces likely contributes to the low HADDOCK score of the top ranked cluster (cluster 1) for the HuGCase-MuLIMP2 and HuL444PGCase-MuLIMP2 complexes (**Fig. 3.12-3.13 E(ii-iii)**). The low HADDOCK score of the top ranked MuGCase-MuLIMP2 cluster (cluster 2) is primarily driven by negative electrostatics energy (**Fig. 3.14 E(ii)**), whilst negative van der Waals-related energy of the top cluster (cluster 5) in the HuGCase-HuLIMP2 complex largely accounts for its low HADDOCK score (**Fig. 3.15 E(iii)**).



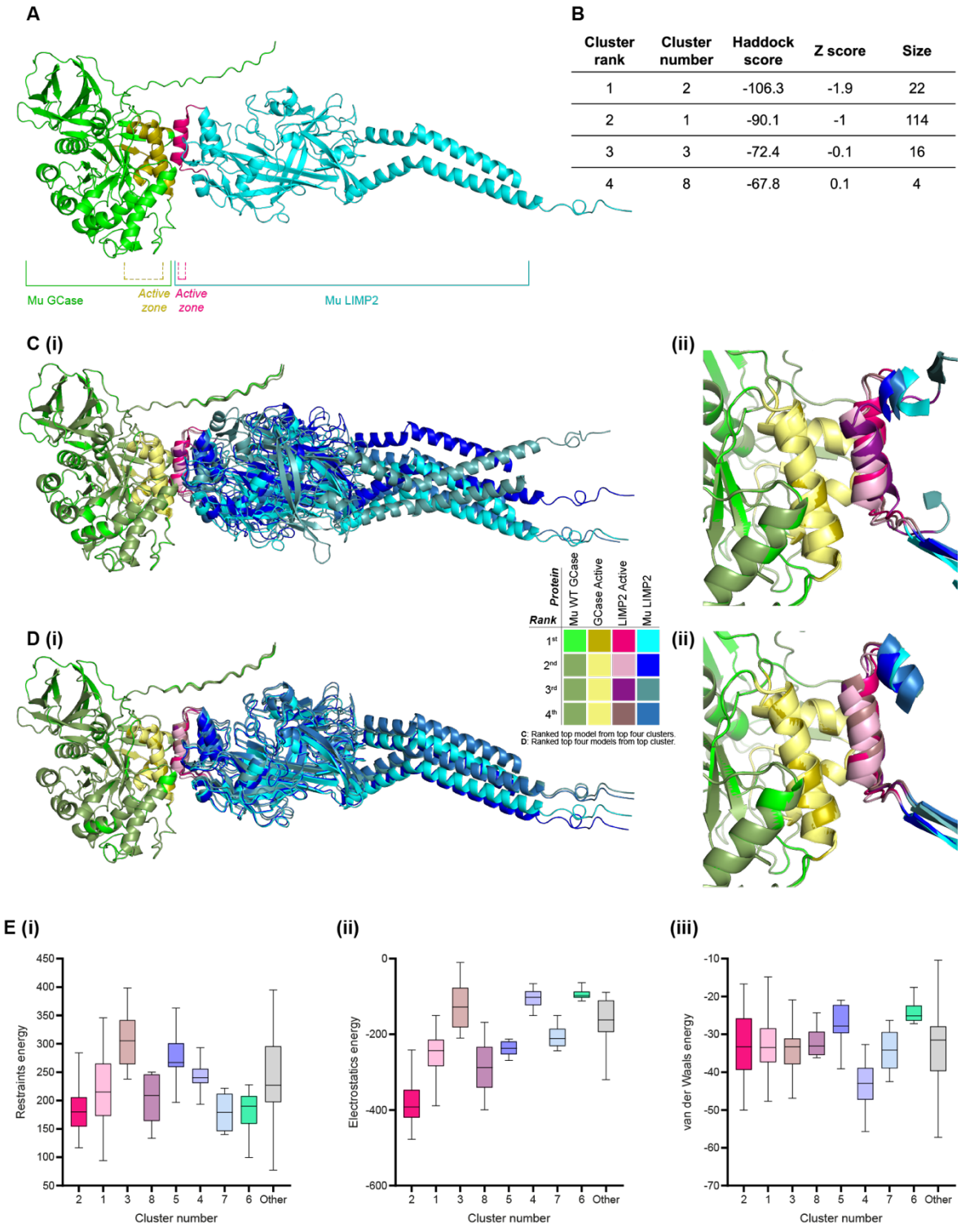
Cluster rank	Cluster number	Haddock score	Z score	Size
1	1	-68.1	-1.0	75
2	2	-65.1	-0.8	48
3	3	-51.9	0.2	46
4	4	-34.3	1.5	10

Figure 3.12: The structure and intermolecular energies of the docked HuGCase-MuLIMP2 complex. (**A**) The model with the lowest HADDOCK score. (**B**) The HADDOCK score, Z score and size of the four top-ranked clusters. Clusters are ranked according to HADDOCK score and numbered according to their size. (**C**) Alignment of the lowest-scoring HADDOCK model from each of the four top-ranked clusters (clusters 1-4), illustrating the complete structure (**i**) and the interaction interface (**ii**). (**D**) Alignment of the four lowest-scoring HADDOCK models in the top-ranked cluster (cluster 1), illustrating the complete structure (**i**) and the interaction interface (**ii**). (**E**) Box-and-whiskers plots quantifying the restraints (**i**), electrostatics (**ii**) and van der Waals (**iii**) energies across clusters that underlie the HADDOCK score of these clusters.



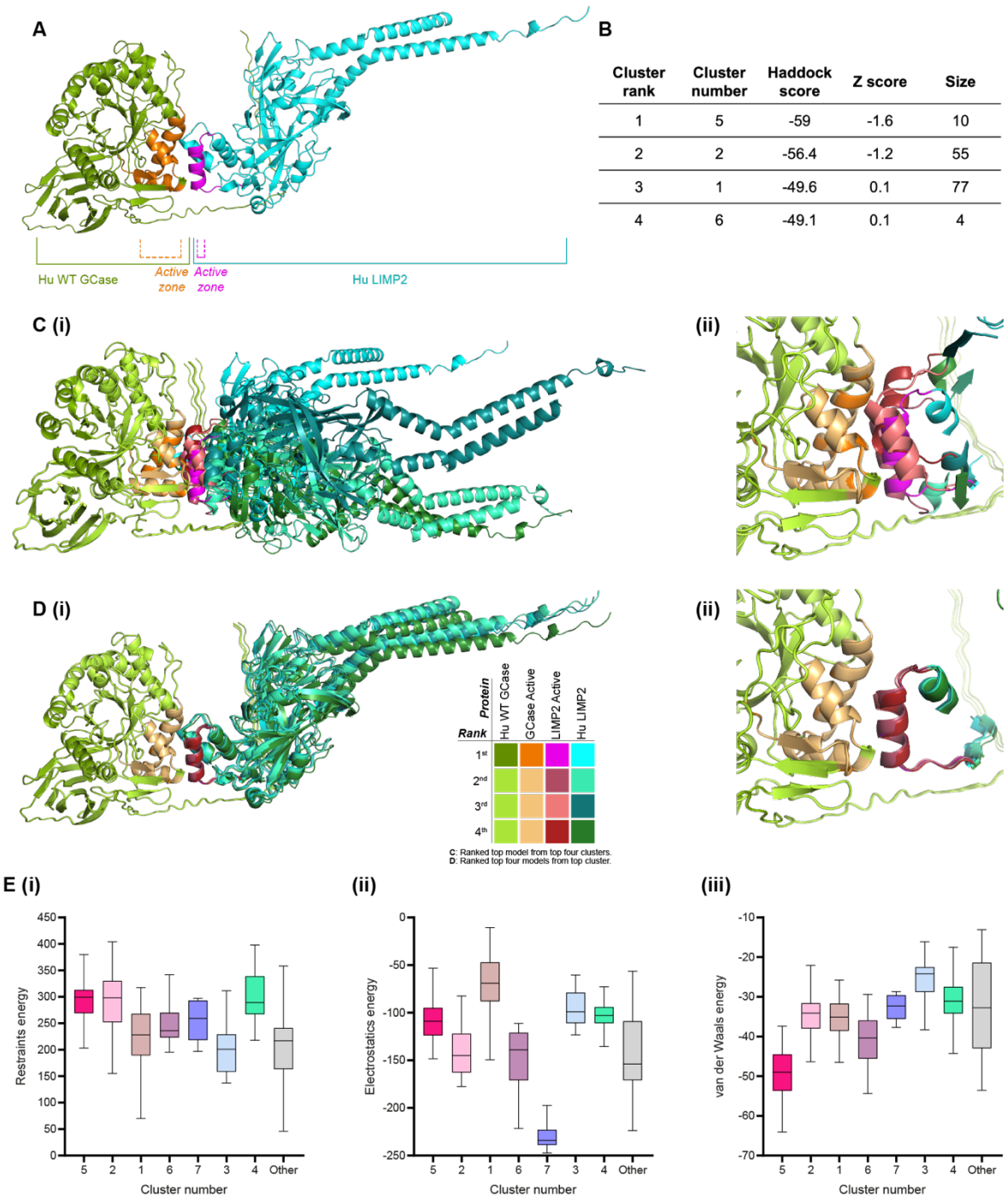
Cluster rank	Cluster number	Haddock score	Z score	Size
1	1	-66.5	-1.2	90
2	3	-62.6	-0.9	37
3	2	-51.8	-0.2	49
4	5	-33.4	1.1	5

Figure 3.13: The structure and intermolecular energies of the docked HuL444PGCase-MuLIMP2 complex. (**A**) The model with the lowest HADDOCK score. (**B**) The HADDOCK score, Z score and size of the four top-ranked clusters. Clusters are ranked according to HADDOCK score and numbered according to their size. (**C**) Alignment of the lowest-scoring HADDOCK model from each of the four top-ranked clusters, illustrating the complete structure (**i**) and the interaction interface (**ii**). (**D**) Alignment of the four lowest-scoring HADDOCK models in the top-ranked cluster, illustrating the complete structure (**i**) and the interaction interface (**ii**). (**E**) Box-and-whiskers plots quantifying the restraints (**i**), electrostatics (**ii**) and van der Waals (**iii**) energies across clusters that underlie the HADDOCK score of these clusters. (**A, C, D**) The L444P mutation is indicated in red.



Cluster rank	Cluster number	Haddock score	Z score	Size
1	2	-106.3	-1.9	22
2	1	-90.1	-1	114
3	3	-72.4	-0.1	16
4	8	-67.8	0.1	4

Figure 3.14: The structure and intermolecular energies of the docked MuGCase-MuLIMP2 complex. (**A**) The model with the lowest HADDOCK score. (**B**) The HADDOCK score, Z score and size of the four top-ranked clusters. Clusters are ranked according to HADDOCK score and numbered according to their size. (**C**) Alignment of the lowest-scoring HADDOCK model from each of the four top-ranked clusters (clusters 2, 1, 3, 8), illustrating the complete structure (**i**) and the interaction interface (**ii**). (**D**) Alignment of the four lowest-scoring HADDOCK models in the top-ranked cluster (cluster 2), illustrating the complete structure (**i**) and the interaction interface (**ii**). (**E**) Box-and-whiskers plots quantifying the restraints (**i**), electrostatics (**ii**) and van der Waals (**iii**) energies across clusters that underlie the HADDOCK score of these clusters.



Cluster rank	Cluster number	Haddock score	Z score	Size
1	5	-59	-1.6	10
2	2	-56.4	-1.2	55
3	1	-49.6	0.1	77
4	6	-49.1	0.1	4

Figure 3.15: The structure and intermolecular energies of the docked HuGCase-HuLIMP2 complex. (**A**) The model with the lowest HADDOCK score. (**B**) The HADDOCK score, Z score and size of the four top-ranked clusters. Clusters are ranked according to HADDOCK score and numbered according to their size. (**C**) Alignment of the lowest-scoring HADDOCK model from each of the four top-ranked clusters (clusters 5, 2, 1, 6), illustrating the complete structure (**i**) and the interaction interface (**ii**). (**D**) Alignment of the four lowest-scoring HADDOCK models in the top-ranked cluster (cluster 5), illustrating the complete structure (**i**) and the interaction interface (**ii**). (**E**) Box-and-whiskers plots quantifying the restraints (**i**), electrostatics (**ii**) and van der Waals (**iii**) energies across clusters that underlie the HADDOCK score of these clusters.

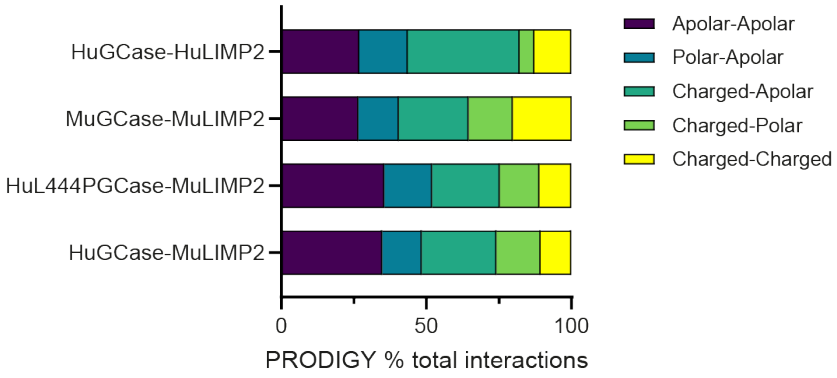
Subsequent analyses were restricted to the model with the lowest HADDOCK score for each complex (**Fig. 3.12-3.15 A**) because these predictions were deemed to best-represent the true conformation of their respective complexes. The affinity of the GCase-LIMP2 interaction (**Fig. 3.16 A**) and the nature of the non-covalent bonds (**Fig. 3.16 B-C**) across the four complexes were computationally determined using the PRODIGY (Vangone and Bonvin, 2017, Vangone and Bonvin, 2015) and RING web servers (Clementel et al., 2022, Martin et al., 2011). The complete list of the interacting residue pairs from these analyses is shown in **Table A-1**.

Firstly, the Kd value of the HuGCase-MuLIMP2 complex is similar, albeit slightly higher than the HuL444PGCase-MuLIMP2 complex (**Fig. 3.16 A**). In accord with this, the number and types non-covalent interactions (**Fig. 3.16**) and the conformation of the interacting interface (**Fig. 3.17 A**) are comparable across these complexes. Additionally, the active residues that form strong polar contacts are well-conserved (**Fig. 3.17 A**) and the lengths of the polar bonds are largely equivalent in both complexes (**Fig. 3.17 B-D**). For instance, residues K161 and Q165 on LIMP2 make strong polar contacts with T193 and K194, respectively, on Helix 2 of hWT and L444P GCase (**Fig. 3.17 B**). Also, E154 on LIMP2 interacts with GCase residues N141 and Q205 across both complexes (**Fig. 3.17 C**). GCase R202 interacts with LIMP2 L155 in the HuGCase-MuLIMP2 complex (**Fig. 3.17 C(i)**) and LIMP2's adjacent residue, E154, in the HuL444PGCase-MuLIMP2 complex (**Fig. 3.17 C(ii)**). Lastly, Y163 on LIMP2 forms a strong polar contact with L133 on hWT GCase (**Fig. 3.17 D(i)**) and its adjacent residue, A134, on L444P GCase (**Fig. 3.17 D(ii)**).

A

	PRODIGY				RING
Complex	**Kd (M)**	**Non Interacting Surface charged**	**Non Interacting Surface apolar**	**Number of interatomic contacts**	**Number of interactions**
HuGCase-MuLIMP2	2.5e-07	22.64	44.02	66	13
HuL444PGCase-MuLIMP2	7.3e-08	22.83	44.12	73	10
MuGCase-MuLIMP2	2.4e-08	23.52	44.01	79	25
HuGCase-HuLIMP2	4e-09	24.44	42.94	78	23

B (i)



(ii)

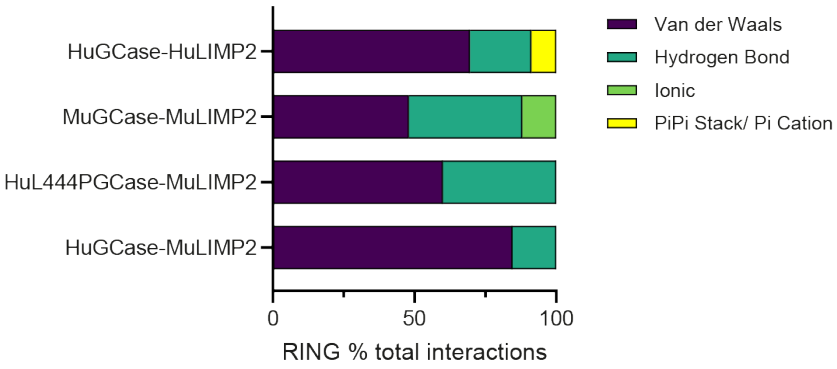


Figure 3.16: Parameters mediating the strength of the GCase-LIMP2 interaction across complexes. (**A**) Summary of results from PRODIGY and RING analyses, demonstrating the binding affinity and number of interacting residue pairs across complexes. (**B**) The proportion of different classes of non-covalent interactions across complexes from PRODIGY (**i**) and RING (**ii**) analyses.

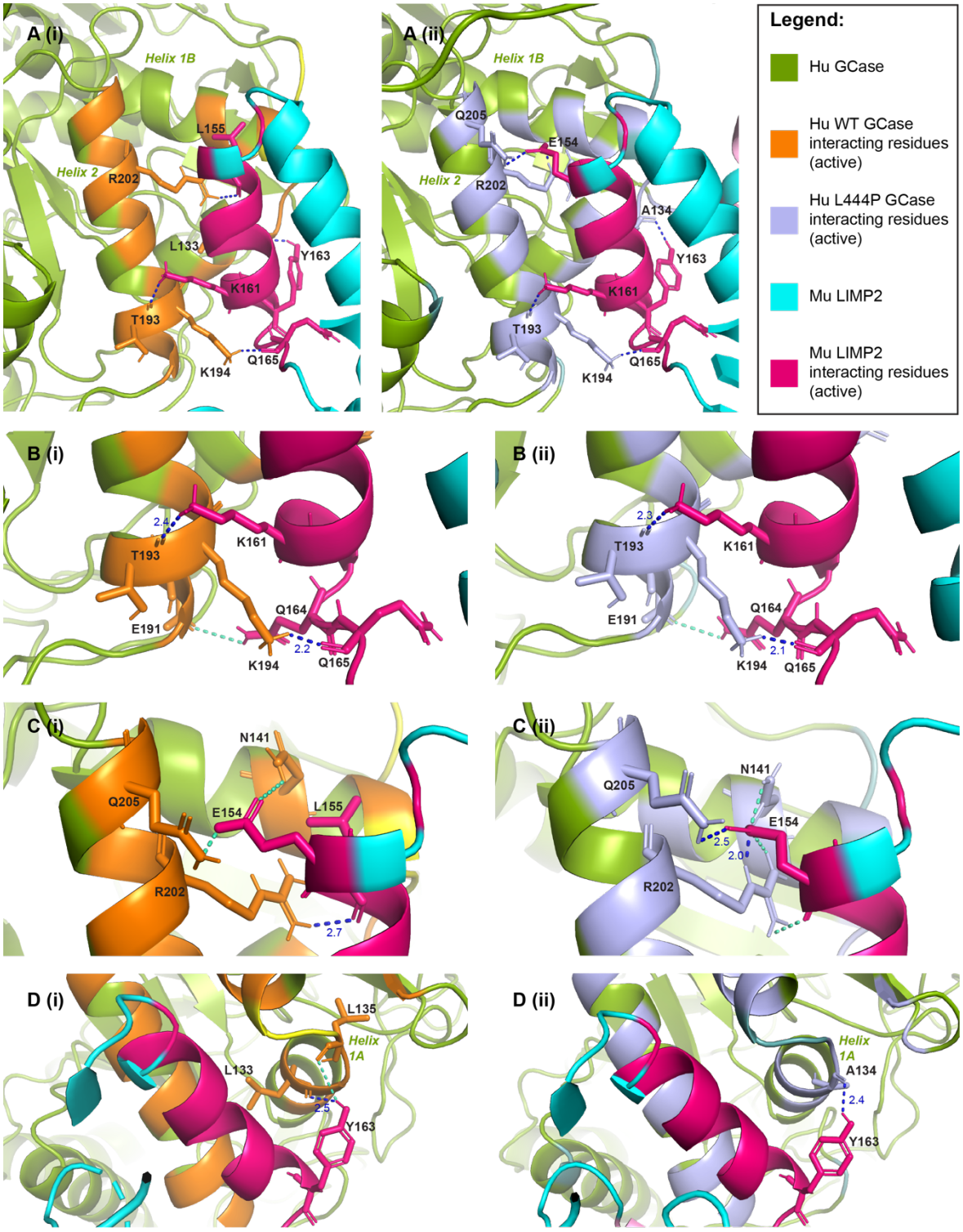


Figure 3.17: The structural conformation and polar interactions of the HuGCase-MuLIMP2 and HuL444PGCase-MuLIMP2 complexes. (**A**) The conformation of the interaction interface for HuGCase-MuLIMP2 (**i**) and HuL444PGCase-MuLIMP2 (**ii**). (**B-D**) Magnified views of key polar contacts in HuGCase-MuLIMP2 (**i**) and HuL444PGCase-MuLIMP2 (**ii**). Active residues are those that have previously been implicated in the GCase-LIMP2 interaction. Strong polar contacts are highlighted in dark blue and weaker polar contacts are coloured light blue.

Following this, species-related differences underlying GCase-LIMP2 binding were characterised. The computationally-predicted binding affinity of the MuGCase-MuLIMP2 interaction is 10-fold higher than the HuGCase-MuLIMP2 interaction (**Fig. 3.16 A**). Accordingly, the MuGCase-MuLIMP2 complex has more interacting residues (**Fig. 3.16 A**) and a higher proportion of "charged" interactions (**Fig. 3.16 B**) and hydrogen bonds (**Fig. 3.16 C**) vs the HuGCase-MuLIMP2 complex. In addition, there are more strong polar contacts formed within the major interaction site in the MuGCase-MuLIMP2 complex (**Fig. 3.18 A(ii)**) vs the HuGCase-MuLIMP2 complex (**Fig. 3.18 A(i)**). Residues that have not previously been implicated in GCase-LIMP2 binding, labelled as "non-active", also formed polar bonds both within (**Fig. 3.18 A(ii)**) and outside (**Fig. A-2 C**) the major interaction interface of the MuGCase-MuLIMP2 complex. On the other hand, strong polar contacts in the HuGCase-MuLIMP2 complex are exclusively formed by active residues in the major binding interface (**Fig. 3.18 A(i) and Fig. A-2 A**). Furthermore, GCase Helix 2 is closer to LIMP2 in the MuGCase-MuLIMP2 complex. This facilitates stronger and more abundant connections between the proteins, which also likely mediates this complex's higher binding affinity. This closer proximity is demonstrated by the shorter bond lengths of the polar contacts between these helices in the MuGCase-MuLIMP2 complex (**Fig. 3.18 B-D**) and is most evident in **Fig. 3.18 B**: K166 on LIMP2 is 2.4 Å from T173 on mouse GCase (**Fig. 3.18 B(ii) ↓**) but is 10.5 Å from T193 on human GCase[4] **(Fig. 3.18 B(i) ↓**). Also, the non-active residues K241 and Q77 are 1.7 Å apart in MuGCase-MuLIMP2 (**Fig. 3.18 B(ii)***) but the distance between the equivalent residues in the HuGCase-MuLIMP2 complex is 14.4 Å (**Fig. 3.18 B(i)***). Mouse LIMP2 also occupies different positions relative to GCase Helix 2 in the MuGCase-MuLIMP2 complex vs the HuGCase-MuLIMP2 complex (**Fig. 3.18 C**).

[4] The equivalent residues on the aligned human and mouse GCase sequences do not have identical position numbers because the chain length of mouse GCase is shorter than human GCase. For example, residues T193 on human GCase and T173 on mouse GCase are equivalent (**Fig. 2.4**).

For instance, in the HuGCase-MuLIMP2 complex, T193 and K161 are horizontally aligned forming a strong polar contact (**Fig. 3.18 C(i) ↓**). But K161 is 7.7 Å away from T173 in MuGCase-MuLIMP2 (**Fig. 3.18 C(ii) ↓**). In turn, this brings LIMP2 in closer proximity to GCase Helix 1B in the MuGCase-MuLIMP2 complex vs the HuGCase-MuLIMP2 complex. This close proximity enables strong polar contacts to form between these helices in MuGCase-MuLIMP2 (**Fig. 3.18 D(ii) ↓↓**), whereas only one weaker polar contact is formed between LIMP2 and GCase Helix 1B in HuGCase-MuLIMP2 (**Fig. 3.18 D(i) ↓**). On the other hand, mouse LIMP2 does not form strong polar interactions with Helix 1A of mouse GCase (**Fig. 3.18E(ii)**), highlighting another difference in the structural conformation of the complexes. HuGCase-MuLIMP2 harbours a strong polar contact between L133 and Y163 (**Fig. 3.18 E(i)**) but the corresponding residues are 7.3 Å apart in MuGCase-MuLIMP2 (**Fig. 3.18E(ii)**).

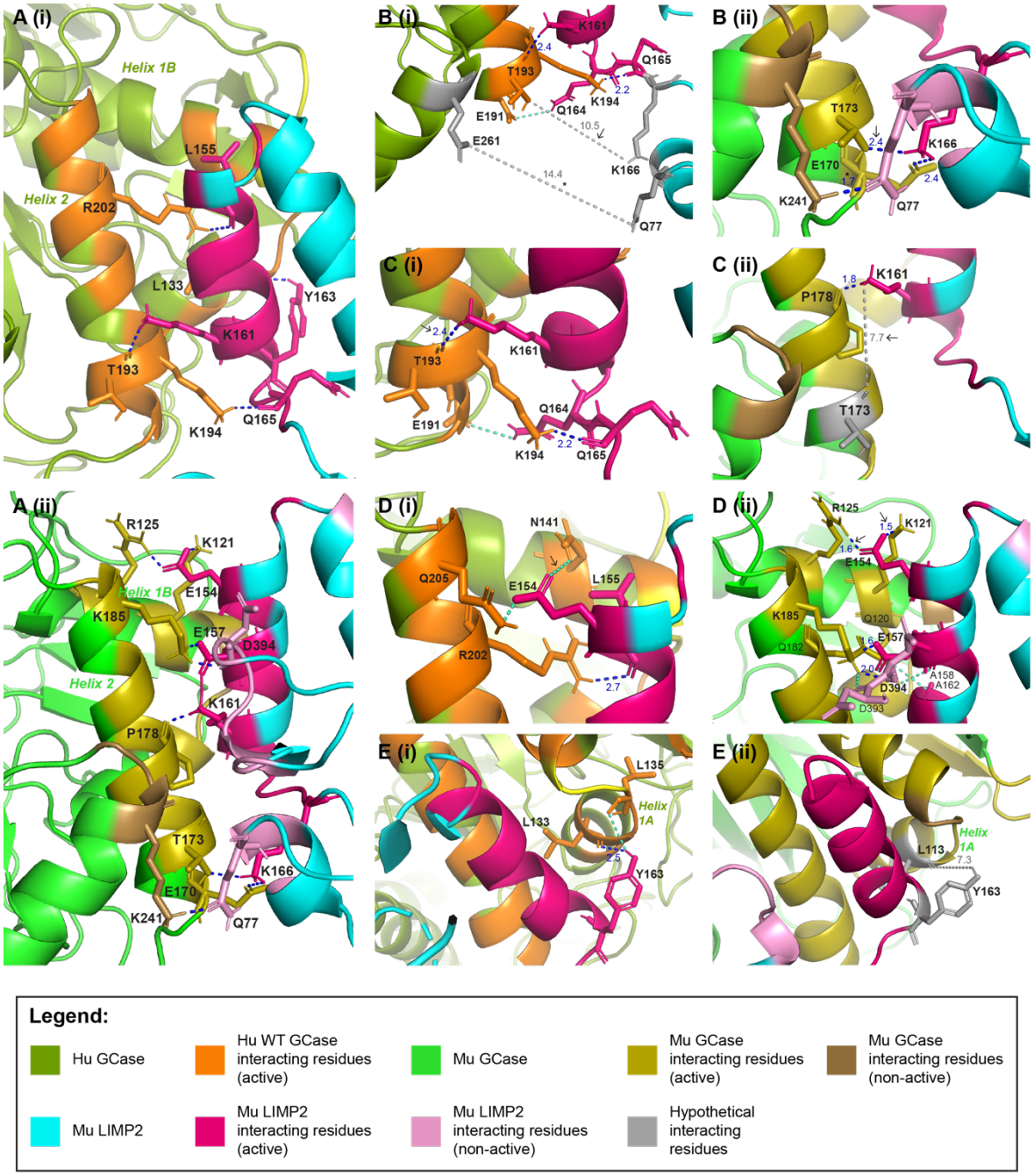


Figure 3.18: The structural conformation and polar interactions of the HuGCase-MuLIMP2 and MuGCase-MuLIMP2 complexes. (**A**) The conformation of the interaction interface for HuGCase-MuLIMP2 (**i**) and MuGCase-MuLIMP2 (**ii**). (**B-E**) Magnified views of key polar contacts in HuGCase-MuLIMP2 (**i**) and MuGCase-MuLIMP2 (**ii**). Active residues are those that have previously been implicated in the GCase-LIMP2 interaction, whereas non-active residues have not. Strong polar contacts are highlighted in dark blue, weaker polar contacts are coloured light blue and illustrative distances between "hypothetical interacting residues" (shown for comparative purposes only) are indicated in grey. (**B-D**) Key interactions are highlighted by an * or ↓. (**D(ii)**) Residues Q182, Q120, A158, A162 and D393 are not bolded to illustrate that they participate in weaker interactions only, whereas bolded residues in this panel mediate strong polar contacts.

Lastly, the conformation and affinity of the HuGCase-MuLIMP2 and HuGCase-HuLIMP2 complexes were compared. Strikingly, the affinity of the HuCase-HuLIMP2 complex is 100-fold higher than the HuCase-MuLIMP2 complex (Kd 4e-09 vs Kd 2.5e-07, respectively) (**Fig. 3.16 A**). Supporting this, HuCase-HuLIMP2 has more interacting residues in total (**Fig. 3.16 A**), a lower proportion of the weaker apolar-apolar interactions (**Fig. 3.16 B**) and a greater proportion of hydrogen bonds (**Fig. 3.16 C**) vs HuGCase-MuLIMP2. Many non-active residues form strong polar contacts both within (**Fig. 3.19 A(ii)**) and outside (**Fig. A-2 D**) the major interacting region of the HuCase-HuLIMP2 complex; whereas, strong polar interactions in the HuCase-MuLIMP2 complex are restricted to the active residues within the primary binding region (**Fig. 3.19 A(i) and Fig. A-2 A**). The polar interactions at the major interaction site are also individually stronger in the HuGCase-HuLIMP2 complex; polar contact bond length is less than 2.0 Å in HuCase-HuLIMP2 (**Fig. 3.19B(ii)**) vs 2.2-2.7 Å in HuCase-MuLIMP2 (**Fig. 3.16 B-D(i)**). All of these factors combined likely underlie the higher affinity of the HuGCase-HuLIMP2 complex. The relative conformation of GCase and LIMP2 is also different across both complexes; the orientation of GCase relative to LIMP2 appears inverted in HuGCase-HuLIMP2 compared to HuGCase-MuLIMP2 (**Fig. 3.19 B**). In the HuGCase-MuLIMP2 complex (**Fig. 3.19 B(i)**), residues T193 and K161 strongly interact (2.4 Å), but these residues are 20.8 Å apart in HuGCase-HuLIMP2 (**Fig. 3.19 B(ii)**). Likewise, the bond length of the polar contact between residues K194 and Q165 in HuGCase-MuLIMP2 is 2.2 Å (**Fig. 3.19 B(i)**) but in HuGCase-HuLIMP2 these residues are 22.1 Å apart (**Fig. 3.19 B(ii)**). It is also noteworthy that H150 on human LIMP2 forms a strong polar contact with K194 on human GCase because this H150 residue is not conserved on mouse LIMP2 (**Fig. 3.19 A-B(ii)**). T150 is the equivalent residue on mouse LIMP2 (**Fig. 2.4**) and this residue does not strongly interact with GCase across any of the other complexes.

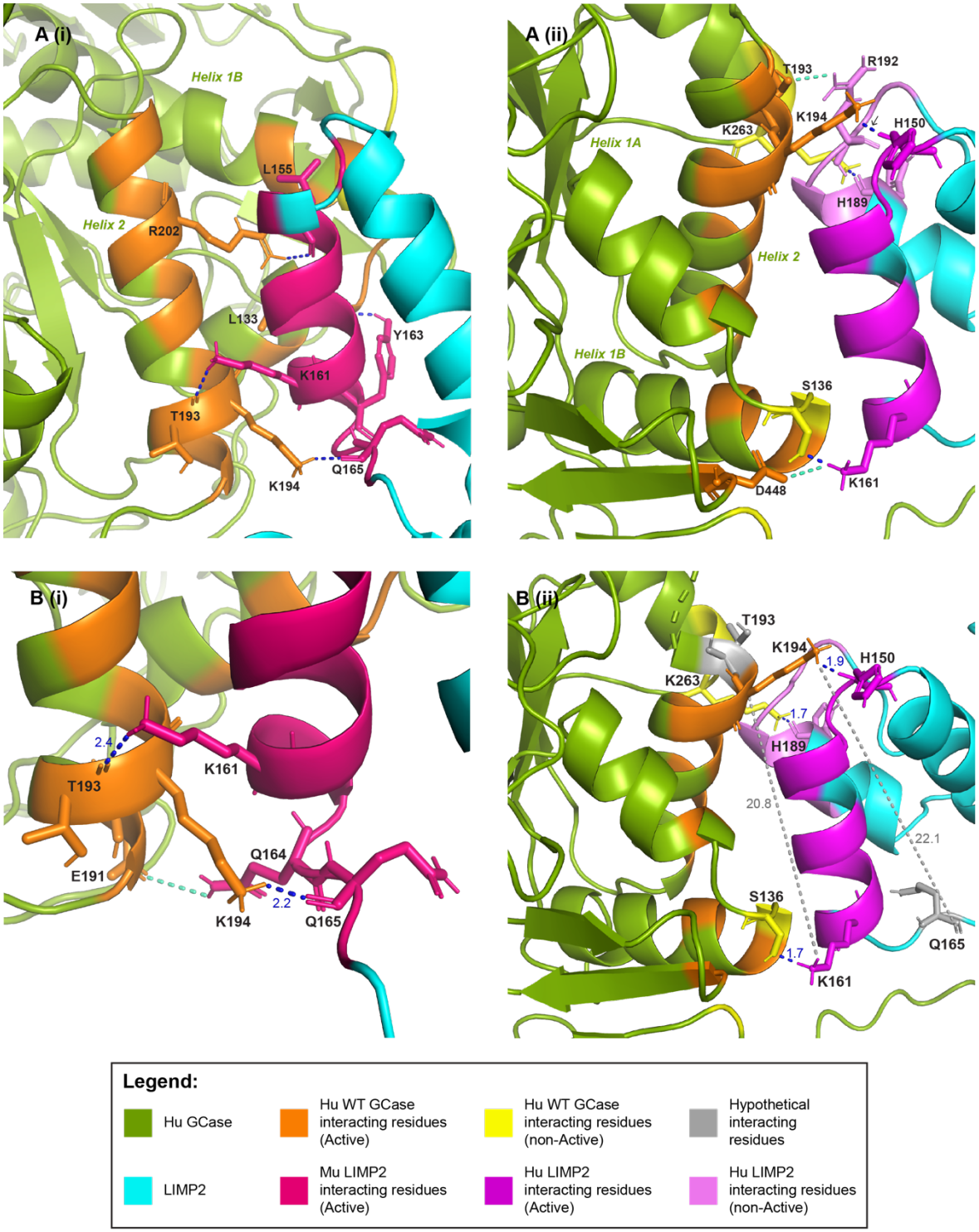


Figure 3.19: The structural conformation and polar interactions of the HuGCase-MuLIMP2 and HuGCase-HuLIMP2 complexes. (**A**) The conformation of the interaction interface for HuGCase-MuLIMP2 (**i**) and HuGCase-HuLIMP2 (**ii**). (**B**) Comparison of the distance between GCase-LIMP2 residue pairs: T193-K161 and K194-Q165, to illustrate differences in the conformation of the complexes. These residues form strong polar contacts (dark blue) in HuGCase-MuLIMP2 (**i**) but are > 20 Å apart (grey, "hypothetical interacting residues") in HuGCase-HuLIMP2 (**ii**). Active residues are those that have previously been implicated in the GCase-LIMP2 interaction, whereas non-active residues have not. Strong polar contacts are highlighted in dark blue, weaker polar contacts are coloured light blue and illustrative distances between "hypothetical interacting residues" are indicated in grey. (**B(ii)**) The interaction between K194 and H150 is marked by an ↓.

3.3 DISCUSSION

3.3.1 L444P MICE DISPLAY PHENOTYPES RELATED TO GAIN-OF-FUNCTION AND LOSS OF GCASE ACTIVITY

As gain- and loss-of-function effects of *GBA* mutations cooperate in the pathology of *GBA*-associated PD (Yoon et al., 2024), this chapter initially explored whether these effects are recapitulated in the cortex of L444P mice. Firstly, I observed that the high MW form of human GCase was significantly elevated in the cortex of L444P vs hWT mice (**Fig. 3.2 B(i)**). This finding corroborates the accumulation of high MW, Endo-H sensitive L444P GCase in the midbrain (**Fig. 3.1 A-B**). Presuming that this high MW cortical GCase is also Endo-H sensitive, this phenotype indicates that mutant GCase is entrapped in the ER, thereby illustrating a gain-of-function effect of the L444P mutation in the cortex of our model. Elevated Endo-H sensitive mutant GCase has previously been observed in iPSC-DAns (Fernandes et al., 2016), fibroblasts (Bendikov-Bar et al., 2011, McNeill et al., 2014, Ron and Horowitz, 2005), *Drosophila* (Maor et al., 2013), and midbrain organoids (Frattini et al., 2024). However, our observations in midbrain and cortex are the first demonstrations of high MW GCase accumulation in a mouse model of *GBA*-associated PD. On the other hand, the comparable levels of total GCase expression in the cortex of hWT and L444P mice reflects the equivalent location and expression levels of the human transgene across these genotypes. This finding also suggests that proteasomal degradation of L444P GCase is not upregulated in this region (**Fig. 3.2 B(ii)**).

Having identified gain-of-function related effects of the L444P mutation, I next examined whether GCase activity is attenuated in the L444P cortex. GCase activity was significantly reduced in primary cortical cultures from L444P and *Gba*$^{+/-}$ mice (**Fig. 3.3 B**). This is the first demonstration of GCase activity deficits in primary cortical cultures from a mouse model harbouring a heterozygous *GBA* mutation. This phenotype also agrees with

previous observations of GCase activity deficits in primary cortical neurons from *Gba*$^{+/-}$ mice (Magalhaes et al., 2018) and in iPSC-DAns and fibroblasts from *GBA*-associated PD patients (Ambrosi et al., 2015, Fernandes et al., 2016, Schondorf et al., 2014). Notably, cortical and hippocampal neurons from *Gba*$^{+/L444P}$ mice have been shown to display mitochondrial, lysosomal and autophagy deficits (Li et al., 2019a, Mahoney-Crane et al., 2023, Yun et al., 2018). Future studies could explore if these phenotypes are also evident in cortical cultures from our L444P model, using live cell imaging approaches. For example, mitochondrial membrane potential and reactive oxygen species (ROS) production could be assessed with JC-10 and MitoSOX dyes, respectively, whereas lysosomal activity could be measured with a DQ-BSA assay (Liao et al., 2020, Sivandzade et al., 2019, Frost et al., 2017). It would also be useful to measure *in situ* GCase activity in our primary cultures, e.g. using the 5-(Pentafluorobenzoylamino) Fluorescein Di-β-D-Glucopyranoside (PFB-FDGlu) fluorescent probe. Live measures of lysosomal GCase activity offer advantages over the *in vitro* 4-MUG assay by accounting for the effect of lysosomal pH and availability of GCase's cofactor SapC (Ysselstein et al., 2021).

3.3.2 AMBROXOL FAILED TO RESCUE GCASE ACTIVITY DEFICITS IN L444P PRIMARY CORTICAL CULTURES

Considering ambroxol's demonstrated effectiveness at enhancing GCase activity in various preclinical models (**Section 1.3.4**), I sought to assess whether this compound could rescue GCase activity deficits in primary cultures from the L444P mice (**Fig. 3.3 B**). Firstly, ambroxol significantly increased GCase activity in cultures from nTG mice, reflecting previous studies in primary cortical cultures and cortex tissue from WT mice (Magalhaes et al., 2018, Migdalska-Richards et al., 2016). On the other hand, the subtle increase in hWT GCase activity following ambroxol exposure (+11%) did not reach significance. This may signal differences in ambroxol's efficacy at human vs mouse GCase, as previously observed

for other GCase activators (Berger et al., 2015). Indeed, studies in transgenic mice have shown that ambroxol significantly enhances mouse L444P GCase activity but not human L444P GCase activity (Migdalska-Richards et al., 2016, Sanders et al., 2013). In accord with this, ambroxol failed to restore GCase activity deficits in cultures from our humanised L444P model, although the inconsistency in ambroxol's effectiveness between Migdalska-Richards et al. (2016) and Sanders et al. (2013) may be due to the different drug dosage regimens employed by these studies. Nevertheless, my findings also mirrored Sanchez-Martinez et al. (2016), who demonstrated that 5 μM ambroxol increased GCase activity in WT, but not L444P, fibroblasts. Taken together, these results may indicate that ambroxol's effect is stronger on WT vs L444P-GCase activity.

However, it should also be noted that using a higher concentration of ambroxol in future studies may significantly improve GCase activity in cultures from L444P and *Gba*$^{+/-}$ mice. A 10 μM concentration was chosen based on previous demonstrations of positive effects in WT mouse primary cortical neurons (Magalhaes et al., 2018). In hindsight, treating cells with 30 μM of ambroxol may have been preferable because this concentration was previously shown to increase GCase activity in *Gba*$^{+/-}$ primary cortical neurons (Magalhaes et al., 2018). Considering that ambroxol can inhibit GCase activity and induce cytotoxicity at high concentrations (Magalhaes et al., 2018, Ysselstein et al., 2021), the optimal concentration of ambroxol for these cultures should be established by measuring GCase activity in response to titrated ambroxol concentrations. Furthermore, investigating ambroxol's effect on GCase activity in isolated lysosomes from our model may also reveal a stronger upregulation of GCase activity vs measurements in whole cell lysates. Indeed, ambroxol previously increased GCase activity to a larger extent in lysosomal vs whole-tissue fractions from *Gba*$^{+/L444P}$ mice (Migdalska-Richards et al., 2016). Future studies could also assess if ambroxol can improve other pathological phenotypes in our L444P model, despite

its inability to restore L444P GCase activity in my cortical cultures. Regarding this, ambroxol decreased ER stress and rescued behavioural deficits, but had no effect on GCase activity, in *Drosophila* expressing L444P- or N370S-GCase (Sanchez-Martinez et al., 2016). The GCase activity deficits observed in primary cultures from our L444P model also provide a platform to test other pharmacological GCase modulators. Non-inhibitory chaperones e.g. NCGC607 (Aflaki et al., 2016) and direct GCase activators e.g. S-181 (Burbulla et al., 2019) are of special interest because, unlike ambroxol, these molecules bind outside of GCase's active site and therefore do not compete with GCase lipid substrates (Han et al., 2020, Martinez-Bailen et al., 2022).

3.3.3 CHANGES TO GCASE ACTIVITY, ER HOMEOSTASIS OR LYSOSOMAL/AUTOPHAGIC FUNCTION WERE NOT DETECTED IN L444P CORTEX TISSUE

As GCase activity was significantly reduced in L444P primary cortical cultures, I next sought to investigate whether this deficit is also evident in cortex tissue from L444P mice aged 3- and 15-21-months-old. Although GCase activity was slightly reduced in L444P cortical tissue, this deficit did not reach significance at either age (**Fig. 3.4**). In contrast to these results, GCase activity is significantly reduced in the cortex of *Gba*$^{+/L444P}$ models (Mahoney-Crane et al., 2023, Migdalska-Richards et al., 2016, Migdalska-Richards et al., 2017b). Differences in GCase vulnerability across cortical subregions could explain the discrepancy between my findings, using whole cortex homogenates, and those of Mahoney-Crane et al. (2023), who detected deficits specifically in prefrontal cortex of *Gba*$^{+/L444P}$ mice. Supporting this theory, GCase activity is also impaired to varying degrees across cortical subregions in post-mortem PD brains (Leyns et al., 2023, Murphy et al., 2014). Moreover, other studies have found that GCase activity is normal in the cortex, but significantly reduced in the SN of PD patient brains vs non-PD brains (Blumenreich et al., 2024,

Chiasserini et al., 2015, Gegg et al., 2012, Moors et al., 2019, Rocha et al., 2015a)[5]. These findings reflect the regional differences in our model, considering that GCase activity is impaired in the midbrain, but not the cortex, of L444P mice. The factors controlling this region-specific GCase vulnerability remain elusive, although GCase activity has been shown to negatively correlate with αS expression levels across brain regions in mice and post-mortem samples (Ikuno et al., 2019, Murphy et al., 2014).

However, it is also possible that GCase activity deficits were not detected in L444P cortex tissue because the enzymatic reaction in my 4-MUG assay was not occurring at its maximum rate throughout. In an *in vitro* enzymatic activity assay, the enzyme concentration should be proportional to the product formed when reactions are occurring within the linear range, i.e. at their maximum rate (Bisswanger, 2014). This might not hold true in my study because the 50% reduction in GCase enzyme levels in the *Gba*$^{+/-}$ mice was not associated with an equivalent impairment in enzymatic activity. We may therefore suspect that genotype-related differences are underestimated in our assay, which could mask potential deficits in the L444P cortex. Future work should optimise the concentration of substrate relative to enzyme to ensure that GCase is saturated and can therefore hydrolyse 4-MUG at its maximum rate throughout the assay. Indeed, a lower concentration of GCase enzyme relative to 4-MUG substrate was used to detect GCase activity deficits in my primary cultures (**Fig. 3.3, Table 2.7**) and by Mahoney-Crane et al. (2023) in cortex tissue. This may explain the discrepancy between these studies and phenotypes observed in cortex tissue from our L444P mice.

Furthermore, my experiments did not find evidence to suggest that the accumulation of high MW GCase or loss of cellular GCase activity was associated with ER stress or

[5] Unaltered cortical GCase activity has not been universally observed, as Leyns et al. (2023) and Murphy et al. (2014) observed GCase activity deficits in post-mortem cortex.

autophagic/lysosomal deficits in the L444P cortex: the expression levels of BiP, LC3 and LAMP1 were similar across genotypes on western blots with cortical tissue homogenates (**Fig. 3.5-3.6**). Supporting these findings, ER stress and autophagic/lysosomal dysfunction have not been widely identified in existing transgenic mouse models of *GBA*-associated PD (**Table 1.3**). Notably, Rocha et al. (2015c) found that LC3-II was elevated in CBE-treated mice; however, studies investigating LC3 levels in *Gba*$^{+/L444P}$ mice have produced largely inconsistent results (**Table 1.3**). Indeed, much of the evidence for these phenotypes derives from cellular models of the disease (Pradas and Martinez-Vicente, 2023) (**Section 1.3.3.1-1.3.3.2**). For example, increased expression of LAMP1, LC3-II and BiP has been demonstrated in iPSC-DAns from *GBA*-associated PD patients (Fernandes et al., 2016, Schondorf et al., 2014, Schondorf et al., 2018). Considering that disease-relevant neuronal changes may therefore be masked when measuring protein levels in whole tissue homogenates, it would be useful to probe lysosomal/autophagic function and ER homeostasis specifically in neurons from our mouse model.

3.3.4 GLCSPH ACCUMULATES IN THE BRAIN AND VISCERA OF *GBA*$^{+/-}$ MICE

Although the build-up of GlcCer and GlcSph due to GCase deficiency is central to GD pathology (Dekker et al., 2011, Revel-Vilk et al., 2020, Rolfs et al., 2013, Stirnemann et al., 2017), the relevance of glycosphingolipid accumulation to the pathology of *GBA*-associated PD is uncertain (**Section 1.3.3.1**) (Blumenreich et al., 2022, Gleason et al., 2022a, Huebecker et al., 2019, Leyns et al., 2023, Milenkovic et al., 2022, Surface et al., 2022). To investigate if defective GCase activity elevates glycosphingolipid species in our L444P model, lipidomic analysis was conducted in the brain, liver and spleen across genotypes.

GlcCer levels were normal in L444P and *Gba*$^{+/-}$ mice (**Fig. 3.7 A, 3.9 A**), whereas GlcSph was significantly elevated in the brain, liver and spleen of *Gba*$^{+/-}$ mice (**Fig. 3.7 C,**

3.9 C). L444P mice also displayed significant GlcSph accumulation in the spleen, whilst GlcSph was elevated in the liver and spleen of hWT mice (**Fig. 3.9 C**). Taken together, these findings largely agree with observations of elevated GlcSph and unchanged GlcCer in other mouse models of *GBA*-associated PD and GD (**Table 1.3**) and in PD patient derived samples and post-mortem brains (**Section 1.3.3.1**). Notably, in the current study, the extent of GlcSph accumulation was typically larger in visceral organs compared to the brain. This may be because more GlcCer is available to be converted to GlcSph in the liver and spleen; GlcCer concentrations were over 10-fold higher in these organs vs the brain (**Fig. 3.7 A, 3.9 A**).

Previously, GCase activity was shown to be the biggest determinant of GlcSph levels in *GBA*-associated PD patient brains (Leyns et al., 2023). This finding may explain why GlcSph accumulation was observed in the midbrain of $Gba^{+/-}$ mice but not L444P mice given that loss of midbrain GCase activity was greater in $Gba^{+/-}$ mice at 3-months-old (**Fig. 3.1 C**). Furthermore, in agreement with Leyns et al. (2023), no significant differences in GCase activity or GlcSph levels were identified in $Gba^{+/-}$ cortex tissue (**Fig. 3.4, 3.7 C(iii))**, whereas significant GCase activity deficits coincided with GlcSph accumulation in the midbrain of these mice (**Fig. 3.1 C, 3.7 C(i)**). Notably, Ikuno et al. (2019) also did not detect changes to GlcSph in the $Gba^{+/-}$ cortex. On the other hand, the elevated GlcSph in the viscera of hWT mice warrants further investigation and is discussed further in **Section 3.3.6**.

As GlcSph progressively accumulates with age in WT mice and $Gba^{+/L444P}$ mice (Hallett et al., 2018, Mahoney-Crane et al., 2023, Lado et al., 2024), it would be interesting for future studies to analyse the impact of ageing on GlcSph levels in our model. Moreover, although the two-fold increase in GlcSph of $Gba^{+/-}$ mice reflects the extent of GlcSph accumulation in a $Gba^{+/L444P}$ mouse model (Mahoney-Crane et al., 2023, Lado et al., 2024) and PD patient plasma (Surface et al., 2022), it is much lower than the >100 fold elevation observed in GD patient plasma (Dekker et al., 2011, Revel-Vilk et al., 2020). Therefore, it

is unclear if the extent of GlcSph accumulation is sufficient to directly confer toxicity in the brains of *Gba*$^{+/-}$ mice, despite previous studies *in vitro* demonstrating that GlcSph can promote αS pathology (**Section 1.3.3.3**) and induce lysosomal/autophagic deficits (Kumar et al., 2023, Srikanth et al., 2021).

Notably, one limitation of our study was that our detection method did not allow for the separation of species with different hydrocarbon chain lengths. Hexosylceramides (glucosyl- and galactosylsphingosine) with shorter acyl chains have been proposed to mediate αS aggregation in *GBA*-associated PD fibroblasts (Galvagnion et al., 2022). Changes in the relative abundance of sphingolipids of different chain lengths have also been reported in post-mortem brains (Abbott et al., 2014, Munoz et al., 2024) and iPSC-DAns and fibroblasts from PD patients (Fernandes et al., 2016, Galvagnion et al., 2022).

On the other hand, a major advantage of our lipidomic analysis was that glucosylated glycosphingolipids (GlcCer and GlcSph) could be separated from their galactosylated isobaric isomers (GalCer and GalSph, respectively) with a HILIC column, as described in Lelieveld et al. (2022). These pairs of isobaric isomers only differ in the stereochemistry of the 4'-hydroxyl group, which makes them challenging to separate without specialised equipment (Boutin et al., 2016, Milenkovic et al., 2022). Changes to GalCer and GalSph have not been widely implicated in *GBA*-associated PD (Leyns et al., 2023), in agreement with **Fig. A-1**. However, as these galactosyl isoforms are more abundant than glucosyl isoforms in the human and mouse brain (Boutin et al., 2016, Matsumoto et al., 2022) (**Fig. 3.7 A, C** and **Fig. A-1**), potential disease-relevant changes to GlcCer and GlcSph can be masked using techniques that do not distinguish between glucosyl- and galactosyl- species.

We also found that GlcChol was unaltered across genotypes (**Fig. 3.8 B**), in agreement with findings in PD patient plasma (Surface et al., 2022). Cholesterol levels were also comparable across genotypes in this study (**Fig. 3.8 A**), in contrast to the elevated cholesterol

levels in *GBA* mutant and GCase deficient cells (Garcia-Sanz et al., 2017, Magalhaes et al., 2016, Navarro-Romero et al., 2022). Notably, Navarro-Romero et al. (2022) has shown that cholesterol was specifically elevated in lysosomal-enriched fractions, and not whole cell lysates from *GBA* mutant neurons. It is also possible that the mixed cell population in our tissue samples conceals neuronal-specific lipid dyshomeostasis in our L444P model (Suzuki et al., 2018). It would therefore be interesting to measure lipid species specifically in neurons or isolated lysosomal fractions from our mice.

3.3.5 THE SUBCELLULAR DISTRIBUTION OF αS WAS UNCHANGED ACROSS GENOTYPES

The relative proportions of $\alpha S_{mem.}$ and $\alpha S_{sol.}$ were investigated across brain regions in mice aged 3 months and 15-22 months (**Fig. 3.10-3.11**). Although the subcellular distribution of αS has not been previously investigated in a *GBA*-associated PD mouse model, multiple lines of evidence suggest that the localisation of αS with lipid membranes may be altered in our L444P or $Gba^{+/-}$ mice.

Firstly, Dr Natalie Connor-Robson has previously shown that mean levels of αS oligomers accumulate in the aged L444P and $Gba^{+/-}$ SN (**Fig. 3.1 D**). This may be associated with increased $\alpha S_{mem.}$ in these mice, considering that αS-membrane binding accelerates the formation of toxic αS oligomers and insoluble aggregates (Galvagnion et al., 2015, Lee et al., 2002, Suzuki et al., 2018). Secondly, GCase deficiency increases levels of aggregation-prone αS monomers through destabilisation of physiological αS tetramers, whereas overexpression of WT GCase improves tetramer stability (Glajch et al., 2021, Kim et al., 2018c). These studies also support a hypothetical heightened association of αS with lipid membranes in L444P cells, given that most membrane-associated αS is monomeric, while αS tetramers are primarily cytosolic (Dettmer et al., 2015, Wang et al., 2011, Bartels et al.,

2011, Westphal and Chandra, 2013). Thirdly, membranes of *GBA*-L444P fibroblasts have a higher abundance of sphingolipids with short acyl chain lengths and incubation of lipids from these cells with αS accelerated αS aggregation (Galvagnion et al., 2022). Given that αS prefers to interact with fluid membranes (Galvagnion et al., 2016), the predominance of short chain sphingolipids in the L444P membrane may also increase αS co-localisation with membranes by increasing membrane fluidity (Galvagnion et al., 2022, Mencarelli and Martinez-Martinez, 2013).

Despite these indications, no changes to the intracellular distribution of αS were observed in the L444P or $Gba^{+/-}$ mice (**Fig. 3.10-3.11**). One possibility is that the mixed cell population in the tissue homogenates is masking neuronal-specific changes. Previously, significant αS accumulation was demonstrated in neuronal cultures, but not in whole brain tissue homogenates, from a $Gba^{+/L444P}SNCA^{A53T}$ mouse model (Fishbein et al., 2014), illustrating the advantage of measuring αS in isolated neurons. It also should be noted that αS is known to be primarily localised to the cytosol, as demonstrated by studies in neuronal cultures (Dettmer et al., 2013) and in mouse (Burre et al., 2013), zebra finch (George et al., 1995) and human brains (Dettmer et al., 2015, Irizarry et al., 1996, Sanderson et al., 2020). In this ELISA-based assay, we would expect $αS_{mem.}$ to represent up to approximately 30% of the total αS present (Dr Tim Bartels, personal communication). However, the mean proportion of $αS_{mem.}$ reached almost 60% in some regions (**Fig. 3.10. A(ii)-(iii)**). Technical factors, including extraction solution composition and the temperature of the ELISA-based MSD immunoassay, can influence these αS proportions and should therefore be optimised in future experiments. Also, this study would have benefitted from the inclusion of samples from *SNCA*-OVX mice (Janezic et al., 2013) and *Snca*-KO mice (Senior et al., 2008) as positive and negative controls, respectively.

As GCase deficiency can promote αS to shift toward its unstable monomeric state (Kim et al., 2018c) and αS monomers have increased propensity to form toxic oligomers (Dettmer et al., 2016), it would be interesting for future studies to investigate if the αS tetramer:monomer ratio is altered in our model, using a disuccinimidyl glutarate (DSG) cross-linking assay (Bartels et al., 2011, Dettmer et al., 2013). Furthermore, pharmacological GCase inhibition and heterozygous *GBA* mutations have been reported to increase αS secretion into the media of neuronal cultures (Fernandes et al., 2016, Gegg et al., 2020, Magalhaes et al., 2016). Future studies could also probe if this is recapitulated in mixed cortical cultures from our L444P or *Gba*$^{+/-}$ mice.

3.3.6 THE STRENGTH AND CONFORMATION OF GCASE-LIMP2 INTERACTIONS IN OUR HUMANISED *GBA* MICE MAY DIFFER FROM THE HUMAN ENVIRONMENT

Impaired ER-lysosomal translocation of mutant GCase is a widely reported feature of *GBA*-associated PD (Chatterjee and Krainc, 2023). Although L444P GCase is capable of binding to LIMP2 (Reczek et al., 2007), no studies have investigated whether the L444P mutation directly reduces the strength of GCase binding to LIMP2. To examine this, the conformation and affinity of the GCase-LIMP2 interaction was compared across docked HuGCase-MuLIMP2 and HuL444PGCase-MuLIMP2 complexes. As the scope of this study was limited to L444P's potential influence on the GCase-LIMP2 interaction in our mouse model, a HuL444PGCase-HuLIMP2 complex was not generated.

This study did not find evidence that the L444P mutation diminishes the strength of the GCase-LIMP2 interaction (**Fig. 3.16 A**). Instead, LIMP2's affinity for L444P-GCase was slightly higher than its affinity for WT GCase. Similarly, previous PRODIGY-based predictions indicated that LIMP2 has a higher affinity for E326K-GCase vs WT GCase, although the functional implications of this finding were not explored (Pietrafesa et al.,

2024). Indeed, the pathophysiological-relevance of LIMP2's predicted higher affinity for L444P-GCase is unclear, especially since many of the residues that form polar contacts are conserved across HuGCase-MuLIMP2 and HuL444PGCase-MuLIMP2 and the structural conformations of these complexes are similar (**Fig. 3.17**). These findings largely reflect the L444P mutation's distant position from the GCase-Limp2 binding interface (**Fig. 3.13**). In contrast, LIMP2 may have lower affinity for D409H-GCase given that the interaction between D409 on WT GCase and K181 on LIMP2 was shown to be integral for the formation of the GCase-LIMP2 complex (Dobert et al., 2025).

Future studies should seek to explore other mechanisms related to L444P-GCase lysosomal trafficking defects in our model. Aside from direct effects of *GBA* mutations on the conformation and strength of GCase-LIMP2 binding, increased ERAD of the GCase-LIMP2 complex also likely contributes to aberrant GCase trafficking in PD. For instance, reduced GCase-LIMP2 co-localisation in L444P-mutant cells was attributed to ER stress and proteolytic degradation of the GCase-LIMP2 complex (Dobert et al., 2024). The D409H mutation has also been indicated to promote ERAD of this complex (Dobert et al., 2025). In addition, αS accumulation has been associated with impaired GCase trafficking in PD (Gegg et al., 2012, Mazzulli et al., 2011, Murphy et al., 2014). On the other hand, it remains controversial whether changes to LIMP2 expression alters GCase transport to the lysosome in PD. Although GCase activity and post-ER GCase levels are reduced in LIMP2-deficient models (Pavan et al., 2024, Reczek et al., 2007, Rothaug et al., 2014, Stojkovska et al., 2022), there are conflicting reports of increased (Rothaug et al., 2014), decreased (Thomas et al., 2021) and unchanged (Gegg et al., 2012, Murphy et al., 2014) LIMP2 levels in PD, with different implications for GCase activity and trafficking.

This chapter also presents the first direct interspecies comparison of GCase-LIMP2 interaction dynamics across human and mouse. Protein interactions were more abundant and

polar bonds were individually stronger in the MuGCase-MuLIMP2 and HuGCase-HuLIMP2 complexes vs the HuGCase-MuLIMP2 complex (**Fig. 3.16, 3.18, 3.19**). Together, these factors contribute to the predicted binding affinity of HuGCase-MuLIMP2 being 10-fold lower than MuGCase-MuLIMP2 and 100 fold lower than HuGCase-HuLIMP2 (**Fig. 3.16 A**). In light of these findings, we could speculate that mouse LIMP2 preferentially traffics mouse vs human GCase to the lysosome in our humanised transgenic mice and that less human GCase reaches the lysosome in our mice vs in the human environment. Aberrant binding of human GCase to mouse LIMP2, and consequential lysosomal translocation deficits, may underlie the elevated GlcSph in the viscera of hWT mice (**Fig. 3.9 C**), considering these mice have normal GCase activity (**Fig. 3.3-3.4**). However, functional relevance cannot be inferred from these computational predictions alone.

Along with the broad spectrum of binding affinities across GCCase-LIMP2 complexes, some remarkable differences in the conformation of the GCase-LIMP2 interaction were observed across species. Also, certain human LIMP2 residues, which are not conserved on mouse LIMP2, formed strong polar contacts in the HuGCase-HuLIMP2 complex (**Fig. 3.19**). This included human LIMP2 H150, which is T150 on mouse LIMP2 (**Fig. 2.4**). H150 is a reported pH sensing residue that has been proposed to trigger conformational changes that mediate binding and lysosomal-dissociation of human LIMP2 and GCase (Liou et al., 2014, Zhao et al., 2014). Interestingly, human H150T-mutant LIMP2 has a weakened binding affinity for human GCase and impaired dissociation from GCase in acidic conditions that mimic the lysosomal environment (Zhao et al., 2014). T150 on mouse LIMP2 may therefore contribute to the lower affinity of the HuGCase-MuLIMP2 complex and disturb the lysosomal separation of human GCase and mouse LIMP2. Overall, these predictions highlight that the pH sensing mechanisms, and related conformational changes, underlying

HuGCase-MuLIMP2 binding and dissociation in our model may be fundamentally different to those governing GCase-LIMP2 interactions in the human environment.

There are some noteworthy limitations to the computational methods used in this study. Firstly, the conformation of the docked GCase-LIMP2 complexes was predicted based on "active residues" that were previously reported to be involved in this interaction (Liou et al., 2014, Reczek et al., 2007, Zunke et al., 2016) (**Fig. 2.3-2.4**). A cryo-TEM structure of the HuGCase-HuLIMP2 complex, published after these predictions were generated, confirmed the involvement of some of these residues (Dobert et al., 2025). However, many of the interfacing residues in the cryo-TEM complex were distinct from those considered in this study. The docked complexes presented in this chapter should therefore be revised in future to account for this updated information. Also, the experimentally-determined structure confirmed that the GCase-LIMP2 interface is composed of a hydrophobic core (Dobert et al., 2025), whereas only polar interactions were explored in this study. Moreover, GCase's glycan chains were not modelled in AlphaFold's predicted structures before conducting protein-protein docking with HADDOCK. Given the importance of glycosylation for GCase structure and stability (Bergfussman et al., 1993, Pol-Fachin et al., 2016), incorporating these glycan chains into the docking predictions may impact the conformation and strength of GCase's interaction with LIMP2. Finally, the active residues on mouse GCase and LIMP2 were defined based on sequence alignment to the previously reported active residues on human GCase and LIMP2, respectively (Liou et al., 2014, Reczek et al., 2007, Zunke et al., 2016) (**Fig. 2.4**). However, whether the interacting residues on mouse GCase and LIMP2 directly map to the interacting residues on their respective human proteins remains to be established because the MuGCase-MuLIMP2 complex has not been experimentally characterised. Nevertheless, this assumption is reasonable considering that the interfacing residues in the human proteins are well-conserved in mice (Dobert et al., 2025). Also, both

proteins have a high level of gene-sequence homology, over 85% amino acid sequence similarity and are structurally alike across human and mouse (Gasteiger et al., 2003, Liou et al., 2019, O'Neill et al., 1989, Tabuchi et al., 1997).

Further experiments are needed to validate my computational predictions and to determine potential functional implications of the identified species-related differences. For example, pull-down assays would provide a simple readout of the extent of the GCase-LIMP2 interaction across complexes. These experiments have previously revealed negative effects of various *GBA* mutations on GCase-LIMP2 binding (Dobert et al., 2024, Dobert et al., 2025). Surface plasmon resonance analyses have also determined the Kd of the HuGCase-HuLIMP2 interaction and can model how GCase-LIMP2 binding changes across distinct cellular compartments by manipulating the pH conditions (Zhao et al., 2014). This approach could help to clarify if lysosomal separation of the HuGCase-MuLIMP2 complex is impaired, as previously observed for HuGCase-HuH150TLIMP2 (Zhao et al., 2014). Moreover, GCase activity assays in lysosomal fractions could elucidate whether the predicted low HuGCase-MuLIMP2 binding affinity translates to impaired lysosomal trafficking of hWT GCase in our model. Such deficits would not be revealed using the *in vitro* 4-MUG GCase assay with whole tissue lysates. Lastly, this study could be expanded in future to investigate the impact of the L444P mutation and interspecies differences on GCase's interaction with its other known binding partners. For example, it would be particularly interesting to elucidate the GCase-SapC interaction in our model, considering that the L444P mutation may directly impair GCase binding to SapC (Atrian et al., 2008, Grace et al., 1994, Liou et al., 2006, Romero et al., 2019).

3.3.7 CONCLUSION

In conclusion, this chapter demonstrated that our L444P mouse model recapitulates gain-of-function and loss-of-function effects of the L444P mutation in the cortex. However, my

experiments did not identify elevated ER stress, dysfunction in the lysosomal-autophagy pathway, glycosphingolipid accumulation or changes to the subcellular distribution of αS in the brains of L444P mice. On the other hand, GlcSph was elevated in the viscera of L444P mice. Moreover, computational predictions indicated that the L444P mutation does not overtly perturb GCase-LIMP2 binding in our model, whereas the conformation and strength of this interaction may fundamentally differ according to species. In future, probing pathology in isolated neurons or lysosomal fractions could unveil genotype-related differences that are potentially masked in whole tissue homogenates. Experiments in the next chapter seek to elucidate the L444P mutation's impact on DA release dynamics in the striatum of our humanised model.

CHAPTER 4: THE IMPACT OF THE L444P MUTATION ON STRIATAL DOPAMINERGIC TRANSMISSION

4.1 INTRODUCTION

Approximately 30-50% of DA neurons in the SN have insidiously degenerated by the time motor symptoms manifest in PD patients (Cheng et al., 2010, Fearnley and Lees, 1991). A complex interplay of dysfunctional and compensatory changes to striatal DA homeostasis has therefore been proposed to occur in the prodromal phase of disease (Cramb et al., 2023, Blesa et al., 2017). Indeed, numerous rodent models of PD display synaptic dysregulation and striatal DA release deficits in the absence of nigral dopaminergic neurodegeneration (Schirinzi et al., 2016, Cramb et al., 2023). Investigating these deficits can provide valuable insights into early-stage PD pathology and may facilitate the development of disease-modifying therapies. FCV, combined with CFMs, has been instrumental to identifying aberrant DA release in the striatum of transgenic rodent models of PD, developed by our lab (Janezic et al., 2013, Sloan et al., 2016, Taylor et al., 2014) and others (Grinevich et al., 2022). This technique can capture electrically-evoked, extracellular DA dynamics, in striatal sections or *in vivo,* at sub-second resolution and with high spatial precision (John and Jones, 2007, Venton and Cao, 2020). However, until now, striatal DA transmission has not been examined in a transgenic mouse model of *GBA*-associated PD.

FCV recordings, conducted prior to this DPhil, revealed that 3-month-old L444P mice have impaired DA release in response to single-pulse (1p) electrical stimulations (**Fig. 4.1,** Dr Bradley Roberts and Dr Katherine Brimblecombe). This deficit was observed exclusively in the dorsolateral striatum (DLS) (**Fig. 4.1 E**), reflecting the selective vulnerability of the

DA neurons that project to this region from the SN (Wong et al., 2019). In contrast, DA release was unaltered in the DLS and nucleus accumbens core (NAcC) of *Gba*$^{+/-}$ mice (**Fig. 4.1 C-D**). This suggests that a gain-of-function effect of the L444P mutation is responsible for impaired DA release in L444P mice. As PD is an age-related disorder (Reeve et al., 2014), and since DA transmission progressively deteriorates with age in other rodent models (Sloan et al., 2016), this chapter first sought to characterise the concentration of extracellular DA ($[DA]_o$) across striatal subregions of 18-22-month-old mice.

Moreover, previous stereology experiments determined that DA neurons of the SN are preserved in L444P mice at 18 months (**Fig. A-3**, Dr Natalie Connor-Robson). Despite this, loss of DA axons in the striatum has been shown to precede nigral dopaminergic neurodegeneration in PD patients and in many rodent models of the disorder (Kordower et al., 2013, Tagliaferro and Burke, 2016, Wong et al., 2019). Therefore, experiments in this chapter also set out to examine the integrity of dopaminergic axons and striatal DA content in our model.

Lastly, striatal DA dynamics are tightly controlled by a concert of regulators in the striatal milieu (**Fig. 4.2**) (Sulzer et al., 2016, Rice et al., 2011). For example, the dopamine transporter (DAT), mediates DA reuptake from the extracellular space and thereby regulates the duration and spatial dynamics of DA transmission (Giros et al., 1996, Cragg and Rice, 2004, Rice and Cragg, 2008). This transporter also modulates neuronal excitability (Carvelli et al., 2004, Ingram et al., 2002) and the short term plasticity of DA release (Condon et al., 2019). In addition, activation of axonal DA D_2 receptors (D_2Rs) on DA axons governs feedback inhibition of DA transmission (Ford, 2014). Striatal DA release is also tonically inhibited by ambient GABA acting at $GABA_A$ and $GABA_B$ receptors on DA axons (Roberts et al., 2021). Changes to DA reuptake by the DAT, D_2R-mediated autoinhibition of DA release and striatal GABA tone have previously been described in rodent models of PD

(Dagra et al., 2021, Lin et al., 2021, Bu et al., 2021, Threlfell et al., 2021, Roberts et al., 2020). I therefore questioned if these regulatory mechanisms are also disturbed in the DLS of our L444P mice.

The specific aims of this chapter are:

1. To determine if the DLS-specific, electrically-evoked DA release deficit persists with age in our L444P mouse model.
2. To assess whether the L444P mutation alters dopaminergic axon density and DA content in the striatum.
3. To investigate if the L444P mutation impacts regulatory mechanisms that govern DA dynamics in the DLS including:
    i) DAT-mediated DA reuptake.
    ii) Inhibition of DA release by D_2Rs.
    iii) Tonic GABAergic inhibition on DA release.

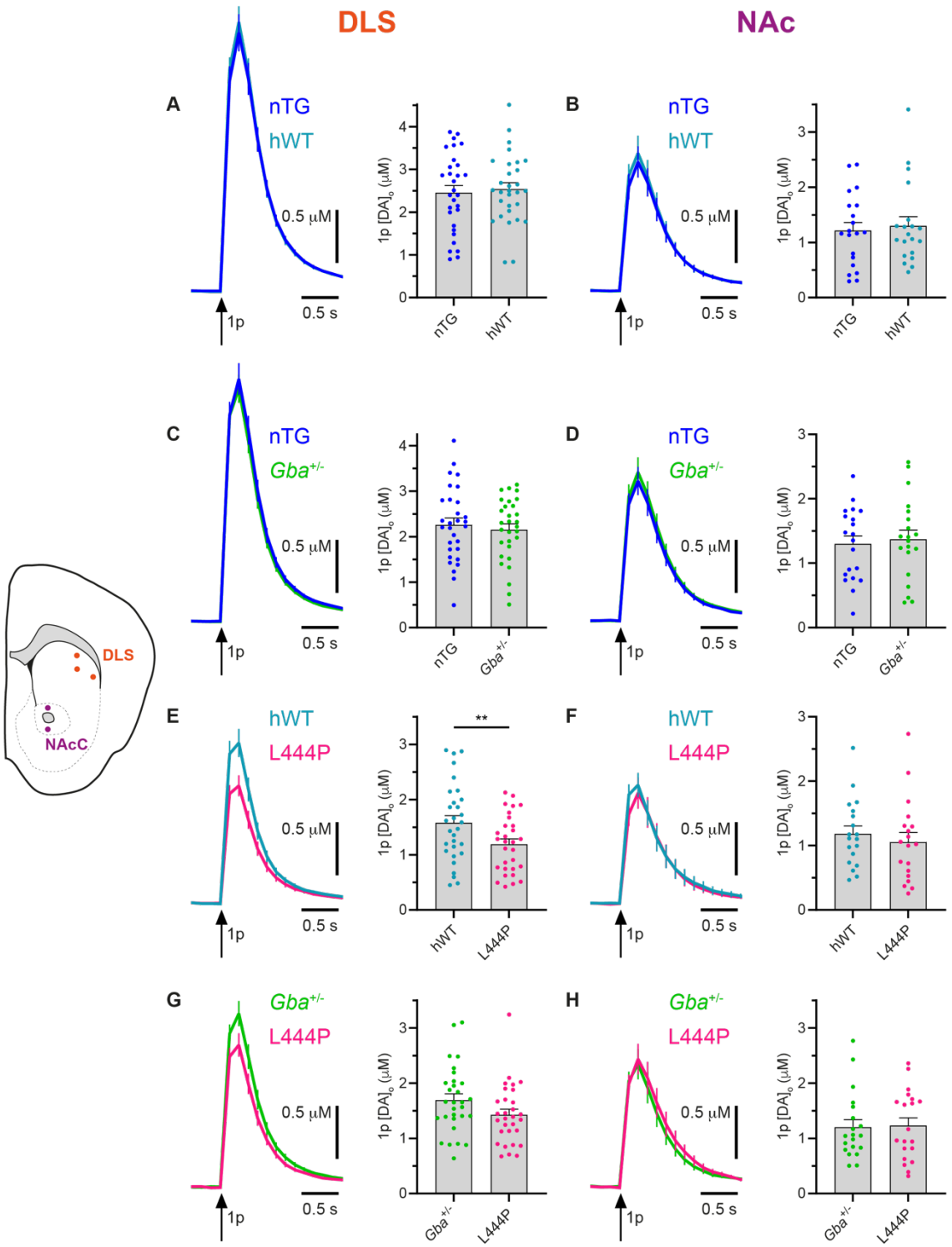


Figure 4.1: Multisite FCV recordings of 1p-evoked $[DA]_o$ in the striatum of 3-month-old mice. Mean $[DA]_o$ transients (*left*) and corresponding mean peak $[DA]_o$ (*right*) across pairwise genotype comparisons in the DLS (**A, C, E, G**) and NAcC (**B, D, F, H**). DLS $[DA]_o$ was significantly reduced in L444P vs hWT mice ($p = 0.0012$) (**E**). No other significant differences were observed ($p > 0.0606$). Inset: schematic of a coronal section illustrating the position of recording sites. (**A, C-F**) Two-tailed paired t-test, (**B, G, H**) Wilcoxon matched-pairs signed rank test; ** $p < 0.01$; across pairwise comparisons 30 DLS recordings and 19-20 NAcC recordings were made per genotype from n = 5 mice per genotype per pairing. Data are presented as mean ± SEM and each datapoint on the bar charts represents one recording site. Data from Dr Bradley Roberts and Dr Katherine Brimblecombe.

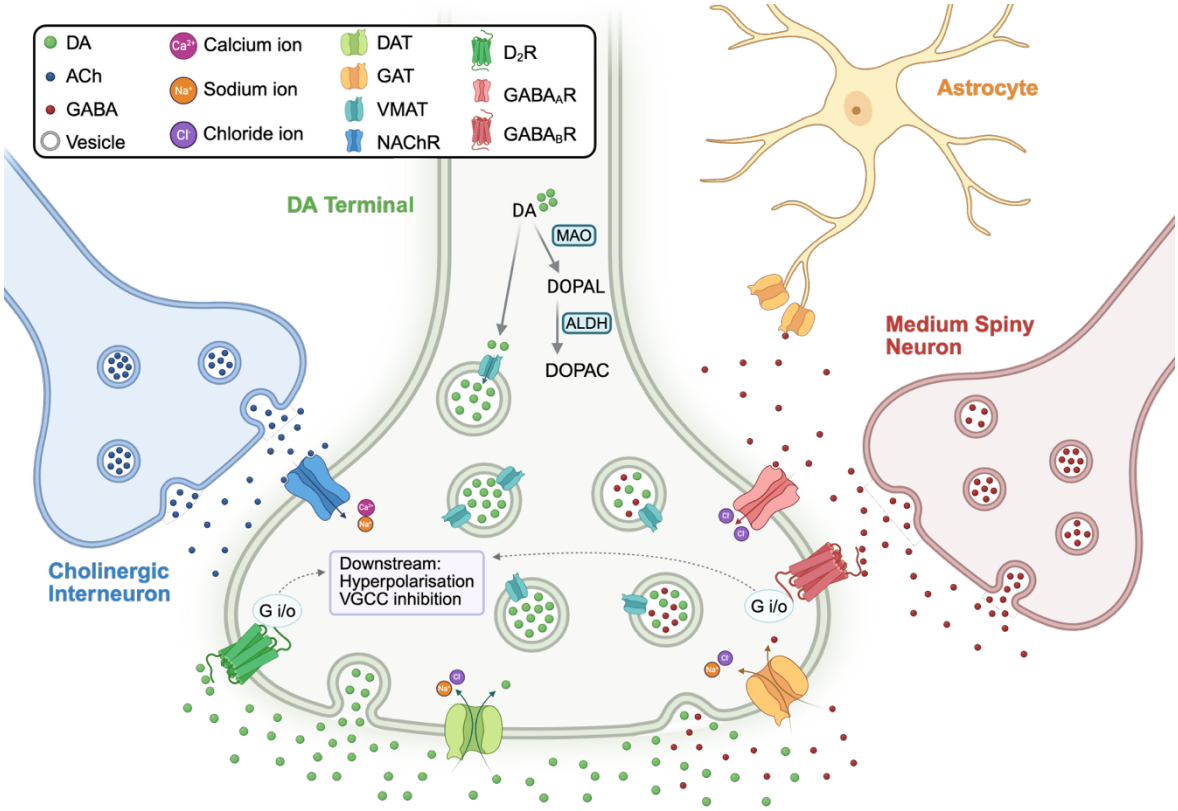


Figure 4.2: Local control of striatal DA release from striatal axons. Intracellular DA can be metabolised to DOPAC or packaged into synaptic vesicles by VMAT. Following synaptic vesicle exocytosis, DATs on the axonal membrane mediate DA reuptake from the extracellular space via sodium chloride co-transport. Axonal DA release is regulated by a concert of neuromodulators in the striatal microcircuitry acting at ionotropic and metabotropic receptors on the surface of DA axons. These include ACh action at nAChRs, DA at D_2Rs and GABA at $GABA_A$Rs and $GABA_B$Rs. The primary source of striatal GABA is medium spiny neurons but GABA co-release from DA axons has also been observed. GATs, located on neurons and astrocytes, remove GABA from the extracellular space. To note, only one DA axon is illustrated on this schematic for simplicity. Therefore, parallel mechanisms in other nearby striatal axons are not represented. Also, this figure exclusively highlights the local regulators of striatal DA dynamics that were explored in this thesis; it is not meant to portray an exhaustive depiction of all regulatory mechanisms that govern axonal DA release. For instance, adenosine, noradrenaline and serotonin also modulate striatal DA transmission and dysregulation of these neurotransmitters is implicated in PD pathology. Striatal DA and DOPAC levels are quantified in **Section 4.2.2** of this thesis, while **Sections 4.2.3-4.2.5** examine the regulation of DA transmission by the DAT, D_2R-mediated inhibition of DA release and the magnitude of inhibitory GABA tone. DA = dopamine, ACh = acetylcholine, MAO = monoamine oxidase, ALDH = aldehyde dehydrogenase, DOPAL = 3,4-dihydroxyphenylacetaldehyde, DOPAC = 3,4-dihydroxyphenylacetic acid, G i/o = $G_{i/o}$ protein alpha subunit, VGCC = voltage-gated calcium channel, DAT = dopamine transporter, GAT = GABA transporter, VMAT = vesicular monoamine transporter, nAChR = nicotinic acetylcholine receptor, D_2R = dopamine D_2 receptor, $GABA_A$R = $GABA_A$ receptor, $GABA_B$R = $GABA_B$ receptor. Created with BioRender.com.

4.2 RESULTS

4.2.1 CHARACTERISATION OF DA RELEASE IN THE AGED STRIATUM WITH MULTISITE FCV RECORDINGS

This chapter first sought to investigate whether the $[DA]_o$ deficit observed in 3-month-old L444P mice (**Fig. 4.1**) is sustained with age. To do this, FCV was used to record 1p-evoked $[DA]_o$ in *ex vivo* hemisected coronal slices from mice aged 18-22 months. The shape of the FCV voltammogram (**Fig. 4.3**, *inset top: representative voltammogram*) confirmed that recorded signals specifically represented DA and not an alternative monoamine transmitter. The oxidation and reduction peaks of voltammograms were typically observed at 0.5-0.6 V and -0.2 V, respectively, consistent with the characteristic peak oxidation and reduction potentials for DA (Venton and Cao, 2020). In each experiment, a pair of striatal sections from different genotypes were simultaneously held in the recording chamber and $[DA]_o$ was measured at three DLS sites and two NAcC sites of individual sections (**Fig. 4.3**, *inset bottom*). Sampling was alternated across sections at each recording site, which enabled $[DA]_o$ to be directly compared across genotypes. Four pairwise genotypic comparisons were studied: nTG vs hWT, nTG vs *Gba*$^{+/-}$, hWT vs L444P and L444P vs *Gba*$^{+/-}$.

The peak magnitude of 1p $[DA]_o$ was similar in the DLS and the NAcC of nTG vs hWT mice (**Fig. 4.3 A-B**). nTG and *Gba*$^{+/-}$ mice also had comparable DA release across regions (**Fig. 4.3 C-D**). On the other hand, the peak amplitude of DLS $[DA]_o$ was significantly lower in aged L444P mice vs hWT mice (median percentage reduction of 13%) (**Fig. 4.3 E**), which corroborated findings in 3-month-old mice (**Fig. 4.1 E**). However, I did not find evidence that peak $[DA]_o$ in L444P mice was attenuated vs *Gba*$^{+/-}$ mice (**Fig. 4.3 G**). In contrast to the $[DA]_o$ deficit in the L444P DLS, peak NAcC $[DA]_o$ was significantly elevated in L444P mice vs hWT mice (**Fig. 4.3 F**). No differences in $[DA]_o$ were observed in the NAcC of L444P vs *Gba*$^{+/-}$ mice (**Fig. 4.3 H**).

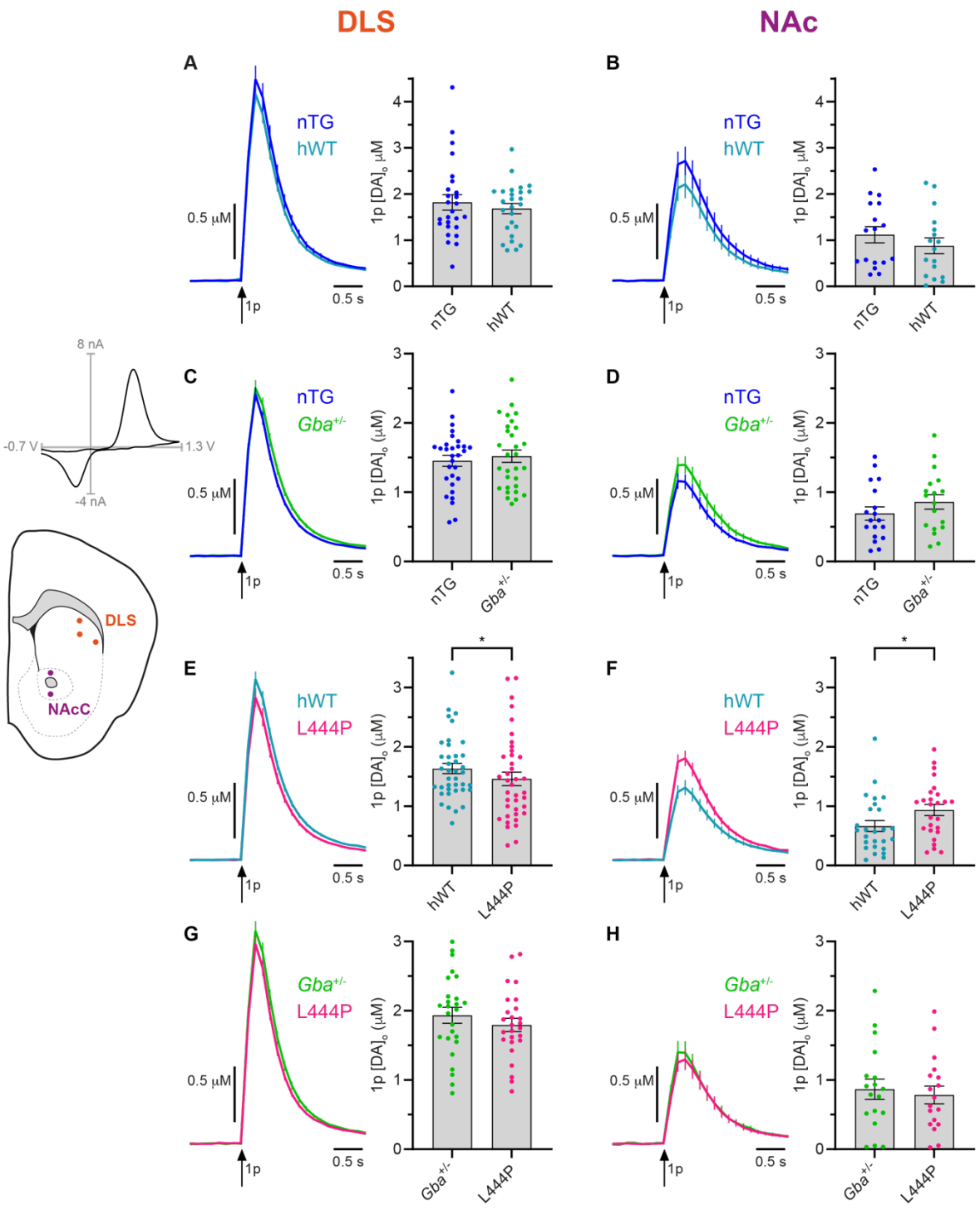


Figure 4.3: Multisite FCV recordings of 1p-evoked $[DA]_o$ in the striatum of aged mice. Mean $[DA]_o$ transients (*left*) and corresponding mean peak $[DA]_o$ (*right*) across pairwise genotype comparisons in the DLS (**A, C, E, G**) and NAcC (**B, D, F, H**). L444P mice displayed significantly reduced DLS $[DA]_o$ ($p = 0.0213$) (**E**) and significantly elevated NAcC $[DA]_o$ ($p = 0.0102$) (**F**). No other genotype-related differences were observed ($p > 0.0544$). Inset: representative DA voltammogram (*top*) and schematic of coronal section illustrating the position of $[DA]_o$ recording sites (*bottom*). (**A, E-F**) Wilcoxon matched-pairs signed rank test, (**B-D, G-H**) two-tailed paired t-test; * $p < 0.05$; across pairwise comparisons 26-39 DLS recordings and 17-26 NAcC recordings were made per genotype from n = 5 mice per genotype per pairing. Data are presented as mean ± SEM and each datapoint on the bar charts represents one recording site.

4.2.2 QUANTIFICATION OF STRIATAL DOPAMINERGIC AXON DENSITY AND STRIATAL DA CONTENT

In many rodent models of PD, the abundance of striatal dopaminergic axons declines before nigral DA neurons degenerate (Tagliaferro and Burke, 2016, Wong et al., 2019). This mirrors axonal loss in patients in the early-disease stages (Kordower et al., 2013). Considering this, I sought to determine if the DLS $[DA]_o$ deficit in young and aged L444P mice was associated with depletion of striatal DA.

Immunofluorescence (IF) in paraffin-embedded sections was first used to visualise the density of dopaminergic axons in the DLS of 3-month-old and 18-month-old mice (**Fig. 4.4 A**). Three images were captured per mouse in distinct DLS subregions and the area occupied by the TH-positive (TH+) signal was averaged across images. The area of the TH+ staining was comparable across genotypes at both ages (**Fig. 4.4 B**), thereby indicating that striatal DA axons are preserved in L444P mice.

The concentration of DA and one of its major metabolites DOPAC (Meiser et al., 2013) were also quantified in the striatum of aged mice (15-22-months-old) with HPLC. These experiments determined that DA and DOPAC levels were similar across genotypes in the CPu (**Fig. 4.5 A-B**) and the NAc (**Fig. 4.5 D-E**). Consequently, the DOPAC:DA ratio (expressed as the proportion of DOPAC relative to DA) was also comparable across genotypes in both regions (**Fig. 4.5 C, F**). An equivalent HPLC dataset in 3-month-old mice, previously collected by Dr Natalie Connor-Robson, also found no genotype-related differences in DA, DOPAC or the DOPAC:DA ratio (**Fig. A-4**).

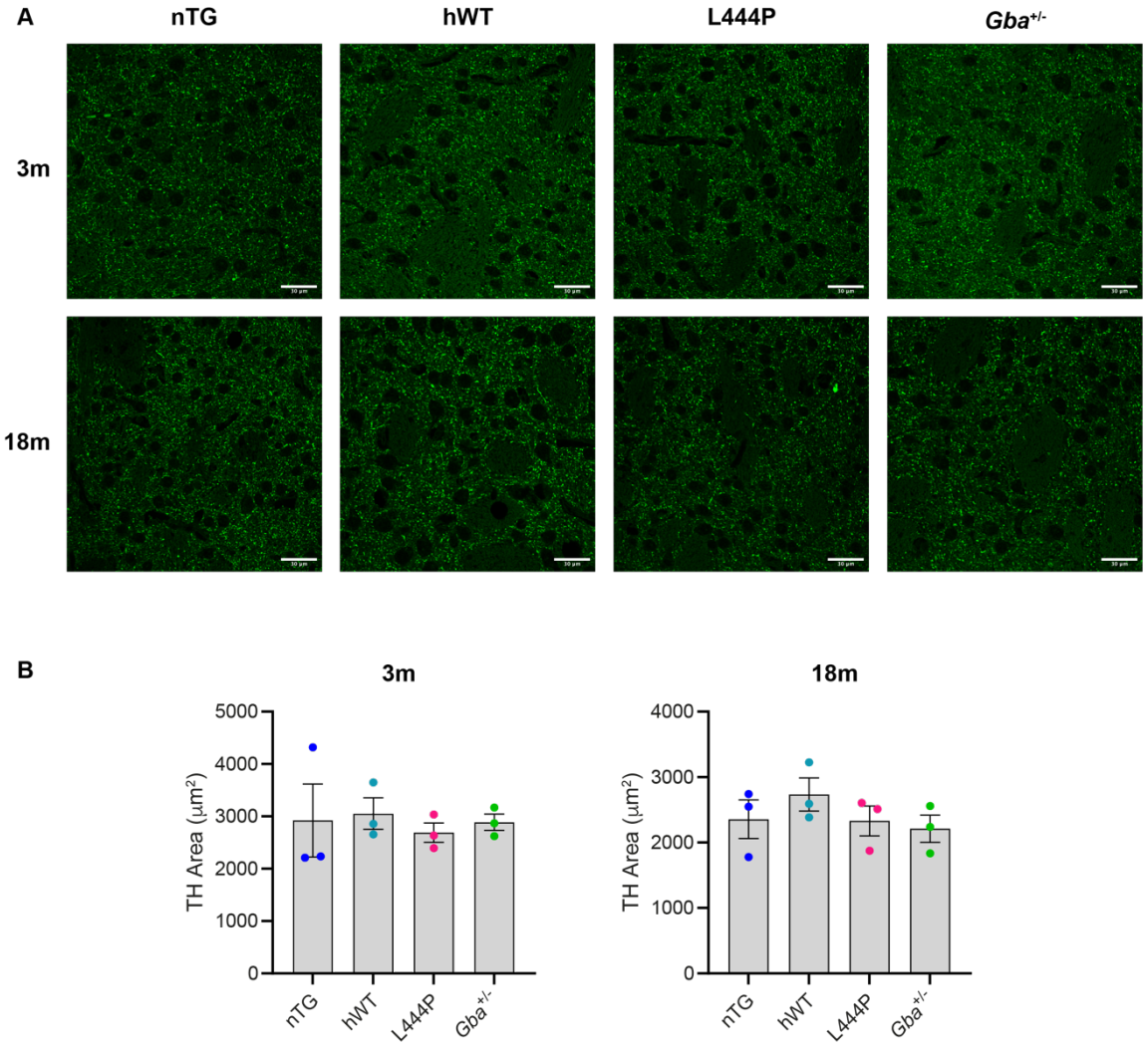


Figure 4.4: Dopaminergic axon area is preserved in the DLS of L444P mice. (**A**) Representative immunofluorescent images of DLS TH+ axons in coronal sections from mice at 3 months (*3m*) and 18 months (*18m*). Scale bars = 30 µm. (**B**) No genotype-related differences in the area of TH+ signal were observed in mice at either age. (**B**) Kruskal-Wallis test (*3m*): Kruskal-Wallis statistic = 1.359 p = 0.7594, one-way ANOVA (*18m*): $F_{(3,8)}$ = 0.8352 p = 0.5113; n = 3 mice per genotype. Data are presented as mean ± SEM and each datapoint represents one mouse.

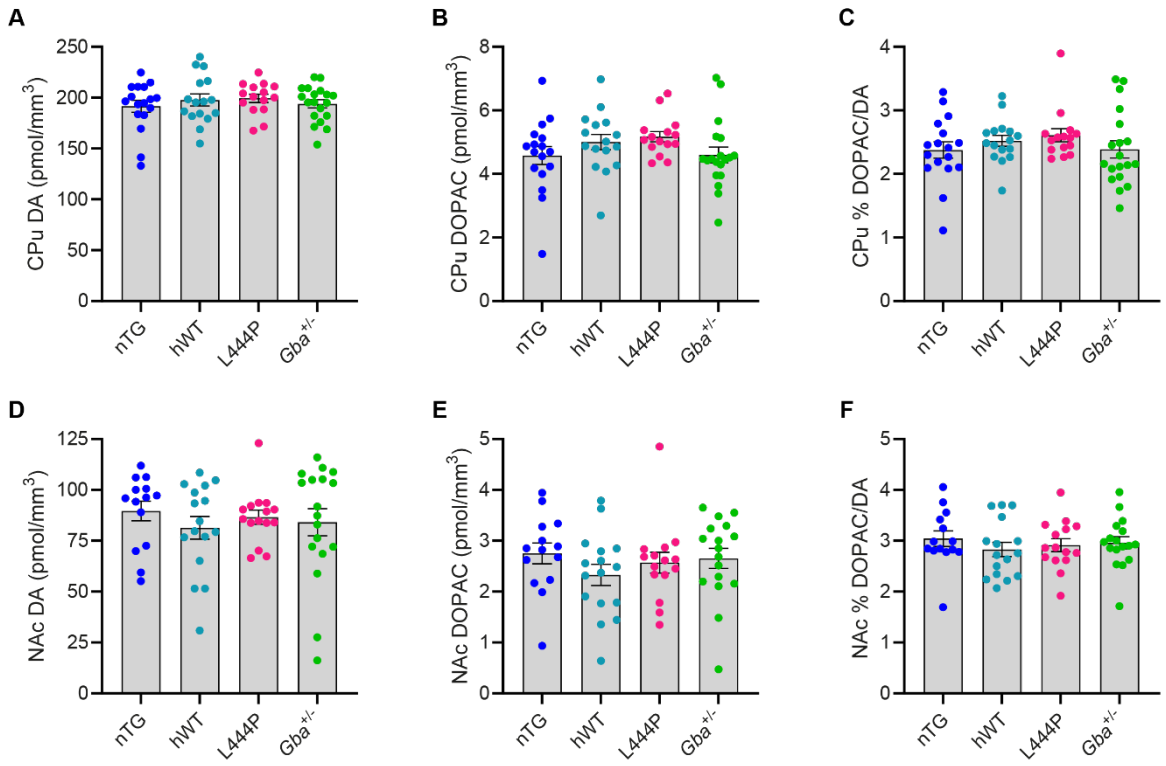


Figure 4.5: DA and DOPAC levels are maintained in the striatum of aged L444P mice. HPLC was used to quantify the concentration of DA and DOPAC in tissue punch homogenates from the dorsal striatum (CPu) (**A-C**) and NAc (**D-F**) of 15–22-month-old mice. The concentration of DA (**A, D**) and DOPAC (**B, E**) and the DOPAC:DA ratio (**C, F**) was similar across genotypes. (**A, C-E**) Kruskal-Wallis test: all Kruskal-Wallis statistics < 4.156 and all $p > 0.2451$, (**B, F**) one-way ANOVA: all $F < 1.451$ and all $p > 0.2364$; (**A-C**) n = 15-19, (**D**) n = 14-18, (**E-F**) n =14-17 mice per genotype. Data are presented as mean ± SEM and each datapoint represents one mouse.

4.2.3 THE REGULATION OF DA REUPTAKE AND SHORT TERM PLASTICITY BY THE DAT

Having demonstrated that striatal DA levels are consistent across genotypes, I next questioned whether the DLS $[DA]_o$ deficit in L444P mice coincided with increased DAT-mediated DA reuptake. To investigate this, the change in 1p $[DA]_o$ was measured in response to DAT inhibition with 5 μM cocaine in the DLS of young (3-6-month-old) and aged (15-19-month-old) mice (**Fig. 4.6-4.7**). Cocaine acts as a nonselective monoamine uptake inhibitor across DA, serotonin and noradrenaline transporters. However, previous observations from our lab have determined that cocaine's effects in the striatum are primarily mediated by the DAT and are comparable to the effects of more selective DAT inhibitors. Cocaine's advantageous physiochemical properties, e.g. high solubility in water and rapid onset of action, also contribute to its popularity as a DAT inhibitor for use in *ex vivo* FCV experiments (Condon et al., 2019, Threlfell et al., 2021). Consistent with previous studies from our lab (Condon et al., 2019, Threlfell et al., 2021), all recordings were made in aCSF containing 1 μM DHβE, a nicotinic acetylcholine receptor (nAChR) antagonist. Acetylcholine (ACh) is a powerful modulator of DA release (Rice and Cragg, 2004, Zhang and Sulzer, 2004, Zhou et al., 2001) and therefore nAChR inhibition served to prevent ACh's influence on DA release in these experiments.

$[DA]_o$ was sampled at 2.5-min intervals at a single recording site in DLS. Prior to cocaine wash-on, $[DA]_o$ was allowed to equilibrate in DHβE to establish a stable baseline (**Fig. 4.6-4.7 A**, *filled datapoints*). The peak $[DA]_o$ increased almost immediately in all genotypes upon cocaine exposure and plateaued within approximately 5 min of wash-on (**Fig. 4.6-4.7 A**, *unfilled datapoints*). Although cocaine increased peak $[DA]_o$ over time, its effect did not differ across genotypes. Accordingly, the mean peak $[DA]_o$, calculated across the final four stimulations in cocaine (**Fig. 4.6-4.7 A**, *grey shaded area*), was approximately

three-fold higher than baseline $[DA]_o$ in all genotypes at both ages (**Fig. 4.6-4.7 B**). Cocaine's similar effect on the amplitude of peak $[DA]_o$ in all genotypes signal that DAT-mediated DA uptake is not altered in our L444P model. Cocaine also slowed the kinetics of $[DA]_o$ dynamics across all genotypes, illustrated by the extended rising and falling phases of the $[DA]_o$ transients (**Fig. 4.6-4.7 C**, *unfilled datapoints*).

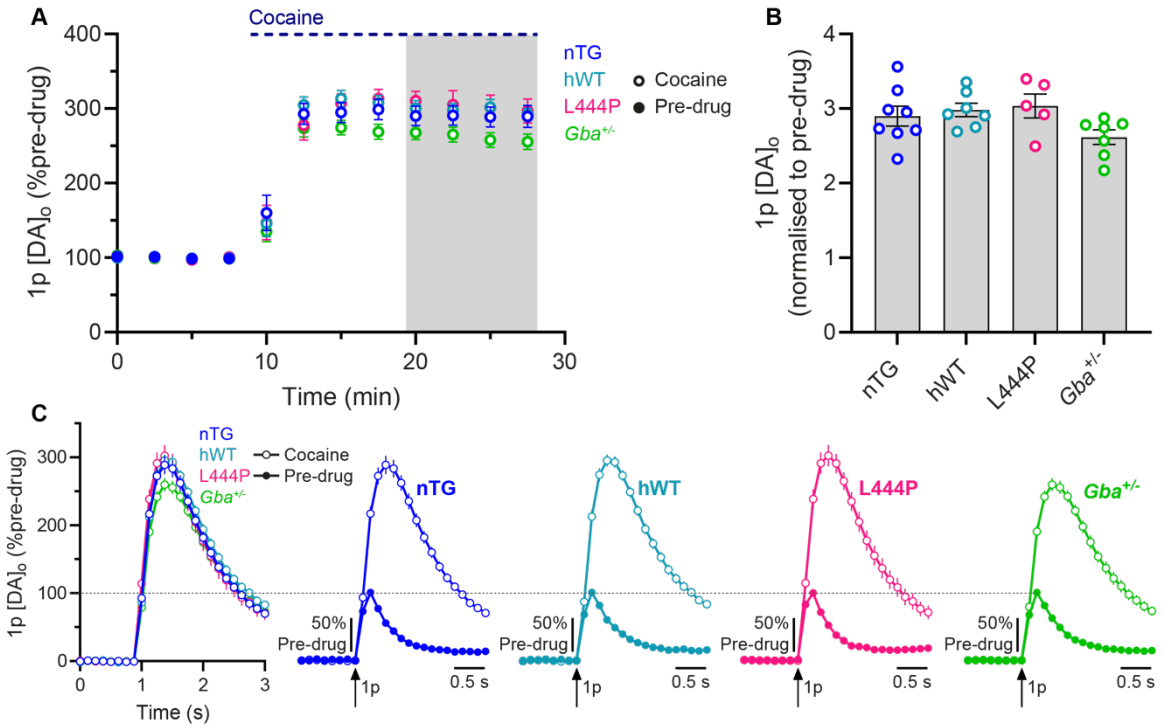


Figure 4.6: The dynamics of DAT-mediated DA uptake is similar across genotypes at 3-6 months. (**A**) DAT inhibition with cocaine produced an immediate and sustained increase in peak 1p $[DA]_o$ (*unfilled datapoints*) in the DLS of all genotypes. (**B**) No genotype-related differences were observed in mean peak $[DA]_o$ in the presence of cocaine. (**C**) Cocaine slowed the kinetics of mean $[DA]_o$ transients to a similar extent in all genotypes. Transients are presented overlayed (*leftmost panel*) and individually across genotypes. (**A-C**) Data are presented normalised within each genotype to the mean peak $[DA]_o$ pre-cocaine wash-on (calculated across *filled datapoints* in **A**). This is represented in **C** by the *grey dashed line*. (**B-C**) The mean $[DA]_o$ in cocaine was calculated across the final four datapoints in the paradigm (*grey shaded area* in **A**). (**A**) Two-way repeated measures ANOVA: genotype $F_{(3,23)} = 1.943$ $p = 0.1508$, time $F_{(2.485,57.15)} = 454.2$ $p < 0.0001$, interaction $F_{(7.454,57.15)} = 1.282$ $p = 0.2735$, (**B**) one-way ANOVA: $F_{(3,23)} = 2.279$ $p = 0.1063$; n = 5-8 slices per genotype from 5-8 mice per genotype (one slice was used per mouse). Data are presented as mean ± SEM and each datapoint in **B** represents one slice.

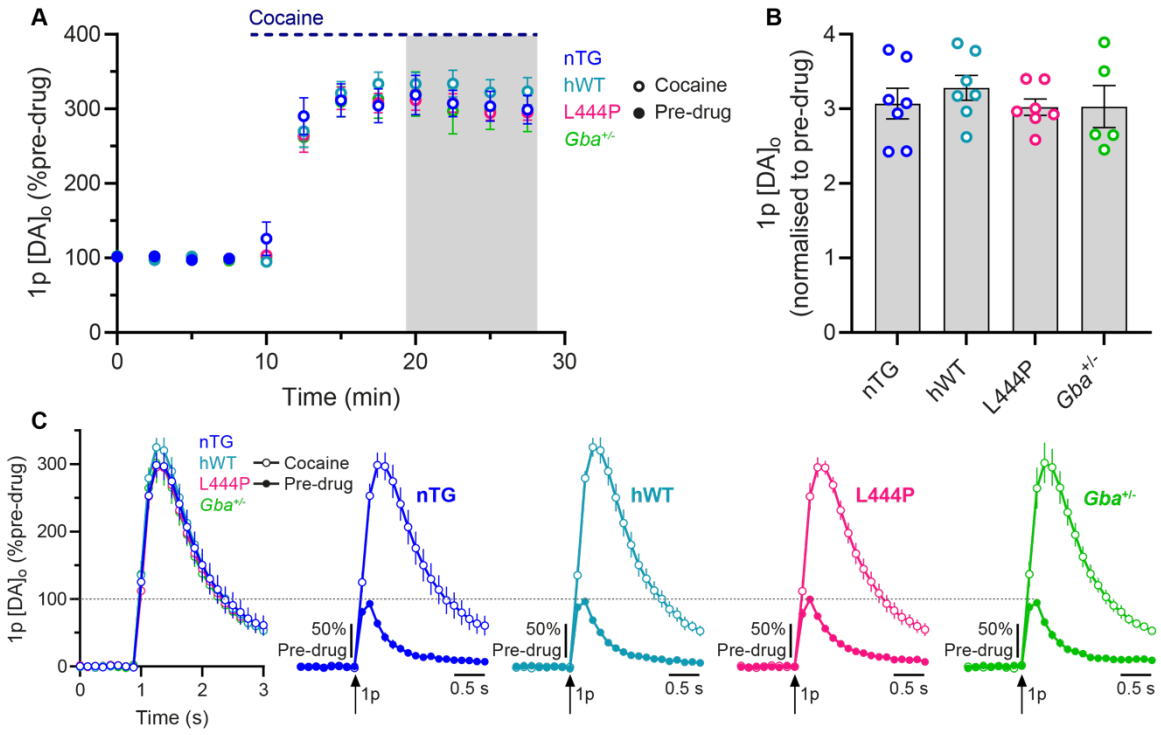


Figure 4.7: No genotype-related differences in DA uptake by the DAT were observed in aged mice. (**A**) The peak 1p DLS $[DA]_o$ increased upon cocaine wash-on (*unfilled datapoints*) across all genotypes in 15-19-month-old mice. (**B**) The mean peak $[DA]_o$ following exposure to cocaine was similar across genotypes. (**C**) Cocaine extended the rise and decay phase of mean $[DA]_o$ transients to a similar degree in all genotypes, as shown overlayed (*leftmost panel*) and individually across genotypes. (**A-C**) Data are presented normalised within each genotype to the mean peak $[DA]_o$ before washing on cocaine (calculated across *filled datapoints* in **A**). This is represented in **C** by the *grey dashed line*. (**B-C**) The mean $[DA]_o$ in cocaine was calculated across the final four timepoints in the paradigm (*grey shaded area* in **A**). (**A**) Two-way repeated measures ANOVA: genotype $F_{(3,22)} = 0.2592$ $p = 0.8539$, time $F_{(2.343,51.54)} = 316.8$ $p < 0.0001$, interaction $F_{(7.028,51.54)} = 0.6013$ $p = 0.7526$, (**B**) one-way ANOVA: $F_{(3,22)} = 0.4448$ $p = 0.7234$; n = 5-7 slices per genotype from 5-6 mice per genotype. Data are presented as mean ± SEM and each datapoint in **B** represents one slice. Dr Emanuel Lopes contributed two experiments to this dataset.

In addition to their role in removing DA from the extracellular space, DATs are also known to modulate the short term plasticity of DA release (Condon et al., 2019). The DAT's influence on short term facilitation was tested across genotypes in aged mice by consecutively alternating 1p stimulations (**Fig. 4.8 A-D,** *circular datapoints*) with pairs of electrical pulses delivered at 10 ms intervals (2p 100 Hz) (**Fig. 4.8 A-D,** *square datapoints*). $[DA]_o$ was sampled before and during cocaine wash-on at the same DLS recording site used in **Fig. 4.7**. $[DA]_o$ attributed to the second pulse of the 2p 100 Hz stimulation, "P_2", was obtained by subtracting the mean $[DA]_o$ transient produced by flanking 1p stimulations from

the intermediate 2p 100 Hz $[DA]_o$ transient. The paired pulse ratio (PPR) was subsequently calculated by dividing the peak P_2 $[DA]_o$ by the mean peak $[DA]_o$ of the flanking 1p stimulations. The PPR is used as a readout of short term plasticity at DA release sites, as previously described (Condon et al., 2019).

Prior to cocaine wash-on, peak P_2 $[DA]_o$ was greater than 1p evoked $[DA]_o$ in all genotypes (**Fig. 4.8 A-D** (*left*), **E**). Consequently, the value of the PPR in DHβE was >1 across genotypes (**Fig. 4.8 G**, *filled datapoints*). This is indicative of short term facilitation of DA release and is in line with previous studies that measured the PPR under conditions of nAChR antagonism with DHβE (Condon et al., 2019, Rice and Cragg, 2004). Notably, no genotype-related differences in the value of the PPR were detected before cocaine wash-on, indicating that the L444P mutation does not alter the short term plasticity of DA release in these conditions.

In all genotypes, cocaine increased the peak amplitude of $[DA]_o$ evoked by 1p stimulations and 2p 100 Hz stimulations (**Fig. 4.8 A-D** (*right*). The kinetics of the 1p $[DA]_o$ and 2p 100 Hz $[DA]_o$ transients were also remarkably slower for all genotypes during cocaine wash-on (**Fig. 4.8 A-D**). Furthermore, in the presence of cocaine, P_2 $[DA]_o$ became equivalent to, or lower than, 1p $[DA]_o$ (**Fig. 4.8 A-D** (*right*), **F**) and consequently the value of the PPR was significantly attenuated across genotypes (**Fig. 4.8 G**, *unfilled datapoints*). These findings indicate that cocaine reduced short term facilitation in all genotypes, consistent with previous reports from our lab (Condon et al., 2019). However, the value of the PPR in the presence of cocaine and the magnitude of cocaine's effect on the PPR was not significantly different across genotypes (**Fig. 4.8 G**). Taken together, these experiments did not find evidence of aberrant short term plasticity of DA release in L444P mice at 10 ms interpulse intervals.

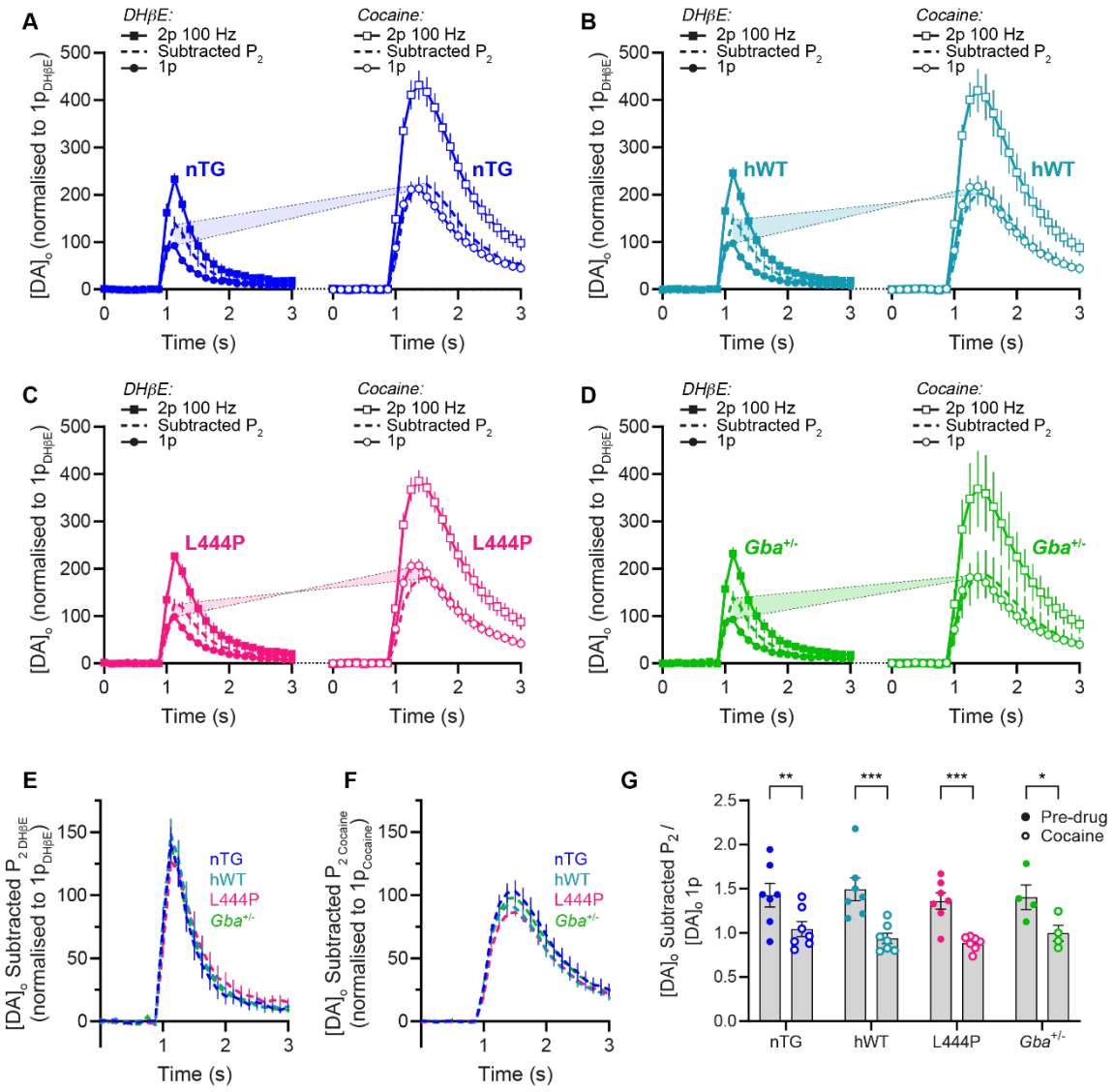


Figure 4.8: Short term plasticity of DA release is comparable across genotypes in aged mice prior to and during cocaine exposure. (**A-D**) Mean $[DA]_o$ transients in DHβE (*left*) and cocaine (*right*) evoked by 1p (*circular datapoints*) and 2p 100 Hz stimulations (*square datapoints*) and $[DA]_o$ attributed to the second pulse of the 2p 100 Hz stimulation ("P_2", *dashed line*) in nTG (**A**), hWT (**B**), L444P (**C**) and *Gba*$^{+/-}$ (**D**) mice, aged 15-19 months. P_2 transients were obtained by subtracting the mean 1p $[DA]_o$ transients from the intermediate 2p 100 Hz $[DA]_o$ transient within each experiment. In all genotypes, cocaine reduced the peak of P_2 $[DA]_o$ relative to 1p $[DA]_o$ (*shaded regions* in **A-D**). (**E-F**) Mean P_2 $[DA]_o$ transients from **A-D** overlayed across genotypes. Peak P_2 $[DA]_o$ is greater than 1p $[DA]_o$ in DHβE (**E**), whereas P_2 $[DA]_o$ is equivalent to or less than 1p $[DA]_o$ in cocaine (**F**); as indicated by the shaded regions in **A-D**. The shape of the transients is comparable across genotypes in both conditions. Data are presented normalised to the peak 1p $[DA]_o$ in DHβE (**A-E**) or the peak 1p $[DA]_o$ in cocaine (**F**). (**G**) Cocaine significantly reduced the paired pulse ratio (P_2 $[DA]_o$ / 1p $[DA]_o$) in all genotypes, but this effect did not significantly differ across genotypes. (**G**) Two-way ANOVA with Tukey's post-hoc test: genotype $F_{(3,42)} = 0.5411$ $p = 0.6568$, drug treatment $F_{(1,42)} = 39.42$ $p < 0.0001$, interaction $F_{(3,42)} = 0.3087$ $p = 0.8189$; * $p < 0.05$, ** $p < 0.01$, *** $p < 0.001$ from Tukey's post-hoc test; n = 4-7 slices per genotype from 4-6 mice per genotype. Data are presented as mean ± SEM and each datapoint in **G** represents one slice. Dr Emanuel Lopes contributed two experiments to this dataset.

In agreement with these functional experiments, no genotype-related changes to DAT expression levels were detected in the DLS using IF (**Fig. 4.9**): the area of the DAT signal was consistent across genotypes in 3- and 18-month-old mice (**Fig. 4.9 B**). Altogether, experiments in this chapter did not identify impairments in the functionality or membrane-availability of the DAT in L444P mice.

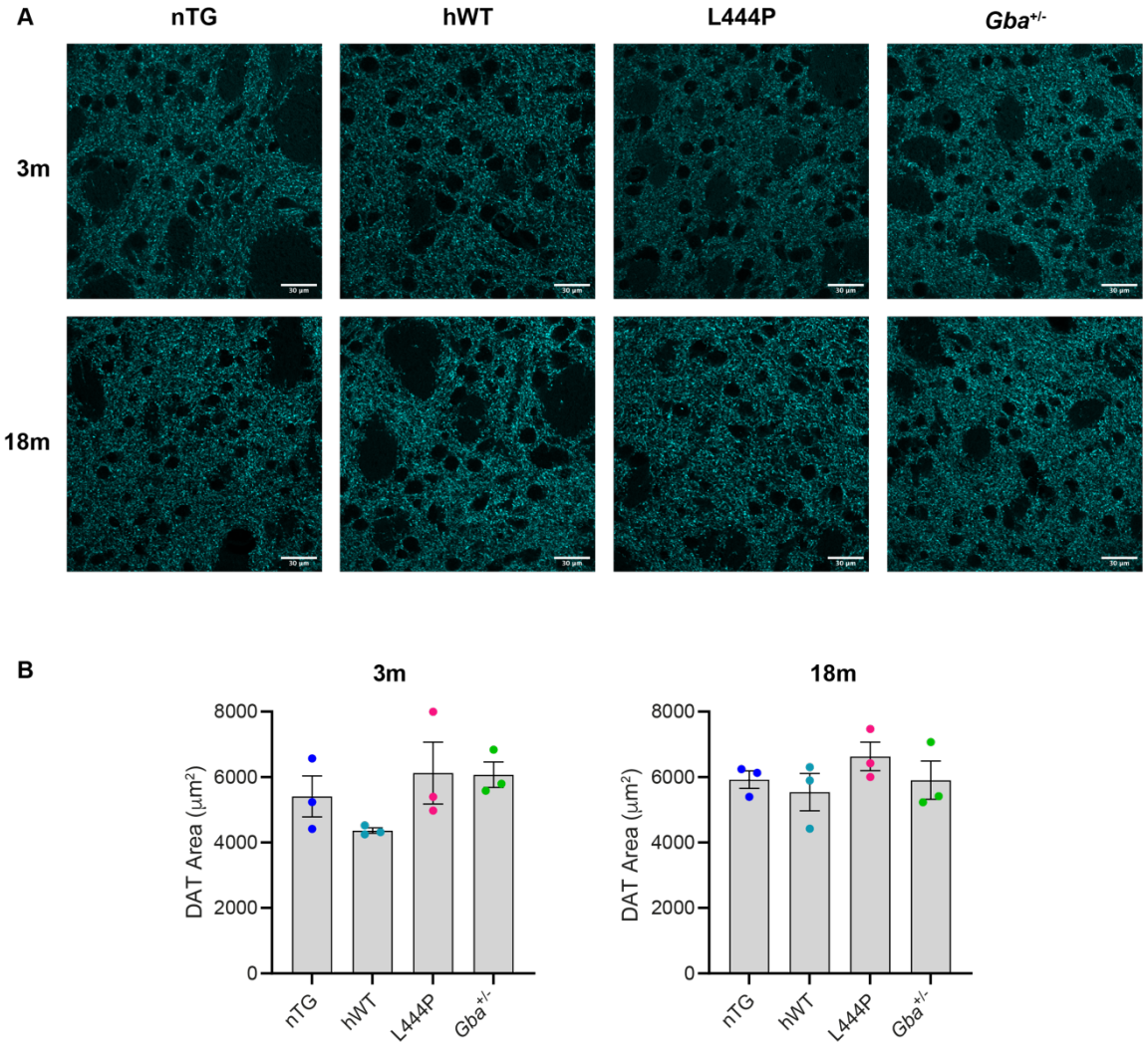


Figure 4.9: DAT expression levels are similar across genotypes in the DLS. Representative images (**A**) and corresponding quantification (**B**) of immunofluorescent DAT staining in 3-month-old (*3m*) and 18-month-old (*18m*) mice. Scale bars = 30 µm in **A**. (**B**) No genotype-related differences were detected in the area of the DAT signal at either age. (**B**) One-way ANOVA: all $F_{(3,8)} < 1.861$ and all $p > 0.2145$; n = 3 mice per genotype. Data are presented as mean ± SEM and each datapoint represents one mouse.

4.2.4 D_2R-MEDIATED INHIBITION OF DA RELEASE

I next sought to investigate whether D_2R-governed feedback inhibition on striatal DA transmission differs across genotypes in young and aged mice. To do this, I measured the effect of pharmacological D_2R agonism with quinpirole on 1p $[DA]_o$. Application of quinpirole at its EC_{50} (44 nM) and subsequently maximum (1 μM) concentration enabled receptor-effector coupling and membrane availability of D_2Rs to be probed, respectively. Drug concentrations were determined based on a dose-response curve illustrating quinpirole's effect on $[DA]_o$ from Dr Michael Clements' DPhil thesis (2008).

$[DA]_o$ was measured at 2.5-min intervals at a single recording site in DLS before and during quinpirole exposure (**Fig. 4.10-4.11 A**). A stable baseline readout of $[DA]_o$ (*filled datapoints*) was achieved prior to drug application. Subsequent quinpirole wash-on progressively deteriorated $[DA]_o$ over time in a concentration-dependent fashion. Although, quinpirole diminished $[DA]_o$ compared to baseline levels at its EC_{50} (*half-filled datapoints*) and maximum concentrations (*unfilled datapoints*), its effect was not different across genotypes. Accordingly, in all genotypes, the mean peak $[DA]_o$ in EC_{50} quinpirole, calculated across the final four EC_{50} stimulations (**Fig. 4.10-4.11 A**, *left grey shaded area*), was approximately 45% of baseline levels in young mice and 55% of baseline in aged mice (**Fig. 4.10-4.11 B**). Following application of 1 μM quinpirole, the mean peak $[DA]_o$, obtained from the final four timepoints (**Fig. 4.10-4.11 A**, *right grey shaded area*), declined to less than 10% of baseline release across genotypes at both ages (**Fig. 4.10-4.11 B**). The similar response to EC_{50} and maximum quinpirole across genotypes at both ages indicates that receptor-effector coupling and membrane availability of D_2Rs is not altered by the L444P mutation. Moreover, quinpirole did not appear to affect the time course of DA signals, despite its striking effect on peak $[DA]_o$ in all genotypes: $[DA]_o$ transients had a similar time to peak and a similar decay rate in EC_{50} quinpirole compared to pre-drug exposure (**Fig.**

4.10-4.11 C, *half-filled datapoints*). Kinetics also appeared comparable in 1 µM quinpirole, although they are more challenging to discern at this concentration given the small amplitude of the $[DA]_o$ transients (**Fig. 4.10-4.11 C**, *unfilled datapoints*). Nevertheless, the shape of the transients at both concentrations was similar across genotypes (**Fig. 4.10-4.11 C**, *leftmost panel*).

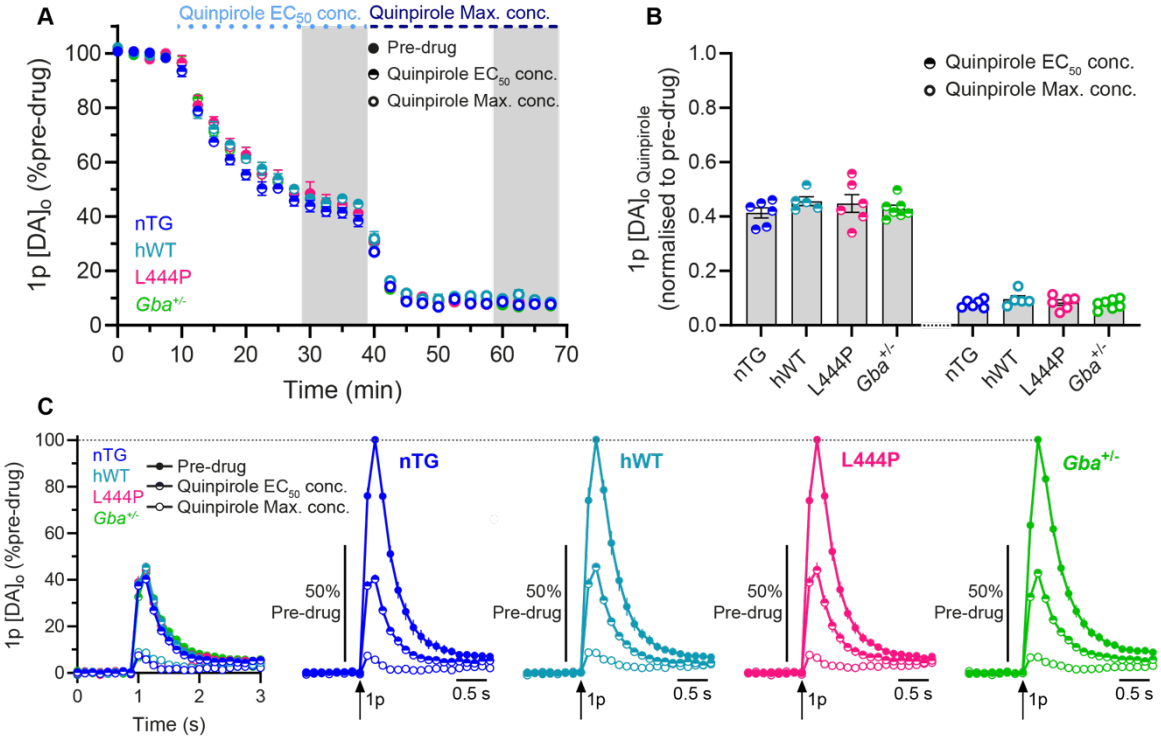


Figure 4.10: Inhibition of DA release by D_2Rs is unaltered in 3-6-month-old L444P mice. (**A**) The peak 1p DLS $[DA]_o$ declined across all genotypes in response to agonism of D_2Rs with quinpirole at its EC_{50} (44 nM) (*half-filled datapoints*) and maximum ("Max.", 1 µM) (*unfilled datapoints*) concentrations. (**B**) The mean peak $[DA]_o$ is similar across genotypes in EC_{50} and Max. quinpirole. (**C**) Mean $[DA]_o$ transients, presented overlayed (*leftmost panel*) and individually across genotypes, have similar kinetics before and during quinpirole treatment. (**A-C**) Data are presented normalised within individual genotypes to the mean peak $[DA]_o$ pre-quinpirole exposure (calculated across *filled datapoints* in **A**). This is represented in **C** by the *grey dashed line*. (**B-C**) Mean $[DA]_o$ in EC_{50} and Max. quinpirole was obtained from the final four stimulations at each concentration (*left and right grey shaded area* in **A**, respectively). (**A**) Two-way repeated measures ANOVA: genotype $F_{(3,20)} = 1.311$ $p = 0.2986$, time $F_{(5.110,102.2)} = 2227$ $p < 0.0001$, interaction $F_{(15.33,102.2)} = 0.9217$ $p = 0.5443$, (**B**) one-way ANOVA (EC_{50} and Max.): all $F_{(3,20)} < 0.8771$ and all $p > 0.4696$; n = 5-7 slices per genotype from 5-7 mice per genotype (one slice was used per mouse). Data are presented as mean ± SEM and each datapoint in **B** represents one slice.

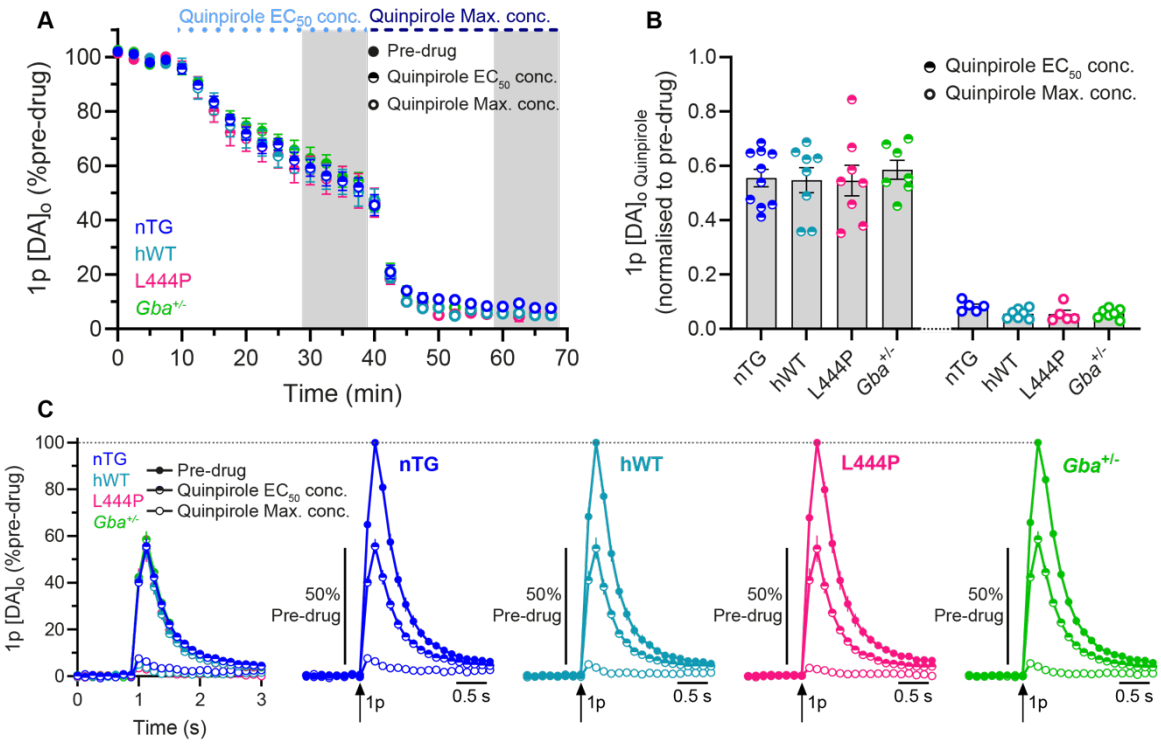


Figure 4.11: D_2R-mediated inhibition of DA release remains similar across genotypes in aged mice. (**A**) D_2R agonism via wash-on of EC_{50} (44 nM) (*half-filled datapoints*) and maximum (Max., 1 µM) (*unfilled datapoints*) quinpirole caused a steady decline in peak 1p $[DA]_o$ in the DLS of 15-19-month-old mice. (**B**) The mean peak $[DA]_o$ was not different across genotypes at both quinpirole concentrations. (**C**) Mean $[DA]_o$ transients had equivalent kinetics across genotypes in all treatment conditions, as illustrated when genotypes are plotted together (*leftmost panel*) and separately. (**A-C**) Data are presented normalised within individual genotypes to the mean peak $[DA]_o$ pre-drug application (calculated across *filled datapoints* in **A**). This is represented in **C** by the *grey dashed line*. (**B-C**) Mean $[DA]_o$ in EC_{50} and Max. quinpirole was obtained from the final four stimulations at each concentration (*left and right grey shaded area* in **A**, respectively). (**A**) Mixed-effects analysis: genotype $F_{(3,29)} = 0.4558$ $p = 0.7153$, time $F_{(1.965,50.86)} = 1038$ $p < 0.0001$, interaction $F_{(5.894,50.86)} = 0.4235$ $p = 0.8571$, (**B**) one-way ANOVA (EC_{50}): $F_{(3,29)} = 0.1644$ $p = 0.9195$, Kruskal-Wallis test (Max.): Kruskal-Wallis statistic = 6.185 $p = 0.1029$; n = 7-10 slices per genotype (EC_{50}) or 5-7 slices per genotype (Max.) from 4-7 mice per genotype (EC_{50}) or from 4-6 mice per genotype (Max.). Data are presented as mean ± SEM and each datapoint in **B** represents one slice. Dr Emanuel Lopes contributed one experiment to this dataset.

Immunofluorescent staining in the DLS of paraffin-embedded sections supported that D_2R availability was comparable across genotypes (**Fig. 4.12**). No significant differences in the area occupied by the D_2R signal were identified in young and aged mice (**Fig. 4.12 B**). Taken together, the experiments presented herein did not find evidence of abnormal D_2R-mediated regulation of DA release in L444P mice.

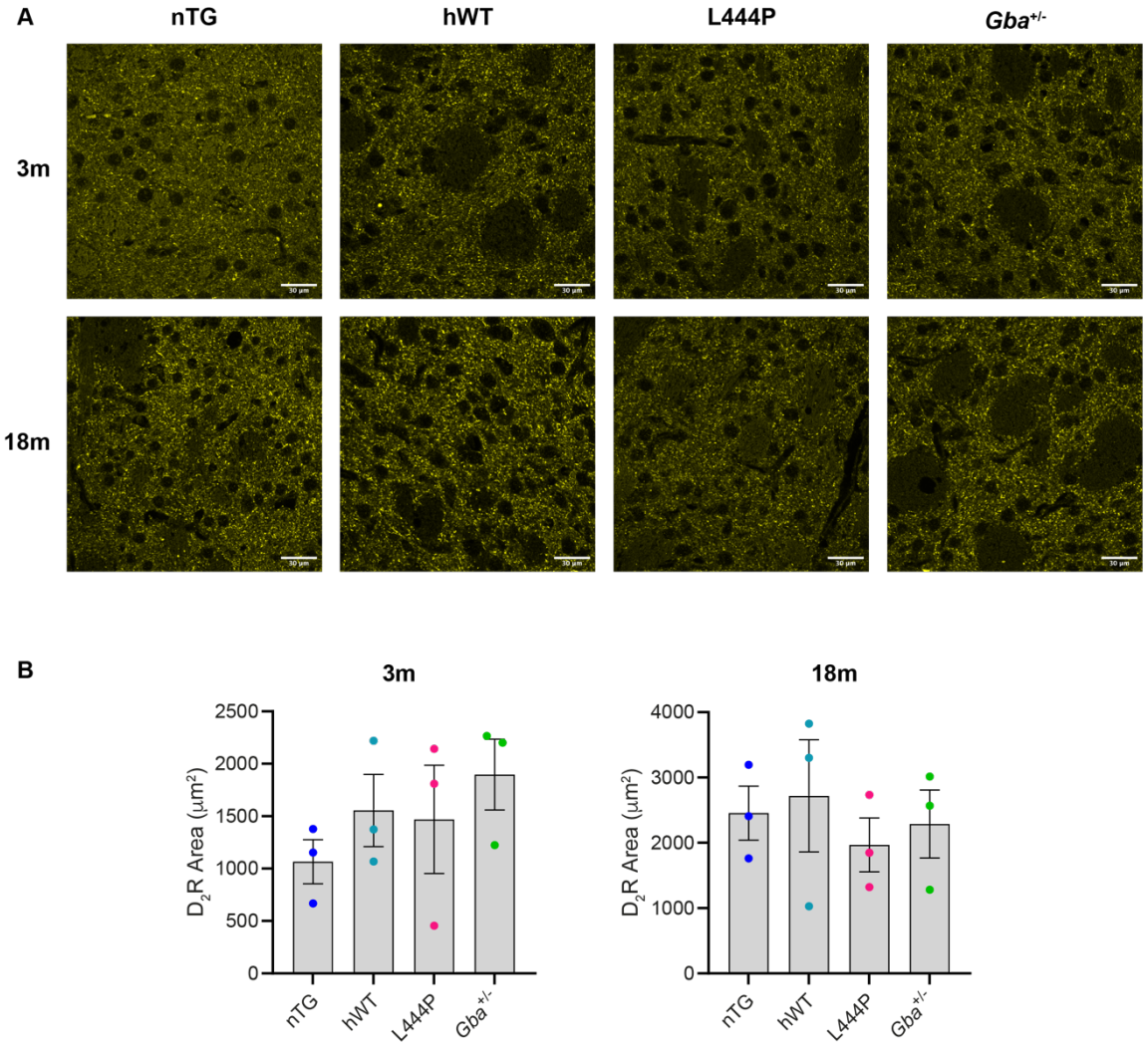


Figure 4.12: The abundance of D_2Rs in the DLS is comparable across genotypes. (**A**) Representative immunofluorescent images of D_2R staining in mice aged 3-months (*3m*) and 18-months (*18m*). Scale bars = 30 µm. (**B**) Corresponding quantification of the area of D_2R signal revealed no significant genotype-related differences across both ages. (**B**) One-way ANOVA: all $F_{(3,8)} < 0.8600$ and all $p > 0.5000$; n = 3 mice per genotype. Data are presented as mean ± SEM and each datapoint represents one mouse.

4.2.5 TONIC GABAERGIC INHIBITION OF DA RELEASE IN RESPONSE TO SINGLE-PULSE AND PHASIC STIMULATIONS

Aside from D_2R-mediated inhibition, striatal DA release is also under tonic inhibition imposed by ambient GABA (Roberts et al., 2021). I therefore sought to explore if the intensity of striatal GABA tone is different across genotypes. To investigate this, I assessed how $[DA]_o$ responds to dual antagonism of the $GABA_A$ and $GABA_B$ receptors ($GABA_{A+B}Rs$) using bicuculine (10 μM) and CGP 55845 (4 μM), respectively. All recordings were conducted under nAChR inhibition with 1 μM DHβE to eliminate ACh-mediated control of $[DA]_o$, as per previous reports (Lopes et al., 2019, Roberts et al., 2020).

1p-evoked $[DA]_o$ was recorded at a single site in the DLS every 2.5 min before and during $GABA_{A+B}R$ inhibition (**Fig. 4.13-4.14 A**). $[DA]_o$ was stable in DHβE before drug wash-on (*filled datapoints*) and co-application of $GABA_{A+B}R$ antagonists produced a modest elevation in $[DA]_o$ over time across all genotypes at both ages (*unfilled datapoints*). However, the extent of increase was not significantly different across genotypes (**Fig. 4.13-4.14 A-B**); the mean peak $[DA]_o$, calculated across the last four recordings in $GABA_{A+B}R$ antagonists (**Fig. 4.12-4.13 A**, *grey shaded area*), was consistently 30-50% higher than baseline $[DA]_o$ (**Fig. 4.13-4.14 B**). As $GABA_{A+B}R$ antagonism evoked a similar increase in the peak amplitude of 1p $[DA]_o$ across genotypes, this indicates the magnitude of GABAergic tonic inhibition of 1p-evoked DA release is not altered in L444P mice. Furthermore, $GABA_{A+B}R$ inhibition did not seem to alter the temporal dynamics of DA signalling: the rise and decay phases of the DA transients were comparable before and during drug application (**Fig. 4.13-4.14 C**). The shape of the transients was also similar across genotypes in the presence of $GABA_{A+B}R$ antagonists (**Fig. 4.13-4.14 C**, *leftmost panel*).

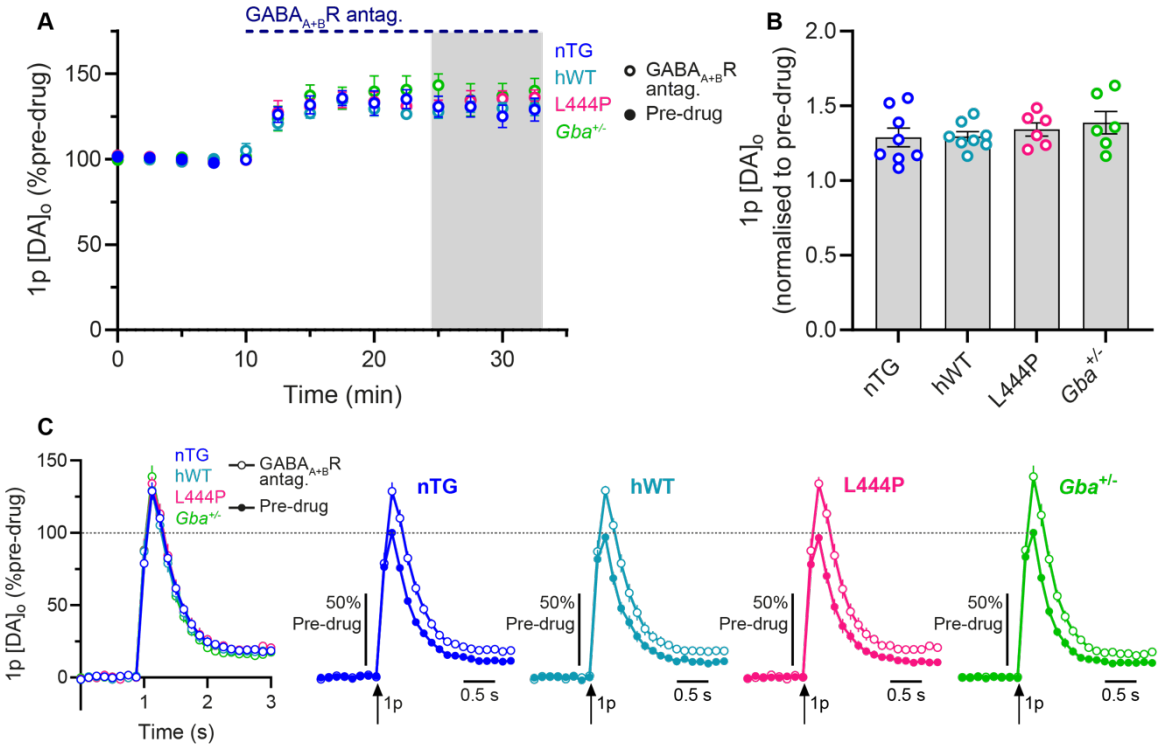


Figure 4.13: The extent of GABAergic inhibition of DA release is not different across genotypes in 3-6-month-old mice. (**A**) Peak 1p [DA]$_o$ was increased in the DLS of all genotypes following co-application of bicuculine (10 µM) and CGP 55845 (4 µM) (GABA$_{A+B}$R antag.) (*unfilled datapoints*). (**B**) The mean peak [DA]$_o$ was similar across genotypes in the presence of GABA$_{A+B}$R antagonists. (**C**) Mean [DA]$_o$ transients, presented overlayed (*leftmost panel*) and individually across genotypes, appeared to have similar kinetics in all genotypes in both treatment conditions. (**A-C**) Data are presented normalised within each genotype to the mean peak [DA]$_o$ pre-drug wash-on (calculated across *filled datapoints* in **A**). This is represented in **C** by the *grey dashed line*. (**B-C**) The mean [DA]$_o$ in GABA$_{A+B}$R antagonists was calculated across the final four stimulations of the drug wash-on (*grey shaded area* in **A**). (**A**) Two-way repeated measures ANOVA: genotype $F_{(3,24)} = 0.4412$ $p = 0.7257$, time $F_{(2.644,63.45)} = 93.89$ $p < 0.0001$, interaction $F_{(7.931, 63.45)} = 0.9319$ $p = 0.4963$, (**B**) one-way ANOVA: $F_{(3,24)} = 0.6637$ $p = 0.5825$; n = 6-8 slices per genotype from 6-8 mice per genotype (one slice was used per mouse). Data are presented as mean ± SEM and each datapoint in **B** represents one slice.

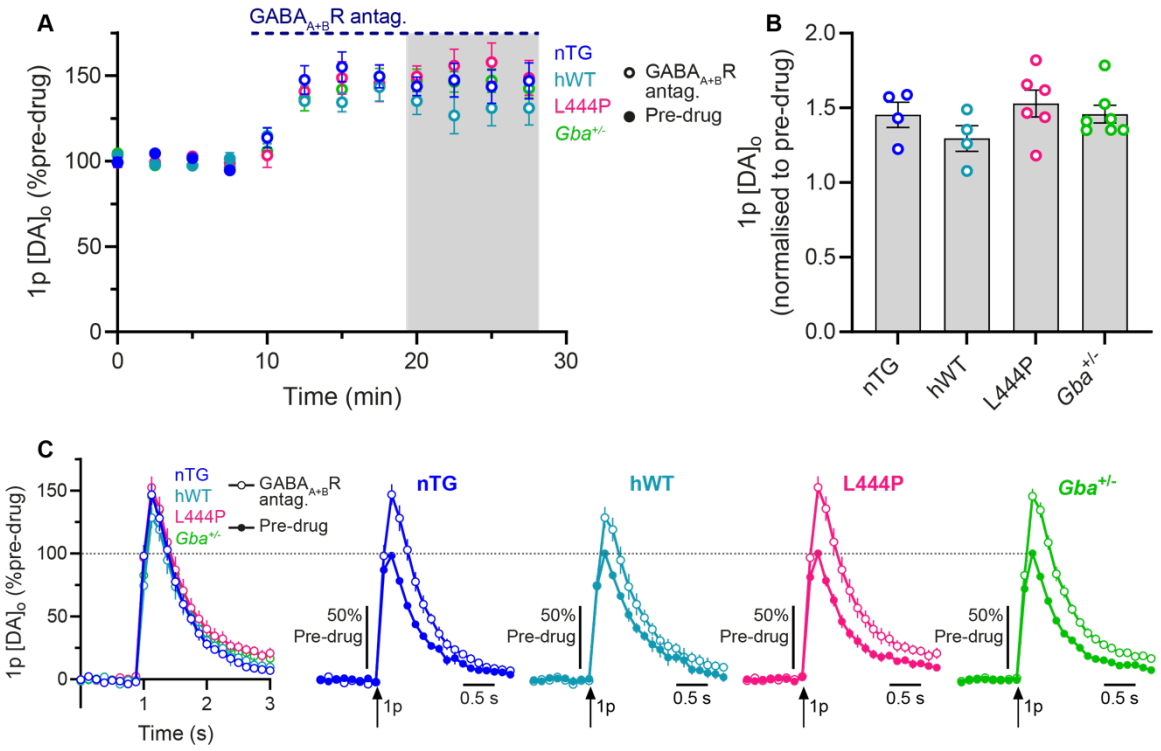


Figure 4.14: The levels of striatal GABA tone remained comparable across genotypes in aged mice. (**A**) Co-exposure to bicuculine (10 µM) and CGP 55845 (4 µM) (GABA$_{A+B}$R antag.) (*unfilled datapoints*) increased peak 1p [DA]$_o$ across all genotypes in 18-22-month-old mice. (**B**) The mean peak 1p [DA]$_o$ following GABA$_{A+B}$R antag. wash-on was not different across genotypes. (**C**) The shape of the mean [DA]$_o$ transients was similar across genotypes in the absence and presence of GABA$_{A+B}$R antagonism, as shown overlayed (*leftmost panel*) and individually in each genotype. (**A-C**) Data are presented normalised within each genotype to the mean peak [DA]$_o$ prior to inhibition of GABA$_{A+B}$Rs (calculated across *filled datapoints* in **A**). This is represented in **C** by the *grey dashed line*. (**B-C**) The mean [DA]$_o$ in GABA$_{A+B}$R antag. was obtained from the final four recordings in the paradigm (*grey shaded area* in **A**). (**A**) Two-way repeated measures ANOVA: genotype $F_{(3,17)}$ = 0.8497 p = 0.4858, time $F_{(2.707,46.03)}$ = 59.13 p < 0.0001, interaction $F_{(8.122, 46.03)}$ = 1.205 p = 0.3171, (**B**) Kruskal-Wallis test: Kruskal-Wallis statistic = 3.591 p = 0.3092; n = 4-7 slices per genotype from 4-5 mice per genotype. Data are presented as mean ± SEM and each datapoint in **B** represents one slice. Dr Emanuel Lopes contributed 10 experiments to this dataset.

As GABA signalling also modulates the activity dependence of DA release (Lopes et al., 2019, Patel et al., 2024, Roberts et al., 2020), subsequent experiments probed if antagonism of GABA$_{A+B}$Rs differentially affects phasic DA release (evoked by 5p 100 Hz stimulation trains) vs 1p [DA]$_o$ across genotypes in 3-6-month-old mice. The frequency sensitivity of DA release was measured by consecutively alternating 1p and 5p 100 Hz stimulations in the absence and presence of GABA$_{A+B}$R antagonists at the same DLS recording site used in **Fig. 4.13**. In DHβE alone, the peak 5p 100 Hz [DA]$_o$ was

approximately 3.5-fold higher than 1p $[DA]_o$ across all genotypes (**Fig. 4.15 A-E**, *left*), in line with previous reports (Lopes et al., 2019, Roberts et al., 2020). The peak magnitude of 5p 100 Hz $[DA]_o$ was higher in the presence of $GABA_{A+B}R$ antagonists compared to DHβE alone (**Fig. 4.15 A-E**, *right*), although no obvious effect of $GABA_{A+B}R$ antagonism on peak 1p $[DA]_o$ was observed in this experiment. This is likely because recordings in the absence and presence of $GABA_{A+B}R$ antagonists in this paradigm were not made consecutively, unlike **Fig. 4.13-4.14**; therefore, the absolute $[DA]_o$ signal naturally declined during the course of the experiment. Nevertheless, $GABA_{A+B}R$ antagonism promoted the frequency dependence of DA release by having a relatively stronger effect on 5p 100 Hz $[DA]_o$ vs 1p $[DA]_o$ (**Fig. 4.15 A-D**, *dashed lines*), which translated to an increase in the 5p 100 Hz/1p ratio following disinhibition of GABAergic signalling (**Fig. 4.15 F**). This effect was significant across all genotypes, apart from L444P mice (**Fig. 4.15 F**). However, no significant effect of genotype or interaction effect between drug and genotype was demonstrated on a two-way ANOVA (**Fig. 4.15 F**). These results therefore show that GABAergic regulation of the frequency sensitivity of DA release was not significantly different across genotypes.

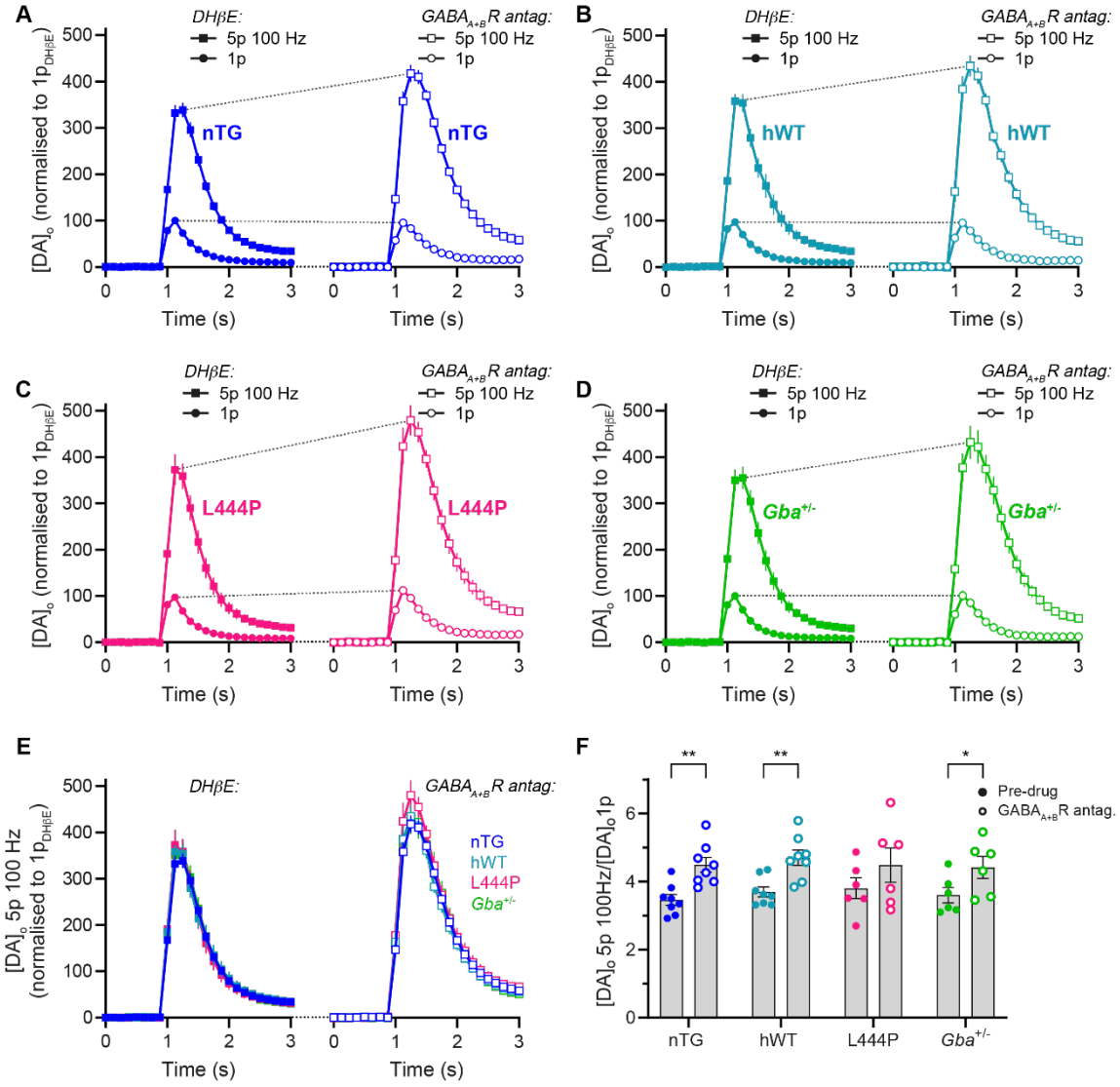


Figure 4.15: The frequency sensitivity of DA release is similar across genotypes in the absence and presence of GABA$_{A+B}$R antagonism. (**A-D**) Mean [DA]$_o$ transients evoked by 1p (*circular datapoints*) and 5p 100 Hz (*square datapoints*) stimulations in DHβE (*left*) and GABA$_{A+B}$R antagonists (*right*, "GABA$_{A+B}$R antag.", 10 μM bicuculine and 4 μM CGP 55845) in mice aged 3-6 months. GABA$_{A+B}$R inhibition increased 5p 100 Hz [DA]$_o$ to a greater extent than 1p [DA]$_o$ (*grey dashed lines*) in nTG (**A**), hWT (**B**), L444P (**C**) and *Gba*$^{+/-}$ (**D**) mice. (**E**) Mean 5p 100 Hz [DA]$_o$ transients from **A-D** overlayed across genotypes in DHβE (*left*) and GABA$_{A+B}$R antagonists (*right*), illustrating the similar peak and kinetics of [DA]$_o$ across genotypes in both conditions. (**A-E**) Data are presented normalised within each genotype to the peak 1p [DA]$_o$ in DHβE. (**F**) Although GABA$_{A+B}$R inhibition tended to increase the ratio of 5p 100 Hz [DA]$_o$ to 1p [DA]$_o$, this effect did not significantly differ across genotypes. (**F**) Two-way ANOVA with Tukey's post-hoc test: genotype $F_{(3,48)} = 0.3490$ $p = 0.7900$, drug treatment $F_{(1,48)} = 22.33$ $p < 0.0001$, interaction $F_{(3,48)} = 0.1975$ $p = 0.8976$; * $p < 0.05$, ** $p < 0.01$ from Tukey's post-hoc test; n = 6-8 slices per genotype from 6-8 mice per genotype (one slice was used per mouse). Data are presented as mean ± SEM and each datapoint in **F** represents one slice.

4.3 DISCUSSION

4.3.1 THE DLS $[DA]_o$ DEFICIT IN L444P MICE IS A MARKER OF EARLY STAGE SELECTIVE VULNERABILITY IN THE ABSENCE OF NEURONAL LOSS

The exploration of early dysfunctional changes in rodent models of PD is of paramount importance for elucidating prodromal pathology and identifying therapeutic targets. Striatal $[DA]_o$ deficits that precede, or are unaccompanied by, neurodegeneration have emerged as an early disease biomarker in a vast array of models, developed by our lab (Sloan et al., 2016, Janezic et al., 2013, Taylor et al., 2014) and others (Cramb et al., 2023, Schirinzi et al., 2016). Indeed, it has previously been demonstrated that 3-month-old L444P mice have impaired $[DA]_o$, exclusively in the DLS (**Fig. 4.1 E**). Building on these observations, experiments in this chapter first investigated if $[DA]_o$ deficits were sustained with age in the L444P mice. To do this, 1p-evoked $[DA]_o$ was recorded across distinct sites in DLS and NAcC using FCV. Two genotypes were compared in each experiment by consecutively alternating recordings across a pair of slices that were simultaneously held in the recording chamber.

Firstly, I confirmed that DLS $[DA]_o$ was not altered by insertion of the human transgene because DA release was similar across nTG and hWT mice (**Fig. 4.3 A**). DA release in the DLS of nTG and *Gba*$^{+/-}$ mice was also comparable (**Fig. 4.3 C**). This indicates that loss of GCase activity was not sufficient to disturb DLS $[DA]_o$ in aged *Gba*$^{+/-}$ mice, consistent with observations at 3 months (**Fig. 4.1 C**). In contrast, DLS $[DA]_o$ was significantly decreased in L444P vs hWT mice (**Fig. 4.3 E**), highlighting that the $[DA]_o$ deficit in L444P mice is sustained with age. However, no significant changes in DLS $[DA]_o$ were observed between L444P and *Gba*$^{+/-}$ mice (**Fig. 4.3 G**). The evoked DLS $[DA]_o$ phenotypes across all pairwise comparisons in aged mice replicate observations in 3-month-old mice (**Fig. 4.1**). Although

$[DA]_o$ did not seem to progressively deteriorate with age in L444P DLS, these studies were not designed to directly compare across ages as they were conducted at different timepoints.

The significantly impaired DA release in young and aged L444P mice are the first demonstrations of evoked $[DA]_o$ deficits in a genetic mouse model of *GBA*-associated PD. In agreement with these findings, diminished DA release was previously observed in heterozygous *GBA*-N370S iPSC-DAns and midbrain organoid models (Rosety et al., 2023, Woodard et al., 2014). The $[DA]_o$ impairment in L444P mice is presumably driven by a gain-of-function effect of the mutation, rather than loss of GCase activity, since we found no evidence of DLS $[DA]_o$ deficits in $Gba^{+/-}$ mice (**Fig. 4.1, 4.3 C**). However, the exact mechanisms underlying this putative gain-of-function effect remain enigmatic and suggestions for future research to unravel this are described further in **Section 4.3.5**. Notably, the normal $[DA]_o$ in $Gba^{+/-}$ mice disagrees with previous reports of impaired DA release in CBE-treated mice (Ginns et al., 2014). The discrepancy between studies may arise due to off-target effects of CBE on GCase2 activity (Kuo et al., 2019, Ridley et al., 2013) or due to differences in the techniques used to measure $[DA]_o$. FCV can record electrically-evoked, relative fluctuations in $[DA]_o$ with millisecond resolution, whereas *in vivo* microdialysis, employed by Ginns et al. (2014), measures absolute $[DA]_o$ collected over a longer timescale (typically minutes) (Bucher and Wightman, 2015). Alternatively, these opposing phenotypes may reflect differences in the extent of GCase deficiency across models, although the magnitude of GCase inhibition achieved with CBE was not reported (Ginns et al., 2014). Notably, considering that no significant differences were detected between L444P and $Gba^{+/-}$ mice at either age (**Fig. 4.1, 4.3 G**), one cannot exclude that $[DA]_o$ may also be mildly diminished in $Gba^{+/-}$ mice. Presuming that this hypothetical impairment is weaker than the L444P deficit, it is possible that my experiments lack sufficient statistical power to uncover a significant difference between $Gba^{+/-}$ vs nTG mice

(**Fig. 4.3 C**). Nevertheless, future FCV studies should further elucidate the relationship between evoked DA release and GCase activity by measuring $[DA]_o$ in response to CBE at titrated concentrations.

On a final note, stereology experiments, conducted prior to this DPhil, confirmed that nigral DA neurons are maintained in L444P mice at 18-months-old (**Fig. A-3**). The striatal $[DA]_o$ deficit in the absence of nigral DA depletion underscores the usefulness of our L444P mice to study early-stage dysfunction in PD. Moreover, pharmacological compounds that target this deficit could be a fruitful disease-modifying therapeutic strategy. It should also be highlighted that the L444P $[DA]_o$ deficit was isolated to the DLS, in agreement with other models developed by our lab (Janezic et al., 2013, Sloan et al., 2016, Taylor et al., 2014). This reflects the PD-related selective vulnerability of the DA neurons that project to this region from the SN (Wong et al., 2019). NAcC $[DA]_o$ phenotypes are discussed further in the next section (**Section 4.3.2**).

4.3.2 Elevated L444P NAcC $[DA]_o$ may be a manifestation of early compensatory mechanisms

$[DA]_o$ was also recorded in the NAcC of aged mice in the multisite FCV experiments presented in **Fig. 4.3**. Consistent with DLS $[DA]_o$ phenotypes, no significant differences were observed between nTG vs hWT, nTG vs *Gba*$^{+/-}$ or L444P vs *Gba*$^{+/-}$ mice (**Fig. 4.3 B, D, H**). However, NAcC $[DA]_o$ was significantly higher in aged L444P vs hWT mice (**Fig. 4.3 F**). It is tempting to speculate that this hyperdopaminergic phenotype may reflect a compensatory or protective process in the aged L444P mice. Indeed, many putative compensatory mechanisms have been described in PD (Blesa et al., 2017), which likely serve to delay neurodegeneration and maintain striatal DA homeostasis during the long prodromal phase (Kalia and Lang, 2015). Moreover, protective factors presumably combat

dopaminergic dysfunction in non-manifesting carriers of *GBA* mutations, considering that most carriers do not develop PD (Balestrino et al., 2020).

Upregulation of the vesicular glutamate transporter 2 (VGLUT2), primarily responsible for glutamate loading into synaptic vesicles, has been proposed to mediate dopaminergic neuroprotection in PD (Buck et al., 2022, Zhao et al., 2023a). VGLUT2 expression in DA neurons enables DA-glutamate co-release and promotes DA loading into synaptic vesicles (Aguilar et al., 2017, Dal Bo et al., 2004, Hnasko et al., 2010). As the vast majority of midbrain VGLUT2-expressing DA neurons are located in the VTA, striatal DA-glutamate co-release is largely isolated to the NAc (Eskenazi et al., 2021, Trudeau et al., 2014, Tecuapetla et al., 2010, Stuber et al., 2010). It follows that a hypothetical protective upregulation of VGLUT2 levels in our L444P mice would preferentially influence dopaminergic transmission in the NAc. Accordingly, VGLUT2 KO in DA neurons of mice deteriorates $[DA]_o$ exclusively in the NAc of *ex vivo* slices (Hnasko et al., 2010, Fortin et al., 2012); however, this $[DA]_o$ deficit is more widespread using *in vivo* recordings (Alsio et al., 2011).

Many lines of evidence have connected VGLUT2 to neuroprotection in PD, although the exact mechanisms remain unclear (Buck et al., 2022, Zhao et al., 2023a). Firstly, VGLUT2-expressing DA neurons are largely spared from degeneration in PD patients, associated with their predominance in the VTA (Brichta and Greengard, 2014, Eskenazi et al., 2021, Trudeau et al., 2014). In rodent models, VGLUT2 KO in DA neurons aggravates MPTP and 6-OHDA-induced pathology (Kouwenhoven et al., 2020, Shen et al., 2018, Steinkellner et al., 2018), whereas VGLUT2-expressing DA neurons are less susceptible to neurotoxins and αS (Buck et al., 2021, Steinkellner et al., 2022). Moreover, VGLUT2 levels are upregulated in DA neurons in response to PD-related insults both *in vitro* and in rodents (Buck et al., 2021, Kouwenhoven et al., 2020, Steinkellner et al., 2022). This has been

proposed to confer neuroprotection and reflects observations of increased VGLUT2 expression in prevailing neurons of postmortem PD brains (Kashani et al., 2007, Steinkellner et al., 2022). Mirroring the phenotype in aged L444P mice, DA release was recently shown to be amplified in heterozygous *GBA*-L444P iPSC-DAns (Rodríguez-Traver et al., 2024). This was accompanied by augmented glutamate release per TH-VGLUT2 co-expressing neuron in the culture, although a corresponding upregulation in VGLUT2 expression was not identified (Rodríguez-Traver et al., 2024). Despite the inconclusive nature of VGLUT2's relation to DA release in these mutant neurons, it would nevertheless be interesting to examine whether VGLUT2 levels are upregulated in L444P NAc axons as a protective mechanism underlying the elevated NAcC $[DA]_o$ in our model.

Non-dopaminergic mechanisms have also been reported to compensate for dysfunctional DA transmission in early phases of PD (Bezard et al., 2003). Supporting this, our lab has demonstrated that the excitability of striatal medium spiny neurons (MSNs) is increased when co-cultured with heterozygous *GBA*-N370S iPSC-DAns (Do et al., 2024). This was suggested to represent a compensatory process considering that it was observed in early, but not late, cultures. In light of this, characterising the electrophysiological properties of MSNs in L444P mice may be an interesting future study.

In contrast to neuroprotective processes, dysfunctional macroautophagy or DAT redistribution on the plasma membrane were reported to underlie hyperdopaminergic phenotypes in αS overexpressing models (Hunn et al., 2019, Medina-Luque et al., 2024). However, these mechanisms are less likely to mediate elevated NAcC $[DA]_o$ in our L444P mice because I found no evidence for gross impairments in autophagy (**Fig. 3.6**) or DAT function and expression in the DLS (**Fig. 4.6-4.9**).

Finally, it is important to note that compensatory changes are largely observed in PD models in response to DA loss (Blesa et al., 2017); however, no changes to the striatal DA

content (**Fig. 4.5**) or nigral DA neurons (**Fig. A-3**) were observed in aged L444P mice. It should also be highlighted that NAc $[DA]_o$ is unaltered in 3-month-old L444P mice (**Fig. 3.1 F, H**) and in previous BAC transgenic rodent models developed by our lab (Janezic et al., 2013, Sloan et al., 2016, Taylor et al., 2014). Additionally, no significant changes to NAcC $[DA]_o$ were observed between L444P and *Gba*$^{+/-}$ mice (**Fig. 3.3 H**). Therefore, the heightened NAcC $[DA]_o$ in L444P mice should be validated in future studies with larger sample sizes before potential underlying mechanisms are explored in greater depth.

4.3.3 Aberrant DA release in L444P mice is not accompanied by striatal DA depletion or perturbed DA turnover

Loss of striatal DA axons has been widely demonstrated to precede SN dopaminergic neurodegeneration in PD patients and rodent models (Kordower et al., 2013, Tagliaferro and Burke, 2016, Wong et al., 2019). I therefore hypothesized that impaired $[DA]_o$ in L444P mice could be attributed to a decline in striatal DA levels, despite the lack of nigral DA neurodegeneration in 18-month-old mice (**Fig. A-3**). However, no detectable changes to the density of DLS dopaminergic axons or the concentration of striatal DA were observed across genotypes using IF and HPLC, respectively (**Fig. 4.4-4.5**). Indeed, it should be noted that my IF measurements provide a relatively crude approach to measuring axonal density. It would therefore be useful for future studies to examine potential changes to the ultrastructure of L444P DA axons with higher resolution imaging e.g. using transmission electron microscopy (TEM). Such an approach may reveal changes to the density of DA release sites, which could inform on the mechanistic-basis of impaired DLS $[DA]_o$ in L444P mice. It would also be advisable to increase the number of mice per group for these experiments, considering that my IF study only incorporated three mice per genotype at each age. Future research directions are discussed further in **Section 4.3.5**.

Nevertheless, my results corroborate previous findings from HPLC experiments conducted in a 3-month-old cohort (**Fig. A-4 A-B**). Similarly, DA levels were normal in the striatum of *Gba*$^{D409V/D409V}$ (Polinski et al., 2021, Polinski et al., 2022) and *Gba*$^{+/L444P}$ mice (Lado et al., 2024, Migdalska-Richards et al., 2017b, Yun et al., 2018), although the L444P mutation can significantly aggravate MPTP-induced striatal DA depletion (Yun et al., 2018). Striatal DA axons were also preserved in CBE-treated mice (Mus et al., 2019). Conversely, intracellular DA was decreased in heterozygous and homozygous *GBA*-N370 iPSC-DAns (Aflaki et al., 2016, Woodard et al., 2014), which was associated with reduced DA uptake (Aflaki et al., 2016). Furthermore, Rosety et al. (2023) demonstrated that TH+ neurons are less abundant in heterozygous *GBA*-N370S midbrain organoids. However, this phenotype arose due to defective differentiation of precursor cells into dopaminergic neurons (Rosety et al., 2023) and therefore lacks construct validity to the age-related neurodegenerative process in PD patients.

Aside from DA depletion in the striatum and SN, there are mixed reports of increased (Lohle et al., 2016, Sossi et al., 2002, Sossi et al., 2004) and decreased (Kremer et al., 2021) DA turnover in PD patients, using ^{18}F-dopa positron emission tomography (PET) imaging or by quantifying relative levels of DA and DOPAC, respectively. Elevated DA turnover in early PD patients has been suggested to represent compensatory changes in response to neurodegeneration (Sossi et al., 2002, Sossi et al., 2004). HPLC experiments in this chapter determined that DOPAC levels and the DOPAC:DA ratio in the CPu and NAc were comparable across genotypes in aged mice (**Fig. 4.5**), thereby indicating that DA turnover was not grossly altered by the L444P mutation. These findings also replicated previous observations in our L444P model at 3-months-old (**Fig. A-4 C-D**) and corroborated reports of normal DOPAC content and DA turnover in *Gba*$^{+/L444P}$ mice (Lado et al., 2024, Migdalska-Richards et al., 2017b, Yun et al., 2018). On the other hand, studies in

Gba$^{D409V/D409V}$ mice have yielded inconsistent results as DA turnover was unchanged or increased across reports (Polinski et al., 2021, Polinski et al., 2022). DA turnover was also heightened in heterozygous *GBA*-N370 iPSC-DAns (Woodard et al., 2014) and CBE-treated SH-SY5Y cells (de la Fuente et al., 2017). However, the concentration of DOPAC was equivalent to, or greater than, DA in these studies (de la Fuente et al., 2017, Woodard et al., 2014); therefore, these results have limited biological validity, given that DOPAC levels are an order of magnitude lower than DA in humans (Fornstedt Wallin, 2024).

To conclude, the absence of genotype-related differences in my IF and HPLC experiments reflect the lack of DA neurodegeneration in the SN of aged L444P mice (**Fig. A-3**) and confirmed that the L444P DLS $[DA]_o$ deficit did not arise due to altered striatal DA levels.

4.3.4 PD-RELATED DISTURBANCES TO THE LOCAL CONTROL OF DA TRANSMISSION BY THE STRIATAL MICROCIRCUITRY

Striatal dopaminergic signalling is regulated by a plethora of transporters and neuromodulators in the microcircuitry of striatal release sites (**Fig. 4.2**). Experiments in this chapter explored if potential changes to these regulatory mechanisms in the DLS coincided with impaired $[DA]_o$ in young and aged L444P mice.

Experiments first sought to investigate the functionality and expression of the DAT, a master regulator of striatal DA homeostasis. DATs are sodium chloride coupled transporters, which are exclusively present on DA neurons (Nirenberg et al., 1996, Hersch et al., 1997, Ciliax et al., 1999, Lohr et al., 2017) and are primarily responsible for DA reuptake from the extracellular space following exocytosis (Cragg and Rice, 2004, Giros et al., 1996, Rice and Cragg, 2008) (**Fig. 4.2**). This has a knock-on influence on vesicular loading and quantal size by controlling levels of intracellular DA stores (Benoit-Marand et al., 2000, Jones et al., 1998). The DAT has also been shown to heighten neuronal excitability (Carvelli et al., 2004,

Ingram et al., 2002) and regulate the short term plasticity of DA release (Condon et al., 2019). Experiments in this chapter determined that DAT-inhibition with cocaine had a similar effect on the amplitude of 1p-evoked and 2p 100 Hz-evoked DA release in all genotypes (**Fig. 4.6-4.8**). The value of the PPR of DA release was also comparable across genotypes in the presence and absence of cocaine (**Fig. 4.8**). Subsequently, no genotype-related differences were observed in the area of DAT immunofluorescent signal in the DLS (**Fig. 4.9**). Altogether, these findings indicate that DAT expression and DAT-mediated control of DA reuptake and short term plasticity is not altered in our L444P mice. Conversely, Aflaki et al. (2016) illustrated that DA reuptake was reduced in homozygous *GBA*-N370S iPSC-DAns. This was associated with a trending downregulation of DAT mRNA levels. Although this was the only previous report examining DA-reuptake in a *GBA* mutant model, dysregulated trafficking and endocytic recycling of the DAT has been shown to accompany aberrant DA transmission in a range of other transgenic PD models (Bu et al., 2021). Furthermore, we and others have demonstrated that the functionality and expression levels of DATs are elevated in other non-*GBA* models of early PD (Harraz, 2023, Threlfell et al., 2021). This contrasts with the DAT decline in PD patients as a correlate of dopaminergic cell loss (Heng et al., 2023). Augmented DAT activity can render DA neurons more susceptible to toxicity by elevating cytosolic DA and related oxidative stress (Masoud et al., 2015) and by transporting the PD-related toxicants, 6-OHDA and MPP+ (the active toxic metabolite of MPTP), into the cell (Cerruti et al., 1993, Gainetdinov et al., 1997, Redman et al., 2006). The mechanisms underlying increased DAT function in models of early PD remain unclear but autophagic deficits and co-accumulation of αS and cholesterol have been proposed to contribute (Harraz, 2023, Threlfell et al., 2021).

DA is known to limit the probability of subsequent DA release in a negative feedback mechanism via activation of D_2Rs on DA axons (**Fig. 4.2**) (Ford, 2014). D_2Rs are $G_{i/o}$

coupled G protein-coupled receptors (GPCRs) whose activation triggers downstream signalling cascades that inhibit calcium channels and mediate hyperpolarisation by G protein-coupled inwardly rectifying potassium channels (GIRKs) (Ford, 2014). These receptors are located on the soma and axons of DA neurons, although the influence of D_2R-mediated autoinhibition is stronger on axonal vs somatodendritic DA release (Cragg and Greenfield, 1997). This chapter demonstrated that pharmacological agonism of axonal D_2Rs with quinpirole suppressed 1p-evoked DLS $[DA]_o$ in a concentration-dependent fashion (**Fig. 4.10-4.11**); however, this effect was similar across genotypes. In agreement with this, no genotype-related differences in area of DLS D_2Rs were observed with immunofluorescent staining (**Fig. 4.12**). This indicates that D_2R-mediated inhibitory effects on striatal DA release and D_2R expression are not altered by the L444P mutation. The regulation of DA transmission by D_2Rs has not previously been investigated in a model of *GBA*-associated PD. However, downregulation of D_2R-mediated autoinhibition disturbed DA release, firing activity and calcium dynamics in DA neurons from mice that overexpress αS (Dagra et al., 2021, Lin et al., 2021). Dysregulated D_2R signalling in non-DA neurons can also induce pathology in PD models. For instance, D_2R expression was reduced in neurons of the prefrontal cortex in *Park7* KO mice, which disrupted calcium signalling and gave rise to anxiety-like behaviour (Li et al., 2019b). It follows that D_2R activation has been shown to confer neuroprotection in a myriad of cell and animal models of PD (Bozzi and Borrelli, 2006). Indeed, DA receptor agonists, many of which are selective for D_2Rs, have been used in the clinic to manage PD symptoms for over 50 years (Isaacson et al., 2023, Woitalla et al., 2023). D_2R agonists have diverse neuroprotective mechanisms, which are largely dependent on their site of action. For instance, studies in preclinical models have shown that activation of D_2Rs on DA neurons attenuates hyperactive neuronal firing and oxidative stress (Dagra et al., 2021, Lin et al., 2021), whereas D_2R agonism on MSNs

improves calcium homeostasis and mitochondrial function by inhibiting cAMP/PKA signalling (Tozzi et al., 2018).

Aside from DA-mediated inhibition, striatal GABA also inhibits DA release primarily via $GABA_{A+B}$Rs on DA axons (**Fig. 4.2**) (Roberts et al., 2021). $GABA_A$ receptors are ionotropic chloride-conducting channels (Ghit et al., 2021), whereas $GABA_B$ receptors are $G_{i/o}$ coupled GPCRs (Gassmann and Bettler, 2012). This tonic inhibition is limited by GABA uptake via GABA uptake transporters (GATs) on neurons and astrocytes (Roberts et al., 2021). This chapter explored if the magnitude of inhibitory striatal GABA tone was altered across genotypes by measuring $[DA]_o$ in response to $GABA_{A+B}$R antagonism with bicuculine and CGP 55845. Co-application of these antagonists increased the peak amplitude of 1p-evoked $[DA]_o$ to a similar extent across genotypes, thereby indicating that the L444P mutation does not alter GABA-mediated tonic inhibition of DA release (**Fig. 4.13-4.14**). This was the first investigation into the influence of GABAergic signalling on striatal DA dynamics in a mouse model of *GBA*-associated PD. However, our lab previously determined that GABA-mediated tonic inhibition on DA release is elevated in *SNCA*-OVX mice, due to GAT downregulation (Roberts et al., 2020). Reduced GAT levels have also been observed in the basal ganglia of 6-OHDA rodent models (Chazalon et al., 2018). Subsequent experiments in this chapter demonstrated that the frequency dependence of DA release was increased following $GABA_{A+B}$R antagonism, which reached significance in all genotypes except for L444P mice (**Fig. 4.15**). These observations were surprising considering that our lab has previously shown that augmenting GABAergic signalling (via $GABA_{A+B}$R agonism or GAT inhibition) also increases the frequency sensitivity of DA release (Lopes et al., 2019, Roberts et al., 2020). Additionally, antagonism of GABAergic signalling previously had no significant effect on the 5p 100 Hz/1p $[DA]_o$ ratio (Lopes et al., 2019). However, in accord with my results, Patel et al. (2024) found that antagonism of $GABA_A$Rs on DA axons

promoted the frequency dependence of DA release by exerting stronger disinhibition of DA evoked by stimulation trains vs single-pulses. This effect was lost following GAT KO on DA axons, indicating that GABA co-released from DA neurons is responsible for autoinhibition at $GABA_A$Rs (Patel et al., 2024). We could therefore hypothesize that GAT levels are reduced on DA neurons of L444P mice, since the activity-dependence of DA release was not significantly altered by $GABA_{A+B}$R antagonism in these mice (**Fig. 4.15**). However, it is likely that my study lacked statistical power to reveal a significant difference in this group: the number of L444P mice was less than nTG and hWT mice and the mean 5p 100 Hz/1p $[DA]_o$ ratio in $GABA_{A+B}$R antagonists was similar to other groups. Furthermore, a two-way ANOVA did not reveal an effect of genotype or a drug x genotype interaction effect. Therefore, my experiments did not find conclusive evidence that GABAergic inhibition of single-pulse and phasic evoked DA release is disturbed in L444P mice.

Acetylcholine (ACh) is another key player in the regulation of striatal DA transmission (**Fig. 4.2**) (Exley and Cragg, 2008). Therefore, future studies could investigate whether changes to cholinergic signalling coexist with the $[DA]_o$ deficit in L444P mice. Cholinergic signalling at nAChRs can directly drive DA release independent of firing activity in the cell body of nigral DA neurons (Threlfell et al., 2012). Therefore, striatal ACh acts via nAChRs on DA axons to directly increase DA release evoked by single-pulse electrical stimulations as part of a dual-release event. ACh action at DA axons also contributes to short term depression of DA release in response to higher frequency stimulation trains (Rice and Cragg, 2004, Zhang and Sulzer, 2004). This effect likely arises because nAChR activation can maintain the DA axons in a depolarised state for approximately 100 ms after the initial depolarisation event, which prevents further action potential generation and DA axon activation (Zhang et al., 2025b). It follows that the effect of nAChR antagonism on DA release probability depends on the firing activity of DA neurons; the peak amplitude of

single-pulse $[DA]_o$ is attenuated but phasic $[DA]_o$ is augmented (Rice and Cragg, 2004, Zhang and Sulzer, 2004). Meanwhile, DA signalling modulates cholinergic interneuron (CIN) excitation either directly, by activating DA receptors on CINs, or indirectly, via co-released glutamate or GABA (Chuhma et al., 2014, Straub et al., 2014, Tritsch and Sabatini, 2012, Wieland et al., 2014). A long standing theory in the pathogenesis of PD is that reciprocal antagonistic interactions between striatal DA and ACh are disrupted (Barbeau, 1962). Consequently, DA depletion gives rise to hypercholinergic activity, which contributes to motor symptoms (Tubert and Murer, 2021). In line with this, anticholinergic therapies were a cornerstone of symptom management before the advent of levodopa (Carlos Giugni and Rodriguez-Cruz, 2016, Duvoisin, 1967). However, studies in recent years have disputed the view that DA and ACh exist purely in opposition in the disorder. Across various rodent models, DA deficiency attenuated the strength of cholinergic signalling at M4 muscarinic receptors (Nielsen and Ford, 2024) and weakened CIN excitability and long term potentiation (Cai et al., 2021, McKinley et al., 2019, Tozzi et al., 2016). Notably, restoring cholinergic activity in some of these models alleviated motor deficits (Cai et al., 2021, Nielsen and Ford, 2024). On the other hand, cholinergic signalling in the striatum of existing *Gba* transgenic mice has not been investigated. Nonetheless, Clarke et al. (2019) suggested that hippocampal cholinergic transmission is impaired in $Gba^{+/D409V}$ mice, due to downregulation of the vesicular acetylcholine transporter (vAChT). Furthermore, the heterozygous *GBA*-N370S mutation impairs GCase activity and causes αS and tau accumulation iPSC-derived cholinergic neurons (Yang et al., 2022). Additionally, *GBA*-associated PD patients have more severe cholinergic degeneration vs non-*GBA* mutation carriers in early disease stages (Slingerland et al., 2024, Slingerland et al., 2025). Cholinergic denervation has also been associated with exacerbated cognitive decline in patients harbouring *GBA* mutations (Slingerland et al., 2025). Considering this, investigations into

striatal and extra-striatal cholinergic transmission in our L444P mice would be interesting lines of future research. The next section (**Section 4.3.5**) explores other suggestions for future experiments focused on elucidating mechanisms underlying the DA release deficit in L444P mice.

4.3.5 FUTURE RESEARCH AVENUES TO SHED LIGHT ON THE MECHANISTIC BASIS OF IMPAIRED $[DA]_o$ IN L444P MICE

The exact gain-of-function effect of the L444P mutation that is responsible for impaired DLS DA release remains unknown. Investigating pathological mechanisms that are implicated in the selective vulnerability of SN DA neurons in PD may provide valuable clues into this. One long standing theory underlying why DA neurons of the SN are more liable to degeneration is that their expansive axonal arbour (Matsuda et al., 2009) increases their susceptibility to bioenergetic impairments (Bolam and Pissadaki, 2012, Wong et al., 2019). Supporting this, mitochondrial oxidative phosphorylation, and resultant oxidative stress, have been shown to positively relate to the extent of axonal arborization of DA neurons (Pacelli et al., 2015). Notably, *GBA* mutations have been demonstrated to impair mitochondrial function in a plethora of cell and animal models (Rubilar et al., 2024). For example, the homozygous L444P mutation directly disturbs mitochondrial complex 1 activity in organoid models (Baden et al., 2023) and heterozygous *GBA*-84GG iPSC-DAns have less axonal mitochondria and reduced ATP production (Kim et al., 2021). Considering this, it is plausible that the energy requirements of DLS axons in L444P mice exceed their bioenergetic capacity. This could, at least in part, underlie the diminished DLS $[DA]_o$ in these mice.

Moreover, spontaneous oxidation of cytosolic DA to reactive quinone species also contributes to the selective vulnerability of DA neurons in PD (Wong et al., 2019). It follows that a hypothetical increase in DA oxidation may contribute to DLS-specific impairments in

DA transmission in our L444P mice. Oxidised DA can also directly perturb cysteine residues in GCase's catalytic site, thereby impairing GCase activity (Burbulla et al., 2017). Additionally, the L444P mutation has been shown to drive synaptic vesicle endocytosis deficits in mice (Vidyadhara et al., 2025), which may exacerbate the accumulation of oxidised DA (Burbulla and Krainc, 2019, Wong et al., 2019).

Furthermore, SN DA neurons are subjected to high calcium influxes due to their endogenous pacemaking activity. This is also thought to be a culprit in mediating selective vulnerability (Chan et al., 2007, Surmeier and Schumacker, 2013). Elevated cytosolic calcium contributes to mitochondrial-related oxidative stress (Guzman et al., 2010) and the accumulation of cytoplasmic DA that is susceptible to oxidation (Mosharov et al., 2009) in SN DA neurons. Indeed, dysregulated calcium signalling was associated with bioenergetic insufficiency and increased oxidative stress in GCase deficient neurons from mice (Plotegher et al., 2020). Calcium dyshomeostasis has also been demonstrated in iPSC-DAns harbouring various *GBA* mutations (Beccano-Kelly et al., 2023, Schondorf et al., 2014). Furthermore, the L-type voltage gated calcium channels that mediate calcium inflow during pacemaking also promote DA release in the DLS (Brimblecombe et al., 2015, Chan et al., 2007) and our lab has shown that inhibiting these channels attenuates DLS $[DA]_o$ in female *Gba*$^{+/-}$ mice (Brimblecombe et al., 2024). This indicates that GCase activity modulates L-type channel-mediated control of DA release, although the underlying mechanisms are unknown. Nevertheless, future investigations into the regulation of calcium homeostasis in our L444P mice may shed light on the mechanistic basis of impaired DLS $[DA]_o$.

An in-depth characterisation of the intrinsic properties of striatal DA axons could also be useful to unveil mechanisms underlying the DLS $[DA]_o$ deficit in L444P mice. Initial experiments, conducted prior to this DPhil, hypothesized that impaired $[DA]_o$ in 3-month-old L444P mice may be reflected by a reduction in the synaptic release machinery. Although

no gross changes to synaptotagmin or SNARE proteins in the L444P striatum were observed on Western blots (Dr Natalie Connor-Robson, *data not shown*), the mixed-cell population in the tissue may be masking dopaminergic-specific deficits. Our lab has recently integrated spatial transcriptomic analysis with translating ribosome affinity purification (TRAP) to identify cell type-specific gene expression signatures in SN and VTA DA neurons (Kilfeather et al., 2024). Such approach may identify that genes implicated in synaptic vesicle recycling are differentially expressed specifically in SN DA neurons of our L444P mice. Notably, RNA sequencing analysis has not been conducted in the midbrain or striatum of *Gba* transgenic mice. However, we have previously demonstrated that genes controlling synaptic function are downregulated in heterozygous *GBA*-N370S iPSC-DAns (Lang et al., 2019) and Vidyadhara et al. (2025) found that genes governing synaptic vesicle recycling and synapse assembly were downregulated in cortical neurons from *Gba*$^{L444P/KO}$ mice. In addition, TEM is a powerful tool for visualising the synaptic vesicle pool and ultrastructure of dopaminergic synaptic boutons in the striatum. This approach revealed that synaptic vesicles were less abundant or re-distributed in striatal dopaminergic axons of other genetic PD rodent models, which coincided with impaired $[DA]_o$ (Connor-Robson et al., 2019, Janezic et al., 2013). Moreover, striatal axons of CBE-treated mice were found to have a smaller post-synaptic density (Ginns et al., 2014), although this study did not distinguish between dopaminergic and non-dopaminergic neurons. Additionally, cortical synapses of *Gba*$^{L444P/KO}$ mice harbour less clathrin coated vesicles, which was associated aberrant synaptic vesicle endocytosis (Vidyadhara et al., 2025). Future studies should explore whether similar changes are also evident in the striatum of our L444P model, considering that striatal dopaminergic axons in existing *Gba* genetic mouse models have not been visualised with TEM.

The magnitude and probability of striatal DA release is also regulated by the firing activity of midbrain dopaminergic neurons (Dreyer et al., 2010, Sulzer et al., 2016). Notably, striatal $[DA]_o$ deficits in other rodent models developed by our lab coexisted with age-related changes to the firing pattern and firing rate of nigral DA neurons (Janezic et al., 2013, Sloan et al., 2016). However, electrophysiological properties of DA neurons in the SN of *GBA*-associated PD mouse models have not been examined. Moreover, studies in *GBA* mutant iPSC-DAns have produced mixed results: the frequency of evoked action potentials was reduced, unchanged or increased across reports in neurons harbouring diverse *GBA* mutations (Beccano-Kelly et al., 2023, Rodríguez-Traver et al., 2024, Rosh et al., 2024). In contrast, the spontaneous excitatory activity of *GBA* mutant iPSC-DAns and pyramidal neurons of $Gba^{+/L444P}$ mice was more consistently attenuated across studies (Beccano-Kelly et al., 2023, Lado et al., 2024, Rosh et al., 2024, Woodard et al., 2014). However, this spontaneous activity has limited relevance to the electrically evoked DA release deficit in L444P mice. Nevertheless, characterising the firing activity of SN DA neurons in our L444P mice would be an interesting line of future research and may help to elucidate the origin of the DA release deficit.

4.3.6 CONCLUSION

Experiments in this chapter first demonstrated that aged L444P mice have impaired DLS $[DA]_o$ and subsequently confirmed that this is not accompanied by loss of striatal DA content. This deficit therefore represents a biomarker of selective early-stage dysfunction and illustrates the usefulness of our model to study pathology in the prodromal phase of PD. It is plausible that a gain-of-function effect of the L444P mutation underpins this impairment, given that $Gba^{+/-}$ mice have normal DA release. On the other hand, increased L444P NAcC $[DA]_o$ may be a telltale sign of underlying protective or compensatory processes. However, the exact mechanisms that govern dysregulated $[DA]_o$ in L444P mice

remain elusive. Furthermore, the regulation of DLS DA transmission by the DAT, D_2Rs and $GABA_{A+B}$Rs was not perturbed in L444P mice, despite being dysregulated in other PD models. This mild pathology likely reflects the role of *GBA* as a risk factor, and not a causal agent, in PD. In future, exploring other local modulators of striatal DA transmission or factors that may be implicated in the selective vulnerability of DLS DA axons could shed further light on the DLS DA release deficit in our L444P model. Indeed, illuminating the pathophysiological basis of impaired $[DA]_o$ in L444P mice may prove fruitful for the development of pharmacological strategies to alleviate early-stage dysfunction in *GBA*-associated PD. The next chapter explores whether impaired DLS $[DA]_o$, and other pathological phenotypes observed in Chapter 3, translate into behavioural deficits in aged L444P mice.

CHAPTER 5: BEHAVIOURAL CHARACTERISATION OF AGED MICE

5.1 INTRODUCTION

The symptomatology of PD comprises both the cardinal motor signs: bradykinesia, tremor, rigidity and postural instability, and a broad spectrum of non-motor symptoms, including GI, cognitive and psychological deficits (Schapira et al., 2017, Sveinbjornsdottir, 2016). Although motor symptoms largely underpin clinical diagnosis of the disease, non-motor symptoms can manifest up to 20 years prior and therefore offer a window into early-stage pathology (Kalia and Lang, 2015, Postuma et al., 2012, Tolosa et al., 2021). *GBA*-associated PD patients have a similar clinical profile to idiopathic PD patients but tend to have faster deterioration of motor function and a higher prevalence of various non-motor symptoms (**Table 1.2, Section 1.2.3**) (Brockmann et al., 2015, Brockmann et al., 2011, Cilia et al., 2016, Petrucci et al., 2020, Straniero et al., 2020, Malek et al., 2018, Jesus et al., 2016, Carandina et al., 2022, Zhang et al., 2018b).

Behavioural characterisation of PD rodent models is crucial for understanding how underlying pathophysiology contributes to symptom onset and progression (Sheta et al., 2024, Zhang et al., 2022c). Behavioural studies are also a cornerstone of preclinical investigations into potential therapeutic compounds for the disease (Guimaraes et al., 2024). Therefore, rodent models that exhibit disease-relevant, reproducible behavioural phenotypes are highly sought after. However, the face validity of PD rodent models has been criticized in recent years and there remains a misalignment between therapeutic efficacy in preclinical and clinical trials (Vingill et al., 2018, Zeiss et al., 2017). This “translation-gap” obstructs the development of neuroprotective therapies and has contributed to debate on the usefulness

of rodent models to PD research (Barker and Bjorklund, 2020, Athauda and Foltynie, 2015). The incomplete penetrance of *GBA* mutations in the disease poses a further challenge to replicating PD symptoms in *Gba* transgenic mice, considering that up to 90% of heterozygous *GBA* mutation carriers do not display any signs of parkinsonism (Balestrino et al., 2020, Farfel-Becker et al., 2019).

Previous chapters of this thesis demonstrated pathological effects of the L444P mutation in cells, tissue homogenates and *ex vivo* sections. In this chapter, I sought to examine whether these findings translated into behavioural deficits in the L444P mice. Prior to the experiments presented herein, conducted in 2021, few studies had characterised behaviour in *Gba* transgenic models (**Table 5.1-5.2, 5.4-5.5**). Only two reports included $Gba^{+/L444P}$ mice (Migdalska-Richards et al., 2017b, Yun et al., 2018) and many early investigations drew insights from mice carrying homozygous or compound heterozygous mutations, including the D409H and D409V mutations (Kim et al., 2018a, Dai et al., 2016, Sardi et al., 2011). Behavioural phenotypes in these mice have limited validity to PD-relevant behaviour because homozygous *GBA* mutations cause GD, whilst heterozygous mutations are more commonly associated with PD (Riboldi and Di Fonzo, 2019). Also, D409H has low prevalence in PD, whereas D409V is a rare mutation only observed once in heteroallelic GD patients and not in PD patients (Parlar et al., 2023, Theophilus et al., 1989b). Moreover, existing *Gba* transgenic mice lack comprehensive gait analysis, in spite of the plethora of gait difficulties in PD patients (Mirelman et al., 2019). The CatWalk XT automated gait analysis system was therefore incorporated into this behavioural test battery, given its ability to detect subtle, PD-relevant gait abnormalities in a wide range of other rodent models (Garrick et al., 2021, Timotius et al., 2023). To optimise the likelihood of observing clinically relevant deficits, behaviour was characterised in aged mice (15-21-months-old). This age range recapitulates the age of symptom onset and progression in *GBA*-

associated PD patients (Sukoff Rizzo and Crawley, 2017, Zhang et al., 2018b). In addition, the comparison of L444P and *Gba*$^{+/-}$ mice in this study may shed light on whether gain- or loss-of-function-effects of the L444P mutation are primarily driving behavioural deficits.

The specific aims of the behavioural assays presented in this chapter are:

1. To characterise various aspects of motor function, including general LMA, coordination, balance, muscle strength and gait.
2. To examine non-motor clinical phenotypes related to GI, cognitive and psychological function.

5.2 RESULTS

5.2.1 CHARACTERISTICS OF THE BEHAVIOURAL COHORT

A cohort of mice was bred and maintained for behavioural characterisation. At the time of testing, all mice were aged between 15-21 months; however, L444P mice were significantly younger than hWT mice (**Fig. 5.1 A**). On the other hand, weight was comparable across genotypes (**Fig. 5.1 B**). The proportion of male and female mice was relatively even in all groups and the sex-distribution was not significantly different across genotypes (**Fig. 5.1 C**). The sample sizes of each group were as follows: nTG = 11 mice, hWT = 15 mice, L444P = 9 mice and *Gba*$^{+/-}$ = 11 mice (**Fig. 5.1 C**).

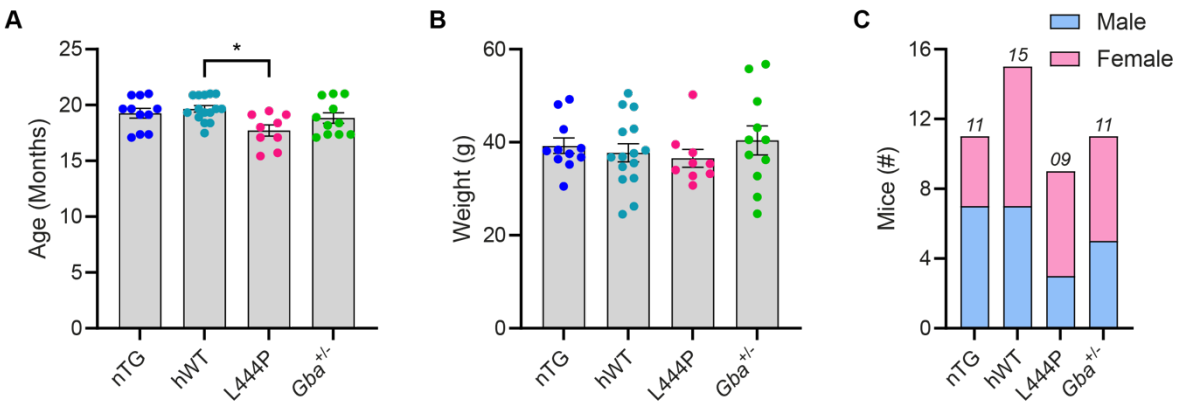


Figure 5.1: The age, weight and sex distribution of the behavioural analysis cohort. (**A**) The mean age of L444P mice was significantly lower than hWT mice. (**B**) The weight of the mice was evenly distributed across genotypes. (**C**) The sex distribution was not significantly different across genotypes. The sample size of each group is given in italics at the top of the bars in (**C**). (**A**) Kruskal-Wallis test with Dunn's post-hoc test: Kruskal-Wallis statistic = 9.452 p = 0.0238, (**B**) Kruskal-Wallis test: Kruskal-Wallis statistic = 1.999 p = 0.5726, (**C**) Fisher's exact test: p = 0.6294; * p < 0.05 from Dunn's post-hoc test; n = 9-15 mice per genotype. Data are presented as mean ± SEM and each datapoint (**A-B**) represents one mouse.

5.2.2 SPONTANEOUS LOCOMOTION IN THE OPEN FIELD

Akinesia, characterised by difficulties in conducting voluntary movements, is typically assessed in rodent models by measuring spontaneous locomotor activity (LMA) (Guimaraes et al., 2024, Sheta et al., 2024). The Photobeam Activity System-Home Cage (PAS-HC) (SD instruments) was used to measure spontaneous LMA in this study. This apparatus automatically tracks ambulation in real-time by recording photobeam breaks made as a mouse freely moves around the open field.

Beam breaks were collated into 15 min intervals over the 4 hour trial. In all genotypes, the accumulative number of beam breaks increased steeply at first but gradually plateaued in later phases of the trial (**Fig. 5.2 A**). This pattern illustrates that LMA steadily declined at a similar rate across genotypes. The total number of beam breaks during the trial was also comparable in all genotypes (**Fig. 5.2 B**). Together, these results demonstrate that spontaneous LMA is not significantly different across genotypes. The open field test can also assess anxiety-related behaviour by measuring rodents' ambulation in the centre vs periphery of the arena (Seibenhener and Wooten, 2015). Typically, mice with higher levels of anxiety display thigmotactic behaviour and therefore avoid exploring the centre of the open field (Simon et al., 1994). In this study, the accumulative number of central beam breaks after each 15 min interval was equivalent across genotypes (**Fig. 5.2 C**). Similar to total LMA, mice's central activity was highest at the start of the trial and then levelled off. On average, all genotypes spent approximately 35% of the total trial in the centre of the field (**Fig. 5.2 D**). Therefore, this study did not identify anxiety-related phenotypes in L444P mice.

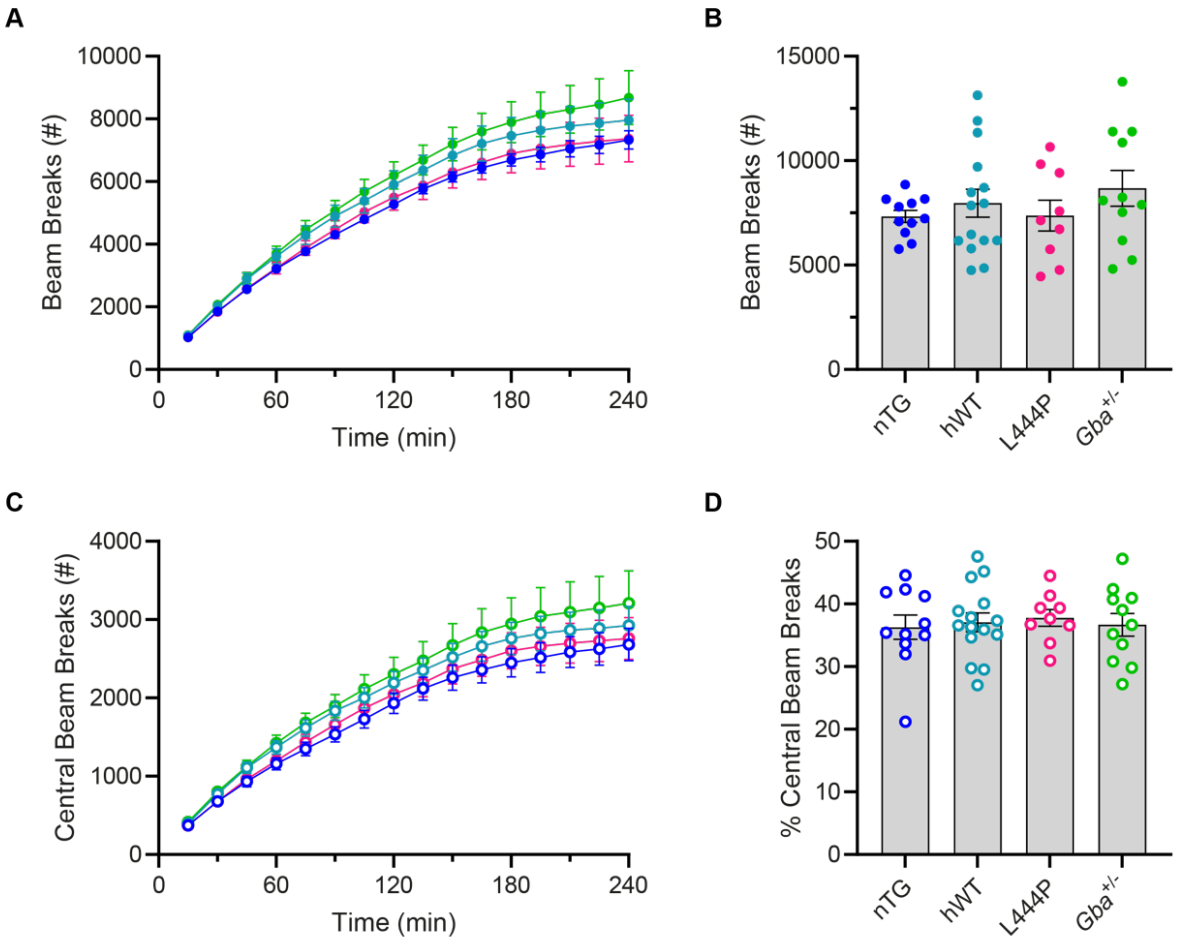


Figure 5.2: Spontaneous LMA is similar across genotypes. Infrared beam breaks caused by locomotion of each mouse were recorded in 15 min intervals across four hours as each mouse spontaneously moved around its own open field. No genotype-related differences were observed in the accumulative increase in beam breaks over time (**A**), the total beam breaks made during the test (**B**), the beam breaks made in the centre of the arena (# central beam breaks) (**C**) and the proportion of central beam breaks expressed normalised to total beam breaks (**D**). (**A, C**) Two-way repeated measures ANOVA: (**A**) genotype $F_{(3,42)} = 1.008$ $p = 0.3986$, time $F_{(1.147,48.17)} = 370.0$ $p < 0.0001$, interaction $F_{(45,630)} = 0.6496$ $p = 0.9636$, (**C**) genotype $F_{(3,42)} = 0.8986$ $p = 0.4499$, time $F_{(1.109,46.57)} = 265.5$ $p < 0.0001$, interaction $F_{(45,630)} = 0.4379$ $p = 0.9995$, (**B, D**) one-way ANOVA: all $F_{(3,42)} < 0.7979$ and all $p > 0.5020$; n = 9-15 mice per genotype. Data are presented as mean ± SEM and each datapoint (**B, D**) represents one mouse.

5.2.3 Motor coordination and balance on the accelerating rotarod

Since its inception over 60 years ago (Dunham and Miya, 1957), the rotarod has become one of the most widely used methods to assess coordination and balance in rodent models of PD (Sheta et al., 2024). This simple test measures the duration that mice can stay on an accelerating, rotating horizontal rod before falling off. This is recorded as the latency to fall

(Deacon, 2013a). This chapter presents the first study to characterise rotarod performance in a mouse model carrying a monogenic L444P mutation[6].

The mice's latency to fall increased during the training phase (trial days 1-3) and remained largely stable during the test phase (trial days 4-5) (**Fig. 5.3 A**). All genotypes improved to a similar extent across trial days, illustrating that L444P mice have normal motor learning abilities. The mean latency to fall across trial days 4-5 was also comparable across genotypes (**Fig. 5.3 B**). These findings therefore indicate that aged L444P mice do not have impaired coordination or balance on the rotarod. The fall latency of C57BL/6 mice has previously been shown to negatively correlate with age (Shoji and Miyakawa, 2019, Shoji et al., 2016, Yanai and Endo, 2021) and bodyweight (McFadyen et al., 2003, Cook et al., 2002). In this cohort, no correlation existed between age and latency to fall (**Fig. A-5 A,C**). However, weight and latency to fall were negatively correlated. This reached significance in all genotypes, except for nTG mice (**Fig. A-5 B-C**). To ensure that age or weight did not confound a potential genotype-effect on rotarod performance, the linear regression lines on each scatterplot (**Fig. A-5 A-B**) were compared across genotypes using ANCOVAs. On both plots (**Fig. A-5 A-B**), the slope and y-intercept of the linear regression lines were not significantly different across genotypes. Therefore, the latency to fall remained comparable across genotypes after including age or weight as a covariate.

[6] These experiments were conducted in 2021, the first published reports on rotarod performance in *Gba*$^{+/L444P}$ and *Gba*$^{L444P/L444P}$ mice were from Lado et al. (2024) and Furderer et al. (2024), respectively.

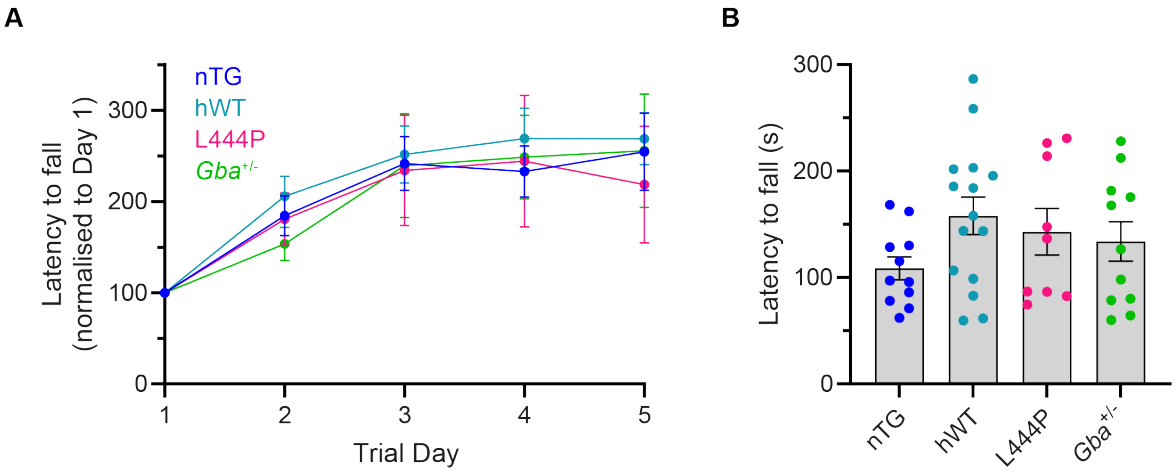


Figure 5.3: Aged L444P mice did not display coordination or balance deficits on the rotarod. The amount of time mice stayed on an accelerating rotarod before falling (latency to fall) was recorded and used as an indicator of coordination and balance. (**A**) The latency to fall increased to a similar extent across genotypes with repeated exposures to the rotarod across trial days. Data are expressed normalised to the latency to fall on day one within each individual mouse. (**B**) The average latency to fall across trial days 4-5 was also similar across genotypes. (**A**) Two-way repeated measures ANOVA: genotype $F_{(3,42)} = 0.1401$ $p = 0.9354$, time $F_{(1.870,78.53)} = 27.80$ $p < 0.0001$, interaction $F_{(12,168)} = 0.2748$ $p = 0.9924$, (**B**) one-way ANOVA: $F_{(3,42)} = 1.489$ $p = 0.2315$; n = 9-15 mice per genotype. Data are presented as mean ± SEM and each datapoint (**B**) represents one mouse.

5.2.4 Speed and Coordination on the Vertical Pole

Bradykinesia, i.e. slowness of movement, is another debilitating cardinal sign of PD (Bologna et al., 2020). This symptom has been widely characterised in rodent models by measuring the time taken to descend a vertical pole (Sheta et al., 2024). The vertical pole test was first described in 1985 and is highly sensitive to impaired motor coordination and speed due to nigrostriatal degeneration (Ogawa et al., 1985, Matsuura et al., 1997). It therefore offers good construct validity to human parkinsonism.

In this study, mice got progressively faster at descending the vertical pole across repeated trials (**Fig. 5.4 A**). Improvement was greatest during the training phase (trial days 1-2) and levelled off by the test day (trial day three). Genotypes did not differ in the extent of improvement across trial days (**Fig. 5.4 A**) or the total descent time on the test day (**Fig. 5.4 B**). The time mice took to complete a T-turn (**Fig. 5.4 C**) (a 180° rotation resulting in the body pointing downwards) and to walk down the pole after the T-turn (**Fig. 5.4 D**) were also

similar across genotypes on the test day. Furthermore, the total descent time did not correlate with bodyweight and remained equivalent across genotypes in an ANCOVA with weight included as a covariate (**Fig. A-6**). Altogether, the vertical pole test did not detect bradykinesia in aged L444P mice.

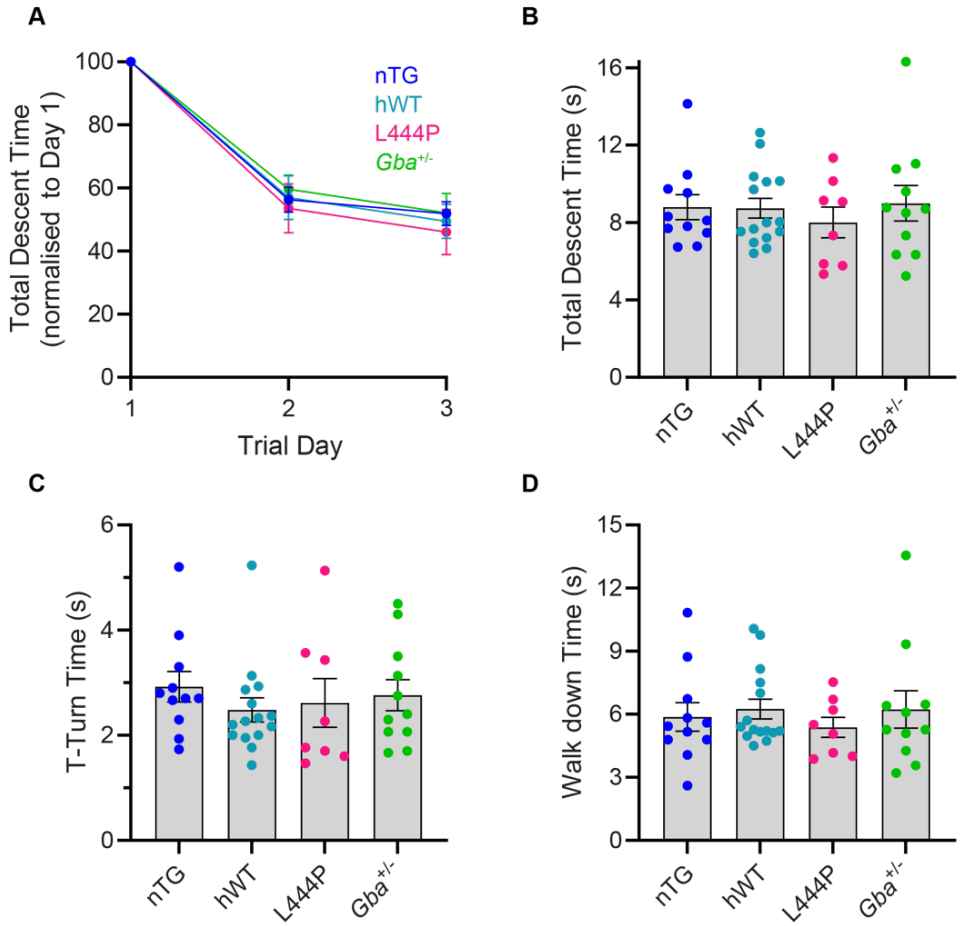


Figure 5.4: No genotype-related differences were observed in the vertical pole test. Briefly, mice were placed facing upwards on the top of a vertical pole and the time required to orient themselves downwards (make a T-turn) and move down the pole was recorded. (**A**) The total time required to descend the vertical pole decreased to a similar extent in all genotypes across trial days. Data are expressed normalised to the total descent time on day one within each individual mouse. (**B-D**) The total descent time (measured from the time of placement on the pole) (**B**), T-turn time (**C**) and walk-down time following the turn (**D**) were similar across genotypes on trial day three. (**A**) Two-way repeated measures ANOVA: genotype $F_{(3,41)} = 0.1672$ $p = 0.9179$, time $F_{(1.515, 62.13)} = 206.3$ $p < 0.0001$, interaction $F_{(6,82)} = 0.1738$ $p = 0.9832$, (**B-D**) Kruskal-Wallis test: all Kruskal-Wallis statistics < 2.309 and all $p > 0.5108$; n = 8-15 mice per genotype. Data are presented as mean ± SEM and each datapoint (**B-D**) represents one mouse.

5.2.5 MUSCLE STRENGTH USING THE INVERTED SCREEN TEST

Muscle weakness is a frequently-reported, but relatively understudied, symptom of PD (Murphy and Lynch, 2023, Alonso-Juarez et al., 2022). Grip strength was investigated in our aged cohort using the inverted screen test (Kondziella, 1964). This test assesses the combined strength of all four limbs by measuring the time mice are able to grip to the underside of an inverted wire-mesh grid before falling (Deacon, 2013b).

Most mice managed to grip to the grid for the maximum trial time of 60 s (**Fig. 5.5 A**). Consequently, muscle strength was not significantly different across genotypes. A heavy bodyweight likely underlies why some mice prematurely fell from the grid, as previously described (Brooks and Dunnett, 2009). Indeed, mice that weighed over 40 g tended to not reach the maximum trial time, while only one mouse lighter than 40 g fell off the grid before 60 s (**Fig. 5.5 B**).

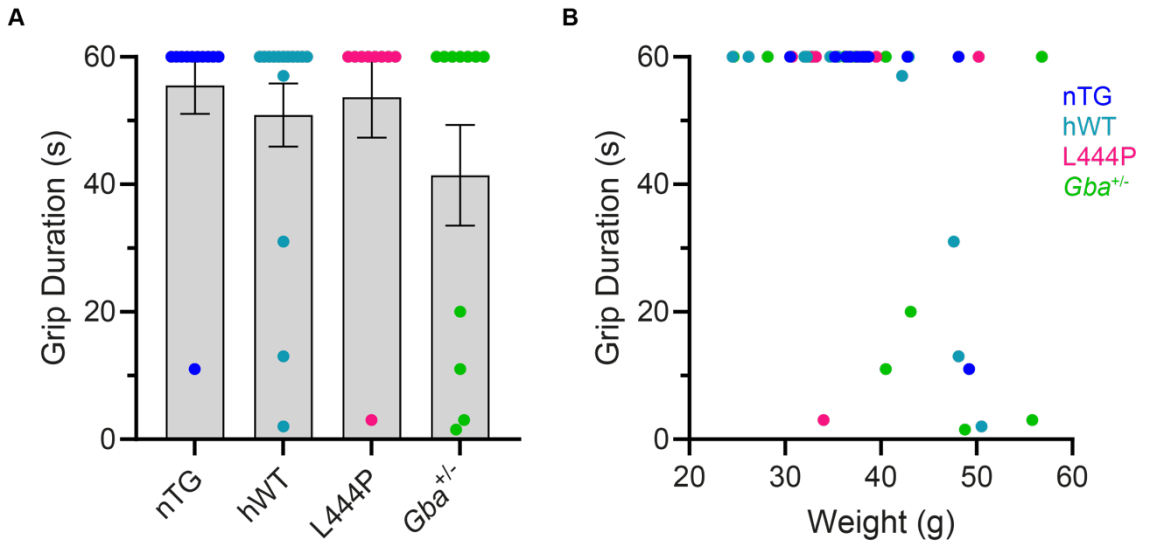


Figure 5.5: Grip strength was normal across genotypes in the inverted screen test. The time that mice were able to cling to the underside of an inverted mesh grid before falling (grip duration) was used to assess muscle strength. (**A**) Grip duration was not significantly different across genotypes, as most mice held on to the grid for the maximum trial time of 60 s. Kruskal-Wallis test: Kruskal-Wallis statistic = 3.181 p = 0.3645. (**B**) Body weight appeared to influence grip duration as mice weighing over 40 g tended to fall before 60 s. (**A-B**) n = 9-15 mice per genotype. Data are presented as mean ± SEM in (**A**) and each datapoint represents one mouse.

5.2.6 AUTOMATED GAIT ANALYSIS WITH THE CATWALK XT

PD patients exhibit early, progressive disturbances in the pace, rhythmicity and smoothness of gait (Mirelman et al., 2019). Many rodent models of PD also display gait abnormalities that reflect early clinical manifestations in PD patients, including reduced stride length and swing speed, along with interlimb asymmetry (Mirelman et al., 2019, Sheta et al., 2024, Timotius et al., 2023, Wenger et al., 2022). Despite this, there is a dearth of evidence for gait deficits in existing mouse models of *GBA*-associated PD (**Table 5.1**). Gait was characterised in our cohort using the CatWalk XT automated gait analysis system (Noldus). This apparatus objectively records over 200 gait parameters in real-time, with high sensitivity and spatiotemporal precision, as the mouse voluntarily transverses a glass platform (Garrick et al., 2021).

Gait parameters of interest were streamlined for analysis based on those that have previously been reported in PD models (Timotius et al., 2023). These parameters can broadly be divided into five categories: temporal, spatial, support, coordination and print and are described further in **Table 5.3**. Each gait parameter was analysed individually across genotypes using either a one-way ANOVA or a Kruskal-Wallis test, depending on whether or not the data followed a normal distribution, respectively. A Tukey's post-hoc test was conducted for parameters where a significant effect of genotype was identified in the preceding ANOVA. The results of these analyses are summarised in **Fig. 5.6**. For parameters where post-hoc tests were performed, significant differences are represented in red or blue according to the multiplicity adjusted p-value of the pairwise genotype comparison. White cells represent no significant changes ($p \geq 0.05$), either in the initial omnibus test or in the post-hoc test, where relevant. The hindlimb swing duration and the hindlimb swing speed were the only parameters that significantly differed across genotypes (**Fig. 5.6-5.7**). Notably, no significant gait changes were observed in *Gba*$^{+/-}$ mice vs nTG or hWT mice (**Fig. 5.6**).

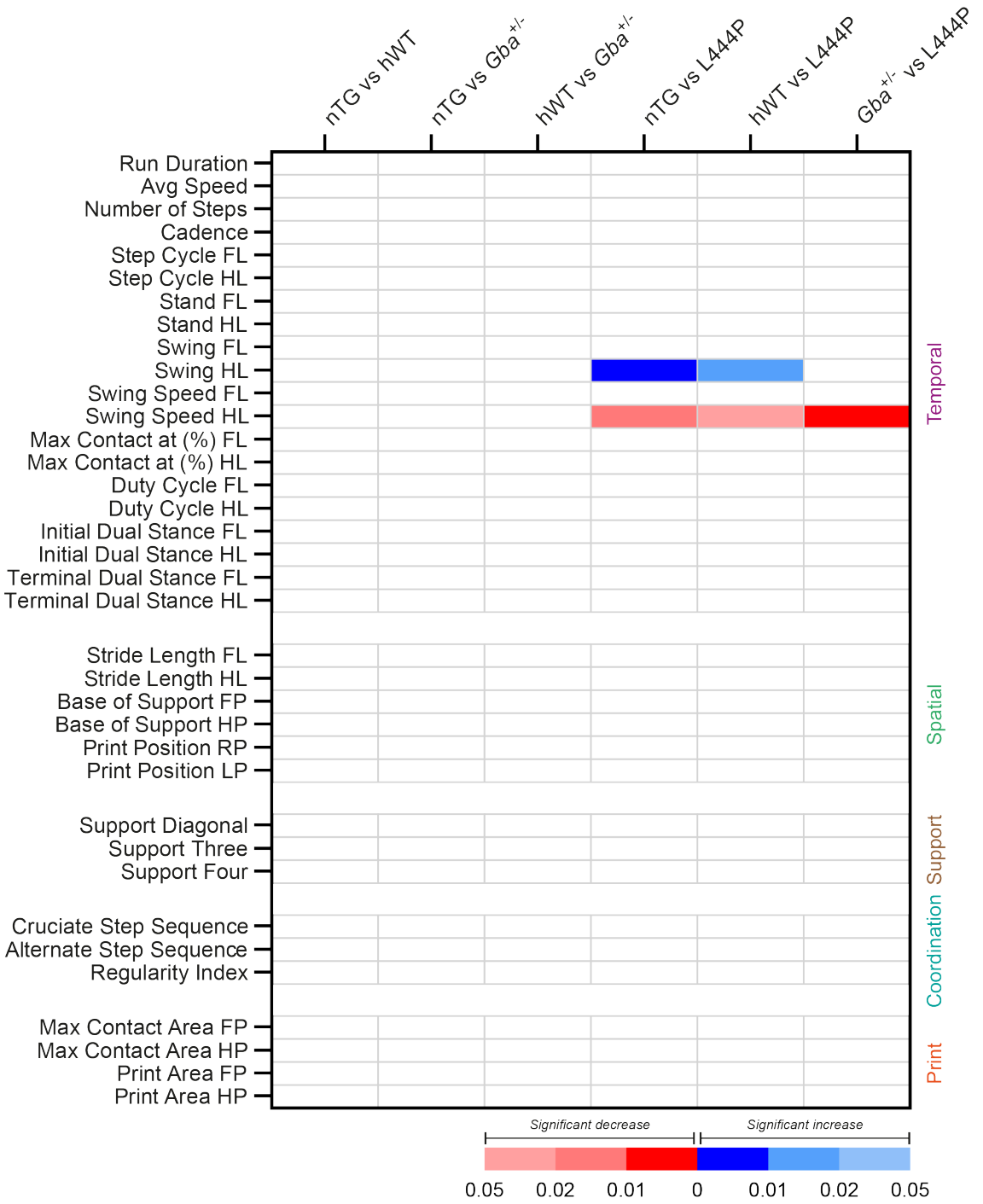


Figure 5.6: Heatmap summarising the results from gait analysis using the CatWalk XT. Various gait parameters were recorded by the CatWalk XT in real-time as mice transversed a glass platform. These parameters are represented in the rows of the heatmap and are grouped into five categories. Each parameter was first analysed individually using a one-way ANOVA or a Kruskal-Wallis test. The swing duration and swing speed of the hindlimbs (Swing HL and Swing Speed HL) were the only gait parameters that significantly differed across genotypes. Tukey's post-hoc tests were subsequently performed for Swing HL and Swing Speed HL and cells representing these parameters are coloured based on the multiplicity adjusted p-value for each pairwise genotype comparison. Red and blue cells represent statistically significant decreases and increases, respectively, in the Tukey's post-hoc test ($p < 0.05$). White cells indicate no significant differences ($p \geq 0.05$) in the initial omnibus test or in the Tukey's post-hoc test (for Swing HL and Swing Speed HL only). FL = Forelimb, HL = Hindlimb, FP = Forepaw, HP = Hindpaw. RP = Right Paw, LP = Left Paw.

L444P mice had a longer hindlimb swing duration, which reached significance vs nTG and hWT mice (**Fig. 5.7 A**). In line with this, the hindlimb swing speed of L444P mice was significantly slower vs all other genotypes (**Fig. 5.7 B**). The swing duration and swing speed of the forelimbs were not different across genotypes (**Fig. 5.7 C-D**). Bar charts illustrating genotype comparisons for all other analysed gait parameters are shown in (**Fig. A-7 – A-10**).

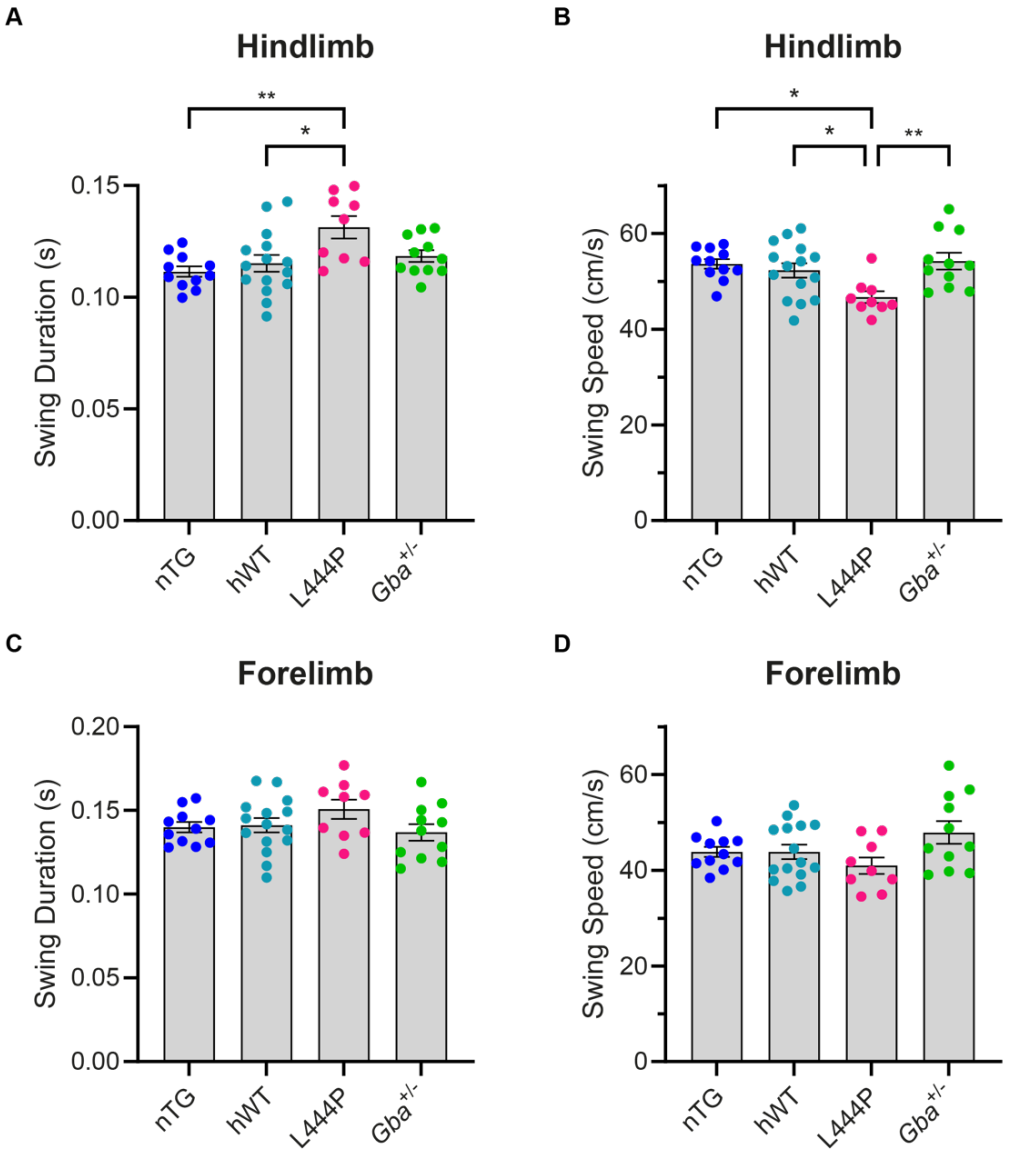


Figure 5.7: Swing duration and swing speed are exclusively altered in the hindlimbs of L444P mice. (**A**) The mean hindlimb swing duration is elevated in L444P mice. This reached significance vs nTG and hWT mice. (**B**) L444P mice have a significantly slower hindlimb swing speed vs nTG, hWT and *Gba*$^{+/-}$ mice. The forelimb swing duration (**C**) and forelimb swing speed (**D**) are not significantly different across genotypes. (**A-B**) One-way ANOVA with Tukey's post-hoc test: (**A**) $F_{(3,42)} = 5.056$ $p = 0.0044$, (**B**) $F_{(3,42)} = 4.642$ $p = 0.0068$, (**C-D**) one-way ANOVA: all $F_{(3,42)} < 2.403$ and all $p > 0.0810$; * $p < 0.05$, ** $p < 0.01$ from Tukey's post-hoc test; n = 9-15 mice per genotype. Data are presented as mean ± SEM and each datapoint represents one mouse.

5.2.7 GI FUNCTION WITH THE STOOL COLLECTION TEST

GI dysfunction in *GBA*-associated PD has not been widely investigated, although there are some reports of increased constipation in patients and in a $Gba^{+/L444P}SNCA^{A53T}$ mouse model (Fishbein et al., 2014, Jesus et al., 2016, Zhou et al., 2023). Therefore, I sought to assess the GI function of our aged mouse cohort by recording the amount, weight and % water content of stool pellets produced during a 60 min trial. L444P mice defecated less frequently on average vs other genotypes, although this only reached statistical significance vs nTG mice (**Fig. 5.8 A**). On the other hand, the wet weight (**Fig. 5.8 B**) and dry weight (**Fig. 5.8 C**) of the stool pellets were consistent in all genotypes. Therefore, the % water content of the stool (((Wet weight – Dry weight)/Wet weight)*100) was also similar across genotypes (**Fig. 5.8 D**).

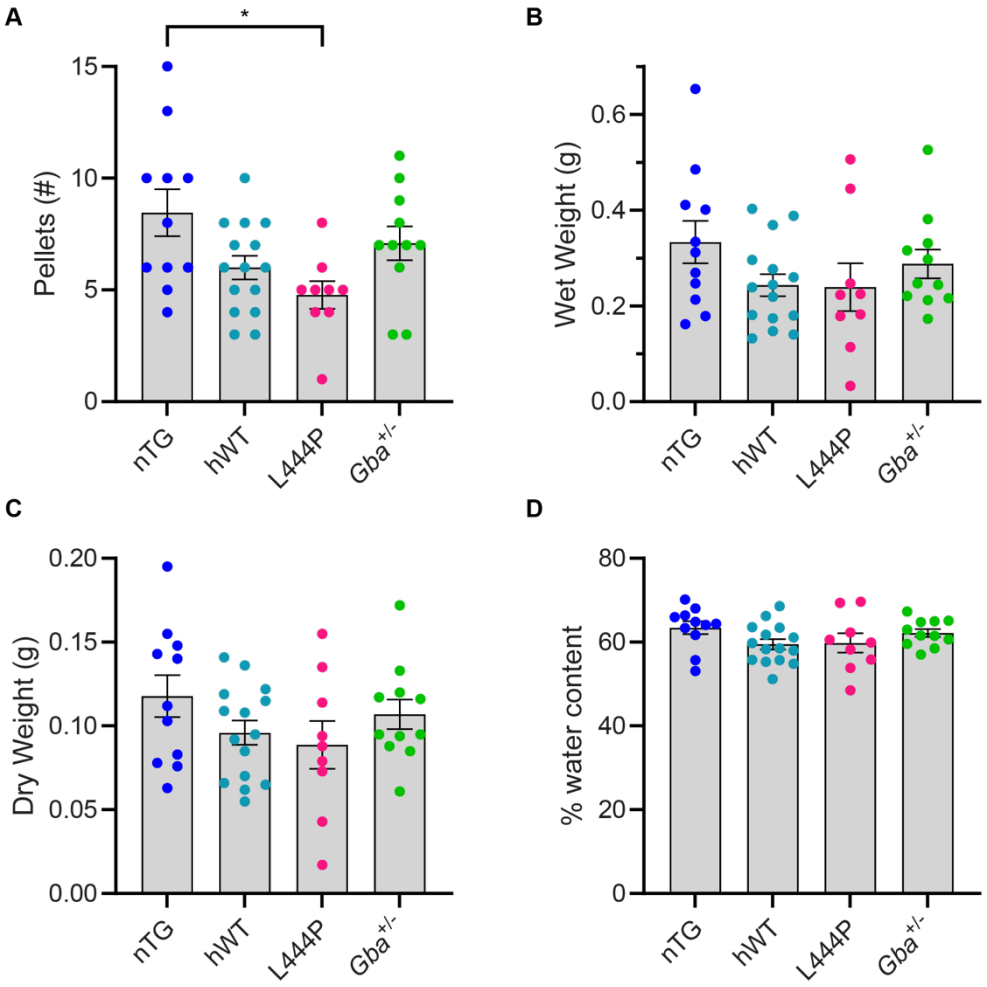


Figure 5.8: Assessment of GI function using the stool collection test. The stool pellets produced by the mice during a 60 min trial were collected and recorded. (**A**) L444P mice produced the lowest number of stool pellets on average during the trial, although this only reached significance vs nTG mice. The wet weight (**B**), dry weight (**C**) and % water content (**D**) of the stool was not significantly different across genotypes. (**A**) one-way ANOVA with Tukey's post-hoc test: $F_{(3,42)} = 3.940$ $p = 0.0145$, (**B-D**) one-way ANOVA: all $F_{(3,42)} < 1.705$ and all $p > 0.1806$; * $p < 0.05$ from Tukey's post-hoc test; n = 9-15 mice per genotype. Data are presented as mean ± SEM and each datapoint represents one mouse.

5.2.8 SPATIAL WORKING MEMORY USING THE T-MAZE SPONTANEOUS ALTERNATION TEST

GBA-L444P PD patients are at increased risk of dementia vs carriers of mild *GBA* mutations and non-carrier patients (**Table 1.2**) (Cilia et al., 2016). Despite this, studies exploring the novel object recognition memory of $Gba^{+/L444P}$ mice have produced conflicting results (Lado et al., 2024, Migdalska-Richards et al., 2017b). Additionally, spatial working memory has not previously been investigated in a mouse model harbouring an L444P mutation. I therefore sought to examine this in our cohort by measuring spontaneous alternation with a T-maze.

Spontaneous alternation refers to rodents' natural tendency to enter opposite goal arms of the T-maze when allowed to voluntarily choose across two successive runs (d'Isa et al., 2021, Dennis, 1939, Tolman, 1925). Each trial was therefore composed of two runs and mice underwent two trials per day. On the first day, all mice, except for one ($Gba^{+/-}$), completed all four runs across the two trials (**Fig. 5.9 A**). However, mice gradually became more reluctant to run the maze upon repeated exposure and only 20-44% of mice in each group completed two trials on the fifth day. Linear regression analysis revealed the rate of decline in participation across days was not significantly different across genotypes (**Fig. 5.9 A**). However, in light of the decrease in participation, the % alternation was only analysed across testing days 1-3. Mice with normal spatial working memory typically alternate 70-80% of the time (d'Isa et al., 2021, Deacon and Rawlins, 2006). Consistent with this, the mean % alternation was 73-78% in all groups (**Fig. 5.9 B**). Therefore, spatial working memory deficits were not observed in aged L444P mice using this test.

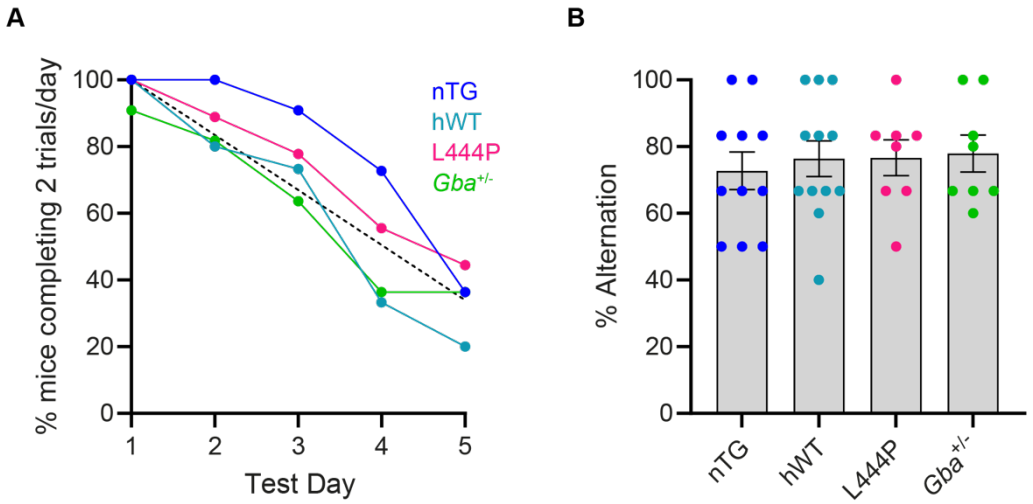


Figure 5.9: All genotypes had similar activity and spontaneous alternation rates in the T-maze. In each run, a mouse was presented with a choice of two goal arms in the T-maze. An alternation was recorded if the mouse entered opposite goal arms of the maze across both runs of the trial. (**A**) The proportion of mice that completed two trials per day declined across days. Linear regression analysis revealed the rate of decline did not differ across genotypes (*coloured solid lines*) and therefore that the data was best represented with the same linear regression line (*black dashed*); n = 9-15 mice per genotype (**B**) The % alternation, i.e. the proportion of trials with an alternation relative to the total number of completed trials across day 1-3, was also not significantly different across genotypes. (**B**) One-way ANOVA: $F_{(3,35)} = 0.1650$ p = 0.9192; n = 8-12 mice per genotype. (**A-B**) Data are presented as mean ± SEM and each datapoint (**B**) represents one mouse.

5.2.9 Anxiety-like behaviour in the EPM

Anxiety is another highly prevalent (Broen et al., 2016) and debilitating (Balestrino and Martinez-Martin, 2017), yet often overlooked (Pontone et al., 2019), non-motor symptom of PD. Although *GBA* mutations are associated with increased risk of anxiety in PD (Brockmann et al., 2011, Petrucci et al., 2020), no studies have investigated this symptom in an existing monogenic *Gba* mouse model that is heterozygous for the L444P mutation. In light of this, anxiety levels were examined in our aged mouse cohort using an EPM (Walf and Frye, 2007). Since the EPM was first described by Handley and Mithani (1984), it has been widely used to characterise anxiety in rodent models of PD (Sheta et al., 2024). The apparatus consists of two open and two closed arms, which are arranged in the shape of a plus sign and elevated above a soft surface (**Section 2.5.8**) (Walf and Frye, 2007). This test assesses anxiety using an approach-avoidant paradigm, leveraging mice's innate inclination

to explore dark, enclosed spaces over open spaces (Handley and Mithani, 1984, Montgomery, 1955, Pellow et al., 1985). Therefore, mice with higher anxiety levels will tend to enter the open arms less frequently and spend less time in the open arms overall.

The total number of entries into all arms (open and closed) did not vary according to genotype during the 5 min trial (**Fig. 5.10 A**). The similar activity levels across genotypes on the EPM corroborates findings in the open field (**Fig. 5.2**). Across all genotypes, mice seldom entered the open arms (**Fig. 5.10 B**) and therefore spent less than 5% of the trial in the open arms on average (**Fig. 5.10 C**). Furthermore, a remarkable proportion of mice did not enter any open arm during the trial, especially in the nTG and hWT groups (**Fig. 5.10 B-C**). Consequently, the mean open arm entries and mean time spent in the open arms was relatively higher for L444P and *Gba*$^{+/-}$ mice. However, these differences were not statistically significant and therefore no genotype-related differences in anxiety-like behaviour were identified in this test.

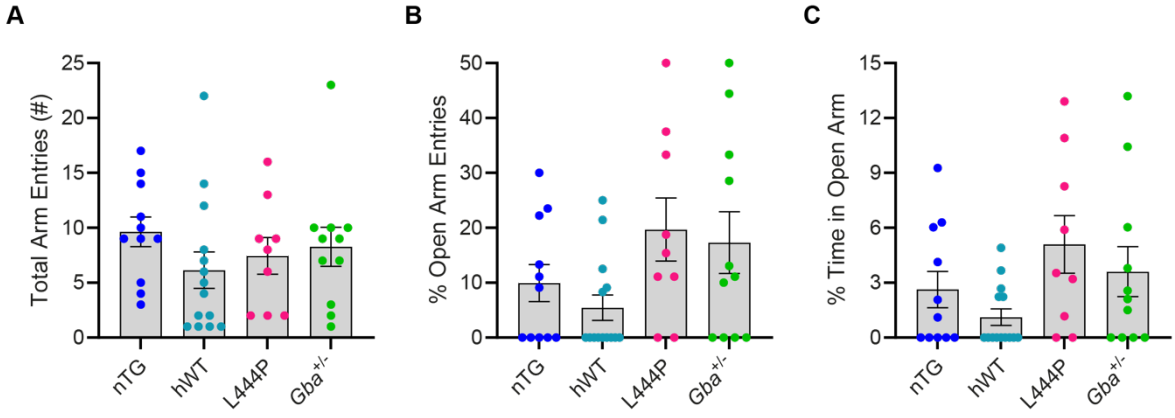


Figure 5.10: Total activity and open arm activity were similar across genotypes in the EPM. Mice were placed in the centre of an EPM and were subsequently allowed to freely choose to move into any of the four arms (two open and two closed) in one trial lasting 5 min. The total number entries into the open and closed arms (**A**), the open arm entries (expressed as a proportion of the total number of arm entries per mouse) (**B**) and time spent in the open arms (expressed as a proportion of the total trial time) (**C**) were similar across genotypes. (**A-C**) Kruskal-Wallis test: all Kruskal-Wallis statistics < 6.458 and all $p > 0.0914$; n = 9-14 mice per genotype. Data are presented as mean ± SEM and each datapoint represents one mouse.

5.3 DISCUSSION

5.3.1 MOTOR DYSFUNCTION IN *GBA*-ASSOCIATED PD IS POORLY RECAPITULATED IN MOUSE MODELS

The cardinal motor signs of PD have been well-studied ever since James Parkinson first described resting tremor and postural instability in patients over 200 years ago (Obeso et al., 2017, Parkinson, 1817). However, attempts to replicate progressive motor deficits in rodent models of the disease have had mixed-success (Guimaraes et al., 2024, Sheta et al., 2024). Prior to this study, conducted in 2021, a limited number of reports characterised motor function in *Gba* transgenic mice (**Table 5.1-5.2**). In light of this, I sought to investigate if our aged L444P mice can recapitulate the motor symptoms of PD.

Firstly, L444P mice displayed no changes to spontaneous LMA or thigmotactic behaviour in the open field (**Fig. 5.2**). These results corroborate findings in other transgenic models (**Table 5.1**), including recent observations in $Gba^{+/L444P}$ mice (Lado et al., 2024, Mahoney-Crane et al., 2023). Subsequently, our L444P mice had normal coordination and balance on the accelerating rotarod, indicated by a similar fall latency across genotypes (**Fig. 5.3**). An influx of studies testing rotarod performance in monogenic *Gba* transgenic mice was published in 2024, all of which agreed with the findings in this thesis (**Table 5.1**). Moreover, coordination and speed were equivalent across genotypes on the vertical pole (**Fig. 5.4**). Bradykinesia has also not been observed in other monogenic *Gba* transgenic mice using this test (**Table 5.1**). L444P mice also had normal grip strength on the inverted screen test (**Fig. 5.5**), consistent with other models (**Table 5.1**). Across all studies in **Table 5.1**, the only indication of motor dysfunction is the impaired balance beam performance in $Gba^{+/-}$ mice (Do et al., 2021). However, this phenotype has questionable validity because it was not observed in more severe models (**Table 5.1**) and the elevated slip frequency has dubious biological significance considering the mean increase was only 1.5 slips.

Table 5.1: Studies investigating motor function in existing genetic mouse models of *GBA*-associated PD and GD.

Behavioural Test	Model (Original Reference)	Direction of change (vs WT): Parameter(s)	Age (n/group)	Reference
Spontaneous LMA	*Gba*$^{+/L444P}$ (*)	NC: Distance travelled, % centre, velocity	3 m (5-7), 12 m (16-22)	(Mahoney-Crane et al., 2023)
	Gba$^{+/L444P}$ (*)	NC: Distance travelled, time in centre, # of rearings	2.5 m (17), 7 m (16)	(Lado et al., 2024)
	Gba$^{D409V/D409V}$ (‡)	NC: total activity, total ambulation (M only) ↑: total activity, total ambulation (M only)	4 m, 12 m (13-15) 8 m (13-15)	(Polinski et al., 2022)
	Gba$^{D409V/D409V}$ (‡‡)	NC: distance travelled, % centre	6 m (ND)	(Sardi et al., 2011)
	Gba$^{+/D409V}$ (‡)	NC: distance travelled, time in perimeter, velocity	12 m (9)	(Clarke et al., 2019)
	Gba$^{+/D409V}$ (‡)	NC: distance travelled, time in centre	9 m (6-11)	(Johnson et al., 2021)
	Gba$^{L444P/KO}$ (*)	NC: distance travelled	3-12 m^ (9-12)	(Vidyadhara et al., 2025)
	GBA^{L444P}*Gba*$^{-/-}$ (***)	NC: time in centre, entries in centre (M only)	ND (5-7)	(Chen et al., 2024)
	Gba$^{E326K/E326K}$ (§)	NC: % centre, distance travelled, velocity	10 m (10-12)	(Kweon et al., 2024)
Rotarod	*Gba*$^{L444P/L444P}$ (**)	NC: latency to fall	16 m (10)	(Furderer et al., 2024)
	Gba$^{+/D409V}$ (‡)	NC: latency to fall	12 m (6-7)	(Clarke et al., 2019)
	Gba$^{+/L444P}$ (*)	NC: latency to fall	2.5 m (10-13), 7 m (20)	(Lado et al., 2024)
	GBA^{L444P}*Gba*$^{-/-}$ (***)	NC: latency to fall (M only)	ND (6-11)	(Chen et al., 2024)
	Gba$^{D409V/D409V}$ (‡)	NC: latency to fall	3 m, 9 m (ND)	(Walton et al., 2024)
	Gba$^{+/D409H}$ (‡‡)	NC: latency to fall	6 m (7)	(Kim et al., 2018a)
	Gba$^{D409H/D409H}$ (‡‡)	NC: latency to fall	6 m (7)	(Kim et al., 2018a)
	Gba$^{E326K/E326K}$ (§)	NC: latency to fall	13 m (10)	(Kweon et al., 2024)
Vertical Pole	*Gba*$^{+/L444P}$ (*)	↓: total descent time, NC: T-turn time, descent time NC: total descent time, T-turn time, descent time	3 m (6-7) 12 m (15-18)	(Mahoney-Crane et al., 2023)
	Gba$^{+/L444P}$ (*)	NC: total descent time	8 m (15)	(Yun et al., 2018)
	Gba$^{+/L444P}$ (*)	NC: total descent time, T-turn time (M only)	22 m (8-10)	(Migdalska-Richards et al., 2017b)

Vertical Pole (cont.)	*Gba*$^{+/-}$ (††)	NC: total descent time, T-turn time (M only)	22 m (9)	(Migdalska-Richards et al., 2017b)
	Gba$^{+/D409H}$ (‡‡)	NC: total descent time	6 m (7)	(Kim et al., 2018a)
	Gba$^{D409H/D409H}$ (‡‡)	NC: total descent time	6 m (7)	(Kim et al., 2018a)
	Gba$^{+/E326K}$ (§)	NC: total descent time	9 m (7-17)	(Kweon et al., 2024)
	Gba$^{E326K/E326K}$ (§)	NC: total descent time	9 m (8-17)	(Kweon et al., 2024)
	DAT-Cre-Gba-KO (¶)	NC: total descent time, T-turn time	18 m (ND)	(Soria et al., 2017)
	GBA^{L444P}*Gba*$^{-/-}$ (***)	NC: total descent time (M only)	ND (7-15)	(Chen et al., 2024)
Balance beam	*Gba*$^{+/-}$ (†)	↑: transverse time at 8 m, slip freq. over time	8-23 m^ (6-9)	(Do et al., 2021)
	Gba$^{L444P/KO}$ (*)	NC: # of runs/min.	3-12 m^ (9-12)	(Vidyadhara et al., 2025)
	Gba$^{L444P/L444P}$ (**)	NC: transverse time	16 m (10)	(Furderer et al., 2024)
	Gba$^{+/L444P}$ (*)	NC: transverse time	7 m (18)	(Lado et al., 2024)
	DAT-Cre-Gba-KO (¶)	NC: transverse time	18 m (ND)	(Soria et al., 2017)
Manual paw print analysis	*Gba*$^{D409V/KO}$ (‡‡)	↑: Paw base width (inconsistent across age and sex) ↑: Stride length (F: 3, 6, 18 m), NC: stride length M	3-18 m^ (7-25)	(Dai et al., 2016)
Grip strength	*Gba*$^{D409V/D409V}$ (‡)	NC: Grip strength (M only) ↑: Grip strength (M only)	4 m, 8 m (13-15) 12 m (13-15)	(Polinski et al., 2022)
	Gba$^{+/L444P}$ (*)	NC: Grip strength	8 m (6)	(Yun et al., 2018)
	Gba$^{L444P/KO}$ (*)	NC: Grip strength	3-12 m^ (9-12)	(Vidyadhara et al., 2025)
	Gba$^{+/E326K}$ (§)	NC: Grip strength	9 m (7-17)	(Kweon et al., 2024)
	Gba$^{E326K/E326K}$ (§)	NC: Grip strength	9 m (8-17), 13 m (10)	(Kweon et al., 2024)
Hindlimb clasp	*Gba*$^{+/-}$ (†)	NC: Hindlimb clasp score	13-20 m^ (6-9)	(Do et al., 2021)
	Gba$^{L444P/KO}$ (*)	NC: % time spent clasping	3-12 m^ (9-12)	(Vidyadhara et al., 2025)

Key: Model: * (Liu et al., 1998); ** (Ginns et al., 2014); *** (Sanders et al., 2013); † (Tybulewicz et al., 1992); †† (Enquist et al., 2007); ‡ (Ikuno et al., 2019, Polinski et al., 2021); ‡‡ (Xu et al., 2003); ¶ (Soria et al., 2017); § (Kweon et al., 2024). NC = no change; ↑ = significant increase; ↓ = significant decrease; m = months; ^ = longitudinal study; ND = not disclosed; M = male; F = female; LMA = locomotor activity.

Table 5.2: Studies investigating motor function in existing multifactorial genetic mouse models of *GBA*-associated PD and GD.

Behavioural Test	Model (Original Reference) x Additional insult	Direction of change: Parameter(s)	Age (n/group)	Reference
Spontaneous LMA	*Gba*$^{+/L444P}$ (*) x PFF IS	NC: Distance travelled, % centre, avg. velocity	12 m (8-22)	(Mahoney-Crane et al., 2023)
	Gba$^{+/L444P}$ (*) x Thy1-*SNCA*	NC: Distance travelled, time in centre, # of rearings (M only)	2.5 m (10-19) 7 m (11-19)	(Lado et al., 2024)
	Gba$^{+/L444P}$ (*) x *SNCA*^{A53T}	NC: Distance travelled, # of rearings ↓: Time spent rearing vs *SNCA*^{A53T}	12-14 m (ND)	(Fishbein et al., 2014)
	Gba$^{+/D409V}$ (‡) x PFF OB	NC: distance travelled, time in centre	9 m (6-11)	(Johnson et al., 2021)
	Gba$^{L444P/KO}$ (*) x *SNCA*^{A30P}	↓: Distance travelled vs WT (9-12 m), *Gba*$^{L444P/KO}$ (12 m) & *SNCA*$^{+/A30P}$ (12 m), NC at other ages	3-12 m^ (9-12)	(Vidyadhara et al., 2025)
	Gba$^{D409V/D409V}$ (‡) x Thy1-*SNCA*	↑: total activity vs *Gba*$^{D409V/D409V}$ & Thy1-*SNCA*, NC vs WT ↑: total ambulation vs WT & Thy1-*SNCA*, NC vs *Gba*$^{D409V/D409V}$	4 m (13-15)	(Polinski et al., 2022)
		NC: total activity, total ambulation (M only for all tests)	8 m, 12 m (13-15)	
	Gba$^{E326K/E326K}$ (§) x PFF GI	↓: % time in centre vs WT & *Gba*$^{E326K/E326K}$, NC vs PFF ↓: % entries in centre vs WT, *Gba*$^{E326K/E326K}$ & PFF	10 m (9-13)	(Kweon et al., 2024)
	Gba$^{+/-}$ (†) x *SNCA*-Tg/Tg	↑: Distance travelled, time in centre vs WT (M only)	15 m (17-20)	(Ikuno et al., 2019)
Rotarod	*Gba*$^{+/L444P}$ (*) x *SNCA*^{A53T}	NC: Latency to fall ↓: Latency to fall vs *SNCA*^{A53T}	7 m (20) 14 m (31-34)	(Fishbein et al., 2014)
	Gba$^{+/L444P}$ (*) x Thy1-*SNCA*	NC: Latency to fall (M only) ↓: Latency to fall vs WT, *Gba*$^{+/L444P}$ & Thy1-*SNCA* (M only)	2.5 m (10-13) 7 m (10-16)	(Lado et al., 2024)
	Gba$^{E326K/E326K}$ (§) x PFF IS	↓: Latency to fall vs WT, *Gba*$^{E326K/E326K}$ & PFF	13 m (8-13)	(Kweon et al., 2024)
	GBA^{L444P}*Gba*$^{-/-}$ (***) x PFF SLD	↓: Latency to fall vs WT, *GBA*^{L444P}*Gba*$^{-/-}$ & PFF (M only)	4 m (ND)	(Chen et al., 2024)
	Gba$^{D409V/D409V}$ (‡) x PFF OB	NC: latency to fall	3 m, 9 m (ND)	(Walton et al., 2024)
	Gba$^{+/D409H}$ (‡‡) x *SNCA*^{A53T}	↓: Latency to fall vs WT, *Gba*$^{+/D409H}$ & *SNCA*^{A53T}	6 m (7)	(Kim et al., 2018a)
	Gba$^{D409H/D409H}$ (‡‡) x *SNCA*^{A53T}	↓: Latency to fall vs WT, *Gba*$^{D409H/D409H}$ & *SNCA*^{A53T}	6 m (7)	(Kim et al., 2018a)
Vertical Pole	*Gba*$^{+/L444P}$ (*) x PFF IS	NC: total descent time, T-turn time, descent time	12 m (8-18)	(Mahoney-Crane et al. 2023)
	GBA^{L444P}*Gba*$^{-/-}$ (***) x PFF	↑: total descent time vs WT, *GBA*^{L444P}*Gba*$^{-/-}$ & PFF (M only)	4 m (ND)	(Chen et al., 2024)

Vertical Pole (cont.)	*Gba*$^{+/L444P}$ (*) x MPTP	↑: total descent time vs WT, *Gba*$^{+/L444P}$ & WT-MPTP	8 m (15)	(Yun et al., 2018)
	Gba$^{+/D409H}$ (‡‡) x *SNCA*^{A53T}	↑: total descent time vs WT, *Gba*$^{+/D409H}$ & *SNCA*^{A53T}	6 m (7)	(Kim et al., 2018a)
	Gba$^{D409H/D409H}$ (‡‡) x *SNCA*^{A53T}	↑: total descent time vs WT, *Gba*$^{D409H/D409H}$ & *SNCA*^{A53T}	6 m (7)	(Kim et al., 2018a)
Balance beam	*Gba*$^{+/-}$ (†) x *SNCA*^{A53T}	↑: transverse time at 8 m, slip freq. over time vs WT, NC vs *Gba*$^{+/-}$ & *SNCA*^{A53T}	8-23 m^ (6-10)	(Do et al., 2021)
	Gba$^{L444P/KO}$ (*) x *SNCA*^{A30P}	↓: # of runs/min. vs WT & *Gba*$^{L444P/KO}$ (≥ 6 m) NC vs *SNCA*^{A30P}	3-12 m^ (9-12)	(Vidyadhara et al., 2025)
Grip strength	*Gba*$^{+/L444P}$ (*) x MPTP	↓: Grip strength vs WT, *Gba*$^{+/L444P}$ & WT-MPTP	8 m (6-7)	(Yun et al., 2018)
	Gba$^{L444P/KO}$ (*) x *SNCA*^{A30P}	↓: Grip strength vs WT & *Gba*$^{L444P/KO}$ (≥ 6 m), NC vs *SNCA*^{A30P}	3-12 m^ (9-12)	(Vidyadhara et al., 2025)
	Gba$^{D409V/D409V}$ (‡) x Thy1-*SNCA*	NC: Grip strength (M only) ↓: Grip strength vs WT, *Gba*$^{D409V/D409V}$ & Thy1-*SNCA* (M only)	4 m, 8 m (13-15) 12 m (13-15)	(Polinski et al., 2022)
	Gba$^{E326K/E326K}$ (§) x PFF IS	↓: Grip strength vs WT, *Gba*$^{E326K/E326K}$ & PFF	13 m (8-13)	(Kweon et al., 2024)
Hindlimb Clasp	*Gba*$^{+/-}$ (†) x *SNCA*^{A53T}	↑: Hindlimb clasp score vs WT, NC vs *Gba*$^{+/-}$ & *SNCA*^{A53T}	13-20 m^ (6-10)	(Do et al., 2021)
	Gba$^{L444P/KO}$ (*) x *SNCA*^{A30P}	↑: % time spent clasping vs WT (3-12 m), *Gba*$^{L444P/KO}$ (12 m) & *SNCA*^{A30P} (3, 9 m), NC at other ages	3-12 m^ (9-12)	(Vidyadhara et al., 2025)

Key: Model: * (Liu et al., 1998); *** (Sanders et al., 2013); † (Tybulewicz et al., 1992); ‡ (Ikuno et al., 2019, Polinski et al., 2021); ‡‡ (Xu et al., 2003); § (Kweon et al., 2024). NC = no change; ↑ = significant increase; ↓ = significant decrease; m = months; ^ = longitudinal study; ND = not disclosed; M = male; LMA = locomotor activity; GI = gastrointestinal; IS = intra-striatal; SLD = sublaterodorsal tegmental nucleus; OB = olfactory bulb. Red font indicates that *Gba* mutation deteriorates behaviour in multifactorial model over all controls.

It should be noted that the cardinal motor signs of PD only become evident in patients once approximately 30-50% of nigrostriatal DA neurons have degenerated (Cheng et al., 2010, Fearnley and Lees, 1991). However, previous stereology revealed that DA neurons of the SN are preserved in our L444P mice at 18-months-old (**Fig. A-3,** Dr Natalie Connor-Robson). Similarly, monogenic *Gba* mutations are not associated with nigral dopaminergic neurodegeneration in other models (**Table 1.3**). Considering this, it is not surprising that rodent models poorly replicate the severe motor decline experienced by *GBA*-associated PD patients (Brockmann et al., 2015, Cilia et al., 2016, Malek et al., 2018). These findings may also reflect the relatively low penetrance of *GBA* mutations in PD vs disease-causing variants in monogenic PD (Balestrino et al., 2020, Day and Mullin, 2021).

A complex interplay of genetic and environmental factors likely gives rise to neurodegeneration, and consequently parkinsonism, in *GBA* mutation carriers who develop PD (Kalia and Lang, 2015). This "multiple hit" hypothesis (Sulzer, 2007) has been explored in various models by combining *Gba* mutations with other insults, including MPTP exposure, PFF injection, αS overexpression and αS mutations (**Section 1.4.2**). These multifactorial models have reduced locomotion, impaired rotarod and vertical pole performances and weaker grip strength (**Table 5.2**). Many of these phenotypes have therefore provided a useful platform to demonstrate the efficacy of AAV-mediated *GBA* overexpression, as a potential gene therapy for the disorder (Chen et al., 2024, Yun et al., 2018). On the other hand, glucosylceramide synthase inhibitors failed to restore behavioural deficits in PFF-injected $Gba^{+/L444P}$ mice (Mahoney-Crane et al., 2023), despite positive effects in $Gba^{D409V/D409V}$ mice (Viel et al., 2021, Sardi et al., 2017). Notably, it can be challenging to discern the extent to which the *Gba* mutation contributes to pathology in these models if appropriate controls are not included in the experiments. For example, Fishbein et al. (2014) compared $Gba^{+/L444P}SNCA^{A53T}$ mice with $SNCA^{A53T}$ mice but not with WT or

Gba$^{+/L444P}$ mice. Also, models combining *Gba* and *SNCA* mutations lack construct validity, since these mutations have not been found to co-occur in PD patients. Nevertheless, future studies could expose our L444P mice to additional stressors to improve their face validity and potential utility in preclinical trials testing therapeutic efficacy (**Section 6.3.2**).

Some technical-constraints and limitations of the assays used to characterise motor behaviour should be considered. In the rotarod test, some mice gripped to the rod and freely rotated without moving their limbs. The duration of this "cartwheeling" behaviour could not be accurately accounted for due to technical issues with the camcorder. Cartwheeling is primarily influenced by the surface-texture (Brooks and Dunnett, 2009, Deacon, 2013a) and diameter (Rustay et al., 2003b) of the rod. Future studies can therefore prevent this by covering the rod's surface with coarse rubber or sandpaper (Brooks and Dunnett, 2009, Bohlen et al., 2009). Also, the acceleration rate of the rotarod was slower in these experiments (2.5-25 rpm) vs previous studies from my lab (4-40 rpm) (Hunn et al., 2019, Janezic et al., 2013, Sloan et al., 2016). Slower acceleration should help to diminish potential confounds of endurance or fatigue on the latency to fall (Brooks and Dunnett, 2009, Deacon, 2013a) and may offer increased sensitivity to detect subtle changes in performance (Rustay et al., 2003a, Rustay et al., 2003b). Acceleration rate may also have influenced cartwheeling in my assessment, although, to the best of my knowledge, this relationship has not previously been investigated. Lastly, the inverted screen test is influenced by bodyweight (**Fig. 5.5 B**) (Brooks and Dunnett, 2009). It also lacks sensitivity to detect muscle weakness, since mice can usually grip for the maximum trial duration (Brooks and Dunnett, 2009, Deacon, 2013b) (**Fig. 5.5**). A modified apparatus and scoring system for this test has been developed, which has improved sensitivity to MPTP-induced muscle weakness (Kim et al., 2010, Tillerson et al., 2002). Alternatively, a grip strength meter (or similar apparatus, (Meyer et al., 1979)) can directly quantify muscle strength of the forelimbs and hindlimbs, either individually or

combined (Vidyadhara et al., 2025, Polinski et al., 2022). These approaches could be used in future studies aiming to assess muscle strength of L444P mice.

5.3.2 ABNORMAL GAIT SIGNATURES OF RODENT MODELS IMITATES GAIT DEFICITS IN PD PATIENTS

The clinical presentation of PD patients has been broadly divided into two subtypes: PIGD-dominant and tremor-dominant (**Section 1.1.2**) (Stebbins et al., 2013). *GBA*-associated PD patients are more likely to display the PIGD-dominant phenotype (**Section 1.2.3**) (Davis et al., 2016, Malek et al., 2018). Patients with this phenotype typically have a slower speed, take shorter and less regular strides and have increased gait instability vs patients with the tremor-dominant phenotype (Rezvanian et al., 2018, Herman et al., 2014). In line with this, Morris et al. (2022) observed that the gait of *GBA*-associated PD patients was slower and more variable than non-carriers of *GBA* mutations. Gait analysis has been largely overlooked in previous behavioural characterisations of transgenic *Gba* mouse models (**Table 5.1**), although Dai et al. (2016) measured gait parameters of $Gba^{D409V/KO}$ mice from a pattern of inked paw prints. This manual approach is time-consuming, limited to few static gait parameters and prone to observer-related bias and errors (Garrick et al., 2021, Mohamed-Fathy Kamal et al., 2025). In light of these limitations, automated approaches to gait analysis, such as the CatWalk XT, have gained popularity in recent years (Timotius et al., 2023).

Table 5.3: Description of CatWalk XT gait parameters analysed in this thesis. Parameters were selected based on previous investigations in PD rodent models.

	Parameter (Units)	Definition	Change in PD (# Studies)
Temporal	Run Duration (s)	Time taken to complete one full run.	↑ (2), NC (1)
	Average Speed (cm/s)	Distance travelled divided by run duration.	↓ (5), NC (2)
	Number of Steps (#)	Total number of steps taken.	↑ (1)
	Cadence (#/s)	Number of steps taken per second.	↓ (3), NC (1)
	Step Cycle (s)	Time between two consecutive contacts of the heel of the same paw with the ground. Consists of a Stand and Swing phase.	↑ (1)
	Stand (s)	Duration that a paw is contacting the ground during the Step Cycle.	↑ (4)
	Swing (s)	Duration that a paw is not contacting the ground during the Step Cycle.	↑ (1), NC (2)
	Swing Speed (cm/s)	Speed of a limb in the Swing Phase of the Step Cycle.	↓ (5)
	Max Contact at (%)	Duration that a paw is in maximum contact with the ground expressed as a percentage of the Stand Phase duration.	↑ (2)
	Duty Cycle (%)	The Stand Phase duration expressed as a percentage of the Step Cycle duration.	↑ (1)
	Initial Dual Stance (s)	Duration that contralateral front or hind paws simultaneously contact the ground for the 1st (Initial), or 2nd time (Terminal) in a Step Cycle.	↑ (1)
	Terminal Dual Stance (s)		↑ (2)
Spatial	Stride Length (cm)	Distance between two consecutive prints made by the same paw.	↓ (4), ↑ (1), NC (2)
	Base of Support FP/HP (cm)	Distance between the two FPs or HPs.	FP: ↑ (2), NC (3)
			HP: ↑ (2), NC (2)
	Print Position (cm)	Distance between a hindpaw print relative to the previous ipsilateral forepaw print.	↑ (1), NC (1)
Support	Support Diagonal (%) (i)	Percentage of the run where two contralateral diagonal paws (i), three paws (ii) or four paws (iii) simultaneously contact the ground.	↓ (2)
	Support Three (%) (ii)		↓ (1), ↑ (1)
	Support Four (%) (iii)		↑ (1)
Coordination	Cruciate Step Sequence (%)	Percentage of the run where mice use a cruciate step sequence pattern.	NC (2)
	Alternate Step Sequence (%)	Percentage of the run where mice use an alternate step sequence pattern.	NC (2)
	Regularity Index (%)	Percentage of the run where the mouse use a cruciate, alternate or rotary step sequence.	↓ (2), NC (3)
Print	Max. Contact Area (cm^2)	Area of the paw print at the point of maximum contact with the ground.	↑ (1), NC (1)
	Print Area (cm^2)	Area of the complete paw print.	↓ (2), NC (1)
Key:	↑ = Significant increase, ↓ = Significant decrease, NC = No significant change, FL = Forelimb, HL = Hindlimb, FP = Forepaw, HP = Hindpaw. Parameters in **bold** are significantly altered in L444P mice. The number of studies reporting changes in PD models is adapted from Timotius et al. (2023) Supplementary Table 6; a meta-analysis of 15 studies using CatWalk XT in PD models.		

In this chapter, gait analysis with the CatWalk XT revealed that L444P mice have increased hindlimb swing time and reduced hindlimb swing speed (**Fig. 5.6-5.7**). Similar reductions in limb swing speed have been identified in other PD models using this system (**Table 5.3**) (Hunn et al., 2019, Timotius et al., 2023). Many gait abnormalities observed in rodents can be mapped to gait impairments in patients, thereby providing a window into clinical symptomatology of the disease (Mirelman et al., 2019, Sheta et al., 2024, Timotius et al., 2023, Wenger et al., 2022). For instance, reduced speed (both average and swing), reduced cadence and increased stand time are among the most common phenotypes across PD mouse models (**Table 5.3**) (Timotius et al., 2023). Together, these gait changes mirror the bradykinesia experienced by PD patients. Reduced stride length is another frequently reported parameter (**Table 5.3**), which recapitulates the shorter shuffling steps taken by PD patients (Boix et al., 2018, Taylor et al., 2010, Timotius et al., 2023). Additionally, some models have a reduced "regularity index" (**Table 5.3**) (Timotius et al., 2023), which indicates a decline in consistency of the step sequences. This may mimic the lower rhythmicity of gait in patients (Plotnik and Hausdorff, 2008). Various gait parameters can also be asymmetrically impaired across rodent models (Broom et al., 2019), replicating the early-stage, unilateral gait deficits in PD patients (Mirelman et al., 2019). Mild gait changes have been identified in rodent models as young as 10-12-weeks-old (Timotius et al., 2019a), although the severity of impairment tends to reflect the extent of neurodegeneration (Gries et al., 2021, Radlicka-Borysewska et al., 2024, Wenger et al., 2022). This likely explains why most gait parameters were unchanged in L444P mice since nigral DA neurons are preserved in these mice at 18 months (**Fig. 5.6**, **A-3**). It also underscores the utility of gait analysis to identify early-stage phenotypic biomarkers and to track disease progression. Future studies could longitudinally-investigate how hindlimb dynamics progressively deteriorate with age in L444P mice.

We may hypothesize that a gain-of-function effect of the mutation drives gait deficits in L444P mice, considering that *Gba*$^{+/-}$ mice had normal gait (**Fig. 5.6**). Other studies, in *Gba*$^{+/-}$, conditional *Gba* KO and CBE-treated mice, have also indicated that loss of GCase activity is not sufficient to impair motor function (Henderson et al., 2020, Migdalska-Richards et al., 2017b, Rockenstein et al., 2016, Soria et al., 2017). However, the exact mechanisms underlying the gait deficits in L444P mice remain elusive. It is also unclear why impairments were isolated to the hindlimbs (**Fig. 5.7**). Some toxin-induced and transgenic models have more severe motor dysfunction in the hindlimbs vs the forelimbs (Amende et al., 2005, Fleming et al., 2004), although this has not been universally observed (Bengoa-Vergniory et al., 2020). The hindlimb-specificity could be related to previous reports of hindlimb muscle weakness (indicated by reduced rearing) or increased hindlimb clasping in multifactorial *Gba* models (Do et al., 2021, Fishbein et al., 2014, Vidyadhara et al., 2025); however, these phenotypes have not been demonstrated in monogenic *Gba* mice (**Table 5.1**).

Finally, it must be highlighted that inherent differences in the gait of bipeds and quadrupeds limits the translational validity of gait abnormalities in rodent models (Broom et al., 2017, Wenger et al., 2022). Moreover, a mouse's weight, size, motivation to run and speed can confound various gait parameters recorded by the CatWalk XT (Batka et al., 2014, Parkkinen et al., 2013, Pitzer et al., 2021, Timotius et al., 2019b). Statistical methods that can account for the influence of body size and speed on gait have been developed (Timotius et al., 2019b, Batka et al., 2014). However, bodyweight and average speed were not factored into the analysis of gait parameters in this study, since they were not different across genotypes (**Fig. 5.1, A-7 B**). Some reports recommend pre-training mice on the CatWalk XT to familiarise them to the apparatus and, consequently, to minimise anxiety and variability across runs (Garrick et al., 2021, Heinzel et al., 2020). Our mice did not undergo training prior to testing; however, runs were excluded from the analysis if the variation in speed

exceeded 35% (**Section 2.5.5**). Moreover, the large number of available gait parameters can increase the likelihood of observing false positive results if specific parameters of interest are not determined prior to analysis (Garrick et al., 2021). In this study, parameters were selected for analysis based on a comprehensive review of CatWalk XT studies in PD models (**Table 5.3**) (Timotius et al., 2023).

5.3.3 MOUSE MODELS OF *GBA*-ASSOCIATED PD HAVE MILD OR INCONSISTENT NON-MOTOR PHENOTYPES

Research into the non-motor symptomatology of PD has grown over the past decade (Li et al., 2024). However, the underlying pathophysiology of these symptoms remains poorly understood, the burden they place on patient quality of life is frequently overlooked and clinical management is inadequate (LeWitt and Chaudhuri, 2020, Martinez-Martin et al., 2011, Todorova et al., 2014). Animal models have potential to help advance future progress, but behavioural phenotyping thus far has produced largely inconsistent findings (Fan et al., 2021, Zhang et al., 2022c).

GI dysfunction was the most reproducible symptom in a systematic review of non-motor phenotypes in rodent models of PD (Zhang et al., 2022c) but remains relatively understudied in *GBA*-associated PD (Fishbein et al., 2014, Jesus et al., 2016, Zhou et al., 2023). Therefore, I set out to investigate this in our aged mouse cohort. L444P mice defecated significantly less frequently than their nTG counterparts during the stool collection test (**Fig. 5.8 A**), signalling a constipation-like phenotype. This would support previous reports of slower colonic motility in $Gba^{+/L444P}SNCA^{A53T}$ mice (Fishbein et al., 2014) and reflect the increased prevalence of constipation in PD patients carrying a *GBA* mutation (Jesus et al., 2016, Zhou et al., 2023). However, my results were inconclusive given that the reduced pellet count in L444P mice did not reach significance vs other genotypes

and because the stool weight and % water content were unchanged across genotypes (**Fig. 5.8 B-D**).

A limitation of this study was that mice were only tested in one trial lasting for 60 min. These experiments could also not account for potential variation introduced by differences in food and water intake before the trial, which were available *ad libitum* until the trial started. To mitigate this, future studies should repeatedly sample stool over a longer time frame. Longitudinal, non-invasive stool collection could be achieved with an adapted home cage apparatus that maintains mice in their natural environment (Frynta et al., 2009). Additionally, combining the stool collection protocol with another measure of GI function, e.g. GI motility time (Fishbein et al., 2014), could increase the validity of the results. Aside from characterising GI symptoms, future studies could use the L444P mice to elucidate mechanisms underlying GI dysfunction in PD. In duodenal PFF-injected mice, αS pathology in the gut and related GI dysfunction were ameliorated by elevating GCase expression (Challis et al., 2020). It would therefore be interesting to determine if the severity of PFF-induced GI pathology is greater in our L444P mice.

Table 5.4: Studies investigating non-motor behaviour in existing genetic mouse models of *GBA*-associated PD and GD.

Behavioural Test	Model (Original Reference)	Direction of change (vs WT): Parameter(s)	Age (n/group)	Reference
Radial water maze	*Gba*$^{+/L444P}$ (*)	↑: # of failures to enter goal arm	7 m (16-19)	(Lado et al., 2024)
Morris water maze	*Gba*$^{+/L444P}$ (*)	NC: escape latency	2.5 m (10-11) 7 m (18-19)	(Lado et al., 2024)
	Gba$^{+/D409V}$ (‡)	NC: escape latency, distance to platform ↑: escape latency, distance to platform	3, 6, 9 m (8-9) 12 m (8-9)	(Clarke et al., 2019)
	Gba$^{E326K/E326K}$ (§)	NC: escape latency	10 m (10-12)	(Kweon et al., 2024)
Probe trial	*Gba*$^{+/D409V}$ (‡)	↓: time in platform quadrant	12 m (8-9)	(Clarke et al., 2019)
	Gba$^{+/L444P}$ (*)	↓: time in platform quadrant	2.5 m (10-11) 7 m (18-19)	(Lado et al., 2024)
	Gba$^{E326K/E326K}$ (§)	NC: time in platform quadrant	10 m (10-12)	(Kweon et al., 2024)
Fear conditioning	*Gba*$^{+/L444P}$ (*)	↓: time freezing contextual FC, NC: cued FC NC: time freezing contextual FC, cued FC	3 m (7) 12 m (18-22)	(Mahoney-Crane et al. 2023)
	Gba$^{+/L444P}$ (*)	↓: time freezing contextual FC, NC: cued FC	2.5 m (10-11), 7 m (18)	(Lado et al., 2024)
	Gba$^{L444P/KO}$ (*)	NC: freeze count (cued) vs *Gba*$^{L444P/KO}$	3, 12 m (6-7)	(Vidyadhara et al., 2025)
	Gba$^{D409V/D409V}$ (‡‡)	↓: time freezing contextual FC, cued FC	6 m (ND)	(Sardi et al., 2011)
	Gba$^{D409V/D409V}$ (‡‡)	↓: time freezing contextual FC	9 m (≥10), 13 m (≥10)	(Sardi et al., 2017)
	Gba$^{D409V/KO}$ (‡‡)	↓: freezing events contextual FC (M only) ↓: freezing events cued FC (M & F)	12 m (11-12)	(Dai et al., 2016)
	Gba$^{E326K/E326K}$ (§)	NC: time freezing contextual FC, cued FC	13 m (10)	(Kweon et al., 2024)
Contextual FC (Passive avoidance)	*Gba*$^{E326K/E326K}$ (§)	NC: latency to enter dark compartment	10 m (10-12)	(Kweon et al., 2024)
Repeated open field habituation	*Gba*$^{D409V/KO}$ (‡‡)	NC: exploratory behaviours ↑: exploratory behaviours	6 m (9-35) 9 m, 12 m (9-35)	(Dai et al., 2016)
Novel object recognition	*Gba*$^{+/L444P}$ (*)	NC: discrimination index (M only)	22 m (8-10)	(Migdalska-Richards et al., 2017b)
	Gba$^{+/L444P}$ (*)	↓: % time exploring novel object, discrimination index	7 m (17-18)	(Lado et al., 2024)

Novel object recognition (cont.)	*Gba*$^{L444P/KO}$ (*)	↓: time exploring novel object NC: time exploring novel object	3 m (9-10) 12 m (7-19)	(Vidyadhara et al., 2025)
	Gba$^{+/-}$ (††)	NC: discrimination index (M only)	22 m (9)	(Migdalska-Richards et al., 2017b)
	Gba$^{+/-}$ (†)	NC: discrimination index	8-23 m^ (6-9)	(Do et al., 2021)
	Gba$^{+/-}$ (††)	NC: % exploration of novel object	6 m (7)	(Sardi et al., 2011)
	Gba$^{+/D409V}$ (‡‡)	NC: % exploration of novel object	6 m (6-7)	(Sardi et al., 2011)
	Gba$^{D409V/D409V}$ (‡‡)	↓: % exploration of novel object	6 m (ND)	(Sardi et al., 2011)
	Gba$^{D409V/D409V}$ (‡‡)	↓: % exploration of novel object ↓: % exploration of novel object ↓: % exploration of novel object	4 m, 6 m, 14 m, (9-12) 3 m, 12 m (≥10) 8 m (≥17)	(Sardi et al., 2013) (Sardi et al., 2017) (Viel et al., 2021)
	GBA^{L444P}*Gba*$^{-/-}$ (***)	NC: discrimination index (M only)	4 m (ND)	(Chen et al., 2024)
	Gba$^{E326K/E326K}$ (§)	NC: time exploring novel object, discrimination index	10 m (10-12)	(Kweon et al., 2024)
Y-maze	*Gba*$^{+/D409V}$ (‡)	NC: % spontaneous alternation ↓: % spontaneous alternation	3, 6, 9 m (8-10) 12 m (8-10)	(Clarke et al., 2019)
	Gba$^{E326K/E326K}$ (§)	NC: % spontaneous alternation	10 m (10-12)	(Kweon et al., 2024)
Elevated plus maze	*Gba*$^{E326K/E326K}$ (§)	NC: % time in open arm, % open arm entries	10 m (10-12)	(Kweon et al., 2024)
Marble burying	*Gba*$^{D409V/KO}$ (‡‡)	↓: latency time (M: 6 m, F: 6, 9 m) ↑: latency time (M, F: 18 m) ↑: # of marbles buried (F: 12, 18 m)	3-18 m^ (8-20)	(Dai et al., 2016)
Forced swimming	*Gba*$^{E326K/E326K}$ (§)	NC: immobility time	10 m (10-12)	(Kweon et al., 2024)
Tail suspension	*Gba*$^{E326K/E326K}$ (§)	NC: immobility time	10 m (10-12)	(Kweon et al., 2024)
Buried pellet test	*Gba*$^{+/L444P}$ (*)	NC: latency to find object (M only)	22 m (8-10)	(Migdalska-Richards et al., 2017b)
	Gba$^{+/-}$ (††)	NC: latency to find object (M only)	22 m (9)	(Migdalska-Richards et al., 2017b)
	Gba$^{+/-}$ (†)	NC: latency to find object	8-23 m^ (6-9)	(Do et al., 2021)

Key: Model: * (Liu et al., 1998); *** (Sanders et al., 2013); † (Tybulewicz et al., 1992); †† (Enquist et al., 2007); ‡ (Ikuno et al., 2019, Polinski et al., 2021); ‡‡ (Xu et al., 2003); § (Kweon et al., 2024). NC = no change; ↑ = significant increase; ↓ = significant decrease; m = months; ^ = longitudinal study; ND = not disclosed; M = male; F = female; FC = fear conditioning.

Table 5.5: Studies investigating non-motor behaviour in existing genetic multifactorial mouse models of *GBA*-associated PD and GD.

Behavioural Test	Model (Original Reference) x Additional insult	Direction of change: Parameter(s)	Age (n/group)	Reference
Morris water maze	*Gba*$^{+/L444P}$ (*) x Thy1-*SNCA*	↑: escape latency vs WT, *Gba*$^{+/L444P}$ & Thy1-*SNCA* ↑: escape latency vs WT, *Gba*$^{+/L444P}$, NC vs Thy1-*SNCA* (M only)	2.5 m (14-16) 7 m (10-14)	(Lado et al., 2024)
	Gba$^{E326K/E326K}$ (§) x PFF GI	↑: escape latency vs WT & *Gba*$^{E326K/E326K}$, NC vs PFF	10 m (9-13)	(Kweon et al., 2024)
Probe trial	*Gba*$^{+/L444P}$ (*) x Thy1-*SNCA*	↓: time in platform quadrant vs WT, *Gba*$^{+/L444P}$ & Thy1-*SNCA* ↓: time in platform quadrant vs WT & *Gba*$^{+/L444P}$, NC vs Thy1-*SNCA* (M only)	2.5 m (14-16) 7 m (10-14)	(Lado et al., 2024)
	Gba$^{E326K/E326K}$ (§) x PFF GI	↓: time in platform quadrant vs WT & *Gba*$^{E326K/E326K}$ NC vs PFF	10 m (9-13)	(Kweon et al., 2024)
Fear conditioning	*Gba*$^{+/L444P}$ (*) x PFF IS	NC: time freezing contextual or cued	12 m (9-22)	(Mahoney-Crane et al. 2023)
	Gba$^{+/L444P}$ (*) x Thy1-*SNCA*	↓: time freezing (contextual) vs WT, *Gba*$^{+/L444P}$ & Thy1-*SNCA* ↓: time freezing (contextual) vs WT & *Gba*$^{+/L444P}$, NC vs Thy1-*SNCA*, NC: cued either age. (M only for all experiments)	2.5 m (13-22) 7 m (10)	(Lado et al., 2024)
	Gba$^{E326K/E326K}$ (§) x PFF IS	↓: time freezing (contextual & cued) vs WT, *Gba*$^{E326K/E326K}$ & PFF	13 m (8-13)	(Kweon et al., 2024)
	Gba$^{L444P/KO}$ (*) x *SNCA*^{A30P}	NC: freeze count (cued) vs *Gba*$^{L444P/KO}$ x *SNCA*$^{+/A30P}$	3 m, 12 m (8-12)	(Vidyadhara et al., 2025)
Contextual FC (Passive avoidance)	*Gba*$^{E326K/E326K}$ (§) x PFF GI	↓: latency to enter dark compartment vs WT, *Gba*$^{E326K/E326K}$ & PFF	10 m (9-13)	(Kweon et al., 2024)
Novel object recognition	*Gba*$^{+/-}$ (†) x *SNCA*^{A53T}	NC: discrimination index	8-23 m^ (6-10)	(Do et al., 2021)
	Gba$^{L444P/KO}$ (*) x *SNCA*^{A30P}	↓: time exploring novel object vs WT & *SNCA*$^{+/A30P}$ NC vs *Gba*$^{L444P/KO}$ *Note: < 5% of trial spent with novel object.*	3 m, 12 m (7-19)	(Vidyadhara et al., 2025)
	GBA^{L444P}*Gba*$^{-/-}$ (***) x PFF SLD	↓: discrimination index vs WT & *GBA*^{L444P}*Gba*$^{-/-}$, NC vs PFF (M only)	4 m (ND)	(Chen et al., 2024)
	Gba$^{E326K/E326K}$ (§) x PFF GI	↓: time exploring novel object and discrimination index vs WT, *Gba*$^{E326K/E326K}$ & PFF	10 m (9-13)	(Kweon et al., 2024)
Y-maze	*Gba*$^{E326K/E326K}$ (§) x PFF GI	↓: spontaneous alternation vs WT, *Gba*$^{E326K/E326K}$ & PFF	10 m (9-13)	(Kweon et al., 2024)
Barnes Maze	*Gba*$^{+/-}$ (†) x *SNCA*-Tg/Tg	NC: time to correct arm (M only)	15 m (17-20)	(Ikuno et al., 2019)
Zero maze	*Gba*$^{+/L444P}$ (*) x *SNCA*^{A53T}	↓: % time open area vs *SNCA*^{A53T} NC: closed area entries, distance travelled	20 m (ND)	(Fishbein et al., 2014)

Elevated plus maze	*Gba*$^{+/L444P}$ (*) x *SNCA*^{A53T}	↓: open arm entries, time centre, % time open arm vs *SNCA*^{A53T} NC: closed arm entries, distance travelled	20 m (ND)	(Fishbein et al., 2014)
	Gba$^{E326K/E326K}$ (§) x PFF GI	↓: % open arm entries, % time open arm vs WT & *Gba*$^{E326K/E326K}$, NC vs PFF	10 m (9-13)	(Kweon et al., 2024)
Forced swimming	*Gba*$^{E326K/E326K}$ (§) x PFF GI	↓: immobility time vs WT & *Gba*$^{E326K/E326K}$, NC vs PFF	10 m (9-13)	(Kweon et al., 2024)
Tail suspension	*Gba*$^{E326K/E326K}$ (§) x PFF GI	↓: immobility time vs WT & *Gba*$^{E326K/E326K}$, NC vs PFF	10 m (9-13)	(Kweon et al., 2024)
GI function	*Gba*$^{+/L444P}$ (*) x *SNCA*^{A53T}	NC: colonic motility time (7 m) ↑: colonic motility time vs *SNCA*^{A53T} (14 m) (M only) NC: whole-gut transit time (15 m)	7 m (16-24) 14 m (14-19) 15 m (ND)	(Fishbein et al., 2014)
Buried pellet test	*Gba*$^{+/-}$ (†) x *SNCA*^{A53T}	↑: latency to find object vs WT (< 20 m), NC vs *Gba*$^{+/-}$, *SNCA*^{A53T}	8-23 m^ (6-10)	(Do et al., 2021)

Key: Model: * (Liu et al., 1998); *** (Sanders et al., 2013); † (Tybulewicz et al., 1992); § (Kweon et al., 2024). NC = no change; ↑ = significant increase; ↓ = significant decrease; m = months; ^ = longitudinal study; ND = not disclosed; M = male; FC = fear conditioning; GI = gastrointestinal; IS = intra-striatal; SLD = sublaterodorsal tegmental nucleus. Red font indicates that *Gba* mutation deteriorates behaviour in multifactorial model over all controls.

I next sought to characterise spatial working memory in our aged cohort given the high prevalence of cognitive difficulties and dementia in *GBA*-associated PD (**Table 1.2**) (Brockmann et al., 2015, Brockmann et al., 2011, Straniero et al., 2020, Zhang et al., 2018b), particularly in patients carrying an L444P mutation (Cilia et al., 2016). Contrary to this, L444P mice alternated in 77% of trials in the T-maze, which aligns with the expected range (70-80%) in mice with normal spatial working memory (d'Isa et al., 2021, Deacon and Rawlins, 2006). These experiments were the first assessment of spatial working memory in a mouse model of *GBA*-associated PD using a T-maze apparatus. Previously, spatial working memory and spatial learning were assessed in these models using a Y-maze and Morris water maze, respectively (**Table 5.4-5.5**). These assays have produced conflicting results across models (Clarke et al., 2019, Kweon et al., 2024, Lado et al., 2024) (**Table 5.4**), although the addition of αS insults consistently deteriorates performance (Kweon et al., 2024, Lado et al., 2024) (**Table 5.5**). In contrast with our model, *Gba*$^{+/D409V}$ mice appeared to develop spatial working memory deficits at 12-months-old in the Y-maze (**Table 5.4**) (Clarke et al., 2019). However, these findings have questionable biological significance because the spontaneous alternation rates of 9-month-old WT mice were highly similar to these 12-month-old *Gba*$^{+/D409V}$ mice in this study.

Since cognitive dysfunction was the least reproducible, albeit most frequently studied, phenotype across mouse models of PD (Zhang et al., 2022c), the inconsistencies across cognitive assessments in *Gba* transgenic models are unsurprising. This largely reflects the variability in the affected cognitive domains and severity of cognitive dysfunction in PD patients (Aarsland et al., 2021). Reproducing cognitive phenotypes across models is also challenging because the type and severity of cognitive deficits are highly sensitive to the specific protocol employed (Fisher and Bannerman, 2019, Zhang et al., 2022c). This can give rise to apparent contradictory phenotypes, even within the same model. For example,

the novel object recognition test can assess both short-term memory and long-term memory, depending on the intertrial interval length (Lueptow, 2017). Differences in the intertrial interval across Lado et al. (2024) and Migdalska-Richards et al. (2017b) (30 min vs 24 hours, respectively) likely contribute to conflicting observations in the novel object recognition test in the same *Gba*$^{+/L444P}$ mouse (**Table 5.4**). However, neither of these studies distinguished between short-term and long-term memory when reporting their findings. The contextual fear conditioning (FC) test has also produced contradictory phenotypes in the same *Gba*$^{+/L444P}$ model (Lado et al., 2024, Mahoney-Crane et al., 2023) (**Table 5.4**). Perhaps 12-month-old mice performed better in Mahoney-Crane et al. (2023) because they were exposed to more tones and subsequent foot shocks during training, vs Lado et al. (2024). On the contrary, it is likely that 3-month-old *Gba*$^{+/L444P}$ mice freeze less in Mahoney-Crane et al. (2023) because they are hyperactive (**Table 5.1, vertical pole**), rather than due to impaired contextual fear memory (Gewirtz et al., 2000, Mahoney-Crane et al., 2023). Indeed, many tests use rodents' time to complete motoric tasks as an indicator of cognitive ability. Therefore, both hyperactivity and (more often) motor deficits displayed by rodent models of PD can confound the characterisation of cognition (Wichmann et al., 2025, Dunnett and Lelos, 2010). The T-maze is advantageous in this regard because performance is not graded according to the time to choose a goal arm. Moreover, by measuring spontaneous alternation, this test leverages the mice's innate motivation to explore new environments and therefore does not require pre-training, food-deprivation or rewards. This reduces stress and the time required to complete the assay (d'Isa et al., 2021, Deacon and Rawlins, 2006).

On the other hand, a common challenge of measuring spontaneous alternation in the T-maze is that rodents gradually stop exploring the maze (**Fig. 5.9 A**) (d'Isa et al., 2021, Deacon and Rawlins, 2006, Wu et al., 2018). This occurs due to a loss of motivation to explore upon

repeated exposure and can be mitigated by regularly changing the floor odour (Deacon and Rawlins, 2006). Cognitive tasks in rodents are also limited by being typically restricted to a single cognitive domain. This simplicity lacks translatability to the complex, multifaceted cognitive dysfunction in patients (Kwak et al., 2016, Zhang et al., 2022c). In addition, executive function has not been widely assessed in PD rodent models (Zhang et al., 2022c), despite being the most prevalent cognitive difficulty in prodromal PD patients (Fengler et al., 2017). Future studies should therefore employ a battery of tests to assess various cognitive abilities in our L444P mice, including executive function. Alternatively, touchscreen-based tests have been described, which can assess various domains of cognition using a single apparatus. This method employs complex tasks that are relevant to human cognition but require minimal motor effort and do not evoke stress (Kwak et al., 2016, Bussey et al., 2012).

Despite the high prevalence of anxiety, depression and other psychiatric disturbances in *GBA*-associated PD patients (Brockmann et al., 2011, Jesus et al., 2016, Petrucci et al., 2020, Zhang et al., 2018b), these symptoms have largely been neglected in behavioural studies with *Gba* transgenic mice (**Table 5.4-5.5**). Only three studies have examined anxiety in these models (Dai et al., 2016, Fishbein et al., 2014, Kweon et al., 2024) and the EPM test presented herein is the sole investigation in a mouse monogenic for the L444P mutation. The EPM assay does not involve pre-training, noxious stimuli or food and water deprivation, and therefore can be completed quickly causing minimal stress (Pellow et al., 1985). There was no indication of increased anxiety in L444P mice, as their activity levels in the open arms were similar to other genotypes (**Fig. 5.10**). These findings corroborate previous observations of normal anxiety levels in *Gba*$^{E326K/E326K}$ mice on the EPM (Kweon et al., 2024). Notably, increased anxiety in PFF-treated *Gba*$^{E326K/E326K}$ mice is likely driven by the PFF injection rather than the *Gba* mutation because these mice had similar anxiety levels to

PFF-treated WT mice (**Table 5.5**). Although, *Gba*$^{+/L444P}$*SNCA*^{A53T} mice were more anxious than *SNCA*^{A53T} on the EPM and zero maze (**Table 5.5**) (Fishbein et al., 2014), these results have questionable validity considering WT and *Gba*$^{+/L444P}$ mice were not included in the study and the sample size was not reported. Also, the increased anxiety observed in *Gba*$^{D409V/KO}$ mice using the marble burying test has limited relevance to PD (**Table 5.4**), considering these mice model neuropathic GD (Dai et al., 2016). Overall, there is no robust evidence demonstrating that PD-relevant *GBA* mutations increase anxiety in transgenic rodent models. Similarly, other PD models also generally fail to display anxiety or depressive phenotypes (Zhang et al., 2022c).

A pitfall of my EPM experiments was that some mice did not explore the open arms (**Fig. 5.10 B-C**). This created a floor effect in the data and thereby limited the sensitivity of the assay to detect potential anxiogenic effects of the L444P mutation. Prior exposure to other behavioural tests can reduce rodent activity in the open arms of the EPM (Shoji and Miyakawa, 2021, Voikar et al., 2004). This may have contributed to the observed floor effect, since the EPM was the final assessment performed in the behavioural testing battery. It would therefore be advisable for future studies to assess mice on the EPM before conducting other behavioural tests. Using an elevated zero maze may also increase the window of detection, since rodents exhibit higher baseline activity in open areas of this maze vs the EPM (Tucker and McCabe, 2017, Braun et al., 2011).

5.3.4 FACTORS INFLUENCING THE VALIDITY AND REPRODUCIBILITY OF BEHAVIOURAL DATA IN PD MODELS

5.3.4.1 The relevance of ageing to symptom manifestation is largely disregarded in behavioural studies with *Gba* rodent models

Typically, *GBA*-associated PD patients develop disease symptoms no sooner than their early to mid 50s (Zhang et al., 2018b). This approximates to 15-16 months in the lifespan of a mouse (Sukoff Rizzo and Crawley, 2017). In this thesis, behaviour was characterised in mice

aged 15-21-months-old (**Fig. 5.1 A**) to replicate the timeframe of symptom onset and progression in patients. On the other hand, I only found seven studies that characterised behaviour in *Gba* genetic mouse models aged 15 months or older (Dai et al., 2016, Do et al., 2021, Fishbein et al., 2014, Furderer et al., 2024, Ikuno et al., 2019, Migdalska-Richards et al., 2017b, Soria et al., 2017) (**Table 5.1-5.2, 5.4-5.5**). Studies in younger mice undermine the effect of ageing on underlying pathological mechanisms and may overlook phenotypes that only manifest in later disease stages (Klaestrup et al., 2022, Reeve et al., 2014). Moreover, behavioural abnormalities observed in younger mice, e.g. hyperactivity on the vertical pole (Mahoney-Crane et al., 2023), have questionable relevance to the disease. Nonetheless, behavioural phenotyping of younger mice can be useful as part of longitudinal assessments to track symptom progression over time. Previous longitudinal analyses in *Gba* mouse models have not identified clear age-related deterioration in motor or non-motor function (Dai et al., 2016, Do et al., 2021, Vidyadhara et al., 2025). Despite this, it may still be interesting to assess younger L444P mice on the CatWalk XT to identify the onset of the observed gait abnormalities (**Fig. 5.6-5.7**).

In this study, L444P mice were significantly younger than their hWT counterparts (**Fig. 5.1 A**). This may limit our ability detect disease-relevant phenotypes, given that C57BL/6 mice display a natural age-related decline in motoric, cognitive and psychological function (Yanai and Endo, 2021, Shoji and Miyakawa, 2019, Shoji et al., 2016); however, many of these behavioural phenotypes tend to stabilise from 16 months onwards (Shoji and Miyakawa, 2019, Yanai and Endo, 2021). I also demonstrated that rotarod performance remained similar across genotypes after accounting for age (**Fig. A-5**). Moreover, the mean spontaneous alternation rate of all genotypes on the T-maze was consistent with the expected rate in cognitively normal mice (70-80%) (d'Isa et al., 2021, Deacon and Rawlins, 2006)

(**Fig. 5.9**). Therefore, this age difference is unlikely to be masking L444P-induced deficits in motor or cognitive function.

5.3.4.2 Behavioural characterisation across both sexes is necessary to encapsulate the diverse clinical profile of PD patients

The higher prevalence of PD in men (Zirra et al., 2023, Dorsey et al., 2018a) may contribute to the overrepresentation of male patients in clinical trials (Smilowska et al., 2025, Tosserams et al., 2018). This bias has translated to behavioural research in preclinical models of PD; approximately 50% of studies investigating non-motor phenotypes used male rodents only (Zhang et al., 2022c). I also came across five previous behavioural studies in *Gba* genetic mouse models that used males only for more than one of their tests (Chen et al., 2024, Ikuno et al., 2019, Lado et al., 2024, Migdalska-Richards et al., 2017b, Polinski et al., 2022) (**Table 5.1-5.2, 5.4-5.5**). As the symptomatology and progression of PD differs across sexes (Iwaki et al., 2021, Picillo et al., 2017), incorporating male and female mice is necessary to adequately capture diversity in the disease. This may be especially relevant for *GBA*-associated PD, as there are mixed reports around the disease prevalence across sexes (Li et al., 2021, Ortega et al., 2022, Straniero et al., 2020), although cognitive deficits may be more common in male patients (Caminiti et al., 2025). In this study, male and female mice were equally distributed across all genotypes (**Fig. 5.1 C**). Future behavioural characterisation of our L444P mice could incorporate larger sample sizes to analyse behaviour in males and females individually. Using this approach, reports in other PD mouse models have demonstrated more severe motor deficits in males (Chen et al., 2019, Geldenhuys et al., 2015, Lamontagne-Proulx et al., 2023). Similar analyses have revealed sex-divergent phenotypes in colonic motility, gait and anxiety in *Gba* transgenic mice, although the disease-relevance of these findings is uncertain (Dai et al., 2016, Fishbein et al., 2014).

Lastly, it should be noted that male rodents are overrepresented in neuroscience and behavioural research at large, not just PD-related studies (Kahnau et al., 2023, Beery and Zucker, 2011). Female mice have often been excluded from experiments due to concerns around variability introduced by the oestrous cycle (Beery, 2018, McCarthy et al., 2012, Wald and Wu, 2010). These beliefs have been refuted by multiple studies demonstrating that the intrinsic variability of both sexes is similar across various physiological and behavioural traits (Kaluve et al., 2022, Levy et al., 2023, Prendergast et al., 2014, Tsao et al., 2023). Many funding bodies now require research plans to incorporate male and female animals, unless a well-justified reason can be given for not doing so (Lee, 2018, Clayton and Collins, 2014). It is hoped that such initiatives will reduce the sex bias in future PD behavioural studies.

5.3.4.3 Many rodent behavioural studies lack adequate power

Neuroscience research has been widely criticized due to the high prevalence of underpowered studies with low sample sizes (Bespalov and Steckler, 2018, Nord et al., 2017, Button et al., 2013). Inadequate reporting of sample sizes also contributes to the reproducibility crisis in animal research (Lin et al., 2024a, Song et al., 2024, Enserink, 2017, Baker et al., 2014), despite the introduction of the "ARRIVE" guidelines in 2010 (Percie du Sert et al., 2020, Kilkenny et al., 2010). Indeed, some of the previous behavioural studies in *Gba* mouse models did not explicitly disclose sample sizes (Chen et al., 2024, Fishbein et al., 2014, Sardi et al., 2011, Soria et al., 2017, Walton et al., 2024) (**Table 5.1-5.2, 5.4-5.5**). The statistical power of the behavioural characterisation presented herein was limited by the relatively small sample size of 9-15 mice per genotype (**Fig. 5.1 C**). As a rule of thumb, 12-15 animals per group has been deemed generally sufficient for behavioural analyses (Sukoff Rizzo and Crawley, 2017). Notably however, my experiments had more mice than most previous reports in *Gba* models (**Table 5.1-5.2, 5.4-5.5**): only seven previous investigations

had 12 mice or more in each group for at least one of their behavioural experiments (Fishbein et al., 2014, Ikuno et al., 2019, Lado et al., 2024, Mahoney-Crane et al., 2023, Polinski et al., 2022, Viel et al., 2021, Yun et al., 2018). The sample size for this study was determined based on previous behavioural studies from my lab (Bengoa-Vergniory et al., 2020, Hunn et al., 2019, Sloan et al., 2016). This approach remains common practise (Festing, 2018, Lado et al., 2024), although it would be advisable to use a power calculation for future behavioural characterisations in L444P mice (NC3Rs, 2023). Notably, it is especially challenging to achieve sufficiently large sample sizes in studies with aged mice. Age-related morbidities, e.g. weight loss, spontaneous tumours, are inevitable and resulted in mice needing to be sacrificed before this study commenced. Also, the extra housing and husbandry required to maintain ageing cohorts is space-, labour- and cost-intensive, which can limit the feasibility of establishing large cohorts for some researchers (Klaestrup et al., 2022). To overcome this, experimental plans should maximise the amount of information gathered per animal, in line with the principles of the 3Rs (Russell, 1959).

5.3.4.4 Novel, automated technologies show promise to improve the reliability of behavioural data

A myriad of factors related to the laboratory environment, experimenter and experimental design can influence behavioural studies (Schellinck, 2010). These include housing conditions, handling techniques and observer-related biases and errors (Gouveia and Hurst, 2017, Crabbe et al., 1999, Chesler et al., 2002). In this study, many steps were taken to reduce or eliminate the effects of these confounds: data was collected blind to genotype, mice were pre-habituated to handling, the mice's housing conditions, lighting and diet were standardized and experiments were performed at consistent times each day. However, these confounds are often overlooked or difficult to control across studies, which limits the reliability of behavioural results (Sare et al., 2021). In light of this, researchers should

embrace advancements in automated technologies to improve the reproducibility of behavioural data. Many video tracking systems are now available that can be used to objectively, accurately and efficiently quantify mouse behaviour in a variety of paradigms (Panadeiro et al., 2021, Noldus et al., 2001, Spink et al., 2001). For instance, these systems have been applied to continuously monitor behaviour in the home-cage environment over long time scales. This non-invasive method alleviates experimenter-related stressors and can decrease variability introduced by diurnal changes in mouse behaviour (Bains et al., 2018, Kahnau et al., 2023, Pernold et al., 2019, Voikar and Gaburro, 2020). The advent of pose estimation software, e.g. DeepLabCut (Nath et al., 2019, Mathis et al., 2018) has also greatly enhanced the behavioural researcher's toolkit. This software, combined with machine learning approaches, can quantify ethologically-relevant, complex phenotypes with equivalent, or better, precision and accuracy than human scoring in a range of behavioural assays (Sturman et al., 2020, von Ziegler et al., 2021). This approach has also identified early motor deficits, undetectable to the naked eye, in a PD mouse model (Bidgood et al., 2024) and therefore also shows promise to improve the face validity of *Gba* transgenic mice.

5.3.5 CONCLUSION

In conclusion, this chapter has demonstrated that aged L444P mice do not display overt motor or non-motor behavioural deficits. These findings largely corroborate phenotypes in other monogenic *Gba* transgenic models (**Table 5.1, 5.4**). On the other hand, automated gait analysis has exclusively revealed that the L444P mutation induces mild deficits in hindlimb swing dynamics. In future, further subtle deficits may be identified by taking advantage of the slew of new behavioural testing technologies and statistical methods. On a final note, the lack of gross behavioural impairments in our model renders it currently unsuitable to use in behavioural studies for preclinical therapeutic trials. Exposure to additional insults may increase the face validity of our model for such trials (**Table 5.2, 5.5**), this is further

discussed in **Section 6.3.2**. Nevertheless, a rodent model that recapitulates the progressive nature of most motor and non-motor symptoms is unlikely to be attainable. Instead, behavioural characterisations should endeavour to robustly identify the strengths and limitations of the model in its ability to recapitulate disease phenotypes. This will enable future research to best-align the choice of model with the specific study requirements (Fisher and Bannerman, 2019).

CHAPTER 6: DISCUSSION

6.1 STRENGTHS OF OUR L444P MODEL AND SUMMARY OF KEY FINDINGS IN THIS THESIS

GBA is the strongest genetic risk factor for PD; however, the mechanisms governing mutant GCase's pathogenic role in this disease remain enigmatic. Until now, the lack of a valid humanised mouse model of *GBA*-associated PD has been a missing puzzle piece in efforts to demystify GCase dysfunction in the disorder. To accelerate progress in this field, our lab used BAC transgenic technology to create a mouse model of *GBA*-associated PD that is hemizygous for a human *GBA*-L444P transgene.

This novel model confers many unique advantages over existing genetically engineered mice used to study *GBA*-associated PD pathology. First and foremost, it is the only humanised mouse model of *GBA*-associated PD that has been created to date. It therefore bestows unprecedented construct validity and translatability to the human condition. Investigations into pharmacological GCase modulators have strongly indicated that mouse and human GCase have different catalytic properties: the efficacy of small molecule GCase activators was higher for human GCase than mouse GCase, whereas CBE's potency was lower at human vs mouse GCase (Berger et al., 2015, Liou et al., 2006). These interspecies-differences substantiate that humanised models of *GBA*-associated PD would grant superior predictive validity in preclinical studies for PD therapies targeting GCase function. *GBA* variants have also been shown to produce divergent effects in mice and humans. For example, GD patients that harbour homozygous *GBA*-N370S mutations can remain asymptomatic until adulthood (Stirnemann et al., 2017), whereas $Gba^{N370S/N370S}$ mice died within 24 hours of birth due to skin barrier defects (Xu et al., 2003). The reasons for this

discrepancy are unclear but they may not be directly related to interspecies differences in GCase's catalytic function (Liou et al., 2006). This is further discussed in **Section 6.2**. Indeed, although human and mouse GCase share approximately 85% amino acid sequence similarity (O'Neill et al., 1989), these findings highlight that protein functionality across species in physiological and disease states cannot be predicted based on sequence homology alone. This is supported by Woeste et al. (2019), who used *Gba2*-KO mice to investigate phenotypes related to hereditary spastic paraplegia and autosomal recessive cerebellar ataxia; diseases that are caused by *GBA2* mutations and related loss of GCase2 activity. This study found that *Gba2*-KO mice displayed reduced GCase2 activity, but poorly replicated phenotypes observed in patients with these conditions. This failure was largely attributed to species-related differences between human and mouse GCase2 function, despite the amino acid sequence of these proteins being 87% identical. Furthermore, pathology in our humanised L444P mice may be more reproducible than phenotypes in pre-existing *Gba* KI or haploinsufficient mice because WT murine GCase activity varies according to strain (Duran et al., 2021). In the future, direct interspecies comparisons of GCase structure and function hold promise to unveil further benefits of using humanised mice to examine *GBA*-associated PD pathology.

Our model also overcomes limitations of previous attempts to model human mutant GCase pathology in mice. For instance, disease features produced by injection of an AAV vector harbouring human *GBA*-N370S are dependent on the viral titre (Papadopoulos et al., 2018, Polissidis et al., 2022). Furthermore, since AAV *GBA*-N370S mice overexpress human *GBA* on a $Gba^{+/+}$ background, their total GCase activity is similar to that of WT mice not administered with an AAV *GBA* vector. Alternatively, others have considered humanised mouse models of GD as suitable candidates to investigate *GBA*-associated PD pathology (Chen et al., 2024). Various pathological phenotypes in these GD mice, including splenic

lesions and Gaucher cell accumulation, serve to highlight their poor face validity for PD (Sanders et al., 2013). Similar to the aforementioned viral *GBA*-N370S overexpressing mice, these humanised GD models express mutant GCase at supraphysiological levels (Sanders et al., 2013), which further limits their relevance to human PD. Conversely, in our humanised mice, the full-length human *GBA* gene, along with its endogenous promoter and regulatory elements, was specifically integrated into the Rosa26 locus. Consequently, GCase expression levels in the L444P mice were physiologically relevant and equivalent to the hWT mice, making these genotypes directly comparable in my experiments.

Our model is also highly translatable to the human disease because the L444P mutation is the most common "severe" variant observed in PD patients (**Section 1.2.2**). Moreover, the relatively high penetrance of this variant in PD likely facilitates the observation of pathological phenotypes in our mice. Lastly, our breeding strategy is advantageous because it produces $Gba^{+/-}$ mice as littermates of humanised transgenic mice (**Section 2.1.2**). This affords the opportunity to probe whether disease features in the L444P mice can be mapped to either a loss- or gain-of-function effect of the mutation (**Fig. 1.4**).

This DPhil project sought to thoroughly characterise pathology in our L444P model from a molecular to a behavioural level. I first confirmed that these transgenic mice can recapitulate loss- and gain-of-function effects of the L444P mutation in the cortex from an early age (**Section 3.2.1-3.2.2**). The significant GCase activity deficits in L444P midbrain tissue and cortical cell cultures align with multiple reports of attenuated GCase activity in other mouse models of *GBA*-associated PD (**Table 1.3**). In contrast, gain-of-function effects of *Gba* mutations have not been widely investigated in pre-existing models (**Table 1.3**). Therefore, a particularly notable phenotype in our L444P mice was the accumulation of high MW GCase in the midbrain and cortex (**Fig. 3.1-3.2**), indicating the retention of mutant GCase in the ER. This is the first demonstration of high MW GCase accumulation in a mouse

model of *GBA*-associated PD, corroborating previous reports of elevated Endo-H sensitive GCase in PD patient-derived fibroblasts, iPSC-DAns and midbrain organoids (Fernandes et al., 2016, Frattini et al., 2024, McNeill et al., 2014) and in *GBA* transgenic *Drosophila* models (Maor et al., 2013).

Our L444P mice also display impaired DA release in the DLS, a phenotype that has not previously been observed in other genetically engineered *Gba* mutant mice (**Fig. 4.1, 4.3**). I validated that this $[DA]_o$ deficit persists with age in the L444P DLS but is absent in $Gba^{+/-}$ mice. This suggests that a gain-of-function effect of the L444P mutation is responsible for driving this phenotype in our humanised model. However, the mechanistic nature of this effect remains unclear since DA transmission deficits were not accompanied by loss of striatal DA content (**Section 4.2.2**) or changes to the regulation of striatal DA dynamics by the DAT, D_2Rs or ambient striatal GABA (**Section 4.2.3-4.2.5**). Although striatal DA release deficits have not previously been identified in genetically engineered models of *GBA*-associated PD, other transgenic mice that harbour the L444P mutation display impaired hippocampal synaptic transmission (Lado et al., 2024) and dysregulated synaptic vesicle endocytosis in the cortex (Vidyadhara et al., 2025).

Lastly, I determined that our L444P mice have subtle gait impairments in their hindlimbs but do not replicate the severe motor dysfunction that manifests in PD patients (**Section 5.2.6**). This is the first time that gait deficits have been identified in a mouse model of *GBA*-associated PD using the CatWalk XT system, although this technology has detected similar gait abnormalities in other genetic models of PD (**Table 5.3**) (Hunn et al., 2019, Timotius et al., 2023). Many of these phenotypes align with the gait difficulties experienced by PD patients (**Section 5.3.2**). For instance, the reduced hindlimb swing speed in our L444P mice may be reminiscent of early-stage bradykinesia. On the other hand, $Gba^{+/-}$ mice did not display difficulties with gait or other aspects of motor function, thereby highlighting that

attenuated GCase activity is likely insufficient to drive motoric impairments. Notably, the mild behavioural deficits in our L444P mice coincides with the lack of DA neurodegeneration in the SN of these mice at 18-months-old (**Fig. A-3**, Dr Natalie Connor-Robson). Consistent with this, many other models of *GBA*-associated PD do not display loss of nigral DA neurons or severe behavioural phenotypes (**Table 1.3, 5.1, 5.2, 5.4, 5.5**). This reflects *GBA*'s nature as a genetic risk factor and not a causal element in the disease.

On the other hand, rodents that harbour mutations in monogenic causal PD genes exhibit variable degrees of neurodegeneration and behavioural impairments, largely according to the specific mutation carried and the strategy used to generate the model. For example, mice harbouring PD-related mutations in *PRKN*, *PINK1* or *DJ-1* typically do not exhibit nigral neurodegeneration but can display slight behavioural impairments (Bobela et al., 2014, Vingill et al., 2018). DA neurons of the SN are also generally preserved in rodents carrying *LRRK2* mutations, although impaired striatal DA release has been observed in *LRRK2*-mutant models developed by our lab and others (Sloan et al., 2016, Vingill et al., 2018, Volta and Melrose, 2017). Behavioural phenotypes in these models are variable. Viral-mediated overexpression of WT or mutant αS is particularly effective at inducing neurodegeneration and motor deficits in rodents, whereas pathology tends to be more mixed in transgenic *SNCA* models (Konnova and Swanberg, 2018, Koprich et al., 2017). In line with this, our lab demonstrated that *SNCA*-OVX, but not *SNCA*-A30P, BAC transgenic mice displayed SN neurodegeneration and motor deficits (Janezic et al., 2013, Taylor et al., 2014). It is also worth noting that neuropathology and behavioural phenotypes in mouse models of *GBA*-associated PD contrast with disease-features in neurotoxicant-based models, which often display severe nigral dopaminergic neurodegeneration and PD-related behavioural deficits (Bobela et al., 2014, Vingill et al., 2018).

Given the heterogenous disease phenotypes across mouse models of PD, the choice of model must be aligned to the study's specific objectives. To do this, it is essential to pinpoint models' unique strengths and limitations by comprehensively characterising their pathology. As our L444P mice recapitulate loss- and gain-of-function effects of the mutation from an early age but do not display nigral DA neurodegeneration, I anticipate that this model will be most useful to investigations of prodromal PD pathology. Improved understanding of early-stage dysfunction in the disease will be key to the discovery of therapeutic targets for disease-modifying compounds that can act before overt neurodegeneration occurs. Early phenotypes in our model, such as the accumulation of high MW GCase, could also act as a biomarker of target engagement and compound effectiveness in preclinical drug testing.

6.2 LIMITATIONS OF OUR L444P MICE AND GENERAL CHALLENGES OF MODELLING *GBA*-ASSOCIATED PD

Like all PD models, our humanised L444P mice have limitations that are important to acknowledge. Firstly, our model retains the expression of endogenous mouse *Gba* and therefore is not fully humanised. For unknown reasons, mice that were homozygous for the human *GBA* transgene on a *Gba* KO background were not viable. This may reflect enigmatic differences in the catalytic mechanisms of human and mouse GCase. Alternatively, it could indicate that regulators of GCase activity diverge across species. Related to this, my computational-based interspecies comparison of the GCase-LIMP2 interaction offered some preliminary insights into how lysosomal trafficking of human GCase may differ in the mouse vs human environment (**Section 3.2.6, 3.3.6**). This study showed that human GCase had a lower predicted binding affinity for mouse LIMP2 compared to human LIMP2 (**Fig. 3.16**). It also highlighted that the putative pH sensing residue on human LIMP2, H150, is replaced with a threonine on mouse LIMP2. These findings are in accord with a previous study that

determined H150T-mutant human LIMP2 had impaired affinity for and dissociation from human GCase (Zhao et al., 2014).

Potential interspecies differences in GCase functionality have also been indicated by pitfalls of early attempts to create genetically engineered models of GD. Mice harbouring homozygous N370S or L444P KI mutations in their native *Gba* gene only survived up to 24-48 hours after birth (Liu et al., 1998, Xu et al., 2003). This unanticipated lethality arose due to defects in the permeability barrier of the mice's epidermis and was later rescued in models that selectively retained GCase expression in the skin (Taguchi et al., 2017). This phenotype was particularly surprising for *Gba*$^{N370S/N370S}$ mice, considering this variant typically predisposes to mild pathology in human patients (**Section 1.2.2**). Indeed, the mechanisms governing these inter-species contrasts remain unclear. It may indicate differences in the distribution of GlcCer species in the skin of mice and humans (Liou et al., 2006) or reflect the later development of the skin permeability barrier during mouse vs human gestation (Liu et al., 1998). Alternatively, perhaps mouse mutant GCase is less efficient than human mutant GCase at hydrolysing GlcCer species with long acyl chains that are particularly abundant in the skin (Xu et al., 2003). Nevertheless, these findings, alongside the species-divergences identified in my computational experiments, reflect that the functionality of a human protein in mice may not align to its functionality in its native human environment. This fundamental principle is worthy of consideration in the general appraisal of humanised transgenic disease models.

The absence of *GBA*'s pseudogene, *GBAP*, in mice is another species-related contrast that should be recognised when modelling *GBA*-associated PD. Similarly, our human *GBA* BAC transgenic constructs did not harbour *GBAP*. As the relevance of this pseudogene to *GBA*-associated PD pathology has not been established (Farfel-Becker et al., 2019), the potential ramifications of its absence in mice and in our humanised model are uncertain.

Notably, Straniero et al. (2017) identified that *GBAP* plays a role in regulating *GBA* expression. Future studies that further elucidate *GBAP's* transcriptome with long-read RNA sequencing should help to establish other physiological functions of this gene (Gustavsson et al., 2024). This may also implicate *GBAP* dysregulation in the pathology of *GBA*-associated PD and thereby indicate advantages of incorporating this pseudogene into future models of the disease.

Lastly, the incomplete penetrance of *GBA* mutations in PD poses a universal challenge to recapitulating patient phenotypes across mouse models of the disorder. *GBA*'s nature as a PD risk factor is reflected in our model, and in pre-existing models, by the preservation of nigral DA neurons and general lack of overt behavioural deficits. Indeed, this weakens our model's face validity for later phases of the disease. It also limits their suitability for measuring compounds' effects on behaviour in preclinical drug testing. Some studies have sought to circumvent this mild pathology in *Gba* mutant mice by exposing these models to additional insults, including MPTP, αS PFFs and other PD-related genetic mutations (**Section 1.4.2**). Potential lines of future research to elevate disease phenotypes in our model and thereby emulate the multifactorial nature of *GBA*-associated PD are discussed in (**Section 6.3.2**).

6.3 FUTURE RESEARCH DIRECTIONS

Our model shows promise as a valuable asset to future studies that aim to unravel GCase dysfunction in PD, especially in the early phase of the disease. Therefore, I think that future investigations should delve further into the mechanisms underlying the disease features presented herein and aim to build on these phenotypes by characterising dysfunction in other pathological pathways and brain regions. On the other hand, the absence of nigral dopaminergic neurodegeneration and severe behavioural deficits in our L444P model limit its face validity for late disease stages. Considering this, exposing our mice to additional

insults may be a fruitful strategy to elevate PD-relevant phenotypes and to elucidate the multi-aetiological nature of *GBA*-associated PD. These broad avenues of future research are discussed in the following sections.

6.3.1 IDENTIFYING NOVEL DISEASE FEATURES IN OUR MODEL AND PROBING THE MECHANISMS OF OBSERVED PHENOTYPES

Firstly, as our L444P mice display early and sustained GCase activity deficits across brain regions, it would be interesting to further probe the impact of GCase deficiency on lysosomal/autophagic function in the model. A useful starting point would be to conduct live cell imaging-based assays of lysosomal homeostasis and activity using primary cortical cultures from neonatal mice (**Section 2.3.1**). For example, lysosomal proteolytic activity could be assessed with fluorescent DQ-BSA and lysosomal pH could be measured using the LysoSensor dye (Albrecht et al., 2020). Indeed, a DQ-BSA assay previously demonstrated late endosomal/ lysosomal activity deficits in primary hippocampal cultures from *Gba*$^{+/L444P}$ mice (Mahoney-Crane et al., 2023). Studies should also consider conducting these assays in isolated lysosomes from our mice, considering that Navarro-Romero et al. (2022) only identified lysosomal deficits in the lysosomal fraction, but not whole cell lysates, of *GBA*-mutant dopaminergic cell lines. It would also be interesting to track age-related changes to lipid homeostasis in our model given that GlcSph was not altered in the brains of 3-month-old L444P mice (**Fig. 3.7**). Indeed, cerebral GlcSph has been shown to progressively accumulate with age in WT and *Gba*$^{+/L444P}$ mice and significantly elevated GlcSph was only evident in *Gba*$^{+/L444P}$ mice from 6 months-old onwards (Hallett et al., 2018, Lado et al., 2024, Mahoney-Crane et al., 2023).

The mechanistic basis of impaired DLS $[DA]_o$ in the L444P mice also deserves further attention. Future lines of research to unravel this have previously been discussed in **Section 4.3.5**. In my opinion, using TEM to examine the ultrastructure of striatal DA axons and the

properties of their synaptic vesicle pools holds particular promise to illuminate the pathological underpinnings of this deficit. Previous TEM studies in *SNCA*-OVX, *LRRK2*-R1441C and *LRRK2*-G2019S models from our lab revealed changes to the abundance or distribution of synaptic vesicles in striatal DA axons (Connor-Robson et al., 2019, Janezic et al., 2013). These phenotypes accompanied attenuated DLS DA release in these models (Janezic et al., 2013, Sloan et al., 2016). It would also be interesting to investigate whether the DLS $[DA]_o$ deficit in L444P mice can be rescued by restoring GCase folding with pharmacological chaperones, such as ambroxol. Small molecule activators of GCase may be less effective, considering that this phenotype cannot be directly attributed to loss of GCase activity in the L444P mice.

Furthermore, evaluating mitochondrial function in our L444P model may also unveil relevant pathological phenotypes. For example, bioenergetic deficits evoked by the L444P mutation could render these mice more vulnerable to impairments in DA transmission, thereby contributing to the observed DLS $[DA]_o$ deficit. Notably, many studies in recent years have linked GCase pathology to mitochondrial dysfunction in PD (Rubilar et al., 2024). Mitochondrial size, complex 1 activity and oxidative phosphorylation were reduced in cortical neurons from *Gba*$^{+/L444P}$ mice (Yun et al., 2018) and hippocampal neurons from the same model displayed mitophagy deficits and elevated mitochondrial superoxide production (Li et al., 2019a). Attenuated mitochondrial complex 1 activity was also observed in midbrain organoid models harbouring the L444P mutation (Baden et al., 2023) and in *GBA*-associated PD patient brains (Li et al., 2019a). In accord with this, WT GCase was recently recognized to localise to mitochondria and maintain mitochondrial complex 1 activity in physiological states (Baden et al., 2023).

Finally, an in-depth characterisation of pathology in the hippocampus of our L444P mice is warranted, considering this brain region has been under-explored in experiments

thus far. As aforementioned, lysosomal and mitochondrial function is impaired in primary hippocampal neuronal cultures from *Gba*$^{+/L444P}$ mice (Li et al., 2019a, Mahoney-Crane et al., 2023). Previous studies have also identified dysregulation of synaptic proteins, depletion of excitatory synapses and consequential impairments in synaptic transmission in the hippocampus of these *Gba*$^{+/L444P}$ mice (Lado et al., 2024, Mahoney-Crane et al., 2023). These synaptic deficits were proposed to underlie cognitive dysfunction in this model (Lado et al., 2024, Mahoney-Crane et al., 2023). Considering this, it would be interesting to investigate if the L444P mutation also impairs excitatory hippocampal transmission in our model, along with the observed striatal dopaminergic release deficit.

6.3.2 Exploring the multifactorial nature of *GBA*-associated PD

It remains an outstanding question why only a minority of *GBA* mutation carriers develop PD, but the answers are highly sought-after. It would therefore be valuable to probe the incomplete penetrance of *GBA* mutations in our model by assessing how exposure to additional insults influences the nature and severity of pathology. Previous studies in *Gba*$^{+/L444P}$ mice have used many approaches to emulate the additional "hits" required for disease-onset in *GBA*-associated PD patients (**Section 1.4.2**), including MPTP administration and co-expression of an *SNCA*-A53T transgene (Fishbein et al., 2014, Yun et al., 2018). However, the acute nature of MPTP toxicity precludes the study of age-related disease progression and *Gba*$^{+/L444P}$ *SNCA*^{A53T} dual mutant mice lack construct validity, since the *SNCA*-A53T variant has not been observed in *GBA*-associated PD patients. Considering this, I would aim to elucidate factors that modulate PD susceptibility in *GBA* mutation carriers by perturbing known regulators of GCase function in our L444P model. This approach may also serve to elevate SN pathology and motor dysfunction in these mice.

LIMP2 and SapC would be prime candidates to target given their roles in GCase transport and lysosomal activation, respectively. Notably, in addition to its physiological function as an allosteric GCase activator, SapC can protect against αS pathology in PD by facilitating αS degradation in the lysosome (Kojima et al., 2022) and hindering αS's interaction with GCase (Yap et al., 2013a). These findings indicate that SapC dysregulation may contribute to PD pathology via mechanisms extrinsic to its direct effects on GCase activity. Furthermore, expression of SapC and LIMP2 was shown to be altered in idiopathic and *GBA*-associated PD patients, thereby implicating these proteins as secondary risk factors in the disease. For instance, SapC was diminished in white blood cells from *GBA*-associated PD patients (Avenali et al., 2021) and non-carrier PD patients (Ruz et al., 2022). To the best of my knowledge, SapC levels have not been investigated in post-mortem PD brains. However, its precursor, PSAP, was depleted in PD post-mortem nigral DA neurons (He et al., 2023). On the other hand, studies investigating LIMP2 levels in PD have produced inconsistent findings, indicating that LIMP2 dysregulation in the disorder may depend on the cell type and disease stage. For example, LIMP2 was depleted in fibroblasts from sporadic PD patients (Thomas et al., 2021), whereas elevated LIMP2 in peripheral blood mononuclear cells (PBMCs) and iPSC-DAns from *GBA*-associated PD patients may represent a compensatory mechanism (Avenali et al., 2021, Fernandes et al., 2016). Furthermore, Rothaug et al. (2014) found that LIMP2 was increased in surviving post-mortem DA neurons from PD patient midbrain but this was not replicated by other post-mortem studies investigating LIMP2 in whole brain tissue from PD patients (Gegg et al., 2012, Murphy et al., 2014). Notably, the mechanisms underlying changes to LIMP2 and SapC expression in the disease remain elusive. Genetic association studies have identified single nucleotide polymorphisms (SNPs) near or in the LIMP2-encoding gene, *SCARB2*, that increase PD risk (Do et al., 2011, Hopfner et al., 2013, Michelakakis et al., 2012) but

these variants have questionable relevance to LIMP2 function because they don't affect LIMP2 expression or alter Gase activity (Alcalay et al., 2016, Maniwang et al., 2013, Thomas et al., 2021). Moreover, SapC variants that are associated with increased PD risk have not been identified (Ouled Amar Bencheikh et al., 2018, Sosero et al., 2020).

Aside from the well-established importance of LIMP2 and SapC for maintaining GCase function, progranulin's (PGRN) impact on GCase activity and lysosomal localisation is increasingly recognized (Jian et al., 2016a, Simon et al., 2023, Zhou et al., 2019). PGRN is a secreted growth factor that has been associated with many cellular processes; however, its physiological role in the lysosome remains incompletely defined (Paushter et al., 2018, Simon et al., 2023, Tayebi et al., 2020). Nevertheless, downregulation of this glycoprotein may contribute to PD by influencing LIMP2 and SapC-mediated regulation of GCase function. Firstly, PGRN deficiency evokes GCase-LIMP2 aggregate formation and reduces localisation of the GCase-LIMP2 complex to the lysosome (Jian et al., 2016a). Secondly, PGRN can recruit PSAP to the lysosome (Zhou et al., 2017) and indirectly affects PSAP processing by promoting the maturation and activity of CTSD (Beel et al., 2017, Butler et al., 2019), a lysosomal protease responsible for PSAP cleavage to saposins A-D (Hiraiwa et al., 1997). It follows that PGRN-mediated perturbations to PSAP function may have harmful downstream consequences on GCase activation by SapC. Supporting this, PSAP processing was reduced in PGRN deficient neurons, resulting in diminished SapC levels and GCase activity (Valdez et al., 2020). PGRN's link to GCase function was first indicated by the high prevalence of SNPs in the PGRN-encoding gene, *GRN*, among GD patients alongside observations of reduced PGRN levels in GD patient serum (Jian et al., 2016b). Since then, SNPs in the vicinity of *GRN* have been identified in PD GWAS, implicating *GRN* downregulation as a susceptibility factor in PD (Nalls et al., 2021, Nalls et al., 2019). Reduced PGRN levels have also been demonstrated in PD patient plasma and the extent of

PGRN deficiency was suggested to act as a biomarker of PD severity (Yao et al., 2020). Considering PGRN's influence on GCase activity and association with PD, it would be interesting to investigate the impact of PGRN deficiency on GCase activity and related phenotypes in our L444P model. Notably, PGRN KO in *Gba*$^{D409V/D409V}$ GD mice was associated with severe GCase activity impairments, αS pathology and neuroinflammation (Zhao et al., 2023b), whereas PGRN KO in *Gba*$^{+/D409V}$ mice produced a milder GCase activity deficit (Lin et al., 2024b).

An alternative approach to studying *GBA* mutations' incomplete penetrance in PD and to heightening pathology in our model would be to introduce additional PD-related genetic mutations that have previously been observed in *GBA*-associated PD patients. For instance, large-scale observational clinical studies identified a subset of PD patients who co-expressed pathogenic variants in *GBA* and *PRKN* (Cook et al., 2024, Westenberger et al., 2024). Dual *GBA-PRKN* mice may also be particularly relevant to *GBA*-associated PD pathology given that L444P-GCase is ubiquitinated by parkin and has been proposed to confer toxicity by hindering the ubiquitination of other parkin substrates (Bendikov-Bar et al., 2014, Ron et al., 2010).

Our L444P mice could also be useful to study the interplay between mutant GCase and LRRK2 kinase activity in PD. PD patients that harbour dual mutations in *GBA* and *LRRK2* have been shown to display milder symptoms vs patients who only carry a *GBA* mutation (Omer et al., 2020, Yahalom et al., 2019). This indicates that *LRRK2* variants may protect against or override the more severe clinical manifestations typically related to *GBA*-associated PD pathology (**Table 1.2**). In agreement with this, GCase activity was heightened in fibroblasts and PBMCs from PD patients that harbour the *LRRK2*-G2019S mutation (Kedariti et al., 2022). However, studies investigating GCase activity in iPSC-DAns and dried blood spots from PD patients with *LRRK2* mutations have produced inconclusive

results (Alcalay et al., 2015, Kedariti et al., 2022, Omer et al., 2022, Ysselstein et al., 2019). There is also no definitive evidence of changes to GCase activity or protein levels in post-mortem brain samples of *LRRK2*-associated PD patients (Leyns et al., 2023, Zhao et al., 2018). On the other hand, GCase protein levels are reduced in *LRRK2*-G2019S mice (Kedariti et al., 2022). Furthermore, *Drosophila* that co-expressed human mutant *GBA* and *LRRK2* transgenes displayed attenuation of the UPR but similar GCase activity vs *Drosophila* that harboured a mutant *GBA* transgene alone (Serebryany-Piavsky et al., 2025). Notably, a dual *GBA-LRRK2* mouse model has not yet been created. As the nature and mechanisms of GCase regulation by LRRK2 remains elusive, introducing mutant *LRRK2* to our L444P model could make a valuable contribution to this area of ongoing research.

6.4 CONCLUDING REMARKS

A myriad of animal models are available in the PD researcher's toolkit (Dovonou et al., 2023, Konnova and Swanberg, 2018). However, a "perfect model" that can recapitulate PD-relevant aetiological factors, underlying molecular mechanisms, progressive DA neurodegeneration and αS pathology alongside age-dependent behavioural deficits does not exist. The field has detached from the notion that replicating most neuropathological and behavioural phenotypes of PD in a single model is "vital" to developing disease-modifying therapies (Beal, 2010). Instead, researchers have capitalised on the diverse range of available animal models in efforts to develop precision-medicine-based interventions for genetic subtypes of PD (Straccia et al., 2022). Emphasis is increasingly placed on recognizing the strengths and limitations of individual models to optimally tailor the choice of model to the study's specific goals (Dovonou et al., 2023, Fisher and Bannerman, 2019). The genotypic and phenotypic diversity of PD animal models also reflects the heterogenous aetiology, neuropathology and symptoms of the disease in humans (Konnova and Swanberg, 2018). The distinctive clinical profile of PD patients carrying *GBA* mutations has recently sparked

the suggestion of a new eponym for *GBA*-associated PD: “Sidransky Syndrome” (Istaiti et al., 2025). This eponym pays homage to Dr Ellen Sidransky’s contributions to establishing the link between *GBA* mutations and PD. However, labelling *GBA*-associated PD as a distinct entity is not justified, in my opinion, because GCase’s role in PD pathology remains elusive. Such an eponym may also detract from observations of GCase deficits in PD patients who don't carry *GBA* mutations (Alcalay et al., 2015, Gegg et al., 2012, Murphy et al., 2014, Parnetti et al., 2017, Rocha et al., 2015a). Indeed, identifying pathological mechanisms that are common to idiopathic and *GBA*-associated PD may also help to establish targets for disease-modifying therapies.

Only time will tell whether this new eponym will be embraced by researchers, clinicians and patients alike. For now, research efforts should continue to focus on illuminating the mechanistic basis of *GBA*-associated PD pathology. I believe that mouse models with high construct validity for the disease, such as the humanised L444P mice characterised in this thesis, will be integral to this pursuit. The findings presented herein have highlighted the usefulness of our *GBA*-L444P BAC transgenic mice as a model of early-stage dysfunction in PD and have laid a solid foundation for future research to build on. Our model will be deposited at The Jackson Laboratory (https://www.jax.org) on publication for distribution to other researchers. We actively encourage members of the scientific community to take advantage of this valuable tool in their work on GCase’s association with PD. I am hopeful that this novel model will facilitate future discoveries that ultimately pave the way to a brighter future for *GBA*-associated PD patients.

APPENDIX

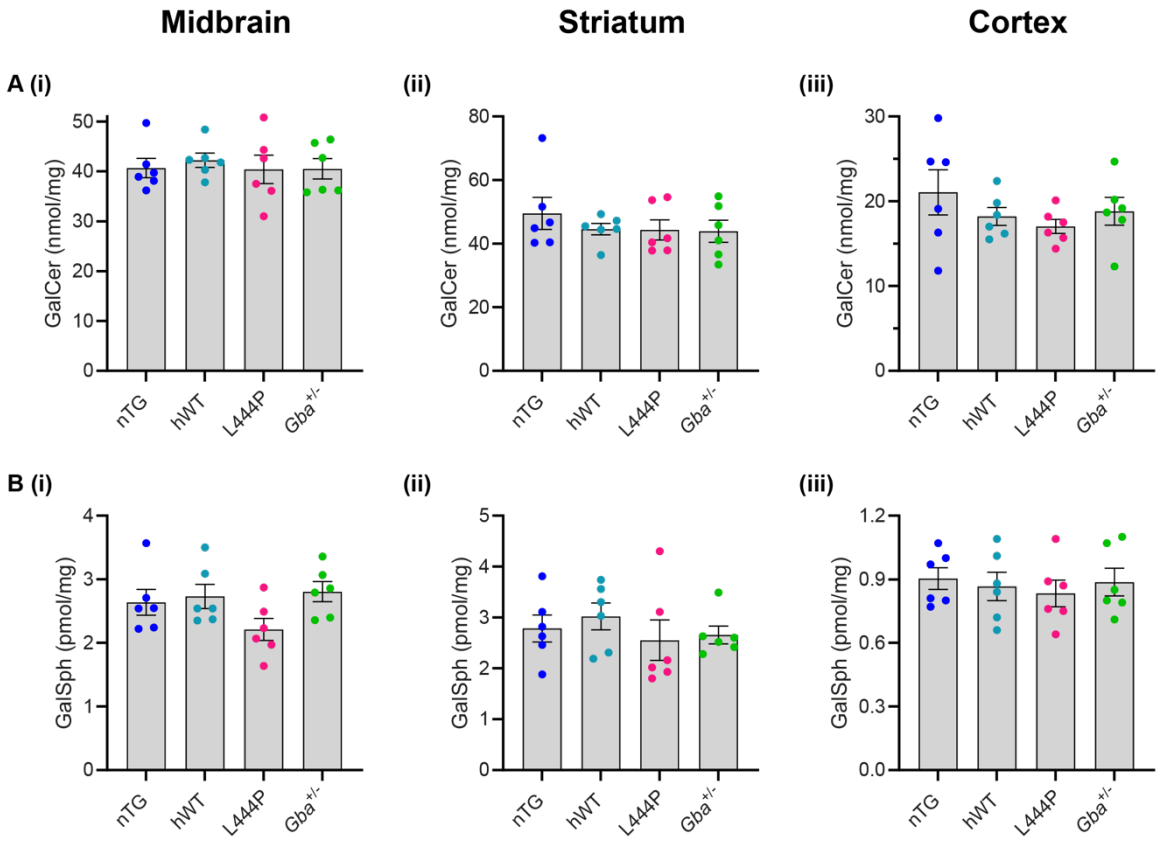


Figure A-1: GalCer and GalSph levels are comparable across genotypes in various brain regions. Lipids were extracted from midbrain (**i**), striatal (**ii**) and cortical (**iii**) tissue lysates from 3-month-old mice and were detected using LC-MS/MS. No genotype-related changes to GalCer (**A**) or GalSph (**B**) were observed in any brain regions investigated. (**A-B**) Lipid species are normalised to protein concentration per sample, determined with a BCA assay. ((**A (i, iii)), (B (i, iii)**)) One-way ANOVA: all $F_{(3,20)} < 2.148$ and all $p > 0.1261$, (**A(ii)**, (**B(ii)**) Kruskal-Wallis test: all Kruskal-Wallis statistics < 2.507 and all $p > 0.4740$; n = 6 mice per genotype. Data are presented as mean ± SEM and each datapoint represents one mouse. Data collected and analysed by Ms. Katerina Bila and Dr Martijn van der Lienden.

Table A-1: List of interacting residues across complexes determined by PRODIGY and RING analyses. Residues previously implicated in GCase-LIMP2 binding (active residues), are in black. Residues not previously implicated in GCase-LIMP2 binding (non-active residues), are in blue. Note: for the HuL444PGCase-MuLIMP2, MuGCase-MuLIMP2 and HuGCase-HuLIMP2 complexes, the *number of interactions* in the RING results (**Fig. 3.16 A**) is greater than the *number of interacting residue pairs* determined by RING in this table because certain residue pairs have multiple interactions. This is accounted for in the RING results (**Fig. 3.16 A**), whereas this table only lists the interacting residue pairs and therefore does not account for more than one interaction per pair.

HuGCase-MuLIMP2			HuL444PGCase-MuLIMP2			MuGCase-MuLIMP2			HuGCase-HuLIMP2		
GCase	LIMP2	Server	GCase	LIMP2	Server	GCase	LIMP2	Server	GCase	LIMP2	Server
SER24	GLY316	PRODIGY	GLY23	GLY316	PRODIGY	ARG4	THR242	PRODIGY	ILE20	ARG121	PRODIGY
SER24	GLU315	PRODIGY	SER24	GLU315	PRODIGY	ARG4	ASP243	PRODIGY	MET21	GLY126	PRODIGY
LEU25	GLU315	PRODIGY & RING	LEU25	THR241	PRODIGY	ARG4	GLU315	PRODIGY & RING	MET21	VAL125	PRODIGY
ALA59	PHE191	PRODIGY	LEU25	GLU315	PRODIGY	ARG4	THR241	PRODIGY & RING	MET21	ARG121	PRODIGY
THR60	PHE191	PRODIGY	ALA59	PHE191	PRODIGY	ILE6	GLU315	PRODIGY	ALA22	GLY126	PRODIGY
LEU130	ALA162	PRODIGY	THR60	PHE191	PRODIGY	PHE11	LEU149	PRODIGY	ALA22	ASP127	PRODIGY
LEU133	TYR163	PRODIGY	LEU130	ALA162	PRODIGY	GLN12	LEU151	PRODIGY	ALA22	VAL125	PRODIGY & RING
LEU133	MET159	PRODIGY	LEU133	ALA162	PRODIGY & RING	ALA13	LEU151	PRODIGY	ALA22	ARG121	PRODIGY & RING
LEU133	ALA162	PRODIGY	LEU133	ALA158	PRODIGY & RING	VAL14	LEU151	PRODIGY	ALA22	ASP131	PRODIGY
LEU133	ALA158	PRODIGY & RING	LEU133	TYR163	PRODIGY	LEU110	GLN164	PRODIGY	GLY23	ILE130	PRODIGY
ALA134	TYR163	PRODIGY	LEU133	MET159	PRODIGY	ILE112	ALA162	PRODIGY	GLY23	GLY126	PRODIGY
ALA134	ALA162	PRODIGY	ALA134	LEU187	PRODIGY	LEU113	TYR163	PRODIGY	GLY23	VAL125	PRODIGY
LEU135	MET159	PRODIGY & RING	ALA134	ALA162	PRODIGY	LEU113	ALA162	PRODIGY & RING	GLY23	ARG121	PRODIGY
LEU135	TYR163	PRODIGY	ALA134	TYR163	PRODIGY & RING	LEU113	LYS161	PRODIGY & RING	GLY23	ASP131	PRODIGY & RING
SER136	MET159	PRODIGY	LEU135	TYR163	PRODIGY	LEU113	GLN164	PRODIGY	GLY23	ASP127	PRODIGY
SER136	PHE191	PRODIGY	LEU135	LEU187	PRODIGY	ALA114	ALA162	PRODIGY	SER24	ASP131	PRODIGY
PRO137	LEU152	PRODIGY & RING	LEU135	MET159	PRODIGY	LEU115	TYR163	PRODIGY	SER24	LEU132	PRODIGY
PRO137	MET159	PRODIGY	SER136	PHE191	PRODIGY	LEU115	ALA162	PRODIGY	SER24	ILE130	PRODIGY

PRO137	ILE156	PRODIGY	SER136	LEU187	PRODIGY	SER116	TYR163	PRODIGY	LEU25	LEU132	PRODIGY
PRO137	LEU155	PRODIGY & RING	SER136	MET159	PRODIGY	SER116	ALA162	PRODIGY	LEU25	ILE130	PRODIGY
PRO138	LEU152	PRODIGY & RING	SER136	ILE190	PRODIGY	PRO117	TYR163	PRODIGY	THR26	LEU132	PRODIGY
PRO138	LEU155	PRODIGY	PRO137	LEU155	PRODIGY	PRO117	LEU155	PRODIGY	THR26	ILE130	PRODIGY
PRO138	PHE191	PRODIGY	PRO137	ILE156	PRODIGY	PRO117	ALA158	PRODIGY	GLY27	LEU132	PRODIGY
GLN140	LEU155	PRODIGY	PRO137	LEU187	PRODIGY	PRO117	MET159	PRODIGY & RING	ALA59	LYS161	PRODIGY
GLN140	ALA158	PRODIGY	PRO137	MET159	PRODIGY	PRO117	ALA162	PRODIGY	LEU133	ALA158	PRODIGY
GLN140	MET159	PRODIGY	PRO137	LEU152	PRODIGY	PRO118	ALA158	PRODIGY	LEU133	GLU154	PRODIGY & RING
ASN141	LEU155	PRODIGY & RING	PRO138	LEU152	PRODIGY	PRO118	LEU155	PRODIGY	LEU133	ILE155	PRODIGY
ASN141	GLU154	PRODIGY	PRO138	LEU155	PRODIGY	GLN120	MET159	PRODIGY	SER136	LYS161	PRODIGY & RING
GLU190	GLN164	PRODIGY	PRO138	PHE191	PRODIGY	GLN120	ALA162	PRODIGY	PRO137	LEU160	PRODIGY
GLU190	GLN165	PRODIGY	GLN140	ALA158	PRODIGY	GLN120	LYS161	PRODIGY	PRO137	ALA158	PRODIGY
GLU190	LYS161	PRODIGY	GLN140	MET159	PRODIGY	GLN120	GLU157	PRODIGY	PRO137	MET159	PRODIGY
GLU191	GLN164	PRODIGY	GLN140	LEU155	PRODIGY	GLN120	ALA158	PRODIGY & RING	PRO137	ALA162	PRODIGY
THR193	VAL396	PRODIGY	ASN141	GLU154	PRODIGY	LYS121	LEU155	PRODIGY	PRO137	LYS161	PRODIGY
THR193	LYS161	PRODIGY & RING	ASN141	LEU155	PRODIGY & RING	LYS121	ALA158	PRODIGY	PRO137	GLU157	PRODIGY & RING
THR193	GLU157	PRODIGY	LEU144	GLU154	PRODIGY	LYS121	GLU154	PRODIGY & RING	PRO138	LYS161	PRODIGY & RING
LYS194	GLU397	PRODIGY	ILE169	GLN164	PRODIGY	ARG125	GLU154	PRODIGY & RING	PRO138	ALA162	PRODIGY
LYS194	LEU160	PRODIGY	GLU190	LYS161	PRODIGY	GLU170	LYS166	PRODIGY & RING	GLN140	ALA158	PRODIGY & RING
LYS194	ALA158	PRODIGY	GLU190	GLN164	PRODIGY	THR173	LYS166	PRODIGY & RING	GLN140	GLU154	PRODIGY
LYS194	GLN165	PRODIGY & RING	GLU190	GLN165	PRODIGY	THR173	GLU73	PRODIGY	ASN141	ALA158	PRODIGY
LYS194	LYS166	PRODIGY	GLU191	GLN164	PRODIGY	THR173	VAL396	PRODIGY	ASN141	MET159	PRODIGY
LYS194	VAL396	PRODIGY	THR193	GLU157	PRODIGY	LYS174	GLN164	PRODIGY & RING	ASN141	ALA162	PRODIGY
LYS194	ALA162	PRODIGY	THR193	LYS161	PRODIGY & RING	LYS174	LYS166	PRODIGY	GLU190	HIS150	PRODIGY
LYS194	GLN164	PRODIGY	THR193	VAL396	PRODIGY	LYS174	GLN165	PRODIGY	GLU190	PHE151	PRODIGY

LYS194	LYS161	PRODIGY & RING	LYS194	LEU160	PRODIGY	LYS174	LYS161	PRODIGY	GLU190	GLU154	PRODIGY
LEU195	ALA162	PRODIGY	LYS194	GLU397	PRODIGY	LEU175	GLN164	PRODIGY	THR193	LEU152	PRODIGY
LEU195	LYS161	PRODIGY	LYS194	GLN165	PRODIGY & RING	ILE177	VAL396	PRODIGY	THR193	ARG192	PRODIGY
LEU195	ALA158	PRODIGY	LYS194	LYS161	PRODIGY & RING	ILE177	LYS161	PRODIGY	THR193	ILE155	PRODIGY
LEU195	TYR163	PRODIGY	LYS194	GLN164	PRODIGY	PRO178	VAL396	PRODIGY	LYS194	GLU154	PRODIGY
PRO198	ALA158	PRODIGY	LYS194	LYS166	PRODIGY	PRO178	GLU157	PRODIGY	LYS194	ARG153	PRODIGY
PRO198	GLU157	PRODIGY	LYS194	ALA158	PRODIGY	PRO178	LYS161	PRODIGY & RING	LYS194	LEU152	PRODIGY & RING
PRO198	LYS161	PRODIGY & RING	LYS194	VAL396	PRODIGY	PRO178	GLU397	PRODIGY	LYS194	HIS150	PRODIGY & RING
LEU199	ALA158	PRODIGY	LYS194	GLU157	PRODIGY	LEU179	LYS161	PRODIGY	LYS194	ILE155	PRODIGY & RING
LEU199	GLU157	PRODIGY	LYS194	ALA162	PRODIGY	HIS181	VAL396	PRODIGY & RING	LYS194	PHE151	PRODIGY
HIS201	GLU154	PRODIGY	LEU195	ALA162	PRODIGY	HIS181	GLU157	PRODIGY	LEU195	ILE155	PRODIGY
ARG202	MET159	PRODIGY	LEU195	ALA158	PRODIGY	HIS181	LYS161	PRODIGY	LEU195	GLU154	PRODIGY
ARG202	ALA158	PRODIGY	LEU195	LYS161	PRODIGY	HIS181	ASP394	PRODIGY	ILE197	PHE191	PRODIGY
ARG202	ILE156	PRODIGY	PRO198	ALA158	PRODIGY & RING	HIS181	ASP393	PRODIGY	PRO198	ILE155	PRODIGY
ARG202	LEU155	PRODIGY & RING	PRO198	GLU157	PRODIGY	GLN182	GLU157	PRODIGY & RING	PRO198	PHE191	PRODIGY & RING
ARG202	GLU157	PRODIGY	PRO198	LYS161	PRODIGY	GLN182	ALA158	PRODIGY	HIS201	VAL190	PRODIGY & RING
ARG202	GLU154	PRODIGY	LEU199	ALA158	PRODIGY	GLN182	GLU154	PRODIGY	HIS201	PHE191	PRODIGY & RING
ALA203	GLU154	PRODIGY	LEU199	GLU157	PRODIGY	GLN182	LYS161	PRODIGY & RING	ARG202	PHE191	PRODIGY & RING
GLN205	GLU154	PRODIGY	HIS201	GLU154	PRODIGY	LYS185	LYS161	PRODIGY	ARG202	ALA158	PRODIGY & RING
LEU206	LEU155	PRODIGY	ARG202	GLU154	PRODIGY & RING	LYS185	ASP394	PRODIGY & RING	ARG202	MET159	PRODIGY
LEU206	GLU154	PRODIGY & RING	ARG202	MET159	PRODIGY	LYS185	ASP393	PRODIGY	GLN205	LEU187	PRODIGY
ASP448	ILE190	PRODIGY	ARG202	GLU157	PRODIGY	LYS185	PHE395	PRODIGY	GLN205	VAL190	PRODIGY & RING
ASP448	PHE191	PRODIGY	ARG202	ILE156	PRODIGY	LYS185	VAL396	PRODIGY	GLN205	PHE191	PRODIGY
			ARG202	LEU155	PRODIGY	LYS185	GLU157	PRODIGY & RING	GLU261	PRO193	PRODIGY
			ARG202	ALA158	PRODIGY	MET186	GLU154	PRODIGY	HIS262	PHE191	PRODIGY

	GLN205	GLU154	PRODIGY	LYS241	GLN77	PRODIGY & RING	HIS262	PRO193	PRODIGY
	LEU206	GLU154	PRODIGY	LYS241	LEU76	PRODIGY	HIS262	ASP194	PRODIGY
	HIS262	VAL396	PRODIGY	LYS241	ASP400	PRODIGY	HIS262	VAL190	PRODIGY
	ILE445	TYR163	PRODIGY	LYS241	GLY399	PRODIGY	HIS262	ARG192	PRODIGY
	ASP448	ILE190	PRODIGY	TYR242	ASP400	PRODIGY	LYS263	ARG192	PRODIGY
				TYR242	GLY399	PRODIGY	LYS263	PHE191	PRODIGY
				TYR242	VAL396	PRODIGY	LYS263	PRO193	PRODIGY & RING
				TYR242	LEU76	PRODIGY	LYS263	VAL190	PRODIGY
				TYR242	LYS166	PRODIGY	LYS263	HIS189	PRODIGY & RING
				TYR242	GLU73	PRODIGY	ASP448	LYS161	PRODIGY
				GLY243	ASP400	PRODIGY			

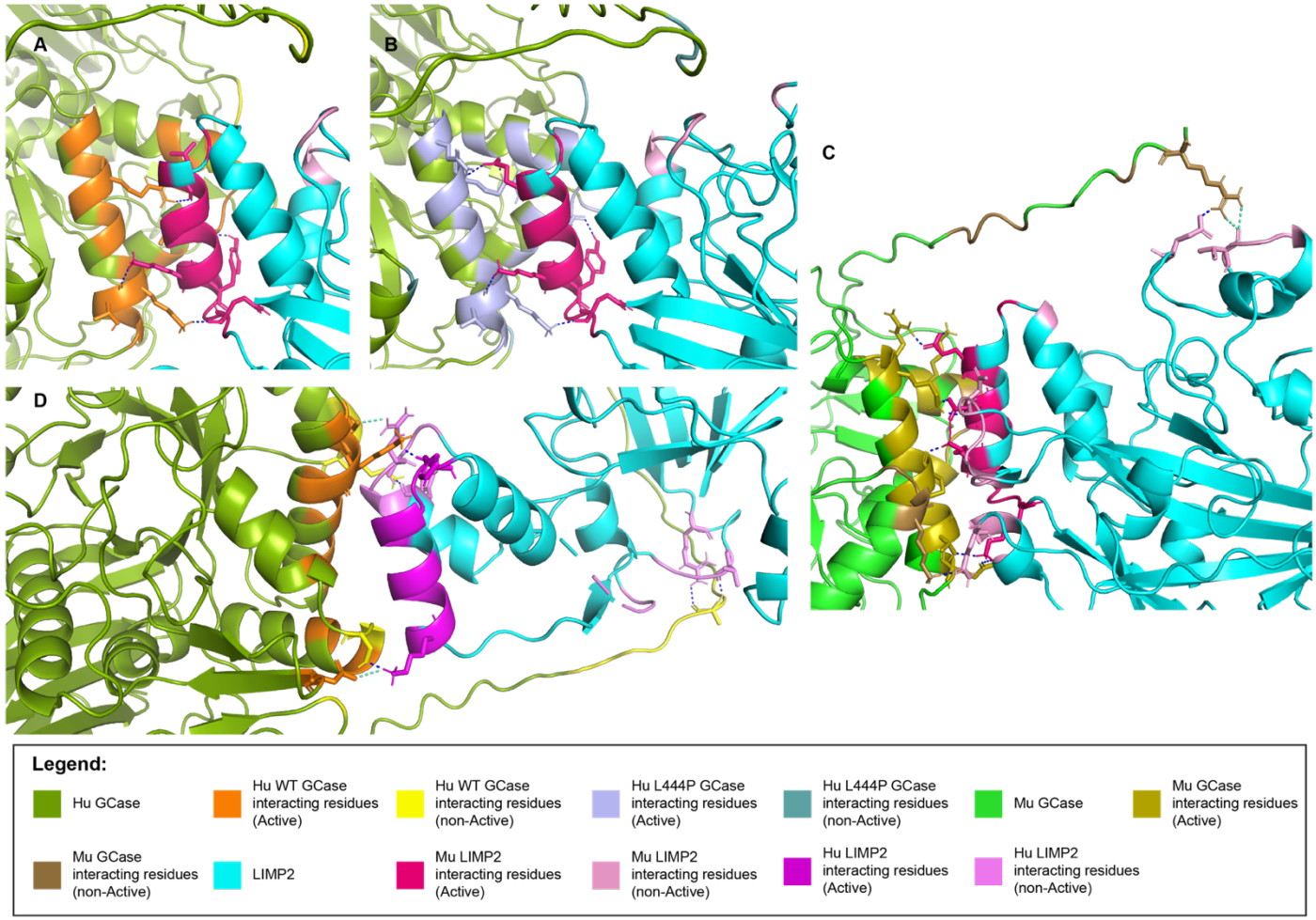


Figure A-2: The structural conformation of the GCase-LIMP2 complexes, illustrating polar contacts within and outside the main interaction interface. (**A**) HuGCase-MuLIMP2, (**B**) HuL444PGCase-MuLIMP2, (**C**) MuGCase-MuLIMP2, (**D**) HuGCase-HuLIMP2. Active residues are those that have previously been implicated in the GCase-LIMP2 interaction, whereas non-active residues have not. Strong polar contacts are highlighted in dark blue and weaker polar contacts are coloured light blue. Residue sticks and bond lengths are only shown for polar contacts < 4.2 Å, accordingly the sticks for non-active residues in (**A-B**) are not shown.

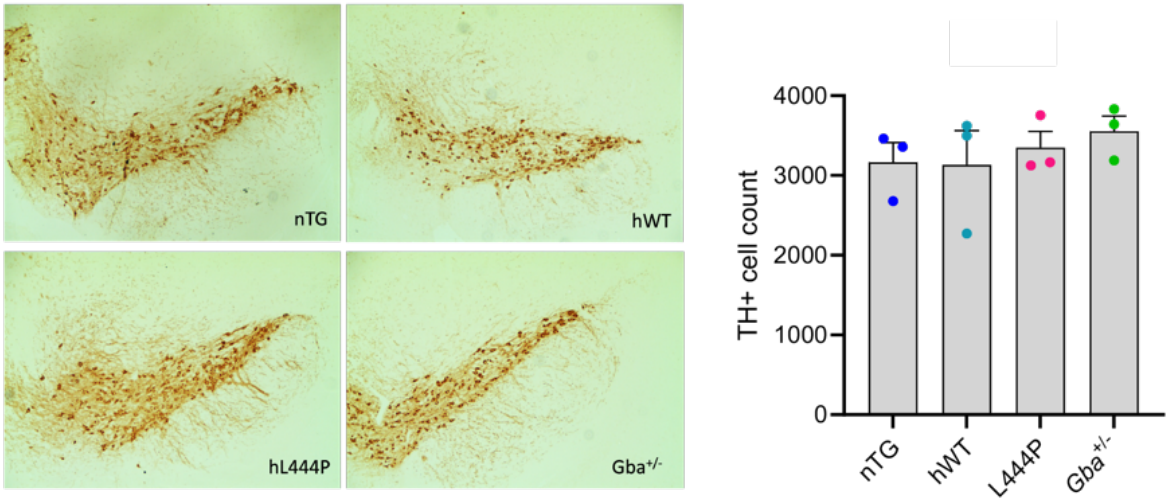


Figure A-3: DA neurons in the SN are preserved in aged L444P mice. Representative stereological images (left) and corresponding quantification (right) of TH+ neurons in the SN of 18-month-old mice. One-way ANOVA: $F_{(3,8)} = 0.4655$ $p = 0.7143$; $n = 3$ mice per genotype. Data are presented as mean ± SEM and each datapoint represents one mouse. Data collected and analysed by Dr Natalie Connor-Robson.

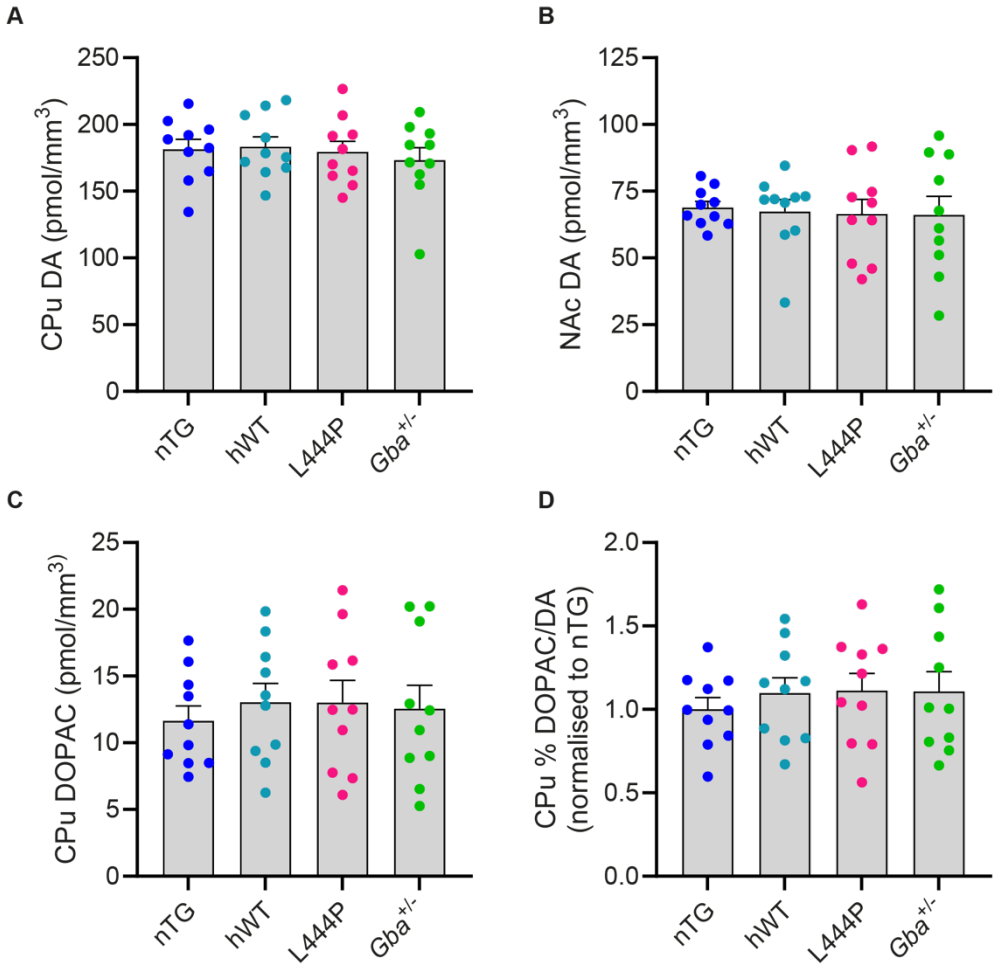
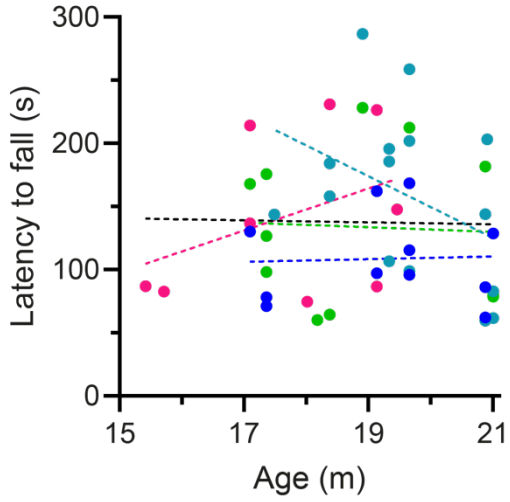
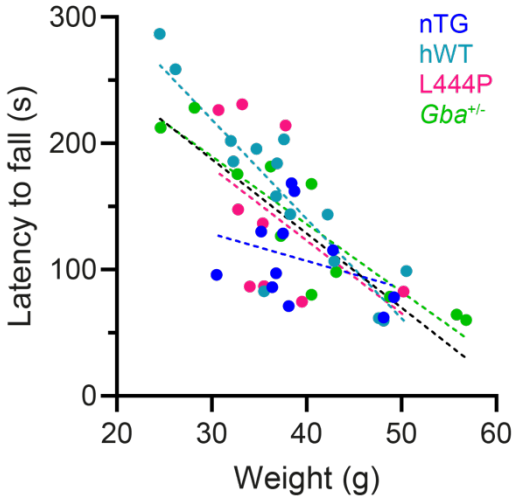


Figure A-4: Striatal DA and DOPAC levels are comparable across genotypes in 3-month-old mice. The concentration of DA and DOPAC were quantified in striatal tissue punch homogenates using HPLC. DA content in the CPu (**A**) and NAc (**B**) were not significantly different across genotypes. The CPu DOPAC concentration (**C**) and DOPAC:DA ratio (**D**) were also similar across genotypes. (**A, C-D**) One-way ANOVA: all $F_{(3,36)} < 0.2969$ and all $p > 0.8274$, (**B**) Kruskal-Wallis test: Kruskal-Wallis statistic = 0.1361 $p = 0.9872$; n = 10 mice per genotype. Data are presented as mean ± SEM and each datapoint represents one mouse. Data collected and analysed by Dr Natalie Connor-Robson.

A



B

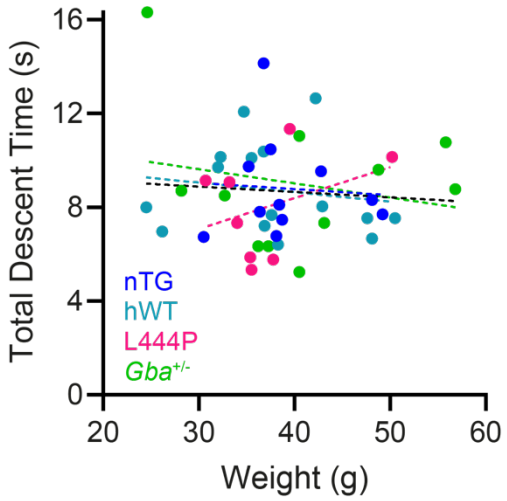


C

	(A) Age vs Latency to fall			(B) Weight vs Latency to fall		
	Equation of the line	r	p	Equation of the line	r	p
nTG	y = 1.068*x + 88.01	-0.055	0.8739	y = -2.141*x + 192.6	-0.200	0.5574
hWT	y = -24.39*x + 637.4	-0.332	0.2255	y = -7.868*x + 454.9	**-0.811**	**0.0004**
L444P	y = 16.64*x - 152.0	-0.345	0.3615	y = -5.762*x + 353.6	**-0.700**	**0.0433**
***Gba*$^{+/-}$**	y = -1.837*x + 168.5	-0.032	0.9289	y = -5.363*x + 350.6	**-0.952**	**< 0.0001**
Shared	y = -0.798*x + 152.6	-0.078	0.6075	y = -5.879*x + 363.9	**-0.691**	**< 0.0001**

Figure A-5: The relationship of rotarod performance with age and bodyweight. Latency to fall from the rotarod did not correlate with age of the mice (**A, C**), but was negatively correlated with body weight (**B, C**). (**A-B**) The slopes and y intercepts of the linear regression lines (dashed lines) on both scatter plots were not significantly different across genotypes using an ANCOVA. Therefore, there remained no effect of genotype on latency to fall after accounting for age and weight. (**A-C**) Linear regression analysis determined the equations of the lines of best fit. Correlation was quantified using Spearman's correlation co-efficient "r", statistically significant correlations ($p < 0.05$) are highlighted in bold in (**C**); n = 9-15 mice per genotype. Each datapoint on the scatterplots (**A-B**) represents one mouse.

A



B

	Weight vs Total Descent Time		
	Equation of the line	r	p
nTG	y = -0.026*x + 9.823	-0.036	0.924
hWT	y = -0.041*x + 10.26	-0.290	0.293
L444P	y = 0.132*x + 3.099	0.167	0.703
***Gba*$^{+/-}$**	y = -0.060*x + 11.43	0.064	0.852
Shared	y = -0.023*x + 9.567	-0.0138	0.928

Figure A-6: Bodyweight did not influence the total descent time from the vertical pole. (**A-B**) Bodyweight did not correlate with vertical pole descent time. There remained no effect of genotype on descent time after including weight as a co-variate in an ANCOVA; the slopes and y intercepts of the linear regression lines (dashed lines) are not significantly different. Linear regression analysis determined the equations of the lines of best fit. Correlation was quantified using Spearman's correlation co-efficient "r"; n = 8-15 mice per genotype. Each datapoint on the scatterplot (**A**) represents one mouse.

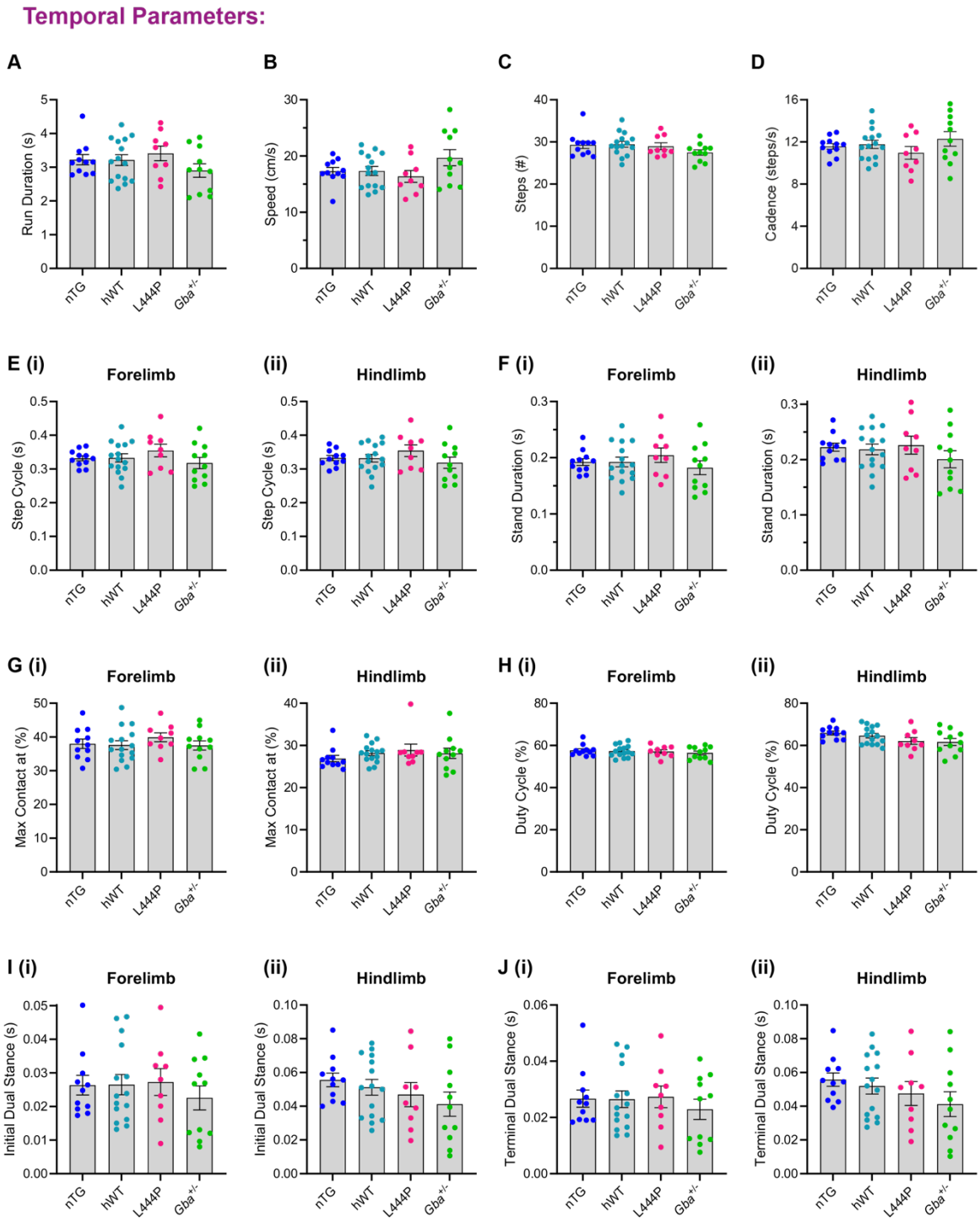


Figure A-7: Various temporal gait parameters recorded by the CatWalk XT were not different across genotypes. (**A, C, G(ii), H(i), I(i), J(i)**) Kruskal-Wallis test: all Kruskal-Wallis statistics < 3.950 and all $p > 0.2669$, (**B, D-F, G(i), H(ii), I(ii), J(ii)**) one-way ANOVA: all $F_{(3,42)} < 2.254$ and all $p > 0.0961$; n = 9-15 mice per genotype. Data are presented as mean ± SEM and each datapoint represents one mouse.

Spatial Parameters:

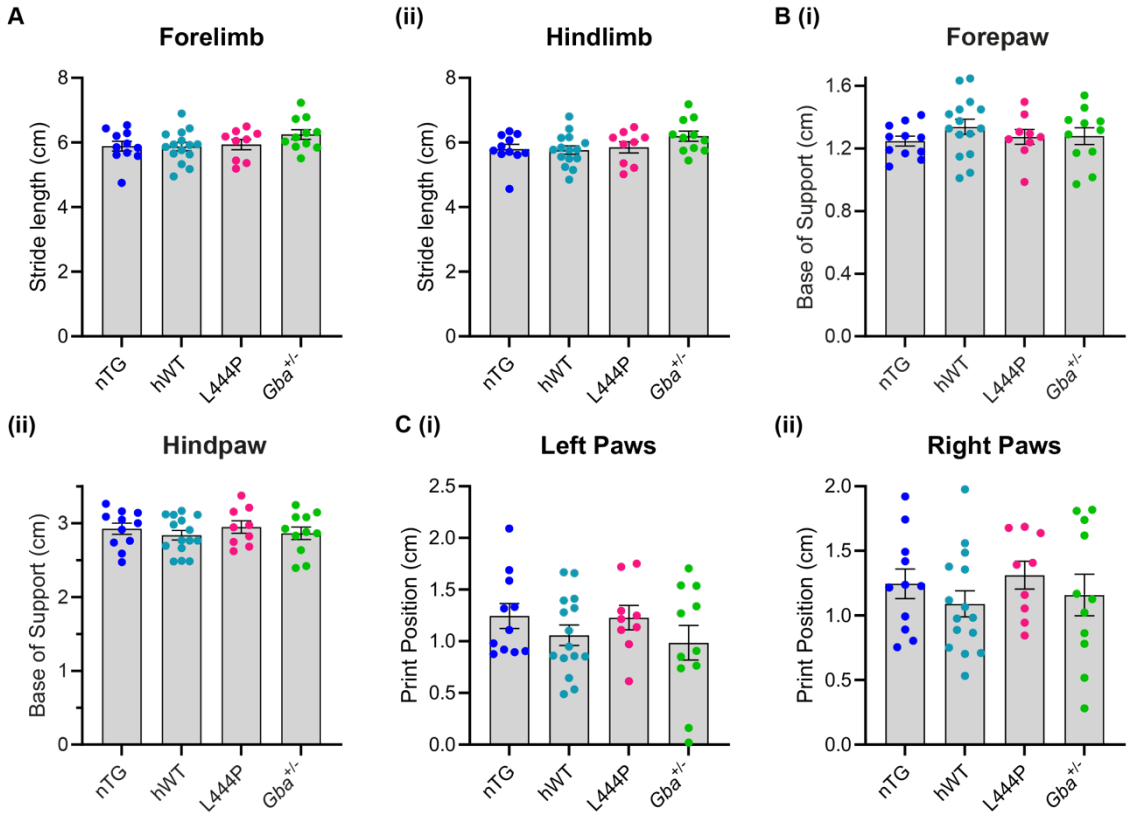


Figure A-8: Spatial gait parameters recorded by the CatWalk XT were not different across genotypes. (**A(i), B-C**) One-way ANOVA: all $F_{(3,42)} < 1.462$ and all $p > 0.2386$, (**A(ii)**) Kruskal-Wallis test: Kruskal-Wallis statistic = 3.703 p = 0.2954; n = 9-15 mice per genotype. Data are presented as mean ± SEM and each datapoint represents one mouse.

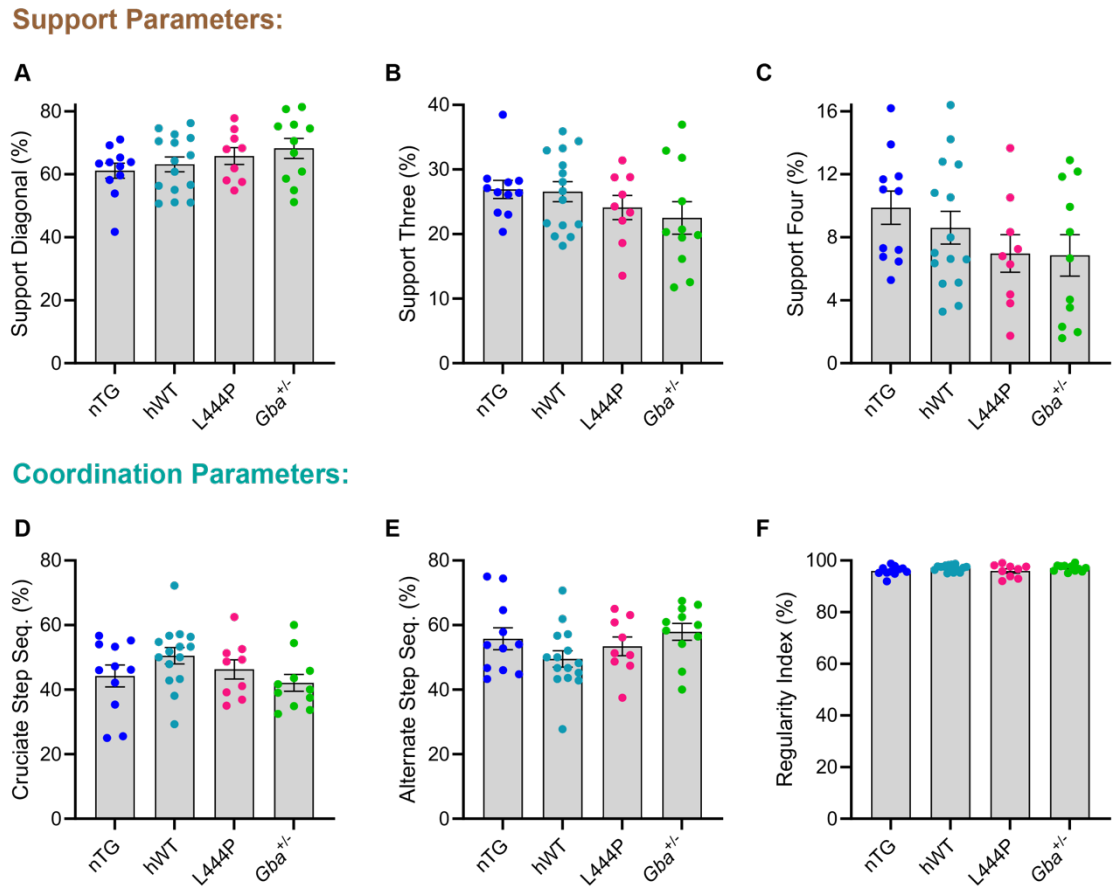


Figure A-9: Support and coordination gait parameters recorded by the CatWalk XT were not different across genotypes. (**A, C-F**) One-way ANOVA: all $F_{(3,42)} < 1.771$ and all $p > 0.1674$, (**B**) Kruskal-Wallis test: Kruskal-Wallis statistic = 3.482 p = 0.3230; n = 9-15 mice per genotype. Data are presented as mean ± SEM and each datapoint represents one mouse.

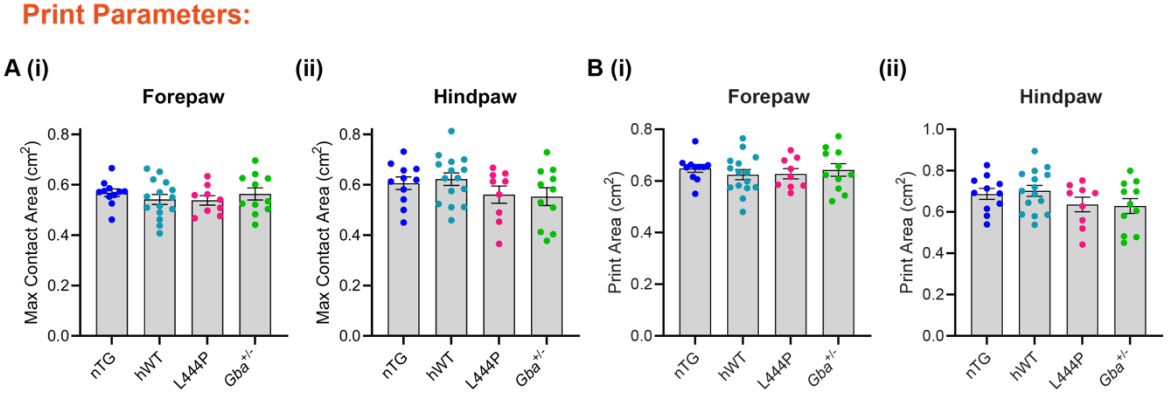


Figure A-10: Print gait parameters recorded by the CatWalk XT were not different across genotypes. (**A-B**) One-way ANOVA: all $F_{(3,42)} < 1.468$ and all $p > 0.2369$; n = 9-15 mice per genotype. Data are presented as mean ± SEM and each datapoint represents one mouse.

REFERENCES

Aamodt, W. W., Willis, A. W. & Dahodwala, N. 2023. Racial and Ethnic Disparities in Parkinson Disease: A Call to Action. *Neurol Clin Pract,* 13**,** e200138.

Aarsland, D., Batzu, L., Halliday, G. M., Geurtsen, G. J., Ballard, C., Ray Chaudhuri, K. & Weintraub, D. 2021. Parkinson disease-associated cognitive impairment. *Nat Rev Dis Primers,* 7**,** 47.

Abbott, S. K., Li, H., Munoz, S. S., Knoch, B., Batterham, M., Murphy, K. E., Halliday, G. M. & Garner, B. 2014. Altered ceramide acyl chain length and ceramide synthase gene expression in Parkinson's disease. *Mov Disord,* 29**,** 518-26.

Abrahamov, A., Elstein, D., Gross-Tsur, V., Farber, B., Glaser, Y., Hadas-Halpern, I., Ronen, S., Tafakjdi, M., Horowitz, M. & Zimran, A. 1995. Gaucher's disease variant characterised by progressive calcification of heart valves and unique genotype. *Lancet,* 346**,** 1000-3.

Aflaki, E., Borger, D. K., Moaven, N., Stubblefield, B. K., Rogers, S. A., Patnaik, S., Schoenen, F. J., Westbroek, W., Zheng, W., Sullivan, P., Fujiwara, H., Sidhu, R., Khaliq, Z. M., Lopez, G. J., Goldstein, D. S., Ory, D. S., Marugan, J. & Sidransky, E. 2016. A New Glucocerebrosidase Chaperone Reduces alpha-Synuclein and Glycolipid Levels in iPSC-Derived Dopaminergic Neurons from Patients with Gaucher Disease and Parkinsonism. *J Neurosci,* 36**,** 7441-52.

Aflaki, E., Westbroek, W. & Sidransky, E. 2017. The Complicated Relationship between Gaucher Disease and Parkinsonism: Insights from a Rare Disease. *Neuron,* 93**,** 737-746.

Aguilar, J. I., Dunn, M., Mingote, S., Karam, C. S., Farino, Z. J., Sonders, M. S., Choi, S. J., Grygoruk, A., Zhang, Y., Cela, C., Choi, B. J., Flores, J., Freyberg, R. J., Mccabe, B. D., Mosharov, E. V., Krantz, D. E., Javitch, J. A., Sulzer, D., Sames, D., Rayport, S. & Freyberg, Z. 2017. Neuronal Depolarization Drives Increased Dopamine Synaptic Vesicle Loading via VGLUT. *Neuron,* 95**,** 1074-1088 e7.

Aharon-Peretz, J., Rosenbaum, H. & Gershoni-Baruch, R. 2004. Mutations in the glucocerebrosidase gene and Parkinson's disease in Ashkenazi Jews. *N Engl J Med,* 351**,** 1972-7.

Akiyama, H., Kobayashi, S., Hirabayashi, Y. & Murakami-Murofushi, K. 2013. Cholesterol glucosylation is catalyzed by transglucosylation reaction of beta-glucosidase 1. *Biochem Biophys Res Commun,* 441**,** 838-43.

Alam, P., Bousset, L., Melki, R. & Otzen, D. E. 2019. alpha-synuclein oligomers and fibrils: a spectrum of species, a spectrum of toxicities. *J Neurochem,* 150**,** 522-534.

Albrecht, L. V., Tejeda-Munoz, N. & De Robertis, E. M. 2020. Protocol for Probing Regulated Lysosomal Activity and Function in Living Cells. *STAR Protoc,* 1**,** 100132.

Alcalay, R. N., Caccappolo, E., Mejia-Santana, H., Tang, M., Rosado, L., Orbe Reilly, M., Ruiz, D., Ross, B., Verbitsky, M., Kisselev, S., Louis, E., Comella, C., Colcher, A., Jennings, D., Nance, M., Bressman, S., Scott, W. K., Tanner, C., Mickel, S., Andrews, H., Waters, C., Fahn, S., Cote, L., Frucht, S., Ford, B., Rezak, M., Novak, K., Friedman, J. H., Pfeiffer, R., Marsh, L., Hiner, B., Siderowf, A., Payami, H., Molho, E., Factor, S., Ottman, R., Clark, L. N. & Marder, K. 2012a. Cognitive performance of GBA mutation carriers with early-onset PD: the CORE-PD study. *Neurology,* 78**,** 1434-40.

Alcalay, R. N., Gu, Y., Mejia-Santana, H., Cote, L., Marder, K. S. & Scarmeas, N. 2012b. The association between Mediterranean diet adherence and Parkinson's disease. *Mov Disord,* 27**,** 771-4.

Alcalay, R. N., Levy, O. A., Waters, C. C., Fahn, S., Ford, B., Kuo, S. H., Mazzoni, P., Pauciulo, M. W., Nichols, W. C., Gan-Or, Z., Rouleau, G. A., Chung, W. K., Wolf, P., Oliva, P., Keutzer, J., Marder, K. & Zhang, X. 2015. Glucocerebrosidase activity in Parkinson's disease with and without GBA mutations. *Brain,* 138**,** 2648-58.

Alcalay, R. N., Levy, O. A., Wolf, P., Oliva, P., Zhang, X. K., Waters, C. H., Fahn, S., Kang, U., Liong, C., Ford, B., Mazzoni, P., Kuo, S., Johnson, A., Xiong, L., Rouleau, G. A., Chung, W., Marder, K. S. & Gan-Or, Z. 2016. SCARB2 variants and glucocerebrosidase activity in Parkinson's disease. *NPJ Parkinsons Dis,* 2**,** 16004-.

Alcalay, R. N., Wolf, P., Chiang, M. S. R., Helesicova, K., Zhang, X. K., Merchant, K., Hutten, S. J., Scherzer, C., Caspell-Garcia, C., Blauwendraat, C., Foroud, T., Nudelman, K., Gan-Or, Z., Simuni, T., Chahine, L. M., Levy, O., Zheng, D., Li, G., Sardi, S. P. & Parkinson's Progression Markers, I. 2020. Longitudinal Measurements of Glucocerebrosidase activity in Parkinson's patients. *Ann Clin Transl Neurol,* 7**,** 1816-1830.

Alonso-Juarez, M., Fekete, R. & Baizabal-Carvallo, J. F. 2022. Objective and self-perceived lower limb weakness in Parkinson's disease. *Ther Adv Neurol Disord,* 15**,** 17562864221136903.

Alsio, J., Nordenankar, K., Arvidsson, E., Birgner, C., Mahmoudi, S., Halbout, B., Smith, C., Fortin, G. M., Olson, L., Descarries, L., Trudeau, L. E., Kullander, K., Levesque, D. & Wallen-Mackenzie, A. 2011. Enhanced sucrose and cocaine self-administration and cue-induced drug seeking after loss of VGLUT2 in midbrain dopamine neurons in mice. *J Neurosci,* 31**,** 12593-603.

Alves, G., Larsen, J. P., Emre, M., Wentzel-Larsen, T. & Aarsland, D. 2006. Changes in motor subtype and risk for incident dementia in Parkinson's disease. *Mov Disord,* 21**,** 1123-30.

Alzforum. 2025. *Research Models: Parkinson's Disease* [Online]. Available: https://www.alzforum.org/research-models/parkinsons-disease [Accessed 01 June 2025].

Ambrosi, G., Ghezzi, C., Zangaglia, R., Levandis, G., Pacchetti, C. & Blandini, F. 2015. Ambroxol-induced rescue of defective glucocerebrosidase is associated with increased LIMP-2 and saposin C levels in GBA1 mutant Parkinson's disease cells. *Neurobiol Dis,* 82**,** 235-242.

Amende, I., Kale, A., Mccue, S., Glazier, S., Morgan, J. P. & Hampton, T. G. 2005. Gait dynamics in mouse models of Parkinson's disease and Huntington's disease. *J Neuroeng Rehabil,* 2**,** 20.

Anderson, C., Checkoway, H., Franklin, G. M., Beresford, S., Smith-Weller, T. & Swanson, P. D. 1999. Dietary factors in Parkinson's disease: the role of food groups and specific foods. *Mov Disord,* 14**,** 21-7.

Anheim, M., Elbaz, A., Lesage, S., Durr, A., Condroyer, C., Viallet, F., Pollak, P., Bonaiti, B., Bonaiti-Pellie, C., Brice, A. & French Parkinson Disease Genetic, G. 2012. Penetrance of Parkinson disease in glucocerebrosidase gene mutation carriers. *Neurology,* 78**,** 417-20.

Antoniades, C. A. & Spering, M. 2024. Eye movements in Parkinson's disease: from neurophysiological mechanisms to diagnostic tools. *Trends Neurosci,* 47**,** 71-83.

Antonini, A., Poewe, W., Chaudhuri, K. R., Jech, R., Pickut, B., Pirtosek, Z., Szasz, J., Valldeoriola, F., Winkler, C., Bergmann, L., Yegin, A., Onuk, K., Barch, D., Odin, P. & Co-Investigators, G. S. 2017. Levodopa-carbidopa intestinal gel in advanced

Parkinson's: Final results of the GLORIA registry. *Parkinsonism Relat Disord,* 45**,** 13-20.

Aquino, C. C. & Fox, S. H. 2015. Clinical spectrum of levodopa-induced complications. *Mov Disord,* 30**,** 80-9.

Aravindan, A., Newell, M. E. & Halden, R. U. 2024. Literature review and meta-analysis of environmental toxins associated with increased risk of Parkinson's disease. *Sci Total Environ,* 931**,** 172838.

Armstrong, M. J. & Okun, M. S. 2020. Diagnosis and Treatment of Parkinson Disease: A Review. *JAMA,* 323**,** 548-560.

Arnold, P. & Zunke, F. 2025. Base and translation of beta-glucocerebrosidase and its transporter LIMP-2 in neuropathies. *Neural Regen Res,* 21**,** 314-315.

Artusi, C. A., Dwivedi, A. K., Romagnolo, A., Pal, G., Kauffman, M., Mata, I., Patel, D., Vizcarra, J. A., Duker, A., Marsili, L., Cheeran, B., Woo, D., Contarino, M. F., Verhagen, L., Lopiano, L., Espay, A. J., Fasano, A. & Merola, A. 2019. Association of Subthalamic Deep Brain Stimulation With Motor, Functional, and Pharmacologic Outcomes in Patients With Monogenic Parkinson Disease: A Systematic Review and Meta-analysis. *JAMA Netw Open,* 2**,** e187800.

Artusi, C. A. & Lopiano, L. 2023. Should we offer deep brain stimulation to Parkinson's disease patients with GBA mutations? *Front Neurol,* 14**,** 1158977.

Ascherio, A. & Schwarzschild, M. A. 2016. The epidemiology of Parkinson's disease: risk factors and prevention. *Lancet Neurol,* 15**,** 1257-1272.

Athauda, D. & Foltynie, T. 2015. The ongoing pursuit of neuroprotective therapies in Parkinson disease. *Nat Rev Neurol,* 11**,** 25-40.

Atrian, S., Lopez-Vinas, E., Gomez-Puertas, P., Chabas, A., Vilageliu, L. & Grinberg, D. 2008. An evolutionary and structure-based docking model for glucocerebrosidase-saposin C and glucocerebrosidase-substrate interactions - relevance for Gaucher disease. *Proteins,* 70**,** 882-91.

Aureli, M., Bassi, R., Loberto, N., Regis, S., Prinetti, A., Chigorno, V., Aerts, J. M., Boot, R. G., Filocamo, M. & Sonnino, S. 2012. Cell surface associated glycohydrolases in normal and Gaucher disease fibroblasts. *J Inherit Metab Dis,* 35**,** 1081-91.

Avenali, M., Cerri, S., Ongari, G., Ghezzi, C., Pacchetti, C., Tassorelli, C., Valente, E. M. & Blandini, F. 2021. Profiling the Biochemical Signature of GBA-Related Parkinson's Disease in Peripheral Blood Mononuclear Cells. *Mov Disord,* 36**,** 1267-1272.

Avenali, M., Toffoli, M., Mullin, S., Mcneil, A., Hughes, D. A., Mehta, A., Blandini, F. & Schapira, A. H. V. 2019. Evolution of prodromal parkinsonian features in a cohort of GBA mutation-positive individuals: a 6-year longitudinal study. *J Neurol Neurosurg Psychiatry,* 90**,** 1091-1097.

Avenali, M., Zangaglia, R., Cuconato, G., Palmieri, I., Albanese, A., Artusi, C. A., Bozzali, M., Calandra-Buonaura, G., Cavallieri, F., Cilia, R., Cocco, A., Cogiamanian, F., Colucci, F., Cortelli, P., Di Fonzo, A., Eleopra, R., Giannini, G., Imarisio, A., Imbalzano, G., Ledda, C., Lopiano, L., Malaguti, M. C., Mameli, F., Minardi, R., Mitrotti, P., Monfrini, E., Spagnolo, F., Tassorelli, C., Valentino, F., Valzania, F., Pacchetti, C., Valente, E. M. & Group, P. S. 2024. Are patients with GBA-Parkinson disease good candidates for deep brain stimulation? A longitudinal multicentric study on a large Italian cohort. *J Neurol Neurosurg Psychiatry,* 95**,** 309-315.

Baden, P., Perez, M. J., Raji, H., Bertoli, F., Kalb, S., Illescas, M., Spanos, F., Giuliano, C., Calogero, A. M., Oldrati, M., Hebestreit, H., Cappelletti, G., Brockmann, K., Gasser, T., Schapira, A. H. V., Ugalde, C. & Deleidi, M. 2023. Glucocerebrosidase is imported into mitochondria and preserves complex I integrity and energy metabolism. *Nat Commun,* 14**,** 1930.

Bae, E. J., Yang, N. Y., Lee, C., Lee, H. J., Kim, S., Sardi, S. P. & Lee, S. J. 2015. Loss of glucocerebrosidase 1 activity causes lysosomal dysfunction and alpha-synuclein aggregation. *Exp Mol Med,* 47**,** e153.

Bae, E. J., Yang, N. Y., Song, M., Lee, C. S., Lee, J. S., Jung, B. C., Lee, H. J., Kim, S., Masliah, E., Sardi, S. P. & Lee, S. J. 2014. Glucocerebrosidase depletion enhances cell-to-cell transmission of alpha-synuclein. *Nat Commun,* 5**,** 4755.

Baggett, D., Olson, A. & Parmar, M. S. 2024. Novel approaches targeting α-Synuclein for Parkinson's Disease: Current progress and future directions for the disease-modifying therapies. *Brain Disorders,* 16.

Bains, R. S., Wells, S., Sillito, R. R., Armstrong, J. D., Cater, H. L., Banks, G. & Nolan, P. M. 2018. Assessing mouse behaviour throughout the light/dark cycle using automated in-cage analysis tools. *J Neurosci Methods,* 300**,** 37-47.

Baker, D., Lidster, K., Sottomayor, A. & Amor, S. 2014. Two years later: journals are not yet enforcing the ARRIVE guidelines on reporting standards for pre-clinical animal studies. *PLoS Biol,* 12**,** e1001756.

Balestrino, R. & Martinez-Martin, P. 2017. Neuropsychiatric symptoms, behavioural disorders, and quality of life in Parkinson's disease. *J Neurol Sci,* 373**,** 173-178.

Balestrino, R., Martone, T., Toffoli, M., Montanaro, E., Fabbri, M., Artusi, C. A., Romagnolo, A., Zibetti, M., Rizzone, M., Goldwurm, S., Lopiano, L. & Schapira, A. H. V. 2024. Levodopa-carbidopa intestinal gel infusion (LCIG) in Parkinson disease with genetic mutations. *Neurol Sci,* 45**,** 1489-1497.

Balestrino, R., Tunesi, S., Tesei, S., Lopiano, L., Zecchinelli, A. L. & Goldwurm, S. 2020. Penetrance of Glucocerebrosidase (GBA) Mutations in Parkinson's Disease: A Kin Cohort Study. *Mov Disord,* 35**,** 2111-2114.

Bandres-Ciga, S., Diez-Fairen, M., Kim, J. J. & Singleton, A. B. 2020. Genetics of Parkinson's disease: An introspection of its journey towards precision medicine. *Neurobiol Dis,* 137**,** 104782.

Bannink, S., Bila, K. O., Van Weperen, J., Ligthart, N. a. M., Ferraz, M. J., Boot, R. G., Van Der Vliet, D., Boer, D. E. C., Overkleeft, H. S., Artola, M. & Aerts, J. 2024. 6-O-alkyl 4-methylumbelliferyl-beta-D-glucosides as selective substrates for GBA1 in the discovery of glycosylated sterols. *J Lipid Res,* 65**,** 100670.

Barbeau, A. 1962. The pathogenesis of Parkinson's disease: a new hypothesis. *Can Med Assoc J,* 87**,** 802-7.

Barbeau, A. 1984. Manganese and extrapyramidal disorders (a critical review and tribute to Dr. George C. Cotzias). *Neurotoxicology,* 5**,** 13-35.

Barber, M. S., Muller, H. M., Gilbert, R. G. & Baldwin, A. J. 2018. Glucocerebrosidase rescues alpha-synuclein from amyloid formation. *bioRxiv,* preprint**,** DOI: 10.1101/363986.

Barker, R. A. & Bjorklund, A. 2020. Animal Models of Parkinson's Disease: Are They Useful or Not? *J Parkinsons Dis,* 10**,** 1335-1342.

Barker, R. A., Bjorklund, A. & Parmar, M. 2024. The history and status of dopamine cell therapies for Parkinson's disease. *Bioessays,* 46**,** e2400118.

Barrett, M. J., Shanker, V. L., Severt, W. L., Raymond, D., Gross, S. J., Schreiber-Agus, N., Kornreich, R., Ozelius, L. J., Bressman, S. B. & Saunders-Pullman, R. 2014. Cognitive and Antipsychotic Medication Use in Monoallelic GBA-Related Parkinson Disease. *JIMD Rep,* 16**,** 31-8.

Bartels, T., Choi, J. G. & Selkoe, D. J. 2011. alpha-Synuclein occurs physiologically as a helically folded tetramer that resists aggregation. *Nature,* 477**,** 107-10.

Batka, R. J., Brown, T. J., Mcmillan, K. P., Meadows, R. M., Jones, K. J. & Haulcomb, M. M. 2014. The need for speed in rodent locomotion analyses. *Anat Rec (Hoboken),* 297**,** 1839-64.

Beal, M. F. 2010. Parkinson's disease: a model dilemma. *Nature,* 466**,** S8-10.

Beavan, M., Mcneill, A., Proukakis, C., Hughes, D. A., Mehta, A. & Schapira, A. H. 2015. Evolution of prodromal clinical markers of Parkinson disease in a GBA mutation-positive cohort. *JAMA Neurol,* 72**,** 201-8.

Beccano-Kelly, D. A., Cherubini, M., Mousba, Y., Cramb, K. M. L., Giussani, S., Caiazza, M. C., Rai, P., Vingill, S., Bengoa-Vergniory, N., Ng, B., Corda, G., Banerjee, A., Vowles, J., Cowley, S. & Wade-Martins, R. 2023. Calcium dysregulation combined with mitochondrial failure and electrophysiological maturity converge in Parkinson's iPSC-dopamine neurons. *iScience,* 26**,** 107044.

Beel, S., Moisse, M., Damme, M., De Muynck, L., Robberecht, W., Van Den Bosch, L., Saftig, P. & Van Damme, P. 2017. Progranulin functions as a cathepsin D chaperone to stimulate axonal outgrowth in vivo. *Hum Mol Genet,* 26**,** 2850-2863.

Beery, A. K. 2018. Inclusion of females does not increase variability in rodent research studies. *Curr Opin Behav Sci,* 23**,** 143-149.

Beery, A. K. & Zucker, I. 2011. Sex bias in neuroscience and biomedical research. *Neurosci Biobehav Rev,* 35**,** 565-72.

Bembi, B., Zambito Marsala, S., Sidransky, E., Ciana, G., Carrozzi, M., Zorzon, M., Martini, C., Gioulis, M., Pittis, M. G. & Capus, L. 2003. Gaucher's disease with Parkinson's disease: clinical and pathological aspects. *Neurology,* 61**,** 99-101.

Ben-Shlomo, Y., Darweesh, S., Llibre-Guerra, J., Marras, C., San Luciano, M. & Tanner, C. 2024. The epidemiology of Parkinson's disease. *Lancet,* 403**,** 283-292.

Bendikov-Bar, I., Rapaport, D., Larisch, S. & Horowitz, M. 2014. Parkin-mediated ubiquitination of mutant glucocerebrosidase leads to competition with its substrates PARIS and ARTS. *Orphanet J Rare Dis,* 9**,** 86.

Bendikov-Bar, I., Ron, I., Filocamo, M. & Horowitz, M. 2011. Characterization of the ERAD process of the L444P mutant glucocerebrosidase variant. *Blood Cells Mol Dis,* 46**,** 4-10.

Bengoa-Vergniory, N., Faggiani, E., Ramos-Gonzalez, P., Kirkiz, E., Connor-Robson, N., Brown, L. V., Siddique, I., Li, Z., Vingill, S., Cioroch, M., Cavaliere, F., Threlfell, S., Roberts, B., Schrader, T., Klarner, F. G., Cragg, S., Dehay, B., Bitan, G., Matute, C., Bezard, E. & Wade-Martins, R. 2020. CLR01 protects dopaminergic neurons in vitro and in mouse models of Parkinson's disease. *Nat Commun,* 11**,** 4885.

Benoit-Marand, M., Jaber, M. & Gonon, F. 2000. Release and elimination of dopamine in vivo in mice lacking the dopamine transporter: functional consequences. *Eur J Neurosci,* 12**,** 2985-92.

Berg, D., Postuma, R. B., Adler, C. H., Bloem, B. R., Chan, P., Dubois, B., Gasser, T., Goetz, C. G., Halliday, G., Joseph, L., Lang, A. E., Liepelt-Scarfone, I., Litvan, I., Marek, K., Obeso, J., Oertel, W., Olanow, C. W., Poewe, W., Stern, M. & Deuschl, G. 2015. MDS research criteria for prodromal Parkinson's disease. *Mov Disord,* 30**,** 1600-11.

Berge-Seidl, V., Pihlstrom, L., Maple-Grodem, J., Forsgren, L., Linder, J., Larsen, J. P., Tysnes, O. B. & Toft, M. 2017. The GBA variant E326K is associated with Parkinson's disease and explains a genome-wide association signal. *Neurosci Lett,* 658**,** 48-52.

Berger, Z., Perkins, S., Ambroise, C., Oborski, C., Calabrese, M., Noell, S., Riddell, D. & Hirst, W. D. 2015. Tool compounds robustly increase turnover of an artificial substrate by glucocerebrosidase in human brain lysates. *PLoS One,* 10**,** e0119141.

Bergfussman, A., Grace, M. E., Ioannou, Y. & Grabowski, G. A. 1993. Human Acid Beta-Glucosidase - N-Glycosylation Site Occupancy and the Effect of Glycosylation on Enzymatic-Activity. *Journal of Biological Chemistry,* 268**,** 14861-14866.

Bergmann, J. E. & Grabowski, G. A. 1989. Posttranslational processing of human lysosomal acid beta-glucosidase: a continuum of defects in Gaucher disease type 1 and type 2 fibroblasts. *Am J Hum Genet,* 44**,** 741-50.

Berry, C., La Vecchia, C. & Nicotera, P. 2010. Paraquat and Parkinson's disease. *Cell Death Differ,* 17**,** 1115-25.

Bespalov, A. & Steckler, T. 2018. Lacking quality in research: Is behavioral neuroscience affected more than other areas of biomedical science? *J Neurosci Methods,* 300**,** 4-9.

Bezard, E., Gross, C. E. & Brotchie, J. M. 2003. Presymptomatic compensation in Parkinson's disease is not dopamine-mediated. *Trends Neurosci,* 26**,** 215-21.

Bezard, E. & Przedborski, S. 2011. A tale on animal models of Parkinson's disease. *Mov Disord,* 26**,** 993-1002.

Bidgood, R., Zubelzu, M., Ruiz-Ortega, J. A. & Morera-Herreras, T. 2024. Automated procedure to detect subtle motor alterations in the balance beam test in a mouse model of early Parkinson's disease. *Sci Rep,* 14**,** 862.

Biggs, D., Chen, C. M. & Davies, B. 2023. Targeted Integration of Transgenes at the Mouse Gt(ROSA)26Sor Locus. *Methods Mol Biol,* 2631**,** 299-323.

Bisswanger, H. 2014. Enzyme assays. *Perspectives in Science,* 1**,** 41-55.

Blanz, J. & Saftig, P. 2016. Parkinson's disease: acid-glucocerebrosidase activity and alpha-synuclein clearance. *J Neurochem,* 139 Suppl 1**,** 198-215.

Blauwendraat, C., Bras, J. M., Nalls, M. A., Lewis, P. A., Hernandez, D. G., Singleton, A. B. & International Parkinson's Disease Genomics, C. 2018a. Coding variation in GBA explains the majority of the SYT11-GBA Parkinson's disease GWAS locus. *Mov Disord,* 33**,** 1821-1823.

Blauwendraat, C., Kia, D. A., Pihlstrom, L., Gan-Or, Z., Lesage, S., Gibbs, J. R., Ding, J., Alcalay, R. N., Hassin-Baer, S., Pittman, A. M., Brooks, J., Edsall, C., Chung, S. J., Goldwurm, S., Toft, M., Schulte, C., International Parkinson's Disease Genomics Consortium, C.-P. D. C., Hernandez, D., Singleton, A. B., Nalls, M. A., Brice, A., Scholz, S. W. & Wood, N. W. 2018b. Insufficient evidence for pathogenicity of SNCA His50Gln (H50Q) in Parkinson's disease. *Neurobiol Aging,* 64**,** 159 e5-159 e8.

Blauwendraat, C., Nalls, M. A. & Singleton, A. B. 2020. The genetic architecture of Parkinson's disease. *Lancet Neurol,* 19**,** 170-178.

Blesa, J. & Przedborski, S. 2014. Parkinson's disease: animal models and dopaminergic cell vulnerability. *Front Neuroanat,* 8**,** 155.

Blesa, J., Trigo-Damas, I., Dileone, M., Del Rey, N. L., Hernandez, L. F. & Obeso, J. A. 2017. Compensatory mechanisms in Parkinson's disease: Circuits adaptations and role in disease modification. *Exp Neurol,* 298**,** 148-161.

Blumenreich, S., Nehushtan, T., Barav, O. B., Saville, J. T., Dingjan, T., Hardy, J., Fuller, M. & Futerman, A. H. 2022. Elevation of gangliosides in four brain regions from Parkinson's disease patients with a GBA mutation. *NPJ Parkinsons Dis,* 8**,** 99.

Blumenreich, S., Nehushtan, T., Kupervaser, M., Shalit, T., Gabashvili, A., Joseph, T., Milenkovic, I., Hardy, J. & Futerman, A. H. 2024. Large-scale proteomics analysis of five brain regions from Parkinson's disease patients with a GBA1 mutation. *NPJ Parkinsons Dis,* 10**,** 33.

Bobela, W., Zheng, L. & Schneider, B. L. 2014. Overview of mouse models of Parkinson's disease. *Curr Protoc Mouse Biol,* 4**,** 121-39.

Bock, M. A., Brown, E. G., Zhang, L. & Tanner, C. 2022. Association of Motor and Nonmotor Symptoms With Health-Related Quality of Life in a Large Online Cohort of People With Parkinson Disease. *Neurology,* 98**,** e2194-e2203.

Bohlen, M., Cameron, A., Metten, P., Crabbe, J. C. & Wahlsten, D. 2009. Calibration of rotational acceleration for the rotarod test of rodent motor coordination. *J Neurosci Methods,* 178**,** 10-4.

Boix, J., Von Hieber, D. & Connor, B. 2018. Gait Analysis for Early Detection of Motor Symptoms in the 6-OHDA Rat Model of Parkinson's Disease. *Front Behav Neurosci,* 12**,** 39.

Bolam, J. P. & Pissadaki, E. K. 2012. Living on the edge with too many mouths to feed: why dopamine neurons die. *Mov Disord,* 27**,** 1478-83.

Bologna, M., Paparella, G., Fasano, A., Hallett, M. & Berardelli, A. 2020. Evolving concepts on bradykinesia. *Brain,* 143**,** 727-750.

Book, A., Guella, I., Candido, T., Brice, A., Hattori, N., Jeon, B., Farrer, M. J. & Consortium, S. M. I. O. T. G. 2018. A Meta-Analysis of alpha-Synuclein Multiplication in Familial Parkinsonism. *Front Neurol,* 9**,** 1021.

Boot, R. G., Verhoek, M., Donker-Koopman, W., Strijland, A., Van Marle, J., Overkleeft, H. S., Wennekes, T. & Aerts, J. M. 2007. Identification of the non-lysosomal glucosylceramidase as beta-glucosidase 2. *J Biol Chem,* 282**,** 1305-12.

Boulos, C., Yaghi, N., El Hayeck, R., Heraoui, G. N. & Fakhoury-Sayegh, N. 2019. Nutritional Risk Factors, Microbiota and Parkinson's Disease: What Is the Current Evidence? *Nutrients,* 11.

Boutin, M., Sun, Y., Shacka, J. J. & Auray-Blais, C. 2016. Tandem Mass Spectrometry Multiplex Analysis of Glucosylceramide and Galactosylceramide Isoforms in Brain Tissues at Different Stages of Parkinson Disease. *Anal Chem,* 88**,** 1856-63.

Bozzi, Y. & Borrelli, E. 2006. Dopamine in neurotoxicity and neuroprotection: what do D2 receptors have to do with it? *Trends Neurosci,* 29**,** 167-74.

Braak, H. & Del Tredici, K. 2017. Neuropathological Staging of Brain Pathology in Sporadic Parkinson's disease: Separating the Wheat from the Chaff. *J Parkinsons Dis,* 7**,** S71-S85.

Braak, H., Del Tredici, K., Rub, U., De Vos, R. A., Jansen Steur, E. N. & Braak, E. 2003a. Staging of brain pathology related to sporadic Parkinson's disease. *Neurobiol Aging,* 24**,** 197-211.

Braak, H., Rub, U., Gai, W. P. & Del Tredici, K. 2003b. Idiopathic Parkinson's disease: possible routes by which vulnerable neuronal types may be subject to neuroinvasion by an unknown pathogen. *J Neural Transm (Vienna),* 110**,** 517-36.

Brady, R. O., Kanfer, J. & Shapiro, D. 1965a. The Metabolism of Glucocerebrosides. I. Purification and Properties of a Glucocerebroside-Cleaving Enzyme from Spleen Tissue. *J Biol Chem,* 240**,** 39-43.

Brady, R. O., Kanfer, J. N. & Shapiro, D. 1965b. Metabolism of Glucocerebrosides. Ii. Evidence of an Enzymatic Deficiency in Gaucher's Disease. *Biochem Biophys Res Commun,* 18**,** 221-5.

Braulke, T. & Bonifacino, J. S. 2009. Sorting of lysosomal proteins. *Biochim Biophys Acta,* 1793**,** 605-14.

Braun, A. A., Skelton, M. R., Vorhees, C. V. & Williams, M. T. 2011. Comparison of the elevated plus and elevated zero mazes in treated and untreated male Sprague-Dawley rats: effects of anxiolytic and anxiogenic agents. *Pharmacol Biochem Behav,* 97**,** 406-15.

Breen, D. P., Halliday, G. M. & Lang, A. E. 2019. Gut-brain axis and the spread of alpha-synuclein pathology: Vagal highway or dead end? *Mov Disord,* 34**,** 307-316.

Brichta, L. & Greengard, P. 2014. Molecular determinants of selective dopaminergic vulnerability in Parkinson's disease: an update. *Front Neuroanat,* 8**,** 152.

Brimblecombe, K. R., Connor-Robson, N., Bataille, C. J. R., Roberts, B. M., Gracie, C., O'connor, B., Te Water Naude, R., Karthik, G., Russell, A. J., Wade-Martins, R. & Cragg, S. J. 2024. Inhibition of striatal dopamine release by the L-type calcium channel inhibitor isradipine co-varies with risk factors for Parkinson's. *Eur J Neurosci,* 59**,** 1242-1259.

Brimblecombe, K. R., Gracie, C. J., Platt, N. J. & Cragg, S. J. 2015. Gating of dopamine transmission by calcium and axonal N-, Q-, T- and L-type voltage-gated calcium channels differs between striatal domains. *J Physiol,* 593**,** 929-46.

Brockmann, K., Srulijes, K., Hauser, A. K., Schulte, C., Csoti, I., Gasser, T. & Berg, D. 2011. GBA-associated PD presents with nonmotor characteristics. *Neurology,* 77**,** 276-80.

Brockmann, K., Srulijes, K., Pflederer, S., Hauser, A. K., Schulte, C., Maetzler, W., Gasser, T. & Berg, D. 2015. GBA-associated Parkinson's disease: reduced survival and more rapid progression in a prospective longitudinal study. *Mov Disord,* 30**,** 407-11.

Broen, M. P., Narayen, N. E., Kuijf, M. L., Dissanayaka, N. N. & Leentjens, A. F. 2016. Prevalence of anxiety in Parkinson's disease: A systematic review and meta-analysis. *Mov Disord,* 31**,** 1125-33.

Brolin, K. A., Backstrom, D., Wallenius, J., Gan-Or, Z., Puschmann, A., Hansson, O. & Swanberg, M. 2025. GBA1 T369M and Parkinson's disease - Further evidence of a lack of association in the Swedish population. *Parkinsonism Relat Disord,* 130**,** 107191.

Brooks, S. P. & Dunnett, S. B. 2009. Tests to assess motor phenotype in mice: a user's guide. *Nat Rev Neurosci,* 10**,** 519-29.

Broom, L., Ellison, B. A., Worley, A., Wagenaar, L., Sorberg, E., Ashton, C., Bennett, D. A., Buchman, A. S., Saper, C. B., Shih, L. C., Hausdorff, J. M. & Vanderhorst, V. G. 2017. A translational approach to capture gait signatures of neurological disorders in mice and humans. *Sci Rep,* 7**,** 3225.

Broom, L., Worley, A., Gao, F., Hernandez, L. D., Ashton, C. E., Shih, L. C. & Vanderhorst, V. G. 2019. Translational methods to detect asymmetries in temporal and spatial walking metrics in parkinsonian mouse models and human subjects with Parkinson's disease. *Sci Rep,* 9**,** 2437.

Bu, M., Farrer, M. J. & Khoshbouei, H. 2021. Dynamic control of the dopamine transporter in neurotransmission and homeostasis. *NPJ Parkinsons Dis,* 7**,** 22.

Bucher, E. S. & Wightman, R. M. 2015. Electrochemical Analysis of Neurotransmitters. *Annu Rev Anal Chem (Palo Alto Calif),* 8**,** 239-61.

Buck, S. A., De Miranda, B. R., Logan, R. W., Fish, K. N., Greenamyre, J. T. & Freyberg, Z. 2021. VGLUT2 Is a Determinant of Dopamine Neuron Resilience in a Rotenone Model of Dopamine Neurodegeneration. *J Neurosci,* 41**,** 4937-4947.

Buck, S. A., Erickson-Oberg, M. Q., Bhatte, S. H., Mckellar, C. D., Ramanathan, V. P., Rubin, S. A. & Freyberg, Z. 2022. Roles of VGLUT2 and Dopamine/Glutamate Co-Transmission in Selective Vulnerability to Dopamine Neurodegeneration. *ACS Chem Neurosci,* 13**,** 187-193.

Bucur, M. & Papagno, C. 2023. Deep Brain Stimulation in Parkinson Disease: A Meta-analysis of the Long-term Neuropsychological Outcomes. *Neuropsychol Rev,* 33**,** 307-346.

Burbulla, L. F., Jeon, S., Zheng, J., Song, P., Silverman, R. B. & Krainc, D. 2019. A modulator of wild-type glucocerebrosidase improves pathogenic phenotypes in dopaminergic neuronal models of Parkinson's disease. *Sci Transl Med,* 11.

Burbulla, L. F. & Krainc, D. 2019. The role of dopamine in the pathogenesis of GBA1-linked Parkinson's disease. *Neurobiol Dis,* 132**,** 104545.

Burbulla, L. F., Song, P., Mazzulli, J. R., Zampese, E., Wong, Y. C., Jeon, S., Santos, D. P., Blanz, J., Obermaier, C. D., Strojny, C., Savas, J. N., Kiskinis, E., Zhuang, X., Kruger, R., Surmeier, D. J. & Krainc, D. 2017. Dopamine oxidation mediates mitochondrial and lysosomal dysfunction in Parkinson's disease. *Science,* 357**,** 1255-1261.

Burke, D. G., Rahim, A. A., Waddington, S. N., Karlsson, S., Enquist, I., Bhatia, K., Mehta, A., Vellodi, A. & Heales, S. 2013. Increased glucocerebrosidase (GBA) 2 activity in GBA1 deficient mice brains and in Gaucher leucocytes. *J Inherit Metab Dis,* 36**,** 869-72.

Burre, J., Sharma, M. & Sudhof, T. C. 2018. Cell Biology and Pathophysiology of alpha-Synuclein. *Cold Spring Harb Perspect Med,* 8.

Burre, J., Vivona, S., Diao, J., Sharma, M., Brunger, A. T. & Sudhof, T. C. 2013. Properties of native brain alpha-synuclein. *Nature,* 498**,** E4-6; discussion E6-7.

Bussey, T. J., Holmes, A., Lyon, L., Mar, A. C., Mcallister, K. A., Nithianantharajah, J., Oomen, C. A. & Saksida, L. M. 2012. New translational assays for preclinical modelling of cognition in schizophrenia: the touchscreen testing method for mice and rats. *Neuropharmacology,* 62**,** 1191-203.

Butler, V. J., Cortopassi, W. A., Argouarch, A. R., Ivry, S. L., Craik, C. S., Jacobson, M. P. & Kao, A. W. 2019. Progranulin Stimulates the In Vitro Maturation of Pro-Cathepsin D at Acidic pH. *J Mol Biol,* 431**,** 1038-1047.

Button, K. S., Ioannidis, J. P., Mokrysz, C., Nosek, B. A., Flint, J., Robinson, E. S. & Munafo, M. R. 2013. Power failure: why small sample size undermines the reliability of neuroscience. *Nat Rev Neurosci,* 14**,** 365-76.

Cai, Y., Nielsen, B. E., Boxer, E. E., Aoto, J. & Ford, C. P. 2021. Loss of nigral excitation of cholinergic interneurons contributes to parkinsonian motor impairments. *Neuron,* 109**,** 1137-1149 e5.

Calabresi, P., Mechelli, A., Natale, G., Volpicelli-Daley, L., Di Lazzaro, G. & Ghiglieri, V. 2023. Alpha-synuclein in Parkinson's disease and other synucleinopathies: from overt neurodegeneration back to early synaptic dysfunction. *Cell Death Dis,* 14**,** 176.

Caminiti, S. P., Avenali, M., Galli, A., Malito, R., Cuconato, G., Galandra, C., Calabrese, R., Pilotto, A., Padovani, A., Blandini, F., Perani, D., Tassorelli, C. & Valente, E. M. 2025. Male sex accelerates cognitive decline in GBA1 Parkinson's disease. *NPJ Parkinsons Dis,* 11**,** 41.

Cao, F., Souders Ii, C. L., Perez-Rodriguez, V. & Martyniuk, C. J. 2018. Elucidating Conserved Transcriptional Networks Underlying Pesticide Exposure and Parkinson's Disease: A Focus on Chemicals of Epidemiological Relevance. *Front Genet,* 9**,** 701.

Carandina, A., Lazzeri, G., Rodrigues, G. D., Franco, G., Monfrini, E., Arienti, F., Frattini, E., Trezzi, I., Da Silva Soares, P. P., Bellocchi, C., Furlan, L., Montano, N., Di Fonzo, A. & Tobaldini, E. 2022. Dysautonomia in Parkinson's Disease: Impact of Glucocerebrosidase Gene Mutations on Cardiovascular Autonomic Control. *Front Neurosci,* 16**,** 842498.

Carlos Giugni, J. & Rodriguez-Cruz, R. L. 2016. Anticholinergic agents in the management of Parkinson’s disease. *In:* GÁLVEZ-JIMÉNEZ, N., FERNANDEZ, H. H., ESPAY, A. J. & FOX, S. H. (eds.) *Parkinson’s Disease: Current and Future Therapeutics and Clinical Trials.* Cambridge: Cambridge University Press.

Carvelli, L., Mcdonald, P. W., Blakely, R. D. & Defelice, L. J. 2004. Dopamine transporters depolarize neurons by a channel mechanism. *Proc Natl Acad Sci U S A,* 101**,** 16046-51.

Casola, S. 2010. Mouse models for miRNA expression: the ROSA26 locus. *Methods Mol Biol,* 667**,** 145-63.

Castillon, G., Chang, S. C. & Moride, Y. 2022. Global Incidence and Prevalence of Gaucher Disease: A Targeted Literature Review. *J Clin Med,* 12.

Cattaneo, C. & Pagonabarraga, J. 2025. Sex Differences in Parkinson's Disease: A Narrative Review. *Neurol Ther,* 14**,** 57-70.

Cerri, S., Ghezzi, C., Ongari, G., Croce, S., Avenali, M., Zangaglia, R., Di Monte, D. A., Valente, E. M. & Blandini, F. 2021. GBA Mutations Influence the Release and Pathological Effects of Small Extracellular Vesicles from Fibroblasts of Patients with Parkinson's Disease. *Int J Mol Sci,* 22.

Cerri, S., Mus, L. & Blandini, F. 2019. Parkinson's Disease in Women and Men: What's the Difference? *J Parkinsons Dis,* 9**,** 501-515.

Cerruti, C., Drian, M. J., Kamenka, J. M. & Privat, A. 1993. Protection by BTCP of cultured dopaminergic neurons exposed to neurotoxins. *Brain Res,* 617**,** 138-42.

Challis, C., Hori, A., Sampson, T. R., Yoo, B. B., Challis, R. C., Hamilton, A. M., Mazmanian, S. K., Volpicelli-Daley, L. A. & Gradinaru, V. 2020. Gut-seeded alpha-synuclein fibrils promote gut dysfunction and brain pathology specifically in aged mice. *Nat Neurosci,* 23**,** 327-336.

Chan, C. S., Guzman, J. N., Ilijic, E., Mercer, J. N., Rick, C., Tkatch, T., Meredith, G. E. & Surmeier, D. J. 2007. 'Rejuvenation' protects neurons in mouse models of Parkinson's disease. *Nature,* 447**,** 1081-6.

Chandler, K. J., Chandler, R. L., Broeckelmann, E. M., Hou, Y., Southard-Smith, E. M. & Mortlock, D. P. 2007. Relevance of BAC transgene copy number in mice: transgene copy number variation across multiple transgenic lines and correlations with transgene integrity and expression. *Mamm Genome,* 18**,** 693-708.

Charcot, J. M. & Vulpian, A. 1861. Revue clinique: De la paralysie agitante, à propos d'un cas tiré de la clinique du Professeur Oppolzer. *Gazette hebdomadaire de Médecine et de Chirurgie,* 8, 765-767 and 816-820 and 9, 54-59.

Chatterjee, D. & Krainc, D. 2023. Mechanisms of Glucocerebrosidase Dysfunction in Parkinson's Disease. *J Mol Biol,* 435**,** 168023.

Chaudhuri, K. R., Azulay, J. P., Odin, P., Lindvall, S., Domingos, J., Alobaidi, A., Kandukuri, P. L., Chaudhari, V. S., Parra, J. C., Yamazaki, T., Oddsdottir, J., Wright, J. & Martinez-Martin, P. 2024. Economic Burden of Parkinson's Disease: A Multinational, Real-World, Cost-of-Illness Study. *Drugs Real World Outcomes,* 11**,** 1-11.

Chaudhuri, K. R., Schrag, A., Weintraub, D., Rizos, A., Rodriguez-Blazquez, C., Mamikonyan, E. & Martinez-Martin, P. 2020. The movement disorder society nonmotor rating scale: Initial validation study. *Mov Disord,* 35**,** 116-133.

Chazalon, M., Paredes-Rodriguez, E., Morin, S., Martinez, A., Cristovao-Ferreira, S., Vaz, S., Sebastiao, A., Panatier, A., Boue-Grabot, E., Miguelez, C. & Baufreton, J. 2018. GAT-3 Dysfunction Generates Tonic Inhibition in External Globus Pallidus Neurons in Parkinsonian Rodents. *Cell Rep,* 23**,** 1678-1690.

Chen, H., O'reilly, E., Mccullough, M. L., Rodriguez, C., Schwarzschild, M. A., Calle, E. E., Thun, M. J. & Ascherio, A. 2007. Consumption of dairy products and risk of Parkinson's disease. *Am J Epidemiol,* 165**,** 998-1006.

Chen, J., Li, W., Zhang, T., Wang, Y. J., Jiang, X. J. & Xu, Z. Q. 2014. Glucocerebrosidase gene mutations associated with Parkinson's disease: a meta-analysis in a Chinese population. *PLoS One,* 9**,** e115747.

Chen, Y., Xie, W. Y., Xia, D., Zhang, M. T., Sun, Y. R., Duan, W. X., Shen, Y., Wang, F., Qu, W. M., Huang, Z. L. & Liu, C. F. 2024. GBA-AAV mitigates sleep disruptions and

motor deficits in mice with REM sleep behavior disorder. *NPJ Parkinsons Dis,* 10**,** 142.

Chen, Y. H., Wang, V., Huang, E. Y., Chou, Y. C., Kuo, T. T., Olson, L. & Hoffer, B. J. 2019. Delayed Dopamine Dysfunction and Motor Deficits in Female Parkinson Model Mice. *Int J Mol Sci,* 20.

Cheng, H. C., Ulane, C. M. & Burke, R. E. 2010. Clinical progression in Parkinson disease and the neurobiology of axons. *Ann Neurol,* 67**,** 715-25.

Chesler, E. J., Wilson, S. G., Lariviere, W. R., Rodriguez-Zas, S. L. & Mogil, J. S. 2002. Identification and ranking of genetic and laboratory environment factors influencing a behavioral trait, thermal nociception, via computational analysis of a large data archive. *Neurosci Biobehav Rev,* 26**,** 907-23.

Chiasserini, D., Paciotti, S., Eusebi, P., Persichetti, E., Tasegian, A., Kurzawa-Akanbi, M., Chinnery, P. F., Morris, C. M., Calabresi, P., Parnetti, L. & Beccari, T. 2015. Selective loss of glucocerebrosidase activity in sporadic Parkinson's disease and dementia with Lewy bodies. *Mol Neurodegener,* 10**,** 15.

Choi, J. M., Kim, W. C., Lyoo, C. H., Kang, S. Y., Lee, P. H., Baik, J. S., Koh, S. B., Ma, H. I., Sohn, Y. H., Lee, M. S. & Kim, Y. J. 2012. Association of mutations in the glucocerebrosidase gene with Parkinson disease in a Korean population. *Neurosci Lett,* 514**,** 12-5.

Chuhma, N., Mingote, S., Moore, H. & Rayport, S. 2014. Dopamine neurons control striatal cholinergic neurons via regionally heterogeneous dopamine and glutamate signaling. *Neuron,* 81**,** 901-12.

Cilia, R., Tunesi, S., Marotta, G., Cereda, E., Siri, C., Tesei, S., Zecchinelli, A. L., Canesi, M., Mariani, C. B., Meucci, N., Sacilotto, G., Zini, M., Barichella, M., Magnani, C., Duga, S., Asselta, R., Solda, G., Seresini, A., Seia, M., Pezzoli, G. & Goldwurm, S. 2016. Survival and dementia in GBA-associated Parkinson's disease: The mutation matters. *Ann Neurol,* 80**,** 662-673.

Ciliax, B. J., Drash, G. W., Staley, J. K., Haber, S., Mobley, C. J., Miller, G. W., Mufson, E. J., Mash, D. C. & Levey, A. I. 1999. Immunocytochemical localization of the dopamine transporter in human brain. *J Comp Neurol,* 409**,** 38-56.

Clark, L. N., Ross, B. M., Wang, Y., Mejia-Santana, H., Harris, J., Louis, E. D., Cote, L. J., Andrews, H., Fahn, S., Waters, C., Ford, B., Frucht, S., Ottman, R. & Marder, K. 2007. Mutations in the glucocerebrosidase gene are associated with early-onset Parkinson disease. *Neurology,* 69**,** 1270-7.

Clarke, E., Jantrachotechatchawan, C., Buhidma, Y., Broadstock, M., Yu, L., Howlett, D., Aarsland, D., Ballard, C. & Francis, P. T. 2019. Age-related neurochemical and behavioural changes in D409V/WT GBA1 mouse: Relevance to lewy body dementia. *Neurochem Int,* 129**,** 104502.

Clayton, J. A. & Collins, F. S. 2014. Policy: NIH to balance sex in cell and animal studies. *Nature,* 509**,** 282-3.

Cleeter, M. W., Chau, K. Y., Gluck, C., Mehta, A., Hughes, D. A., Duchen, M., Wood, N. W., Hardy, J., Mark Cooper, J. & Schapira, A. H. 2013. Glucocerebrosidase inhibition causes mitochondrial dysfunction and free radical damage. *Neurochem Int,* 62**,** 1-7.

Clementel, D., Del Conte, A., Monzon, A. M., Camagni, G. F., Minervini, G., Piovesan, D. & Tosatto, S. C. E. 2022. RING 3.0: fast generation of probabilistic residue interaction networks from structural ensembles. *Nucleic Acids Res,* 50**,** W651-W656.

Colacios, C., Sabourdy, F., Andrieu-Abadie, N. & Ségui, B., Levade, T. 2015. Basics of Sphingolipid Metabolism and Signalling. *In:* HANNUN, Y., LUBERTO, C., MAO,

C. & OBEID, L. (eds.) *Bioactive Sphingolipids in Cancer Biology and Therapy.* Springer, Cham.

Collins, L. M., Drouin-Ouellet, J., Kuan, W. L., Cox, T. & Barker, R. A. 2017. Dermal fibroblasts from patients with Parkinson's disease have normal GCase activity and autophagy compared to patients with PD and GBA mutations. *F1000Res,* 6**,** 1751.

Colucci, F., Avenali, M., De Micco, R., Fusar Poli, M., Cerri, S., Stanziano, M., Bacila, A., Cuconato, G., Franco, V., Franciotta, D., Ghezzi, C., Gastaldi, M., Elia, A. E., Romito, L., Devigili, G., Leta, V., Garavaglia, B., Golfre Andreasi, N., Cazzaniga, F., Reale, C., Galandra, C., Germani, G., Mitrotti, P., Ongari, G., Palmieri, I., Picascia, M., Pichiecchio, A., Verri, M., Esposito, F., Cirillo, M., Di Nardo, F., Aloisio, S., Siciliano, M., Prioni, S., Amami, P., Piacentini, S., Bruzzone, M. G., Grisoli, M., Moda, F., Eleopra, R., Tessitore, A., Valente, E. M. & Cilia, R. 2023. Ambroxol as a disease-modifying treatment to reduce the risk of cognitive impairment in GBA-associated Parkinson's disease: a multicentre, randomised, double-blind, placebo-controlled, phase II trial. The AMBITIOUS study protocol. *BMJ Neurol Open,* 5**,** e000535.

Condon, M. D., Platt, N. J., Zhang, Y. F., Roberts, B. M., Clements, M. A., Vietti-Michelina, S., Tseu, M. Y., Brimblecombe, K. R., Threlfell, S., Mann, E. O. & Cragg, S. J. 2019. Plasticity in striatal dopamine release is governed by release-independent depression and the dopamine transporter. *Nat Commun,* 10**,** 4263.

Connor-Robson, N., Booth, H., Martin, J. G., Gao, B., Li, K., Doig, N., Vowles, J., Browne, C., Klinger, L., Juhasz, P., Klein, C., Cowley, S. A., Bolam, P., Hirst, W. & Wade-Martins, R. 2019. An integrated transcriptomics and proteomics analysis reveals functional endocytic dysregulation caused by mutations in LRRK2. *Neurobiol Dis,* 127**,** 512-526.

Cook, L., Verbrugge, J., Schwantes-An, T. H., Schulze, J., Foroud, T., Hall, A., Marder, K. S., Mata, I. F., Mencacci, N. E., Nance, M. A., Schwarzschild, M. A., Simuni, T., Bressman, S., Wills, A. M., Fernandez, H. H., Litvan, I., Lyons, K. E., Shill, H. A., Singer, C., Tropea, T. F., Vanegas Arroyave, N., Carbonell, J., Cruz Vicioso, R., Katus, L., Quinn, J. F., Hodges, P. D., Meng, Y., Strom, S. P., Blauwendraat, C., Lohmann, K., Casaceli, C., Rao, S. C., Ghosh Galvelis, K., Naito, A., Beck, J. C. & Alcalay, R. N. 2024. Parkinson's disease variant detection and disclosure: PD GENEration, a North American study. *Brain,* 147**,** 2668-2679.

Cook, M. N., Bolivar, V. J., Mcfadyen, M. P. & Flaherty, L. 2002. Behavioral differences among 129 substrains: implications for knockout and transgenic mice. *Behav Neurosci,* 116**,** 600-11.

Cookson, M. R. 2011. A feedforward loop links Gaucher and Parkinson's diseases? *Cell,* 146**,** 9-11.

Correia Guedes, L., Ferreira, J. J., Rosa, M. M., Coelho, M., Bonifati, V. & Sampaio, C. 2010. Worldwide frequency of G2019S LRRK2 mutation in Parkinson's disease: a systematic review. *Parkinsonism Relat Disord,* 16**,** 237-42.

Cotzias, G. C., Papavasiliou, P. S. & Gellene, R. 1969. Modification of Parkinsonism--chronic treatment with L-dopa. *N Engl J Med,* 280**,** 337-45.

Crabbe, J. C., Wahlsten, D. & Dudek, B. C. 1999. Genetics of mouse behavior: interactions with laboratory environment. *Science,* 284**,** 1670-2.

Crabtree, D. M. & Zhang, J. 2012. Genetically engineered mouse models of Parkinson's disease. *Brain Res Bull,* 88**,** 13-32.

Cragg, S. J. & Greenfield, S. A. 1997. Differential autoreceptor control of somatodendritic and axon terminal dopamine release in substantia nigra, ventral tegmental area, and striatum. *J Neurosci,* 17**,** 5738-46.

Cragg, S. J. & Rice, M. E. 2004. DAncing past the DAT at a DA synapse. *Trends Neurosci,* 27**,** 270-7.

Cramb, K. M. L., Beccano-Kelly, D., Cragg, S. J. & Wade-Martins, R. 2023. Impaired dopamine release in Parkinson's disease. *Brain,* 146**,** 3117-3132.

Creese, B., Bell, E., Johar, I., Francis, P., Ballard, C. & Aarsland, D. 2018. Glucocerebrosidase mutations and neuropsychiatric phenotypes in Parkinson's disease and Lewy body dementias: Review and meta-analyses. *Am J Med Genet B Neuropsychiatr Genet,* 177**,** 232-241.

Crosiers, D., Verstraeten, A., Wauters, E., Engelborghs, S., Peeters, K., Mattheijssens, M., De Deyn, P. P., Theuns, J., Van Broeckhoven, C. & Cras, P. 2016. Mutations in glucocerebrosidase are a major genetic risk factor for Parkinson's disease and increase susceptibility to dementia in a Flanders-Belgian cohort. *Neurosci Lett,* 629**,** 160-164.

Crouse, J. J., Phillips, J. R., Jahanshahi, M. & Moustafa, A. A. 2016. Postural instability and falls in Parkinson's disease. *Rev Neurosci,* 27**,** 549-55.

Cullen, V., Sardi, S. P., Ng, J., Xu, Y. H., Sun, Y., Tomlinson, J. J., Kolodziej, P., Kahn, I., Saftig, P., Woulfe, J., Rochet, J. C., Glicksman, M. A., Cheng, S. H., Grabowski, G. A., Shihabuddin, L. S. & Schlossmacher, M. G. 2011. Acid beta-glucosidase mutants linked to Gaucher disease, Parkinson disease, and Lewy body dementia alter alpha-synuclein processing. *Ann Neurol,* 69**,** 940-53.

D'isa, R., Comi, G. & Leocani, L. 2021. Apparatus design and behavioural testing protocol for the evaluation of spatial working memory in mice through the spontaneous alternation T-maze. *Sci Rep,* 11**,** 21177.

Dagra, A., Miller, D. R., Lin, M., Gopinath, A., Shaerzadeh, F., Harris, S., Sorrentino, Z. A., Stoier, J. F., Velasco, S., Azar, J., Alonge, A. R., Lebowitz, J. J., Ulm, B., Bu, M., Hansen, C. A., Urs, N., Giasson, B. I. & Khoshbouei, H. 2021. alpha-Synuclein-induced dysregulation of neuronal activity contributes to murine dopamine neuron vulnerability. *NPJ Parkinsons Dis,* 7**,** 76.

Dai, M., Liou, B., Swope, B., Wang, X., Zhang, W., Inskeep, V., Grabowski, G. A., Sun, Y. & Pan, D. 2016. Progression of Behavioral and CNS Deficits in a Viable Murine Model of Chronic Neuronopathic Gaucher Disease. *PLoS One,* 11**,** e0162367.

Dai, X., Gakidou, E. & Lopez, A. D. 2022. Evolution of the global smoking epidemic over the past half century: strengthening the evidence base for policy action. *Tob Control,* 31**,** 129-137.

Dal Bo, G., St-Gelais, F., Danik, M., Williams, S., Cotton, M. & Trudeau, L. E. 2004. Dopamine neurons in culture express VGLUT2 explaining their capacity to release glutamate at synapses in addition to dopamine. *J Neurochem,* 88**,** 1398-405.

Darweesh, S. K., Koudstaal, P. J., Stricker, B. H., Hofman, A. & Ikram, M. A. 2016. Trends in the Incidence of Parkinson Disease in the General Population: The Rotterdam Study. *Am J Epidemiol,* 183**,** 1018-26.

Daubner, S. C., Le, T. & Wang, S. 2011. Tyrosine hydroxylase and regulation of dopamine synthesis. *Arch Biochem Biophys,* 508**,** 1-12.

Davis, M. Y., Johnson, C. O., Leverenz, J. B., Weintraub, D., Trojanowski, J. Q., Chen-Plotkin, A., Van Deerlin, V. M., Quinn, J. F., Chung, K. A., Peterson-Hiller, A. L., Rosenthal, L. S., Dawson, T. M., Albert, M. S., Goldman, J. G., Stebbins, G. T., Bernard, B., Wszolek, Z. K., Ross, O. A., Dickson, D. W., Eidelberg, D., Mattis, P. J., Niethammer, M., Yearout, D., Hu, S. C., Cholerton, B. A., Smith, M., Mata, I. F., Montine, T. J., Edwards, K. L. & Zabetian, C. P. 2016. Association of GBA Mutations and the E326K Polymorphism With Motor and Cognitive Progression in Parkinson Disease. *JAMA Neurol,* 73**,** 1217-1224.

Dawson, T. M., Ko, H. S. & Dawson, V. L. 2010. Genetic animal models of Parkinson's disease. *Neuron,* 66**,** 646-61.

Day, J. O. & Mullin, S. 2021. The Genetics of Parkinson's Disease and Implications for Clinical Practice. *Genes (Basel),* 12.

Daykin, E. C., Ryan, E. & Sidransky, E. 2021. Diagnosing neuronopathic Gaucher disease: New considerations and challenges in assigning Gaucher phenotypes. *Mol Genet Metab,* 132**,** 49-58.

De Bie, R. M. A., Clarke, C. E., Espay, A. J., Fox, S. H. & Lang, A. E. 2020. Initiation of pharmacological therapy in Parkinson's disease: when, why, and how. *Lancet Neurol,* 19**,** 452-461.

De La Fuente, C., Burke, D. G., Eaton, S. & Heales, S. J. R. 2017. Inhibition of neuronal mitochondrial complex I or lysosomal glucocerebrosidase is associated with increased dopamine and serotonin turnover. *Neurochem Int,* 109**,** 94-100.

De Miranda, B. R., Goldman, S. M., Miller, G. W., Greenamyre, J. T. & Dorsey, E. R. 2022. Preventing Parkinson's Disease: An Environmental Agenda. *J Parkinsons Dis,* 12**,** 45-68.

De Santis, T., Cocco, A., Castiglioni, P., Ferrarin, M., Mineri, R., Morenghi, E., Avenali, M. & Albanese, A. 2025. Parasympathetic Dysfunction Prevails in GBA1-Associated Parkinson's Disease. *Mov Disord Clin Pract,* 12**,** 364-370.

Deacon, R. M. 2013a. Measuring motor coordination in mice. *J Vis Exp***,** e2609.

Deacon, R. M. 2013b. Measuring the strength of mice. *J Vis Exp*.

Deacon, R. M. & Rawlins, J. N. 2006. T-maze alternation in the rodent. *Nat Protoc,* 1**,** 7-12.

Dekker, N., Van Dussen, L., Hollak, C. E., Overkleeft, H., Scheij, S., Ghauharali, K., Van Breemen, M. J., Ferraz, M. J., Groener, J. E., Maas, M., Wijburg, F. A., Speijer, D., Tylki-Szymanska, A., Mistry, P. K., Boot, R. G. & Aerts, J. M. 2011. Elevated plasma glucosylsphingosine in Gaucher disease: relation to phenotype, storage cell markers, and therapeutic response. *Blood,* 118**,** e118-27.

Den Dunnen, J. T. & Antonarakis, S. E. 2001. Nomenclature for the description of human sequence variations. *Hum Genet,* 109**,** 121-4.

Den Dunnen, J. T., Dalgleish, R., Maglott, D. R., Hart, R. K., Greenblatt, M. S., Mcgowan-Jordan, J., Roux, A. F., Smith, T., Antonarakis, S. E. & Taschner, P. E. 2016. HGVS Recommendations for the Description of Sequence Variants: 2016 Update. *Hum Mutat,* 37**,** 564-9.

Den Heijer, J. M., Cullen, V. C., Pereira, D. R., Yavuz, Y., De Kam, M. L., Grievink, H. W., Moerland, M., Leymarie, N., Khatri, K., Sollomoni, I., Spitalny, L., Dungeon, L., Hilt, D. C., Justman, C., Lansbury, P. & Groeneveld, G. J. 2023a. A Biomarker Study in Patients with GBA1-Parkinson's Disease and Healthy Controls. *Mov Disord,* 38**,** 783-795.

Den Heijer, J. M., Cullen, V. C., Quadri, M., Schmitz, A., Hilt, D. C., Lansbury, P., Berendse, H. W., Van De Berg, W. D. J., De Bie, R. M. A., Boertien, J. M., Boon, A. J. W., Contarino, M. F., Van Hilten, J. J., Hoff, J. I., Van Mierlo, T., Munts, A. G., Van Der Plas, A. A., Ponsen, M. M., Baas, F., Majoor-Krakauer, D., Bonifati, V., Van Laar, T. & Groeneveld, G. J. 2020. A Large-Scale Full GBA1 Gene Screening in Parkinson's Disease in the Netherlands. *Mov Disord,* 35**,** 1667-1674.

Den Heijer, J. M., Kruithof, A. C., Moerland, M., Walker, M., Dudgeon, L., Justman, C., Solomini, I., Splitalny, L., Leymarie, N., Khatri, K., Cullen, V. C., Hilt, D. C., Groeneveld, G. J. & Lansbury, P. 2023b. A Phase 1B Trial in GBA1-Associated Parkinson's Disease of BIA-28-6156, a Glucocerebrosidase Activator. *Mov Disord,* 38**,** 1197-1208.

Den Heijer, J. M., Kruithof, A. C., Van Amerongen, G., De Kam, M. L., Thijssen, E., Grievink, H. W., Moerland, M., Walker, M., Been, K., Skerlj, R., Justman, C., Dudgeon, L., Lansbury, P., Cullen, V. C., Hilt, D. C. & Groeneveld, G. J. 2021. A randomized single and multiple ascending dose study in healthy volunteers of LTI-291, a centrally penetrant glucocerebrosidase activator. *Br J Clin Pharmacol,* 87**,** 3561-3573.

Deng, H., Wang, P. & Jankovic, J. 2018. The genetics of Parkinson disease. *Ageing Res Rev,* 42**,** 72-85.

Dennis, W. 1939. Spontaneous alternation in rats as an indicator of the persistence of stimulus effects. *Journal of Comparative Psychology,* 28**,** 305-312.

Dermentzaki, G., Dimitriou, E., Xilouri, M., Michelakakis, H. & Stefanis, L. 2013. Loss of beta-glucocerebrosidase activity does not affect alpha-synuclein levels or lysosomal function in neuronal cells. *PLoS One,* 8**,** e60674.

Dettmer, U., Newman, A. J., Luth, E. S., Bartels, T. & Selkoe, D. 2013. In vivo cross-linking reveals principally oligomeric forms of alpha-synuclein and beta-synuclein in neurons and non-neural cells. *J Biol Chem,* 288**,** 6371-85.

Dettmer, U., Newman, A. J., Soldner, F., Luth, E. S., Kim, N. C., Von Saucken, V. E., Sanderson, J. B., Jaenisch, R., Bartels, T. & Selkoe, D. 2015. Parkinson-causing alpha-synuclein missense mutations shift native tetramers to monomers as a mechanism for disease initiation. *Nat Commun,* 6**,** 7314.

Dettmer, U., Selkoe, D. & Bartels, T. 2016. New insights into cellular alpha-synuclein homeostasis in health and disease. *Curr Opin Neurobiol,* 36**,** 15-22.

Devigili, G., Straccia, G., Cereda, E., Garavaglia, B., Fedeli, A., Elia, A. E., Piacentini, S., Prioni, S., Amami, P., Invernizzi, F., Andreasi, N. G., Romito, L. M., Eleopra, R. & Cilia, R. 2023. Unraveling Autonomic Dysfunction in GBA-Related Parkinson's Disease. *Mov Disord Clin Pract,* 10**,** 1620-1638.

Do, C. B., Tung, J. Y., Dorfman, E., Kiefer, A. K., Drabant, E. M., Francke, U., Mountain, J. L., Goldman, S. M., Tanner, C. M., Langston, J. W., Wojcicki, A. & Eriksson, N. 2011. Web-based genome-wide association study identifies two novel loci and a substantial genetic component for Parkinson's disease. *PLoS Genet,* 7**,** e1002141.

Do, J., Perez, G., Berhe, B., Tayebi, N. & Sidransky, E. 2021. Behavioral Phenotyping in a Murine Model of GBA1-Associated Parkinson Disease. *Int J Mol Sci,* 22.

Do, Q. B., Noor, H., Marquez-Gomez, R., Cramb, K. M. L., Ng, B., Abbey, A., Ibarra-Aizpurua, N., Caiazza, M. C., Sharifi, P., Lang, C., Beccano-Kelly, D., Baleriola, J., Bengoa-Vergniory, N. & Wade-Martins, R. 2024. Early deficits in an in vitro striatal microcircuit model carrying the Parkinson's GBA-N370S mutation. *NPJ Parkinsons Dis,* 10**,** 82.

Dobert, J. P., Bub, S., Machtel, R., Januliene, D., Steger, L., Regensburger, M., Wilfling, S., Chen, J. X., Dejung, M., Plotz, S., Hehr, U., Moeller, A., Arnold, P. & Zunke, F. 2024. Activation and Purification of ss-Glucocerebrosidase by Exploiting its Transporter LIMP-2 - Implications for Novel Treatment Strategies in Gaucher's and Parkinson's Disease. *Adv Sci (Weinh),* 11**,** e2401641.

Dobert, J. P., Schafer, J. H., Dal Maso, T., Ravindran, P., Huard, D. J. E., Socher, E., Schildmeyer, L. A., Lieberman, R. L., Versees, W., Moeller, A., Zunke, F. & Arnold, P. 2025. Cryo-TEM structure of beta-glucocerebrosidase in complex with its transporter LIMP-2. *Nat Commun,* 16**,** 3074.

Dobrowsky, R. T., Kamibayashi, C., Mumby, M. C. & Hannun, Y. A. 1993. Ceramide Activates Heterotrimeric Protein Phosphatase-2a. *Journal of Biological Chemistry,* 268**,** 15523-15530.

Dominguez, C., Boelens, R. & Bonvin, A. M. 2003. HADDOCK: a protein-protein docking approach based on biochemical or biophysical information. *J Am Chem Soc,* 125**,** 1731-7.

Dorsey, E. R. & Bloem, B. R. 2018. The Parkinson Pandemic-A Call to Action. *JAMA Neurol,* 75**,** 9-10.

Dorsey, E. R., Elbaz, A. & Gbd 2016 Parkinson's Disease Collaborators 2018a. Global, regional, and national burden of Parkinson's disease, 1990-2016: a systematic analysis for the Global Burden of Disease Study 2016. *Lancet Neurol,* 17**,** 939-953.

Dorsey, E. R., Sherer, T., Okun, M. S. & Bloem, B. R. 2018b. The Emerging Evidence of the Parkinson Pandemic. *J Parkinsons Dis,* 8**,** S3-S8.

Dovonou, A., Bolduc, C., Soto Linan, V., Gora, C., Peralta Iii, M. R. & Levesque, M. 2023. Animal models of Parkinson's disease: bridging the gap between disease hallmarks and research questions. *Transl Neurodegener,* 12**,** 36.

Dreyer, J. K., Herrik, K. F., Berg, R. W. & Hounsgaard, J. D. 2010. Influence of phasic and tonic dopamine release on receptor activation. *J Neurosci,* 30**,** 14273-83.

Du, T. T., Wang, L., Duan, C. L., Lu, L. L., Zhang, J. L., Gao, G., Qiu, X. B., Wang, X. M. & Yang, H. 2015. GBA deficiency promotes SNCA/alpha-synuclein accumulation through autophagic inhibition by inactivated PPP2A. *Autophagy,* 11**,** 1803-20.

Dunham, N. W. & Miya, T. S. 1957. A note on a simple apparatus for detecting neurological deficit in rats and mice. *J Am Pharm Assoc Am Pharm Assoc,* 46**,** 208-9.

Dunnett, S. B. & Lelos, M. 2010. Behavioral analysis of motor and non-motor symptoms in rodent models of Parkinson's disease. *Prog Brain Res,* 184**,** 35-51.

Duran, A., Rebolledo-Jaramillo, B., Olguin, V., Rojas-Herrera, M., Las Heras, M., Calderon, J. F., Zanlungo, S., Priestman, D. A., Platt, F. M. & Klein, A. D. 2021. Identification of genetic modifiers of murine hepatic beta-glucocerebrosidase activity. *Biochem Biophys Rep,* 28**,** 101105.

Duran, R., Mencacci, N. E., Angeli, A. V., Shoai, M., Deas, E., Houlden, H., Mehta, A., Hughes, D., Cox, T. M., Deegan, P., Schapira, A. H., Lees, A. J., Limousin, P., Jarman, P. R., Bhatia, K. P., Wood, N. W., Hardy, J. & Foltynie, T. 2013. The glucocerobrosidase E326K variant predisposes to Parkinson's disease, but does not cause Gaucher's disease. *Mov Disord,* 28**,** 232-236.

Duvoisin, R. C. 1967. Cholinergic-anticholinergic antagonism in parkinsonism. *Arch Neurol,* 17**,** 124-36.

Duvoisin, R. C. 1984. Is Parkinson's disease acquired or inherited? *Can J Neurol Sci,* 11**,** 151-5.

Dvir, H., Harel, M., Mccarthy, A. A., Toker, L., Silman, I., Futerman, A. H. & Sussman, J. L. 2003. X-ray structure of human acid-beta-glucosidase, the defective enzyme in Gaucher disease. *EMBO Rep,* 4**,** 704-9.

Enquist, I. B., Lo Bianco, C., Ooka, A., Nilsson, E., Mansson, J. E., Ehinger, M., Richter, J., Brady, R. O., Kirik, D. & Karlsson, S. 2007. Murine models of acute neuronopathic Gaucher disease. *Proc Natl Acad Sci U S A,* 104**,** 17483-8.

Enserink, M. 2017. Sloppy reporting on animal studies proves hard to change. *Science,* 357**,** 1337-1338.

Erickson, A. H., Ginns, E. I. & Barranger, J. A. 1985. Biosynthesis of the lysosomal enzyme glucocerebrosidase. *J Biol Chem,* 260**,** 14319-24.

Eskenazi, D., Malave, L., Mingote, S., Yetnikoff, L., Ztaou, S., Velicu, V., Rayport, S. & Chuhma, N. 2021. Dopamine Neurons That Cotransmit Glutamate, From Synapses to Circuits to Behavior. *Front Neural Circuits,* 15**,** 665386.

Exley, R. & Cragg, S. J. 2008. Presynaptic nicotinic receptors: a dynamic and diverse cholinergic filter of striatal dopamine neurotransmission. *Br J Pharmacol,* 153 Suppl 1**,** S283-97.

Eyal, N., Wilder, S. & Horowitz, M. 1990. Prevalent and rare mutations among Gaucher patients. *Gene,* 96**,** 277-83.

Fabrega, S., Durand, P., Codogno, P., Bauvy, C., Delomenie, C., Henrissat, B., Martin, B. M., Mckinney, C., Ginns, E. I., Mornon, J. P. & Lehn, P. 2000. Human glucocerebrosidase: heterologous expression of active site mutants in murine null cells. *Glycobiology,* 10**,** 1217-24.

Fahn, S. 2018. The 200-year journey of Parkinson disease: Reflecting on the past and looking towards the future. *Parkinsonism Relat Disord,* 46 Suppl 1**,** S1-S5.

Fan, J. Q. 2003. A contradictory treatment for lysosomal storage disorders: inhibitors enhance mutant enzyme activity. *Trends Pharmacol Sci,* 24**,** 355-60.

Fan, Y., Han, J., Zhao, L., Wu, C., Wu, P., Huang, Z., Hao, X., Ji, Y., Chen, D. & Zhu, M. 2021. Experimental Models of Cognitive Impairment for Use in Parkinson's Disease Research: The Distance Between Reality and Ideal. *Front Aging Neurosci,* 13**,** 745438.

Farfel-Becker, T., Do, J., Tayebi, N. & Sidransky, E. 2019. Can GBA1-Associated Parkinson Disease Be Modeled in the Mouse? *Trends Neurosci,* 42**,** 631-643.

Farfel-Becker, T., Vitner, E., Dekel, H., Leshem, N., Enquist, I. B., Karlsson, S. & Futerman, A. H. 2009. No evidence for activation of the unfolded protein response in neuronopathic models of Gaucher disease. *Hum Mol Genet,* 18**,** 1482-8.

Fasano, A., Garcia-Ramos, R., Gurevich, T., Jech, R., Bergmann, L., Sanchez-Solino, O., Parra, J. C. & Simu, M. 2023. Levodopa-carbidopa intestinal gel in advanced Parkinson's disease: long-term results from COSMOS. *J Neurol,* 270**,** 2765-2775.

Fasano, A., Visanji, N. P., Liu, L. W., Lang, A. E. & Pfeiffer, R. F. 2015. Gastrointestinal dysfunction in Parkinson's disease. *Lancet Neurol,* 14**,** 625-39.

Fauvet, B., Mbefo, M. K., Fares, M. B., Desobry, C., Michael, S., Ardah, M. T., Tsika, E., Coune, P., Prudent, M., Lion, N., Eliezer, D., Moore, D. J., Schneider, B., Aebischer, P., El-Agnaf, O. M., Masliah, E. & Lashuel, H. A. 2012. alpha-Synuclein in central nervous system and from erythrocytes, mammalian cells, and Escherichia coli exists predominantly as disordered monomer. *J Biol Chem,* 287**,** 15345-64.

Fearnley, J. M. & Lees, A. J. 1991. Ageing and Parkinson's disease: substantia nigra regional selectivity. *Brain,* 114 (Pt 5)**,** 2283-301.

Feigin, V. L., Abajobir, A. A. & Gbd 2015 Neurological Disorders Collaborator Group 2017. Global, regional, and national burden of neurological disorders during 1990-2015: a systematic analysis for the Global Burden of Disease Study 2015. *Lancet Neurol,* 16**,** 877-897.

Fengler, S., Liepelt-Scarfone, I., Brockmann, K., Schaffer, E., Berg, D. & Kalbe, E. 2017. Cognitive changes in prodromal Parkinson's disease: A review. *Mov Disord,* 32**,** 1655-1666.

Fernandes, H. J., Hartfield, E. M., Christian, H. C., Emmanoulidou, E., Zheng, Y., Booth, H., Bogetofte, H., Lang, C., Ryan, B. J., Sardi, S. P., Badger, J., Vowles, J., Evetts, S., Tofaris, G. K., Vekrellis, K., Talbot, K., Hu, M. T., James, W., Cowley, S. A. & Wade-Martins, R. 2016. ER Stress and Autophagic Perturbations Lead to Elevated Extracellular alpha-Synuclein in GBA-N370S Parkinson's iPSC-Derived Dopamine Neurons. *Stem Cell Reports,* 6**,** 342-56.

Ferraz, M. J., Marques, A. R., Appelman, M. D., Verhoek, M., Strijland, A., Mirzaian, M., Scheij, S., Ouairy, C. M., Lahav, D., Wisse, P., Overkleeft, H. S., Boot, R. G. & Aerts,

J. M. 2016. Lysosomal glycosphingolipid catabolism by acid ceramidase: formation of glycosphingoid bases during deficiency of glycosidases. *FEBS Lett,* 590**,** 716-25.

Festing, M. F. 2018. On determining sample size in experiments involving laboratory animals. *Lab Anim,* 52**,** 341-350.

Fields, C. R., Bengoa-Vergniory, N. & Wade-Martins, R. 2019. Targeting Alpha-Synuclein as a Therapy for Parkinson's Disease. *Front Mol Neurosci,* 12**,** 299.

Fishbein, I., Kuo, Y. M., Giasson, B. I. & Nussbaum, R. L. 2014. Augmentation of phenotype in a transgenic Parkinson mouse heterozygous for a Gaucher mutation. *Brain,* 137**,** 3235-47.

Fisher, E. M. C. & Bannerman, D. M. 2019. Mouse models of neurodegeneration: Know your question, know your mouse. *Sci Transl Med,* 11.

Fleming, S. M., Salcedo, J., Fernagut, P. O., Rockenstein, E., Masliah, E., Levine, M. S. & Chesselet, M. F. 2004. Early and progressive sensorimotor anomalies in mice overexpressing wild-type human alpha-synuclein. *J Neurosci,* 24**,** 9434-40.

Foo, J. N., Chew, E. G. Y., Chung, S. J., Peng, R., Blauwendraat, C., Nalls, M. A., Mok, K. Y., Satake, W., Toda, T., Chao, Y., Tan, L. C. S., Tandiono, M., Lian, M. M., Ng, E. Y., Prakash, K. M., Au, W. L., Meah, W. Y., Mok, S. Q., Annuar, A. A., Chan, A. Y. Y., Chen, L., Chen, Y., Jeon, B. S., Jiang, L., Lim, J. L., Lin, J. J., Liu, C., Mao, C., Mok, V., Pei, Z., Shang, H. F., Shi, C. H., Song, K., Tan, A. H., Wu, Y. R., Xu, Y. M., Xu, R., Yan, Y., Yang, J., Zhang, B., Koh, W. P., Lim, S. Y., Khor, C. C., Liu, J. & Tan, E. K. 2020. Identification of Risk Loci for Parkinson Disease in Asians and Comparison of Risk Between Asians and Europeans: A Genome-Wide Association Study. *JAMA Neurol,* 77**,** 746-754.

Ford, C. P. 2014. The role of D2-autoreceptors in regulating dopamine neuron activity and transmission. *Neuroscience,* 282**,** 13-22.

Fornstedt Wallin, B. 2024. Oxidation of dopamine and related catechols in dopaminergic brain regions in Parkinson's disease and during ageing in non-Parkinsonian subjects. *J Neural Transm (Vienna),* 131**,** 213-228.

Fortin, G. M., Bourque, M. J., Mendez, J. A., Leo, D., Nordenankar, K., Birgner, C., Arvidsson, E., Rymar, V. V., Berube-Carriere, N., Claveau, A. M., Descarries, L., Sadikot, A. F., Wallen-Mackenzie, A. & Trudeau, L. E. 2012. Glutamate corelease promotes growth and survival of midbrain dopamine neurons. *J Neurosci,* 32**,** 17477-91.

Fox, S. H., Katzenschlager, R., Lim, S. Y., Barton, B., De Bie, R. M. A., Seppi, K., Coelho, M., Sampaio, C. & Movement Disorder Society Evidence-Based Medicine, C. 2018. International Parkinson and movement disorder society evidence-based medicine review: Update on treatments for the motor symptoms of Parkinson's disease. *Mov Disord,* 33**,** 1248-1266.

Frattini, E., Faustini, G., Lopez, G., Carsana, E. V., Tosi, M., Trezzi, I., Magni, M., Solda, G., Straniero, L., Facchi, D., Samarani, M., Marta-Ariza, M., De Luca, C. M. G., Vezzoli, E., Pittaro, A., Stepanyan, A., Silipigni, R., Rosety, I., Schwamborn, J. C., Sardi, S. P., Moda, F., Corti, S., Comi, G. P., Blandini, F., Tritsch, N. X., Bortolozzi, M., Ferrero, S., Cribiu, F. M., Wisniewski, T., Asselta, R., Aureli, M., Bellucci, A. & Di Fonzo, A. 2024. Lewy pathology formation in patient-derived GBA1 Parkinson's disease midbrain organoids. *Brain*.

Freeze, H. H. & Kranz, C. 2010. Endoglycosidase and glycoamidase release of N-linked glycans. *Curr Protoc Mol Biol,* Chapter 17**,** Unit 17 13A.

Frigerio, R., Sanft, K. R., Grossardt, B. R., Peterson, B. J., Elbaz, A., Bower, J. H., Ahlskog, J. E., De Andrade, M., Maraganore, D. M. & Rocca, W. A. 2006. Chemical exposures

and Parkinson's disease: a population-based case-control study. *Mov Disord,* 21**,** 1688-92.

Frost, L. S., Dhingra, A., Reyes-Reveles, J. & Boesze-Battaglia, K. 2017. The Use of DQ-BSA to Monitor the Turnover of Autophagy-Associated Cargo. *Methods Enzymol,* 587**,** 43-54.

Frynta, D., Novakova, M., Kutalova, H., Palme, R. & Sedlacek, F. 2009. Apparatus for collection of fecal samples from undisturbed spiny mice (Acomys cahirinus) living in a complex social group. *J Am Assoc Lab Anim Sci,* 48**,** 196-201.

Fujita, H., Ezaki, J., Noguchi, Y., Kono, A., Himeno, M. & Kato, K. 1991. Isolation and sequencing of a cDNA clone encoding 85kDa sialoglycoprotein in rat liver lysosomal membranes. *Biochem Biophys Res Commun,* 178**,** 444-52.

Fullard, M. E., Morley, J. F. & Duda, J. E. 2017. Olfactory Dysfunction as an Early Biomarker in Parkinson's Disease. *Neurosci Bull,* 33**,** 515-525.

Furderer, M. L., Berhe, B., Chen, T. C., Wincovitch, S., Jiang, X., Tayebi, N., Sidransky, E. & Han, T. U. 2024. A Comparative Biochemical and Pathological Evaluation of Brain Samples from Knock-In Murine Models of Gaucher Disease. *Int J Mol Sci,* 25.

Furderer, M. L., Hertz, E., Lopez, G. J. & Sidransky, E. 2022. Neuropathological Features of Gaucher Disease and Gaucher Disease with Parkinsonism. *Int J Mol Sci,* 23.

Gabbert, C., Schaake, S., Luth, T., Much, C., Klein, C., Aasly, J. O., Farrer, M. J. & Trinh, J. 2023. GBA1 in Parkinson's disease: variant detection and pathogenicity scoring matters. *BMC Genomics,* 24**,** 322.

Gainetdinov, R. R., Fumagalli, F., Jones, S. R. & Caron, M. G. 1997. Dopamine transporter is required for in vivo MPTP neurotoxicity: evidence from mice lacking the transporter. *J Neurochem,* 69**,** 1322-5.

Galvagnion, C., Brown, J. W., Ouberai, M. M., Flagmeier, P., Vendruscolo, M., Buell, A. K., Sparr, E. & Dobson, C. M. 2016. Chemical properties of lipids strongly affect the kinetics of the membrane-induced aggregation of alpha-synuclein. *Proc Natl Acad Sci U S A,* 113**,** 7065-70.

Galvagnion, C., Buell, A. K., Meisl, G., Michaels, T. C., Vendruscolo, M., Knowles, T. P. & Dobson, C. M. 2015. Lipid vesicles trigger alpha-synuclein aggregation by stimulating primary nucleation. *Nat Chem Biol,* 11**,** 229-34.

Galvagnion, C., Marlet, F. R., Cerri, S., Schapira, A. H. V., Blandini, F. & Di Monte, D. A. 2022. Sphingolipid changes in Parkinson L444P GBA mutation fibroblasts promote alpha-synuclein aggregation. *Brain,* 145**,** 1038-1051.

Gan-Or, Z., Amshalom, I., Kilarski, L. L., Bar-Shira, A., Gana-Weisz, M., Mirelman, A., Marder, K., Bressman, S., Giladi, N. & Orr-Urtreger, A. 2015a. Differential effects of severe vs mild GBA mutations on Parkinson disease. *Neurology,* 84**,** 880-7.

Gan-Or, Z., Bar-Shira, A., Mirelman, A., Gurevich, T., Kedmi, M., Giladi, N. & Orr-Urtreger, A. 2010. LRRK2 and GBA mutations differentially affect the initial presentation of Parkinson disease. *Neurogenetics,* 11**,** 121-5.

Gan-Or, Z., Giladi, N., Rozovski, U., Shifrin, C., Rosner, S., Gurevich, T., Bar-Shira, A. & Orr-Urtreger, A. 2008. Genotype-phenotype correlations between GBA mutations and Parkinson disease risk and onset. *Neurology,* 70**,** 2277-83.

Gan-Or, Z., Mirelman, A., Postuma, R. B., Arnulf, I., Bar-Shira, A., Dauvilliers, Y., Desautels, A., Gagnon, J. F., Leblond, C. S., Frauscher, B., Alcalay, R. N., Saunders-Pullman, R., Bressman, S. B., Marder, K., Monaca, C., Hogl, B., Orr-Urtreger, A., Dion, P. A., Montplaisir, J. Y., Giladi, N. & Rouleau, G. A. 2015b. GBA mutations are associated with Rapid Eye Movement Sleep Behavior Disorder. *Ann Clin Transl Neurol,* 2**,** 941-5.

Gao, X., Chen, H., Fung, T. T., Logroscino, G., Schwarzschild, M. A., Hu, F. B. & Ascherio, A. 2007. Prospective study of dietary pattern and risk of Parkinson disease. *Am J Clin Nutr,* 86**,** 1486-94.

Garcia-Ruiz, P. J. & Espay, A. J. 2017. Parkinson Disease: An Evolutionary Perspective. *Front Neurol,* 8**,** 157.

Garcia-Sanz, P., Orgaz, L., Bueno-Gil, G., Espadas, I., Rodriguez-Traver, E., Kulisevsky, J., Gutierrez, A., Davila, J. C., Gonzalez-Polo, R. A., Fuentes, J. M., Mir, P., Vicario, C. & Moratalla, R. 2017. N370S-GBA1 mutation causes lysosomal cholesterol accumulation in Parkinson's disease. *Mov Disord,* 32**,** 1409-1422.

Garrick, J. M., Costa, L. G., Cole, T. B. & Marsillach, J. 2021. Evaluating Gait and Locomotion in Rodents with the CatWalk. *Curr Protoc,* 1**,** e220.

Gary, S. E., Ryan, E., Steward, A. M. & Sidransky, E. 2018. Recent advances in the diagnosis and management of Gaucher disease. *Expert Rev Endocrinol Metab,* 13**,** 107-118.

Gash, D. M., Rutland, K., Hudson, N. L., Sullivan, P. G., Bing, G., Cass, W. A., Pandya, J. D., Liu, M., Choi, D. Y., Hunter, R. L., Gerhardt, G. A., Smith, C. D., Slevin, J. T. & Prince, T. S. 2008. Trichloroethylene: Parkinsonism and complex 1 mitochondrial neurotoxicity. *Ann Neurol,* 63**,** 184-92.

Gassmann, M. & Bettler, B. 2012. Regulation of neuronal GABA(B) receptor functions by subunit composition. *Nat Rev Neurosci,* 13**,** 380-94.

Gasteiger, E., Gattiker, A., Hoogland, C., Ivanyi, I., Appel, R. D. & Bairoch, A. 2003. ExPASy: The proteomics server for in-depth protein knowledge and analysis. *Nucleic Acids Res,* 31**,** 3784-8.

Gaucher, P. C. E. 1882. De l'Epithelioma Primitif de la Rate: Hypertrophie Idiopathique de la Rate sans Leucémie [French]. Thesis**,** Faculté de Medécine de Paris.

Gegg, M. E., Burke, D., Heales, S. J., Cooper, J. M., Hardy, J., Wood, N. W. & Schapira, A. H. 2012. Glucocerebrosidase deficiency in substantia nigra of parkinson disease brains. *Ann Neurol,* 72**,** 455-63.

Gegg, M. E., Sweet, L., Wang, B. H., Shihabuddin, L. S., Sardi, S. P. & Schapira, A. H. 2015. No evidence for substrate accumulation in Parkinson brains with GBA mutations. *Mov Disord,* 30**,** 1085-9.

Gegg, M. E., Verona, G. & Schapira, A. H. V. 2020. Glucocerebrosidase deficiency promotes release of alpha-synuclein fibrils from cultured neurons. *Hum Mol Genet,* 29**,** 1716-1728.

Geldenhuys, W. J., Guseman, T. L., Pienaar, I. S., Dluzen, D. E. & Young, J. W. 2015. A novel biomechanical analysis of gait changes in the MPTP mouse model of Parkinson's disease. *PeerJ,* 3**,** e1175.

George, J. M., Jin, H., Woods, W. S. & Clayton, D. F. 1995. Characterization of a novel protein regulated during the critical period for song learning in the zebra finch. *Neuron,* 15**,** 361-72.

Gerfen, C. R. & Bolam, J. P. 2010. The Neuroanatomical Organization of the Basal Ganglia. *Handbook of Basal Ganglia Structure and Function,* 20**,** 3-28.

Gething, M. J. 1999. Role and regulation of the ER chaperone BiP. *Semin Cell Dev Biol,* 10**,** 465-72.

Gewirtz, J. C., Mcnish, K. A. & Davis, M. 2000. Is the hippocampus necessary for contextual fear conditioning? *Behav Brain Res,* 110**,** 83-95.

Ghit, A., Assal, D., Al-Shami, A. S. & Hussein, D. E. E. 2021. GABA(A) receptors: structure, function, pharmacology, and related disorders. *J Genet Eng Biotechnol,* 19**,** 123.

Gibson, L. L., Weintraub, D., Lemmen, R., Perera, G., Chaudhuri, K. R., Svenningsson, P. & Aarsland, D. 2024. Risk of Dementia in Parkinson's Disease: A Systematic Review and Meta-Analysis. *Mov Disord,* 39**,** 1697-1709.

Giguere, N., Burke Nanni, S. & Trudeau, L. E. 2018. On Cell Loss and Selective Vulnerability of Neuronal Populations in Parkinson's Disease. *Front Neurol,* 9**,** 455.

Giladi, N., Alcalay, R. N., Cutter, G., Gasser, T., Gurevich, T., Hoglinger, G. U., Marek, K., Pacchetti, C., Schapira, A. H. V., Scherzer, C. R., Simuni, T., Minini, P., Sardi, S. P. & Peterschmitt, M. J. 2023. Safety and efficacy of venglustat in GBA1-associated Parkinson's disease: an international, multicentre, double-blind, randomised, placebo-controlled, phase 2 trial. *Lancet Neurol,* 22**,** 661-671.

Ginns, E. I., Choudary, P. V., Tsuji, S., Martin, B., Stubblefield, B., Sawyer, J., Hozier, J. & Barranger, J. A. 1985. Gene mapping and leader polypeptide sequence of human glucocerebrosidase: implications for Gaucher disease. *Proc Natl Acad Sci U S A,* 82**,** 7101-5.

Ginns, E. I., Mak, S. K., Ko, N., Karlgren, J., Akbarian, S., Chou, V. P., Guo, Y., Lim, A., Samuelsson, S., Lamarca, M. L., Vazquez-Derose, J. & Manning-Bog, A. B. 2014. Neuroinflammation and alpha-synuclein accumulation in response to glucocerebrosidase deficiency are accompanied by synaptic dysfunction. *Mol Genet Metab,* 111**,** 152-62.

Giros, B., Jaber, M., Jones, S. R., Wightman, R. M. & Caron, M. G. 1996. Hyperlocomotion and indifference to cocaine and amphetamine in mice lacking the dopamine transporter. *Nature,* 379**,** 606-12.

Glajch, K. E., Moors, T. E., Chen, Y., Bechade, P. A., Nam, A. Y., Rajsombath, M. M., Mccaffery, T. D., Dettmer, U., Weihofen, A., Hirst, W. D., Selkoe, D. J. & Nuber, S. 2021. Wild-type GBA1 increases the alpha-synuclein tetramer-monomer ratio, reduces lipid-rich aggregates, and attenuates motor and cognitive deficits in mice. *Proc Natl Acad Sci U S A,* 118.

Gleason, A., Tayebi, N., Lopez, G. & Sidransky, E. 2022a. No Evidence That Glucosylsphingosine Is a Biomarker for Parkinson's Disease: Statistical Differences Do Not Necessarily Indicate Biological Significance. *Mov Disord,* 37**,** 653.

Gleason, A. M., Tayebi, N., Lopez, G. J. & Sidransky, E. 2022b. Reply to: "Overlapping Ranges in Levels Indicate That Hexosylsphingosine Is Not a Clinically Relevant Biomarker for GBA1-Associated Parkinson's Disease". *Mov Disord,* 37**,** 1781-1782.

Goedert, M., Spillantini, M. G., Del Tredici, K. & Braak, H. 2013. 100 years of Lewy pathology. *Nat Rev Neurol,* 9**,** 13-24.

Goker-Alpan, O., Schiffmann, R., Lamarca, M. E., Nussbaum, R. L., Mcinerney-Leo, A. & Sidransky, E. 2004. Parkinsonism among Gaucher disease carriers. *J Med Genet,* 41**,** 937-40.

Goldman, S. M. 2014. Environmental toxins and Parkinson's disease. *Annu Rev Pharmacol Toxicol,* 54**,** 141-64.

Goldman, S. M., Weaver, F. M., Stroupe, K. T., Cao, L., Gonzalez, B., Colletta, K., Brown, E. G. & Tanner, C. M. 2023. Risk of Parkinson Disease Among Service Members at Marine Corps Base Camp Lejeune. *JAMA Neurol,* 80**,** 673-681.

Goldstein, O., Gana-Weisz, M., Cohen-Avinoam, D., Shiner, T., Thaler, A., Cedarbaum, J. M., John, S., Lalioti, M., Gurevich, T., Bar-Shira, A., Mirelman, A., Giladi, N. & Orr-Urtreger, A. 2019. Revisiting the non-Gaucher-GBA-E326K carrier state: Is it sufficient to increase Parkinson's disease risk? *Mol Genet Metab,* 128**,** 470-475.

Gouveia, K. & Hurst, J. L. 2017. Optimising reliability of mouse performance in behavioural testing: the major role of non-aversive handling. *Sci Rep,* 7**,** 44999.

Grabowski, G. A., Zimran, A. & Ida, H. 2015. Gaucher disease types 1 and 3: Phenotypic characterization of large populations from the ICGG Gaucher Registry. *Am J Hematol,* 90 Suppl 1**,** S12-8.

Grace, M. E., Newman, K. M., Scheinker, V., Berg-Fussman, A. & Grabowski, G. A. 1994. Analysis of human acid beta-glucosidase by site-directed mutagenesis and heterologous expression. *J Biol Chem,* 269**,** 2283-91.

Gray, R., Ives, N., Rick, C., Patel, S., Gray, A., Jenkinson, C., Mcintosh, E., Wheatley, K., Williams, A., Clarke, C. E. & Pd Med Collaborative Group 2014. Long-term effectiveness of dopamine agonists and monoamine oxidase B inhibitors compared with levodopa as initial treatment for Parkinson's disease (PD MED): a large, open-label, pragmatic randomised trial. *Lancet,* 384**,** 1196-205.

Gries, M., Christmann, A., Schulte, S., Weyland, M., Rommel, S., Martin, M., Baller, M., Roth, R., Schmitteckert, S., Unger, M., Liu, Y., Sommer, F., Muhlhaus, T., Schroda, M., Timmermans, J. P., Pintelon, I., Rappold, G. A., Britschgi, M., Lashuel, H., Menger, M. D., Laschke, M. W., Niesler, B. & Schafer, K. H. 2021. Parkinson mice show functional and molecular changes in the gut long before motoric disease onset. *Mol Neurodegener,* 16**,** 34.

Grinevich, V. P., Zakirov, A. N., Berseneva, U. V., Gerasimova, E. V., Gainetdinov, R. R. & Budygin, E. A. 2022. Applying a Fast-Scan Cyclic Voltammetry to Explore Dopamine Dynamics in Animal Models of Neuropsychiatric Disorders. *Cells,* 11.

Groninger, M., Sabin, J., Kaaks, R., Amiano, P., Aune, D., Castro, N. C., Guevara, M., Hansen, J., Homann, J., Masala, G., Nicolas, G., Peters, S., Sacerdote, C., Sanchez, M. J., De Magistris, M. S., Sieri, S., Vermeulen, R., Zhao, Y., Lill, C. M. & Katzke, V. A. 2024. Associations of milk, dairy products, calcium and vitamin D intake with risk of developing Parkinson s disease within the EPIC4ND cohort. *Eur J Epidemiol,* 39**,** 1251-1265.

Grosso Jasutkar, H., Oh, S. E. & Mouradian, M. M. 2022. Therapeutics in the Pipeline Targeting alpha-Synuclein for Parkinson's Disease. *Pharmacol Rev,* 74**,** 207-237.

Guimaraes, R. P., Resende, M. C. S., Tavares, M. M., Belardinelli De Azevedo, C., Ruiz, M. C. M. & Mortari, M. R. 2024. Construct, Face, and Predictive Validity of Parkinson's Disease Rodent Models. *Int J Mol Sci,* 25.

Guo, H. B., Perminov, A., Bekele, S., Kedziora, G., Farajollahi, S., Varaljay, V., Hinkle, K., Molinero, V., Meister, K., Hung, C., Dennis, P., Kelley-Loughnane, N. & Berry, R. 2022. AlphaFold2 models indicate that protein sequence determines both structure and dynamics. *Sci Rep,* 12**,** 10696.

Gupta, N., Oppenheim, I. M., Kauvar, E. F., Tayebi, N. & Sidransky, E. 2011. Type 2 Gaucher disease: phenotypic variation and genotypic heterogeneity. *Blood Cells Mol Dis,* 46**,** 75-84.

Gustavsson, E. K., Sethi, S., Gao, Y., Brenton, J. W., Garcia-Ruiz, S., Zhang, D., Garza, R., Reynolds, R. H., Evans, J. R., Chen, Z., Grant-Peters, M., Macpherson, H., Montgomery, K., Dore, R., Wernick, A. I., Arber, C., Wray, S., Gandhi, S., Esselborn, J., Blauwendraat, C., Douse, C. H., Adami, A., Atacho, D. a. M., Kouli, A., Quaegebeur, A., Barker, R. A., Englund, E., Platt, F., Jakobsson, J., Wood, N. W., Houlden, H., Saini, H., Bento, C. F., Hardy, J. & Ryten, M. 2024. The annotation of GBA1 has been concealed by its protein-coding pseudogene GBAP1. *Sci Adv,* 10**,** eadk1296.

Guzman, J. N., Sanchez-Padilla, J., Wokosin, D., Kondapalli, J., Ilijic, E., Schumacker, P. T. & Surmeier, D. J. 2010. Oxidant stress evoked by pacemaking in dopaminergic neurons is attenuated by DJ-1. *Nature,* 468**,** 696-700.

Haaxma, C. A., Bloem, B. R., Borm, G. F., Oyen, W. J., Leenders, K. L., Eshuis, S., Booij, J., Dluzen, D. E. & Horstink, M. W. 2007. Gender differences in Parkinson's disease. *J Neurol Neurosurg Psychiatry,* 78**,** 819-24.

Hallett, P. J., Huebecker, M., Brekk, O. R., Moloney, E. B., Rocha, E. M., Priestman, D. A., Platt, F. M. & Isacson, O. 2018. Glycosphingolipid levels and glucocerebrosidase activity are altered in normal aging of the mouse brain. *Neurobiol Aging,* 67**,** 189-200.

Halperin, A., Elstein, D. & Zimran, A. 2006. Increased incidence of Parkinson disease among relatives of patients with Gaucher disease. *Blood Cells Mol Dis,* 36**,** 426-8.

Han, F., Grimes, D. A., Li, F., Wang, T., Yu, Z., Song, N., Wu, S., Racacho, L. & Bulman, D. E. 2016. Mutations in the glucocerebrosidase gene are common in patients with Parkinson's disease from Eastern Canada. *Int J Neurosci,* 126**,** 415-21.

Han, T. U., Sam, R. & Sidransky, E. 2020. Small Molecule Chaperones for the Treatment of Gaucher Disease and GBA1-Associated Parkinson Disease. *Front Cell Dev Biol,* 8**,** 271.

Handley, S. L. & Mithani, S. 1984. Effects of alpha-adrenoceptor agonists and antagonists in a maze-exploration model of 'fear'-motivated behaviour. *Naunyn Schmiedebergs Arch Pharmacol,* 327**,** 1-5.

Hariz, M. & Blomstedt, P. 2022. Deep brain stimulation for Parkinson's disease. *J Intern Med,* 292**,** 764-778.

Harraz, M. M. 2023. Selective dopaminergic vulnerability in Parkinson's disease: new insights into the role of DAT. *Front Neurosci,* 17**,** 1219441.

Harris, S., Narayanan, N. S. & Tranel, D. 2023. Does Black vs. White race affect practitioners' appraisal of Parkinson's disease? *NPJ Parkinsons Dis,* 9**,** 106.

Hauser, R. A., Rascol, O., Korczyn, A. D., Jon Stoessl, A., Watts, R. L., Poewe, W., De Deyn, P. P. & Lang, A. E. 2007. Ten-year follow-up of Parkinson's disease patients randomized to initial therapy with ropinirole or levodopa. *Mov Disord,* 22**,** 2409-17.

Hawkins-Salsbury, J. A., Parameswar, A. R., Jiang, X., Schlesinger, P. H., Bongarzone, E., Ory, D. S., Demchenko, A. V. & Sands, M. S. 2013. Psychosine, the cytotoxic sphingolipid that accumulates in globoid cell leukodystrophy, alters membrane architecture. *J Lipid Res,* 54**,** 3303-11.

He, Y., Kaya, I., Shariatgorji, R., Lundkvist, J., Wahlberg, L. U., Nilsson, A., Mamula, D., Kehr, J., Zareba-Paslawska, J., Biverstal, H., Chergui, K., Zhang, X., Andren, P. E. & Svenningsson, P. 2023. Prosaposin maintains lipid homeostasis in dopamine neurons and counteracts experimental parkinsonism in rodents. *Nat Commun,* 14**,** 5804.

Healy, D. G., Falchi, M., O'sullivan, S. S., Bonifati, V., Durr, A., Bressman, S., Brice, A., Aasly, J., Zabetian, C. P., Goldwurm, S., Ferreira, J. J., Tolosa, E., Kay, D. M., Klein, C., Williams, D. R., Marras, C., Lang, A. E., Wszolek, Z. K., Berciano, J., Schapira, A. H., Lynch, T., Bhatia, K. P., Gasser, T., Lees, A. J., Wood, N. W. & International, L. C. 2008. Phenotype, genotype, and worldwide genetic penetrance of LRRK2-associated Parkinson's disease: a case-control study. *Lancet Neurol,* 7**,** 583-90.

Heinrich, M., Wickel, M., Schneider-Brachert, W., Sandberg, C., Gahr, J., Schwandner, R., Weber, T., Saftig, P., Peters, C., Brunner, J., Kronke, M. & Schutze, S. 1999. Cathepsin D targeted by acid sphingomyelinase-derived ceramide. *EMBO J,* 18**,** 5252-63.

Heinzel, J., Langle, G., Oberhauser, V., Hausner, T., Kolbenschlag, J., Prahm, C., Grillari, J. & Hercher, D. 2020. Use of the CatWalk gait analysis system to assess functional recovery in rodent models of peripheral nerve injury - a systematic review. *J Neurosci Methods,* 345**,** 108889.

Hely, M. A., Reid, W. G., Adena, M. A., Halliday, G. M. & Morris, J. G. 2008. The Sydney multicenter study of Parkinson's disease: the inevitability of dementia at 20 years. *Mov Disord,* 23**,** 837-44.

Henderson, M. X., Sedor, S., Mcgeary, I., Cornblath, E. J., Peng, C., Riddle, D. M., Li, H. L., Zhang, B., Brown, H. J., Olufemi, M. F., Bassett, D. S., Trojanowski, J. Q. & Lee, V. M. Y. 2020. Glucocerebrosidase Activity Modulates Neuronal Susceptibility to Pathological alpha-Synuclein Insult. *Neuron,* 105**,** 822-836 e7.

Heng, N., Malek, N., Lawton, M. A., Nodehi, A., Pitz, V., Grosset, K. A., Ben-Shlomo, Y. & Grosset, D. G. 2023. Striatal Dopamine Loss in Early Parkinson's Disease: Systematic Review and Novel Analysis of Dopamine Transporter Imaging. *Mov Disord Clin Pract,* 10**,** 539-546.

Herman, T., Weiss, A., Brozgol, M., Giladi, N. & Hausdorff, J. M. 2014. Gait and balance in Parkinson's disease subtypes: objective measures and classification considerations. *J Neurol,* 261**,** 2401-10.

Hersch, S. M., Yi, H., Heilman, C. J., Edwards, R. H. & Levey, A. I. 1997. Subcellular localization and molecular topology of the dopamine transporter in the striatum and substantia nigra. *J Comp Neurol,* 388**,** 211-27.

Hertz, E., Chen, Y. & Sidransky, E. 2024. Gaucher disease provides a unique window into Parkinson disease pathogenesis. *Nat Rev Neurol,* 20**,** 526-540.

Hiraiwa, M., Martin, B. M., Kishimoto, Y., Conner, G. E., Tsuji, S. & O'brien, J. S. 1997. Lysosomal proteolysis of prosaposin, the precursor of saposins (sphingolipid activator proteins): its mechanism and inhibition by ganglioside. *Arch Biochem Biophys,* 341**,** 17-24.

Hnasko, T. S., Chuhma, N., Zhang, H., Goh, G. Y., Sulzer, D., Palmiter, R. D., Rayport, S. & Edwards, R. H. 2010. Vesicular glutamate transport promotes dopamine storage and glutamate corelease in vivo. *Neuron,* 65**,** 643-56.

Ho, M. W. & O'brien, J. S. 1971. Gaucher's disease: deficiency of 'acid' -glucosidase and reconstitution of enzyme activity in vitro. *Proc Natl Acad Sci U S A,* 68**,** 2810-3.

Honorato, R. V., Trellet, M. E., Jimenez-Garcia, B., Schaarschmidt, J. J., Giulini, M., Reys, V., Koukos, P. I., Rodrigues, J., Karaca, E., Van Zundert, G. C. P., Roel-Touris, J., Van Noort, C. W., Jandova, Z., Melquiond, A. S. J. & Bonvin, A. 2024. The HADDOCK2.4 web server for integrative modeling of biomolecular complexes. *Nat Protoc,* 19**,** 3219-3241.

Hopfner, F., Schulte, E. C., Mollenhauer, B., Bereznai, B., Knauf, F., Lichtner, P., Zimprich, A., Haubenberger, D., Pirker, W., Brucke, T., Peters, A., Gieger, C., Kuhlenbaumer, G., Trenkwalder, C. & Winkelmann, J. 2013. The role of SCARB2 as susceptibility factor in Parkinson's disease. *Mov Disord,* 28**,** 538-40.

Horowitz, M., Braunstein, H., Zimran, A., Revel-Vilk, S. & Goker-Alpan, O. 2022. Lysosomal functions and dysfunctions: Molecular and cellular mechanisms underlying Gaucher disease and its association with Parkinson disease. *Adv Drug Deliv Rev,* 187**,** 114402.

Horowitz, M., Wilder, S., Horowitz, Z., Reiner, O., Gelbart, T. & Beutler, E. 1989. The human glucocerebrosidase gene and pseudogene: structure and evolution. *Genomics,* 4**,** 87-96.

Hruska, K. S., Lamarca, M. E., Scott, C. R. & Sidransky, E. 2008. Gaucher disease: mutation and polymorphism spectrum in the glucocerebrosidase gene (GBA). *Hum Mutat,* 29**,** 567-83.

Huang, Y., Deng, L., Zhong, Y. & Yi, M. 2018. The Association between E326K of GBA and the Risk of Parkinson's Disease. *Parkinsons Dis,* 2018**,** 1048084.

Huebecker, M., Moloney, E. B., Van Der Spoel, A. C., Priestman, D. A., Isacson, O., Hallett, P. J. & Platt, F. M. 2019. Reduced sphingolipid hydrolase activities, substrate accumulation and ganglioside decline in Parkinson's disease. *Mol Neurodegener,* 14**,** 40.

Hughes, D. A. & Pastores, G. M. 2023. Gaucher Disease. *In:* ADAM, M. P., FELDMAN, J. & MIRZAA, G. M. (eds.) *GeneReviews [Internet].* Seattle (WA): University of Washington.

Hughes, K. C., Gao, X., Kim, I. Y., Wang, M., Weisskopf, M. G., Schwarzschild, M. A. & Ascherio, A. 2017. Intake of dairy foods and risk of Parkinson disease. *Neurology,* 89**,** 46-52.

Huh, Y. E., Park, H., Chiang, M. S. R., Tuncali, I., Liu, G., Locascio, J. J., Shirvan, J., Hutten, S. J., Rotunno, M. S., Viel, C., Shihabuddin, L. S., Wang, B., Sardi, S. P. & Scherzer, C. R. 2021. Glucosylceramide in cerebrospinal fluid of patients with GBA-associated and idiopathic Parkinson's disease enrolled in PPMI. *NPJ Parkinsons Dis,* 7**,** 102.

Hunn, B. H. M., Vingill, S., Threlfell, S., Alegre-Abarrategui, J., Magdelyns, M., Deltheil, T., Bengoa-Vergniory, N., Oliver, P. L., Cioroch, M., Doig, N. M., Bannerman, D. M., Cragg, S. J. & Wade-Martins, R. 2019. Impairment of Macroautophagy in Dopamine Neurons Has Opposing Effects on Parkinsonian Pathology and Behavior. *Cell Rep,* 29**,** 920-931 e7.

Hustad, E. & Aasly, J. O. 2020. Clinical and Imaging Markers of Prodromal Parkinson's Disease. *Front Neurol,* 11**,** 395.

Ibanez, P., Bonnet, A. M., Debarges, B., Lohmann, E., Tison, F., Pollak, P., Agid, Y., Durr, A. & Brice, A. 2004. Causal relation between alpha-synuclein gene duplication and familial Parkinson's disease. *Lancet,* 364**,** 1169-71.

Ikuno, M., Yamakado, H., Akiyama, H., Parajuli, L. K., Taguchi, K., Hara, J., Uemura, N., Hatanaka, Y., Higaki, K., Ohno, K., Tanaka, M., Koike, M., Hirabayashi, Y. & Takahashi, R. 2019. GBA haploinsufficiency accelerates alpha-synuclein pathology with altered lipid metabolism in a prodromal model of Parkinson's disease. *Hum Mol Genet,* 28**,** 1894-1904.

Imbalzano, G., Ledda, C., Romagnolo, A., Covolo, A., Lopiano, L. & Artusi, C. A. 2024. Neurological symptoms in adults with Gaucher disease: a systematic review. *J Neurol,* 271**,** 3897-3907.

Ingram, S. L., Prasad, B. M. & Amara, S. G. 2002. Dopamine transporter-mediated conductances increase excitability of midbrain dopamine neurons. *Nat Neurosci,* 5**,** 971-8.

Irizarry, M. C., Kim, T. W., Mcnamara, M., Tanzi, R. E., George, J. M., Clayton, D. F. & Hyman, B. T. 1996. Characterization of the precursor protein of the non-A beta component of senile plaques (NACP) in the human central nervous system. *J Neuropathol Exp Neurol,* 55**,** 889-95.

Isaacson, S. H., Hauser, R. A., Pahwa, R., Gray, D. & Duvvuri, S. 2023. Dopamine agonists in Parkinson's disease: Impact of D1-like or D2-like dopamine receptor subtype selectivity and avenues for future treatment. *Clin Park Relat Disord,* 9**,** 100212.

Istaiti, M., Yahalom, G., Cohen, M., Skrahina, V., Skrahin, A., Lukas, J., Rolfs, A. & Zimran, A. 2025. Sidransky Syndrome-GBA1-Related Parkinson's Disease and Its Targeted Therapies. *Int J Mol Sci,* 26.

Iwaki, H., Blauwendraat, C., Leonard, H. L., Liu, G., Maple-Grodem, J., Corvol, J. C., Pihlstrom, L., Van Nimwegen, M., Hutten, S. J., Nguyen, K. H., Rick, J., Eberly, S., Faghri, F., Auinger, P., Scott, K. M., Wijeyekoon, R., Van Deerlin, V. M., Hernandez, D. G., Day-Williams, A. G., Brice, A., Alves, G., Noyce, A. J., Tysnes, O. B., Evans,

J. R., Breen, D. P., Estrada, K., Wegel, C. E., Danjou, F., Simon, D. K., Ravina, B., Toft, M., Heutink, P., Bloem, B. R., Weintraub, D., Barker, R. A., Williams-Gray, C. H., Van De Warrenburg, B. P., Van Hilten, J. J., Scherzer, C. R., Singleton, A. B. & Nalls, M. A. 2019. Genetic risk of Parkinson disease and progression:: An analysis of 13 longitudinal cohorts. *Neurol Genet,* 5**,** e348.

Iwaki, H., Blauwendraat, C., Leonard, H. L., Makarious, M. B., Kim, J. J., Liu, G., Maple-Grodem, J., Corvol, J. C., Pihlstrom, L., Van Nimwegen, M., Smolensky, L., Amondikar, N., Hutten, S. J., Frasier, M., Nguyen, K. H., Rick, J., Eberly, S., Faghri, F., Auinger, P., Scott, K. M., Wijeyekoon, R., Van Deerlin, V. M., Hernandez, D. G., Gibbs, R. J., Day-Williams, A. G., Brice, A., Alves, G., Noyce, A. J., Tysnes, O. B., Evans, J. R., Breen, D. P., Estrada, K., Wegel, C. E., Danjou, F., Simon, D. K., Andreassen, O. A., Ravina, B., Toft, M., Heutink, P., Bloem, B. R., Weintraub, D., Barker, R. A., Williams-Gray, C. H., Van De Warrenburg, B. P., Van Hilten, J. J., Scherzer, C. R., Singleton, A. B. & Nalls, M. A. 2021. Differences in the Presentation and Progression of Parkinson's Disease by Sex. *Mov Disord,* 36**,** 106-117.

Jackson, A., Forsyth, C. B., Shaikh, M., Voigt, R. M., Engen, P. A., Ramirez, V. & Keshavarzian, A. 2019. Diet in Parkinson's Disease: Critical Role for the Microbiome. *Front Neurol,* 10**,** 1245.

James, S. L., Abate, D. & Collaborators, G. D. a. I. I. a. P. 2018. Global, regional, and national incidence, prevalence, and years lived with disability for 354 diseases and injuries for 195 countries and territories, 1990-2017: a systematic analysis for the Global Burden of Disease Study 2017. *Lancet,* 392**,** 1789-1858.

Janezic, S., Threlfell, S., Dodson, P. D., Dowie, M. J., Taylor, T. N., Potgieter, D., Parkkinen, L., Senior, S. L., Anwar, S., Ryan, B., Deltheil, T., Kosillo, P., Cioroch, M., Wagner, K., Ansorge, O., Bannerman, D. M., Bolam, J. P., Magill, P. J., Cragg, S. J. & Wade-Martins, R. 2013. Deficits in dopaminergic transmission precede neuron loss and dysfunction in a new Parkinson model. *Proc Natl Acad Sci U S A,* 110**,** E4016-25.

Jankovic, J. 2008. Parkinson's disease: clinical features and diagnosis. *J Neurol Neurosurg Psychiatry,* 79**,** 368-76.

Jankovic, J. & Kapadia, A. S. 2001. Functional decline in Parkinson disease. *Arch Neurol,* 58**,** 1611-5.

Jankovic, J., Mcdermott, M., Carter, J., Gauthier, S., Goetz, C., Golbe, L., Huber, S., Koller, W., Olanow, C., Shoulson, I. & Et Al. 1990. Variable expression of Parkinson's disease: a base-line analysis of the DATATOP cohort. The Parkinson Study Group. *Neurology,* 40**,** 1529-34.

Janssen Daalen, J. M., Van Den Bergh, R., Prins, E. M., Moghadam, M. S. C., Van Den Heuvel, R., Veen, J., Mathur, S., Meijerink, H., Mirelman, A., Darweesh, S. K. L., Evers, L. J. W. & Bloem, B. R. 2024. Digital biomarkers for non-motor symptoms in Parkinson's disease: the state of the art. *NPJ Digit Med,* 7**,** 186.

Jellinger, K. A. 2019. Is Braak staging valid for all types of Parkinson's disease? *J Neural Transm (Vienna),* 126**,** 423-431.

Jenkins, B., Ronis, M. & Koulman, A. 2020. LC-MS Lipidomics: Exploiting a Simple High-Throughput Method for the Comprehensive Extraction of Lipids in a Ruminant Fat Dose-Response Study. *Metabolites,* 10.

Jesus, S., Huertas, I., Bernal-Bernal, I., Bonilla-Toribio, M., Caceres-Redondo, M. T., Vargas-Gonzalez, L., Gomez-Llamas, M., Carrillo, F., Calderon, E., Carballo, M., Gomez-Garre, P. & Mir, P. 2016. GBA Variants Influence Motor and Non-Motor Features of Parkinson's Disease. *PLoS One,* 11**,** e0167749.

Jia, F., Fellner, A. & Kumar, K. R. 2022. Monogenic Parkinson's Disease: Genotype, Phenotype, Pathophysiology, and Genetic Testing. *Genes (Basel),* 13.

Jian, J., Tian, Q. Y., Hettinghouse, A., Zhao, S., Liu, H., Wei, J., Grunig, G., Zhang, W., Setchell, K. D. R., Sun, Y., Overkleeft, H. S., Chan, G. L. & Liu, C. J. 2016a. Progranulin Recruits HSP70 to beta-Glucocerebrosidase and Is Therapeutic Against Gaucher Disease. *EBioMedicine,* 13**,** 212-224.

Jian, J., Zhao, S., Tian, Q. Y., Liu, H., Zhao, Y., Chen, W. C., Grunig, G., Torres, P. A., Wang, B. C., Zeng, B., Pastores, G., Tang, W., Sun, Y., Grabowski, G. A., Kong, M. X., Wang, G., Chen, Y., Liang, F., Overkleeft, H. S., Saunders-Pullman, R., Chan, G. L. & Liu, C. J. 2016b. Association Between Progranulin and Gaucher Disease. *EBioMedicine,* 11**,** 127-137.

John, C. E. & Jones, S. R. 2007. Fast Scan Cyclic Voltammetry of Dopamine and Serotonin in Mouse Brain Slices. *In:* MICHAEL, A. C. & BORLAND, L. M., EDITORS (eds.) *Electrochemical Methods for Neuroscience.* Boca Raton (Fl): CRC Press/Taylor & Francis.

Johnson, M. E., Bergkvist, L., Stetzik, L., Steiner, J. A., Meyerdirk, L., Schulz, E., Wolfrum, E., Luk, K. C., Wesson, D. W., Krainc, D. & Brundin, P. 2021. Heterozygous GBA D409V and ATP13a2 mutations do not exacerbate pathological alpha-synuclein spread in the prodromal preformed fibrils model in young mice. *Neurobiol Dis,* 159**,** 105513.

Jones, S. R., Gainetdinov, R. R., Jaber, M., Giros, B., Wightman, R. M. & Caron, M. G. 1998. Profound neuronal plasticity in response to inactivation of the dopamine transporter. *Proc Natl Acad Sci U S A,* 95**,** 4029-34.

Jonsson, L. M., Murray, G. J., Sorrell, S. H., Strijland, A., Aerts, J. F., Ginns, E. I., Barranger, J. A., Tager, J. M. & Schram, A. W. 1987. Biosynthesis and maturation of glucocerebrosidase in Gaucher fibroblasts. *Eur J Biochem,* 164**,** 171-9.

Jumper, J., Evans, R., Pritzel, A., Green, T., Figurnov, M., Ronneberger, O., Tunyasuvunakool, K., Bates, R., Zidek, A., Potapenko, A., Bridgland, A., Meyer, C., Kohl, S. a. A., Ballard, A. J., Cowie, A., Romera-Paredes, B., Nikolov, S., Jain, R., Adler, J., Back, T., Petersen, S., Reiman, D., Clancy, E., Zielinski, M., Steinegger, M., Pacholska, M., Berghammer, T., Bodenstein, S., Silver, D., Vinyals, O., Senior, A. W., Kavukcuoglu, K., Kohli, P. & Hassabis, D. 2021. Highly accurate protein structure prediction with AlphaFold. *Nature,* 596**,** 583-589.

Kahnau, P., Mieske, P., Wilzopolski, J., Kalliokoski, O., Mandillo, S., Holter, S. M., Voikar, V., Amfim, A., Badurek, S., Bartelik, A., Caruso, A., Cater, M., Ey, E., Golini, E., Jaap, A., Hrncic, D., Kiryk, A., Lang, B., Loncarevic-Vasiljkovic, N., Meziane, H., Radzeviciene, A., Rivalan, M., Scattoni, M. L., Torquet, N., Trifkovic, J., Ulfhake, B., Thone-Reineke, C., Diederich, K., Lewejohann, L. & Hohlbaum, K. 2023. A systematic review of the development and application of home cage monitoring in laboratory mice and rats. *BMC Biol,* 21**,** 256.

Kalia, L. V. & Lang, A. E. 2015. Parkinson's disease. *Lancet,* 386**,** 896-912.

Kaluve, A. M., Le, J. T. & Graham, B. M. 2022. Female rodents are not more variable than male rodents: A meta-analysis of preclinical studies of fear and anxiety. *Neurosci Biobehav Rev,* 143**,** 104962.

Kamath, S. D., Holla, V. V., Phulpagar, P., Kamble, N., Yadav, R., Muthusamy, B. & Pal, P. K. 2024. Clinicogenetic Characterization of Patients with PD and Heterozygous GBA1 Variants in an Indian Cohort. *Mov Disord,* 39**,** 628-630.

Kashani, A., Betancur, C., Giros, B., Hirsch, E. & El Mestikawy, S. 2007. Altered expression of vesicular glutamate transporters VGLUT1 and VGLUT2 in Parkinson disease. *Neurobiol Aging,* 28**,** 568-78.

Keatinge, M., Bui, H., Menke, A., Chen, Y. C., Sokol, A. M., Bai, Q., Ellett, F., Da Costa, M., Burke, D., Gegg, M., Trollope, L., Payne, T., Mctighe, A., Mortiboys, H., De

Jager, S., Nuthall, H., Kuo, M. S., Fleming, A., Schapira, A. H., Renshaw, S. A., Highley, J. R., Chacinska, A., Panula, P., Burton, E. A., O'neill, M. J. & Bandmann, O. 2015. Glucocerebrosidase 1 deficient Danio rerio mirror key pathological aspects of human Gaucher disease and provide evidence of early microglial activation preceding alpha-synuclein-independent neuronal cell death. *Hum Mol Genet,* 24**,** 6640-52.

Kedariti, M., Frattini, E., Baden, P., Cogo, S., Civiero, L., Ziviani, E., Zilio, G., Bertoli, F., Aureli, M., Kaganovich, A., Cookson, M. R., Stefanis, L., Surface, M., Deleidi, M., Di Fonzo, A., Alcalay, R. N., Rideout, H., Greggio, E. & Plotegher, N. 2022. LRRK2 kinase activity regulates GCase level and enzymatic activity differently depending on cell type in Parkinson's disease. *NPJ Parkinsons Dis,* 8**,** 92.

Kelly, V. E., Johnson, C. O., Mcgough, E. L., Shumway-Cook, A., Horak, F. B., Chung, K. A., Espay, A. J., Revilla, F. J., Devoto, J., Wood-Siverio, C., Factor, S. A., Cholerton, B., Edwards, K. L., Peterson, A. L., Quinn, J. F., Montine, T. J., Zabetian, C. P. & Leverenz, J. B. 2015. Association of cognitive domains with postural instability/gait disturbance in Parkinson's disease. *Parkinsonism Relat Disord,* 21**,** 692-7.

Kilfeather, P., Khoo, J. H., Wagner, K., Liang, H., Caiazza, M. C., An, Y., Zhang, X., Chen, X., Connor-Robson, N., Shang, Z. & Wade-Martins, R. 2024. Single-cell spatial transcriptomic and translatomic profiling of dopaminergic neurons in health, aging, and disease. *Cell Rep,* 43**,** 113784.

Kilkenny, C., Browne, W. J., Cuthill, I. C., Emerson, M. & Altman, D. G. 2010. Improving bioscience research reporting: The ARRIVE guidelines for reporting animal research. *J Pharmacol Pharmacother,* 1**,** 94-9.

Kim, D., Hwang, H., Choi, S., Kwon, S. H., Lee, S., Park, J. H., Kim, S. & Ko, H. S. 2018a. D409H GBA1 mutation accelerates the progression of pathology in A53T alpha-synuclein transgenic mouse model. *Acta Neuropathol Commun,* 6**,** 32.

Kim, J. J., Vitale, D., Otani, D. V., Lian, M. M., Heilbron, K., Andme Research, T., Iwaki, H., Lake, J., Solsberg, C. W., Leonard, H., Makarious, M. B., Tan, E. K., Singleton, A. B., Bandres-Ciga, S., Noyce, A. J., Global Parkinson's Genetics, P., Blauwendraat, C., Nalls, M. A., Foo, J. N. & Mata, I. 2024a. Multi-ancestry genome-wide association meta-analysis of Parkinson's disease. *Nat Genet,* 56**,** 27-36.

Kim, M. J., Jeon, S., Burbulla, L. F. & Krainc, D. 2018b. Acid ceramidase inhibition ameliorates alpha-synuclein accumulation upon loss of GBA1 function. *Hum Mol Genet,* 27**,** 1972-1988.

Kim, M. J., Kim, S., Reinheckel, T. & Krainc, D. 2024b. Inhibition of cysteine protease cathepsin L increases the level and activity of lysosomal glucocerebrosidase. *JCI Insight,* 9.

Kim, S., Wong, Y. C., Gao, F. & Krainc, D. 2021. Dysregulation of mitochondria-lysosome contacts by GBA1 dysfunction in dopaminergic neuronal models of Parkinson's disease. *Nat Commun,* 12**,** 1807.

Kim, S., Yun, S. P., Lee, S., Umanah, G. E., Bandaru, V. V. R., Yin, X., Rhee, P., Karuppagounder, S. S., Kwon, S. H., Lee, H., Mao, X., Kim, D., Pandey, A., Lee, G., Dawson, V. L., Dawson, T. M. & Ko, H. S. 2018c. GBA1 deficiency negatively affects physiological alpha-synuclein tetramers and related multimers. *Proc Natl Acad Sci U S A,* 115**,** 798-803.

Kim, S. T., Son, H. J., Choi, J. H., Ji, I. J. & Hwang, O. 2010. Vertical grid test and modified horizontal grid test are sensitive methods for evaluating motor dysfunctions in the MPTP mouse model of Parkinson's disease. *Brain Res,* 1306**,** 176-83.

Kin, K., Yasuhara, T., Kameda, M. & Date, I. 2019. Animal Models for Parkinson's Disease Research: Trends in the 2000s. *Int J Mol Sci,* 20.

Kitatani, K., Idkowiak-Baldys, J. & Hannun, Y. A. 2008. The sphingolipid salvage pathway in ceramide metabolism and signaling. *Cell Signal,* 20**,** 1010-8.

Klaestrup, I. H., Just, M. K., Holm, K. L., Alstrup, A. K. O., Romero-Ramos, M., Borghammer, P. & Van Den Berge, N. 2022. Impact of aging on animal models of Parkinson's disease. *Front Aging Neurosci,* 14**,** 909273.

Kmiecik, M. J., Micheletti, S., Coker, D., Heilbron, K., Shi, J., Stagaman, K., Filshtein Sonmez, T., Fontanillas, P., Shringarpure, S., Wetzel, M., Rowbotham, H. M., Cannon, P., Shelton, J. F., Hinds, D. A., Tung, J. Y., Andme Research, T., Holmes, M. V., Aslibekyan, S. & Norcliffe-Kaufmann, L. 2024. Genetic analysis and natural history of Parkinson's disease due to the LRRK2 G2019S variant. *Brain,* 147**,** 1996-2008.

Kojima, R., Zurbruegg, M., Li, T., Paslawski, W., Zhang, X. & Svenningsson, P. 2022. Prosaposin Reduces alpha-Synuclein in Cells and Saposin C Dislodges it from Glucosylceramide-enriched Lipid Membranes. *J Mol Neurosci,* 72**,** 2313-2325.

Kondziella, W. 1964. [a New Method for the Measurement of Muscle Relaxation in White Mice]. *Arch Int Pharmacodyn Ther,* 152**,** 277-84.

Konnova, E. A. & Swanberg, M. 2018. Animal Models of Parkinson's Disease. *In:* STOKER, T. B. & GREENLAND, J. C. (eds.) *Parkinson's Disease: Pathogenesis and Clinical Aspects.* Brisbane (AU).

Koprich, J. B., Kalia, L. V. & Brotchie, J. M. 2017. Animal models of alpha-synucleinopathy for Parkinson disease drug development. *Nat Rev Neurosci,* 18**,** 515-529.

Koprivica, V., Stone, D. L., Park, J. K., Callahan, M., Frisch, A., Cohen, I. J., Tayebi, N. & Sidransky, E. 2000. Analysis and classification of 304 mutant alleles in patients with type 1 and type 3 Gaucher disease. *Am J Hum Genet,* 66**,** 1777-86.

Kopytova, A. E., Usenko, T. S., Baydakova, G. V., Nikolaev, M. A., Senkevich, K. A., Izyumchenko, A. D., Tyurin, A. A., Miliukhina, I. V., Emelyanov, A. K., Zakharova, E. Y. & Pchelina, S. N. 2022. Could Blood Hexosylsphingosine Be a Marker for Parkinson's Disease Linked with GBA1 Mutations? *Mov Disord,* 37**,** 1779-1781.

Kordower, J. H., Olanow, C. W., Dodiya, H. B., Chu, Y., Beach, T. G., Adler, C. H., Halliday, G. M. & Bartus, R. T. 2013. Disease duration and the integrity of the nigrostriatal system in Parkinson's disease. *Brain,* 136**,** 2419-31.

Koros, C., Bougea, A., Alefanti, I., Simitsi, A. M., Papagiannakis, N., Pachi, I., Sfikas, E., Antonelou, R. & Stefanis, L. 2024. A Global Perspective of GBA1-Related Parkinson's Disease: A Narrative Review. *Genes (Basel),* 15.

Korschen, H. G., Yildiz, Y., Raju, D. N., Schonauer, S., Bonigk, W., Jansen, V., Kremmer, E., Kaupp, U. B. & Wachten, D. 2013. The non-lysosomal beta-glucosidase GBA2 is a non-integral membrane-associated protein at the endoplasmic reticulum (ER) and Golgi. *J Biol Chem,* 288**,** 3381-93.

Kotagal, V. 2016. Is PIGD a legitimate motor subtype in Parkinson disease? *Ann Clin Transl Neurol,* 3**,** 473-7.

Kouli, A., Torsney, K. M. & Kuan, W. L. 2018. Parkinson's Disease: Etiology, Neuropathology, and Pathogenesis. *In:* STOKER, T. B. & GREENLAND, J. C. (eds.) *Parkinson's Disease: Pathogenesis and Clinical Aspects.* Brisbane (AU): Codon Publications.

Kouwenhoven, W. M., Fortin, G., Penttinen, A. M., Florence, C., Delignat-Lavaud, B., Bourque, M. J., Trimbuch, T., Luppi, M. P., Salvail-Lacoste, A., Legault, P., Poulin, J. F., Rosenmund, C., Awatramani, R. & Trudeau, L. E. 2020. VGluT2 Expression in Dopamine Neurons Contributes to Postlesional Striatal Reinnervation. *J Neurosci,* 40**,** 8262-8275.

Kremer, T., Taylor, K. I., Siebourg-Polster, J., Gerken, T., Staempfli, A., Czech, C., Dukart, J., Galasko, D., Foroud, T., Chahine, L. M., Coffey, C. S., Simuni, T., Weintraub, D., Seibyl, J., Poston, K. L., Toga, A. W., Tanner, C. M., Marek, K., Hutten, S. J., Dziadek, S., Trenkwalder, C., Pagano, G. & Mollenhauer, B. 2021. Longitudinal Analysis of Multiple Neurotransmitter Metabolites in Cerebrospinal Fluid in Early Parkinson's Disease. *Mov Disord,* 36**,** 1972-1978.

Kresojevic, N., Markovic, V., Dobricic, V., Stankovic, I., Stojkovic, T., Tomic, A., Lukic, M. J., Jankovic, M., Marjanovic, A., Brankovic, M., Novakovic, I., Petrovic, I., Dragasevic, N., Svetel, M. & Kostic, V. 2023. Reply to: "Differences in Sex-Specific Frequency of Glucocerebrosidase Variant Carriers and Familial Parkinsonism". *Mov Disord,* 38**,** 712-713.

Krohn, L., Ruskey, J. A., Rudakou, U., Leveille, E., Asayesh, F., Hu, M. T. M., Arnulf, I., Dauvilliers, Y., Hogl, B., Stefani, A., Monaca, C. C., Abril, B., Plazzi, G., Antelmi, E., Ferini-Strambi, L., Heidbreder, A., Boeve, B. F., Espay, A. J., De Cock, V. C., Mollenhauer, B., Sixel-Doring, F., Trenkwalder, C., Sonka, K., Kemlink, D., Figorilli, M., Puligheddu, M., Dijkstra, F., Viaene, M., Oertel, W., Toffoli, M., Gigli, G. L., Valente, M., Gagnon, J. F., Desautels, A., Montplaisir, J. Y., Postuma, R. B., Rouleau, G. A. & Gan-Or, Z. 2020. GBA variants in REM sleep behavior disorder: A multicenter study. *Neurology,* 95**,** e1008-e1016.

Kumar, M., Srikanth, M. P., Deleidi, M., Hallett, P. J., Isacson, O. & Feldman, R. A. 2023. Acid ceramidase involved in pathogenic cascade leading to accumulation of alpha-synuclein in iPSC model of GBA1-associated Parkinson's disease. *Hum Mol Genet,* 32**,** 1888-1900.

Kuo, C. L., Kallemeijn, W. W., Lelieveld, L. T., Mirzaian, M., Zoutendijk, I., Vardi, A., Futerman, A. H., Meijer, A. H., Spaink, H. P., Overkleeft, H. S., Aerts, J. & Artola, M. 2019. In vivo inactivation of glycosidases by conduritol B epoxide and cyclophellitol as revealed by activity-based protein profiling. *FEBS J,* 286**,** 584-600.

Kuo, S. H., Tasset, I., Cheng, M. M., Diaz, A., Pan, M. K., Lieberman, O. J., Hutten, S. J., Alcalay, R. N., Kim, S., Ximenez-Embun, P., Fan, L., Kim, D., Ko, H. S., Yacoubian, T., Kanter, E., Liu, L., Tang, G., Munoz, J., Sardi, S. P., Li, A., Gan, L., Cuervo, A. M. & Sulzer, D. 2022. Mutant glucocerebrosidase impairs alpha-synuclein degradation by blockade of chaperone-mediated autophagy. *Sci Adv,* 8**,** eabm6393.

Kurolap, A., Del Toro, M., Spiegel, R., Gutstein, A., Shafir, G., Cohen, I. J., Barrabes, J. A. & Feldman, H. B. 2019. Gaucher disease type 3c: New patients with unique presentations and review of the literature. *Mol Genet Metab,* 127**,** 138-146.

Kwak, C., Lim, C. S. & Kaang, B. K. 2016. Assessments of cognitive abilities in a mouse model of Parkinson's disease with a touch screen test. *Behav Brain Res,* 301**,** 63-71.

Kweon, S. H., Ryu, H. G., Kwon, S. H., Park, H., Lee, S., Kim, N. S., Ma, S. X., Jee, H. J., Kim, S. & Ko, H. S. 2024. Gba1 E326K renders motor and non-motor symptoms with pathological alpha-synuclein, tau and glial activation. *Brain,* 147**,** 4072-4083.

Kwon, D., Zhang, K., Paul, K. C., Folle, A. D., Del Rosario, I., Jacobs, J. P., Keener, A. M., Bronstein, J. M. & Ritz, B. 2024. Diet and the gut microbiome in patients with Parkinson's disease. *NPJ Parkinsons Dis,* 10**,** 89.

Labrador-Garrido, A., Zhong, S., Hughes, L., Keshiya, S., Kim, W. S., Halliday, G. M. & Dzamko, N. 2023. Live cell in situ lysosomal GCase activity correlates to alpha-synuclein levels in human differentiated neurons with LRRK2 and GBA1 mutations. *Front Cell Neurosci,* 17**,** 1229213.

Lachenmayer, M. L., Murset, M., Antih, N., Debove, I., Muellner, J., Bompart, M., Schlaeppi, J. A., Nowacki, A., You, H., Michelis, J. P., Dransart, A., Pollo, C.,

Deuschl, G. & Krack, P. 2021. Subthalamic and pallidal deep brain stimulation for Parkinson's disease-meta-analysis of outcomes. *NPJ Parkinsons Dis,* 7**,** 77.

Lado, W., Ham, A., Li, H., Zhang, H., Chang, A. Y., Sardi, S. P., Alcalay, R. N., Arancio, O., Przedborsky, S. & Tang, G. 2024. Synaptic and cognitive impairment associated with L444P heterozygous glucocerebrosidase mutation. *Brain*.

Lahue, S. C., Comella, C. L. & Tanner, C. M. 2016. The best medicine? The influence of physical activity and inactivity on Parkinson's disease. *Mov Disord,* 31**,** 1444-1454.

Lama, J., Buhidma, Y., Fletcher, E. J. R. & Duty, S. 2021. Animal models of Parkinson's disease: a guide to selecting the optimal model for your research. *Neuronal Signal,* 5**,** NS20210026.

Lamontagne-Proulx, J., Coulombe, K., Morissette, M., Rieux, M., Calon, F., Di Paolo, T. & Soulet, D. 2023. Sex and Age Differences in a Progressive Synucleinopathy Mouse Model. *Biomolecules,* 13.

Lampropoulos, I. C., Malli, F., Sinani, O., Gourgoulianis, K. I. & Xiromerisiou, G. 2022. Worldwide trends in mortality related to Parkinson's disease in the period of 1994-2019: Analysis of vital registration data from the WHO Mortality Database. *Front Neurol,* 13**,** 956440.

Lang, C., Campbell, K. R., Ryan, B. J., Carling, P., Attar, M., Vowles, J., Perestenko, O. V., Bowden, R., Baig, F., Kasten, M., Hu, M. T., Cowley, S. A., Webber, C. & Wade-Martins, R. 2019. Single-Cell Sequencing of iPSC-Dopamine Neurons Reconstructs Disease Progression and Identifies HDAC4 as a Regulator of Parkinson Cell Phenotypes. *Cell Stem Cell,* 24**,** 93-106 e6.

Langston, J. W. 2017. The MPTP Story. *J Parkinsons Dis,* 7**,** S11-S19.

Langston, J. W., Ballard, P., Tetrud, J. W. & Irwin, I. 1983. Chronic Parkinsonism in humans due to a product of meperidine-analog synthesis. *Science,* 219**,** 979-80.

Lashuel, H. A. 2020. Do Lewy bodies contain alpha-synuclein fibrils? and Does it matter? A brief history and critical analysis of recent reports. *Neurobiol Dis,* 141**,** 104876.

Latham, T., Grabowski, G. A., Theophilus, B. D. & Smith, F. I. 1990. Complex alleles of the acid beta-glucosidase gene in Gaucher disease. *Am J Hum Genet,* 47**,** 79-86.

Lazic, S. E., Clarke-Williams, C. J. & Munafo, M. R. 2018. What exactly is 'N' in cell culture and animal experiments? *PLoS Biol,* 16**,** e2005282.

Lee, H. J., Choi, C. & Lee, S. J. 2002. Membrane-bound alpha-synuclein has a high aggregation propensity and the ability to seed the aggregation of the cytosolic form. *J Biol Chem,* 277**,** 671-8.

Lee, K. W., Chen, W., Junn, E., Im, J. Y., Grosso, H., Sonsalla, P. K., Feng, X., Ray, N., Fernandez, J. R., Chao, Y., Masliah, E., Voronkov, M., Braithwaite, S. P., Stock, J. B. & Mouradian, M. M. 2011. Enhanced phosphatase activity attenuates alpha-synucleinopathy in a mouse model. *J Neurosci,* 31**,** 6963-71.

Lee, S. K. 2018. Sex as an important biological variable in biomedical research. *BMB Rep,* 51**,** 167-173.

Lelieveld, L. T., Gerhardt, S., Maas, S., Zwiers, K. C., De Wit, C., Beijk, E. H., Ferraz, M. J., Artola, M., Meijer, A. H., Tudorache, C., Salvatori, D., Boot, R. G. & Aerts, J. 2022. Consequences of excessive glucosylsphingosine in glucocerebrosidase-deficient zebrafish. *J Lipid Res,* 63**,** 100199.

Leocadi, M., Canu, E., Donzuso, G., Stojkovic, T., Basaia, S., Kresojevic, N., Stankovic, I., Sarasso, E., Piramide, N., Tomic, A., Markovic, V., Petrovic, I., Stefanova, E., Kostic, V. S., Filippi, M. & Agosta, F. 2022. Longitudinal clinical, cognitive, and neuroanatomical changes over 5 years in GBA-positive Parkinson's disease patients. *J Neurol,* 269**,** 1485-1500.

Lerche, S., Schulte, C., Wurster, I., Machetanz, G., Roeben, B., Zimmermann, M., Deuschle, C., Hauser, A. K., Bohringer, J., Krageloh-Mann, I., Waniek, K., Lachmann, I., Petterson, X. T., Chiang, R., Park, H., Wang, B., Liepelt-Scarfone, I., Maetzler, W., Galasko, D., Scherzer, C. R., Gasser, T., Mielke, M. M., Hutten, S. J., Mollenhauer, B., Sardi, S. P., Berg, D. & Brockmann, K. 2021. The Mutation Matters: CSF Profiles of GCase, Sphingolipids, alpha-Synuclein in PD(GBA). *Mov Disord,* 36**,** 1216-1228.

Leroi, I., Mcdonald, K., Pantula, H. & Harbishettar, V. 2012. Cognitive impairment in Parkinson disease: impact on quality of life, disability, and caregiver burden. *J Geriatr Psychiatry Neurol,* 25**,** 208-14.

Lesage, S., Anheim, M., Condroyer, C., Pollak, P., Durif, F., Dupuits, C., Viallet, F., Lohmann, E., Corvol, J. C., Honore, A., Rivaud, S., Vidailhet, M., Durr, A., Brice, A. & French Parkinson's Disease Genetics Study, G. 2011. Large-scale screening of the Gaucher's disease-related glucocerebrosidase gene in Europeans with Parkinson's disease. *Hum Mol Genet,* 20**,** 202-10.

Lesage, S., Durr, A., Tazir, M., Lohmann, E., Leutenegger, A. L., Janin, S., Pollak, P., Brice, A. & French Parkinson's Disease Genetics Study, G. 2006. LRRK2 G2019S as a cause of Parkinson's disease in North African Arabs. *N Engl J Med,* 354**,** 422-3.

Lesage, S., Houot, M., Mangone, G., Tesson, C., Bertrand, H., Forlani, S., Anheim, M., Brefel-Courbon, C., Broussolle, E., Thobois, S., Damier, P., Durif, F., Roze, E., Tison, F., Grabli, D., Ory-Magne, F., Degos, B., Viallet, F., Cormier-Dequaire, F., Ouvrard-Hernandez, A. M., Vidailhet, M., Lohmann, E., Singleton, A., Corvol, J. C., Brice, A. & French Parkinson Disease Genetics Study, G. 2020. Genetic and Phenotypic Basis of Autosomal Dominant Parkinson's Disease in a Large Multi-Center Cohort. *Front Neurol,* 11**,** 682.

Levy, D. R., Hunter, N., Lin, S., Robinson, E. M., Gillis, W., Conlin, E. B., Anyoha, R., Shansky, R. M. & Datta, S. R. 2023. Mouse spontaneous behavior reflects individual variation rather than estrous state. *Curr Biol,* 33**,** 1358-1364 e4.

Lewitt, P. A. 2015. Levodopa therapy for Parkinson's disease: Pharmacokinetics and pharmacodynamics. *Mov Disord,* 30**,** 64-72.

Lewitt, P. A. & Chaudhuri, K. R. 2020. Unmet needs in Parkinson disease: Motor and non-motor. *Parkinsonism Relat Disord,* 80 Suppl 1**,** S7-S12.

Lewy, F. H. 1912. Paralysis agitans. I. Pathologische Anatomie. *In:* LEWANDOWSKY, M. (ed.) *Handbuch der Neurologie.* Berlin: Springer.

Leyns, C. E. G., Prigent, A., Beezhold, B., Yao, L., Hatcher, N. G., Tao, P., Kang, J., Suh, E., Van Deerlin, V. M., Trojanowski, J. Q., Lee, V. M. Y., Kennedy, M. E., Fell, M. J. & Henderson, M. X. 2023. Glucocerebrosidase activity and lipid levels are related to protein pathologies in Parkinson's disease. *NPJ Parkinsons Dis,* 9**,** 74.

Li, H., Ham, A., Ma, T. C., Kuo, S. H., Kanter, E., Kim, D., Ko, H. S., Quan, Y., Sardi, S. P., Li, A., Arancio, O., Kang, U. J., Sulzer, D. & Tang, G. 2019a. Mitochondrial dysfunction and mitophagy defect triggered by heterozygous GBA mutations. *Autophagy,* 15**,** 113-130.

Li, M., Xu, H., Chen, G., Sun, S., Wang, Q., Liu, B., Wu, X., Zhou, L., Chai, Z., Sun, X., Lu, Y., Younus, M., Zheng, L., Zhu, F., Jia, H., Chen, X., Wang, C. & Zhou, Z. 2019b. Impaired D2 receptor-dependent dopaminergic transmission in prefrontal cortex of awake mouse model of Parkinson's disease. *Brain,* 142**,** 3099-3115.

Li, M., Ye, X., Huang, Z., Ye, L. & Chen, C. 2025. Global burden of Parkinson's disease from 1990 to 2021: a population-based study. *BMJ Open,* 15**,** e095610.

Li, Q., Jing, Y., Lun, P., Liu, X. & Sun, P. 2021. Association of gender and age at onset with glucocerebrosidase associated Parkinson's disease: a systematic review and meta-analysis. *Neurol Sci,* 42**,** 2261-2271.

Li, X., Chen, C., Pan, T., Zhou, X., Sun, X., Zhang, Z., Wu, D. & Chen, X. 2024. Trends and hotspots in non-motor symptoms of Parkinson's disease: a 10-year bibliometric analysis. *Front Aging Neurosci,* 16**,** 1335550.

Li, X., Li, W., Liu, G., Shen, X. & Tang, Y. 2015. Association between cigarette smoking and Parkinson's disease: A meta-analysis. *Arch Gerontol Geriatr,* 61**,** 510-6.

Liao, P. C., Franco-Iborra, S., Yang, Y. & Pon, L. A. 2020. Live cell imaging of mitochondrial redox state in mammalian cells and yeast. *Methods Cell Biol,* 155**,** 295-319.

Lieberman, R. L. 2011. A Guided Tour of the Structural Biology of Gaucher Disease: Acid-beta-Glucosidase and Saposin C. *Enzyme Res,* 2011**,** 973231.

Lieberman, R. L., Wustman, B. A., Huertas, P., Powe, A. C., Jr., Pine, C. W., Khanna, R., Schlossmacher, M. G., Ringe, D. & Petsko, G. A. 2007. Structure of acid beta-glucosidase with pharmacological chaperone provides insight into Gaucher disease. *Nat Chem Biol,* 3**,** 101-7.

Lim, J. L., Lohmann, K., Tan, A. H., Tay, Y. W., Ibrahim, K. A., Abdul Aziz, Z., Mawardi, A. S., Puvanarajah, S. D., Lim, T. T., Looi, I., Ooi, J. C. E., Chia, Y. K., Muthusamy, K. A., Bauer, P., Rolfs, A., Klein, C., Ahmad-Annuar, A. & Lim, S. Y. 2022. Glucocerebrosidase (GBA) gene variants in a multi-ethnic Asian cohort with Parkinson's disease: mutational spectrum and clinical features. *J Neural Transm (Vienna),* 129**,** 37-48.

Lim, S. S., Allen, K. & Gbd 2015 Sdg Collaborators 2016. Measuring the health-related Sustainable Development Goals in 188 countries: a baseline analysis from the Global Burden of Disease Study 2015. *Lancet,* 388**,** 1813-1850.

Lin, M., Mackie, P. M., Shaerzadeh, F., Gamble-George, J., Miller, D. R., Martyniuk, C. J. & Khoshbouei, H. 2021. In Parkinson's patient-derived dopamine neurons, the triplication of alpha-synuclein locus induces distinctive firing pattern by impeding D2 receptor autoinhibition. *Acta Neuropathol Commun,* 9**,** 107.

Lin, Y., Yang, F., Shang, B., Speich, J. E., Wan, Y. Y., Hashida, H., Braun, T., Sadoughi, A., Puehler, T., Lue, T. F. & Zhang, K. 2024a. Reporting quality of animal research in journals that published the ARRIVE 1.0 or ARRIVE 2.0 guidelines: a cross-sectional analysis of 943 studies. *Cardiovasc Diagn Ther,* 14**,** 1070-1082.

Lin, Y., Zhao, X., Liou, B., Fannin, V., Zhang, W., Setchell, K. D. R., Wang, X., Pan, D., Grabowski, G. A., Liu, C. J. & Sun, Y. 2024b. Intrinsic link between PGRN and Gba1 D409V mutation dosage in potentiating Gaucher disease. *Hum Mol Genet,* 33**,** 1771-1788.

Liou, B. & Grabowski, G. A. 2009. Participation of asparagine 370 and glutamine 235 in the catalysis by acid beta-glucosidase: the enzyme deficient in Gaucher disease. *Mol Genet Metab,* 97**,** 65-74.

Liou, B., Haffey, W. D., Greis, K. D. & Grabowski, G. A. 2014. The LIMP-2/SCARB2 binding motif on acid beta-glucosidase: basic and applied implications for Gaucher disease and associated neurodegenerative diseases. *J Biol Chem,* 289**,** 30063-74.

Liou, B., Kazimierczuk, A., Zhang, M., Scott, C. R., Hegde, R. S. & Grabowski, G. A. 2006. Analyses of variant acid beta-glucosidases: effects of Gaucher disease mutations. *J Biol Chem,* 281**,** 4242-53.

Liou, B., Zhang, W., Fannin, V., Quinn, B., Ran, H., Xu, K., Setchell, K. D. R., Witte, D., Grabowski, G. A. & Sun, Y. 2019. Combination of acid beta-glucosidase mutation and Saposin C deficiency in mice reveals Gba1 mutation dependent and tissue-specific disease phenotype. *Sci Rep,* 9**,** 5571.

Liu, G., Boot, B., Locascio, J. J., Jansen, I. E., Winder-Rhodes, S., Eberly, S., Elbaz, A., Brice, A., Ravina, B., Van Hilten, J. J., Cormier-Dequaire, F., Corvol, J. C., Barker,

R. A., Heutink, P., Marinus, J., Williams-Gray, C. H., Scherzer, C. R. & International Genetics of Parkinson Disease Progression, C. 2016. Specifically neuropathic Gaucher's mutations accelerate cognitive decline in Parkinson's. *Ann Neurol,* 80**,** 674-685.

Liu, Y., Suzuki, K., Reed, J. D., Grinberg, A., Westphal, H., Hoffmann, A., Doring, T., Sandhoff, K. & Proia, R. L. 1998. Mice with type 2 and 3 Gaucher disease point mutations generated by a single insertion mutagenesis procedure. *Proc Natl Acad Sci U S A,* 95**,** 2503-8.

Liu, Y. H., Jensen, G. L., Na, M., Mitchell, D. C., Wood, G. C., Still, C. D. & Gao, X. 2021. Diet Quality and Risk of Parkinson's Disease: A Prospective Study and Meta-Analysis. *J Parkinsons Dis,* 11**,** 337-347.

Loesch, D. P., Horimoto, A., Heilbron, K., Sarihan, E. I., Inca-Martinez, M., Mason, E., Cornejo-Olivas, M., Torres, L., Mazzetti, P., Cosentino, C., Sarapura-Castro, E., Rivera-Valdivia, A., Medina, A. C., Dieguez, E., Raggio, V., Lescano, A., Tumas, V., Borges, V., Ferraz, H. B., Rieder, C. R., Schumacher-Schuh, A., Santos-Lobato, B. L., Velez-Pardo, C., Jimenez-Del-Rio, M., Lopera, F., Moreno, S., Chana-Cuevas, P., Fernandez, W., Arboleda, G., Arboleda, H., Arboleda-Bustos, C. E., Yearout, D., Zabetian, C. P., Andme Research, T., Cannon, P., Thornton, T. A., O'connor, T. D., Mata, I. F. & Latin American Research Consortium on the Genetics of Parkinson's, D. 2021. Characterizing the Genetic Architecture of Parkinson's Disease in Latinos. *Ann Neurol,* 90**,** 353-365.

Lohle, M., Mende, J., Wolz, M., Beuthien-Baumann, B., Oehme, L., Van Den Hoff, J., Kotzerke, J., Reichmann, H. & Storch, A. 2016. Putaminal dopamine turnover in de novo Parkinson disease predicts later motor complications. *Neurology,* 86**,** 231-40.

Lohr, K. M., Masoud, S. T., Salahpour, A. & Miller, G. W. 2017. Membrane transporters as mediators of synaptic dopamine dynamics: implications for disease. *Eur J Neurosci,* 45**,** 20-33.

Lopes, E. F., Roberts, B. M., Siddorn, R. E., Clements, M. A. & Cragg, S. J. 2019. Inhibition of Nigrostriatal Dopamine Release by Striatal GABA(A) and GABA(B) Receptors. *J Neurosci,* 39**,** 1058-1065.

Louis, E. D. 1997. The shaking palsy, the first forty-five years: a journey through the British literature. *Mov Disord,* 12**,** 1068-72.

Lueptow, L. M. 2017. Novel Object Recognition Test for the Investigation of Learning and Memory in Mice. *J Vis Exp*.

Lunati, A., Lesage, S. & Brice, A. 2018. The genetic landscape of Parkinson's disease. *Rev Neurol (Paris),* 174**,** 628-643.

Lunde, K. A., Chung, J., Dalen, I., Pedersen, K. F., Linder, J., Domellof, M. E., Elgh, E., Macleod, A. D., Tzoulis, C., Larsen, J. P., Tysnes, O. B., Forsgren, L., Counsell, C. E., Alves, G. & Maple-Grodem, J. 2018. Association of glucocerebrosidase polymorphisms and mutations with dementia in incident Parkinson's disease. *Alzheimers Dement,* 14**,** 1293-1301.

Lunghi, G., Carsana, E. V., Loberto, N., Cioccarelli, L., Prioni, S., Mauri, L., Bassi, R., Duga, S., Straniero, L., Asselta, R., Solda, G., Di Fonzo, A., Frattini, E., Magni, M., Liessi, N., Armirotti, A., Ferrari, E., Samarani, M. & Aureli, M. 2022. beta-Glucocerebrosidase Deficiency Activates an Aberrant Lysosome-Plasma Membrane Axis Responsible for the Onset of Neurodegeneration. *Cells,* 11.

Luo, Y., Qiao, L., Li, M., Wen, X., Zhang, W. & Li, X. 2024. Global, regional, national epidemiology and trends of Parkinson's disease from 1990 to 2021: findings from the Global Burden of Disease Study 2021. *Front Aging Neurosci,* 16**,** 1498756.

Lwin, A., Orvisky, E., Goker-Alpan, O., Lamarca, M. E. & Sidransky, E. 2004. Glucocerebrosidase mutations in subjects with parkinsonism. *Mol Genet Metab,* 81**,** 70-3.

Lythe, V., Athauda, D., Foley, J., Mencacci, N. E., Jahanshahi, M., Cipolotti, L., Hyam, J., Zrinzo, L., Hariz, M., Hardy, J., Limousin, P. & Foltynie, T. 2017. GBA-Associated Parkinson's Disease: Progression in a Deep Brain Stimulation Cohort. *J Parkinsons Dis,* 7**,** 635-644.

Machado, F. A. & Reppold, C. T. 2015. The effect of deep brain stimulation on motor and cognitive symptoms of Parkinson's disease: A literature review. *Dement Neuropsychol,* 9**,** 24-31.

Maegawa, G. H., Tropak, M. B., Buttner, J. D., Rigat, B. A., Fuller, M., Pandit, D., Tang, L., Kornhaber, G. J., Hamuro, Y., Clarke, J. T. & Mahuran, D. J. 2009. Identification and characterization of ambroxol as an enzyme enhancement agent for Gaucher disease. *J Biol Chem,* 284**,** 23502-16.

Maetzler, W., Mirelman, A., Pilotto, A. & Bhidayasiri, R. 2024. Identifying Subtle Motor Deficits Before Parkinson's Disease is Diagnosed: What to Look for? *J Parkinsons Dis,* 14**,** S287-S296.

Magalhaes, J., Gegg, M. E., Migdalska-Richards, A., Doherty, M. K., Whitfield, P. D. & Schapira, A. H. 2016. Autophagic lysosome reformation dysfunction in glucocerebrosidase deficient cells: relevance to Parkinson disease. *Hum Mol Genet,* 25**,** 3432-3445.

Magalhaes, J., Gegg, M. E., Migdalska-Richards, A. & Schapira, A. H. 2018. Effects of ambroxol on the autophagy-lysosome pathway and mitochondria in primary cortical neurons. *Sci Rep,* 8**,** 1385.

Mahlknecht, P., Foltynie, T., Limousin, P. & Poewe, W. 2022. How Does Deep Brain Stimulation Change the Course of Parkinson's Disease? *Mov Disord,* 37**,** 1581-1592.

Mahoney-Crane, C. L., Viswanathan, M., Russell, D., Curtiss, R. a. C., Freire, J., Bobba, S. S., Coyle, S. D., Kandebo, M., Yao, L., Wan, B. L., Hatcher, N. G., Smith, S. M., Marcus, J. N. & Volpicelli-Daley, L. A. 2023. Neuronopathic GBA1L444P Mutation Accelerates Glucosylsphingosine Levels and Formation of Hippocampal Alpha-Synuclein Inclusions. *J Neurosci,* 43**,** 501-521.

Malek, N., Weil, R. S., Bresner, C., Lawton, M. A., Grosset, K. A., Tan, M., Bajaj, N., Barker, R. A., Burn, D. J., Foltynie, T., Hardy, J., Wood, N. W., Ben-Shlomo, Y., Williams, N. W., Grosset, D. G., Morris, H. R. & Consortium, P. R. C. 2018. Features of GBA-associated Parkinson's disease at presentation in the UK Tracking Parkinson's study. *J Neurol Neurosurg Psychiatry,* 89**,** 702-709.

Mallett, V., Ross, J. P., Alcalay, R. N., Ambalavanan, A., Sidransky, E., Dion, P. A., Rouleau, G. A. & Gan-Or, Z. 2016. GBA p.T369M substitution in Parkinson disease: Polymorphism or association? A meta-analysis. *Neurol Genet,* 2**,** e104.

Maniwang, E., Tayebi, N. & Sidransky, E. 2013. Is Parkinson disease associated with lysosomal integral membrane protein type-2?: challenges in interpreting association data. *Mol Genet Metab,* 108**,** 269-71.

Manning-Bog, A. B., Schule, B. & Langston, J. W. 2009. Alpha-synuclein-glucocerebrosidase interactions in pharmacological Gaucher models: a biological link between Gaucher disease and parkinsonism. *Neurotoxicology,* 30**,** 1127-32.

Mansouri, A., Taslimi, S., Badhiwala, J. H., Witiw, C. D., Nassiri, F., Odekerken, V. J. J., De Bie, R. M. A., Kalia, S. K., Hodaie, M., Munhoz, R. P., Fasano, A. & Lozano, A. M. 2018. Deep brain stimulation for Parkinson's disease: meta-analysis of results of randomized trials at varying lengths of follow-up. *J Neurosurg,* 128**,** 1199-1213.

Maor, G., Cabasso, O., Krivoruk, O., Rodriguez, J., Steller, H., Segal, D. & Horowitz, M. 2016. The contribution of mutant GBA to the development of Parkinson disease in Drosophila. *Hum Mol Genet,* 25**,** 2712-2727.

Maor, G., Rencus-Lazar, S., Filocamo, M., Steller, H., Segal, D. & Horowitz, M. 2013. Unfolded protein response in Gaucher disease: from human to Drosophila. *Orphanet J Rare Dis,* 8**,** 140.

Maple-Grodem, J., Dalen, I., Tysnes, O. B., Macleod, A. D., Forsgren, L., Counsell, C. E. & Alves, G. 2021a. Association of GBA Genotype With Motor and Functional Decline in Patients With Newly Diagnosed Parkinson Disease. *Neurology,* 96**,** e1036-e1044.

Maple-Grodem, J., Paul, K. C., Dalen, I., Ngo, K. J., Wong, D., Macleod, A. D., Counsell, C. E., Backstrom, D., Forsgren, L., Tysnes, O. B., Kusters, C. D. J., Fogel, B. L., Bronstein, J. M., Ritz, B. & Alves, G. 2021b. Lack of Association Between GBA Mutations and Motor Complications in European and American Parkinson's Disease Cohorts. *J Parkinsons Dis,* 11**,** 1569-1578.

Marques, A. R., Mirzaian, M., Akiyama, H., Wisse, P., Ferraz, M. J., Gaspar, P., Ghauharali-Van Der Vlugt, K., Meijer, R., Giraldo, P., Alfonso, P., Irun, P., Dahl, M., Karlsson, S., Pavlova, E. V., Cox, T. M., Scheij, S., Verhoek, M., Ottenhoff, R., Van Roomen, C. P., Pannu, N. S., Van Eijk, M., Dekker, N., Boot, R. G., Overkleeft, H. S., Blommaart, E., Hirabayashi, Y. & Aerts, J. M. 2016. Glucosylated cholesterol in mammalian cells and tissues: formation and degradation by multiple cellular beta-glucosidases. *J Lipid Res,* 57**,** 451-63.

Martin, A. J., Vidotto, M., Boscariol, F., Di Domenico, T., Walsh, I. & Tosatto, S. C. 2011. RING: networking interacting residues, evolutionary information and energetics in protein structures. *Bioinformatics,* 27**,** 2003-5.

Martin, I., Kim, J. W., Dawson, V. L. & Dawson, T. M. 2014. LRRK2 pathobiology in Parkinson's disease. *J Neurochem,* 131**,** 554-65.

Martinez-Bailen, M., Clemente, F., Matassini, C. & Cardona, F. 2022. GCase Enhancers: A Potential Therapeutic Option for Gaucher Disease and Other Neurological Disorders. *Pharmaceuticals (Basel),* 15.

Martinez-Martin, P., Rodriguez-Blazquez, C., Kurtis, M. M., Chaudhuri, K. R. & Group, N. V. 2011. The impact of non-motor symptoms on health-related quality of life of patients with Parkinson's disease. *Mov Disord,* 26**,** 399-406.

Masoud, S. T., Vecchio, L. M., Bergeron, Y., Hossain, M. M., Nguyen, L. T., Bermejo, M. K., Kile, B., Sotnikova, T. D., Siesser, W. B., Gainetdinov, R. R., Wightman, R. M., Caron, M. G., Richardson, J. R., Miller, G. W., Ramsey, A. J., Cyr, M. & Salahpour, A. 2015. Increased expression of the dopamine transporter leads to loss of dopamine neurons, oxidative stress and l-DOPA reversible motor deficits. *Neurobiol Dis,* 74**,** 66-75.

Mata, I. F., Leverenz, J. B., Weintraub, D., Trojanowski, J. Q., Chen-Plotkin, A., Van Deerlin, V. M., Ritz, B., Rausch, R., Factor, S. A., Wood-Siverio, C., Quinn, J. F., Chung, K. A., Peterson-Hiller, A. L., Goldman, J. G., Stebbins, G. T., Bernard, B., Espay, A. J., Revilla, F. J., Devoto, J., Rosenthal, L. S., Dawson, T. M., Albert, M. S., Tsuang, D., Huston, H., Yearout, D., Hu, S. C., Cholerton, B. A., Montine, T. J., Edwards, K. L. & Zabetian, C. P. 2016. GBA Variants are associated with a distinct pattern of cognitive deficits in Parkinson's disease. *Mov Disord,* 31**,** 95-102.

Mathers, C. D., Stevens, G. A., Boerma, T., White, R. A. & Tobias, M. I. 2015. Causes of international increases in older age life expectancy. *Lancet,* 385**,** 540-8.

Mathis, A., Mamidanna, P., Cury, K. M., Abe, T., Murthy, V. N., Mathis, M. W. & Bethge, M. 2018. DeepLabCut: markerless pose estimation of user-defined body parts with deep learning. *Nat Neurosci,* 21**,** 1281-1289.

Matsuda, W., Furuta, T., Nakamura, K. C., Hioki, H., Fujiyama, F., Arai, R. & Kaneko, T. 2009. Single nigrostriatal dopaminergic neurons form widely spread and highly dense axonal arborizations in the neostriatum. *J Neurosci,* 29**,** 444-53.

Matsumoto, S. I., Sato, S., Otake, K. & Kosugi, Y. 2022. Highly-sensitive simultaneous quantitation of glucosylsphingosine and galactosylsphingosine in human cerebrospinal fluid by liquid chromatography/tandem mass spectrometry. *J Pharm Biomed Anal,* 217**,** 114852.

Matsuura, K., Kabuto, H., Makino, H. & Ogawa, N. 1997. Pole test is a useful method for evaluating the mouse movement disorder caused by striatal dopamine depletion. *J Neurosci Methods,* 73**,** 45-8.

Mazzulli, J. R., Xu, Y. H., Sun, Y., Knight, A. L., Mclean, P. J., Caldwell, G. A., Sidransky, E., Grabowski, G. A. & Krainc, D. 2011. Gaucher disease glucocerebrosidase and alpha-synuclein form a bidirectional pathogenic loop in synucleinopathies. *Cell,* 146**,** 37-52.

Mazzulli, J. R., Zunke, F., Isacson, O., Studer, L. & Krainc, D. 2016. alpha-Synuclein-induced lysosomal dysfunction occurs through disruptions in protein trafficking in human midbrain synucleinopathy models. *Proc Natl Acad Sci U S A,* 113**,** 1931-6.

Mccarthy, M. M., Arnold, A. P., Ball, G. F., Blaustein, J. D. & De Vries, G. J. 2012. Sex differences in the brain: the not so inconvenient truth. *J Neurosci,* 32**,** 2241-7.

Mcfadyen, M. P., Kusek, G., Bolivar, V. J. & Flaherty, L. 2003. Differences among eight inbred strains of mice in motor ability and motor learning on a rotorod. *Genes Brain Behav,* 2**,** 214-9.

Mcgregor, M. M. & Nelson, A. B. 2019. Circuit Mechanisms of Parkinson's Disease. *Neuron,* 101**,** 1042-1056.

Mckeran, R. O., Bradbury, P., Taylor, D. & Stern, G. 1985. Neurological involvement in type 1 (adult) Gaucher's disease. *J Neurol Neurosurg Psychiatry,* 48**,** 172-5.

Mckinley, J. W., Shi, Z., Kawikova, I., Hur, M., Bamford, I. J., Sudarsana Devi, S. P., Vahedipour, A., Darvas, M. & Bamford, N. S. 2019. Dopamine Deficiency Reduces Striatal Cholinergic Interneuron Function in Models of Parkinson's Disease. *Neuron,* 103**,** 1056-1072 e6.

Mcneill, A., Duran, R., Proukakis, C., Bras, J., Hughes, D., Mehta, A., Hardy, J., Wood, N. W. & Schapira, A. H. 2012. Hyposmia and cognitive impairment in Gaucher disease patients and carriers. *Mov Disord,* 27**,** 526-32.

Mcneill, A., Magalhaes, J., Shen, C., Chau, K. Y., Hughes, D., Mehta, A., Foltynie, T., Cooper, J. M., Abramov, A. Y., Gegg, M. & Schapira, A. H. 2014. Ambroxol improves lysosomal biochemistry in glucocerebrosidase mutation-linked Parkinson disease cells. *Brain,* 137**,** 1481-95.

Medina-Luque, J., Piechocinski, P., Feyen, P., Sgobio, C. & Herms, J. 2024. Striatal dopamine neurotransmission is altered in age- and region-specific manner in a Parkinson's disease transgenic mouse. *Sci Rep,* 14**,** 164.

Meiser, J., Weindl, D. & Hiller, K. 2013. Complexity of dopamine metabolism. *Cell Commun Signal,* 11**,** 34.

Mencarelli, C. & Martinez-Martinez, P. 2013. Ceramide function in the brain: when a slight tilt is enough. *Cell Mol Life Sci,* 70**,** 181-203.

Menozzi, E., Toffoli, M. & Schapira, A. H. V. 2023. Targeting the GBA1 pathway to slow Parkinson disease: Insights into clinical aspects, pathogenic mechanisms and new therapeutic avenues. *Pharmacol Ther,* 246**,** 108419.

Meredith, G. E. & Rademacher, D. J. 2011. MPTP mouse models of Parkinson's disease: an update. *J Parkinsons Dis,* 1**,** 19-33.

Meyer, O. A., Tilson, H. A., Byrd, W. C. & Riley, M. T. 1979. A method for the routine assessment of fore- and hindlimb grip strength of rats and mice. *Neurobehav Toxicol,* 1**,** 233-6.

Miao, S. C., Mccarter, J. D., Grace, M. E., Grabowski, G. A., Aebersold, R. & Withers, S. G. 1994. Identification of Glu(340) as the Active-Site Nucleophile in Human Glucocerebrosidase by Use of Electrospray Tandem Mass-Spectrometry. *Journal of Biological Chemistry,* 269**,** 10975-10978.

Michelakakis, H., Moraitou, M., Dimitriou, E., Santamaria, R., Sanchez, G., Gort, L., Chabas, A., Grinberg, D., Dassopoulou, M., Fotopoulos, S. & Vilageliu, L. 2006. Homozygosity for the double D409H+H255Q allele in type II Gaucher disease. *J Inherit Metab Dis,* 29**,** 591.

Michelakakis, H., Xiromerisiou, G., Dardiotis, E., Bozi, M., Vassilatis, D., Kountra, P. M., Patramani, G., Moraitou, M., Papadimitriou, D., Stamboulis, E., Stefanis, L., Zintzaras, E. & Hadjigeorgiou, G. M. 2012. Evidence of an association between the scavenger receptor class B member 2 gene and Parkinson's disease. *Mov Disord,* 27**,** 400-5.

Migdalska-Richards, A., Daly, L., Bezard, E. & Schapira, A. H. 2016. Ambroxol effects in glucocerebrosidase and alpha-synuclein transgenic mice. *Ann Neurol,* 80**,** 766-775.

Migdalska-Richards, A., Ko, W. K. D., Li, Q., Bezard, E. & Schapira, A. H. V. 2017a. Oral ambroxol increases brain glucocerebrosidase activity in a nonhuman primate. *Synapse,* 71.

Migdalska-Richards, A., Wegrzynowicz, M., Harrison, I. F., Verona, G., Bellotti, V., Spillantini, M. G. & Schapira, A. H. V. 2020. L444P Gba1 mutation increases formation and spread of alpha-synuclein deposits in mice injected with mouse alpha-synuclein pre-formed fibrils. *PLoS One,* 15**,** e0238075.

Migdalska-Richards, A., Wegrzynowicz, M., Rusconi, R., Deangeli, G., Di Monte, D. A., Spillantini, M. G. & Schapira, A. H. V. 2017b. The L444P Gba1 mutation enhances alpha-synuclein induced loss of nigral dopaminergic neurons in mice. *Brain,* 140**,** 2706-2721.

Mignot, C., Gelot, A., Bessieres, B., Daffos, F., Voyer, M., Menez, F., Fallet Bianco, C., Odent, S., Le Duff, D., Loget, P., Fargier, P., Costil, J., Josset, P., Roume, J., Vanier, M. T., Maire, I. & Billette De Villemeur, T. 2003. Perinatal-lethal Gaucher disease. *Am J Med Genet A,* 120A**,** 338-44.

Milenkovic, I., Blumenreich, S. & Futerman, A. H. 2022. GBA mutations, glucosylceramide and Parkinson's disease. *Curr Opin Neurobiol,* 72**,** 148-154.

Mirelman, A., Bonato, P., Camicioli, R., Ellis, T. D., Giladi, N., Hamilton, J. L., Hass, C. J., Hausdorff, J. M., Pelosin, E. & Almeida, Q. J. 2019. Gait impairments in Parkinson's disease. *Lancet Neurol,* 18**,** 697-708.

Mirzaian, M., Wisse, P., Ferraz, M. J., Marques, A. R. A., Gaspar, P., Oussoren, S. V., Kytidou, K., Codee, J. D. C., Van Der Marel, G., Overkleeft, H. S. & Aerts, J. M. 2017. Simultaneous quantitation of sphingoid bases by UPLC-ESI-MS/MS with identical (13)C-encoded internal standards. *Clin Chim Acta,* 466**,** 178-184.

Mistry, P. K., Cappellini, M. D., Lukina, E., Ozsan, H., Mach Pascual, S., Rosenbaum, H., Helena Solano, M., Spigelman, Z., Villarrubia, J., Watman, N. P. & Massenkeil, G. 2011. A reappraisal of Gaucher disease-diagnosis and disease management algorithms. *Am J Hematol,* 86**,** 110-5.

Mistry, P. K., Liu, J., Sun, L., Chuang, W. L., Yuen, T., Yang, R., Lu, P., Zhang, K., Li, J., Keutzer, J., Stachnik, A., Mennone, A., Boyer, J. L., Jain, D., Brady, R. O., New, M. I. & Zaidi, M. 2014. Glucocerebrosidase 2 gene deletion rescues type 1 Gaucher disease. *Proc Natl Acad Sci U S A,* 111**,** 4934-9.

Mitsui, J., Mizuta, I., Toyoda, A., Ashida, R., Takahashi, Y., Goto, J., Fukuda, Y., Date, H., Iwata, A., Yamamoto, M., Hattori, N., Murata, M., Toda, T. & Tsuji, S. 2009. Mutations for Gaucher disease confer high susceptibility to Parkinson disease. *Arch Neurol,* 66**,** 571-6.

Mogi, K., Tomita, H., Yoshihara, M., Kajiyama, H. & Hara, A. 2025. Advances in bacterial artificial chromosome (BAC) transgenic mice for gene analysis and disease research. *Gene,* 934**,** 149014.

Mohamed-Fathy Kamal, O., Ojeda-Hernandez, D. D., Selma-Calvo, B., Benito-Martin, M. S., Fuente-Martin, S., Garcia-Martin, M., Larriba-Gonzalez, T., Sancho-Bielsa, F., Matias-Guiu, J. A., Matias-Guiu, J. & Gomez-Pinedo, U. 2025. Technical Assessment of Motor and Behavioral Tests in Rodent Models of Multiple Sclerosis. *J Integr Neurosci,* 24**,** 26429.

Montgomery, K. C. 1955. The Relation between Fear Induced by Novel Stimulation and Exploratory Behavior. *Journal of Comparative and Physiological Psychology,* 48**,** 254-260.

Moors, T. E., Paciotti, S., Ingrassia, A., Quadri, M., Breedveld, G., Tasegian, A., Chiasserini, D., Eusebi, P., Duran-Pacheco, G., Kremer, T., Calabresi, P., Bonifati, V., Parnetti, L., Beccari, T. & Van De Berg, W. D. J. 2019. Characterization of Brain Lysosomal Activities in GBA-Related and Sporadic Parkinson's Disease and Dementia with Lewy Bodies. *Mol Neurobiol,* 56**,** 1344-1355.

Morabito, G., Giannelli, S. G., Ordazzo, G., Bido, S., Castoldi, V., Indrigo, M., Cabassi, T., Cattaneo, S., Luoni, M., Cancellieri, C., Sessa, A., Bacigaluppi, M., Taverna, S., Leocani, L., Lanciego, J. L. & Broccoli, V. 2017. AAV-PHP.B-Mediated Global-Scale Expression in the Mouse Nervous System Enables GBA1 Gene Therapy for Wide Protection from Synucleinopathy. *Mol Ther,* 25**,** 2727-2742.

Moran, E. E., Bressman, S. B., Ortega, R. A., Raymond, D., Nichols, W. C., Palmese, C. A., Elango, S., Swan, M., Shanker, V., Perera, I., Wang, C., Zimmerman, M. E. & Saunders-Pullman, R. 2021. Cognitive Functioning of Glucocerebrosidase (GBA) Non-manifesting Carriers. *Front Neurol,* 12**,** 635958.

Morris, A. D. 1989. *James Parkinson His Life and Times,* Boston, MA., Birkhauser.

Morris, R., Martini, D. N., Ramsey, K., Kelly, V. E., Smulders, K., Hiller, A., Chung, K. A., Hu, S. C., Zabetian, C. P., Poston, K. L., Mata, I. F., Edwards, K. L., Lapidus, J., Cholerton, B., Montine, T. J., Quinn, J. F. & Horak, F. 2022. Cognition as a mediator for gait and balance impairments in GBA-related Parkinson's disease. *NPJ Parkinsons Dis,* 8**,** 78.

Mosharov, E. V., Larsen, K. E., Kanter, E., Phillips, K. A., Wilson, K., Schmitz, Y., Krantz, D. E., Kobayashi, K., Edwards, R. H. & Sulzer, D. 2009. Interplay between cytosolic dopamine, calcium, and alpha-synuclein causes selective death of substantia nigra neurons. *Neuron,* 62**,** 218-29.

Mosley, P. E., Moodie, R. & Dissanayaka, N. 2017. Caregiver Burden in Parkinson Disease: A Critical Review of Recent Literature. *J Geriatr Psychiatry Neurol,* 30**,** 235-252.

Motulsky, H. J. 2025. *Multiplicity adjusted P values* [Online]. GraphPad Statistics Guide. Available: https://www.graphpad.com/guides/prism/latest/statistics/stat_multiplicity_adjusted_p_values.htm [Accessed 16 September 2025].

Mullin, S., Smith, L., Lee, K., D'souza, G., Woodgate, P., Elflein, J., Hallqvist, J., Toffoli, M., Streeter, A., Hosking, J., Heywood, W. E., Khengar, R., Campbell, P., Hehir, J., Cable, S., Mills, K., Zetterberg, H., Limousin, P., Libri, V., Foltynie, T. & Schapira, A. H. V. 2020. Ambroxol for the Treatment of Patients With Parkinson Disease With

and Without Glucocerebrosidase Gene Mutations: A Nonrandomized, Noncontrolled Trial. *JAMA Neurol,* 77**,** 427-434.

Munoz, S. S., Marlet, F. R., Bilgin, M., Dreier, J. E., Bezard, E., Dehay, B., Jaunmuktane, Z., Maeda, K. & Galvagnion, C. 2024. Lipidomic Profiling Reveals Shared and Distinct Pathological Signatures in Sporadic Parkinson's Disease and GBA Mutation Carriers: Implications for Disease Mechanisms. *bioRxiv,* preprint**,** https://doi.org/10.1101/2024.10.11.617800.

Munoz, S. S., Petersen, D., Marlet, F. R., Kucukkose, E. & Galvagnion, C. 2021. The interplay between Glucocerebrosidase, alpha-synuclein and lipids in human models of Parkinson's disease. *Biophys Chem,* 273**,** 106534.

Murphy, K. E., Gysbers, A. M., Abbott, S. K., Tayebi, N., Kim, W. S., Sidransky, E., Cooper, A., Garner, B. & Halliday, G. M. 2014. Reduced glucocerebrosidase is associated with increased alpha-synuclein in sporadic Parkinson's disease. *Brain,* 137**,** 834-48.

Murphy, K. T. & Lynch, G. S. 2023. Impaired skeletal muscle health in Parkinsonian syndromes: clinical implications, mechanisms and potential treatments. *J Cachexia Sarcopenia Muscle,* 14**,** 1987-2002.

Mus, L., Siani, F., Giuliano, C., Ghezzi, C., Cerri, S. & Blandini, F. 2019. Development and biochemical characterization of a mouse model of Parkinson's disease bearing defective glucocerebrosidase activity. *Neurobiol Dis,* 124**,** 289-296.

Muslimovic, D., Post, B., Speelman, J. D. & Schmand, B. 2005. Cognitive profile of patients with newly diagnosed Parkinson disease. *Neurology,* 65**,** 1239-45.

Nalls, M. A., Blauwendraat, C., Sargent, L., Vitale, D., Leonard, H., Iwaki, H., Song, Y., Bandres-Ciga, S., Menden, K., Faghri, F., Heutink, P., Cookson, M. R. & Singleton, A. B. 2021. Evidence for GRN connecting multiple neurodegenerative diseases. *Brain Commun,* 3**,** fcab095.

Nalls, M. A., Blauwendraat, C., Vallerga, C. L., Heilbron, K., Bandres-Ciga, S., Chang, D., Tan, M., Kia, D. A., Noyce, A. J., Xue, A., Bras, J., Young, E., Von Coelln, R., Simon-Sanchez, J., Schulte, C., Sharma, M., Krohn, L., Pihlstrom, L., Siitonen, A., Iwaki, H., Leonard, H., Faghri, F., Gibbs, J. R., Hernandez, D. G., Scholz, S. W., Botia, J. A., Martinez, M., Corvol, J. C., Lesage, S., Jankovic, J., Shulman, L. M., Sutherland, M., Tienari, P., Majamaa, K., Toft, M., Andreassen, O. A., Bangale, T., Brice, A., Yang, J., Gan-Or, Z., Gasser, T., Heutink, P., Shulman, J. M., Wood, N. W., Hinds, D. A., Hardy, J. A., Morris, H. R., Gratten, J., Visscher, P. M., Graham, R. R., Singleton, A. B., Andme Research, T., System Genomics of Parkinson's Disease, C. & International Parkinson's Disease Genomics, C. 2019. Identification of novel risk loci, causal insights, and heritable risk for Parkinson's disease: a meta-analysis of genome-wide association studies. *Lancet Neurol,* 18**,** 1091-1102.

Nam, Y., Na, J., Ma, S. X., Park, H., Park, H., Lee, E., Kim, H., Jang, S. M., Ko, H. S. & Kim, S. 2024. DJ-1 protects cell death from a mitochondrial oxidative stress due to GBA1 deficiency. *Genes Genomics,* 46**,** 519-529.

Nassery, A., Palmese, C. A., Sarva, H., Groves, M., Miravite, J. & Kopell, B. H. 2016. Psychiatric and Cognitive Effects of Deep Brain Stimulation for Parkinson's Disease. *Curr Neurol Neurosci Rep,* 16**,** 87.

Nath, T., Mathis, A., Chen, A. C., Patel, A., Bethge, M. & Mathis, M. W. 2019. Using DeepLabCut for 3D markerless pose estimation across species and behaviors. *Nat Protoc,* 14**,** 2152-2176.

Navarro-Romero, A., Fernandez-Gonzalez, I., Riera, J., Montpeyo, M., Albert-Bayo, M., Lopez-Royo, T., Castillo-Sanchez, P., Carnicer-Caceres, C., Arranz-Amo, J. A., Castillo-Ribelles, L., Pradas, E., Casas, J., Vila, M. & Martinez-Vicente, M. 2022. Lysosomal lipid alterations caused by glucocerebrosidase deficiency promote

lysosomal dysfunction, chaperone-mediated-autophagy deficiency, and alpha-synuclein pathology. *NPJ Parkinsons Dis,* 8**,** 126.

Nc3rs. 2023. *Group and sample size* [Online]. Available: https://eda.nc3rs.org.uk/experimental-design-group [Accessed 15 April 2024].

Neculai, D., Schwake, M., Ravichandran, M., Zunke, F., Collins, R. F., Peters, J., Neculai, M., Plumb, J., Loppnau, P., Pizarro, J. C., Seitova, A., Trimble, W. S., Saftig, P., Grinstein, S. & Dhe-Paganon, S. 2013. Structure of LIMP-2 provides functional insights with implications for SR-BI and CD36. *Nature,* 504**,** 172-6.

Neudorfer, O., Giladi, N., Elstein, D., Abrahamov, A., Turezkite, T., Aghai, E., Reches, A., Bembi, B. & Zimran, A. 1996. Occurrence of Parkinson's syndrome in type I Gaucher disease. *QJM,* 89**,** 691-4.

Neumann, J., Bras, J., Deas, E., O'sullivan, S. S., Parkkinen, L., Lachmann, R. H., Li, A., Holton, J., Guerreiro, R., Paudel, R., Segarane, B., Singleton, A., Lees, A., Hardy, J., Houlden, H., Revesz, T. & Wood, N. W. 2009. Glucocerebrosidase mutations in clinical and pathologically proven Parkinson's disease. *Brain,* 132**,** 1783-94.

Ng, M., Freeman, M. K., Fleming, T. D., Robinson, M., Dwyer-Lindgren, L., Thomson, B., Wollum, A., Sanman, E., Wulf, S., Lopez, A. D., Murray, C. J. & Gakidou, E. 2014. Smoking prevalence and cigarette consumption in 187 countries, 1980-2012. *JAMA,* 311**,** 183-92.

Nielsen, B. E. & Ford, C. P. 2024. Reduced striatal M4-cholinergic signaling following dopamine loss contributes to parkinsonian and l-DOPA-induced dyskinetic behaviors. *Sci Adv,* 10**,** eadp6301.

Nijhuis, F. a. P., Esselink, R., De Bie, R. M. A., Groenewoud, H., Bloem, B. R., Post, B. & Meinders, M. J. 2021. Translating Evidence to Advanced Parkinson's Disease Patients: A Systematic Review and Meta-Analysis. *Mov Disord,* 36**,** 1293-1307.

Nilsson, O., Mansson, J. E., Hakansson, G. & Svennerholm, L. 1982. The occurrence of psychosine and other glycolipids in spleen and liver from the three major types of Gaucher's disease. *Biochim Biophys Acta,* 712**,** 453-63.

Nilsson, O. & Svennerholm, L. 1982. Accumulation of glucosylceramide and glucosylsphingosine (psychosine) in cerebrum and cerebellum in infantile and juvenile Gaucher disease. *J Neurochem,* 39**,** 709-18.

Nirenberg, M. J., Vaughan, R. A., Uhl, G. R., Kuhar, M. J. & Pickel, V. M. 1996. The dopamine transporter is localized to dendritic and axonal plasma membranes of nigrostriatal dopaminergic neurons. *J Neurosci,* 16**,** 436-47.

Noldus, L. P., Spink, A. J. & Tegelenbosch, R. A. 2001. EthoVision: a versatile video tracking system for automation of behavioral experiments. *Behav Res Methods Instrum Comput,* 33**,** 398-414.

Nord, C. L., Valton, V., Wood, J. & Roiser, J. P. 2017. Power-up: A Reanalysis of 'Power Failure' in Neuroscience Using Mixture Modeling. *J Neurosci,* 37**,** 8051-8061.

Noyce, A. J., Bestwick, J. P., Silveira-Moriyama, L., Hawkes, C. H., Giovannoni, G., Lees, A. J. & Schrag, A. 2012. Meta-analysis of early nonmotor features and risk factors for Parkinson disease. *Ann Neurol,* 72**,** 893-901.

Nutt, J. G. 2016. Motor subtype in Parkinson's disease: Different disorders or different stages of disease? *Mov Disord,* 31**,** 957-61.

Nyholm, D., Askmark, H., Gomes-Trolin, C., Knutson, T., Lennernas, H., Nystrom, C. & Aquilonius, S. M. 2003. Optimizing levodopa pharmacokinetics: intestinal infusion versus oral sustained-release tablets. *Clin Neuropharmacol,* 26**,** 156-63.

O'neill, R. R., Tokoro, T., Kozak, C. A. & Brady, R. O. 1989. Comparison of the chromosomal localization of murine and human glucocerebrosidase genes and of the deduced amino acid sequences. *Proc Natl Acad Sci U S A,* 86**,** 5049-53.

Obeso, J. A., Stamelou, M., Goetz, C. G., Poewe, W., Lang, A. E., Weintraub, D., Burn, D., Halliday, G. M., Bezard, E., Przedborski, S., Lehericy, S., Brooks, D. J., Rothwell, J. C., Hallett, M., Delong, M. R., Marras, C., Tanner, C. M., Ross, G. W., Langston, J. W., Klein, C., Bonifati, V., Jankovic, J., Lozano, A. M., Deuschl, G., Bergman, H., Tolosa, E., Rodriguez-Violante, M., Fahn, S., Postuma, R. B., Berg, D., Marek, K., Standaert, D. G., Surmeier, D. J., Olanow, C. W., Kordower, J. H., Calabresi, P., Schapira, A. H. V. & Stoessl, A. J. 2017. Past, present, and future of Parkinson's disease: A special essay on the 200th Anniversary of the Shaking Palsy. *Mov Disord,* 32**,** 1264-1310.

Oeda, T., Umemura, A., Mori, Y., Tomita, S., Kohsaka, M., Park, K., Inoue, K., Fujimura, H., Hasegawa, H., Sugiyama, H. & Sawada, H. 2015. Impact of glucocerebrosidase mutations on motor and nonmotor complications in Parkinson's disease. *Neurobiol Aging,* 36**,** 3306-3313.

Offman, M. N., Krol, M., Silman, I., Sussman, J. L. & Futerman, A. H. 2010. Molecular basis of reduced glucosylceramidase activity in the most common Gaucher disease mutant, N370S. *J Biol Chem,* 285**,** 42105-14.

Oftedal, L., Maple-Grodem, J., Dalen, I., Tysnes, O. B., Pedersen, K. F., Alves, G. & Lange, J. 2023. Association of CSF Glucocerebrosidase Activity With the Risk of Incident Dementia in Patients With Parkinson Disease. *Neurology,* 100**,** e388-e395.

Ogawa, N., Hirose, Y., Ohara, S., Ono, T. & Watanabe, Y. 1985. A simple quantitative bradykinesia test in MPTP-treated mice. *Res Commun Chem Pathol Pharmacol,* 50**,** 435-41.

Okunoye, O., Marston, L., Walters, K. & Schrag, A. 2022. Change in the incidence of Parkinson's disease in a large UK primary care database. *NPJ Parkinsons Dis,* 8**,** 23.

Olszewska, D. A., Mccarthy, A., Soto-Beasley, A. I., Walton, R. L., Magennis, B., Mclaughlin, R. L., Hardiman, O., Ross, O. A. & Lynch, T. 2020. Association Between Glucocerebrosidase Mutations and Parkinson's Disease in Ireland. *Front Neurol,* 11**,** 527.

Omer, N., Giladi, N., Gurevich, T., Bar-Shira, A., Gana-Weisz, M., Glinka, T., Goldstein, O., Kestenbaum, M., Cedarbaum, J. M., Mabrouk, O. S., Fraser, K. B., Shirvan, J. C., Orr-Urtreger, A., Mirelman, A. & Thaler, A. 2022. Glucocerebrosidase Activity is not Associated with Parkinson's Disease Risk or Severity. *Mov Disord,* 37**,** 190-195.

Omer, N., Giladi, N., Gurevich, T., Bar-Shira, A., Gana-Weisz, M., Goldstein, O., Kestenbaum, M., Cedarbaum, J. M., Orr-Urtreger, A., Mirelman, A. & Thaler, A. 2020. A Possible Modifying Effect of the G2019S Mutation in the LRRK2 Gene on GBA Parkinson's Disease. *Mov Disord,* 35**,** 1249-1253.

Ortega, R. A., Bressman, S. B., Raymond, D., Ozelius, L. J., Katsnelson, V., Leaver, K., Swan, M. C., Shanker, V., Miravite, J., Wang, C., Bennett, S. a. L. & Saunders-Pullman, R. 2022. Differences in Sex-Specific Frequency of Glucocerebrosidase Variant Carriers and Familial Parkinsonism. *Mov Disord,* 37**,** 2217-2225.

Orvisky, E., Park, J. K., Lamarca, M. E., Ginns, E. I., Martin, B. M., Tayebi, N. & Sidransky, E. 2002. Glucosylsphingosine accumulation in tissues from patients with Gaucher disease: correlation with phenotype and genotype. *Mol Genet Metab,* 76**,** 262-70.

Ou, Z., Pan, J., Tang, S., Duan, D., Yu, D., Nong, H. & Wang, Z. 2021. Global Trends in the Incidence, Prevalence, and Years Lived With Disability of Parkinson's Disease in 204 Countries/Territories From 1990 to 2019. *Front Public Health,* 9**,** 776847.

Ouled Amar Bencheikh, B., Leveille, E., Ruskey, J. A., Spiegelman, D., Liong, C., Fon, E. A., Rouleau, G. A., Dauvilliers, Y., Dupre, N., Alcalay, R. N. & Gan-Or, Z. 2018.

Sequencing of the GBA coactivator, Saposin C, in Parkinson disease. *Neurobiol Aging,* 72**,** 187 e1-187 e3.

Pacelli, C., Giguere, N., Bourque, M. J., Levesque, M., Slack, R. S. & Trudeau, L. E. 2015. Elevated Mitochondrial Bioenergetics and Axonal Arborization Size Are Key Contributors to the Vulnerability of Dopamine Neurons. *Curr Biol,* 25**,** 2349-60.

Pachi, I., Koros, C., Simitsi, A. M., Papadimitriou, D., Bougea, A., Prentakis, A., Papagiannakis, N., Bozi, M., Antonelou, R., Angelopoulou, E., Beratis, I., Stamelou, M., Trapali, X. G., Papageorgiou, S. G. & Stefanis, L. 2021. Apathy: An underestimated feature in GBA and LRRK2 non-manifesting mutation carriers. *Parkinsonism Relat Disord,* 91**,** 1-8.

Pagano, G., Ferrara, N., Brooks, D. J. & Pavese, N. 2016. Age at onset and Parkinson disease phenotype. *Neurology,* 86**,** 1400-1407.

Pal, G., Mangone, G., Hill, E. J., Ouyang, B., Liu, Y., Lythe, V., Ehrlich, D., Saunders-Pullman, R., Shanker, V., Bressman, S., Alcalay, R. N., Garcia, P., Marder, K. S., Aasly, J., Mouradian, M. M., Link, S., Rosenbaum, M., Anderson, S., Bernard, B., Wilson, R., Stebbins, G., Nichols, W. C., Welter, M. L., Sani, S., Afshari, M., Verhagen, L., De Bie, R. M. A., Foltynie, T., Hall, D., Corvol, J. C. & Goetz, C. G. 2022. Parkinson Disease and Subthalamic Nucleus Deep Brain Stimulation: Cognitive Effects in GBA Mutation Carriers. *Ann Neurol,* 91**,** 424-435.

Palakurthi, B. & Burugupally, S. P. 2019. Postural Instability in Parkinson's Disease: A Review. *Brain Sci,* 9.

Panadeiro, V., Rodriguez, A., Henry, J., Wlodkowic, D. & Andersson, M. 2021. A review of 28 free animal-tracking software applications: current features and limitations. *Lab Anim (NY),* 50**,** 246-254.

Pankratz, N., Beecham, G. W., Destefano, A. L., Dawson, T. M., Doheny, K. F., Factor, S. A., Hamza, T. H., Hung, A. Y., Hyman, B. T., Ivinson, A. J., Krainc, D., Latourelle, J. C., Clark, L. N., Marder, K., Martin, E. R., Mayeux, R., Ross, O. A., Scherzer, C. R., Simon, D. K., Tanner, C., Vance, J. M., Wszolek, Z. K., Zabetian, C. P., Myers, R. H., Payami, H., Scott, W. K., Foroud, T. & Consortium, P. G. 2012. Meta-analysis of Parkinson's disease: identification of a novel locus, RIT2. *Ann Neurol,* 71**,** 370-84.

Panteghini, C., Reale, C., Colangelo, I., Suerz, M., Catania, A., Garavaglia, B. & Invernizzi, F. 2023. Sex distribution and classification of GBA1 variants in an Italian cohort of Parkinson's disease patients analyzed over the last seventeen years. *Parkinsonism Relat Disord,* 117**,** 105919.

Papadopoulos, V. E., Nikolopoulou, G., Antoniadou, I., Karachaliou, A., Arianoglou, G., Emmanouilidou, E., Sardi, S. P., Stefanis, L. & Vekrellis, K. 2018. Modulation of beta-glucocerebrosidase increases alpha-synuclein secretion and exosome release in mouse models of Parkinson's disease. *Hum Mol Genet,* 27**,** 1696-1710.

Park, J. K., Orvisky, E., Tayebi, N., Kaneski, C., Lamarca, M. E., Stubblefield, B. K., Martin, B. M., Schiffmann, R. & Sidransky, E. 2003. Myoclonic epilepsy in Gaucher disease: genotype-phenotype insights from a rare patient subgroup. *Pediatr Res,* 53**,** 387-95.

Park, J. K., Tayebi, N., Stubblefield, B. K., Lamarca, M. E., Mackenzie, J. J., Stone, D. L. & Sidransky, E. 2002. The E326K mutation and Gaucher disease: mutation or polymorphism? *Clin Genet,* 61**,** 32-4.

Parkinson, J. 1817. An essay on the shaking palsy. 1817. London: Sherwood, Neely and Jones. *Reprinted (2002) in J Neuropsychiatry Clin Neurosci,* 14**,** 223-36; discussion 222.

Parkinson Study Group, C. C. I. 2009. Long-term effect of initiating pramipexole vs levodopa in early Parkinson disease. *Arch Neurol,* 66**,** 563-70.

Parkkinen, S., Ortega, F. J., Kuptsova, K., Huttunen, J., Tarkka, I. & Jolkkonen, J. 2013. Gait impairment in a rat model of focal cerebral ischemia. *Stroke Res Treat,* 2013**,** 410972.

Parlar, S. C., Grenn, F. P., Kim, J. J., Baluwendraat, C. & Gan-Or, Z. 2023. Classification of GBA1 Variants in Parkinson's Disease: The GBA1-PD Browser. *Mov Disord,* 38**,** 489-495.

Parnetti, L., Paciotti, S., Eusebi, P., Dardis, A., Zampieri, S., Chiasserini, D., Tasegian, A., Tambasco, N., Bembi, B., Calabresi, P. & Beccari, T. 2017. Cerebrospinal fluid beta-glucocerebrosidase activity is reduced in parkinson's disease patients. *Mov Disord,* 32**,** 1423-1431.

Patel, J. C., Sherpa, A. D., Melani, R., Witkovsky, P., Wiseman, M. R., O'neill, B., Aoki, C., Tritsch, N. X. & Rice, M. E. 2024. GABA co-released from striatal dopamine axons dampens phasic dopamine release through autoregulatory GABA(A) receptors. *Cell Rep,* 43**,** 113834.

Paul, A., Jacoby, G., Laor Bar-Yosef, D., Beck, R., Gazit, E. & Segal, D. 2021. Glucosylceramide Associated with Gaucher Disease Forms Amyloid-like Twisted Ribbon Fibrils That Induce alpha-Synuclein Aggregation. *ACS Nano,* 15**,** 11854-11868.

Paushter, D. H., Du, H., Feng, T. & Hu, F. 2018. The lysosomal function of progranulin, a guardian against neurodegeneration. *Acta Neuropathol,* 136**,** 1-17.

Pavan, E., Peruzzo, P., Cattarossi, S., Bergamin, N., Bordugo, A., Sechi, A., Scarpa, M., Biasizzo, J., Colucci, F. & Dardis, A. 2024. Deficiency of Glucocerebrosidase Activity beyond Gaucher Disease: PSAP and LIMP-2 Dysfunctions. *Int J Mol Sci,* 25.

Pedersen, K. F., Larsen, J. P., Tysnes, O. B. & Alves, G. 2017. Natural course of mild cognitive impairment in Parkinson disease: A 5-year population-based study. *Neurology,* 88**,** 767-774.

Pellow, S., Chopin, P., File, S. E. & Briley, M. 1985. Validation of open:closed arm entries in an elevated plus-maze as a measure of anxiety in the rat. *J Neurosci Methods,* 14**,** 149-67.

Peng, S., Liu, P., Wang, X. & Li, K. 2025. Global, regional and national burden of Parkinson's disease in people over 55 years of age: a systematic analysis of the global burden of disease study, 1991-2021. *BMC Neurol,* 25**,** 178.

Percie Du Sert, N., Hurst, V., Ahluwalia, A., Alam, S., Avey, M. T., Baker, M., Browne, W. J., Clark, A., Cuthill, I. C., Dirnagl, U., Emerson, M., Garner, P., Holgate, S. T., Howells, D. W., Karp, N. A., Lazic, S. E., Lidster, K., Maccallum, C. J., Macleod, M., Pearl, E. J., Petersen, O. H., Rawle, F., Reynolds, P., Rooney, K., Sena, E. S., Silberberg, S. D., Steckler, T. & Wurbel, H. 2020. The ARRIVE guidelines 2.0: Updated guidelines for reporting animal research. *Exp Physiol,* 105**,** 1459-1466.

Pereira, G. M., Teixeira-Dos-Santos, D., Soares, N. M., Marconi, G. A., Friedrich, D. C., Saffie Awad, P., Santos-Lobato, B. L., Brandao, P. R. P., Noyce, A. J., Marras, C., Mata, I. F., Rieder, C. R. M. & Schuh, A. F. S. 2024. A systematic review and meta-analysis of the prevalence of Parkinson's disease in lower to upper-middle-income countries. *NPJ Parkinsons Dis,* 10**,** 181.

Perlman, R. L. 2016. Mouse models of human disease: An evolutionary perspective. *Evol Med Public Health,* 2016**,** 170-6.

Pernold, K., Iannello, F., Low, B. E., Rigamonti, M., Rosati, G., Scavizzi, F., Wang, J., Raspa, M., Wiles, M. V. & Ulfhake, B. 2019. Towards large scale automated cage monitoring - Diurnal rhythm and impact of interventions on in-cage activity of C57BL/6J mice recorded 24/7 with a non-disrupting capacitive-based technique. *PLoS One,* 14**,** e0211063.

Peterschmitt, M. J., Saiki, H., Hatano, T., Gasser, T., Isaacson, S. H., Gaemers, S. J. M., Minini, P., Saubadu, S., Sharma, J., Walbillic, S., Alcalay, R. N., Cutter, G., Hattori, N., Hoglinger, G. U., Marek, K., Schapira, A. H. V., Scherzer, C. R., Simuni, T., Giladi, N., Sardi, S. P., Fischer, T. Z. & Investigators, M.-P. 2022. Safety, Pharmacokinetics, and Pharmacodynamics of Oral Venglustat in Patients with Parkinson's Disease and a GBA Mutation: Results from Part 1 of the Randomized, Double-Blinded, Placebo-Controlled MOVES-PD Trial. *J Parkinsons Dis,* 12**,** 557-570.

Petrucci, S., Ginevrino, M., Trezzi, I., Monfrini, E., Ricciardi, L., Albanese, A., Avenali, M., Barone, P., Bentivoglio, A. R., Bonifati, V., Bove, F., Bonanni, L., Brusa, L., Cereda, C., Cossu, G., Criscuolo, C., Dati, G., De Rosa, A., Eleopra, R., Fabbrini, G., Fadda, L., Garbellini, M., Minafra, B., Onofrj, M., Pacchetti, C., Palmieri, I., Pellecchia, M. T., Petracca, M., Picillo, M., Pisani, A., Vallelunga, A., Zangaglia, R., Di Fonzo, A., Morgante, F., Valente, E. M. & Group, I.-G.-P. S. 2020. GBA-Related Parkinson's Disease: Dissection of Genotype-Phenotype Correlates in a Large Italian Cohort. *Mov Disord,* 35**,** 2106-2111.

Picillo, M., Nicoletti, A., Fetoni, V., Garavaglia, B., Barone, P. & Pellecchia, M. T. 2017. The relevance of gender in Parkinson's disease: a review. *J Neurol,* 264**,** 1583-1607.

Pietrafesa, D., Casamassa, A., Benassi, B., Santoro, M., Marano, M., Consales, C., Rosati, J. & Arcangeli, C. 2024. Investigating the Impact of the Parkinson's-Associated GBA1 E326K Mutation on beta-Glucocerebrosidase Dimerization and Interactome Dynamics Through an In Silico Approach. *Int J Mol Sci,* 25.

Piovesan, D., Minervini, G. & Tosatto, S. C. 2016. The RING 2.0 web server for high quality residue interaction networks. *Nucleic Acids Res,* 44**,** W367-74.

Pitzer, C., Kurpiers, B. & Eltokhi, A. 2021. Gait performance of adolescent mice assessed by the CatWalk XT depends on age, strain and sex and correlates with speed and body weight. *Sci Rep,* 11**,** 21372.

Plotegher, N., Perocheau, D., Ferrazza, R., Massaro, G., Bhosale, G., Zambon, F., Rahim, A. A., Guella, G., Waddington, S. N., Szabadkai, G. & Duchen, M. R. 2020. Impaired cellular bioenergetics caused by GBA1 depletion sensitizes neurons to calcium overload. *Cell Death Differ,* 27**,** 1588-1603.

Plotnik, M. & Hausdorff, J. M. 2008. The role of gait rhythmicity and bilateral coordination of stepping in the pathophysiology of freezing of gait in Parkinson's disease. *Mov Disord,* 23 Suppl 2**,** S444-50.

Poewe, W., Seppi, K., Tanner, C. M., Halliday, G. M., Brundin, P., Volkmann, J., Schrag, A. E. & Lang, A. E. 2017. Parkinson disease. *Nat Rev Dis Primers,* 3**,** 17013.

Pol-Fachin, L., Siebert, M., Verli, H. & Saraiva-Pereira, M. L. 2016. Glycosylation is crucial for a proper catalytic site organization in human glucocerebrosidase. *Glycoconj J,* 33**,** 237-44.

Polinski, N. K., Martinez, T. N., Gorodinsky, A., Gareus, R., Sasner, M., Herberth, M., Switzer, R., Ahmad, S. O., Cosden, M., Kandebo, M., Drolet, R. E., Buckett, P. D., Shan, W., Chen, Y., Pellegrino, L. J., Ellsworth, G. D., Dungan, L. B., Hirst, W. D., Clark, S. W. & Dave, K. D. 2021. Decreased glucocerebrosidase activity and substrate accumulation of glycosphingolipids in a novel GBA1 D409V knock-in mouse model. *PLoS One,* 16**,** e0252325.

Polinski, N. K., Martinez, T. N., Ramboz, S., Sasner, M., Herberth, M., Switzer, R., Ahmad, S. O., Pelligrino, L. J., Clark, S. W., Marcus, J. N., Smith, S. M., Dave, K. D. & Frasier, M. A. 2022. The GBA1 D409V mutation exacerbates synuclein pathology to differing extents in two alpha-synuclein models. *Dis Model Mech,* 15.

Polissidis, A., Koronaiou, E., Nikolopoulou, G., Viel, C., Nikatou, M., Bogiongko, M., Sardi, S. P., Xilouri, M., Vekrellis, K. & Stefanis, L. 2022. A double-hit in vivo model of GBA viral microRNA-mediated downregulation and human alpha-synuclein overexpression demonstrates nigrostriatal degeneration. *Neurobiol Dis,* 163**,** 105612.

Polymeropoulos, M. H., Lavedan, C., Leroy, E., Ide, S. E., Dehejia, A., Dutra, A., Pike, B., Root, H., Rubenstein, J., Boyer, R., Stenroos, E. S., Chandrasekharappa, S., Athanassiadou, A., Papapetropoulos, T., Johnson, W. G., Lazzarini, A. M., Duvoisin, R. C., Di Iorio, G., Golbe, L. I. & Nussbaum, R. L. 1997. Mutation in the alpha-synuclein gene identified in families with Parkinson's disease. *Science,* 276**,** 2045-7.

Pontone, G. M., Dissanayka, N., Apostolova, L., Brown, R. G., Dobkin, R., Dujardin, K., Friedman, J. H., Leentjens, A. F. G., Lenze, E. J., Marsh, L., Mari, L., Monchi, O., Richard, I. H., Schrag, A., Strafella, A. P., Vernaleo, B., Weintraub, D. & Mari, Z. 2019. Report from a multidisciplinary meeting on anxiety as a non-motor manifestation of Parkinson's disease. *NPJ Parkinsons Dis,* 5**,** 30.

Porras, G., Li, Q. & Bezard, E. 2012. Modeling Parkinson's disease in primates: The MPTP model. *Cold Spring Harb Perspect Med,* 2**,** a009308.

Postuma, R. B., Aarsland, D., Barone, P., Burn, D. J., Hawkes, C. H., Oertel, W. & Ziemssen, T. 2012. Identifying prodromal Parkinson's disease: pre-motor disorders in Parkinson's disease. *Mov Disord,* 27**,** 617-26.

Postuma, R. B. & Berg, D. 2016. Advances in markers of prodromal Parkinson disease. *Nat Rev Neurol,* 12**,** 622-634.

Postuma, R. B., Berg, D., Stern, M., Poewe, W., Olanow, C. W., Oertel, W., Obeso, J., Marek, K., Litvan, I., Lang, A. E., Halliday, G., Goetz, C. G., Gasser, T., Dubois, B., Chan, P., Bloem, B. R., Adler, C. H. & Deuschl, G. 2015. MDS clinical diagnostic criteria for Parkinson's disease. *Mov Disord,* 30**,** 1591-601.

Pradas, E. & Martinez-Vicente, M. 2023. The Consequences of GBA Deficiency in the Autophagy-Lysosome System in Parkinson's Disease Associated with GBA. *Cells,* 12.

Premkumar, L., Sawkar, A. R., Boldin-Adamsky, S., Toker, L., Silman, I., Kelly, J. W., Futerman, A. H. & Sussman, J. L. 2005. X-ray structure of human acid-beta-glucosidase covalently bound to conduritol-B-epoxide. Implications for Gaucher disease. *J Biol Chem,* 280**,** 23815-9.

Prendergast, B. J., Onishi, K. G. & Zucker, I. 2014. Female mice liberated for inclusion in neuroscience and biomedical research. *Neurosci Biobehav Rev,* 40**,** 1-5.

Pringsheim, T., Day, G. S., Smith, D. B., Rae-Grant, A., Licking, N., Armstrong, M. J., De Bie, R. M. A., Roze, E., Miyasaki, J. M., Hauser, R. A., Espay, A. J., Martello, J. P., Gurwell, J. A., Billinghurst, L., Sullivan, K., Fitts, M. S., Cothros, N., Hall, D. A., Rafferty, M., Hagerbrant, L., Hastings, T., O'brien, M. D., Silsbee, H., Gronseth, G., Lang, A. E. & Guideline Subcommittee of The, A. a. N. 2021. Dopaminergic Therapy for Motor Symptoms in Early Parkinson Disease Practice Guideline Summary: A Report of the AAN Guideline Subcommittee. *Neurology,* 97**,** 942-957.

Pringsheim, T., Jette, N., Frolkis, A. & Steeves, T. D. 2014. The prevalence of Parkinson's disease: a systematic review and meta-analysis. *Mov Disord,* 29**,** 1583-90.

Proteinatlas.Org. 2024. *The Human Protein Atlas* [Online]. Available: https://www.proteinatlas.org/ [Accessed 11 March 2025].

Quinn, P. M. J., Moreira, P. I., Ambrosio, A. F. & Alves, C. H. 2020. PINK1/PARKIN signalling in neurodegeneration and neuroinflammation. *Acta Neuropathol Commun,* 8**,** 189.

Radlicka-Borysewska, A., Jablonska, J., Lenarczyk, M., Szumiec, L., Harda, Z., Baginska, M., Barut, J., Pera, J., Kreiner, G., Wojcik, D. K. & Rodriguez Parkitna, J. 2024. Non-motor symptoms associated with progressive loss of dopaminergic neurons in a mouse model of Parkinson's disease. *Front Neurosci,* 18**,** 1375265.

Ran, C., Brodin, L., Forsgren, L., Westerlund, M., Ramezani, M., Gellhaar, S., Xiang, F., Fardell, C., Nissbrandt, H., Soderkvist, P., Puschmann, A., Ygland, E., Olson, L., Willows, T., Johansson, A., Sydow, O., Wirdefeldt, K., Galter, D., Svenningsson, P. & Belin, A. C. 2016. Strong association between glucocerebrosidase mutations and Parkinson's disease in Sweden. *Neurobiol Aging,* 45**,** 212 e5-212 e11.

Reczek, D., Schwake, M., Schroder, J., Hughes, H., Blanz, J., Jin, X., Brondyk, W., Van Patten, S., Edmunds, T. & Saftig, P. 2007. LIMP-2 is a receptor for lysosomal mannose-6-phosphate-independent targeting of beta-glucocerebrosidase. *Cell,* 131**,** 770-83.

Redman, P. T., Jefferson, B. S., Ziegler, C. B., Mortensen, O. V., Torres, G. E., Levitan, E. S. & Aizenman, E. 2006. A vital role for voltage-dependent potassium channels in dopamine transporter-mediated 6-hydroxydopamine neurotoxicity. *Neuroscience,* 143**,** 1-6.

Reed, X., Bandres-Ciga, S., Blauwendraat, C. & Cookson, M. R. 2019. The role of monogenic genes in idiopathic Parkinson's disease. *Neurobiol Dis,* 124**,** 230-239.

Reeve, A., Simcox, E. & Turnbull, D. 2014. Ageing and Parkinson's disease: why is advancing age the biggest risk factor? *Ageing Res Rev,* 14**,** 19-30.

Ren, J., Zhang, R., Pan, C., Xu, J., Sun, H., Hua, P., Zhang, L., Zhang, W., Xu, P., Ma, C. & Liu, W. 2022. Prevalence and genotype-phenotype correlations of GBA-related Parkinson disease in a large Chinese cohort. *Eur J Neurol,* 29**,** 1017-1024.

Revel-Vilk, S., Fuller, M. & Zimran, A. 2020. Value of Glucosylsphingosine (Lyso-Gb1) as a Biomarker in Gaucher Disease: A Systematic Literature Review. *Int J Mol Sci,* 21.

Reza, S., Ugorski, M. & Suchanski, J. 2021. Glucosylceramide and galactosylceramide, small glycosphingolipids with significant impact on health and disease. *Glycobiology,* 31**,** 1416-1434.

Rezvanian, S., Lockhart, T., Frames, C., Soangra, R. & Lieberman, A. 2018. Motor Subtypes of Parkinson's Disease Can Be Identified by Frequency Component of Postural Stability. *Sensors (Basel),* 18.

Riboldi, G. M. & Di Fonzo, A. B. 2019. GBA, Gaucher Disease, and Parkinson's Disease: From Genetic to Clinic to New Therapeutic Approaches. *Cells,* 8.

Rice, M. E. & Cragg, S. J. 2004. Nicotine amplifies reward-related dopamine signals in striatum. *Nat Neurosci,* 7**,** 583-4.

Rice, M. E. & Cragg, S. J. 2008. Dopamine spillover after quantal release: rethinking dopamine transmission in the nigrostriatal pathway. *Brain Res Rev,* 58**,** 303-13.

Rice, M. E., Patel, J. C. & Cragg, S. J. 2011. Dopamine release in the basal ganglia. *Neuroscience,* 198**,** 112-37.

Ridley, C. M., Thur, K. E., Shanahan, J., Thillaiappan, N. B., Shen, A., Uhl, K., Walden, C. M., Rahim, A. A., Waddington, S. N., Platt, F. M. & Van Der Spoel, A. C. 2013. beta-Glucosidase 2 (GBA2) activity and imino sugar pharmacology. *J Biol Chem,* 288**,** 26052-26066.

Rietdijk, C. D., Perez-Pardo, P., Garssen, J., Van Wezel, R. J. & Kraneveld, A. D. 2017. Exploring Braak's Hypothesis of Parkinson's Disease. *Front Neurol,* 8**,** 37.

Rizig, M., Bandres-Ciga, S., Makarious, M. B., Ojo, O. O., Crea, P. W., Abiodun, O. V., Levine, K. S., Abubakar, S. A., Achoru, C. O., Vitale, D., Adeniji, O. A., Agabi, O. P., Koretsky, M. J., Agulanna, U., Hall, D. A., Akinyemi, R. O., Xie, T., Ali, M. W., Shamim, E. A., Ani-Osheku, I., Padmanaban, M., Arigbodi, O. M., Standaert, D. G.,

Bello, A. H., Dean, M. N., Erameh, C. O., Elsayed, I., Farombi, T. H., Okunoye, O., Fawale, M. B., Billingsley, K. J., Imarhiagbe, F. A., Jerez, P. A., Iwuozo, E. U., Baker, B., Komolafe, M. A., Malik, L., Nwani, P. O., Daida, K., Nwazor, E. O., Miano-Burkhardt, A., Nyandaiti, Y. W., Fang, Z. H., Obiabo, Y. O., Kluss, J. H., Odeniyi, O. A., Hernandez, D. G., Odiase, F. E., Tayebi, N., Ojini, F. I., Sidranksy, E., Onwuegbuzie, G. A., D'souza, A. M., Osaigbovo, G. O., Berhe, B., Osemwegie, N., Reed, X., Oshinaike, O. O., Leonard, H. L., Otubogun, F. M., Alvarado, C. X., Oyakhire, S. I., Ozomma, S. I., Samuel, S. C., Taiwo, F. T., Wahab, K. W., Zubair, Y. A., Iwaki, H., Kim, J. J., Morris, H. R., Hardy, J., Nalls, M. A., Heilbron, K., Norcliffe-Kaufmann, L., Nigeria Parkinson Disease Research, N., International Parkinson's Disease Genomics Consortium, A., Black, African American Connections to Parkinson's Disease Study, G., Andme Research, T., Blauwendraat, C., Houlden, H., Singleton, A., Okubadejo, N. U. & Global Parkinson's Genetics, P. 2023. Identification of genetic risk loci and causal insights associated with Parkinson's disease in African and African admixed populations: a genome-wide association study. *Lancet Neurol,* 22**,** 1015-1025.

Roberts, B. M., Doig, N. M., Brimblecombe, K. R., Lopes, E. F., Siddorn, R. E., Threlfell, S., Connor-Robson, N., Bengoa-Vergniory, N., Pasternack, N., Wade-Martins, R., Magill, P. J. & Cragg, S. J. 2020. GABA uptake transporters support dopamine release in dorsal striatum with maladaptive downregulation in a parkinsonism model. *Nat Commun,* 11**,** 4958.

Roberts, B. M., Lopes, E. F. & Cragg, S. J. 2021. Axonal Modulation of Striatal Dopamine Release by Local gamma-Aminobutyric Acid (GABA) Signalling. *Cells,* 10.

Roberts, R. F., Bengoa-Vergniory, N. & Alegre-Abarrategui, J. 2019. Alpha-Synuclein Proximity Ligation Assay (AS-PLA) in Brain Sections to Probe for Alpha-Synuclein Oligomers. *Methods Mol Biol,* 1948**,** 69-76.

Rocha, E. M., Smith, G. A., Park, E., Cao, H., Brown, E., Hallett, P. & Isacson, O. 2015a. Progressive decline of glucocerebrosidase in aging and Parkinson's disease. *Ann Clin Transl Neurol,* 2**,** 433-8.

Rocha, E. M., Smith, G. A., Park, E., Cao, H., Brown, E., Hayes, M. A., Beagan, J., Mclean, J. R., Izen, S. C., Perez-Torres, E., Hallett, P. J. & Isacson, O. 2015b. Glucocerebrosidase gene therapy prevents alpha-synucleinopathy of midbrain dopamine neurons. *Neurobiol Dis,* 82**,** 495-503.

Rocha, E. M., Smith, G. A., Park, E., Cao, H., Graham, A. R., Brown, E., Mclean, J. R., Hayes, M. A., Beagan, J., Izen, S. C., Perez-Torres, E., Hallett, P. J. & Isacson, O. 2015c. Sustained Systemic Glucocerebrosidase Inhibition Induces Brain alpha-Synuclein Aggregation, Microglia and Complement C1q Activation in Mice. *Antioxid Redox Signal,* 23**,** 550-64.

Rockenstein, E., Clarke, J., Viel, C., Panarello, N., Treleaven, C. M., Kim, C., Spencer, B., Adame, A., Park, H., Dodge, J. C., Cheng, S. H., Shihabuddin, L. S., Masliah, E. & Sardi, S. P. 2016. Glucocerebrosidase modulates cognitive and motor activities in murine models of Parkinson's disease. *Hum Mol Genet,* 25**,** 2645-2660.

Rodrigues, J. P., Trellet, M., Schmitz, C., Kastritis, P., Karaca, E., Melquiond, A. S. & Bonvin, A. M. 2012. Clustering biomolecular complexes by residue contacts similarity. *Proteins,* 80**,** 1810-7.

Rodríguez-Traver, E., Suárez, L. M., Crespo, C., González-Burgos, I., Vecino, R., Jurado-Coronel, J. C., Galán, M., González-González, M., Moratalla, R. & Vicario, C. 2024. GBA1 mutations alter neuronal firing and structure, regulating VGLUT2 and CRYAB in dopamine neurons. *bioRxiv,* preprint**,** DOI: 10.1101/2024.08.05.606574.

Roeben, B., Liepelt-Scarfone, I., Lerche, S., Zimmermann, M., Wurster, I., Sunkel, U., Schulte, C., Deuschle, C., Eschweiler, G. W., Maetzler, W., Gasser, T., Berg, D. & Brockmann, K. 2024. Longitudinal cognitive decline characterizes the profile of non-PD-manifest GBA1 mutation carriers. *NPJ Parkinsons Dis,* 10**,** 88.

Rolfs, A., Giese, A. K., Grittner, U., Mascher, D., Elstein, D., Zimran, A., Bottcher, T., Lukas, J., Hubner, R., Golnitz, U., Rohle, A., Dudesek, A., Meyer, W., Wittstock, M. & Mascher, H. 2013. Glucosylsphingosine is a highly sensitive and specific biomarker for primary diagnostic and follow-up monitoring in Gaucher disease in a non-Jewish, Caucasian cohort of Gaucher disease patients. *PLoS One,* 8**,** e79732.

Romero, R., Ramanathan, A., Yuen, T., Bhowmik, D., Mathew, M., Munshi, L. B., Javaid, S., Bloch, M., Lizneva, D., Rahimova, A., Khan, A., Taneja, C., Kim, S. M., Sun, L., New, M. I., Haider, S. & Zaidi, M. 2019. Mechanism of glucocerebrosidase activation and dysfunction in Gaucher disease unraveled by molecular dynamics and deep learning. *Proc Natl Acad Sci U S A,* 116**,** 5086-5095.

Ron, I. & Horowitz, M. 2005. ER retention and degradation as the molecular basis underlying Gaucher disease heterogeneity. *Hum Mol Genet,* 14**,** 2387-98.

Ron, I., Rapaport, D. & Horowitz, M. 2010. Interaction between parkin and mutant glucocerebrosidase variants: a possible link between Parkinson disease and Gaucher disease. *Hum Mol Genet,* 19**,** 3771-81.

Rosborough, K., Patel, N. & Kalia, L. V. 2017. alpha-Synuclein and Parkinsonism: Updates and Future Perspectives. *Curr Neurol Neurosci Rep,* 17**,** 31.

Rosety, I., Zagare, A., Saraiva, C., Nickels, S., Antony, P., Almeida, C., Glaab, E., Halder, R., Velychko, S., Rauen, T., Scholer, H. R., Bolognin, S., Sauter, T., Jarazo, J., Kruger, R. & Schwamborn, J. C. 2023. Impaired neuron differentiation in GBA-associated Parkinson's disease is linked to cell cycle defects in organoids. *NPJ Parkinsons Dis,* 9**,** 166.

Rosh, I., Tripathi, U., Hussein, Y., Rike, W. A., Djamus, J., Shklyar, B., Manole, A., Houlden, H., Winkler, J., Gage, F. H. & Stern, S. 2024. Synaptic dysfunction and extracellular matrix dysregulation in dopaminergic neurons from sporadic and E326K-GBA1 Parkinson's disease patients. *NPJ Parkinsons Dis,* 10**,** 38.

Ross, O. A., Braithwaite, A. T., Skipper, L. M., Kachergus, J., Hulihan, M. M., Middleton, F. A., Nishioka, K., Fuchs, J., Gasser, T., Maraganore, D. M., Adler, C. H., Larvor, L., Chartier-Harlin, M. C., Nilsson, C., Langston, J. W., Gwinn, K., Hattori, N. & Farrer, M. J. 2008. Genomic investigation of alpha-synuclein multiplication and parkinsonism. *Ann Neurol,* 63**,** 743-50.

Rossi, A., Berger, K., Chen, H., Leslie, D., Mailman, R. B. & Huang, X. 2018. Projection of the prevalence of Parkinson's disease in the coming decades: Revisited. *Mov Disord,* 33**,** 156-159.

Rossi, M., Castillo-Torres, S. A. & Merello, M. 2022. Early motor response to dopamine replacement therapy in Parkinson's disease patients carrying GBA variants. *J Neurol Sci,* 440**,** 120354.

Rossi, M., Schaake, S., Usnich, T., Boehm, J., Steffen, N., Schell, N., Kruger, C., Gul-Demirkale, T., Bahr, N., Kleinz, T., Madoev, H., Laabs, B. H., Gan-Or, Z., Alcalay, R. N., Lohmann, K. & Klein, C. 2025. Classification and Genotype-Phenotype Relationships of GBA1 Variants: MDSGene Systematic Review. *Mov Disord,* 40**,** 605-618.

Rothaug, M., Zunke, F., Mazzulli, J. R., Schweizer, M., Altmeppen, H., Lullmann-Rauch, R., Kallemeijn, W. W., Gaspar, P., Aerts, J. M., Glatzel, M., Saftig, P., Krainc, D., Schwake, M. & Blanz, J. 2014. LIMP-2 expression is critical for beta-

glucocerebrosidase activity and alpha-synuclein clearance. *Proc Natl Acad Sci U S A,* 111**,** 15573-8.

Rubilar, J. C., Outeiro, T. F. & Klein, A. D. 2024. The lysosomal beta-glucocerebrosidase strikes mitochondria: implications for Parkinson's therapeutics. *Brain,* 147**,** 2610-2620.

Ruskey, J. A., Greenbaum, L., Ronciere, L., Alam, A., Spiegelman, D., Liong, C., Levy, O. A., Waters, C., Fahn, S., Marder, K. S., Chung, W., Yahalom, G., Israeli-Korn, S., Livneh, V., Fay-Karmon, T., Alcalay, R. N., Hassin-Baer, S. & Gan-Or, Z. 2019. Increased yield of full GBA sequencing in Ashkenazi Jews with Parkinson's disease. *Eur J Med Genet,* 62**,** 65-69.

Russell, W. M. S., Burch, R.L., Hume, C.W. 1959. *The principles of humane experimental technique,* London, Methuen.

Rustay, N. R., Wahlsten, D. & Crabbe, J. C. 2003a. Assessment of genetic susceptibility to ethanol intoxication in mice. *Proc Natl Acad Sci U S A,* 100**,** 2917-22.

Rustay, N. R., Wahlsten, D. & Crabbe, J. C. 2003b. Influence of task parameters on rotarod performance and sensitivity to ethanol in mice. *Behav Brain Res,* 141**,** 237-49.

Ruz, C., Barrero, F. J., Pelegrina, J., Bandres-Ciga, S., Vives, F. & Duran, R. 2022. Saposin C, Key Regulator in the Alpha-Synuclein Degradation Mediated by Lysosome. *Int J Mol Sci,* 23.

Salat, D., Noyce, A. J., Schrag, A. & Tolosa, E. 2016. Challenges of modifying disease progression in prediagnostic Parkinson's disease. *Lancet Neurol,* 15**,** 637-48.

Salat, D. & Tolosa, E. 2013. Levodopa in the treatment of Parkinson's disease: current status and new developments. *J Parkinsons Dis,* 3**,** 255-69.

Salvioli, R., Tatti, M., Scarpa, S., Moavero, S. M., Ciaffoni, F., Felicetti, F., Kaneski, C. R., Brady, R. O. & Vaccaro, A. M. 2005. The N370S (Asn370-->Ser) mutation affects the capacity of glucosylceramidase to interact with anionic phospholipid-containing membranes and saposin C. *Biochem J,* 390**,** 95-103.

Sanchez, A. V., Ison, J. M., Hemley, H., Willis, A., Siddiqi, B., Macklin, E. A., Ulysse, C., Reynolds, M., Schwarzschild, M. A. & Jackson, J. D. 2022. Designing the Fostering Inclusivity in Research Engagement for Underrepresented Populations in Parkinson's Disease study. *Contemp Clin Trials,* 115**,** 106713.

Sanchez-Martinez, A., Beavan, M., Gegg, M. E., Chau, K. Y., Whitworth, A. J. & Schapira, A. H. 2016. Parkinson disease-linked GBA mutation effects reversed by molecular chaperones in human cell and fly models. *Sci Rep,* 6**,** 31380.

Sanders, A., Hemmelgarn, H., Melrose, H. L., Hein, L., Fuller, M. & Clarke, L. A. 2013. Transgenic mice expressing human glucocerebrosidase variants: utility for the study of Gaucher disease. *Blood Cells Mol Dis,* 51**,** 109-15.

Sanderson, J. B., De, S., Jiang, H., Rovere, M., Jin, M., Zaccagnini, L., Hays Watson, A., De Boni, L., Lagomarsino, V. N., Young-Pearse, T. L., Liu, X., Pochapsky, T. C., Hyman, B. T., Dickson, D. W., Klenerman, D., Selkoe, D. J. & Bartels, T. 2020. Analysis of alpha-synuclein species enriched from cerebral cortex of humans with sporadic dementia with Lewy bodies. *Brain Commun,* 2**,** fcaa010.

Sang, S., Ba, Y. & Yang, N. 2024. Longitudinal faster anxiety progression of GBA variant carriers in the early Parkinson's disease cohort. *Front Neurosci,* 18**,** 1353759.

Sardi, S. P., Clarke, J., Kinnecom, C., Tamsett, T. J., Li, L., Stanek, L. M., Passini, M. A., Grabowski, G. A., Schlossmacher, M. G., Sidman, R. L., Cheng, S. H. & Shihabuddin, L. S. 2011. CNS expression of glucocerebrosidase corrects alpha-synuclein pathology and memory in a mouse model of Gaucher-related synucleinopathy. *Proc Natl Acad Sci U S A,* 108**,** 12101-6.

Sardi, S. P., Clarke, J., Viel, C., Chan, M., Tamsett, T. J., Treleaven, C. M., Bu, J., Sweet, L., Passini, M. A., Dodge, J. C., Yu, W. H., Sidman, R. L., Cheng, S. H. & Shihabuddin, L. S. 2013. Augmenting CNS glucocerebrosidase activity as a therapeutic strategy for parkinsonism and other Gaucher-related synucleinopathies. *Proc Natl Acad Sci U S A,* 110**,** 3537-42.

Sardi, S. P., Viel, C., Clarke, J., Treleaven, C. M., Richards, A. M., Park, H., Olszewski, M. A., Dodge, J. C., Marshall, J., Makino, E., Wang, B., Sidman, R. L., Cheng, S. H. & Shihabuddin, L. S. 2017. Glucosylceramide synthase inhibition alleviates aberrations in synucleinopathy models. *Proc Natl Acad Sci U S A,* 114**,** 2699-2704.

Sare, R. M., Lemons, A. & Smith, C. B. 2021. Behavior Testing in Rodents: Highlighting Potential Confounds Affecting Variability and Reproducibility. *Brain Sci,* 11.

Sasco, A. J., Paffenbarger, R. S., Jr., Gendre, I. & Wing, A. L. 1992. The role of physical exercise in the occurrence of Parkinson's disease. *Arch Neurol,* 49**,** 360-5.

Satake, W., Nakabayashi, Y., Mizuta, I., Hirota, Y., Ito, C., Kubo, M., Kawaguchi, T., Tsunoda, T., Watanabe, M., Takeda, A., Tomiyama, H., Nakashima, K., Hasegawa, K., Obata, F., Yoshikawa, T., Kawakami, H., Sakoda, S., Yamamoto, M., Hattori, N., Murata, M., Nakamura, Y. & Toda, T. 2009. Genome-wide association study identifies common variants at four loci as genetic risk factors for Parkinson's disease. *Nat Genet,* 41**,** 1303-7.

Savica, R., Grossardt, B. R., Bower, J. H., Ahlskog, J. E. & Rocca, W. A. 2013. Risk factors for Parkinson's disease may differ in men and women: an exploratory study. *Horm Behav,* 63**,** 308-14.

Savica, R., Grossardt, B. R., Bower, J. H., Ahlskog, J. E. & Rocca, W. A. 2016. Time Trends in the Incidence of Parkinson Disease. *JAMA Neurol,* 73**,** 981-9.

Sawamoto, N., Doi, D., Nakanishi, E., Sawamura, M., Kikuchi, T., Yamakado, H., Taruno, Y., Shima, A., Fushimi, Y., Okada, T., Kikuchi, T., Morizane, A., Hiramatsu, S., Anazawa, T., Shindo, T., Ueno, K., Morita, S., Arakawa, Y., Nakamoto, Y., Miyamoto, S., Takahashi, R. & Takahashi, J. 2025. Phase I/II trial of iPS-cell-derived dopaminergic cells for Parkinson's disease. *Nature,* 641**,** 971-977.

Schapira, A. H. V., Chaudhuri, K. R. & Jenner, P. 2017. Non-motor features of Parkinson disease. *Nat Rev Neurosci,* 18**,** 435-450.

Schellinck, H. M., Cyr, D. P., Brown, R. E. 2010. Chapter 7 - How Many Ways Can Mouse Behavioral Experiments Go Wrong? Confounding Variables in Mouse Models of Neurodegenerative Diseases and How to Control Them. *Advances in the Study of Behavior.* Academic Press.

Schenck, C. H., Boeve, B. F. & Mahowald, M. W. 2013. Delayed emergence of a parkinsonian disorder or dementia in 81% of older men initially diagnosed with idiopathic rapid eye movement sleep behavior disorder: a 16-year update on a previously reported series. *Sleep Med,* 14**,** 744-8.

Schiess, N., Cataldi, R., Okun, M. S., Fothergill-Misbah, N., Dorsey, E. R., Bloem, B. R., Barretto, M., Bhidayasiri, R., Brown, R., Chishimba, L., Chowdhary, N., Coslov, M., Cubo, E., Di Rocco, A., Dolhun, R., Dowrick, C., Fung, V. S. C., Gershanik, O. S., Gifford, L., Gordon, J., Khalil, H., Kuhn, A. A., Lew, S., Lim, S. Y., Marano, M. M., Micallef, J., Mokaya, J., Moukheiber, E., Nwabuobi, L., Okubadejo, N., Pal, P. K., Shah, H., Shalash, A., Sherer, T., Siddiqui, B., Thompson, T., Ullrich, A., Walker, R. & Dua, T. 2022. Six Action Steps to Address Global Disparities in Parkinson Disease: A World Health Organization Priority. *JAMA Neurol,* 79**,** 929-936.

Schindelin, J., Arganda-Carreras, I., Frise, E., Kaynig, V., Longair, M., Pietzsch, T., Preibisch, S., Rueden, C., Saalfeld, S., Schmid, B., Tinevez, J. Y., White, D. J.,

Hartenstein, V., Eliceiri, K., Tomancak, P. & Cardona, A. 2012. Fiji: an open-source platform for biological-image analysis. *Nat Methods,* 9**,** 676-82.

Schirinzi, T., Madeo, G., Martella, G., Maltese, M., Picconi, B., Calabresi, P. & Pisani, A. 2016. Early synaptic dysfunction in Parkinson's disease: Insights from animal models. *Mov Disord,* 31**,** 802-13.

Schmitz, M., Alfalah, M., Aerts, J. M., Naim, H. Y. & Zimmer, K. P. 2005. Impaired trafficking of mutants of lysosomal glucocerebrosidase in Gaucher's disease. *Int J Biochem Cell Biol,* 37**,** 2310-20.

Schonauer, S., Korschen, H. G., Penno, A., Rennhack, A., Breiden, B., Sandhoff, K., Gutbrod, K., Dormann, P., Raju, D. N., Haberkant, P., Gerl, M. J., Brugger, B., Zigdon, H., Vardi, A., Futerman, A. H., Thiele, C. & Wachten, D. 2017. Identification of a feedback loop involving beta-glucosidase 2 and its product sphingosine sheds light on the molecular mechanisms in Gaucher disease. *J Biol Chem,* 292**,** 6177-6189.

Schondorf, D. C., Aureli, M., Mcallister, F. E., Hindley, C. J., Mayer, F., Schmid, B., Sardi, S. P., Valsecchi, M., Hoffmann, S., Schwarz, L. K., Hedrich, U., Berg, D., Shihabuddin, L. S., Hu, J., Pruszak, J., Gygi, S. P., Sonnino, S., Gasser, T. & Deleidi, M. 2014. iPSC-derived neurons from GBA1-associated Parkinson's disease patients show autophagic defects and impaired calcium homeostasis. *Nat Commun,* 5**,** 4028.

Schondorf, D. C., Ivanyuk, D., Baden, P., Sanchez-Martinez, A., De Cicco, S., Yu, C., Giunta, I., Schwarz, L. K., Di Napoli, G., Panagiotakopoulou, V., Nestel, S., Keatinge, M., Pruszak, J., Bandmann, O., Heimrich, B., Gasser, T., Whitworth, A. J. & Deleidi, M. 2018. The NAD+ Precursor Nicotinamide Riboside Rescues Mitochondrial Defects and Neuronal Loss in iPSC and Fly Models of Parkinson's Disease. *Cell Rep,* 23**,** 2976-2988.

Schrag, A., Hovris, A., Morley, D., Quinn, N. & Jahanshahi, M. 2006. Caregiver-burden in parkinson's disease is closely associated with psychiatric symptoms, falls, and disability. *Parkinsonism Relat Disord,* 12**,** 35-41.

Schueler, U. H., Kolter, T., Kaneski, C. R., Blusztajn, J. K., Herkenham, M., Sandhoff, K. & Brady, R. O. 2003. Toxicity of glucosylsphingosine (glucopsychosine) to cultured neuronal cells: a model system for assessing neuronal damage in Gaucher disease type 2 and 3. *Neurobiol Dis,* 14**,** 595-601.

Schulze, H., Kolter, T. & Sandhoff, K. 2009. Principles of lysosomal membrane degradation: Cellular topology and biochemistry of lysosomal lipid degradation. *Biochim Biophys Acta,* 1793**,** 674-83.

Schumacher, A. E., Kyu, H. H. & Collaborators, G. D. 2024. Global age-sex-specific mortality, life expectancy, and population estimates in 204 countries and territories and 811 subnational locations, 1950-2021, and the impact of the COVID-19 pandemic: a comprehensive demographic analysis for the Global Burden of Disease Study 2021. *Lancet,* 403**,** 1989-2056.

Schumacher-Schuh, A. F., Bieger, A., Okunoye, O., Mok, K. Y., Lim, S. Y., Bardien, S., Ahmad-Annuar, A., Santos-Lobato, B. L., Strelow, M. Z., Salama, M., Rao, S. C., Zewde, Y. Z., Dindayal, S., Azar, J., Prashanth, L. K., Rajan, R., Noyce, A. J., Okubadejo, N., Rizig, M., Lesage, S., Mata, I. F. & Global Parkinson's Genetics, P. 2022. Underrepresented Populations in Parkinson's Genetics Research: Current Landscape and Future Directions. *Mov Disord,* 37**,** 1593-1604.

Schwake, M., Schroder, B. & Saftig, P. 2013. Lysosomal membrane proteins and their central role in physiology. *Traffic,* 14**,** 739-48.

Seibenhener, M. L. & Wooten, M. C. 2015. Use of the Open Field Maze to measure locomotor and anxiety-like behavior in mice. *J Vis Exp***,** e52434.

Seidl, S. E., Santiago, J. A., Bilyk, H. & Potashkin, J. A. 2014. The emerging role of nutrition in Parkinson's disease. *Front Aging Neurosci,* 6**,** 36.

Senior, S. L., Ninkina, N., Deacon, R., Bannerman, D., Buchman, V. L., Cragg, S. J. & Wade-Martins, R. 2008. Increased striatal dopamine release and hyperdopaminergic-like behaviour in mice lacking both alpha-synuclein and gamma-synuclein. *Eur J Neurosci,* 27**,** 947-57.

Serebryany-Piavsky, V., Egulsky, L., Manoim-Wolkovitz, J. E., Anis, S., Hassin-Baer, S., Parnas, M. & Horowitz, M. 2025. The modifying effect of mutant LRRK2 on mutant GBA1-associated Parkinson disease. *Hum Mol Genet,* 34**,** 1184-1203.

Serratos, I. N., Hernandez-Perez, E., Campos, C., Aschner, M. & Santamaria, A. 2022. An Update on the Critical Role of alpha-Synuclein in Parkinson's Disease and Other Synucleinopathies: from Tissue to Cellular and Molecular Levels. *Mol Neurobiol,* 59**,** 620-642.

Sevlever, D., Jiang, P. & Yen, S. H. 2008. Cathepsin D is the main lysosomal enzyme involved in the degradation of alpha-synuclein and generation of its carboxy-terminally truncated species. *Biochemistry,* 47**,** 9678-87.

Shahmoradian, S. H., Lewis, A. J., Genoud, C., Hench, J., Moors, T. E., Navarro, P. P., Castano-Diez, D., Schweighauser, G., Graff-Meyer, A., Goldie, K. N., Sutterlin, R., Huisman, E., Ingrassia, A., Gier, Y., Rozemuller, A. J. M., Wang, J., Paepe, A., Erny, J., Staempfli, A., Hoernschemeyer, J., Grosseruschkamp, F., Niedieker, D., El-Mashtoly, S. F., Quadri, M., Van, I. W. F. J., Bonifati, V., Gerwert, K., Bohrmann, B., Frank, S., Britschgi, M., Stahlberg, H., Van De Berg, W. D. J. & Lauer, M. E. 2019. Lewy pathology in Parkinson's disease consists of crowded organelles and lipid membranes. *Nat Neurosci,* 22**,** 1099-1109.

Sharma, M. & Burre, J. 2023. alpha-Synuclein in synaptic function and dysfunction. *Trends Neurosci,* 46**,** 153-166.

Shen, H., Marino, R. a. M., Mcdevitt, R. A., Bi, G. H., Chen, K., Madeo, G., Lee, P. T., Liang, Y., De Biase, L. M., Su, T. P., Xi, Z. X. & Bonci, A. 2018. Genetic deletion of vesicular glutamate transporter in dopamine neurons increases vulnerability to MPTP-induced neurotoxicity in mice. *Proc Natl Acad Sci U S A,* 115**,** E11532-E11541.

Sheta, R., Berard, M., Musiol, D., Martinez-Drudis, L. & Oueslati, A. 2024. Behavioral analysis of motor and non-motor impairment in rodent models of Parkinson's disease. *Front Aging Neurosci,* 16**,** 1464706.

Shin, J. H., Ko, H. S., Kang, H., Lee, Y., Lee, Y. I., Pletinkova, O., Troconso, J. C., Dawson, V. L. & Dawson, T. M. 2011. PARIS (ZNF746) repression of PGC-1alpha contributes to neurodegeneration in Parkinson's disease. *Cell,* 144**,** 689-702.

Shoji, H. & Miyakawa, T. 2019. Age-related behavioral changes from young to old age in male mice of a C57BL/6J strain maintained under a genetic stability program. *Neuropsychopharmacol Rep,* 39**,** 100-118.

Shoji, H. & Miyakawa, T. 2021. Effects of test experience, closed-arm wall color, and illumination level on behavior and plasma corticosterone response in an elevated plus maze in male C57BL/6J mice: a challenge against conventional interpretation of the test. *Mol Brain,* 14**,** 34.

Shoji, H., Takao, K., Hattori, S. & Miyakawa, T. 2016. Age-related changes in behavior in C57BL/6J mice from young adulthood to middle age. *Mol Brain,* 9**,** 11.

Siddiqi, S., Ortiz, Z., Simard, S., Li, J., Lawrence, K., Redmond, M., Tomlinson, J. J., Schlossmacher, M. G. & Salmaso, N. 2025. Race and ethnicity matter! Moving Parkinson's risk research towards diversity and inclusiveness. *NPJ Parkinsons Dis,* 11**,** 45.

Sidransky, E., Arkadir, D., Bauer, P., Dinur, T., Lopez, G., Rolfs, A. & Zimran, A. 2020. Substrate reduction therapy for GBA1-associated Parkinsonism: Are we betting on the wrong mouse? *Mov Disord,* 35**,** 228-230.

Sidransky, E., Nalls, M. A., Aasly, J. O., Aharon-Peretz, J., Annesi, G., Barbosa, E. R., Bar-Shira, A., Berg, D., Bras, J., Brice, A., Chen, C. M., Clark, L. N., Condroyer, C., De Marco, E. V., Durr, A., Eblan, M. J., Fahn, S., Farrer, M. J., Fung, H. C., Gan-Or, Z., Gasser, T., Gershoni-Baruch, R., Giladi, N., Griffith, A., Gurevich, T., Januario, C., Kropp, P., Lang, A. E., Lee-Chen, G. J., Lesage, S., Marder, K., Mata, I. F., Mirelman, A., Mitsui, J., Mizuta, I., Nicoletti, G., Oliveira, C., Ottman, R., Orr-Urtreger, A., Pereira, L. V., Quattrone, A., Rogaeva, E., Rolfs, A., Rosenbaum, H., Rozenberg, R., Samii, A., Samaddar, T., Schulte, C., Sharma, M., Singleton, A., Spitz, M., Tan, E. K., Tayebi, N., Toda, T., Troiano, A. R., Tsuji, S., Wittstock, M., Wolfsberg, T. G., Wu, Y. R., Zabetian, C. P., Zhao, Y. & Ziegler, S. G. 2009. Multicenter analysis of glucocerebrosidase mutations in Parkinson's disease. *N Engl J Med,* 361**,** 1651-61.

Siemeling, O., Slingerland, S., Van Der Zee, S. & Van Laar, T. 2024. Study protocol of the GRoningen early-PD Ambroxol treatment (GREAT) trial: a randomized, double-blind, placebo-controlled, single center trial with ambroxol in Parkinson patients with a GBA mutation. *BMC Neurol,* 24**,** 146.

Sievers, F., Wilm, A., Dineen, D., Gibson, T. J., Karplus, K., Li, W., Lopez, R., Mcwilliam, H., Remmert, M., Soding, J., Thompson, J. D. & Higgins, D. G. 2011. Fast, scalable generation of high-quality protein multiple sequence alignments using Clustal Omega. *Mol Syst Biol,* 7**,** 539.

Silveira, C. R. A., Coleman, K. K. L., Borron, K., Tirona, R. G., Rupar, C. A., Zou, G., Hegele, R. A., Wellington, C., Stukas, S., Finger, E. C., Bartha, R., Morrow, S. A., Wells, J. L., Borrie, M. J., Mahuran, D., Macdonald, P. A., Jenkins, M. E., Jog, M. S., Dresser, G., Fox, S., Camicioli, R., Feagan, B., Mendonca, D. A., Mayich, M., Sharma, M. D., Pandey, S. K. & Pasternak, S. H. 2025. Ambroxol as a Treatment for Parkinson Disease Dementia: A Randomized Clinical Trial. *JAMA Neurol*.

Silveira, C. R. A., Mackinley, J., Coleman, K., Li, Z., Finger, E., Bartha, R., Morrow, S. A., Wells, J., Borrie, M., Tirona, R. G., Rupar, C. A., Zou, G., Hegele, R. A., Mahuran, D., Macdonald, P., Jenkins, M. E., Jog, M. & Pasternak, S. H. 2019. Ambroxol as a novel disease-modifying treatment for Parkinson's disease dementia: protocol for a single-centre, randomized, double-blind, placebo-controlled trial. *BMC Neurol,* 19**,** 20.

Simon, M. J., Logan, T., Devos, S. L. & Di Paolo, G. 2023. Lysosomal functions of progranulin and implications for treatment of frontotemporal dementia. *Trends Cell Biol,* 33**,** 324-339.

Simon, P., Dupuis, R. & Costentin, J. 1994. Thigmotaxis as an index of anxiety in mice. Influence of dopaminergic transmissions. *Behav Brain Res,* 61**,** 59-64.

Simon-Sanchez, J., Schulte, C., Bras, J. M., Sharma, M., Gibbs, J. R., Berg, D., Paisan-Ruiz, C., Lichtner, P., Scholz, S. W., Hernandez, D. G., Kruger, R., Federoff, M., Klein, C., Goate, A., Perlmutter, J., Bonin, M., Nalls, M. A., Illig, T., Gieger, C., Houlden, H., Steffens, M., Okun, M. S., Racette, B. A., Cookson, M. R., Foote, K. D., Fernandez, H. H., Traynor, B. J., Schreiber, S., Arepalli, S., Zonozi, R., Gwinn, K., Van Der Brug, M., Lopez, G., Chanock, S. J., Schatzkin, A., Park, Y., Hollenbeck, A., Gao, J., Huang, X., Wood, N. W., Lorenz, D., Deuschl, G., Chen, H., Riess, O., Hardy, J. A., Singleton, A. B. & Gasser, T. 2009. Genome-wide association study reveals genetic risk underlying Parkinson's disease. *Nat Genet,* 41**,** 1308-12.

Simpson, C., Vinikoor-Imler, L., Nassan, F. L., Shirvan, J., Lally, C., Dam, T. & Maserejian, N. 2022. Prevalence of ten LRRK2 variants in Parkinson's disease: A comprehensive review. *Parkinsonism Relat Disord,* 98**,** 103-113.

Simuni, T., Uribe, L., Cho, H. R., Caspell-Garcia, C., Coffey, C. S., Siderowf, A., Trojanowski, J. Q., Shaw, L. M., Seibyl, J., Singleton, A., Toga, A. W., Galasko, D., Foroud, T., Tosun, D., Poston, K., Weintraub, D., Mollenhauer, B., Tanner, C. M., Kieburtz, K., Chahine, L. M., Reimer, A., Hutten, S. J., Bressman, S., Marek, K. & Investigators, P. 2020. Clinical and dopamine transporter imaging characteristics of non-manifest LRRK2 and GBA mutation carriers in the Parkinson's Progression Markers Initiative (PPMI): a cross-sectional study. *Lancet Neurol,* 19**,** 71-80.

Singleton, A. B., Farrer, M., Johnson, J., Singleton, A., Hague, S., Kachergus, J., Hulihan, M., Peuralinna, T., Dutra, A., Nussbaum, R., Lincoln, S., Crawley, A., Hanson, M., Maraganore, D., Adler, C., Cookson, M. R., Muenter, M., Baptista, M., Miller, D., Blancato, J., Hardy, J. & Gwinn-Hardy, K. 2003. alpha-Synuclein locus triplication causes Parkinson's disease. *Science,* 302**,** 841.

Sittig, L. J., Carbonetto, P., Engel, K. A., Krauss, K. S., Barrios-Camacho, C. M. & Palmer, A. A. 2016. Genetic Background Limits Generalizability of Genotype-Phenotype Relationships. *Neuron,* 91**,** 1253-1259.

Sivandzade, F., Bhalerao, A. & Cucullo, L. 2019. Analysis of the Mitochondrial Membrane Potential Using the Cationic JC-1 Dye as a Sensitive Fluorescent Probe. *Bio Protoc,* 9.

Slingerland, S., Van Der Zee, S., Carli, G., Slomp, A. C., Boertien, J. M., D'angremont, E., Bohnen, N. I., Albin, R. L. & Van Laar, T. 2024. Cholinergic innervation topography in GBA-associated de novo Parkinson's disease patients. *Brain,* 147**,** 900-910.

Slingerland, S., Van Der Zee, S., Carli, G., Slomp, A. C., D'angremont, E., Boertien, J. M. & Van Laar, T. 2025. Cholinergic Degeneration and Cognitive Function in Early GBA1-Related Parkinson's Disease. *Ann Neurol*.

Sloan, M., Alegre-Abarrategui, J., Potgieter, D., Kaufmann, A. K., Exley, R., Deltheil, T., Threlfell, S., Connor-Robson, N., Brimblecombe, K., Wallings, R., Cioroch, M., Bannerman, D. M., Bolam, J. P., Magill, P. J., Cragg, S. J., Dodson, P. D. & Wade-Martins, R. 2016. LRRK2 BAC transgenic rats develop progressive, L-DOPA-responsive motor impairment, and deficits in dopamine circuit function. *Hum Mol Genet,* 25**,** 951-63.

Smilowska, K., Carvalho, V., Szejko, N., Costa, J., Moro, E. & Antonini, A. 2025. How well is the female population represented in clinical trials with infusion therapies for Parkinson's disease? A systematic review and metanalysis. *Eur J Neurol,* 32**,** e70024.

Smith, L., Mullin, S. & Schapira, A. H. V. 2017. Insights into the structural biology of Gaucher disease. *Exp Neurol,* 298**,** 180-190.

Smith, L. J., Bolsinger, M. M., Chau, K. Y., Gegg, M. E. & Schapira, A. H. V. 2023. The GBA variant E326K is associated with alpha-synuclein aggregation and lipid droplet accumulation in human cell lines. *Hum Mol Genet,* 32**,** 773-789.

Soh, S. E., Morris, M. E. & Mcginley, J. L. 2011. Determinants of health-related quality of life in Parkinson's disease: a systematic review. *Parkinsonism Relat Disord,* 17**,** 1-9.

Solch, R. J., Aigbogun, J. O., Voyiadjis, A. G., Talkington, G. M., Darensbourg, R. M., O'connell, S., Pickett, K. M., Perez, S. R. & Maraganore, D. M. 2022. Mediterranean diet adherence, gut microbiota, and Alzheimer's or Parkinson's disease risk: A systematic review. *J Neurol Sci,* 434**,** 120166.

Song, J., Solmi, M., Carvalho, A. F., Shin, J. I. & Ioannidis, J. P. 2024. Twelve years after the ARRIVE guidelines: Animal research has not yet arrived at high standards. *Lab Anim,* 58**,** 109-115.

Sorge, J., Gross, E., West, C. & Beutler, E. 1990. High level transcription of the glucocerebrosidase pseudogene in normal subjects and patients with Gaucher disease. *J Clin Invest,* 86**,** 1137-41.

Sorge, J. A., West, C., Kuhl, W., Treger, L. & Beutler, E. 1987. The human glucocerebrosidase gene has two functional ATG initiator codons. *Am J Hum Genet,* 41**,** 1016-24.

Soria, F. N., Engeln, M., Martinez-Vicente, M., Glangetas, C., Lopez-Gonzalez, M. J., Dovero, S., Dehay, B., Normand, E., Vila, M., Favereaux, A., Georges, F., Lo Bianco, C., Bezard, E. & Fernagut, P. O. 2017. Glucocerebrosidase deficiency in dopaminergic neurons induces microglial activation without neurodegeneration. *Hum Mol Genet,* 26**,** 2603-2615.

Sosero, Y. L., Bandres-Ciga, S., Hassin-Baer, S., Alcalay, R. N., Gan-Or, Z. & International Parkinson's Disease Genomics, C. 2020. Lack of evidence for genetic association of saposins A, B, C and D with Parkinson's disease. *Brain,* 143**,** e72.

Sossi, V., De La Fuente-Fernandez, R., Holden, J. E., Doudet, D. J., Mckenzie, J., Stoessl, A. J. & Ruth, T. J. 2002. Increase in dopamine turnover occurs early in Parkinson's disease: evidence from a new modeling approach to PET 18 F-fluorodopa data. *J Cereb Blood Flow Metab,* 22**,** 232-9.

Sossi, V., De La Fuente-Fernandez, R., Holden, J. E., Schulzer, M., Ruth, T. J. & Stoessl, J. 2004. Changes of dopamine turnover in the progression of Parkinson's disease as measured by positron emission tomography: their relation to disease-compensatory mechanisms. *J Cereb Blood Flow Metab,* 24**,** 869-76.

Spillantini, M. G., Crowther, R. A., Jakes, R., Hasegawa, M. & Goedert, M. 1998. alpha-Synuclein in filamentous inclusions of Lewy bodies from Parkinson's disease and dementia with lewy bodies. *Proc Natl Acad Sci U S A,* 95**,** 6469-73.

Spillantini, M. G., Schmidt, M. L., Lee, V. M., Trojanowski, J. Q., Jakes, R. & Goedert, M. 1997. Alpha-synuclein in Lewy bodies. *Nature,* 388**,** 839-40.

Spink, A. J., Tegelenbosch, R. A., Buma, M. O. & Noldus, L. P. 2001. The EthoVision video tracking system--a tool for behavioral phenotyping of transgenic mice. *Physiol Behav,* 73**,** 731-44.

Srikanth, M. P., Jones, J. W., Kane, M., Awad, O., Park, T. S., Zambidis, E. T. & Feldman, R. A. 2021. Elevated glucosylsphingosine in Gaucher disease induced pluripotent stem cell neurons deregulates lysosomal compartment through mammalian target of rapamycin complex 1. *Stem Cells Transl Med,* 10**,** 1081-1094.

Stebbins, G. T., Goetz, C. G., Burn, D. J., Jankovic, J., Khoo, T. K. & Tilley, B. C. 2013. How to identify tremor dominant and postural instability/gait difficulty groups with the movement disorder society unified Parkinson's disease rating scale: comparison with the unified Parkinson's disease rating scale. *Mov Disord,* 28**,** 668-70.

Stefani, A. & Hogl, B. 2020. Sleep in Parkinson's disease. *Neuropsychopharmacology,* 45**,** 121-128.

Steinkellner, T., Conrad, W. S., Kovacs, I., Rissman, R. A., Lee, E. B., Trojanowski, J. Q., Freyberg, Z., Roy, S., Luk, K. C., Lee, V. M. & Hnasko, T. S. 2022. Dopamine neurons exhibit emergent glutamatergic identity in Parkinson's disease. *Brain,* 145**,** 879-886.

Steinkellner, T., Zell, V., Farino, Z. J., Sonders, M. S., Villeneuve, M., Freyberg, R. J., Przedborski, S., Lu, W., Freyberg, Z. & Hnasko, T. S. 2018. Role for VGLUT2 in selective vulnerability of midbrain dopamine neurons. *J Clin Invest,* 128**,** 774-788.

Steinmetz, J. D., Seeher, K. M. & Gbd 2021 Nervous System Disorders Collaborators 2024. Global, regional, and national burden of disorders affecting the nervous system,

1990-2021: a systematic analysis for the Global Burden of Disease Study 2021. *Lancet Neurol,* 23**,** 344-381.

Stern, M. B., Lang, A. & Poewe, W. 2012. Toward a redefinition of Parkinson's disease. *Mov Disord,* 27**,** 54-60.

Stirnemann, J., Belmatoug, N., Camou, F., Serratrice, C., Froissart, R., Caillaud, C., Levade, T., Astudillo, L., Serratrice, J., Brassier, A., Rose, C., Billette De Villemeur, T. & Berger, M. G. 2017. A Review of Gaucher Disease Pathophysiology, Clinical Presentation and Treatments. *Int J Mol Sci,* 18.

Stocchi, F., Bravi, D., Emmi, A. & Antonini, A. 2024. Parkinson disease therapy: current strategies and future research priorities. *Nat Rev Neurol,* 20**,** 695-707.

Stojkovska, I., Wani, W. Y., Zunke, F., Belur, N. R., Pavlenko, E. A., Mwenda, N., Sharma, K., Francelle, L. & Mazzulli, J. R. 2022. Rescue of alpha-synuclein aggregation in Parkinson's patient neurons by synergistic enhancement of ER proteostasis and protein trafficking. *Neuron,* 110**,** 436-451 e11.

Stoker, T. B. & Barker, R. A. 2020. Recent developments in the treatment of Parkinson's Disease. *F1000Res,* 9.

Stoker, T. B., Camacho, M., Winder-Rhodes, S., Liu, G., Scherzer, C. R., Foltynie, T., Evans, J., Breen, D. P., Barker, R. A. & Williams-Gray, C. H. 2020. Impact of GBA1 variants on long-term clinical progression and mortality in incident Parkinson's disease. *J Neurol Neurosurg Psychiatry,* 91**,** 695-702.

Stowe, R. L., Ives, N. J., Clarke, C., Van Hilten, J., Ferreira, J., Hawker, R. J., Shah, L., Wheatley, K. & Gray, R. 2008. Dopamine agonist therapy in early Parkinson's disease. *Cochrane Database Syst Rev***,** CD006564.

Straccia, G., Colucci, F., Eleopra, R. & Cilia, R. 2022. Precision Medicine in Parkinson's Disease: From Genetic Risk Signals to Personalized Therapy. *Brain Sci,* 12.

Straniero, L., Asselta, R., Bonvegna, S., Rimoldi, V., Melistaccio, G., Solda, G., Aureli, M., Della Porta, M., Lucca, U., Di Fonzo, A., Zecchinelli, A., Pezzoli, G., Cilia, R. & Duga, S. 2020. The SPID-GBA study: Sex distribution, Penetrance, Incidence, and Dementia in GBA-PD. *Neurol Genet,* 6**,** e523.

Straniero, L., Rimoldi, V., Samarani, M., Goldwurm, S., Di Fonzo, A., Kruger, R., Deleidi, M., Aureli, M., Solda, G., Duga, S. & Asselta, R. 2017. The GBAP1 pseudogene acts as a ceRNA for the glucocerebrosidase gene GBA by sponging miR-22-3p. *Sci Rep,* 7**,** 12702.

Straub, C., Tritsch, N. X., Hagan, N. A., Gu, C. & Sabatini, B. L. 2014. Multiphasic modulation of cholinergic interneurons by nigrostriatal afferents. *J Neurosci,* 34**,** 8557-69.

Strikwerda, A. J., Dommershuijsen, L. J., Ikram, M. K. & Voortman, T. 2021. Diet Quality and Risk of Parkinson's Disease: The Rotterdam Study. *Nutrients,* 13.

Stuber, G. D., Hnasko, T. S., Britt, J. P., Edwards, R. H. & Bonci, A. 2010. Dopaminergic terminals in the nucleus accumbens but not the dorsal striatum corelease glutamate. *J Neurosci,* 30**,** 8229-33.

Sturman, O., Von Ziegler, L., Schlappi, C., Akyol, F., Privitera, M., Slominski, D., Grimm, C., Thieren, L., Zerbi, V., Grewe, B. & Bohacek, J. 2020. Deep learning-based behavioral analysis reaches human accuracy and is capable of outperforming commercial solutions. *Neuropsychopharmacology,* 45**,** 1942-1952.

Subramanian, I., Mathur, S., Oosterbaan, A., Flanagan, R., Keener, A. M. & Moro, E. 2022. Unmet Needs of Women Living with Parkinson's Disease: Gaps and Controversies. *Mov Disord,* 37**,** 444-455.

Sukoff Rizzo, S. J. & Crawley, J. N. 2017. Behavioral Phenotyping Assays for Genetic Mouse Models of Neurodevelopmental, Neurodegenerative, and Psychiatric Disorders. *Annu Rev Anim Biosci,* 5**,** 371-389.

Sulzer, D. 2007. Multiple hit hypotheses for dopamine neuron loss in Parkinson's disease. *Trends Neurosci,* 30**,** 244-50.

Sulzer, D., Cragg, S. J. & Rice, M. E. 2016. Striatal dopamine neurotransmission: regulation of release and uptake. *Basal Ganglia,* 6**,** 123-148.

Sun, C. & Armstrong, M. J. 2021. Treatment of Parkinson's Disease with Cognitive Impairment: Current Approaches and Future Directions. *Behav Sci (Basel),* 11.

Sun, Y., Qi, X. & Grabowski, G. A. 2003. Saposin C is required for normal resistance of acid beta-glucosidase to proteolytic degradation. *J Biol Chem,* 278**,** 31918-23.

Surface, M., Balwani, M., Waters, C., Haimovich, A., Gan-Or, Z., Marder, K. S., Hsieh, T., Song, L., Padmanabhan, S., Hsieh, F., Merchant, K. M. & Alcalay, R. N. 2022. Plasma Glucosylsphingosine in GBA1 Mutation Carriers with and without Parkinson's Disease. *Mov Disord,* 37**,** 416-421.

Surmeier, D. J. & Schumacker, P. T. 2013. Calcium, bioenergetics, and neuronal vulnerability in Parkinson's disease. *J Biol Chem,* 288**,** 10736-41.

Suzuki, M., Fujikake, N., Takeuchi, T., Kohyama-Koganeya, A., Nakajima, K., Hirabayashi, Y., Wada, K. & Nagai, Y. 2015. Glucocerebrosidase deficiency accelerates the accumulation of proteinase K-resistant alpha-synuclein and aggravates neurodegeneration in a Drosophila model of Parkinson's disease. *Hum Mol Genet,* 24**,** 6675-86.

Suzuki, M., Sango, K., Wada, K. & Nagai, Y. 2018. Pathological role of lipid interaction with alpha-synuclein in Parkinson's disease. *Neurochem Int,* 119**,** 97-106.

Sveinbjornsdottir, S. 2016. The clinical symptoms of Parkinson's disease. *J Neurochem,* 139 Suppl 1**,** 318-324.

Swan, M., Doan, N., Ortega, R. A., Barrett, M., Nichols, W., Ozelius, L., Soto-Valencia, J., Boschung, S., Deik, A., Sarva, H., Cabassa, J., Johannes, B., Raymond, D., Marder, K., Giladi, N., Miravite, J., Severt, W., Sachdev, R., Shanker, V., Bressman, S. & Saunders-Pullman, R. 2016. Neuropsychiatric characteristics of GBA-associated Parkinson disease. *J Neurol Sci,* 370**,** 63-69.

Szwedo, A. A., Dalen, I., Pedersen, K. F., Camacho, M., Backstrom, D., Forsgren, L., Tzoulis, C., Winder-Rhodes, S., Hudson, G., Liu, G., Scherzer, C. R., Lawson, R. A., Yarnall, A. J., Williams-Gray, C. H., Macleod, A. D., Counsell, C. E., Tysnes, O. B., Alves, G., Maple-Grodem, J. & Parkinson's Incidence Cohorts, C. 2022. GBA and APOE Impact Cognitive Decline in Parkinson's Disease: A 10-Year Population-Based Study. *Mov Disord,* 37**,** 1016-1027.

Tabar, V., Sarva, H., Lozano, A. M., Fasano, A., Kalia, S. K., Yu, K. K. H., Brennan, C., Ma, Y., Peng, S., Eidelberg, D., Tomishima, M., Irion, S., Stemple, W., Abid, N., Lampron, A., Studer, L. & Henchcliffe, C. 2025. Phase I trial of hES cell-derived dopaminergic neurons for Parkinson's disease. *Nature,* 641**,** 978-983.

Tabuchi, N., Akasaki, K., Sasaki, T., Kanda, N. & Tsuji, H. 1997. Identification and characterization of a major lysosomal membrane glycoprotein, LGP85/LIMP II in mouse liver. *J Biochem,* 122**,** 756-63.

Tagliaferro, P. & Burke, R. E. 2016. Retrograde Axonal Degeneration in Parkinson Disease. *J Parkinsons Dis,* 6**,** 1-15.

Taguchi, Y. V., Liu, J., Ruan, J., Pacheco, J., Zhang, X., Abbasi, J., Keutzer, J., Mistry, P. K. & Chandra, S. S. 2017. Glucosylsphingosine Promotes alpha-Synuclein Pathology in Mutant GBA-Associated Parkinson's Disease. *J Neurosci,* 37**,** 9617-9631.

Tajima, A., Yokoi, T., Ariga, M., Ito, T., Kaneshiro, E., Eto, Y. & Ida, H. 2009. Clinical and genetic study of Japanese patients with type 3 Gaucher disease. *Mol Genet Metab,* 97**,** 272-7.

Takasaki, S., Murray, G. J., Furbish, F. S., Brady, R. O., Barranger, J. A. & Kobata, A. 1984. Structure of the N-asparagine-linked oligosaccharide units of human placental beta-glucocerebrosidase. *J Biol Chem,* 259**,** 10112-7.

Tamargo, R. J., Velayati, A., Goldin, E. & Sidransky, E. 2012. The role of saposin C in Gaucher disease. *Mol Genet Metab,* 106**,** 257-63.

Tan, A. H., Lim, S. Y. & Lang, A. E. 2022. The microbiome-gut-brain axis in Parkinson disease - from basic research to the clinic. *Nat Rev Neurol,* 18**,** 476-495.

Tanida, I., Ueno, T. & Kominami, E. 2008. LC3 and Autophagy. *Methods Mol Biol,* 445**,** 77-88.

Tanner, C. M., Kamel, F., Ross, G. W., Hoppin, J. A., Goldman, S. M., Korell, M., Marras, C., Bhudhikanok, G. S., Kasten, M., Chade, A. R., Comyns, K., Richards, M. B., Meng, C., Priestley, B., Fernandez, H. H., Cambi, F., Umbach, D. M., Blair, A., Sandler, D. P. & Langston, J. W. 2011. Rotenone, paraquat, and Parkinson's disease. *Environ Health Perspect,* 119**,** 866-72.

Tayebi, N., Callahan, M., Madike, V., Stubblefield, B. K., Orvisky, E., Krasnewich, D., Fillano, J. J. & Sidransky, E. 2001. Gaucher disease and parkinsonism: a phenotypic and genotypic characterization. *Mol Genet Metab,* 73**,** 313-21.

Tayebi, N., Lopez, G., Do, J. & Sidransky, E. 2020. Pro-cathepsin D, Prosaposin, and Progranulin: Lysosomal Networks in Parkinsonism. *Trends Mol Med,* 26**,** 913-923.

Tayebi, N., Parisiadou, L., Berhe, B., Gonzalez, A. N., Serra-Vinardell, J., Tamargo, R. J., Maniwang, E., Sorrentino, Z., Fujiwara, H., Grey, R. J., Hassan, S., Blech-Hermoni, Y. N., Chen, C., Mcglinchey, R., Makariou-Pikis, C., Brooks, M., Ginns, E. I., Ory, D. S., Giasson, B. I. & Sidransky, E. 2017. Glucocerebrosidase haploinsufficiency in A53T alpha-synuclein mice impacts disease onset and course. *Mol Genet Metab,* 122**,** 198-208.

Tayebi, N., Stubblefield, B. K., Park, J. K., Orvisky, E., Walker, J. M., Lamarca, M. E. & Sidransky, E. 2003. Reciprocal and nonreciprocal recombination at the glucocerebrosidase gene region: implications for complexity in Gaucher disease. *Am J Hum Genet,* 72**,** 519-34.

Taylor, T. N., Greene, J. G. & Miller, G. W. 2010. Behavioral phenotyping of mouse models of Parkinson's disease. *Behav Brain Res,* 211**,** 1-10.

Taylor, T. N., Potgieter, D., Anwar, S., Senior, S. L., Janezic, S., Threlfell, S., Ryan, B., Parkkinen, L., Deltheil, T., Cioroch, M., Livieratos, A., Oliver, P. L., Jennings, K. A., Davies, K. E., Ansorge, O., Bannerman, D. M., Cragg, S. J. & Wade-Martins, R. 2014. Region-specific deficits in dopamine, but not norepinephrine, signaling in a novel A30P alpha-synuclein BAC transgenic mouse. *Neurobiol Dis,* 62**,** 193-207.

Te Vruchte, D., Sturchio, A., Priestman, D. A., Tsitsi, P., Hertz, E., Andreasson, M., Markaki, I., Wallom, K. L., Platt, F. & Svenningsson, P. 2022. Glycosphingolipid Changes in Plasma in Parkinson's Disease Independent of Glucosylceramide Levels. *Mov Disord,* 37**,** 2129-2134.

Tecuapetla, F., Patel, J. C., Xenias, H., English, D., Tadros, I., Shah, F., Berlin, J., Deisseroth, K., Rice, M. E., Tepper, J. M. & Koos, T. 2010. Glutamatergic signaling by mesolimbic dopamine neurons in the nucleus accumbens. *J Neurosci,* 30**,** 7105-10.

Thaler, A., Anis, S., Ponger, P., Fay-Karmon, T., Livneh, V., Faust-Socher, A., Greenbaum, L., Reiner, J., Hilel, A., Shabtai, H., Alcalay, R. N., Djaldetti, R., Hassin-Baer, S., Ezra, A., Mirelman, A., Giladi, N. & Gurevich, T. 2024. Levodopa-carbidopa

intestinal gel for advanced Parkinson's disease: Impact of LRRK2 and GBA1 mutations. *Parkinsonism Relat Disord,* 127**,** 107115.

Thaler, A., Bregman, N., Gurevich, T., Shiner, T., Dror, Y., Zmira, O., Gan-Or, Z., Bar-Shira, A., Gana-Weisz, M., Orr-Urtreger, A., Giladi, N. & Mirelman, A. 2018. Parkinson's disease phenotype is influenced by the severity of the mutations in the GBA gene. *Parkinsonism Relat Disord,* 55**,** 45-49.

Thaler, A., Mirelman, A. & Alcalay, R. N. 2023. Differences in Sex-Specific Frequency of Glucocerebrosidase Variant Carriers and Familial Parkinsonism. *Mov Disord,* 38**,** 713-714.

Thenganatt, M. A. & Jankovic, J. 2014. Parkinson disease subtypes. *JAMA Neurol,* 71**,** 499-504.

Theophilus, B., Latham, T., Grabowski, G. A. & Smith, F. I. 1989a. Gaucher disease: molecular heterogeneity and phenotype-genotype correlations. *Am J Hum Genet,* 45**,** 212-25.

Theophilus, B. D., Latham, T., Grabowski, G. A. & Smith, F. I. 1989b. Comparison of RNase A, a chemical cleavage and GC-clamped denaturing gradient gel electrophoresis for the detection of mutations in exon 9 of the human acid beta-glucosidase gene. *Nucleic Acids Res,* 17**,** 7707-22.

Thomas, R., Moloney, E. B., Macbain, Z. K., Hallett, P. J. & Isacson, O. 2021. Fibroblasts from idiopathic Parkinson's disease exhibit deficiency of lysosomal glucocerebrosidase activity associated with reduced levels of the trafficking receptor LIMP2. *Mol Brain,* 14**,** 16.

Threlfell, S., Lalic, T., Platt, N. J., Jennings, K. A., Deisseroth, K. & Cragg, S. J. 2012. Striatal dopamine release is triggered by synchronized activity in cholinergic interneurons. *Neuron,* 75**,** 58-64.

Threlfell, S., Mohammadi, A. S., Ryan, B. J., Connor-Robson, N., Platt, N. J., Anand, R., Serres, F., Sharp, T., Bengoa-Vergniory, N., Wade-Martins, R., Ewing, A., Cragg, S. J. & Brimblecombe, K. R. 2021. Striatal Dopamine Transporter Function Is Facilitated by Converging Biology of alpha-Synuclein and Cholesterol. *Front Cell Neurosci,* 15**,** 658244.

Tillerson, J. L., Caudle, W. M., Reveron, M. E. & Miller, G. W. 2002. Detection of behavioral impairments correlated to neurochemical deficits in mice treated with moderate doses of 1-methyl-4-phenyl-1,2,3,6-tetrahydropyridine. *Exp Neurol,* 178**,** 80-90.

Timotius, I. K., Canneva, F., Minakaki, G., Moceri, S., Plank, A. C., Casadei, N., Riess, O., Winkler, J., Klucken, J., Eskofier, B. & Von Horsten, S. 2019a. Systematic data analysis and data mining in CatWalk gait analysis by heat mapping exemplified in rodent models for neurodegenerative diseases. *J Neurosci Methods,* 326**,** 108367.

Timotius, I. K., Moceri, S., Plank, A. C., Habermeyer, J., Canneva, F., Winkler, J., Klucken, J., Casadei, N., Riess, O., Eskofier, B. & Von Horsten, S. 2019b. Silhouette-Length-Scaled Gait Parameters for Motor Functional Analysis in Mice and Rats. *eNeuro,* 6.

Timotius, I. K., Roelofs, R. F., Richmond-Hacham, B., Noldus, L., Von Horsten, S. & Bikovski, L. 2023. CatWalk XT gait parameters: a review of reported parameters in pre-clinical studies of multiple central nervous system and peripheral nervous system disease models. *Front Behav Neurosci,* 17**,** 1147784.

Todorova, A., Jenner, P. & Ray Chaudhuri, K. 2014. Non-motor Parkinson's: integral to motor Parkinson's, yet often neglected. *Pract Neurol,* 14**,** 310-22.

Tolman, E. C. 1925. Purpose and cognition: The determiners of animal learning. *Psychological Review,* 32**,** 285-297.

Tolosa, E., Garrido, A., Scholz, S. W. & Poewe, W. 2021. Challenges in the diagnosis of Parkinson's disease. *Lancet Neurol,* 20**,** 385-397.

Tonin, R., Ramat, S., Rinaldi, M., Falliano, S., Feo, F., Cardona, F., Matassini, C., Mannaioni, G., Grigioni, G., Caremani, L., Govoni, A., Della Bona, M. L., La Marca, G., Guerrini, R. & A., M. 2025. GBA genotype-Parkinson's phenotype correlation in a cohort of 252 Italian patients from the Tuscany region. *Clinical Parkinsonism & Related Disorders,* 12.

Tosserams, A., Araujo, R., Pringsheim, T., Post, B., Darweesh, S. K. L., Inthout, J. & Bloem, B. R. 2018. Underrepresentation of women in Parkinson's disease trials. *Mov Disord,* 33**,** 1825-1826.

Tozzi, A., De Iure, A., Bagetta, V., Tantucci, M., Durante, V., Quiroga-Varela, A., Costa, C., Di Filippo, M., Ghiglieri, V., Latagliata, E. C., Wegrzynowicz, M., Decressac, M., Giampa, C., Dalley, J. W., Xia, J., Gardoni, F., Mellone, M., El-Agnaf, O. M., Ardah, M. T., Puglisi-Allegra, S., Bjorklund, A., Spillantini, M. G., Picconi, B. & Calabresi, P. 2016. Alpha-Synuclein Produces Early Behavioral Alterations via Striatal Cholinergic Synaptic Dysfunction by Interacting With GluN2D N-Methyl-D-Aspartate Receptor Subunit. *Biol Psychiatry,* 79**,** 402-414.

Tozzi, A., Tantucci, M., Marchi, S., Mazzocchetti, P., Morari, M., Pinton, P., Mancini, A. & Calabresi, P. 2018. Dopamine D2 receptor-mediated neuroprotection in a G2019S Lrrk2 genetic model of Parkinson's disease. *Cell Death Dis,* 9**,** 204.

Trinh, J., Zeldenrust, F. M. J., Huang, J., Kasten, M., Schaake, S., Petkovic, S., Madoev, H., Grunewald, A., Almuammar, S., Konig, I. R., Lill, C. M., Lohmann, K., Klein, C. & Marras, C. 2018. Genotype-phenotype relations for the Parkinson's disease genes SNCA, LRRK2, VPS35: MDSGene systematic review. *Mov Disord,* 33**,** 1857-1870.

Tritsch, N. X. & Sabatini, B. L. 2012. Dopaminergic modulation of synaptic transmission in cortex and striatum. *Neuron,* 76**,** 33-50.

Troster, A. I. 2024. Developments in the prediction of cognitive changes following deep brain stimulation in persons with Parkinson's disease. *Expert Rev Neurother,* 24**,** 643-659.

Trudeau, L. E., Hnasko, T. S., Wallen-Mackenzie, A., Morales, M., Rayport, S. & Sulzer, D. 2014. The multilingual nature of dopamine neurons. *Prog Brain Res,* 211**,** 141-64.

Tsao, C. H., Wu, K. Y., Su, N. C., Edwards, A. & Huang, G. J. 2023. The influence of sex difference on behavior and adult hippocampal neurogenesis in C57BL/6 mice. *Sci Rep,* 13**,** 17297.

Tsitsi, P., Markaki, I., Waldthaler, J., Machaczka, M. & Svenningsson, P. 2022. Neurocognitive profile of adults with the Norrbottnian type of Gaucher disease. *JIMD Rep,* 63**,** 93-100.

Tsuji, S., Choudary, P. V., Martin, B. M., Stubblefield, B. K., Mayor, J. A., Barranger, J. A. & Ginns, E. I. 1987. A mutation in the human glucocerebrosidase gene in neuronopathic Gaucher's disease. *N Engl J Med,* 316**,** 570-5.

Tsuji, S., Martin, B. M., Barranger, J. A., Stubblefield, B. K., Lamarca, M. E. & Ginns, E. I. 1988. Genetic heterogeneity in type 1 Gaucher disease: multiple genotypes in Ashkenazic and non-Ashkenazic individuals. *Proc Natl Acad Sci U S A,* 85**,** 2349-52.

Tubert, C. & Murer, M. G. 2021. What's wrong with the striatal cholinergic interneurons in Parkinson's disease? Focus on intrinsic excitability. *Eur J Neurosci,* 53**,** 2100-2116.

Tucker, L. B. & Mccabe, J. T. 2017. Behavior of Male and Female C57BL/6J Mice Is More Consistent with Repeated Trials in the Elevated Zero Maze than in the Elevated Plus Maze. *Front Behav Neurosci,* 11**,** 13.

Turpin, J. C., Dubois, G., Brice, A., Masson, M., Nadaud, M. C., Boutry, J. M., Schram, A. W., Tager, J. M. & Baumann, N. 1988. Parkinsonian Symptomatology in a Patient

with Type I (Adult) Gaucher's Disease. *In:* SALVAYRE, R., DOUSTE-BLAZY, L. & GATT, S. (eds.) *Lipid Storage Disorders.* Boston, MA: Springer.

Tybulewicz, V. L., Tremblay, M. L., Lamarca, M. E., Willemsen, R., Stubblefield, B. K., Winfield, S., Zablocka, B., Sidransky, E., Martin, B. M., Huang, S. P. & Et Al. 1992. Animal model of Gaucher's disease from targeted disruption of the mouse glucocerebrosidase gene. *Nature,* 357**,** 407-10.

Uhlen, M., Fagerberg, L., Hallstrom, B. M., Lindskog, C., Oksvold, P., Mardinoglu, A., Sivertsson, A., Kampf, C., Sjostedt, E., Asplund, A., Olsson, I., Edlund, K., Lundberg, E., Navani, S., Szigyarto, C. A., Odeberg, J., Djureinovic, D., Takanen, J. O., Hober, S., Alm, T., Edqvist, P. H., Berling, H., Tegel, H., Mulder, J., Rockberg, J., Nilsson, P., Schwenk, J. M., Hamsten, M., Von Feilitzen, K., Forsberg, M., Persson, L., Johansson, F., Zwahlen, M., Von Heijne, G., Nielsen, J. & Ponten, F. 2015. Proteomics. Tissue-based map of the human proteome. *Science,* 347**,** 1260419.

Ullah, S., Park, T. J., Park, J. S., Atiq, A., Ali, J., Kang, M. H., Ali, W., Choe, K. & Kim, M. O. 2025. Ambroxol attenuates detrimental effect of LPS-induced glia-mediated neuroinflammation, oxidative stress, and cognitive dysfunction in mice brain. *Front Immunol,* 16**,** 1494114.

Usnich, T., Hanssen, H., Lohmann, K., Lohse, C., Klein, C., Kasten, M., Bruggemann, N. & Group, E. S. 2022. Pronounced Orthostatic Hypotension in GBA-Related Parkinson's Disease. *J Parkinsons Dis,* 12**,** 1539-1544.

Uspenskaya, O., Mahoney, E., Verselis, L., Lowrey, M., Velaga, J. & Sevigny, J. 2020. Design of Phase 1/2a Study of AAV9-Based Gene Therapy for Parkinson's Disease with Pathogenic GBA1 Mutations (PROPEL Trial) (1624). *Neurology,* 94.

Vaccaro, A. M., Muscillo, M. & Suzuki, K. 1985. Characterization of human glucosylsphingosine glucosyl hydrolase and comparison with glucosylceramidase. *Eur J Biochem,* 146**,** 315-21.

Vaccaro, A. M., Tatti, M., Ciaffoni, F., Salvioli, R., Maras, B. & Barca, A. 1993. Function of saposin C in the reconstitution of glucosylceramidase by phosphatidylserine liposomes. *FEBS Lett,* 336**,** 159-62.

Valdez, C., Ysselstein, D., Young, T. J., Zheng, J. & Krainc, D. 2020. Progranulin mutations result in impaired processing of prosaposin and reduced glucocerebrosidase activity. *Hum Mol Genet,* 29**,** 716-726.

Van Kampen, J. M. & Robertson, H. A. 2017. The BSSG rat model of Parkinson's disease: progressing towards a valid, predictive model of disease. *EPMA J,* 8**,** 261-271.

Van Weely, S., Brandsma, M., Strijland, A., Tager, J. M. & Aerts, J. M. 1993. Demonstration of the existence of a second, non-lysosomal glucocerebrosidase that is not deficient in Gaucher disease. *Biochim Biophys Acta,* 1181**,** 55-62.

Van Zundert, G. C. P., Rodrigues, J., Trellet, M., Schmitz, C., Kastritis, P. L., Karaca, E., Melquiond, A. S. J., Van Dijk, M., De Vries, S. J. & Bonvin, A. 2016. The HADDOCK2.2 Web Server: User-Friendly Integrative Modeling of Biomolecular Complexes. *J Mol Biol,* 428**,** 720-725.

Vangone, A. & Bonvin, A. 2017. PRODIGY: A Contact-based Predictor of Binding Affinity in Protein-protein Complexes. *Bio Protoc,* 7**,** e2124.

Vangone, A. & Bonvin, A. M. 2015. Contacts-based prediction of binding affinity in protein-protein complexes. *Elife,* 4**,** e07454.

Vangone, A., Rodrigues, J. P., Xue, L. C., Van Zundert, G. C., Geng, C., Kurkcuoglu, Z., Nellen, M., Narasimhan, S., Karaca, E., Van Dijk, M., Melquiond, A. S., Visscher, K. M., Trellet, M., Kastritis, P. L. & Bonvin, A. M. 2017. Sense and simplicity in HADDOCK scoring: Lessons from CASP-CAPRI round 1. *Proteins,* 85**,** 417-423.

Varadi, M., Bertoni, D., Magana, P., Paramval, U., Pidruchna, I., Radhakrishnan, M., Tsenkov, M., Nair, S., Mirdita, M., Yeo, J., Kovalevskiy, O., Tunyasuvunakool, K., Laydon, A., Zidek, A., Tomlinson, H., Hariharan, D., Abrahamson, J., Green, T., Jumper, J., Birney, E., Steinegger, M., Hassabis, D. & Velankar, S. 2024. AlphaFold Protein Structure Database in 2024: providing structure coverage for over 214 million protein sequences. *Nucleic Acids Res,* 52**,** D368-D375.

Vardi, A., Zigdon, H., Meshcheriakova, A., Klein, A. D., Yaacobi, C., Eilam, R., Kenwood, B. M., Rahim, A. A., Massaro, G., Merrill, A. H., Jr., Vitner, E. B. & Futerman, A. H. 2016. Delineating pathological pathways in a chemically induced mouse model of Gaucher disease. *J Pathol,* 239**,** 496-509.

Varkonyi, J., Rosenbaum, H., Baumann, N., Mackenzie, J. J., Simon, Z., Aharon-Peretz, J., Walker, J. M., Tayebi, N. & Sidransky, E. 2003. Gaucher disease associated with parkinsonism: four further case reports. *Am J Med Genet A,* 116A**,** 348-51.

Velez-Pardo, C., Lorenzo-Betancor, O., Jimenez-Del-Rio, M., Moreno, S., Lopera, F., Cornejo-Olivas, M., Torres, L., Inca-Martinez, M., Mazzetti, P., Cosentino, C., Yearout, D., Waldherr, S. M., Zabetian, C. P. & Mata, I. F. 2019. The distribution and risk effect of GBA variants in a large cohort of PD patients from Colombia and Peru. *Parkinsonism Relat Disord,* 63**,** 204-208.

Venton, B. J. & Cao, Q. 2020. Fundamentals of fast-scan cyclic voltammetry for dopamine detection. *Analyst,* 145**,** 1158-1168.

Vidovic, M. & Rikalovic, M. G. 2022. Alpha-Synuclein Aggregation Pathway in Parkinson's Disease: Current Status and Novel Therapeutic Approaches. *Cells,* 11.

Vidyadhara, D. J., Backstrom, D., Chakraborty, R., Ruan, J., Park, J. M., Mistry, P. K. & Chandra, S. S. 2025. Synaptic vesicle endocytosis deficits underlie GBA-linked cognitive dysfunction in Parkinson's disease and Dementia with Lewy bodies. *bioRxiv,* preprint**,** DOI: 10.1101/2024.10.23.619548.

Viel, C., Clarke, J., Kayatekin, C., Richards, A. M., Chiang, M. S. R., Park, H., Wang, B., Shihabuddin, L. S. & Sardi, S. P. 2021. Preclinical pharmacology of glucosylceramide synthase inhibitor venglustat in a GBA-related synucleinopathy model. *Sci Rep,* 11**,** 20945.

Vijiaratnam, N., Simuni, T., Bandmann, O., Morris, H. R. & Foltynie, T. 2021. Progress towards therapies for disease modification in Parkinson's disease. *Lancet Neurol,* 20**,** 559-572.

Vingill, S., Connor-Robson, N. & Wade-Martins, R. 2018. Are rodent models of Parkinson's disease behaving as they should? *Behav Brain Res,* 352**,** 133-141.

Voikar, V. & Gaburro, S. 2020. Three Pillars of Automated Home-Cage Phenotyping of Mice: Novel Findings, Refinement, and Reproducibility Based on Literature and Experience. *Front Behav Neurosci,* 14**,** 575434.

Voikar, V., Vasar, E. & Rauvala, H. 2004. Behavioral alterations induced by repeated testing in C57BL/6J and 129S2/Sv mice: implications for phenotyping screens. *Genes Brain Behav,* 3**,** 27-38.

Volta, M. & Melrose, H. 2017. LRRK2 mouse models: dissecting the behavior, striatal neurochemistry and neurophysiology of PD pathogenesis. *Biochem Soc Trans,* 45**,** 113-122.

Von Ziegler, L., Sturman, O. & Bohacek, J. 2021. Big behavior: challenges and opportunities in a new era of deep behavior profiling. *Neuropsychopharmacology,* 46**,** 33-44.

Wald, C. & Wu, C. 2010. Biomedical research. Of mice and women: the bias in animal models. *Science,* 327**,** 1571-2.

Walf, A. A. & Frye, C. A. 2007. The use of the elevated plus maze as an assay of anxiety-related behavior in rodents. *Nat Protoc,* 2**,** 322-8.

Walker, J. M., Lwin, A., Tayebi, N., Lamarca, M. E., Orvisky, E. & Sidransky, E. 2003. Glucocerebrosidase mutation T369M appears to be another polymorphism. *Clin Genet,* 63**,** 237-8.

Walton, S., Fenyi, A., Tittle, T., Sidransky, E., Pal, G., Choi, S., Melki, R., Killinger, B. A. & Kordower, J. H. 2024. Neither alpha-synuclein fibril strain nor host murine genotype influences seeding efficacy. *NPJ Parkinsons Dis,* 10**,** 105.

Walusinski, O. 2018. Jean-Martin Charcot and Parkinson's disease: Teaching and teaching materials. *Rev Neurol (Paris),* 174**,** 491-505.

Wang, C., Cai, Y., Gu, Z., Ma, J., Zheng, Z., Tang, B. S., Xu, Y., Zhou, Y., Feng, T., Wang, T., Chen, S. D., Chan, P. & Chinese Parkinson Study, G. 2014. Clinical profiles of Parkinson's disease associated with common leucine-rich repeat kinase 2 and glucocerebrosidase genetic variants in Chinese individuals. *Neurobiol Aging,* 35**,** 725 e1-6.

Wang, H. F., Yu, J. T., Tang, S. W., Jiang, T., Tan, C. C., Meng, X. F., Wang, C., Tan, M. S. & Tan, L. 2015. Efficacy and safety of cholinesterase inhibitors and memantine in cognitive impairment in Parkinson's disease, Parkinson's disease dementia, and dementia with Lewy bodies: systematic review with meta-analysis and trial sequential analysis. *J Neurol Neurosurg Psychiatry,* 86**,** 135-43.

Wang, J. W., Zhang, Y. Q., Zhang, X. H., Wang, Y. P., Li, J. P. & Li, Y. J. 2016. Cognitive and Psychiatric Effects of STN versus GPi Deep Brain Stimulation in Parkinson's Disease: A Meta-Analysis of Randomized Controlled Trials. *PLoS One,* 11**,** e0156721.

Wang, P., Chen, X., Na, M., Flores-Torres, M. H., Bjornevik, K., Zhang, X., Chen, X., Khandpur, N., Rossato, S. L., Zhang, F. F., Ascherio, A. & Gao, X. 2025. Long-Term Consumption of Ultraprocessed Foods and Prodromal Features of Parkinson Disease. *Neurology,* 104**,** e213562.

Wang, W., Perovic, I., Chittuluru, J., Kaganovich, A., Nguyen, L. T., Liao, J., Auclair, J. R., Johnson, D., Landeru, A., Simorellis, A. K., Ju, S., Cookson, M. R., Asturias, F. J., Agar, J. N., Webb, B. N., Kang, C., Ringe, D., Petsko, G. A., Pochapsky, T. C. & Hoang, Q. Q. 2011. A soluble alpha-synuclein construct forms a dynamic tetramer. *Proc Natl Acad Sci U S A,* 108**,** 17797-802.

Wasner, K., Grunewald, A. & Klein, C. 2020. Parkin-linked Parkinson's disease: From clinical insights to pathogenic mechanisms and novel therapeutic approaches. *Neurosci Res,* 159**,** 34-39.

Wei, H., Kim, S. J., Zhang, Z., Tsai, P. C., Wisniewski, K. E. & Mukherjee, A. B. 2008. ER and oxidative stresses are common mediators of apoptosis in both neurodegenerative and non-neurodegenerative lysosomal storage disorders and are alleviated by chemical chaperones. *Hum Mol Genet,* 17**,** 469-77.

Wei, R. R., Hughes, H., Boucher, S., Bird, J. J., Guziewicz, N., Van Patten, S. M., Qiu, H., Pan, C. Q. & Edmunds, T. 2011. X-ray and biochemical analysis of N370S mutant human acid beta-glucosidase. *J Biol Chem,* 286**,** 299-308.

Weiner, W. J. 2008. There is no Parkinson disease. *Arch Neurol,* 65**,** 705-8.

Weintraub, D., Aarsland, D., Chaudhuri, K. R., Dobkin, R. D., Leentjens, A. F., Rodriguez-Violante, M. & Schrag, A. 2022. The neuropsychiatry of Parkinson's disease: advances and challenges. *Lancet Neurol,* 21**,** 89-102.

Weiss, K., Gonzalez, A., Lopez, G., Pedoeim, L., Groden, C. & Sidransky, E. 2015. The clinical management of Type 2 Gaucher disease. *Mol Genet Metab,* 114**,** 110-122.

Wenger, N., Vogt, A., Skrobot, M., Garulli, E. L., Kabaoglu, B., Salchow-Hommen, C., Schauer, T., Kroneberg, D., Schuhmann, M. K., Ip, C. W., Harms, C., Endres, M.,

Isaias, I. U., Tovote, P. & Blum, R. 2022. Rodent models for gait network disorders in Parkinson's disease - a translational perspective. *Exp Neurol,* 352**,** 114011.

West, A. B., Moore, D. J., Biskup, S., Bugayenko, A., Smith, W. W., Ross, C. A., Dawson, V. L. & Dawson, T. M. 2005. Parkinson's disease-associated mutations in leucine-rich repeat kinase 2 augment kinase activity. *Proc Natl Acad Sci U S A,* 102**,** 16842-7.

Westenberger, A., Skrahina, V., Usnich, T., Beetz, C., Vollstedt, E. J., Laabs, B. H., Paul, J. J., Curado, F., Skobalj, S., Gaber, H., Olmedillas, M., Bogdanovic, X., Ameziane, N., Schell, N., Aasly, J. O., Afshari, M., Agarwal, P., Aldred, J., Alonso-Frech, F., Anderson, R., Araujo, R., Arkadir, D., Avenali, M., Balal, M., Benizri, S., Bette, S., Bhatia, P., Bonello, M., Braga-Neto, P., Brauneis, S., Cardoso, F. E. C., Cavallieri, F., Classen, J., Cohen, L., Coletta, D., Crosiers, D., Cullufi, P., Dashtipour, K., Demirkiran, M., De Carvalho Aguiar, P., De Rosa, A., Djaldetti, R., Dogu, O., Dos Santos Ghilardi, M. G., Eggers, C., Elibol, B., Ellenbogen, A., Ertan, S., Fabiani, G., Falkenburger, B. H., Farrow, S., Fay-Karmon, T., Ferencz, G. J., Fonoff, E. T., Fragoso, Y. D., Genc, G., Gorospe, A., Grandas, F., Gruber, D., Gudesblatt, M., Gurevich, T., Hagenah, J., Hanagasi, H. A., Hassin-Baer, S., Hauser, R. A., Hernandez-Vara, J., Herting, B., Hinson, V. K., Hogg, E., Hu, M. T., Hummelgen, E., Hussey, K., Infante, J., Isaacson, S. H., Jauma, S., Koleva-Alazeh, N., Kuhlenbaumer, G., Kuhn, A., Litvan, I., Lopez-Manzanares, L., Luxmore, M., Manandhar, S., Marcaud, V., Markopoulou, K., Marras, C., Mckenzie, M., Matarazzo, M., Merello, M., Mollenhauer, B., Morgan, J. C., Mullin, S., Musacchio, T., Myers, B., Negrotti, A., Nieves, A., Nitsan, Z., Oskooilar, N., Oztop-Cakmak, O., Pal, G., Pavese, N., et al. 2024. Relevance of genetic testing in the gene-targeted trial era: the Rostock Parkinson's disease study. *Brain,* 147**,** 2652-2667.

Westphal, C. H. & Chandra, S. S. 2013. Monomeric synucleins generate membrane curvature. *J Biol Chem,* 288**,** 1829-40.

Wichmann, T., Nelson, A., Torres, E. R. S., Svenningsson, P. & Marongiu, R. 2025. Leveraging animal models to understand non-motor symptoms of Parkinson's disease. *Neurobiol Dis,* 208**,** 106848.

Wieland, S., Du, D., Oswald, M. J., Parlato, R., Kohr, G. & Kelsch, W. 2014. Phasic dopaminergic activity exerts fast control of cholinergic interneuron firing via sequential NMDA, D2, and D1 receptor activation. *J Neurosci,* 34**,** 11549-59.

Wilkening, G., Linke, T. & Sandhoff, K. 1998. Lysosomal degradation on vesicular membrane surfaces. Enhanced glucosylceramide degradation by lysosomal anionic lipids and activators. *J Biol Chem,* 273**,** 30271-8.

Willis, A. W., Evanoff, B. A., Lian, M., Galarza, A., Wegrzyn, A., Schootman, M. & Racette, B. A. 2010. Metal emissions and urban incident Parkinson disease: a community health study of Medicare beneficiaries by using geographic information systems. *Am J Epidemiol,* 172**,** 1357-63.

Willis, A. W., Schootman, M., Evanoff, B. A., Perlmutter, J. S. & Racette, B. A. 2011. Neurologist care in Parkinson disease: a utilization, outcomes, and survival study. *Neurology,* 77**,** 851-7.

Winder-Rhodes, S. E., Evans, J. R., Ban, M., Mason, S. L., Williams-Gray, C. H., Foltynie, T., Duran, R., Mencacci, N. E., Sawcer, S. J. & Barker, R. A. 2013. Glucocerebrosidase mutations influence the natural history of Parkinson's disease in a community-based incident cohort. *Brain,* 136**,** 392-9.

Winfield, S. L., Tayebi, N., Martin, B. M., Ginns, E. I. & Sidransky, E. 1997. Identification of three additional genes contiguous to the glucocerebrosidase locus on chromosome 1q21: implications for Gaucher disease. *Genome Res,* 7**,** 1020-6.

Woeste, M. A., Stern, S., Raju, D. N., Grahn, E., Dittmann, D., Gutbrod, K., Dormann, P., Hansen, J. N., Schonauer, S., Marx, C. E., Hamzeh, H., Korschen, H. G., Aerts, J., Bonigk, W., Endepols, H., Sandhoff, R., Geyer, M., Berger, T. K., Bradke, F. & Wachten, D. 2019. Species-specific differences in nonlysosomal glucosylceramidase GBA2 function underlie locomotor dysfunction arising from loss-of-function mutations. *J Biol Chem,* 294**,** 3853-3871.

Woeste, M. A. & Wachten, D. 2017. The Enigmatic Role of GBA2 in Controlling Locomotor Function. *Front Mol Neurosci,* 10**,** 386.

Woitalla, D., Buhmann, C., Hilker-Roggendorf, R., Hoglinger, G., Koschel, J., Muller, T. & Weise, D. 2023. Role of dopamine agonists in Parkinson's disease therapy. *J Neural Transm (Vienna),* 130**,** 863-873.

Wong, Y. C., Luk, K., Purtell, K., Burke Nanni, S., Stoessl, A. J., Trudeau, L. E., Yue, Z., Krainc, D., Oertel, W., Obeso, J. A. & Volpicelli-Daley, L. A. 2019. Neuronal vulnerability in Parkinson disease: Should the focus be on axons and synaptic terminals? *Mov Disord,* 34**,** 1406-1422.

Woo, E. G., Tayebi, N. & Sidransky, E. 2021. Next-Generation Sequencing Analysis of GBA1: The Challenge of Detecting Complex Recombinant Alleles. *Front Genet,* 12**,** 684067.

Woodard, C. M., Campos, B. A., Kuo, S. H., Nirenberg, M. J., Nestor, M. W., Zimmer, M., Mosharov, E. V., Sulzer, D., Zhou, H., Paull, D., Clark, L., Schadt, E. E., Sardi, S. P., Rubin, L., Eggan, K., Brock, M., Lipnick, S., Rao, M., Chang, S., Li, A. & Noggle, S. A. 2014. iPSC-derived dopamine neurons reveal differences between monozygotic twins discordant for Parkinson's disease. *Cell Rep,* 9**,** 1173-82.

Wu, C. Y. C., Lerner, F. M., Couto, E. S. A., Possoit, H. E., Hsieh, T. H., Neumann, J. T., Minagar, A., Lin, H. W. & Lee, R. H. C. 2018. Utilizing the Modified T-Maze to Assess Functional Memory Outcomes After Cardiac Arrest. *J Vis Exp*.

Wu, Y. R., Chen, C. M., Chao, C. Y., Ro, L. S., Lyu, R. K., Chang, K. H. & Lee-Chen, G. J. 2007. Glucocerebrosidase gene mutation is a risk factor for early onset of Parkinson disease among Taiwanese. *J Neurol Neurosurg Psychiatry,* 78**,** 977-9.

Xu, T., Dong, W., Liu, J., Yin, P., Wang, Z., Zhang, L. & Zhou, M. 2024. Disease burden of Parkinson's disease in China and its provinces from 1990 to 2021: findings from the global burden of disease study 2021. *Lancet Reg Health West Pac,* 46**,** 101078.

Xu, Y. H., Quinn, B., Witte, D. & Grabowski, G. A. 2003. Viable mouse models of acid beta-glucosidase deficiency: the defect in Gaucher disease. *Am J Pathol,* 163**,** 2093-101.

Xu, Y. H., Sun, Y., Ran, H., Quinn, B., Witte, D. & Grabowski, G. A. 2011. Accumulation and distribution of alpha-synuclein and ubiquitin in the CNS of Gaucher disease mouse models. *Mol Genet Metab,* 102**,** 436-47.

Yahalom, G., Greenbaum, L., Israeli-Korn, S., Fay-Karmon, T., Livneh, V., Ruskey, J. A., Ronciere, L., Alam, A., Gan-Or, Z. & Hassin-Baer, S. 2019. Carriers of both GBA and LRRK2 mutations, compared to carriers of either, in Parkinson's disease: Risk estimates and genotype-phenotype correlations. *Parkinsonism Relat Disord,* 62**,** 179-184.

Yamaguchi, Y., Sasagasako, N., Goto, I. & Kobayashi, T. 1994. The synthetic pathway for glucosylsphingosine in cultured fibroblasts. *J Biochem,* 116**,** 704-10.

Yanai, S. & Endo, S. 2021. Functional Aging in Male C57BL/6J Mice Across the Life-Span: A Systematic Behavioral Analysis of Motor, Emotional, and Memory Function to Define an Aging Phenotype. *Front Aging Neurosci,* 13**,** 697621.

Yang, S. Y., Gegg, M., Chau, D. & Schapira, A. 2020a. Glucocerebrosidase activity, cathepsin D and monomeric alpha-synuclein interactions in a stem cell derived neuronal model of a PD associated GBA1 mutation. *Neurobiol Dis,* 134**,** 104620.

Yang, S. Y., Taanman, J. W., Gegg, M. & Schapira, A. H. V. 2022. Ambroxol reverses tau and alpha-synuclein accumulation in a cholinergic N370S GBA1 mutation model. *Hum Mol Genet,* 31**,** 2396-2405.

Yang, W., Hamilton, J. L., Kopil, C., Beck, J. C., Tanner, C. M., Albin, R. L., Ray Dorsey, E., Dahodwala, N., Cintina, I., Hogan, P. & Thompson, T. 2020b. Current and projected future economic burden of Parkinson's disease in the U.S. *NPJ Parkinsons Dis,* 6**,** 15.

Yang, X. W. & Gong, S. 2005. An overview on the generation of BAC transgenic mice for neuroscience research. *Curr Protoc Neurosci,* Chapter 5**,** Unit 5 20.

Yang, X. W., Model, P. & Heintz, N. 1997. Homologous recombination based modification in Escherichia coli and germline transmission in transgenic mice of a bacterial artificial chromosome. *Nat Biotechnol,* 15**,** 859-65.

Yao, Y. N., Wang, M. D., Tang, X. C., Wu, B. & Sun, H. M. 2020. Reduced plasma progranulin levels are associated with the severity of Parkinson's disease. *Neurosci Lett,* 725**,** 134873.

Yap, T. L., Gruschus, J. M., Velayati, A., Sidransky, E. & Lee, J. C. 2013a. Saposin C protects glucocerebrosidase against alpha-synuclein inhibition. *Biochemistry,* 52**,** 7161-3.

Yap, T. L., Gruschus, J. M., Velayati, A., Westbroek, W., Goldin, E., Moaven, N., Sidransky, E. & Lee, J. C. 2011. Alpha-synuclein interacts with Glucocerebrosidase providing a molecular link between Parkinson and Gaucher diseases. *J Biol Chem,* 286**,** 28080-8.

Yap, T. L., Jiang, Z., Heinrich, F., Gruschus, J. M., Pfefferkorn, C. M., Barros, M., Curtis, J. E., Sidransky, E. & Lee, J. C. 2015. Structural features of membrane-bound glucocerebrosidase and alpha-synuclein probed by neutron reflectometry and fluorescence spectroscopy. *J Biol Chem,* 290**,** 744-54.

Yap, T. L., Velayati, A., Sidransky, E. & Lee, J. C. 2013b. Membrane-bound alpha-synuclein interacts with glucocerebrosidase and inhibits enzyme activity. *Mol Genet Metab,* 108**,** 56-64.

Yildiz, Y., Matern, H., Thompson, B., Allegood, J. C., Warren, R. L., Ramirez, D. M., Hammer, R. E., Hamra, F. K., Matern, S. & Russell, D. W. 2006. Mutation of beta-glucosidase 2 causes glycolipid storage disease and impaired male fertility. *J Clin Invest,* 116**,** 2985-94.

Yoon, J., Lee, C. Y. & Ah, V. S. 2024. Biochemical consequences of glucocerebrosidase 1 mutations in Parkinson's disease. *Neural Regen Res,* 19**,** 725-727.

Ysselstein, D., Nguyen, M., Young, T. J., Severino, A., Schwake, M., Merchant, K. & Krainc, D. 2019. LRRK2 kinase activity regulates lysosomal glucocerebrosidase in neurons derived from Parkinson's disease patients. *Nat Commun,* 10**,** 5570.

Ysselstein, D., Young, T. J., Nguyen, M., Padmanabhan, S., Hirst, W. D., Dzamko, N. & Krainc, D. 2021. Evaluation of Strategies for Measuring Lysosomal Glucocerebrosidase Activity. *Mov Disord,* 36**,** 2719-2730.

Yun, S. P., Kim, D., Kim, S., Kim, S., Karuppagounder, S. S., Kwon, S. H., Lee, S., Kam, T. I., Lee, S., Ham, S., Park, J. H., Dawson, V. L., Dawson, T. M., Lee, Y. & Ko, H. S. 2018. alpha-Synuclein accumulation and GBA deficiency due to L444P GBA mutation contributes to MPTP-induced parkinsonism. *Mol Neurodegener,* 13**,** 1.

Zachos, C., Blanz, J., Saftig, P. & Schwake, M. 2012. A critical histidine residue within LIMP-2 mediates pH sensitive binding to its ligand beta-glucocerebrosidase. *Traffic,* 13**,** 1113-23.

Zambrowicz, B. P., Imamoto, A., Fiering, S., Herzenberg, L. A., Kerr, W. G. & Soriano, P. 1997. Disruption of overlapping transcripts in the ROSA beta geo 26 gene trap strain

leads to widespread expression of beta-galactosidase in mouse embryos and hematopoietic cells. *Proc Natl Acad Sci U S A,* 94**,** 3789-94.

Zampieri, S., Cattarossi, S., Bembi, B. & Dardis, A. 2017. GBA Analysis in Next-Generation Era: Pitfalls, Challenges, and Possible Solutions. *J Mol Diagn,* 19**,** 733-741.

Zeiss, C. J., Allore, H. G. & Beck, A. P. 2017. Established patterns of animal study design undermine translation of disease-modifying therapies for Parkinson's disease. *PLoS One,* 12**,** e0171790.

Zhang, C., Chen, S., Li, X., Xu, Q., Lin, Y., Lin, F., Yuan, M., Zi, Y. & Cai, J. 2022a. Progress in Parkinson's disease animal models of genetic defects: Characteristics and application. *Biomed Pharmacother,* 155**,** 113768.

Zhang, H. & Sulzer, D. 2004. Frequency-dependent modulation of dopamine release by nicotine. *Nat Neurosci,* 7**,** 581-2.

Zhang, H. B., Ding, X. B., Jin, J., Guo, W. P., Yang, Q. L., Chen, P. C., Yao, H., Ruan, L., Tao, Y. T. & Chen, X. 2022b. Predicted mouse interactome and network-based interpretation of differentially expressed genes. *PLoS One,* 17**,** e0264174.

Zhang, R., Shu, L., Zhu, Q. & Li, N. 2025a. Adherence to a priori and a posteriori dietary patterns and risk of Parkinson's disease: a systematic review and meta-analysis of observational studies. *Front Nutr,* 12**,** 1600955.

Zhang, T. D., Kolbe, S. C., Beauchamp, L. C., Woodbridge, E. K., Finkelstein, D. I. & Burrows, E. L. 2022c. How Well Do Rodent Models of Parkinson's Disease Recapitulate Early Non-Motor Phenotypes? A Systematic Review. *Biomedicines,* 10.

Zhang, Y., Shu, L., Sun, Q., Zhou, X., Pan, H., Guo, J. & Tang, B. 2018a. Integrated Genetic Analysis of Racial Differences of Common GBA Variants in Parkinson's Disease: A Meta-Analysis. *Front Mol Neurosci,* 11**,** 43.

Zhang, Y., Shu, L., Zhou, X., Pan, H., Xu, Q., Guo, J., Tang, B. & Sun, Q. 2018b. A Meta-Analysis of GBA-Related Clinical Symptoms in Parkinson's Disease. *Parkinsons Dis,* 2018**,** 3136415.

Zhang, Y., Sun, Q. Y., Zhao, Y. W., Shu, L., Guo, J. F., Xu, Q., Yan, X. X. & Tang, B. S. 2015. Effect of GBA Mutations on Phenotype of Parkinson's Disease: A Study on Chinese Population and a Meta-Analysis. *Parkinsons Dis,* 2015**,** 916971.

Zhang, Y. F., Luan, P., Qiao, Q., He, Y., Zatka-Haas, P., Zhang, G., Lin, M. Z., Lak, A., Jing, M., Mann, E. O. & Cragg, S. J. 2025b. An axonal brake on striatal dopamine output by cholinergic interneurons. *Nat Neurosci,* 28**,** 783-794.

Zhao, C., Wang, C., Zhang, H. & Yan, W. 2023a. A mini-review of the role of vesicular glutamate transporters in Parkinson's disease. *Front Mol Neurosci,* 16**,** 1118078.

Zhao, J., Peng, Y., Lin, Z. & Gong, Y. 2025. Association between Mediterranean diet adherence and Parkinson's disease: a systematic review and meta-analysis. *J Nutr Health Aging,* 29**,** 100451.

Zhao, X., Lin, Y., Liou, B., Fu, W., Jian, J., Fannie, V., Zhang, W., Setchell, K. D. R., Grabowski, G. A., Sun, Y. & Liu, C. J. 2023b. PGRN deficiency exacerbates, whereas a brain penetrant PGRN derivative protects, GBA1 mutation-associated pathologies and diseases. *Proc Natl Acad Sci U S A,* 120**,** e2210442120.

Zhao, Y., Perera, G., Takahashi-Fujigasaki, J., Mash, D. C., Vonsattel, J. P. G., Uchino, A., Hasegawa, K., Jeremy Nichols, R., Holton, J. L., Murayama, S., Dzamko, N. & Halliday, G. M. 2018. Reduced LRRK2 in association with retromer dysfunction in post-mortem brain tissue from LRRK2 mutation carriers. *Brain,* 141**,** 486-495.

Zhao, Y., Qin, L., Pan, H., Liu, Z., Jiang, L., He, Y., Zeng, Q., Zhou, X., Zhou, X., Zhou, Y., Fang, Z., Wang, Z., Xiang, Y., Yang, H., Wang, Y., Zhang, K., Zhang, R., He, R., Zhou, X., Zhou, Z., Yang, N., Liang, D., Chen, J., Zhang, X., Zhou, Y., Liu, H., Deng, P., Xu, K., Xu, K., Zhou, C., Zhong, J., Xu, Q., Sun, Q., Li, B., Zhao, G., Wang, T.,

Chen, L., Shang, H., Liu, W., Chan, P., Xue, Z., Wang, Q., Guo, L., Wang, X., Xu, C., Zhang, Z., Chen, T., Lei, L., Zhang, H., Wang, C., Tan, J., Yan, X., Shen, L., Jiang, H., Zhang, Z., Hu, Z., Xia, K., Yue, Z., Li, J., Guo, J. & Tang, B. 2020. The role of genetics in Parkinson's disease: a large cohort study in Chinese mainland population. *Brain,* 143**,** 2220-2234.

Zhao, Y., Ren, J., Padilla-Parra, S., Fry, E. E. & Stuart, D. I. 2014. Lysosome sorting of beta-glucocerebrosidase by LIMP-2 is targeted by the mannose 6-phosphate receptor. *Nat Commun,* 5**,** 4321.

Zhou, F. M., Liang, Y. & Dani, J. A. 2001. Endogenous nicotinic cholinergic activity regulates dopamine release in the striatum. *Nat Neurosci,* 4**,** 1224-9.

Zhou, X., Paushter, D. H., Pagan, M. D., Kim, D., Nunez Santos, M., Lieberman, R. L., Overkleeft, H. S., Sun, Y., Smolka, M. B. & Hu, F. 2019. Progranulin deficiency leads to reduced glucocerebrosidase activity. *PLoS One,* 14**,** e0212382.

Zhou, X., Sun, L., Bracko, O., Choi, J. W., Jia, Y., Nana, A. L., Brady, O. A., Hernandez, J. C. C., Nishimura, N., Seeley, W. W. & Hu, F. 2017. Impaired prosaposin lysosomal trafficking in frontotemporal lobar degeneration due to progranulin mutations. *Nat Commun,* 8**,** 15277.

Zhou, Y., Wang, Y., Wan, J., Zhao, Y., Pan, H., Zeng, Q., Zhou, X., He, R., Zhou, X., Xiang, Y., Zhou, Z., Chen, B., Sun, Q., Xu, Q., Tan, J., Shen, L., Jiang, H., Yan, X., Li, J., Guo, J., Tang, B., Wu, H. & Liu, Z. 2023. Mutational spectrum and clinical features of GBA1 variants in a Chinese cohort with Parkinson's disease. *NPJ Parkinsons Dis,* 9**,** 129.

Zhu, J., Cui, Y., Zhang, J., Yan, R., Su, D., Zhao, D., Wang, A. & Feng, T. 2024. Temporal trends in the prevalence of Parkinson's disease from 1980 to 2023: a systematic review and meta-analysis. *Lancet Healthy Longev,* 5**,** e464-e479.

Zirra, A., Rao, S. C., Bestwick, J., Rajalingam, R., Marras, C., Blauwendraat, C., Mata, I. F. & Noyce, A. J. 2023. Gender Differences in the Prevalence of Parkinson's Disease. *Mov Disord Clin Pract,* 10**,** 86-93.

Zunke, F., Andresen, L., Wesseler, S., Groth, J., Arnold, P., Rothaug, M., Mazzulli, J. R., Krainc, D., Blanz, J., Saftig, P. & Schwake, M. 2016. Characterization of the complex formed by beta-glucocerebrosidase and the lysosomal integral membrane protein type-2. *Proc Natl Acad Sci U S A,* 113**,** 3791-6.

Zunke, F., Moise, A. C., Belur, N. R., Gelyana, E., Stojkovska, I., Dzaferbegovic, H., Toker, N. J., Jeon, S., Fredriksen, K. & Mazzulli, J. R. 2018. Reversible Conformational Conversion of alpha-Synuclein into Toxic Assemblies by Glucosylceramide. *Neuron,* 97**,** 92-107 e10.